TEXTE
123/2024

Final report

Manual on Methodologies and Criteria for Modelling and Mapping Critical Loads and Levels and Air Pollution Effects, Risks, and Trends

Update 2024

by:
UNECE Convention on Long-range Transboundary Air Pollution (CLRTAP)

publisher:
German Environment Agency

German Environment Agency

45 YEARS 1979-2024 AIR CONVENTION

Umwelt Bundesamt

TEXTE 123/2024

Final report

Manual on Methodologies and Criteria for Modelling and Mapping Critical Loads and Levels and Air Pollution Effects, Risks, and Trends

Update 2024

by

UNECE Convention on Long-range Transboundary Air Pollution (CLRTAP)

On behalf of the German Environment Agency

Imprint

Publisher
Umweltbundesamt
Wörlitzer Platz 1
06844 Dessau-Roßlau
Tel: +49 340-2103-0
Fax: +49 340-2103-2285
buergerservice@uba.de
Internet: www.umweltbundesamt.de

Report updated by:
Coordination Centre for Effects (CCE)
Wörlitzer Platz 1
06844 Dessau-Roßlau
Germany

Report completed in:
December 2022

Edited by:
Coordination Centre for Effects (CCE)

Publication as pdf:
http://www.umweltbundesamt.de/publikationen

ISSN 1862-4804

Dessau-Roßlau, September 2024

Abstract: Manual on Methodologies and Criteria for Modelling and Mapping Critical Loads and Levels and Air Pollution Effects, Risks, and Trends

This Manual presents methods that are recommended for use by the Parties to the Convention, represented by their National Focal Centres. The Modelling and Mapping Manual can help and assist NFCs to:

1. Model and map critical levels and loads in the ECE region;
2. Model and map areas with air pollution values exceeding critical levels or loads;
3. Develop, harmonize and apply methods and procedures (including dynamic modelling) to assess recovery and risk of future damage on specific targets including biodiversity in a context of climate change;
4. Determine and identify sensitive receptors and locations.

Thus, it provides a scientific basis on the application of critical levels and loads, their interrelationships, and the consequences for abatement strategies, e.g., for the assessment of optimized allocation of emission reductions.

This Manual includes methodologies used by ICP Materials to assess the impact of pollution on corrosion and soiling of building materials (Ch. 4) and by ICP Vegetation concerning the impact of air pollutants, and especially ozone, on crops and semi-natural vegetation (Ch. 3). In contrast to Manuals (or comparable methodological documents) of other ICPs and EMEP CCC, this manual does not contain information on methods of measurements nor on detailed data generation. This reflects the aims and tasks of the ICP Modelling and Mapping within the Convention.

Specific technical information as well as detailed results and other information by National Focal Centres can be found in CCE Status Reports and publications (www.umweltbundesamt.de/en/cce-manual and bibliographic references therein).

Kurzbeschreibung: Handbuch zu Methoden und Kriterien für die Modellierung und Kartierung von Critical Loads und Levels, sowie von Auswirkungen, Risiken und Trends der Luftverschmutzung

In diesem Handbuch werden Methoden vorgestellt, die den Vertragsparteien der Genfer Luftreinhaltekonvention, vertreten durch ihre National Focal Centres, zur Anwendung empfohlen werden. Das Modellierungs- und Kartierungshandbuch kann den NFCs helfen und sie unterstützen bei:

1. Der Modellierung und Kartierung von Critical Levels und Loads in der ECE-Region
2. Der Modellierung und Kartierung von Gebieten mit Luftverschmutzungswerten, die Critical Levels oder Loads überschreiten;
3. Der Entwicklung, Harmonisierung und Anwendung von Methoden und Verfahren (einschließlich dynamischer Modelle) zur Bewertung der Erholung und des Risikos künftiger Schäden an spezifischen Zielen, einschließlich der biologischen Vielfalt, im Zusammenhang mit dem Klimawandel;
4. Der Bestimmung und Identifizierung empfindlicher Rezeptoren und Standorte.

Damit bietet es eine wissenschaftliche Grundlage für die Anwendung von Critical Levels und Loads, ihre Wechselbeziehungen und die Folgen für Vermeidungsstrategien, z. B. für die Bewertung einer optimierten Zuteilung von Emissionsreduktionen.

Dieses Handbuch enthält Methoden, die von der ICP Materials zur Bewertung der Auswirkungen der Verschmutzung auf Korrosion und Verschmutzung von Baumaterialien (Kap. 4) und von der ICP Vegetation zur Bewertung der Auswirkungen von Luftschadstoffen, insbesondere von Ozon, auf Pflanzen und naturnahe Vegetation (Kap. 3) verwendet werden. Im Gegensatz zu den

Handbüchern (oder vergleichbaren methodischen Dokumenten) anderer ICPs und des EMEP CCC enthält dieses Handbuch keine Informationen zu Messmethoden oder zur detaillierten Datengenerierung. Dies spiegelt die Ziele und Aufgaben des ICP Modelling and Mapping im Rahmen des Übereinkommens wider.

Spezifische technische Informationen sowie detaillierte Ergebnisse und andere Informationen der Nationalen Zentren sind in den Statusberichten und Veröffentlichungen des CCE zu finden (www.umweltbundesamt.de/en/cce-manual und darin enthaltene bibliographische Hinweise).

Table of Contents

List of Figures

List of Tables

List of Abbreviations

CO_2	Carbon dioxide
COP	Conference of the Parties
EU-ETS	EU Emissions Trading Scheme

CO_2	Carbon dioxide
F-gases	Fluorinated greenhouse gases
FTIP	Federal Transport Infrastructure Plan
GHG	Greenhouse gas
HGV	Heavy goods vehicle
ICAO	International Civil Aviation Organization
IMO	International Maritime Organization
KSBV	UBA-study Klimaschutzbeitrag des Verkehrs bis 2050 [UBA, 2016a]
NDC	Nationally Determined Contributions (in Paris-Agreement)
NEDC	New European Driving Cycle
N_2O	Nitrous oxide (laughing gas)
PJ	Petajoule (energy measuring unit)
PtG	Power-to-Gas (any power-based gaseous fuels)
PtL	Power-to-Liquid (any power-based liquid fuels)
RDE	Real Driving Emissions
TWh	Terawatt hours (measuring units for energy)
UNFCCC	United Nations Framework Convention on Climate Change
WLTP	Worldwide Harmonized Light-Duty Vehicles Test Procedure

1 Introduction

Last updated in 2015 by Anne Christine Le Gall, Chairwoman of the Task Force on Modelling and Mapping and Jean Paul Hettelingh, CCE, from initial text by Till Spranger, Mapping Manual 2004.

Please refer to this document as: CLRTAP, 2015. Introduction, Chapter 1 of Manual on methodologies and criteria for modelling and mapping critical loads and levels and air pollution effects, risks, and trends. UNECE Convention on Long-range Transboundary Air Pollution; accessed on [date of consultation] on the Web at www.umweltbundesamt.de/en/cce-manual.

1.1 Overview

The critical loads and levels concept is an effect-based approach by which the need for the reduction of atmospheric depositions can be quantified. As a consequence, the concept allows the quantification of atmospheric pollutants emission abatement at their source. The critical load and level concept were developed under the Convention on Long-range Transboundary Air Pollution (LRTAP-Convention) and was first applied under its effect-oriented scientific programmes (Hettelingh et al, 2004). The concept has been used for defining emission reductions aimed at protecting ecosystems and other receptors, such as materials and human health. It is based on indicators defined for specific pollutants, effects, and receptors. Critical loads and levels provide a reference point for the sustainability of air pollution against which actual as well as modelled pollution levels can be compared. They have been used in a framework to address the sustainability of (combinations of) pollution drivers and effects and in particular in the effect-based support of the Protocol to Abate Acidification, Eutrophication and Ground level Ozone under the LRTAP-Convention (e.g., Reiss et al, 2012) and the national Emission Ceiling Directive of the European Commission (e.g., Hettelingh et al. 2013). This support consisted of calculating emission ceilings for individual countries with respect to acceptable air pollution levels (e.g., defined reductions of critical load/level exceedances). Critical loads and levels have been designed to support the setting of ambition levels and assess the efficiency of air pollution reduction policies. In policy frameworks such as the LRTAP-Convention, they have been developed and applied for scenario analyses or optimization of effect-based emission reduction, as shown in Figure 1.1.

Definition of the critical load concept

Critical loads are related to indirect, soil-mediated effects of elevated deposition and are defined as “a quantitative estimate of an exposure to one or more pollutants below which significant harmful effects on specified sensitive elements of the environment do not occur according to present knowledge” (Nilsson and Grennfelt 1988). Critical levels are defined almost similarly, i.e., as ambient concentrations above which damage may occur.

Critical loads and levels correspond to a maximum allowable exposure of a receptor to deposition or ambient concentration respectively. The implications of these definitions in terms of calculations and applications within scientific and policy frameworks are presented in Chapters 3, 5 and 6.

Figure 1.1: Effect based emission reduction optimization and scenario analysis (adapted from Harald Sverdrup)

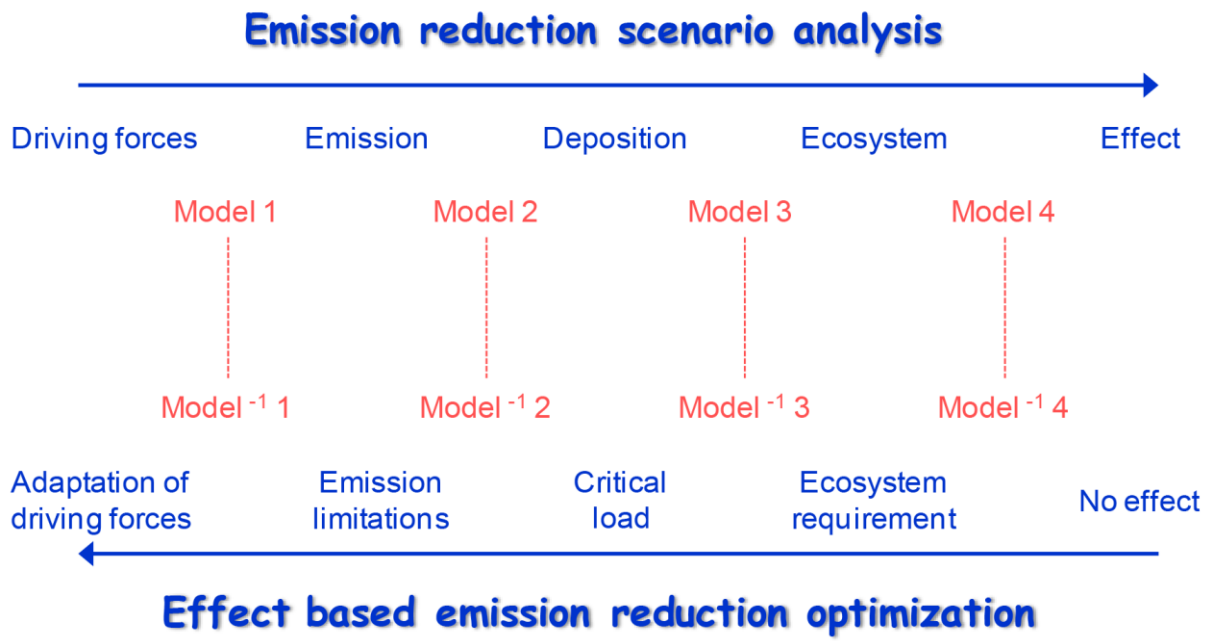

Source: This figure is adopted from a previous version of Chapter 1 of the Mapping Manual

1.2 The critical load and level concept in the UNECE Convention on Long-range Transboundary Air Pollution

During the 1970s, it was recognised that trans-boundary air pollution has ecological and economic consequences (e.g., for the forest and fish industries) caused by acidifying air pollutants. In response to this, the countries of the UN Economic Commission for Europe (UNECE) developed a legal, organisational, and scientific framework to deal with this problem. The UNECE Convention on Long-range Transboundary Air Pollution (LRTAP) was the first international legally binding instrument to deal with problems of air pollution on a broad regional basis. Signed in 1979, it entered into effect in 1983.

The Convention requires that its Parties cooperate in research on the effects of sulphur compounds and other major air pollutants on human health and the environment, including agriculture, forestry, natural vegetation, aquatic ecosystems, and materials (Article 7(d) of the Convention). The Convention also calls for the exchange of information on the physical-chemical and biological data relating to the effects of LRTAP and the extent of damage which these data indicate can be attributed to LRTAP (Article 8(f) of the Convention). To this end, the Executive Body for the Convention established a Working Group on Effects (WGE) that is supported by a number of International Cooperative Programmes (ICPs, cf. Figure 1.2). These ICPs provide monitoring and modelling methodologies and results on effects of air pollution to establish a sound scientific basis in support of effect oriented European emission abatement policies of the LRTAP-Convention. More recently, the Long-Term Strategy of the LRTAP-Convention calls for effect-based knowledge on the interaction between changes of air pollution, climate, and biodiversity.

In 1986, a work programme under the Nordic Council of Ministers agreed on scientific definitions of critical loads for sulphur and nitrogen (Nilsson, 1986). This stimulated the work under the Convention and in March 1988 two Convention workshops were held to further

evaluate the critical levels and loads concept and to provide up-to-date figures. The Bad Harzburg (Germany) workshop dealt with critical levels for direct effects of air pollutants on forests, crops, materials, and natural vegetation, and the Skokloster (Sweden) workshop on critical loads for sulphur and nitrogen compounds (Nilsson and Grennfelt 1988). Furthermore, at the Bad Harzburg workshop the first discussions took place on the possible use of critical level/load maps for defining areas at risk. It was foreseen that these could play an important role in the development of air policy.

As a result of these workshops, in 1988 the Executive Body for the Convention approved the establishment of a programme for mapping critical loads and levels (Task Force on Mapping) under the Working Group for Effects (WGE) with Germany as the lead country. In 1989 the Executive Body welcomed the offer of the Netherlands to host a Coordination Centre for Effects (CCE) that was established in 1990 at RIVM in Bilthoven, The Netherlands. From 1990 to 2015, the CCE organised 25 so-called CCE workshops dedicated to the development of policy relevant critical thresholds and other effect-based methodologies. These workshops also aimed to help reach scientific consensuses on modelling and mapping methods and databases. In 2018, the CCE was transferred from RIVM to the German Environment Agency (UBA, located in Dessau, Germany) where the CCE tasks continue to be fulfilled. More information on CCE activities and the latest version of the Mapping Manual can be found on the CCE homepage: https://www.umweltbundesamt.de/en/Coordination_Centre_for_Effects

In 1999, the Executive Body replaced the Task Force on Mapping with the Task Force of the International Cooperative Programme on Modelling and Mapping of Critical Loads and Levels and their Air Pollution Effects, Risks, and Trends (ICP M&M). In September 2009, France became the lead country of this programme.

The mandates of the ICP M&M[1], the CCE and its National Focal Centres are described further below (see also Hettelingh *et al*, 2004). The Programme and the CCE positions within the Convention are shown in Figure 1.2.

[1] established by the Executive Body in 1999 to replace the Task Force on Mapping, see Ch. 1.3

Figure 1.2: LRTAP organisation chart showing the position of the ICP M&M Task Force within the WGE

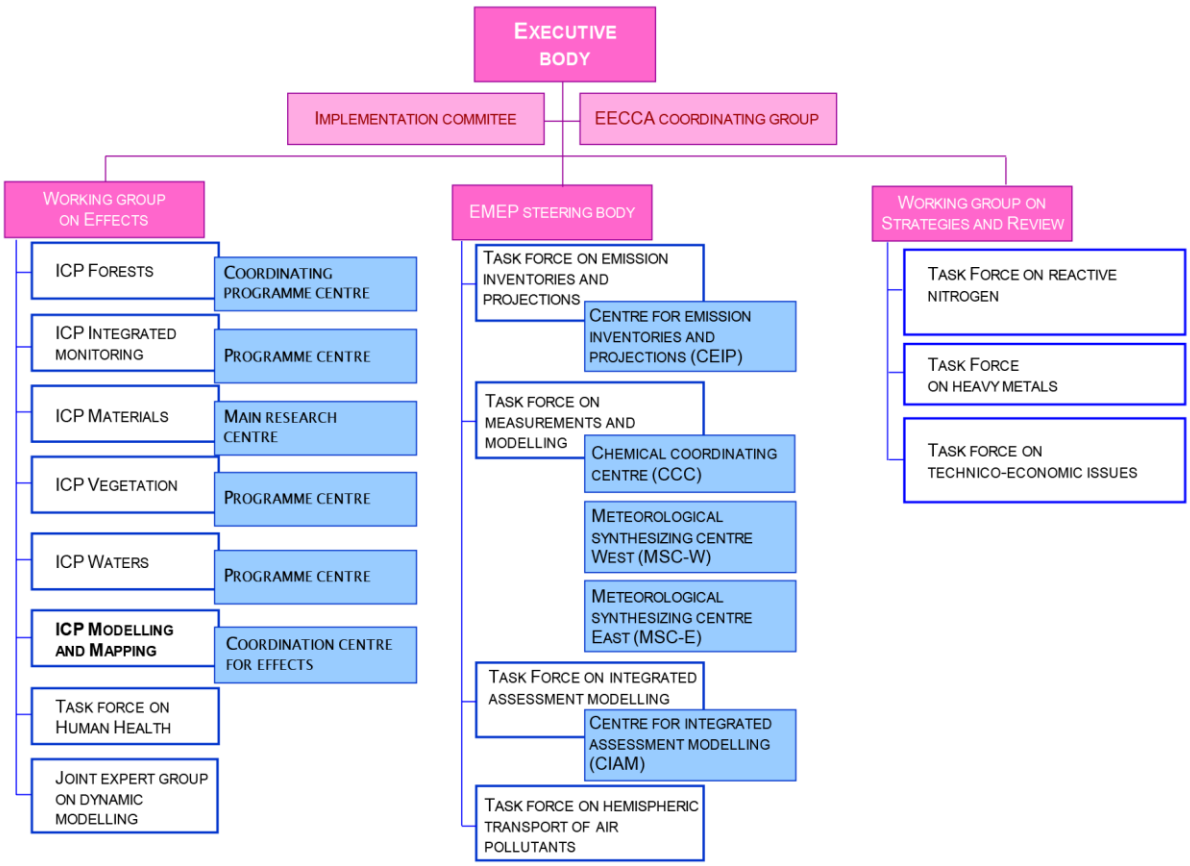

Source: This figure is adopted from a previous version of Chapter 1 of the Mapping Manual

The LRTAP-Convention brings states together with a common purpose and provides a forum for solving issues that cannot be addressed by countries and sub-regions alone (UN, 2004). By 2014, the Convention was extended with eight protocols, three of which have been revised once (cf. http://www.unece.org/env/lrtap/status/lrtap_s.html). The first substance-specific protocols were negotiated on the basis of economic and technological information (e.g., best available techniques). These set the same emission reduction targets for all Parties relative to an emission level of a reference year. These technology-based protocols do not take effects to ecosystems or human health into account. A second generation of protocols came into being when, in June 1994, a second protocol for reducing sulphur emissions (the 'Oslo protocol') was signed by 30 countries. This identified effects-based, cost-effective abatement measures anchored in the analysis of impacts using critical loads. The long-term objective for negotiating national emission reductions was to eliminate the excess sulphur deposition over critical loads for sulphur, i.e., to avoid future exceedances. While cutting sulphur dioxide emissions to achieve deposition levels below critical loads was not feasible for all ecosystems in Europe, policies aimed at reducing effects. The negotiations were based on both the assessment of environmental effects and the protection of ecosystems, as well as technical and economic considerations.

Three of the eight protocols (Heavy Metals, POP, and the Gothenburg Protocol to abate acidification, eutrophication, and ground level ozone) have been amended between 2009 and 2012. The revised protocols will enter into force when two thirds of the parties have ratified, accepted, or approved them.

The application of the critical levels and loads concept and the role of critical level/load maps for the development and implementation of air pollution control strategies are shown in Figure 1.3.

Figure 1.3: Critical Loads and Abatement strategies

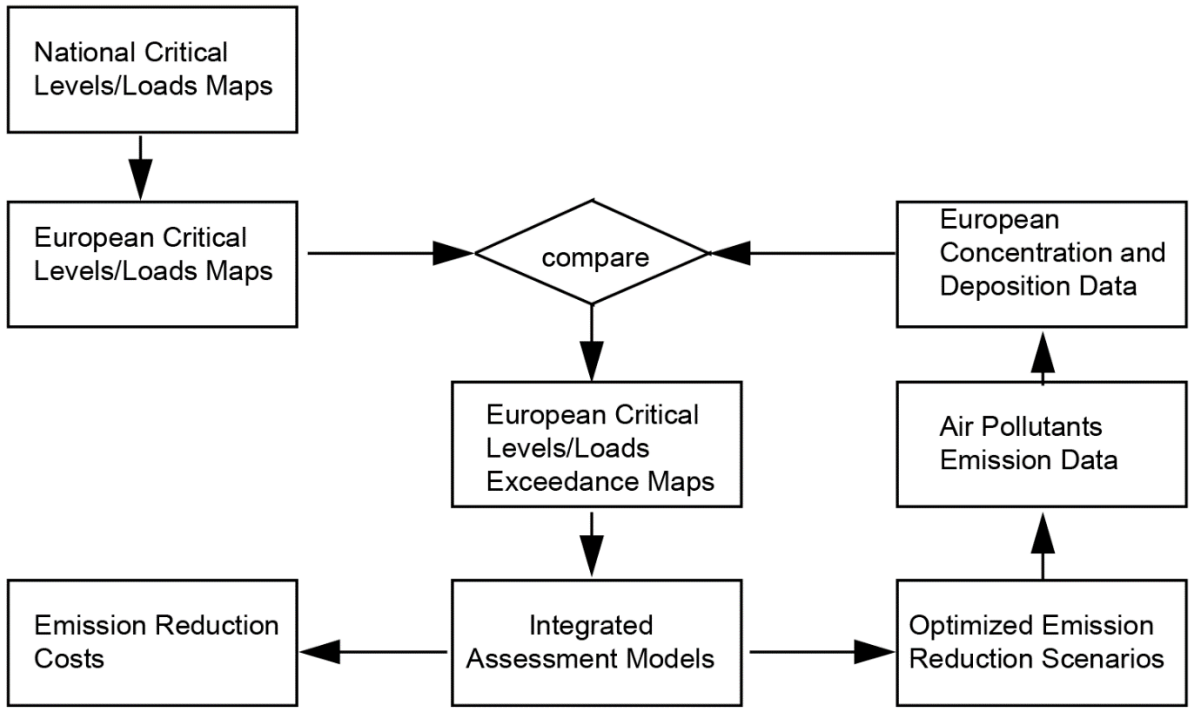

Source: This figure is adopted from a previous version of Chapter 1 of the Mapping Manual

Summarising this figure, the following "crucial steps" are involved:

- Define methods and criteria to determine and map critical loads and levels (Convention and CCE workshops).
- Obtain international approval (Working Group on Effects and Executive Body).
- Perform a mapping exercise (based on this Manual and on the proceedings of critical levels/loads and mapping workshops; see https://www.umweltbundesamt.de/en/Coordination_Centre_for_Effects).
- Calculate excess deposition/concentration per unit area. This can be done in a scenario or optimization mode (Figure 1.1) of integrated assessment models (see Hettelingh et al 2009), such as the GAINS model (Amann *et al., 2011*).
- Use the results for emission reduction strategies in support of European Air pollution policy agreements under the LRTAP Convention and in the European Union.

In practice, maps of critical loads have been used as yardsticks to assess the need for reducing depositions in each EMEP grid cell. An emission reduction scenario can be assessed by comparing a computed scenario-specific European deposition map with the European critical loads map. In support of the Oslo protocol (1994), the negotiators started to use computer models to assess national and European abatement costs of sulphur emission reduction and the effectiveness of alternative emission reduction scenarios. In particular, the RAINS model (**R**egional **A**cidification **IN**formation and **S**imulation) and its successor, the GAINS model

(**G**reenhouse Gas and **A**ir Pollution **In**teractions and **S**ynergies), have been applied to assist key policy negotiations on improving air quality in UNECE and in Europe (Amann et al., 2011).

A full description of the GAINS model is given in Amann et al. (2011) and on the model website (http://gains.iiasa.ac.at/models/) from which the following information is adapted. The GAINS Model is an integrated assessment model that simultaneously addresses health and ecosystem impacts of particulate pollution, acidification, eutrophication, and tropospheric ozone. The GAINS Model also considers greenhouse gas emission rates. Thus, pollutants included are:

- Carbon dioxide (CO_2)
- Methane (CH_4)
- Nitrogen oxides (NOx)
- Nitrous oxide (N_2O)
- Particulate matter (TSP, PM_{10}, $PM_{2.5}$ and PM_1)
- Sulphur dioxide (SO_2)
- Volatile organic compounds (VOC)
- Ozone (O_3)

Certain versions of the GAINS Model also address:

- Ammonia (NH_3)
- Carbon monoxide (CO)
- Fluorinated greenhouse gases (F-Gases)

GAINS has the ability to address various pollutants, emission reduction alternatives, abatement costs and impacts in a consistent systematic framework. By this GAINS provides useful information on trade-offs between pollution sources, costs, and benefits of pollutant reductions as well as impacts of different pollutants to human health and the environment. The GAINS model calculates emissions on a medium-term time horizon. Emission projections are specified in regular time (e.g., five year) intervals through a future policy-defined target year. Emission abatement alternatives and emission control costs can be simulated taking a variety of optional emission reduction technologies into account. Atmospheric dispersion processes are modelled exogenously by EMEP and integrated into the GAINS model framework in a simplified way (e.g., by means of Source-Receptor relationships between country emissions and EMEP grid cells). Critical load and critical level data are compiled exogenously under the Working Group on Effects and incorporated into the GAINS Model framework.

The CCE Environmental Impact Assessment scheme (Figure 1.4) shows how the GAINS data may be used in conjunction with critical loads established under the Modelling and Mapping Programme by the CCE and its network of National Focal Centres. Critical loads are stored in the European Critical Loads database held at the CCE. The CCE tailors the European critical load database for use by GAINS and other integrated assessment models, in support of European air pollution policies. More recently, the European critical load database is also considered in national programmes that address protected European natural areas.

Figure 1.4: The CCE Environmental impact assessment illustrates the links between the GAINS model and critical loads exceedance evaluation (Hettelingh et al., 2008).

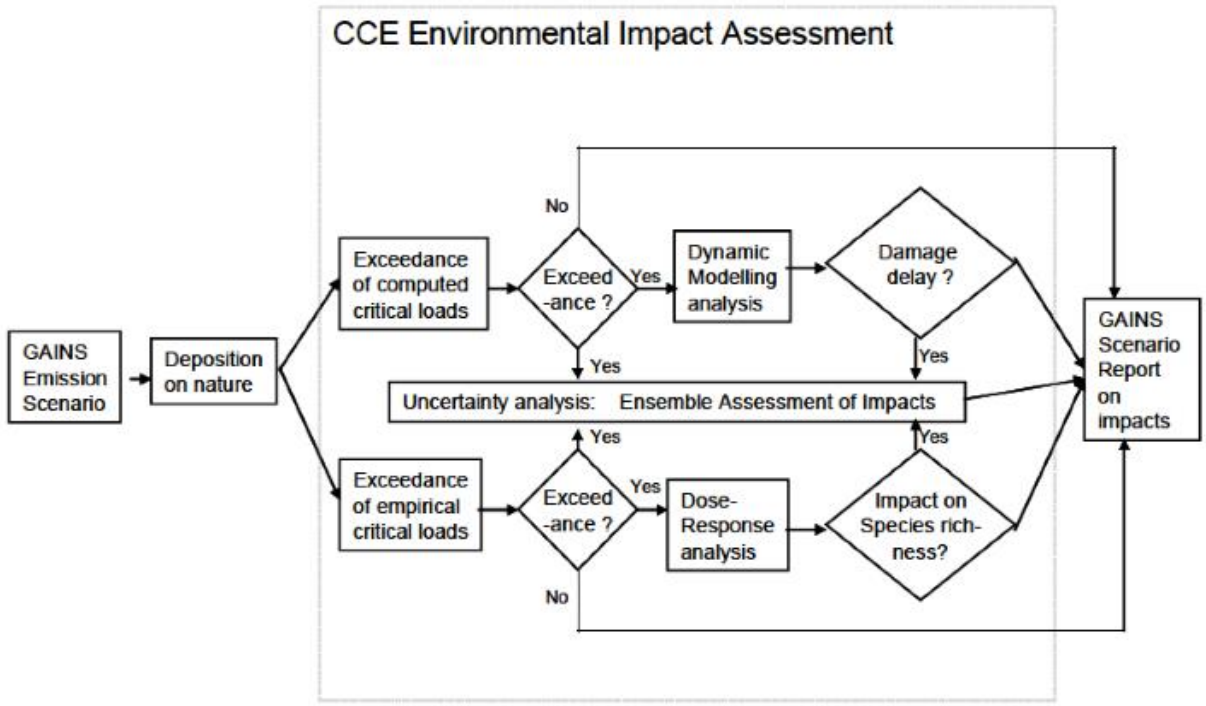

Source: This figure is adopted from a previous version of Chapter 1 of the Mapping Manual

The GAINS Model can be operated in two modes, i.e., the "scenario assessment" and "optimization mode" (see Figure 1.1). The "scenario assessment" mode follows the pathways of the emissions from their sources to their impacts. In this case, the model provides estimates of regional costs and environmental benefits of several emission control strategies. The GAINS model can also operate in the "optimization mode" which identifies cost-optimal allocations of emission reductions in order to achieve specified deposition levels, concentration targets or GHG emissions ceilings. The current version of the model can be used for viewing activity levels and emission control strategies, as well as calculating emissions and control costs for those strategies.

Since 1994 and the Oslo Protocol negotiations, the complexity of the work under the ICP M&M has increased, together with the scientific knowledge mobilized to support policy.

First, the critical load approach had to be completed for use in support of the 1999 Protocol to Abate Acidification, Eutrophication and Ground-level Ozone (the "Gothenburg Protocol"). It recognizes that:

- sulphur as well as oxidized and reduced nitrogen contribute to acidification. Therefore, two critical loads for acidity had to be distinguished, the critical load of sulphur-based acidity and the critical load of nitrogen-based acidity (see Ch. 5.1 - 5.4);
- both oxidized and reduced nitrogen contribute to eutrophication when critical loads of nutrient nitrogen are exceeded (see 5.1 – 5.3);
- both oxidized nitrogen and volatile organic compounds contribute to the formation of tropospheric ozone, for which a critical level was identified for forests, crops, and natural vegetation (see Ch. 3.2.4).

Second, integrated assessment modelling with GAINS is commonly used to assess relationships between economic activities, pollutants emissions, their dispersion, their deposition and ambient concentration and their impacts on biological endpoints.

Third, climate change and the loss of biodiversity have become major issues in the European environmental policies in general and the long-term strategy of the LRTAP-Convention (LRTAP, 2010) in particular. Relevant indicators have been (and still are being) developed (cf. chapter 3 to 8). These new indicators are provided to policy makers, as they complete the information issued from GAINS.

Furthermore, there have also been major activities to develop effects-based approaches for heavy metals in preparation of the review and revision of the 1998 Århus Protocol on Heavy Metals. Critical limits, transfer functions and adapted methods to determine and apply critical loads of heavy metals are being developed and are listed in Ch. 5.5.

1.3 Aims and organization of the Modelling and Mapping Programme

The aims and objectives of the ICP on Modelling and Mapping were approved by the WGE at its nineteenth session in 2000 (Annex VII of document EB.AIR/WG.1/2000/4):

"To provide the Working Group on Effects and the Executive Body for the Convention and its subsidiary bodies with comprehensive information on critical loads and levels and their exceedances for selected pollutants, on the development and application of other methods for effect-based approaches, and on the modelling and mapping of the present status and trends in impacts of air pollution."

Short-term and specific aims are defined in the convention work plan, agreed at sessions of the Working Group and approved by the Executive Body. These are in line with the Convention Long Term Strategy and respond to policy needs (LRTAP, 2010). Bi-annual work plans are available on the Convention web pages.

1.3.1 Division of tasks within the programme

A network of National Focal Centres (NFCs) under the ICP M&M is responsible for the generation of national data sets. NFCs cooperate with the Coordination Centre for Effects to develop modelling methodologies and European databases for critical loads. CCE reports on this work to the Task Force of the ICP M&M in yearly meetings held back-to-back with CCE workshops.

The Programme's organization and division of tasks between its subsidiary bodies, as approved by the WGE (EB.AIR/WG.1/2000/4) are as follows:

"The International Cooperative Programme on Modelling and Mapping was established in 1999 (ECE/EB.AIR/68, para. 52 (f)) to further develop and expand activities so far carried out by the Task Force on Mapping of Critical Levels and Loads and their Exceedances and by the Coordination Centre for Effects, pursuant to their original mandates (EB.AIR/WG.1/18), amended to reflect the present structure of the Executive Body and the new requirements."

1.3.2 Mandate for the Task Force of the ICP Modelling and Mapping

1. The Programme Task Force supports the Working Group on Effects, the Working Group on Strategies and Review and other subsidiary bodies under the Convention by modelling, mapping, reviewing, and assessing the critical loads and levels and their exceedances and by making recommendations on the further development of effect-based approaches, and on future modelling and mapping requirements.

2. The Task Force plans, coordinates, and evaluates the Programme's activities. It is responsible for updating the Programme Manual, as well as for quality assurance.
3. The Task Force prepares regular reports, presenting, and, where appropriate, interpreting programme data.

1.3.3 Mandate for the Coordination Centre for Effects

1. The Coordination Centre for Effects (CCE) assists the Task Force of the ICP on Modelling and Mapping. It also gives scientific and technical support in collaboration with the Programme Centres under the Convention, to the Working Group on Effects and, as required, to the Working Group on Strategies and Review, as well as to other relevant subsidiary bodies under the Convention. In their work related to the effects of air pollution, including the practical development of methods and models for calculating critical loads and levels and the application of other effect-based approaches.
2. In support of the critical loads/levels mapping and modelling exercise, the CCE is focusing on the items listed below.
    a. Provides guidance and documentation on the methodologies and data used in developing critical loads and critical levels of relevant pollutants, and their exceedances.
    b. Collects and assesses national and European data used in the modelling and mapping of critical loads and levels of relevant pollutants. The Centre circulates draft maps and modelling methodologies for review and comment by National Focal Centres, and updates modelling methodologies and maps as appropriate.
    c. Produces reports and maps on critical loads/levels documenting mapping and modelling methodologies, with the assistance of the National Focal Centres and in cooperation with the Task Force on ICP on Modelling and Mapping.
    d. Provides, upon request, the Working Group on Effects and the Task Force on ICP on Modelling and Mapping, the Working Group on Strategies and Review and the Task Force on Integrated Assessment Modelling, with scientific advice regarding the use and interpretation of data and modelling methodologies for critical loads and levels.
    e. Maintains and updates relevant databases and methodologies, and serves as a clearing house for data collection and exchange regarding critical loads and levels among Parties to the Convention, in consultation with the International Cooperative Programmes and EMEP.
    f. Conducts periodic training sessions and workshops to assist National Focal Centres in their work, reviews activities and also develops and refines methodologies used in conjunction with the critical load and critical level mapping exercise.
3. The CCE reports to the Working Group on Effects and the Task Force of ICP on Modelling and Mapping, and receives guidance and instruction from them concerning tasks, priorities and timetables. It also assists the Working Group on Strategies and Review, the Task Force on Integrated Assessment Modelling, and other bodies under the Convention, when appropriate.

1.3.4 Responsibilities of the National Focal Centres

The tasks of the National Focal Centres were defined in the 1996 version of the Mapping Manual. The National Focal Centres are responsible for:

- the collection and archiving of data needed to obtain maps in accordance with the Mapping Manual guidelines and in collaboration with the Coordination Centre for Effects;
- the communication of national mapping procedures (data, formats, models, maps) to the Coordination Centre for Effects;
- the provision of written reports on the methods and models used to obtain national maps;
- organising training facilities for national experts in collaboration with the Coordination Centre for Effects;
- making the necessary provisions to obtain national maps in accordance with the resolution and standards (measurement units, periodicity, etc.) described in the Mapping Manual;
- collaborating with the Coordination Centre for Effects to permit assessment of the methods applied in order to perform multinational mapping exercises (e.g. using GIS) and model comparisons;
- updating the Mapping Manual as appropriate, in collaboration with the Task Force on Mapping and the Coordination Centre for Effects.

1.4 Objectives of the manual

The principal objectives of this Mapping Manual are to describe methods that are recommended for use by the Parties to the Convention, represented by their National Focal Centres. The Modelling and Mapping Manual can help and assist NFCs to:

- model and map critical levels and loads in the ECE region;
- model and map areas with air pollution values exceeding critical levels or loads;
- develop, harmonize and apply methods and procedures (including dynamic modelling) to assess recovery and risk of future damage on specific targets including biodiversity in a context of climate change;
- determine and identify sensitive receptors and locations.

Thus, it provides a scientific basis on the application of critical levels and loads, their interrelationships, and the consequences for abatement strategies, e.g., for the assessment of optimized allocation of emission reductions.

This Mapping Manual includes methodologies used by ICP Materials to assess the impact of pollution on corrosion and the soiling of building materials (Ch. 4). Furthermore, it contains methodologies used by ICP Vegetation concerning the impact of air pollutants, and especially ozone, on crops and semi-natural vegetation (Ch. 3). In contrast to manuals (or comparable methodological documents) of other ICPs and the EMEP CCC, this manual does not contain information on methods of measurements nor on detailed data generation. This reflects the aims and tasks of the ICP Modelling and Mapping within the Convention.

Specific technical information as well as detailed results and other information by the National Focal Centres can be found in CCE Status Reports and publications (www.umweltbundesamt.de/en/cce-manual and bibliographic references therein).

1.5 Structure and scope of the manual

Chapter 1 has given an overview of the Convention's focal points on impact assessment and ICP M&M activities within the Convention. These include the development of impact indicators, including the critical loads and levels, whose calculation methods are presented in the following chapters.

Chapter 2 describes methods to map pollutant concentrations and depositions. These may be used to generate exceedance maps by subtracting critical levels/loads from them. At the European scale, chemistry transport models, such as the EMEP model, are used to construct maps (cf. http://www.emep.int/mscw/). The modelled pollutant concentrations and depositions are derived from national emissions, which provide the link to negotiations on emission controls. In addition, NFCs are encouraged to produce high resolution maps which can be used for effects assessments in specific ecosystems at the national and local level. This chapter was produced by experts, including those from EMEP.

Chapter 3 describes the methods developed for the quantification and mapping of critical levels and fluxes of gaseous pollutants for vegetation. It is largely based on the conclusions and recommendations of Convention workshops while ozone recommendations are based on the intensive work coordinated by ICP Vegetation in cooperation with EMEP. This chapter has been prepared by ICP Vegetation experts (http://icpvegetation.ceh.ac.uk/).

Chapter 4 describes the derivation and application of acceptable levels for effects on materials. It is part of the Manual of ICP on Materials (https://www.ri.se/en/icp-materials). It has been prepared by ICP Materials experts.

Chapter 5 describes how to quantify and map critical loads of nutrient nitrogen, acidity, and heavy metals. The structure of the chapter takes into account three main elements: ecosystem types (aquatic and terrestrial), impacts (eutrophication, acidification, pollution by heavy metals) and methods (empirical and modelling). The chapter starts with an overview that includes definitions (5.1), followed by a subchapter on Empirical Critical Loads (5.2) with sections on nutrient nitrogen (results of a workshop organized by the CCE in Noordwijkerhout in 2010; Bobbink and Hettelingh, 2011) and acidity (results of a workshop in York in 2000). Chapter 5.3 describes methods to model critical loads for terrestrial ecosystems (SMB model) and is divided into subchapters on eutrophication and acidification. Chapter 5.4 deals with critical loads for surface waters (developed in close cooperation with ICP Waters). Again, the chapter is divided into subchapters on eutrophication and acidification. Finally, Chapter 5.5 describes methods to model and map critical loads of heavy metals. New and preliminary approaches to assess the impact of nitrogen on biodiversity are described here. This chapter is at the core of ICP M&M activity and has been mainly written by CCE.

Chapter 6 describes dynamic models for acidification and eutrophication and the use of their results. The authors developed it in close cooperation with the Joint Expert Group on dynamic modelling.

The last two chapters present issues common to the use and the calculation of critical loads for all type of effects (acidification, eutrophication, heavy metals).

Chapter 7 describes how to identify critical load exceedance and parameters derived from exceedance (protection isolines, [average] accumulated exceedances).

Chapter 8 describes procedures needed to produce maps, including map geometry / projections, spatial generalisation and representativity, and the estimation of uncertainty and bias.

1.6 Historical bibliography and websites

For historical details on the establishment of the Task Force on Mapping and the mandates of the cooperating partners in the modelling and mapping exercise see EB Air/R.18/Annex IV, Section 3.6 and EB Air/WG.1/R.18/Annex I, as well as document EB.AIR/WG.1/2004/3.

The historical development of the programme and the approaches used for calculating critical loads and levels can be followed by consulting the following background material:

1. Nilsson J (ed) (1986) Critical Loads of Nitrogen and Sulphur. Environmental Report 1986: 11, Nordic Council of Ministers, Copenhagen, 232 pp.
2. Report of the Initial ECE Mapping Workshop, Bad Harzburg 1989.
3. Mapping Vademecum 1992, available at the Coordination Centre for Effects, Bilthoven, The Netherlands, RIVM Report No. 259101002.
4. Manual on Methodologies and Criteria for Mapping Critical Loads/Levels (First Edition); *Texte Umweltbundesamt 25/93,* Federal Environmental Agency (UBA)(ed.), Berlin, Germany.
5. Manual on Methodologies and Criteria for Mapping Critical Loads/Levels and Geographical Areas Where They Are Exceeded (fully revised in 1995/1996); *Texte Umweltbundesamt 71/96,* Federal Environmental Agency (UBA)(ed.), Berlin, Germany.
6. CLRTAP (2004). Manual on methodologies and criteria for modelling and mapping critical loads and levels and air pollution effects, risks and trends. ICP Mapping and Modelling 251 p.
7. Numerous scientific articles referenced in the following chapters.

Status, results, and the agenda of the ICP Modelling and Mapping are described in various documents to be found on the Convention's web site. Various aspects concerning technical and scientific background and detailed results also of National Focal Centres can be found in CCE publications, especially the CCE Status Reports, found on the CCE web site (https://www.umweltbundesamt.de/en/Coordination_Centre_for_Effects).

1.6.1 Gains model

About the GAINS model as developed by the IIASA, see:
http://gains.iiasa.ac.at/gains/EUN/index.login?logout=1

1.6.2 References

Amann, M., Bertok, I., Borken-Kleefeld, J., Cofala, J., Heyes, C., Höglund-Isaksson, L., Klimont, Z., Nguyen, B., Posch, M., Rafaj, P., Sandler, R., Schöpp, W., Wagner, F., Winiwarter, W., 2011. Cost-effective control of air quality and greenhouse gases in Europe: Modeling and policy applications. Environmental Modelling & Software 26, 1489-1501.

Bobbink R and Hettelingh J-P (eds), 2011. Review and revision of empirical critical loads and dose response relationships. Proceedings of an international expert workshop, Noordwijkerhout, 23-25 Juni 2010, RIVM-report 680359002, Coordination Centre for Effects, RIVM, Bilthoven.

CLRTAP, 2015. Introduction, Chapter 1 of Manual on methodologies and criteria for modelling and mapping critical loads and levels and air pollution effects, risks and trends. UNECE Convention on Long-range Transboundary Air Pollution.

Gauger, T., Anshelm, F., Schuster, H., Erisman, J.W., Vermeulen, A.T., Draaijers, G.P.J., Bleeker, A., Nagel, H.-D., 2002. Mapping of ecosystem specific long-term trends in deposition loads and concentrations of air pollutants in Germany and their comparison with Critical Loads and Critical Levels Part 1: Deposition Loads 1990-1999. UBA, Umweltbundesamt.

Hettelingh J-P, Bull K, Chrast R, Gregor H-D, Grennfelt P, Mill W (2004) Air Pollution effects drive abatement strategies, in: Sliggers J and Kakebeeke W (eds.), Clearing the Air: 25 years of the Convention on Long-range Transboundary Air Pollution, UN Economic Commission for Europe, United Nations Publication, ISBN 92-1-116910-0, Geneva, Switzerland, 167 pp.

Hettelingh, J.P., Posch, M., Slootweg, J., 2008. Status of the critical loads database and impact assessment. In: Hettelingh, J.P., Posch, M., Slootweg, J. (Eds.), Critical load, dynamic modelling and impact assessment in Europe. CCE Status Report 2008. PBL Netherlands Environmental Assessment Agency, Bilthoven, The Netherlands, pp. 15-28.

Hettelingh J-P, De Vries B, Hordijk L, 2009. Integrated Assessment, in: Boersema J and Reijnders L (eds.), Principles of Environmental Sciences, Springer, ISBN 978-1-4020-9157-5, pp. 385-417

Hettelingh J-P, Posch M, Velders JM, Ruyssenaars, Adam M, de Leeuw, F, Lükewille A, Maas R, Sliggers J, Slootweg J, 2013. Assessing interim objectives for acidification, eutrophication and ground-level ozone of the EU National Emissions Ceilings Directive with 2001 and 2012 knowledge, Atmospheric Environment 75: 129-140

LRTAP, 2010. Long-term strategy for the Convention. Moving forward: a strategic vision for the Convention for 2010–2020. Convention on Long-range Transboundary Air Pollution; United Nations, European economic commission, Geneva, Switzerland, p. 9.

Nilsson, J. (Ed.), 1986. Critical loads of nitrogen and sulphur. Nordic Council of Ministers, Copenhagen, Denmark.

Nilsson, J., Grennfelt, P., 1988. Critical loads for sulphur and nitrogen. Nordic council of Ministers, Report from a workshop held at Skokloster, Sweden, 19-24 March 1988. Miljorapport 15, pp. 1-418

Reiss S, Grennfelt P, Klimont Z, Amann M, ApSimon H, Hettelingh J-P, Holland M, Le Gall A-C, Maas R, Posch M, Spranger T, Sutton MA, Williams M (2012) From Acid Rain to Climate Change, Science, 338: 1153-1154

2 Guidance on mapping concentration levels and deposition levels

Last update in 2014 by Anne Christine Le Gall, Chairwoman of the Task Force on Modelling and Mapping, from initial text edited by D. Fowler and R. Smith, Mapping Manual 2004.

Please refer to this document as: CLRTAP, 2014. Guidance on mapping concentrations levels and deposition levels, Chapter 2 of Manual on methodologies and criteria for modelling and mapping critical loads and levels and air pollution effects, risks and trends. UNECE Convention on Long-range Transboundary Air Pollution; accessed on [date of consultation] on the Web at www.umweltbundesamt.de/en/cce-manual.

2.1 Information relative to modelling and mapping concentration as well as deposition

2.1.1 General remarks and objectives

The purpose of this chapter is to provide general information to the participating countries on the generation and use of concentration level and deposition maps for a range of pollutants. These maps may be used for different purposes, such as assessment of air quality for human health and assessment of ecosystems via critical loads exceedances. Depositions are then compared with critical level/load maps. In this chapter, the main principles of mapping concentrations levels and deposition are described and discussed. A range of different techniques are described for the provision of maps of concentration and deposition. These techniques provided depend on the resources and ambition of the country. Modelling procedures are outlined, and the reader is referred to specialist publications for further measurement and modelling approaches. Note that within the LRTAP Convention, modelling and mapping of air pollutant concentrations and their deposition is an EMEP mandate. The reader is therefore referred to EMEP documents and website for further details.

There are three main objectives for mapping concentrations and depositions over a territory within the LRTAP Convention.

The first aim is to construct exceedance maps relative to critical levels and loads. When used within a large scale, such as when covering several countries, transfer coefficients may be calculated. They allocate critical load exceedances in each grid cell of a transport chemistry model to emissions in all European countries. This approach is particularly well suited to assess policy scenarios in integrated assessment modelling. It therefore provides scientific results for a) the implementation of, and compliance with, existing LRTAP Convention protocols and b) their review and extension.

The second aim is to map concentrations and depositions which can be used for effects assessments in specific ecosystems. Such data are needed with a much better spatial and temporal resolutions than required for integrated assessment modelling. National Focal Centres should aim at a sufficient spatial resolution for the assessment process, making use of national models and measurement networks. Large scale transport chemistry models provide background, long-range transported air components which can be used as boundary conditions for such national models.

The third aim is to gain information on deposition at site level. This is particularly important for “monitoring” ICPs, such as ICP Forests and ICP Integrated Monitoring. Then concentration measurements, coupled with wet, dry and throughfall deposition measurements are used for

deriving process parametrisations (mainly micrometeorological measurements) and for independent model validation (mainly throughfall measurements; see Chapter 2.3.1, 2.3.2 and 2.3.10). This chapter does not detail field and laboratory methods for concentrations and deposition measurements. The interested reader is referred to specific ICPs manuals and to the EMEP publications on monitoring methodology (ICP Integrated Monitoring; ICP Forests; ICP Waters; ICP Materials; EMEP/CCC).

2.1.2 UN-ECE EMEP model: a LRTAP chemistry-transport model

The EMEP model is the reference chemistry-transport model for the LRTAP Convention and European air pollution policy assessments. The model covers all of Europe. Its geographic resolution has increased over the years (initially it was 150 x 150 km^2). Since 1999, the EMEP model was run on a 50 x 50 km^2 grid (1.0° long x 0.5° lat) although local air pollution emission and chemistry may now be simulated on a 7 x 7 km^2 grid (0.125° long x 0.0625° lat). Its vertical resolution extends from ground level to the tropopause (100 hPa or arout 16 000 m). It is divided in 20 layers, the lowest having a thickness of about 90m.

The model has changed extensively over the last ten years, with flexible processing of chemical schemes, meteorological inputs (from European Centre for Medium- Range Weather Forecasts[2]) and nesting capability. The model is used to simulate photo-oxidants and both inorganic and organic aerosols. It considers land use (source CCE/SEI for Europe, Global Land Cover 2000 elsewhere, or the CCE harmonised land cover map), at a resolution of about 5 km.

The EMEP model is now available as public domain code, along with all required input data for model runs for one year. It is extensively documented in EMEP status reports, EMEP publications and in the scientific literature (EMEP, 2013; Simpson et al., 2012).

Since 2003, the methodology has been revised for the simulation of dry deposition for particles, the emissions of hydrocarbons from vegetation, NO emissions from soils, co-deposition of SO2 and NH3, the calculation of mixing heights, and the introduction of pH response during sulphate formation. Smaller changes in the equations or parameters values have also been carried out.

The EMEP model is the fruit of 30 years of discussions and intense scientific work carried out within the LRTAP Convention, and in particular within the MSC West and East Centres of the European Monitoring and Evaluation Programme (EMEP programme, http://emep.int). It is continuously evolving. A recent update of the model characteristics has been given by Simpson et al., 2012. Initial work is described in proceedings from several UN- ECE workshops dealing with this subject, most notably the 1992 “Workshop on Deposition” in Göteborg, Sweden (Lövblad et al. 1993), the 1993 “Workshop on the Accuracy of Measurements” with WMO sponsored sessions on “Determining the Representativeness of Measured Parameters in a Given Grid Square as Compared to Model Calculations” in Passau, Germany (Berg and Schaug 1994), and in Erisman and Draaijers (1995), Sutton et al. (1998), Slanina (1996), Fowler et al. (1995a, 2001a) and ICP Forests Manual (UN-ECE 1999). The model characteristics and performances have also been discussed within the task Force on measurements and modelling and as part of European Research Programmes (such as EC4MACS, EURODELTA). Supplementary information can be found in other workshop proceedings and in scientific journals.

Many other national chemistry-transport models are also available. A large number of inter-comparisons in recent years have discussed their strengths and weaknesses (Colette et al., 2011; Colette et al., 2012; Cuvelier et al., 2013; Cuvelier et al., 2007; Fiore et al., 2009; Huijnen et al., 2010; Jonson et al., 2010; Langner et al., 2012; van Loon et al., 2007). In terms of performance,

[2] http://www.ecmwf.int/

the EMEP model has ranked well in these studies, with consistently good performances for different pollutants (ozone, PM, etc.). In terms of complexity, the EMEP model is fairly similar to other regional-scale European chemistry-transport models, such as MATCH (Robertson et al., 1999), CHIMERE (Bessagnet et al., 2004) or DEHM (Christensen, 1997; Frohn et al., 2001). All of these models have some flexibility with regard to chemical schemes and have zooming-capabilities.

Within the LRTAP convention, the EMEP values are regarded as default data, allowing the assessment process to be completed everywhere. In the following sections, references to chemistry- transport models are references to the EMEP model.

Further description of the EMEP grid is given in chapter 8.

The EMEP model has been developed together with the EMEP monitoring network. This is managed by the Chemical Coordinating Centre[3] (CCC), who are responsible for collating contributing parties' data, as well as developing monitoring methods and standards.

2.1.3 Mapped items in long-range chemistry-transport models relevant to critical loads

In order to fulfil their role, long-range chemistry-transport models simulate reactions between a large number of natural and anthropogenic substances and consider many processes. Several items are mapped within this text, in the context of the calculation of critical levels/loads and their exceedances.

For critical level exceedance maps:

- Ozone flux (PODy for vegetation, SOMO35 for human health) and ozone concentration (AOT40 values),
- Sulphur dioxide concentration,
- Nitrogen dioxide concentration,
- Ammonia concentration.

For critical load exceedance maps:

- Oxidized sulphur (SO_x) deposition (total and non-sea-salt),
- Oxidized nitrogen (NO_x) deposition,
- Reduced nitrogen (NH_y) deposition,
- Total nitrogen deposition,
- Base cation and chloride deposition (total and non-sea-salt),
- Total potential acid deposition.

Heavy metal deposition:

- Total deposition of mercury, lead and cadmium,
- Other priority heavy metals as data become available and policy needs are expressed (such as copper, nickel, zinc, arsenic, chromium, and selenium).

[3] http://www.nilu.no/projects/ccc/index.html

Black carbon is also included amongst the species for which concentrations and deposition are calculated. Although its impact was initially mainly calculated for human health, this pollutant also intervenes in material soiling to an extent that now remains to be defined in ecosystem functioning.

As input into deposition and critical load computations:

- Precipitation amount and other meteorological parameters;
- Wet, dry, cloud water/fog and aerosol deposition;
- In the context of biodiversity and climate changes, meteorological parameters such as temperature, light availability, soil wetness become relevant.

2.1.4 Processes relevant to airborne pollutant concentrations and deposition

The behaviour and the fate of each chemical species depend on its physical-chemical properties. They are also the consequences of the processes the substance undergoes in the atmosphere or at the interface with the ecosystems. These processes may be measured at monitoring stations and/or considered in the chemistry-transport models. They are described in the following sections.

2.1.4.1 Meteorology

Meteorological parameters are required inputs for most critical level or critical load calculations, whether at site level or for modelling on a wide geographical area. The data requirements and data provision will vary from country to country. Data are generally available from national weather services. European data can be obtained from the European Centre for Medium-Range Weather Forecasts (ECMWF[4]), who provides modelled data based on observations within Europe. There are other sources for some data such as the US National Centre for Atmospheric Research global precipitation database[5].

Precipitation amounts are needed for critical load computations, for wet deposition mapping and for surface wetness parametrisations.

Fog and cloud occurrence are needed for cloud water/fog deposition estimates.

Wind speed, temperature and *radiation* are basic requirements for the inferential modelling of dry deposition. Additionally, *relative humidity, soil water deficit* and *atmospheric stability* are often required.

2.1.4.2 Emissions

The precise knowledge of quantities as well as localisation of substance sources is essential to model their fate in the atmosphere. For less well-known sources, emission factors may be used. Recent work has shown that the importance of biogenic emissions in the total budget of substance exchanges between the atmosphere and ecosystems (Fowler et al., 2009).

Within the LRTAP Convention, emissions are compiled by the Task Force on Emission Inventories and Projection[6]. Data reported following the "SNAP" nomenclature[7] from each party is compiled, provided to the EMEP and integrated by assessment modelling teams. This Task

[4] http://www.ecmwf.int/
[5] https://climatedataguide.ucar.edu/climate-data/gpcc-global-precipitation-climatology-centre
[6] http://www.UN-ECE.org/env/lrtap/taskforce/tfeip/welcome.html
[7] SNAP: "Selected Nomenclature for Air Pollutants" nomenclature, which consists of yearly masses per surfaces for various domains and resolutions.

Force also provides guidance on estimating emissions from both anthropogenic and natural emission sources, with default methods and emissions factors (TFEIP, 2013).

Total emissions include:

- Anthropic emissions – these are emissions issued from human activities, including industry, transport, energy, urban activities. They are essential in pollution management since they are the sources that can most easily be reduced.

The availability of accurate local meteorological data is often a constraint to detailed local high-resolution modelling. Therefore, the success of models in improving deposition estimates to specific ecosystems may depend as much on the availability of quality meteorological data as on the quality of the local concentration estimates or measurements.

- Biogenic emissions – the vegetation and the soil are receptors for substances but are also emitters. They are dependent on surface types and meteorology. Biogenic emissions are of particular importance for mapping ozone because of VOC emissions and for mapping ammonia, which is emitted as well as absorbed by vegetation. Biogenic emissions are therefore linked to the type of vegetation and soil present over the area modelled. Their quality is therefore linked to that of the land use map.

2.1.4.3 Sea salts

Primary marine aerosols are composed of sea salt and organic material, including sulphur compounds such as dimethyl sulphate (DMS). They are an important contributor to the global aerosol load (Barthel et al., 2014). In the framework of critical loads, marine aerosols are important as they include acid anions (sulphate and chloride) as well as base cations. Consequently, the base cation and chloride deposition in the charge balance from which critical loads are derived have to be corrected for sea salt contributions, since critical loads are compared with anthropogenic inputs only (thus excluding also dust from erosion, especially from Sahara).

There are two main mechanisms for sea salts generation: bubble bursting during whitecap formation and through spume drops under the wave breaking (Simpson et al., 2012). In the EMEP model, sea salts calculations include particles with diameters up to 10 μm that originate mainly from the bubble mediated sea spray (Tsyro et al., 2011).

Depositions of base cations, sulphur and chloride (given in equivalents) are corrected by assuming that either all sodium or all chloride is derived from sea salts, and that the relations between ions are the same as in sea water (after Lyman and Fleming 1940, cited in Sverdrup 1946). Details on how to carry out this correction is given in Chapter 5.

2.1.4.4 Deposition of airborne substances

Deposition is the various processes through which airborne substances are transferred from the atmosphere to the vegetation, the soil or the water. These processes occur within different time and space scales. It is once that they are deposited that these substances may impact ecosystem functioning and human health or damage materials.

Total deposition is the sum of all dry and wet deposition processes. Distinction between the different “depositions” type is as much a matter of the physical-chemical characteristics of the deposition as a matter of measurement technique. Some of these are briefly described below. Information given below is largely inspired by the ICP Forests Manual (chapter 14: Sampling and analysis of deposition) as well as the World Meteorological Office Manual (WMO, 2008 – updated in 2010). The interested reader will find more detailed information in these references.

For information related to the simulation of these parameters, see Simpson et al., 2012 for the EMEP model, as well as Hertel et al., 2013; Hertel et al., 2006; Pacyna et al., 2008; Vet et al., 2013).

2.1.4.4.1 Bulk deposition

Bulk deposition includes parts of particulate and gaseous deposition during dry periods as well as wet deposition. It is sampled continuously in an open area with a plastic funnel connected to a sample bottle. This cheap and simple method makes its implementation easy. However, the method is sensitive to dust from neighbouring areas. In regions with calcareous soils, bulk deposition gives incorrect information on the pH and chemistry of atmospheric deposition.

2.1.4.4.2 Dry deposition

Dry deposition is the settling due to gravity (sedimentation), impaction (due to turbulence) and interception (via chemical and biological processes) of aerosols and gases on a surface during dry periods. These processes are strongly influenced by the type of surfaces (leaves, needles, rocks, water. etc), the humidity of surfaces, the macro- and micrometeorology (stomata closure), and the bio-physical-chemical characteristics of the substances.

Dry deposition is a slow but continuous flux of contaminants to the soil, water or biogenic surfaces. It involves pollutants carried in the lowest part of the atmosphere and is thought to be of particular importance close to the sources of emissions.

These processes are simulated through a resistance analogy, including aerodynamic, surface and substance specific canopy resistances and stomatal conductance (Menut et al., 2013; Simpson et al., 2012). Resistances are modelled using observations of meteorological parameters and parametrisation of surface exchange processes for different receptor surfaces and pollution climates as described in Erisman et al (1994a), Smith et al. (2000), Nemitz et al. (2001), Emberson et al. (2000), Grünhage and Haenel (1997), Gauger et al. (2003).

2.1.4.4.3 Wet deposition

Wet deposition occurs when gaseous or particulate contaminants are scavenged from the atmosphere by rain, snow, cloud and/or fog and subsequently deposited to surfaces with the subsequent rain drops, snowflakes or fog droplets. Due to the scavenging process involved, wet deposition is a good integrator of the atmosphere's chemical content and is potentially influenced by long-range transport of chemicals. Also, wet deposition leads to rapid delivery of pollutants, highly concentrated in precipitation, during the short times in which precipitation events occur.

The simulation of wet deposition integrates both in-cloud and below-cloud scavenging of gases and particles (Simpson et al., 2012).

There are different sampling methods possible for wet deposition. They are not exactly equivalent as they do not sample exactly the same fraction of wet deposition.

2.1.4.4.3.1 Wet-only deposition

Wet-only deposition determines the fluxes of dissolved components from the atmosphere in rain, snow, and hail in the open field. It gives valuable information on the chemistry of atmospheric deposition and on long-range transport of air masses. It requires collectors that open automatically at the onset of precipitation by the use of a sensor and close at the end after the rain, snow, and/or hail has stopped. It thus excludes the deposition of particles and gases during dry periods. This technical equipment requires electrical power and maintenance.

They may not work properly in the case of heavy snow.

Wet deposition is a function of precipitation rates. If wet deposition is assessed from field monitoring, it would be inferred from relatively dense meteorological data and less dense monitoring of concentrations in rain, snow, and hail.

Measured solute concentrations may then be interpolated and wet deposition may be estimated from a function of the mapped solute concentration and the precipitation amount, the latter provided by the meteorological service for the country (cf. for instance in Kopacek et al., 2012).

A very important increase of wet deposition occurs over wind exposed hills and mountains, particularly in the Northern Europe uplands, due to the washing out of topographic clouds by falling rain or snow. As networks do not generally measure at high elevation in complex terrain, these effects are generally omitted from network measurements. The underlying physical process is well documented and the effects may be modelled using the network data (Dore et al. 1992, Fowler et al. 1995b, Kryza et al., 2011).

2.1.4.4.3.2 Occult deposition

Cloud, fog, rime, mist droplets also scavenge the atmosphere from aerosols and gases. When they come into contact of a surface (as the air mass meets a hill or passes through a forest), droplets are deposited with their chemical charge. This is occult deposition. Although amounts deposited are relatively small, concentrations in occult deposition can be very high, which could lead to direct impacts.

This deposition can be estimated from concentration measurements of airborne substances by *micrometeorological measurements* at the process level (for SO_2: Fowler et al. 2001c; for NH_3: Flechard and Fowler 1998; for cloud: Beswick et al. 1991). Micro meteorologically based long-term flux measurements (i.e. continuous flux measurements over more than a year) are possible for O_3, NO_x and SO_2 (LIFE project, Erisman et al. 1998a) and for CO_2 and H_2O (Aubinet et al. 2000). Such measurements give information about the seasonal and interannual variability in the fluxes. Low-cost micrometeorological methods, such as the Time Averaged Gradient (TAG) system (Fowler et al. 2001b), provide the means of obtaining deposition parameters for many more representative terrestrial surfaces in Europe.

The methods mentioned here only work if stringent prerequisites concerning micrometeorological variables (e.g. surface homogeneity) are fulfilled. They cannot be directly extrapolated but the process knowledge obtained from such measurements can be parametrized in inferential models and fluxes can be mapped using this information (see high resolution modelling above).

The deposition velocities of cloud water/fog droplets can be similarly estimated by modelling momentum transfer (Fowler et al. 1993) and a similar technique has been used to estimate base cation deposition (Draaijers et al. 1995). Parameters determining the deposition velocity include atmospheric parameters (e.g. wind speed, temperature, radiation, relative humidity, atmospheric stability, cloud and/or fog frequency) and surface conditions (e.g. roughness, wetness, stomatal response, soil water).

2.1.4.4.3.3 Throughfall and stemflow measurements

Throughfall deposition gives an estimate of the total deposition (bulk, leached through the canopy, dry depositions) that reaches forest floor.

Stemflow is wet deposition sampled on stems, usually at the trunk base. As water flows along the tree stems, it washes off gases and aerosols previously deposited by rain, snow or occult deposition. Stemflow also includes leachates from the bark and leaves. In beech forests, stemflow is an important contributor to the deposition on the forest floor.

The combination of throughfall and stemflow give an estimate of the deposition to the forest floor. Throughfall is sampled beneath the canopy, stemflow near the base of the trunk, both via cheap, simple, low maintenance devices.

According to ICP Forests, the main drawback of the throughfall method is the interaction between the canopy and the throughfall water for nitrogen, potassium, calcium, magnesium, manganese, and protons. However, the results from throughfall monitoring can still be used as a valuable indicator for the nitrogen and base cation deposition to the forest. Throughfall deposition can give information on the lower limit of the true deposition of nitrogen and the upper limit of true deposition of base cations other than sodium. For sodium and sulphur the canopy uptake and leaching are considered to be negligible. Consequently, the throughfall flux is used to estimate the total deposition.

The data will provide knowledge on the seasonal variation and the trends of deposition. In many cases throughfall monitoring is considered to be sufficient, and stemflow is only measured for some tree species, for which it is known to be of importance (e.g., beech trees).

Throughfall measurements give a good overview of the deposition situation in the forest, not only for sulphur but also for nitrogen compounds. Recent Swedish experiences have highlighted the problems with comparing throughfall measurements with wet deposition when the dry deposition contribution to the total is very low (Westling *pers. comm.*), as is now the case for sulphur in many areas of Europe. Large uncertainties in wet deposition at wind-exposed sites have been shown with field intercomparing studies (Draaijers et al. 2001). Even if it is not possible to estimate the total deposition of nitrogen with this method, a lower limit can be set. Sampling considerations (e.g., location of collectors, species composition, spatial variability) are very important for achieving good results. Sampling requirements are described in detail in the ICP Forests Manual (UN-ECE 1999), in review articles such as Draaijers et al. (1996a), and Erisman et al. (1994b).

2.1.4.4.4 Total deposition

Total deposition is the sum of wet-only and dry deposition. It excludes ion exchanges within the canopy. It may be inferred from the values of the depositions described above.

The relation between total deposition and throughfall can be expressed as:

(II.1) Total DEP = DRY + WET + Cl/Fog = THF - CEX

where:

THF = Flux in throughfall plus stemflow

DRY, WET, Cl/Fog = dry, wet, cloud water/fog deposition

CEX = canopy exchange; *CEX* > 0 for leaching, *CEX* < 0 for uptake

When CEX=0, the dry deposition can be estimated as the difference between total flux in throughfall and independent measurements of wet and cloud water/fog deposition. If CEX differs from 0, dry deposition cannot be distinguished from internal cycling. This method can give large overestimates of the true deposition flux (CEX>0) due to canopy leaching (for some base cations). It can also give large underestimates of the true deposition flux (CEX<0) due to canopy uptake (e.g., for nitrogen compounds and protons). The sum of throughfall and stemflow is considered to be equal to total deposition only for sodium and sulphur. For other substances, throughfall plus stemflow fluxes may be interpreted as the upper bounds of total base cation deposition and as the lower bounds of total nitrogen and proton deposition.

In some cases, the total deposition to plant canopies can be deduced from throughfall and precipitation measurements in the open field using empirical *canopy budget models* (based on equation II.1, see Adriaenssens et al., 2013; Draaijers and Erisman, 1995). There are different possible approaches, some being more reliable than others. For instance, special care should be given to the choice of main tracer.

2.1.4.5 Stomatal conductance

Stomatal conductance is the process through which gas and water may enter leaf cells. It is dependent on the plant species, its phenology (including leaf nitrogen content) and environmental drivers such as water, CO2 and light availability.

Stomatal conductance increases when leaf surface is wet (due to humidity in the air being greater than 90%) and when soil humidity is high. Then the flux is mostly determined by atmospheric resistances (Erisman et al. 1994a).

2.1.4.6 Land use roughness and topography

Deposition increases with the roughness of the vegetation, as it filters airborne substances. As a consequence, forests receive larger quantities of dry and wet depositions than grasslands or bare soils. These effects will influence results from a monitoring station and may be assessed by modelling, with the help of land use maps. It is then essential that the land use map being used for modelling deposition is the same as the one used for calculating critical loads and exceedances. Within the LRTAP Convention, land use maps are issued from Corine Land Cover in Europe, Global Land Cover 2000 elsewhere. The development of work on biodiversity has led to map vegetation types at a very fine scale (100 x 100 m^2) over Europe. The "harmonised land cover map" now used under ICP M&M is available from the CCE and is further described in Chapter 5.

Topography influences the exposition of a site to air masses. In valleys, air may be stagnant. Coasts are submitted to high winds. Rainfall is more abundant on the windward rather than the downwind side of mountains. At high altitudes, the air mass might be "connected" to the substance (ozone in particular) reservoir in the boundary layer. Those aspects are therefore to be considered when setting up a monitoring site and inferring deposition from collected data.

2.1.4.7 Temporal variability

Annual deposition rates are sufficient when determining critical load exceedances, whereas for critical level exceedances, short-term information is sometimes needed. However, since there can be substantial variability from year to year with deposition and climatic conditions, a three-year average deposition for calculation of critical load exceedances may be used.

For some substances (ozone for instance), it is essential to monitor and simulate diurnal concentration variability. A time step may then be a minimum of one hour.

2.1.4.8 Geographical variability

Geographical variability is induced by the spatial variability of climate, soil conditions, topography, and land use for example. These parameters are considered in critical load and level calculations as input data. Geographic variability is the result of the sources localisation as well as climatic, geo-pedologic, topographic conditions.

2.1.5 Complementing methods to assess air pollution: long-range modelling, nested models, and monitoring

Several methods are available to estimate boundary layer atmospheric concentrations and wet, dry, and cloud-water/fog deposition on different scales of time and space. In the context of long-range air pollution, one main characteristic is whether the methods take emission inventories into account or whether they are based on site measurements and monitoring. Two groups of methods can be defined on these characteristics:

- Group A: Long-range chemistry- transport modelling
  - Objectives: (1) regional past, present, and future situation analysis, (2) basis for scenario analysis, (3) contribution to field processes understanding.
  - Simulations are based on emission inventories.
  - Examples: EMEP, national long-range transport models or hemispheric models.
- Group B: Monitoring based methods
  - Objectives: (1) model evaluation and validation, (2) site-specific effects analysis at a very fine scale (1 to 1000 ha), (3) monitoring and analysing trends.
  - Measuring concentrations and depositions directly on site: Air pollution representation is independent from inventories but interpolated (by kriging) from field measurements when the monitoring network is dense enough.
  - Examples: Monitoring networks of air concentration and wet deposition including EMEP and national networks and their interpolation (for instance, by kriging).
- Group C: High-resolution models
  - Objectives: (1) simulate air pollution at high spatial resolution (ca. 1 x 1 km^2 or higher), (2) analysis of local impacts of emissions scenarios.
  - Either based on increasing the griding of LRT models or on extrapolating (kriging) data from dense monitoring network.
  - Simulations are based on local emission inventories and on LRT models for boundary conditions.
  - Examples: most LRT models now have the ability to run in nested mode, allowing zooming on specific areas, including the EMEP Model (Simpson et al., 2012).

Nested models are Group A models, in which simulations cover a wide area on a coarse scale and a smaller area (nest) at a finer scale. Thus, they use LRT models for their boundary conditions, while focusing their calculations on smaller areas. Nowadays, EMEP has the ability to run in nested mode with, for instance, its 7 x 7 km^2 grid. It allows zooming around urban areas (Cuvelier et al., 2013; Simpson et al., 2012).

These three approaches are essential and complementary to provide information to policy makers. Modelling may not be robust without validation via monitoring, while monitoring alone cannot be used for scenario analysis. Modelling and monitoring may be used to map concentrations and deposition. The accuracy of the results will be strongly dependant on the model's grid size and on the density of points in the monitoring network.

Well-structured monitoring networks are set up within the LRTAP Convention (EMEP, ICP Forests, ICP Waters, ICP Integrated Monitoring, ICP Materials) and provide a wealth of results. They provide measurements that are necessary to test, validate and improve steady state model parameterisations. They also provide long term trends that are essential for assessments of policy efficiency and sufficiency as well as dynamic modelling tests, validation, and improvement. Parties who are developing existing or new monitoring networks may improve their data robustness and completion by combining their results with these existing networks.

2.1.5.1 Long-range chemistry transport models

Long-range chemistry transport models are most suitable for scenario analyses and country to country budgets ('blame matrices') used in emission reduction negotiations (if the model domain is more than one country). They calculate patterns of concentration and deposition across large regions of the world. Within the Convention, the EMEP model is used for the UN-ECE region.

Standard multiannual concentrations from long-range chemistry transport models are given as one number per year per component per grid square. Deposition fluxes are provided either as average deposition to the grid square or as ecosystem specific deposition estimates. These model outputs can be provided for shorter time periods. However, there is the overall constraint that the emissions inventory, as one of the most important inputs, is often provided only as an annual total.

2.1.5.2 UN-ECE-monitoring based methods

There are several techniques that may be used to carry out site sampling and monitoring of pollutant concentrations and deposition. It is beyond the scope of this manual to describe them here. The interested reader is referred to EMEP-CCC[8], to ICP Forests[9] and ICP integrated monitoring relevant documentations as well as specific literature (setting up a network: Anshelm and Gauger, 2001). We will give here only some general aspects which are essential in the framework of critical load calculations.

In the framework of long-range air pollution, monitoring stations are set at a rural location, avoiding local sources, including farms (for NHy) and roads (for Nox and Sox). However, in order to get a monitoring network representative of the whole range of existing situations, stations may be located at various altitudes and/or at various distances from the emitters of pollutant sources and precursors (Table II.1). Stations at urban locations are not representative of extensive areas but they may be required for differentiating areas with rural and urban pollution conditions. They are also essential for population and material exposure assessments.

Table 2.1: Minimum distance to emission and contamination sources as recommended by EMEP, 2001. All values are indicative as optimum distances and also depend on sources intensities, meteorological, and topographic site characteristics.

Type	Minimum distance	Comment
Large pollution sources (towns, power plants, major motorways)	50 km	Depending on prevailing wind directions
Small scale domestic heating with coal, fuel oil or wood	100 m	Only one emission source at minimum distance

[8] http://www.nilu.no/projects/ccc/manual/
[9] http://icp-forests.net/page/icp-forests-manual

Type	Minimum distance	Comment
Minor roads	100 m	Up to 50 vehicles/day
Main roads	500 m	Up to 500 vehicles/day
Application of manure, stabling of animals.	2 km	Depending on the number of animals and size of fertilized field or pastures
Grazing by domestic animals on fertilized pasture	500 m	Depending on the number of animals and size of fertilized field or pastures

The preferred sampling height is 3-5 m and the monitoring station requires an open aspect without the presence of trees or other tall vegetation in the proximity of the sample intake. The elevation of a particular location determines the extent to which it experiences the influence of air from the free troposphere and from the boundary layer.

Maps may be produced directly from point measurements, but only if the network is dense enough to account for spatial (and temporal) variations. This may be the case for networks measuring air concentrations of compounds with little spatial variation or for measurements of wet deposition in areas of simple terrain. Network (point) measurements should be interpolated using the kriging technique and it may be helpful to include monitoring data from neighbouring countries for interpolation. For some air concentrations, such as ammonia or ozone, or for rain concentrations in complex terrain, the required density of the measurement network could be too dense for practical application. In these cases, it is recommended that concentrations are obtained from less dense networks and that simple models are used to assist the interpolation, using, for example, altitude dependences. It is preferable to interpolate concentrations in rain or in air and then calculate the deposition at the receptor site using local estimates of rainfall and land- use specific ground-level dry deposition rates (see above).

Data assimilation, combining observed and LRT modelled concentrations, is another method applied to provide improved pollutant concentration fields (Flemming, 2003, Rouil et al., 2009).

In areas with clearly delineated watersheds, the “calibrated watershed method” integrates deposition fluxes over a scale compatible to critical load computations, for example for lakes and surface waters. Major fluxes to the groundwater and soil exchange must then be accounted for. It is most useful for conservative elements (e.g., S, Na, Cl). The data are useful to validate deposition estimates derived from modelling.

Catchment mass balance is an alternative approach, valid at a small (catchment) scale. It combines information from monitoring to local modelling.

2.1.6 Characteristics of substances maps in relation to exceedances calculations

Specificities for mapping substance concentrations and deposition are given below, in the context of the calculation of critical loads and levels exceedances.

Usually the relevant information is provided either from the EMEP model, from small scale modelling or from monitoring network.

2.1.6.1 Mapping ozone (O_3) concentrations and deposition

Data on ozone concentrations may be available from photochemistry/transport modelling or from monitoring networks.

The concentrations of ozone close to terrestrial surfaces (e.g. within 1 m) show large spatial variability in both rural and urban areas. For urban areas, this variability is mainly caused by the

rapid chemical consumption of ozone by NO, which is locally emitted. For rural areas away from local sources, this variability is largely caused by spatial and temporal changes in the degree to which individual sites are vertically 'connected' to the main reservoir of ozone in the boundary layer. Like in urban areas, O_3 might be consumed by the reaction with NO which can be emitted from bacterial processes in the soil (PORG 1997).

An ozone concentration field of, at least, a grid of 1 x 1 km^2 cell-size is useful when providing a spatial resolution of the ozone exposure on a horizontal scale which reflects the variations in the orography. As the critical levels are based on the concentration measured in the turbulent layer near the receptor, ozone levels modelled or measured at higher distances from the ground are not directly related to the observed effects. The supply of ozone to vegetation is provided by atmospheric turbulence and hence wind speed and the thermal structure of air close to the ground are considered. The deposition of ozone on terrestrial surfaces and vegetation causes a vertical gradient of the ozone concentration, which is largely determined by the sink activity of the soil-vegetation system.

2.1.6.2 Mapping sulphur dioxide (SO_2) concentrations and oxidised sulphur (SO_X) deposition

Data on SO_2 gas concentrations, sulphate (SO_4^{2-}) aerosol concentrations, and SO_4^{2-} concentrations in rain are available from long-range transport modelling, possibly coupled to small-scale modelling.

SO_2, in contrast to ozone or sulphate aerosol, is a primary pollutant. It is emitted by both high (e.g., power plants) and low (e.g., household) sources. Therefore, the spatial variability of concentrations tends to be higher than that of ozone and sulphate aerosol but lower than that of ammonia. Close to urban areas, the concentrations of rural sulphur dioxide are elevated. This effect should be modelled explicitly where possible, for example, by using urban concentration measurements and areas of urbanisation to model the urban effect.

For rural areas away from local sources, spatial variability is largely caused by spatial and temporal changes in the degree to which individual sites are vertically 'connected' to the main reservoir in the boundary layer.

As for ozone, the SO_2 levels measured 3-5 m above ground are not directly related to the observed effects, since dry deposition causes a systematic vertical concentration gradient towards the surface, while the critical levels are based on the concentration measured close to the receptor. However, surface-type specific corrections are not generally applied and measured/modelled values usually taken uncorrected.

2.1.6.3 Mapping nitrogen oxides (NO_X) concentrations and deposition of oxidised nitrogen (NO_Y)

Data on nitrogen oxides are available from long-range transport modelling, possibly coupled to small-scale modelling or from monitoring networks.

Like SO_2, nitrogen oxides (NO_x=NO+NO_2) are emitted by both high (e.g., power plants) and low (e.g., traffic) sources, mostly as NO and, to a lesser extend as NO_2. The spatial variability of NO_x concentrations is mainly controlled by reactions of NO with O_3. It tends to be higher than that of ozone and nitrate but lower than that of ammonia. In rural areas, emission of NO from soils (both agricultural and semi-natural) can likewise contribute to local NO_2 levels.

Many national modelling activities are able to provide estimates of surface concentrations of NO_2 at a high resolution of at least 5 x 5 km^2. These can incorporate models to adjust concentrations for local emissions by using, for example, distance to major roads.

The reaction products of NO_x in the atmosphere are collectively called NO_y. The main chemical species of NO_y are NO_x, NO_{3-}, NO_{2-}, HONO and HNO_3. Species of secondary importance for deposition (but essential if atmospheric chemistry is to be modelled) are organic oxidised compounds, such as PAN (peroxy acetyl nitrates) and its homologues (peroxy alkyl nitrates, alkyl nitrates) dinitrogen peroxide N_2O_5 and the nitrate radical NO_3 (Hertel et al., 2011; Seinfeld and Pandis, 1998).

Dry deposition modelling includes principally NO_x, NO_{3-} aerosol, and HNO_3 (ideally also HONO). Reactions with ozone will affect both NO_2 and NO concentrations fields.

2.1.6.4 Mapping ammonia (NH_3) concentration, reduced nitrogen (NH_x) deposition and total nitrogen deposition

Ammonia is emitted primarily from agricultural sources that may be grouped as (Hertel et al., 2011):

- Point sources, i.e. animal houses and manure storages,
- Application of manure and mineral fertilizers to the fields,
- Grazing animals,
- Other sources, including plants.

Emissions from these sources vary with agricultural practices and meteorological conditions, as NH_3 emissions is a process that is highly temperature dependant. Gaseous NH_3 has a short atmospheric residence time (Erisman and Draaijers 1995) and, as a result, its concentrations in air may show steep horizontal and vertical gradients (Asman et al. 1988). Even in areas not affected by strong local sources, the ambient concentrations of ammonia may vary by a factor of three to four on scales less than a few kilometres.

The very localised pattern of ammonia concentration, and also of ammonia dry deposition, has consequences for mapping procedures. Mapping of ammonia concentrations by interpolation from measurements alone requires an extremely high measurement network density and the method is only feasible over small areas.

A long-range transport model with, for example, a 50 x 50 km^2 spatial resolution, will not resolve these large variations, neither for ammonia concentrations nor for the dry deposition of ammonia, which will be the major fraction of total reduced nitrogen deposition close to an ammonia source. Therefore, assessments of the exceedances of critical loads will be biased when using such LRT models. In the absence of very detailed emission data (on the level of the individual farm), measurements in a dense network are needed to obtain accurate exceedance levels (Asman et al. 1988).

It is also important to note that ammonia may be emitted by, as well as deposited onto, vegetation, and therefore surface– atmosphere exchange modelling must be used to quantify the net exchange over the landscape. The background developments that allow these processes to be simulated use a compensation point approach (Schjorring et al. 1998; Sutton et al. 2000).

2.1.6.5 Mapping total reactive nitrogen

Total reactive nitrogen (N_r) released in atmosphere consists in three main parts (NH_x, NO_x and N_2O). Organic compounds form a fourth, poorly quantified, fraction of Nr. N_2O takes part of the atmospheric cycle of nitrogen and is important as a greenhouse gas but not for the critical loads and levels calculations. Organic compounds and N_2O will not be discussed further within this text.

The deposition of total nitrogen is needed for many applications in the critical load framework. It is defined as the sum of total deposition of reduced (NH_x) nitrogen [NH_3 dry deposition, NH_4^+ aerosol deposition, NH_4^+ wet deposition, NH_4^+ cloud water/fog deposition] and oxidised (NO_y) nitrogen [NO_2 dry deposition, HNO_3 dry deposition, NO_3^- aerosol deposition, NO_3^- wet deposition, NO_3^- cloud water/fog deposition]. The methodological considerations concerning NH_x and NO_y deposition mapping apply accordingly.

2.1.6.6 Mapping base cation and chloride deposition

The deposition of physiologically active basic cations (Bc = Ca + Mg + K[10], i.e. the sum of calcium, magnesium and potassium) counteracts impacts of acid deposition and can improve the nutrient status of ecosystems with respect to eutrophication by nitrogen inputs. Sodium (Na) fluxes are needed for estimating the sea-salt fraction of sulphur, chloride (Cl) and Bc inputs, and as a tracer for canopy and soil budget models. In addition, inputs of Bc as well as sodium and chloride determine the potential acidity of deposition.

Emissions of base cations are from anthropogenic and natural processes, such as rock weathering, sea salts, biomass burning, volcanic dust, industrial emission, vehicle emissions. Base cations occur in the air in the particulate phase and are deposited in dry and wet processes. In precipitation, they are largely dissolved and occur as ions. In Europe, depositions of base cations are strongly influenced by Saharan dust, especially in countries around the Mediterranean. Sea salt depositions tend to be correlated with the distance to the sea, with highest depositions at western European coastal sites (Torseth et al., 2012; Vet et al., 2013).

As the aim of the Convention is to minimize acid deposition irrespective of other man- made emissions, base cation inputs not linked to emissions of acidifying compounds (for example from emissions of Sahara dust, large-scale wind erosion of basic topsoil particles, etc.,) should, in principle, not be accounted for within the critical load framework. The non- anthropogenic, non-sea-salt atmospheric input of base cations is defined as a property of the receptor ecosystem and indirectly enters the critical load equation for acidity (see Chapter 5, section 5.3).

Base cation particle deposition can be estimated from concentrations in wet deposition and empirical scavenging ratios (Eder and Dennis 1990, Draaijers et al. 1995). Dry deposition velocities can be inferred as for SO_4^{2-} aerosol and the obtained dry deposition estimates added to measured and interpolated wet deposition estimates (e.g. Gauger et al. 2003, RGAR 1997, CLAG 1997).

Deposition of base cations have been estimated for Europe, and especially for the Nordic countries based on monitoring data on concentrations of base cations in precipitation and air-borne particles (Draaijers et al., 1997; Hellsten et al., 2007; Van Leeuwen et al., 1996; Van Leeuwen et al., 1995; Van Loon et al., 2005; Vet et al., 2013; Werner et al., 2011, Lövblad et al., 2004).

2.1.6.7 Mapping total potential acid deposition

Total Potential Acid Deposition is defined as the sum of the total deposition of strong acid anions plus ammonium minus non-sea-salt base cations.

As stated in the preceding subchapter, most chloride inputs are assumed to be of sea-salt origin, and these are removed from the equation by removing all other sea-salt inputs (i.e., of sulphate and base cations including Na) using a “sea-salt correction” with Na as a tracer. The implicit

[10] Na is not taken up by plant (and therefore not « physiologically active »). It is not included in the Bc sum. However, it is a base cation and included in the critical loads calculations in Chapter 5 in the BC sum : BC = Ca + Mg + K + Na).

assumption is that sea-salt is neutral and contains no carbonates. Surplus chloride inputs (Cl^*_{dep}) are assumed to be due to anthropogenic HCl emissions.

The sum of critical load (for sulphur) and background (non-anthropogenic) base cation deposition has formerly been defined as critical (sulphur) deposition, as used for the negotiations for the Second Sulphur Protocol (Oslo, 1994). For comparison to CL(S) + CL(N), as defined in Chapter 5.3.2 (eq. V.19), only deposition values of S and N are needed. However, if the amount of total acid input is of interest (e.g., for comparison to $CL(Ac_{pot})$, as defined in Chapter 5.3.2), non-sea-salt base cation and chloride deposition then has to be included into the input side of the potential acidity exceedance equation:

(II.3) $Ac(pot)_{dep} = SO^*_{x\ dep} + NO_{y\ dep} + NH_{x\ dep} - BC^*_{dep} + Cl^*_{dep}$

where:

$SO^*_{x,\ dep}$ = non-sea-salt sulphate deposition

$NO_{y\ dep}$, $NH_{x\ dep}$ = total oxidized/reduced nitrogen deposition

BC^*_{dep}, Cl^*_{dep} = non-sea-salt base cation/chloride deposition

In areas strongly affected by sea spray (high sea-salt Na, Cl, S inputs), the Total Potential Acid Depostion definition of eq. II.3 becomes problematic, since base cations have a beneficial nutrifying effect irrespective of their chemical form (e.g., CaCl vs. $CaCO_3$). At the Grange-over-Sands Workshop in 1994, it was concluded that *total* Mg+Ca+K deposition rates should be used to determine critical loads for acidity (Sverdrup et al. 1995) (see Chapter 5.3.2).

As stated in Chapter 5.3.2, eq. II.3 assumes that deposited NH_x is completely nitrified and exported from the system as NO_3^-, thereby acidifying the system. Thus, with respect to soil acidification, it is assumed that 1 mol of SO^*_x is forming 2 mols of H^+, and 1 mol of NO_y, NH_x and Cl^* each 1 mol of H^+.

It is important to be consistent when determining total acid inputs. If results are determined on a site and process level, and if H^+ deposition rates are determined separately, NH_4^+ inputs (max. 2 equivalents H^+ per mol) have to be distinguished from NH_3 inputs (max. 1 equivalent H^+ per mol). The same applies to SO_2 (2 equivalents H^+ per mol) vs. SO_4^{2-} (0 equivalents H^+ per mol). On a larger scale, this may be neglected. Note that the emission and subsequent deposition of 1 mol SO_2 and 2 mols NH_3 yields the same potential acid deposition as the deposition of 1 mol of their reaction product $(NH_4)_2SO_4$, namely 4 equivalents.

2.1.7 Use of deposition and concentration maps

2.1.7.1 Issues related to map scales

Deposition and concentration maps are designed to be used in combination with critical load and critical level maps to show where and by how much critical loads and critical levels are exceeded. The use of deposition data with critical loads data very often involves different scales of the different data sources and, in most cases, the critical loads data are provided at a finer resolution than the deposition data, resulting in an underestimation of the critical load exceedance. These issues have been discussed above and improved deposition estimates, for example by using national models at a finer spatial resolution, can improve the quality of the critical load exceedances. One important point reiterated here is that it is essential to note any different scales in the legends to figures and maps.

The scale at which critical levels/loads and concentration/deposition are mapped greatly influences the magnitude of exceedance values (Spranger et al. 2001, Bak 2001, Lövblad 1996,

Smith et al. 1995). For example, if the average value from a 50 x 50 km² grid square is matched to critical loads on the 250 squares of 1 x 1 km² within the 50 x 50 km² grid square, there will generally be less critical load exceedance than if the deposition were available at the 1 x 1 km² scale. The only circumstance in which this underestimate would not occur would be if the high deposition locations matched the high critical load locations. Over many areas of Europe, exactly the opposite occurs. In many areas of complex terrain, the parts of the landscape receiving the largest deposition, such as the higher areas in the mountains of north-western Europe, are also the most sensitive to the effects of deposition such as, for example, acidification. The same holds true for forested areas, which tend to correlate with poor soils in large parts of Europe. This problem is worse for components with local sources (NH_3, NO_x) because the within-grid distribution of sources is not reflected in the grid average estimation from a LRT model but does markedly increase the within-grid variability of deposition and hence potentially increases critical load exceedances over local sensitive areas. As the current deposition estimates from EMEP are provided at a scale which is much larger than the scale of this spatial variability, depositions are averaged over large areas and "hot spots" are smoothed down. The critical loads exceedances for these areas tend to be underestimated.

These effects are minimised by estimating deposition to the smallest spatial scale possible. They are therefore becoming less acute with the use of finer scale in new chemical transport models (the latest version of EMEP is now based on a 0.1° x 0.1° grid). However, there is an underlying relationship that the critical load exceedances will increase as the spatial resolution of the deposition gets closer to that of the critical loads. Beyond the effects caused by a change in grid resolution, it has been shown that the constant improvement in scientific knowledge can modify air pollution risk assessment results. When comparing assessments of environmental situation, it is therefore important to make sure that different assessments are carried out with similar tools and based on similar hypotheses (Hettelingh et al., 2013).

The comparison of national maps and model outputs with data from the EMEP model is a source of science and policy relevant information. Identification of differences between model outputs may lead to model, parameterization, and methodology improvements. These may be of particular significance at borders between countries and may help to avoid "border effects". National data may also complete the information provided to policy makers through EMEP. Whether national data confirm or infirm European integrated assessments, they are part of the information national representatives may use during protocol negotiations or their implementation. Models and approaches intercomparisons are commonly carried out within the LRTAP groups and subgroups.

2.1.7.2 Some preliminary remarks regarding the use of model results by parties

Within UN-ECE countries, the expertise, and facilities for measurement of concentrations and fluxes of pollutants is variable. The extent to which the methods presented in monitoring manuals can be applied is therefore variable. In each country, it is necessary to assess the range of options available. It is important to stress that involvement in measurement alongside modelling activities is highly desirable, as both are complementary.

Besides, the cooperation of all parties in the air pollution impact assessment process is necessary to develop satisfactory and efficient strategies for control of pollutant emissions. These require full participation in the underlying science as well as in the political process.

National Focal Centres are strongly advised to ensure that the monitoring and modelling methodologies described in the publications listed above are documented in the development or validation of a database for national concentration and deposition (and critical level and load exceedance) maps. Compatibility of these maps with other national maps within the Mapping

Programme as well as with monitoring methods employed within other deposition monitoring programmes under the Convention (ICPs on Forests and on Integrated Monitoring; EMEP) is very important.

2.1.7.3 Identifying ecosystems position for critical load calculations and their exceedances

The land use maps used for deposition modelling should be identical to the stock- at-risk maps used for critical level/load mapping. Land use maps based on Corine Land Cover in Europe and Global Land Cover 2000 elsewhere are used within the LRTAP Convention (cf. Section 2.2.4.6 and cf. Chapter 5, section 5.6.3). Vegetation types are then identified using EUNIS nomenclature. In addition to the geographical position of sensitive ecosystems, land use type/vegetation type, vegetation height, and crown coverage also are mapped on a scale that allows for correct allocation of deposition to all ecosystem types in the model domain.

For all maps, the most recent available data should be used. Should data not be available for a given year, data set filling should not go back in time further than five years unless, of course, the objective is to prepare time series.

2.1.7.4 Uncertainties of mapping methods

Since the 2004 version of the Mapping Manual, modelling has significantly improved. The EMEP/MSC-W 50 x 50 km^2 Eulerian LRT has been used, tested, compared to other chemistry transport models, and calibrated to a greater number of monitoring stations over longer periods. At the time this manual's update, finer grid scales at around 28 x 28 km^2 (0.5° Long x 0.25° Lat), or finer, are being implemented in the EMEP model.

There are, of course, a number of persistent issues in chemistry transport model uncertainties that lead to uncertainties in critical load exceedance calculations. There are of course also some uncertainties in critical load calculations. They are discussed in relevant chapters and sections. The following points are mentioned in recent literature, including those related to the EMEP Model, as potential sources of uncertainties (Cuvelier et al., 2013; Hertel et al., 2011; Simpson et al., 2012):

- Emission data
- Climate
- Atmospheric processes (and their non-linearities)
- Pollutant dispersion and vertical resolution
- Deposition and its relation to interactions of pollutants with surfaces and vegetation and aerosol size distributions

When evaluating model-measurement intercomparisons, it is important to recall that

there are also uncertainties with the measurements,

the model may be estimating something rather different from what is being measured.

For instance, the NO_2 concentration at a single site in a (50 x 50 km^2) grid square is only an estimate from a sample of size one of the 'average' NO_2 concentration in the square, which is the value the EMEP/MSC- W model is attempting to match. An evaluation of the overall uncertainty of the model requires that some further information is available on the effects of the spatial distribution of measurement sites.

2.1.8 References

Adriaenssens, S., Staelens, J., Baeten, L., Verstraeten, A., Boeckx, P., Samson, R., and Verheyen, K. (2013). Influence of canopy budget model approaches on atmospheric deposition estimates to forests. *Biogeochemistry*, **116,** 1-3, 215-229.

Anshelm, F. and Th. Gauger (2001): Mapping of ecosystem specific long- term trends in deposition loads and concentrations of air pollutants in Germany and their comparison with Critical Loads and Critical Levels. Part 2: Mapping Critical Levels exceedances. Final Report of Project 29942210. Inst. for Navigation, Stuttgart University and Umweltbundesamt.

Asman, W.A.H. and H.A. van Jaarsveld (1992): A variable-resolution transport model applied for NHx in Europe. Atmos. Environ. Part A-General Topics, 26, 445-464.

Asman, W.A.H., Drukker, B. and A.J. Janssen (1988): Modeled historical concentrations and depositions of ammonia and ammonium in Europe. Atmos. Environ., 22, 725-735.

Aubinet, M., Grelle, A., Ibrom, A., Rannik, U., Moncrieff, J., Foken, T., Kowalski, A.S., Martin, P.H., Berbigier, P., Bernhofer, C., Clement, R., Elbers, J., Granier, A., Grunwald, T., Morgenstern, K., Pilegaard, K., Rebmann, C., Snijders, W., Valentini, R. and Vesala, T. (2000): Estimates of the annual net carbon and water exchange of forests: The EUROFLUX methodology. Adv. Ecol. Res., 30: 113-175.

Bak, J. (2001): Uncertainties in large scale assessments of critical loads exceedances. Water, Air, and Soil Pollution Focus, Vol. 1 Nos. 1-2, 265-280.

Barthel, S., Tegen, I., Wolke, R., and van Pinxteren, M. (2014). Model study on the dependence of primary marine aerosol emission on the sea surface temperature. *Atmospheric chemistry and physics Discussions*, **14,** 377-434.

Barrett, K., Seland, Ø., Foss, A., Mylona, S, Sandnes, H., Styve, H. and Tarrasòn, L. (1995): European transboundary acidifying air pollution. EMEP/MSC-W Report 1/95. The Norwegian Meteorological Institute, Oslo, Norway.

Beier, C., P. Gundersen and Rasmussen L. (1992): A new method for estimation of dry deposition of particles based on throughfall measurements in a forest edge. Atmos. Environ. 26A, 1553-1559.

Berg, T. and Schaug J. (eds.) (1994): Proceedings of the EMEP Workshop on the Accuracy of Measurements with WMO sponsored sessions on Determining the Representativeness of Measured Parameters in a Given Grid Square as Compared to Model Calculations, Passau, Germany, 22-26 Nov. 1993.

Bessagnet, B., Hodzic, A., Vautard, R., Beekmann, M., Cheinet, S., Honoré, C., Liousse, C., and Rouïl, L. (2004). Aerosol modeling with CHIMERE- preliminary evaluation at the continental scale. *Atmospheric Environment*, **38,** 18, 2803-2817.

Beswick, K.M., Hargreaves, K., Gallagher, M.W., Choularton, T.W. & Fowler, D. 1991. Size resolved measurements of cloud droplet deposition velocity to a forest using an eddy correlation technique. Q. J. Roy. Meteor. Soc., 117, 623-645.

Bredemeier, M. (1988): forest canopy transformation of atmospheric deposition. Water Air Soil Poll., 40, 121-138.

Christensen, J. H. (1997). The Danish eulerian hemispheric model – a three-dimensional air pollution model used for the arctic. *Atmospheric Environment*, **31,** 24, 4169-4191.

CLAG (1997): Deposition fluxes in the United Kingdom: A compilation of the current deposition maps and mapping methods (1992-1994) used for Critical Loads exceedance assessment in the United Kingdom. Critical Loads Advisory Group Sub-group report on Depositon Fluxes. 45 pp. Penicuik: Institute of Terrestrial Ecology.

Colette, A., Granier, C., Hodnebrog, Ã., Jakobs, H., Maurizi, A., Nyiri, A., Bessagnet, B., D'Angiola, A., D'Isidoro, M., Gauss, M., Meleux, F., Memmesheimer, M., Mieville, A., Rouïl, L., Russo, F., Solberg, S., Stordal, F., and Tampieri, F. (2011). Air quality trends in Europe over the past decade: a first multi-model assessment. *Atmos. Chem. Phys.*, **11,** 22, 11657-11678.

Colette, A., Granier, C., Hodnebrog, Ã., Jakobs, H., Maurizi, A., Nyiri, A., Rao, S., Amann, M., Bessagnet, B., D'Angiola, A., Gauss, M., Heyes, C., Klimont, Z., Meleux, F., Memmesheimer, M., Mieville, A., Rouïl, L., Russo, F., Schucht, S., Simpson, D., Stordal, F., Tampieri, F., and Vrac, M. (2012). Future air quality in Europe: a multi-model assessment of projected exposure to ozone. *Atmos. Chem. Phys.*, **12,** 21, 10613-10630.

Coyle, M., Smith, R.I., Stedman, J.R., Weston, K.J., and Fowler, D. (2002): Quantifying the spatial distribution of surface ozone concentration in the UK. Atmos. Environ., 36, 1013-1024.

Cuvelier, C., Thunis, P., Karam, D., Shaap, M., Hendricks, C. M. A., Kranenbourg, R., Fagerli, H., Nyiri, A., Simpson, D., Wind, P., Schulz, M., Bessagnet, B., Collette, A., Terrenoire, E., Rouïl, L., Stern, R., Graff, A., Baldasano, J. M., and Pay, M. T. (2013). ScaleDep: Performance of European chemistry-transport models as function of horizontal spatial resolution. Technical report EMEP MSC-W Rep. No. 1/2013, Technical report 1/2013, 62 p.

Cuvelier, C., Thunis, P., Vautard, R., Amann, M., Bessagnet, B., Bedogni, M., Berkowicz, R., Brandt, J., Brocheton, F., Builtjes, P., Carnavale, C., Coppalle, A., Denby, B., Douros, J., Graf, A., Hellmuth, O., Hodzic, A., Honoré, C., Jonson, J., Kerschbaumer, A., de Leeuw, F., Minguzzi, E., Moussiopoulos, N., Pertot, C., Peuch, V. H., Pirovano, G., Rouil, L., Sauter, F., Schaap, M., Stern, R., Tarrason, L., Vignati, E., Volta, M., White, L., Wind, P., and Zuber, A. (2007). CityDelta: A model intercomparison study to explore the impact of emission reductions in European cities in 2010. *Atmospheric Environment*, **41,** 1, 189-207.

Dore, A.J., T.W. Choularton and Fowler, D. (1992): An improved wet deposition map of the United Kingdom incorporating the topographic dependence of rainfall concentrations. Atmos. Environ., 26A, 1375-1381.

Draaijers, G.P.J. and Erisman J.W. (1993): Atmospheric sulphur deposition to forest stands - throughfall estimates compared to estimates from inference. Atmos. Environ., 27A, 43-55.

Draaijers, G. P. J., and Erisman, J. W. (1995). A canopy budget model to assess atmospheric deposition from throughfall measurements. *Water, Air, and Soil Pollution*, **85,** 4, 2253-2258.

Draaijers, G.P.J., van Leeuwen, E.P., Potma, C., van Pul, W.A.J. and Erisman, J.W. (1995): Mapping base cation deposition in Europe on a 10x20 km grid. Water Air Soil Pollut., 85, 2389-2394.

Draaijers, G.P.J., Erisman, J.W., Spranger, T. and Wyers, G.P. (1996a): The application of throughfall measurements. Atmos. Environ., 30, 3349-3361.

Draaijers, G.P.J., Erisman, J.W., van Leeuwen, N.F.M., Römer, F.G., te Winkel, B.H., Veltkamp, A.C., Vermeulen, A.T. and Wyers G.P. (1996b): The impact of canopy exchange on differences observed between atmospheric deposition and throughfall fluxes. Atmos. Environ., 31, 387-397.

Draaijers, G. P. J., Van Leeuwen, E. P., De Jong, P. G. H., and Erisman, J. W. (1997). Base cation deposition in europe-part I. Model description, results and uncertainties. *Atmospheric Environment*, **31,** 24, 4139-4157.

Draaijers, G.P.J., Bleeker, A., van der Veen, D., Erisman, J.W, Möls, H., Fonteijn, P. and Geusenbrock, M. (2001): Field intecomparison of throughfall, stemflow and precipitation measurements performed within the framework of the Pan European Intensive Monitoring Programme of EU/ICP Forests TNO report R2001/140.

Dragosits, U., Theobald, M.R., Place, C.J., Lord, E., Webb, J., Hill, J., ApSimon, H.M. and Sutton, M.A. (2002): Ammonia emission, deposition and impact assessment at the field scale: a case study of sub-grid spatial variablility. Environ. Pollut., 117, 147-158.

Duyzer, J.H., Deinum, G. and Baak, J. (1995): The interpretation of measurements of surface exchange of nitrogen oxides; corrections for chemical reactions. Philosophical Transactions of the Royal Society of London A 351, 1-18

Duyzer, J., Nijenhuis, B. and Weststrate, H. (2001): Monitoring and modelling of ammonia concentrations and deposition in agricultural areas of the Netherlands. Water, Air and Soil Pollution Focus, Vol 1 Nos. 5-6, 131-144.

EDC (Environmental Data Centre) (1993): Manual for Integrated Monitoring. Programme Phase 1993-1996. National Board of Waters and the Environment, Helsinki.

Eder, B.K. and Dennis R.L. (1990): On the use of scavenging ratios for the inference of surface level concentration. Water Air Soil Pollut., 52, 197-215.

Emberson, L.D., Ashmore, M.R., Cambridge, H.M., Simpson, D. and Tuovinen J.-P. (2000): Modelling stomatal ozone flux across Europe. Environ. Pollut., 109, 403-413.

EMEP/CCC (1996): EMEP Manual for Sampling and Analysis. EMEP/CCC Report 1/95.

EMEP (2001). EMEP manual for sampling and chemical analysis. EMEP - Chemical coordinating centre (CCC) EMEP/CCC-Report 1/95, 95 p.

EMEP (2013). Transboundary Acidification, Eutrophication and Ground Level Ozone in Europe in 2011. Norwegian Meteorological Institute 205 p.

Erisman, J.W. and Draaijers G. (1995): Atmospheric deposition in relation to acidification and eutrophication. Studies in Environmental Science 63, Elsevier, Amsterdam.

Erisman, J.W., A. van Pul and Wyers P. (1994a): Parameterization of dry deposition mechanisms for the quantification of atmospheric input to ecosystems. Atmos. Environ., 28, 2595-2607.

Erisman, J.W., Beier, C., Draaijers, G.P.J. and Lindberg, S. (1994b): Review of deposition monitoring methods. Tellus, 46B, 79-93.

Erisman, J.W., Draaijers, G., Duyzer, J., Hofschreuder, P., van Leeuwen, N., Römer, F., Ruijgrok, W. and Wyers, P. (1995): Particle deposition to forests. In: Heij, G.J. and Erisman J.W.(eds.): Proceedings of the conference “Acid rain research: do we have enough answers?”, ’s-Hertogenbosch, The Netherlands, 10-12 Oct. 1994. Studies in Environmental Science 64, 115-126.

Erisman, J.W., Mennen, M.G., Fowler, D., Flechard, C.R., Spindler, G., Grűner, A., Duyzer, J.H., Ruigrok, W. and Wyers, G.P. (1998a): Deposition Monitoring in Europe. Environ. Monit. Assess., 53, 279-295.

Erisman, J.W., Bleeker, A. and Van Jaarsveld, H. (1998b): Atmospheric deposition of ammonia to semi-natural vegetation in the Netherlands-methods for mapping and evaluation. Atmos. Environ., 32, 481-489.

Ferm M. (2001): Validation of a diffusive sampler for ozone in workplace atmospheres according to EN838. Proceedings from International Conference Measuring Air Pollutants by Diffusive Sampling, Montpellier, France 26-28 September 2001, 298-303.

Ferm, M. and Svanberg P.-A. (1998): Cost- efficient techniques for urban and background measurements of SO2 and NO2. Atmos. Environ., 32, 1377-1381.

Fiore, A. M., Dentener, F. J., Wild, O., Cuvelier, C., Schultz, M. G., Hess, P., Textor, C., Schulz, M., Doherty, R. M., Horowitz, L. W., MacKenzie, I. A., Sanderson, M. G., Shindell, D. T., Stevenson, D. S., Szopa, S., Van Dingenen, R., Zeng, G., Atherton, C., Bergmann, D., Bey, I., Carmichael, G., Collins, W. J., Duncan, B. N., Faluvegi, G., Folberth, G., Gauss, M., Gong, S., Hauglustaine, D., Holloway, T., Isaksen, I. S. A., Jacob, D. J., Jonson, J. E., Kaminski, J. W., Keating, T. J., Lupu, A., Marmer, E., Montanaro, V., Park, R. J., Pitari, G., Pringle, K. J., Pyle, J. A., Schroeder, S., Vivanco, M. G., Wind, P., Wojcik, G., Wu, S., and Zuber, A. (2009). Multimodel estimates of intercontinental source-receptor relationships for ozone pollution. *Journal of Geophysical Research: Atmospheres*, **114,** D4, D04301.

Flechard, C.R. and Fowler, D. (1998): Atmospheric ammonia at a moorland site. II: Long-term surface/atmosphere micrometeorological flux measurements. Q. J. Roy. Meteor. Soc., 124, 733-757.

Flemming, J. (2003): Immissionsfelder aus Beobachtung, Modellierung und deren Kombination, PhD thesis, Free University Berlin, FB Geowissenschaften (in German).

Fowler, D., Granat, L., Koble, R., Lovett, G., Moldan, F., Simmons, C., Slanina, S.J. & Zapletal, M. (1993): Wet, cloud water and fog deposition. (Working Group report). In: Models and methods for the quantification of atmospheric input to ecosystems, edited by G.Lovblad, J.W. Erisman & Fowler, 9-12. Copenhagen: Nordic Council of Ministers.

Fowler, D., Jenkinson, D.S., Monteith, J.L. and Unsworth, M.H. eds. (1995a): The exchange of trace gases between land and atmosphere. Proceedings of a Royal Society discussion meeting. Philos. T. Roy. Soc. A, 351 (1696), pp. 205-416.

Fowler, D., Leith, I.D., Binnie, J., Crossley, A., Inglis, D.W.F., Choularton, T.W., Gay, M., Longhurst, J.W.S. and Conland, D.E. (1995b): Orographic enhancement of wet deposition in the United Kingdom: continuouse monitoring. Water Air Soil Pollut., 85, 2107-2112.

Fowler, D., R.I. Smith and Weston K.J. (1995c): Quantifying the spatial distribution of surface ozone exposure at the 1kmx1km scale. In: Fuhrer and Achermann (eds.)(1995), 196-205.

Fowler, D., Pitcairn, C.E.R. and Erisman, J-W. eds. (2001a): Air-Surface Exchange of Gases and Priticles (2000). Proceedings of the Sixth International Conference on Air-Surface Exchange of Gases and Particles, Edinburgh 3-7 July, 2000. Water Air and Soil Pollution Focus, Vol. 1 Nos. 5-6, 1-464.

Fowler, D., Coyle, M., Flechard, C., Hargreaves, K., Storeton-West, R., Sutton, M. and Erisman, J.W. (2001b): Advances in micrometeorological methods for the measurement and interpretation of gas and particles nitrogen fluxes. Plant Soil, 228, 117-129.

Fowler, D., Sutton, M.A., Flechard, C., Cape, J.N., Storeton-West, R., Coyle, M. and Smith, R.I. (2001c): The Control of SO2 dry deposition on to natural surfaces and its effects on regional deposition. Water, Air, and Soil Pollution Focus, Vol. 1 Nos. 5-6, 39-48.

Fowler, D., Pilegaard, K., Sutton, M. A., Ambus, P., Raivonen, M., Duyzer, J., Simpson, D., Fagerli, H., Fuzzi, S., Schjoerring, J. K., Granier, C., Neftel, A., Isaksen, I. S. A., Laj, P., Maione, M., Monks, P. S., Burkhardt, J., Daemmgen, U., Neirynck, J., Personne, E., Wichink- Kruit, R., Butterbach-Bahl, K., Flechard, C., Tuovinen, J. P., Coyle, M., Gerosa, G., Loubet, B., Altimir, N., Gruenhage, L., Ammann, C., Cieslik, S., Paoletti, E., Mikkelsen, T. N., Ro-Poulsen, H., Cellier, P., Cape, J. N., Horvath, L., Loreto, F., Niinemets, U., Palmer, P. I., Rinne, J., Misztal, P., Nemitz, E., Nilsson, D., Pryor, S., Gallagher, M. W., Vesala, T., Skiba, U., Brüggemann, N., Zechmeister-Boltenstern, S., Williams, J., O'Dowd, C., Facchini, M. C., de Leeuw, G., Flossman, A., Chaumerliac, N., and Erisman, J. W. (2009). Atmospheric composition change: Ecosystems - Atmosphere interactions. *Atmospheric Environment*, **43,** 33, 5193-5267.

Frohn, L. M., Christensen, J. H., Brandt, J., and Hertel, O. (2001). Development of a high resolution integrated nested model for studying air pollution in Denmark. *Physics and Chemistry of the Earth, Part B: Hydrology, Oceans and Atmosphere*, **26,** 10, 769-774.

Fuhrer, J. (2002): Ozone impacts on vegetation. Ozone-Sci. Eng., 24, 69-74.

Gallagher, M., Fontan, J., Wyers, P., Ruijgrok, W., Duyzer, J., Hummelsh, P. and Fowler, D. (1997): Atmospheric Particles and their Interactions with Natural Surfaces. In: Biosphere- Atmosphere Exchange of Pollutants and Trace Substances, (ed. S. Slanina), 45-92. Springer-Verlag.

Gauger, Th., F. Anshelm, H. Schuster, J.W. Erisman, A.T. Vermeulen, G.P.J. Draaijers, A. Bleeker and H.-D. Nagel (2003): Mapping of ecosystem specific long-term trends in deposition loads and concentrations of air pollutants

in Germany and their comparison with Critical Loads and Critical Levels. Part 1: Deposition Loads 1990-1999. Final Report of Project 29942210. Inst. for Navigation, Stuttgart University and Umweltbundesamt.

Grunhage, L. and Haenel H.D. (1997): Platin (plant-atmosphere interaction) I: A model of plant-atmosphere interaction for estimating absorbed doses of gaseous air pollutants. Environ. Pollut., 98, 37-50.

Hertel, O., Geels, C., Frohn, L. M., Ellermann, T., Skjoth, C. A., Lofstrom, P., Christensen, J. H., Andersen, H. V., and Peel, R. G. (2013). Assessing atmospheric nitrogen deposition to natural and semi-natural ecosystems – Experience from Danish studies using the DAMOS. *Atmospheric Environment*, **66,** 151-160.

Hertel, O., Reis, S., Skjoth, C. A., Bleekers, A., Harrison, R., Cape, J. N., Fowler, D., Skiba, U., Simpson, D., Jickells, T. D., Baker, A. R., Kulmala, M., Gyldenkærne, S., Lotte Sorensen, L., and Erisman, J. W. (2011). Nitrogen processing in the atmosphere. *In* "European Nitrogen Assessment" Cambridge University Press, Cambridge, UK. pp. 177-207.

Hertel, O., Skjoth, C. A., Lofstrom, P., Geels, C., Frohn, L. M., Ellermann, T., and Madsen, P. V. (2006). Modelling nitrogen deposition on a local scale - A review of the current state of the art. *Environmental Chemistry*, **3,** 5, 317-337.

Hettelingh, J. P., Posch, M., Velders, G. J. M., Ruyssenaars, P., Adams, M., de Leeuw, F., Lükewille, A., Maas, R., Sliggers, J., and Slootweg, J. (2013). Assessing interim objectives for acidification, eutrophication and ground-level ozone of the EU National Emissions Ceilings Directive with 2001 and 2012 knowledge. *Atmospheric Environment*.

Hellsten, S., Van Loon, M., Tarrason, L., Vestreng, V., Torseth, K., Kindborn, K., and Aas, W. (2007). Base cations deposition in Europe. IVL Swedish Environmental Research Institute, Göteborg, Sweden.

Hicks, B.B., Baldocchi, D.D., Meyers, T.P., Matt, D.R. and Hosker, Jr. R.P. (1987): A preliminary multiple resistance routine for deriving dry deposition velocities from measured quantities. Water Air Soil Pollut., 36, 311-330.

Hicks, B.B., McMillen, R., Turner, R.S., Holdren, Jr. G.R. and Strickland, T.C. (1993): A national critical loads framework for atmospheric deposition effects assessment: III. Deposition characterization. Environ. Manage., 17, No.3, 343-353.

Huijnen, V., Eskes, H. J., Poupkou, A., Elbern, H., Boersma, K. F., Foret, G., Sofiev, M., Valdebenito, A., Flemming, J., Stein, O., Gross, A., Robertson, L., D'Isidoro, M., Kioutsioukis, I., Friese, E., Amstrup, B., Bergstrom, R., Strunk, A., Vira, J., Zyryanov, D., Maurizi, A., Melas, D., Peuch, V. H., and Zerefos, C. (2010). Comparison of OMI NO2 tropospheric columns with an ensemble of global and European regional air quality models. *Atmos. Chem. Phys.*, **10,** 7, 3273-3296.

Iversen, T. (editor) (1991): Comparison of three models for long term photochemical oxidants in Europe. EMEP/MSC-W Report 3/91. The Norwegian Meteorological Institute, Oslo, Norway.

Jonson, J. E., Stohl, A., Fiore, A. M., Hess, P., Szopa, S., Wild, O., Zeng, G., Dentener, F. J., Lupu, A., Schultz, M. G., Duncan, B. N., Sudo, K., Wind, P., Schulz, M., Marmer, E., Cuvelier, C., Keating, T., Zuber, A., Valdebenito, A., Dorokhov, V., De Backer, H., Davies, J., Chen, G. H., Johnson, B., Tarasick, D. W., Newchurch, M. J., von der Gathen, P., Steinbrecht, W., and Claude, H. (2010). A multi-model analysis of vertical ozone profiles. *Atmos. Chem. Phys.*, **10,** 12, 5759-5783.

Kopacek, J., Posch, M., Hejzlar, J., Oulehle, F., and Volkova, A. (2012). An elevation-based regional model for interpolating sulphur and nitrogen deposition. *Atmospheric Environment*, **50,** 287-296.

Kryza, M., Dore, A. J., Blas, M., and Sobik, M. (2011). Modelling deposition and air concentration of reduced nitrogen in Poland and sensitivity to variability in annual meteorology. *Journal of Environmental Management*, **92,** 4, 1225-1236.

Langner, J., Engardt, M., Baklanov, A., Christensen, J. H., Gauss, M., Geels, C., Hedegaard, G. B., Nuterman, R., Simpson, D., Soares, J., Sofiev, M., Wind, P., and Zakey, A. (2012). A multi- model study of impacts of climate change on surface ozone in Europe. *Atmos. Chem. Phys.*, **12,** 21, 10423-10440.

Loibl, W. and Smidt, S. (1996): Ozone exposure - Areas of potential ozone risk for selected tree species. Environ. Sci. Pollut. R., 3, 213-217.

Lövblad, G. (1996): In: Knoflacher, M., Schneider, J., and Soja, G. (eds.): Exceedance of Critical Loads and Levels - Spatial and Temporal Interpretation of Elements in Landscape Sensitive to Atmospheric Pollutants. Report from a UN-ECE Workshop held in Vienna, Austria, 22-24 November 1995. Federal Ministry for Environment, Youth and Family, Austria, Conference Papers 15, 236

Lövblad, G. and Erisman J.W. (1992): Deposition of Nitrogen in Europe. Background document; In Grennfelt, P. and Thörnelöf E.(eds.) (1992): Critical Loads for Nitrogen; report from a workshop held at Lökeberg, Sweden, 6-10 April 1992. Nord 1992: 41.

Lövblad, G., J. W. Erisman and Fowler D.(eds.)(1993): Models and Methods for the Quantification of Atmospheric Input to Ecosystems. Proceedings of an international workshop on the deposition of acidifying substances, Göteborg 4-6 November 1992. Nordiske Seminar- og Arbejdsrapporter 1993:573, Nordic Council of Ministers.

Lövblad, G., Grennfelt, P., Kärenlampi, L., Laurila, T., Mortensen, L., Ojanperä, K., Pleijel, H., Semb, A., Simpson, D., Skärby, L., Tuovinen, J.P.and Tørseth, K. (1996): Ozone exposure mapping in the Nordic Countries, Report from a Nordic cooperation project finanaced by the Nordic Council of Miisters, Report Tema Nord 1996:528.

Lyman, J., Fleming, R. H. (1940): Composition of sea water. Journal of Marine Research 3: 134-146.

Menut, L., Bessagnet, B., Khvorostyanov, D., Beekmann, M., Blond, N., Colette, A., Coll, I., Curci, G., Foret, G., Hodzic, A., Mailler, S., Meleux, F., Monge, J. L., Pison, I., Siour, G., Turquety, S., Valari, M., Vautard, R., and Vivanco, M. G. (2013). CHIMERE 2013: a model for regional atmospheric composition modelling. *Geoscientific Model Development* **6,** 4, 981-1028.

Nemitz, E., Milford, C. and Sutton, M.A. (2001): A two-layer canopy compensation point model for describing bi-directional biosphere-atmosphere exchange of ammonia. Q. J. Roy. Meteor. Soc., 127, 815-833.

Pacyna, J. M. (2008). Atmospheric Deposition. *In* "Encyclopedia of Ecology" Academic Press, Oxford. pp. 275-285.

PORG (1997): Ozone in the UK. Fourth report of the Photochemical Oxidants Review Group. 234pp. DETR (ITE Edinburgh).

RGAR (1997): Acid Deposition in the United Kingdom 1992-1994. Fourth Report of the Review Group on Acid Rain. 176 pp. HMSO, London.

Robertson, L., Langner, J., and Engardt, M. (1999). An Eulerian Limited-Area Atmospheric Transport Model. *Journal of Applied Meteorology*, **38,** 2, 190-210.

Rouil, L., Honore, C., Vautard, R., Beekmann, M., Bessagnet, B., Malherbe, L., Meleux, F., Dufour, A., Elichegaray, C., Flaud, J.-M., Menut, L., Martin, D., Peuch, A., Peuch, V.-H., and Poisson, N. (2009). PREV'AIR An Operational Forecasting and Mapping System for Air Quality in Europe. *Bulletin of the American Meteorological Society*, **90,** 1, 73-83.

Ruijgrok, W., Tieben, H. and Eisinga, P. (1996): The dry deposition of particles to a forest canopy: a comparison of model and experimental results. Atmos. Environ., 31, 399-415.

Schaug, J., Iversen, T. and Pedersen, U. (1993): Comparison of measurements and model results for airborne sulphur and nitrogen components with Kriging. Atmos. Environ., 27A, 831-844.

Schjoerring, J.K., Husted, S. and Mattsson, M. (1998): Physiological parameters controlling plant-atmosphere ammonia exchange. Atmos. Environ., 32, 491-498.

Seinfeld, J. H., and Pandis, S. N. (1998). "Atmospheric chemistry and physics. From air pollution to climate change," John Wiley and sons, Inc, New York, USA, 1326 p. Simpson, D., Benedictow, A., Berge, H., Bergström, R., Emberson, L. D., Fagerli, H., Flechard, C. R., Hayman, G. D., Gauss, M., Jonson, J. E., Jenkin, M. E., Nyiri, A., Richter, C., Semeena, V. S., Tsyro, S., Tuovinen, J. P., Valdebenito, A., and Wind, P. (2012). The EMEP MSC-W chemical transport model - technical description. *Atmospheric Chemistry and Physics*, **12,** 16, 7825-7865.

Singles, R, Sutton, M.A. and Weston, K.J. (1998): A multi-layer model to describe the atmospheric transport and deposition of ammonia in Great Britain. Atmos. Environ., 32, 393-399.

Sjöberg K., Lövblad G., Ferm M., Ulrich E., Cecchini S. and Dalstein L. (2001) Ozone measurements at forest plots using diffusive samplers. Proc. from International Conference Measuring Air Pollutants by Diffusive Sampling, Montpellier, France 26-28 September 2001. p116-123.

Slanina, S. ed. (1997): Biosphere- Atmosphere Exchange of Pollutants and Trace Substances. Springer-Verlag

Slinn, W.G.N. (1982): Predictions for particle deposition to vegetativ surfaces. Atmos. Environ., 16, 1785-1794.

Smith, R.I. and Fowler, D. (2001): Uncertainty in estimation of wet deposition of sulphur. Water, Air and Soil Pollution Focus, Vol 1. Nos. 5-6, 341-354.

Smith, R.I., D. Fowler and Bull K.R. (1995): Quantifying the scale dependence in estimates of wet and dry deposition and the implication for critical load exceedances. In: Heij, G.J. and Erisman J.W. (eds.): Proceedings of the conference "Acid rain research: do we have enough answers?", `s-Hertogenbosch, The Netherlands, 10-12 Oct. 1994. Studies in Environmental Science 64, 175-186.

Smith, R.I., D. Fowler, M.A. Sutton, C. Flechard and Coyle, M. (2000): Regional estimation of pollutant gas dry deposition in the UK: model description, sensitivity analyses and outputs. Atmos. Environ., 34, 3757-3777.

Spranger, T. (1992), Erfassung und ökosystemare Bewertung der atmosphärischen Deposition und weiterer oberirdischer Stoffflüsse im Bereich der Bornhöveder Seenkette. Ph.D. thesis, Christian-Albrechts Universität, Kiel, Germany (in German).

Spranger, T., F. Kunze, Th. Gauger, H.-D. Nagel, A. Bleeker and G.P.J. Draaijers (2001): Critical Loads exceedances in Germany and their dependence on the scale of input data. Water, Air, and Soil Pollution Focus, Vol. 1 Nos. 1-2, 335-351.

Stedman, J.R., Vincent, K.J., Campbell, G.W., Goodwin, J.W.L. and C.E.H Downing. (1997): New high-resolution maps of estimated background ambient Nox and NO2 concentrations in the UK. Atmos. Environ., 31,3591-3602.

Sutton, M.A., Lee, D.S., Dollard, G.J. and Fowler D. eds. (1998): International conference on atmospheric ammonia: emmison, deposition and environmental impacts. Atmos. Environ., 32, 269-594.

Sutton, M.A., Nemitz, E., Fowler, D., Wyers, G.P., Otjes, R.P., Schjoerring, J.K., Husted, S., Nielsen, K.H., San José, Moreno, J., Gallagher, M.W. and Gut, A. (2000): Fluxes of ammonia over oilseed rape Overview of the EXAMINE experiment. Agr. Forest Meteorol., 105, 327-349.

Sutton, M.A., Miners B., Tang Y.S., Milford C., Wyers G.P., Duyzer J.H. and Fowler D. (2001a): Comparison of low-cost measurement techniques for long-term monitoring of atmospheric ammonia. J. Environ. Monitor., 3, 446-453.

Sutton, M.A., Tang, Y.S., Dragosits, U., Fournier, N., Dore, T., Smith, R.I., Weston, K.J. and Fowler, D. (2001b): A spat ial analysis of atmospheric ammonia and ammonium in the UK. The Scientific World, 1 (S2), 275-286.

Sverdrup, H., de Vries, W., Hornung, M., Cresser, M., Langan, S., Reynolds, B., Skeffington, R and Robertson, W. (1995): Modification of the simple mass- balance equation for calculation of critical loads of acidity. In: M.

Hornung, M.A. Sutton and R.B. Wilson (eds.) Mapping and modelling of critical loads for nitrogen: a Workshop Report, Grange-over-Sands, October 1994. Penicuik: Instsitute of Terrestrial Ecology. 87-92.

Sverdrup, H. U., Johnson, M. W., Fleming, R.H. (1946): The Oceans - Their Physics Chemistry and General Biology. Prentice-Hall, New York, 1087 pp.

TFEIP (2013). EMEP/EEA air pollutant emission inventory guidebook 2013. Technical guidance to prepare national emission inventories. European Environment Agency Technical report 12/2013,p.

Torseth, K., Aas, W., Breivik, K., Fjaeraa, A. M., Fiebig, M., Hjellbrekke, A. G., Lund Myhre, C., Solberg, S., and Yttri, K. E. (2012). Introduction to the European Monitoring and Evaluation Programme (EMEP) and observed atmospheric composition change during 1972 - 2009. *Atmospheric chemistry and physics*, **12,** 12, 5447-5481.

Tsyro, S., Aas, W., Soares, J., Sofiev, M., Berge, H., and Spindler, G. (2011). Modelling of sea salt concentrations over Europe: key uncertainties and comparison with observations. *Atmos. Chem. Phys.*, **11,** 20, 10367-10388.

UBA (1996): Manual on Methodologies and Criteria for Mapping Critical Levels/Loads and geographical areas where they are exceeded. UBA-Texte 71/96.

Ulrich, B. (1983): Interaction of forest canopies with atmospheric constituents: SO2 , alkali and earth alkali cations and chloride. In: B. Ulrich and Pankrath J.(eds.): Effects of accumulation af air pollutants in forest ecosystems, 33-45

UN-ECE ICP Forests (1999): Manual on methods and criteria for harmonized sampling, assessment, monitoring and analysis of the effects of air pollution on forests. Part VI: Measurement of Deposition and Air Pollution

van Leeuwen, E.P., J.W. Erisman, G.P.J. Draaijers, C.J.M. Potma and van Pul W.A.J. (1995): European wet deposition maps based on measurements. Report No. 722108006, National Institute of Public Health and Environmental Protection, Bilthoven, The Netherlands.

Van Leeuwen, E. P., Potma, C. J. M., Draaijers, G. P. J., Erisman, J. W., and van Pul, W. A. J. (1995). European Wet Deposition Maps Based on Measurements. RIVM (National Institute for Public Health and the Environment), Bilthoven, the Netherlands. RIVM Report 722108006, p.

Van Leeuwen, E. P., Draaijers, G. P. J., and Erisman, J. W. (1996). Mapping wet deposition of acidifying components and base cations over Europe using measurements. *Atmospheric Environment*, **30,** 14, 2495-2511.

Van Loon, M., Tarrason, L., and Posch, M. (2005). Modelling Base Cations in Europe. EMEP; CCE Technical report 2, 58 p.

van Loon, M., Vautard, R., Schaap, M., Bergström, R., Bessagnet, B., Brandt, J., Builtjes, P. J. H., Christensen, J. H., Cuvelier, C., Graff, A., Jonson, J. E., Krol, M., Langner, J., Roberts, P., Rouïl, L., Stern, R., Tarrason, L., Thunis, P., Vignati, E., White, L., and Wind, P. (2007). Evaluation of long-term ozone simulations from seven regional air quality models and their ensemble. *Atmospheric Environment*, **41,** 10, 2083-2097.

van Pul, W.A.J., C. Potma, E. van Leeuwen, Draaijers, G., and Erisman J.W. (1995): EDACS: European deposition maps of acidifying components on a small scale. Model description and preliminary results. RIVM Report no. 722401005, Bilthoven, The Netherlands

Vet, R., Artz, R. S., Carou, S., Shaw, M., Ro, C.-U., Aas, W., Baker, A. R., Bowersox, V. C., Dentener, F., Galy-Lacaux, C., Hou, A., Pienaar, J. J., Gillett, R., Forti, M. C., Gromov, S., Hara, H., Khodzher, T., Mahowald, N. M., Nickovic, S., Rao, P. S. P., and Reid, N. W. (2013). A global assessment of precipitation chemistry and deposition of sulphur, nitrogen, sea salt, base cations, organic acids, acidity and pH, and phosphorus. *Atmospheric Environment*, 1352-2310.

Walton, S., Gallagher, M.W. and Duyzer, J.H. (1997): Use of a detailed model to study the exchange of Nox and O3 above and below a deciduous canopy. Atmos. Environ., 31, 2915-2932.

Werner, M., Kryza, M., Dore, A. J., Blas, M., Hallsworth, S., Vieno, M., Tang, Y. S., and Smith, R. I. (2011). Modelling of marine base cation emissions, concentrations and deposition in the UK. *Atmospheric Chemistry and Physics*, **11,** 3, 1023-1037.

WMO (2008 - updated in 2010). Guide to Meteorological Instruments and Methods of Observation. World meteorological office, Geneva, Switzerland. WMO-No. 8, 716 p.

3 Mapping critical levels for vegetation and lichens

Chapter 3 was prepared under the leadership of the ICP Vegetation[11] and led by Gina Mills, Head of the ICP Vegetation Programme Coordination Centre (PCC), Centre for Ecology & Hydrology, Bangor, UK, with support from the editorial team members Harry Harmens (Chair of the ICP Vegetation), Felicity Hayes (PCC), Håkan Pleijel (Chair Crops Working Group), Patrick Büker (Chair Forest Trees Working Group) and Ignacio González-Fernández (Chair (Semi-)natural Vegetation Working Group). Many other ozone experts from the ICP vegetation also contributed to the chapter, including Rocio Alonso, Jürgen Bender, Elke Bergmann, Viki Bermejo, Sabine Braun, Helena Danielsson, Giacomo Gerosa, Ludger Grünhage, Per Erik Karlsson and Riccardo Marzuoli, together with contributions from ICP Forests (Marcus Schaub) and EMEP (David Simpson).

This fully revised version of Chapter 3 includes updates to the critical levels for ozone agreed at the 30th ICP Vegetation Task Force Meeting on 14-17 February 2017 in Poznan, Poland. The critical levels for SO_2, NO_X, and NH_3, and associated text have not been changed since the previous version. This version was published in April 2017 (minor edits October 2017).

Note: in addition to this chapter, two additional scientific background documents (SBD) are available on the ICP Vegetation web site (https://icpvegetation.ceh.ac.uk/):

- SBD-A: Supplementary material to Chapter 3 of Modelling and Mapping Manual;
- SBD-B: Developing areas and new directions of ozone research.

Please refer to this document as: CLRTAP, 2017. Mapping critical levels for vegetation, Chapter 3 of Manual on methodologies and criteria for modelling and mapping critical loads and levels and air pollution effects, risks and trends. UNECE Convention on Long-range Transboundary Air Pollution; accessed on [date of consultation] on Web at www.umweltbundesamt.de/en/cce-manual.

3.1 Introduction to critical levels for vegetation

The purpose of this chapter is to provide information on the critical levels of air pollutants for vegetation and the methodology for calculating critical level exceedance. Methods for mapping pollutant concentrations, deposition, and exceedance are provided in Chapter II. The International Cooperative Programme on Effects of Air Pollution on Natural Vegetation and Crops (ICP Vegetation) has editorial responsibility for this chapter. Further information supporting the critical levels for ozone (O_3) and associated methodology can be found in the Chapter 3 Scientific Background Document A (SBD-A), whilst information on new developments in research for ozone critical levels is presented in the Chapter 3 Scientific background Document B (SBD-B), both are available on the ICP Vegetation website (http://icpvegetation.ceh.ac.uk).

Excessive exposure to atmospheric pollutants has harmful effects on many types of vegetation, as well as the ecosystem and food services that vegetation provides. Critical levels are described in different ways for different pollutants, including mean concentrations, cumulative exposures and cumulative uptake through small pores in leaves (stomatal flux). The effects vary between vegetation type or species and pollutant and include changes in growth for trees and (semi-) natural vegetation, yield (quality and quantity) for crops, flower number and seed production for (semi-)natural vegetation, and vulnerability to abiotic stresses such as frost or drought and

[11] International Cooperative Programme on Effects of Air Pollution on Natural Vegetation and Crops

biotic stresses such as pests and diseases. Critical levels are defined as indicated in Box 1. Critical level exceedance maps show the difference between the critical level and the monitored or modelled air pollutant concentration, cumulative exposure or cumulative stomatal flux.

Box 1: Definition of critical levels for vegetation

Critical levels for vegetation are the "concentration, cumulative exposure or cumulative stomatal flux of atmospheric pollutants above which direct adverse effects on sensitive vegetation may occur according to present knowledge".

For **sulphur dioxide (SO_2)**, **nitrogen oxides (NO_x)** and **ammonia (NH_3)**, recommendations are made for concentration-based critical levels. For information on critical loads for sulphur and nitrogen acidity, and eutrophication due to nitrogen deposition see Chapter 5. For **ozone (O_3)**, two types of critical levels are described for crops, forest trees and (semi-) natural vegetation: cumulative stomatal flux-based and cumulative concentration-based critical levels. Calculation of both incorporates the concept that the effects of O_3 are cumulative and values are summed over a specific threshold flux or concentration during daylight hours for a defined time period. As described in Section 3.3.1, cumulative stomatal O_3 fluxes are considered biologically more relevant as they provide an estimate of the amount of O_3 entering the leaf pores and causing damage inside the plant (Mills et al., 2011a,b).

The critical levels have been set, reviewed and revised at a series of UNECE Workshops and ICP Vegetation Task Force Meetings, starting with Bad Harzburg (1988) and most recently in Madrid (2016) and at the 30th ICP Vegetation Task Force meeting in Poznan (2017); see Annex for a list of workshops. The critical levels for O_3 and associated methodology have been primarily developed by the ICP Vegetation, with those for forests developed in collaboration with the ICP Forests (International Cooperative Programme on Assessment and Monitoring of Air Pollution Effects on Forests). Following agreement at ICP Vegetation Task Force Meetings or workshops, new or amended critical levels were subsequently put forward for approval at Task Force meetings of ICP Modelling and Mapping (International Cooperative Programme on Modelling and Mapping of Critical Levels and Loads and Air Pollution Effects, Risks and Trends), the joint meeting of the EMEP (The European Monitoring and Evaluation Programme) Steering Body and the WGE (Working Group on Effects) and the meeting of the Executive Body of the LRTAP Convention (http://www.unece.org/env/lrtap/welcome.html).

3.2 Critical levels for sulphur dioxide (SO_2), nitrogen oxides (NO_X), and ammonia (NH_3)

3.2.1 Sulphur dioxide (SO_2)

The critical levels for SO_2 that were established in Egham in 1992 (Ashmore & Wilson, 1993) are still valid (Table 3.1). There are critical levels for four categories of vegetation types – for sensitive groups of lichens, for forest ecosystems, (semi-)natural vegetation and for agricultural crops. These critical levels have been adopted by WHO (2000).

Exceedance of the critical level for (semi-)natural vegetation, forests, and, when appropriate, agricultural crops occurs when either the annual mean concentration or the winter half-year mean concentration is greater than the critical level; this is because of the greater impact of SO_2 under winter conditions.

Table 3.1: Critical levels for SO_2 (µg m^{-3}) by vegetation category.

Vegetation Type	Critical level SO_2 [µg m^{-3}]	Time period
Cyanobacterial lichens	10	Annual mean
Forest ecosystems*	20	Annual mean and Half-year mean (October-March)
(Semi-)natural	20	Annual mean and Half-year mean (October-March)
Agricultural crops	30	Annual mean and Half-year mean (October-March)

*The forest ecosystem includes the response of the understorey vegetation.

3.2.2 Nitrogen oxides (NOx)

The critical levels for NO_x are based on the sum of the NO and NO_2 concentrations because there is insufficient knowledge to establish separate critical levels for the two pollutants. Since the type of response varies from growth stimulation to toxicity depending on concentration, all effects were considered to be adverse. Growth stimulations were of greatest concern for (semi-) natural vegetation because of the likelihood of changes in interspecific competition.

Separate critical levels were not set for classes of vegetation because of the lack of available information. However, the following ranking of sensitivity was established:

(semi-)natural vegetation > forests > crops

Critical levels for NOx were established in 1992 at the Egham Workshop. The background papers on NO_x and NH_3 presented at the Egham Workshop (Ashmore & Wilson, 1993) were further developed as the basis of the Air Quality Guidelines for Europe, published by the WHO in 2000. This further analysis incorporated a formal statistical model to identify concentrations to protect 95% of species at a 95% confidence level. In this re-analysis, growth stimulation was also considered as a potentially adverse ecological effect. Furthermore, a critical level based on 24h mean concentrations was considered to be more effective than one based on 4h mean concentrations as included in the earlier version of the Mapping Manual (UNECE, 1996). Since the WHO guidelines were largely based on analysis extending the background information presented at the Egham Workshop, the critical levels in Table 3.2, which are identical to those of WHO (2000), should now be used.

Table 3.2: Critical levels for NO_x (NO and NO_2 added, expressed as NO_2 (µg m^{-3})).

Vegetation Type	Critical level NOx (expressed as NO_2) [µg m^{-3}]	Time period
All	30	Annual mean
All	75	24-hour mean

For application for mapping critical levels and their exceedance, it is strongly recommended that only the annual mean values are used, as mapped and modelled values of this parameter have much greater reliability, and the long-term effects of NO_x are thought to be more significant than the short-term effects.

Some biochemical changes may occur at concentrations lower than the critical levels, but there is presently insufficient evidence to interpret such effects in terms of critical levels.

3.2.3 Ammonia (NH_3)

The fertilization effect of NH_3 can, in the longer-term, lead to a variety of adverse effects on vegetation, including direct toxic effects on epiphytic lichens through the increase of extracellular pH and fertilization effects such as growth stimulation (which can alter species balance with some species being potentially out-competed) and increased susceptibility to abiotic (drought, frost) and biotic stresses. As for NO_x, for application for mapping critical levels and their exceedance, it is strongly recommended that only the annual mean values of NH_3 are used. This is because mapped and modelled values of the longer-term critical levels have much greater reliability, and the long-term effects of NH_3 are thought to be more significant than the short-term effects.

The critical levels in Table 3.3 refer to ecosystems with the most sensitive lichens and bryophytes and vascular plants. The aim of these critical levels is to protect the functioning of plant and lichen individuals and communities. Lichens and bryophyte species were found to be more sensitive than vascular plants (Table 3.3). Critical levels are currently not set for intensively managed agricultural grasslands (pastures) and arable crops, which are often sources rather than sinks of ammonia and are less likely to contain sensitive species.

Table 3.3: Critical levels for NH_3 (µg m^{-3}).

Plant and lichen individuals and communities	Critical level NH_3 [µg m^{-3}]	Time period
Lichens and bryophytes (including ecosystems where lichens and bryophytes are a key part of ecosystem integrity)	1	Annual mean
Vascular plants (including ecosystems where lichens and bryophytes are not a key part of ecosystem integrity)	3*	Annual mean
Provisional critical levels		
Lichens and bryophytes	12##	Monthly mean
Vascular plants	23	Monthly mean

*An explicit uncertainty range of 2-4 µg m^{-3} was set for vascular plants. The uncertainty range is intended to be useful when applying the critical level in different assessment contexts (e.g. precautionary approach or balance of evidence).
##This value is not derived from experiments or observations, unlike other critical levels. It is highlighted here to be mathematically consistent with the annual level for lichens and bryophytes.

The critical levels presented in Table 3.3, except that for the monthly mean for lichens and bryophytes, were recommended for inclusion in this manual at a workshop, held in Edinburgh from 4-6 December in 2006: *Atmospheric ammonia: Detecting emission changes and environmental impacts* (UNECE, 2007). Their inclusion was subsequently approved at the 20th Task Force meeting of the ICP Vegetation (Dubna, Russian Federation, 5-8 March, 2007) and adopted at the 23rd meeting of the Task Force on Modelling and Mapping (Sofia, Bulgaria, 26-27 April, 2007).

15 years later, the critical levels in Table 3.3 were reviewed and confirmed at an Ammonia Expert Workshop, prepared by the Coordination Center for Effects (CCE) and held in Dessau, Germany and online 28-29 March 2022. The monthly mean critical level for lichens and

bryophytes was added. Amendments to this chapter, based on the Dessau Workshop conclusions, were presented and approved at the 36th Task Force Meeting of the ICP Vegetation (13-15 February 2023) and the 39th ICP Modelling & Mapping Task Force meeting in Prague (28-30 March 2023).

The following recommendations were given by the Edinburgh meeting (December, 2006) and confirmed by the Dessau Workshop (March 2022):

- The definition of a long-term critical level for lichens and bryophytes, including ecosystems where lichens and bryophytes are a key part of the ecosystem integrity, of 1 µg m^{-3} (annual mean);
- The definition of a long-term critical level for vascular plants, of 3 µg m^{-3}, with an uncertainty range of 2-4 µg m^{-3} (annual mean);
- Long-term critical level values are based on observation of actual species changes from both field surveys and long-term exposure experiments, where effects were related to measured ammonia concentrations and could not be assumed to provide a protection for longer than 20-30 years;
- To retain the monthly critical level (23 µg NH3 m^{-3}) for vascular plants only as a provisional value. This value is based on the assessment of adverse effects of short-term exposures as discussed at the UNECE Workshop on Critical Levels held in 1992 in Egham, United Kingdom (Van der Eerden et al., 1994). The monthly critical level was estimated with the "envelope" method using exposure-response data from mainly short-term fumigation experiments. Thus, it does not have the same relevance as the long-term critical levels (annual averages of 1 and 3 µg NH3 m^{-3}) derived from long-term field studies. The provisionally retained monthly value has to be considered as expert judgement to allow the assessment of effects of short-term peak concentrations which can occur, for example, during periods of manure application (e.g., in spring).

The following recommendations were added following the Dessau Workshop (March, 2022):

- The monthly critical level of 23 µg m^{-3} had been derived for vascular plants, and does not apply to lichens, bryophytes and ecosystems where these are important to ecosystem integrity, e.g. peatlands. It can easily be seen that one month of 23 µg m^{-3}, would give a minimum annual average of 1.9 µg m^{-3}, which already exceeds the long-term critical level for lichens and bryophytes. Therefore, to be mathematically consistent with the long-term critical level for those very sensitive elements, a maximum monthly value of 12 µg m^{-3} would apply, though further evidence would be needed to assess whether this value is sufficiently precautionary for sensitive lichen and bryophyte species.
- To remove ambiguity (e.g. where lichens and bryophytes are considered to be a key part of heathlands and other habitats), references to "*heathland, grassland and forest ground flora*" in the table 3.3 were removed in comparison to the previous version of this chapter. Additionally, references to the term "*vegetation*" as a standalone term as well as to "*lower and higher plants*" were removed, referring instead to 'lichens and bryophytes' and 'vascular plants' respectively and acknowledging that lichens are not part of the vegetation in the strict sense.
- In the background information as well as in the presentations of the Dessau Workshop, both published within the workshop proceedings, the latest supporting scientific literature of the past 15 years has been compiled (Franzaring and Kösler, 2023, Chapters 2 and 4)[1]. This

literature review focused on studies in which the effects of ammonia on plants and lichens were investigated. While many investigations were done in the field using e.g. lichens and gradient studies in the lee of farms, there were only a few controlled fumigation experiments published, in which reference concentrations of ammonia were set to derive dose-response relationships. The compiled research results since the 2009 revision to the ammonia critical levels, corroborates the changes made previously. As such, the key evidence (Table 3.4) remains unchanged.

- It must be noted that the effects of ammonia will be modified by concurrent elevated NO_x concentrations (e.g., Sutton et al., see Section 4.4.1 in Franzaring and Kösler, 2023)[1], for which further evidence is needed before setting of critical levels that integrate both gases. In addition, effects of ammonia depend on the wider ecological status of the ecosystem (e.g. combined impacts of management, drought and natural pH preferences). Since most research was based on Northwestern European peat bogs and heathlands, it is recommended that future revisions of critical levels should include other important European habitat types.

The proceedings of the UNECE Workshop on Ammonia (Edinburgh, December 2006) were published in Sutton et al. (2009) by Springer: Sutton M.A., Baker S., Reis S. (eds.), Atmospheric Ammonia: Detecting emission changes and environmental impacts. This book includes details of the evidence used to justify the change in critical levels, as summarized in Table 3.4.

The proceedings of the Dessau Workshop in March 2022 were published by the German Environment Agency. The report "Review of internationally proposed critical levels for ammonia - proceedings of an Expert Workshop held in Dessau and online on 28/29 March 2022" was collated by Franzaring and Kösler (2023) and can be downloaded from the website of the German Environment Agency[12].

Table 3.4: Key evidence based on observations of changes in species composition (a true ecological endpoint) in response to measured air concentrations of ammonia and for justifying separate critical levels for ecosystems where lichens and bryophytes are a key part of ecosystem integrity.

Location	Receptor type	Lowest measured NH_3 concentration [µg m^{-3}]	Estimated NOEC * [µg m^{-3}]	Reference
SE Scotland, poultry farm	Epiphytic lichens	0.6	0.7 (on twigs) 1.8 (on trunks)	(Pitcairn et al., 2004, Sutton et al., 2009)
Devon, SW England	Epiphytic lichens diversity (twig)	0.8 (modelled)	1.6	(Wolseley et al., 2006)
United Kingdom, national NH_3 network	Epiphytic lichens	0.1	1.0	(Leith et al., 2005, Sutton et al., 2009)
Switzerland	Lichen population index	1.9 (modelled)	2.4	(Rihm et al., 2009)
SE Scotland, field NH_3 experiment, Whim bog	Lichens and bryophytes	0.5	< 4	(Sheppard et al., 2009)

[12] https://www.umweltbundesamt.de/publikationen/review-of-internationally-proposed-critical-levels

Location	Receptor type	Lowest measured NH_3 concentration [µg m^{-3}]	Estimated NOEC * [µg m^{-3}]	Reference
	– damage and death			
Corroborative evidence **				
SW England	Epiphytic lichens	1.5	ca. 2	(Leith et al., 2005)
South Portugal	Epiphytic lichens	0.5	1	(Pinho et al., 2009)
Italy, pig farm	Epiphytic lichens	0.7	2.5	(Frati et al., 2007)

*NOECs were directly estimated from exposure/response curves or calculated with regression analysis. The data are from recent experimental studies, both field surveys and controlled field experiments on the impact of NH_3 on vegetation.
**In these cases, NH_3 concentration data were available for less than one year, which is why these results are categorised as "corroborative evidence".

3.3 Critical levels for ozone (O_3)

3.3.1 Overview

3.3.1.1 O_3 damage to vegetation and consequences for food production and ecosystem services

A large body of evidence has shown that ambient O_3 causes damage to O_3-sensitive vegetation. O_3 enters leaves via the stomatal pores on the leaf surface. Once inside the leaf, a series of chemical reactions occur leading to cell membrane damage and other negative impacts on plant metabolism, including photosynthesis. These effects can be in response to short-term episodes or cumulative during the growing season, and can lead to:

- Visible leaf damage and premature aging of leaves;
- Reductions in above- and below-ground growth and biomass;
- Changes in the ratio between shoot and root biomass (including carbon allocation);
- Reductions in flower number, flower biomass and seed production;
- Reductions in crop yield quantity and quality, including cereal grains, potato tubers and tomato fruit;
- Changes in forage quantity and quality for pasture;
- Altered tolerance to abiotic stresses such as drought and frost and biotic stresses such as pest attacks and diseases.

Reviews of O_3 effects on vegetation have been published for crops (Ainsworth, 2016), trees (Matyssek et al., 2012, Wittig et al., 2009), and (semi-)natural vegetation (Bassin et al., 2007, Fuhrer et al., 2016), whilst effects on carbon sequestration are reviewed by Ainsworth et al. (2012). ICP Vegetation has published a series of reports on O_3 effects on vegetation, including food security (Mills & Harmens, 2011), carbon sequestration (Harmens & Mills, 2012), ecosystem services, and biodiversity (Mills et al., 2013).

Widespread evidence of O_3 damage to vegetation in Europe was reported (Mills et al., 2011a) including visible leaf injury on crops, trees (Gottardini et al., 2016) and (semi-) natural

vegetation, reductions in growth of O_3-sensitive compared to resistant cultivars and biotypes, and beneficial effects on yield and growth of reducing the ambient O_3 concentration by filtration. O_3 effects have also been reported in the field in the USA (Fuhrer et al., 2016; Temple et al., 2005; U.S. Environmental Protection Agency, 2014) and southeast Asia (Emberson et al., 2009, Feng et al., 2015) and are present in other regions of the world (Fuhrer et al., 2016). Meta-analyses of published data have also indicated that ambient O_3 is reducing crop yield (Pleijel, 2011) and tree biomass production (Wittig et al., 2009), whilst analysis of survey data has shown how O_3 is reducing tree growth (Braun et al., 2014) and changing species composition, a biodiversity indicator (Payne et al., 2011).

The many impacts of O_3 have been considered when developing critical levels. Here, we provide critical levels for the potential O_3 effects on:

- Crop yield quantity and quality, for food security applications, including economic valuation;
- Tree biomass for timber production and potentially as a starting point for carbon sequestration and biodiversity application;
- Grassland biomass, potentially as a starting point for carbon sequestration and flower and seed production, potentially as a starting point for biodiversity application.

3.3.1.2 Metrics for critical levels of O_3 for vegetation

A glossary for all terms used for O_3 critical levels is provided in Annex III.2.

For O_3, two types of metrics are available for risk assessment, either based on the cumulative stomatal flux or the cumulative exposure. Scientific evidence suggests that observed effects of O_3 on vegetation **are more strongly related to the uptake of O_3 through the stomatal leaf pores (stomatal flux) than to the concentration** in the atmosphere around the plants (Mills et al., 2011b). Stomata are physiologically controlled and respond to environmental conditions such as temperature, light, air humidity, and soil moisture, as well as plant growth stage. For example, under hot and dry conditions, plants close their stomata to reduce water loss and as a consequence O_3 uptake is reduced. The DO_3SE model (Deposition of O_3 for Stomatal Exchange) has been developed to account for the variation in stomatal opening and closing with climatic, soil and plant factors (Büker et al., 2012; Emberson et al., 2000a,b, 2001, 2007). This model is described in Section 3.3.4.3, and available as an online version at: https://www.sei-international.org/do3se. It is used to determine the Phytotoxic O_3 Dose above a threshold flux of Y (POD_Y) which is the accumulated stomatal O_3 uptake during a specified time period. Different metrics have been developed for POD_Y depending on the complexity of the model and its application; see Box 2 for definitions.

Box 2: Metrics for stomatal flux-based critical levels

POD_Y (Phytotoxic O_3 Dose) is the accumulated plant uptake (flux) of O_3 above a threshold of Y during a specified time or growth period.

POD_YSPEC is a species or group of species-specific POD_Y that requires comprehensive input data and is suitable for detailed risk assessment.

POD_YIAM is a vegetation-type specific POD_Y that requires less input data and is suitable for large-scale modelling, including integrated assessment modelling.

The flux-based POD_Y metrics are preferred in risk assessment over the concentration-based AOT40 exposure index (defined in Box 3). AOT40 accounts for the atmospheric O_3 concentration above the leaf surface and is therefore biologically less relevant for O_3 impact assessment than POD_Y as it does not take into account how O_3 uptake is affected by climate, soil, and plant factors. This is particularly relevant on the pan-European scale with large climate differences between different regions. AOT40 can be used in cases where only O_3 concentration data are available (when meteorological and/or vegetation-specific information to calculate POD_Y are not available) and/or areas where no climatic or water restrictions to stomatal O_3 flux are expected. This approach predicts a different spatial pattern of impacts on the pan-European scale than POD_Y (Mills et al., 2011a; Simpson et al., 2007).

Box 3: Metric for concentration-based critical levels

AOT40 is the sum of the differences between the hourly mean O_3 concentration (in ppb) and a threshold value of 40 ppb O_3 when the concentration exceeds 40 ppb during daylight hours, accumulated over a stated time period.

Different types of evidence show that the relationships between effects and exposure are improved by consideration of the defence capacity of the plants, whereby a certain amount of absorbed O_3 is detoxified in the plants and does not impact on the overall effect (Mills et al., 2011b). This is variable by species and is accounted for by including an hourly cut-off Y flux in POD_Y and concentration X in AOT_X (with X being 40 ppb in AOT40).

3.3.1.3 Establishment of critical levels for O_3

The methods described in this chapter have been developed by:

- Combining data from available field studies to calibrate species-, vegetation type- and biogeographical region specific-models of leaf stomatal opening to quantify the stomatal O_3 flux for different plant species;
- Combining the results from available studies in Europe where plants were exposed to different levels of O_3 under field conditions to derive response functions from which critical levels are derived;
- Testing the critical levels using observations in the field under ambient conditions, wherever feasible.

Metric-response relationships have been established using experimental data from exposure systems, such as open-top chambers, that enable plants to be grown under naturally varying climatic conditions for one or more growing seasons. Data from several countries and years of experiments have been combined, wherever possible, for a single species/vegetation type. The approach described by Fuhrer (1994) for calculating relative effect (e.g., yield or biomass), now expressed as a percentage, has been used for each experimental dataset. The relative effect was obtained per data point by dividing the observed values of the response variables by the intercept of the linear regression between the response variable and O_3 exposure for each experiment (i.e., for a hypothetical cumulative stomatal flux or exposure equal to zero) and converted to percentage, to provide a relative effect for each data point. After this transformation, the data from all experiments were combined to derive a common response function for each species/vegetation type and effect. The 95% confidence intervals are shown on flux-effect relationships to give an indication of the strength of the relationship and the range of significance of effect for a given POD_Y (SPEC or IAM). Response functions used to derive the AOT40-based critical levels are provided in the scientific background document A (SBD-A).

In some circumstances when the POD_Y is being calculated, reference against a POD_Y of 0 could theoretically lead to a critical level that is not achievable, as the O_3 concentrations needed to achieve this could be lower than the estimated "pre-industrial" O_3 concentration. Hence, at the O_3 Critical Level workshop in Madrid in November 2016, it was decided that an accumulated flux value calculated at a constant 10 ppb O_3 (estimated pre-industrial mean O_3 concentration) should be set as a reference value (Ref10 POD_Y) for determining flux-based critical levels (SBD-A). Ref10 POD_Y was first determined for the same set of experimental data used for derivation of flux-effect relationships by calculating POD_Y using a constant O_3 concentration of 10 ppb and the climatic conditions in the experiment. If data from several experiments were combined from different climates, the mean of the Ref10 POD_Y was used as the Ref10 POD_Y for that function. The application of this approach in the derivation of a critical level is shown in Figure 3.1. This approach is not needed for AOT40-based critical levels as the cut-off concentration of 40 ppb in calculating AOT40 is substantially higher than estimated pre-industrial O_3 concentration (SBD-A).

Each critical level was derived from a response function using a species or vegetation-specific percentage effect. The choice of percentage value for each critical level is explained in the separate sections.

Figure 3.1: Method for using Ref10 POD_Y (i.e. POD_Y at 10 ppb constant O_3) as reference point for O_3 critical level derivation.

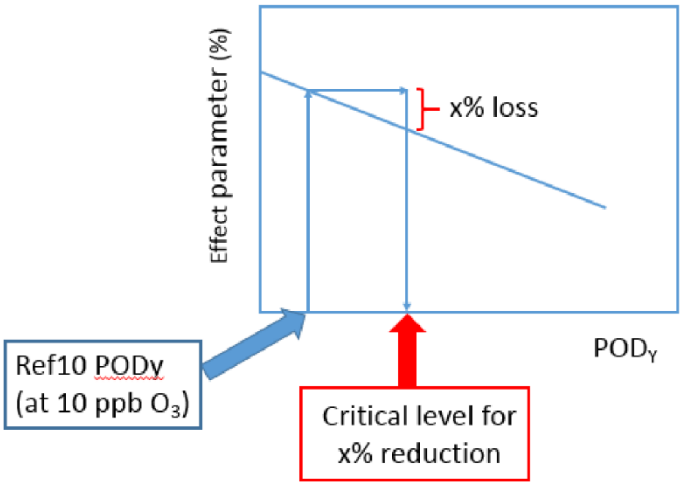

Source: This figure is adopted from a previous version of Chapter 3 of the Mapping Manual

3.3.2 Which metric to choose and the input data required

The flow chart below (Figure 3.2) and table of input requirements (Table 3.5) are provided to help users choose which metric to use, depending on data availability and application.

Figure 3.2: **Flow chart describing which metric and critical level should be used to assess the risk of O3 damage to vegetation, depending on availability of hourly input data and application. Additional information required for PODYSPEC and PODYIAM include biogeographical region, land cover, average canopy height, and average leaf dimension and for PODYSPEC also detailed info on plant phenology. * At canopy height; ** VPD = vapour pressure deficit; *** Med. = Mediterranean.**

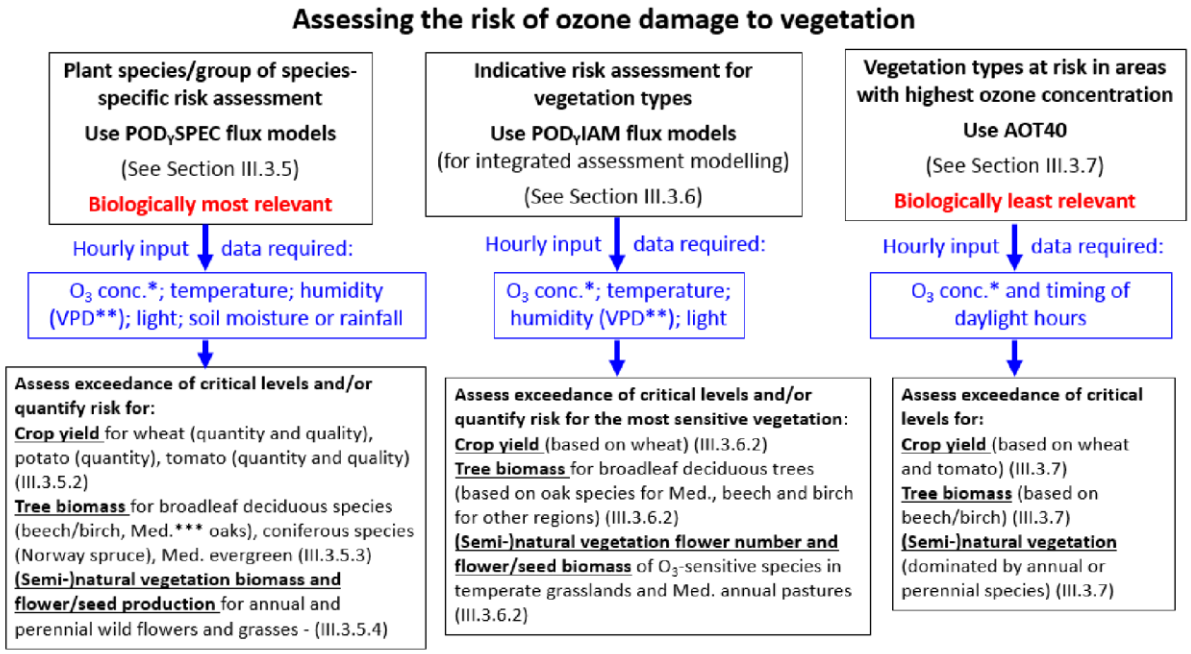

Source: This figure is adopted from a previous version of Chapter 3 of the Mapping Manual

The biologically most relevant risk assessment will be achieved by calculating POD_YSPEC, using biogeographical region-specific O_3 flux models and critical levels for individual plant species or groups (Section 3.3.5). An indicative risk assessment is achieved when using POD_YIAM, using O_3 flux models and critical levels developed for use in large-scale modelling, including integrated risk assessment (IAM; Section 3.3.6). The least biologically relevant risk assessment involves calculating the O_3 concentration-based metric AOT40 (Section 3.3.7). However, as mentioned before, AOT40 can be used in cases where only O_3 concentration data are available and/or areas where no climatic or water restrictions to stomatal O_3 flux are expected.

Table 3.5: Overview of hourly mean input variables required to calculate the Phytotoxic O_3 Dose above a threshold of Y (POD_YSPEC and POD_YIAM; with reference to tables - T) and to calculate AOT40.

	Data types*	POD_YSPEC	POD_YIAM	AOT40
Tables to refer to for further information		Crops (T 3.9), Trees (T 3.11), (Semi-)natural vegetation (T 3.13)	Crops, Trees, (Semi-)natural vegetation (All T 3.15)	Crops, Trees, (Semi-)natural vegetation
O_3 concentration at the top of the canopy (ppb)	Measured or scaledto canopy height from measurements	√	√	√
Temperature (°C)	Measured	√	√	
Vapour pressure deficit (humidity parameter, kPa)	Calculated from measured relative humidity, temperature and atmospheric pressure	√	√	
Light (PPFD, µmol m^{-2} s^{-1})	Measured or estimated from time and geographical position	√	√	√ (astronomic daytime can also be used).
Soil water potential (kPa) or plant available water (%)	Measured or calculated using models (e.g., within DO_3SE) from rainfall and soil characteristics	√	**	

* Additional (non-hourly) information required for POD_YSPEC and POD_YIAM include biogeographical region, land cover, average canopy height and average leaf dimension and for POD_YSPEC also detailed info on plant phenology.
** Some chemical transport models (e.g. EMEP) used for application in integrated assessment modelling (IAM) use a simplified metric for soil water (e.g. soil moisture index; SBD-B, Simpson et al., 2012).

3.3.3 POD_YSPEC, POD_YIAM and AOT40-based critical levels forvegetation

Table 3.6 lists for which effects O_3 critical levels are currently available for different types of vegetation from different biogeographic regions of Europe; currently, no critical levels are available for alpine regions. The final column of the table indicates the sections with further details, the table of the relevant flux-model parameterisation and the figure that contains the response function from which the critical level was derived.

Table 3.6: List of effects for which O_3 critical levels are available for vegetation.

Species or vegetation type	Effect parameter	Biogeographical region*	Ozone metric	Section	Flux model parameters, critical levels (Table - T), response functions (Figure - F)
Species-specific critical levels, using $POD_Y SPEC$ (mmol m^{-2} PLA)					
Crops					
Wheat	Grain yield, 1000-grain weight, protein yield	A, B, C, M (S, P)**	POD_6SPEC	3.3.5.2	T 3.9-10, F 3.10
Potato	Tuber yield	A, B, C (M, S, P)	POD_6SPEC	3.3.5.2	T 3.9-10, F 3.11
Tomato	Fruit yield, fruit quality	M (A, B, C, S, P)	POD_6SPEC	3.3.5.2	T 3.9-10, F 3.11
Forest trees					
Beech/birch	Total biomass	B, C (A, S, P)	POD_1SPEC	3.3.5.3	T 3.11-12, F 3.12
Norway spruce	Total biomass	B, C (A, S, P)	POD_1SPEC	3.3.5.3	T 3.11-12, F 3.12
Deciduous oak species	Root biomass, total biomass	M	POD_1SPEC	3.3.5.3	T 3.11-12, F 3.12
Evergreen tree species	Above-ground biomass	M	POD_1SPEC	3.3.5.3	T 3.11-12, F 3.12
(Semi-)natural vegetation					
Temperate perennial grasslands (O_3-sensitive species)	Above-ground biomass, total biomass, flower number	A, B, C (S, P)	POD_1SPEC	3.3.5.4	T 3.13-14, F 3.13
Mediterranean annual pasture (O_3-sensitive species)	Above-ground biomass, flower/seed biomass	M	POD_1SPEC	3.3.5.4	T 3.13-14, F 3.14
Vegetation-type critical levels, using $POD_Y IAM$ (mmol m^{-2} PLA)					
Crops	Grain yield	A, B, C, M (S, P)**	POD_3IAM	3.3.6.2	T 3.15-16, F 3.15
Forest trees					
Broadleaf deciduous	Total biomass	B, C (A, S, P)	POD_1IAM	3.3.6.2	T 3.15-16, F 3.15
		M	POD_1IAM	3.3.6.2	T 3.15-16, F 3.15
(Semi-)natural vegetation					
Temperate perennial grasslands	Flower number	A, B, C (S, P)	POD_1IAM	3.3.6.2	T 3.15-16, F 3.15

Species or vegetation type	Effect parameter	Biogeographical region*	Ozone metric	Section	Flux model parameters, critical levels (Table - T), response functions (Figure - F)
Mediterranean annual pasture	Seed/flower biomass	M	POD_1IAM	3.3.6.2	T 3.15-16, F 3.15
Concentration-based critical levels, using AOT40 (ppm h)					
Agricultural crops	Yield	All	AOT40	3.3.7.3	T 3.17
Horticultural crops	Yield	All	AOT40	3.3.7.3	T 3.17
Forest trees	Total biomass	All	AOT40	3.3.7.3	T 3.17
(Semi-)natural vegetation dominated by annuals	Above-ground biomass	All	AOT40	3.3.7.3	T 3.17
(Semi-)natural vegetation dominated by perennials	Above-ground biomass	All	AOT40	3.3.7.3	T 3.17

* A= Atlantic, B = Boreal, C = Continental, M = Mediterranean, P = Pannonian, S = Steppic; critical levels are alsoconsidered applicable to regions shown in brackets, based on expert judgement.

** Different parameterisations for Mediterranean and non-Mediterranean species or varieties.

3.3.4 Method for modelling stomatal O_3 flux andcalculating critical level exceedance

O_3 stomatal flux is calculated at the leaf level at the top of the canopy using the DO3SE (Deposition of O_3 for Stomatal Exchange) model (Büker et al., 2015; Emberson et al., 2000a, b, 2001, 2007). The DO3SE model is available in downloadable form at .

Several steps (1-6) are required to model the stomatal flux of O_3 at leaf level at the top of the canopy and calculate critical level exceedance, and to calculate the percentage of effect (step 7) based on the slope of the flux-effect relationships, as listed in Box 4 and described in detail in Sections 3.3.4.1 to 3.3.4.7.

Box 4: Steps to be taken to calculate exceedance of flux-based (POD_YSPEC or POD_YIAM) critical levels and quantification of the risk of effect

- Decide on the species and biogeographical region(s) to be included
- Obtain the O_3 concentrations at the top of the canopy for the species or vegetation-specific accumulation period
- Calculate the hourly stomatal conductance of O_3 (g_{sto})
- Model the hourly stomatal flux of O_3 (F_{st})
- Calculation of POD_Y (POD_YSPEC or POD_YIAM) from F_{st}
- Calculation of exceedance of flux-based critical levels
- Quantification the extent of risk and calculating percentage effect due to O_3

3.3.4.1 Step 1: decide on the species and biogeographicalregion(s) to be included

Plant stomatal functioning varies per plant species and can vary by biogeographical region, reflecting different adaptations of plants to climate and soil water in these regions. To accommodate these differences, separate parameterisations and accumulation periods have been developed for stomatal O_3 flux models for different species and biogeographical regions. The EEA (2016) classification of biogeographical zones is recommended for application to risk assessments for Europe (Figure 3.3); similar classifications should be applied outside of this region. For derivation of the critical levels, no data were available from Steppic and Pannonian regions, hence the applicability of critical levels for these regions is less certain. Currently, no critical levels are available for Alpine regions.

Note: In earlier versions of this Chapter, countries were assigned to a climate zone (Northern Europe, Atlantic Central Europe, Continental Central Europe, Eastern and Western Mediterranean). This classification has now been replaced by the use of biogeographical zones.

Figure 3.3: Biographic regions in Europe

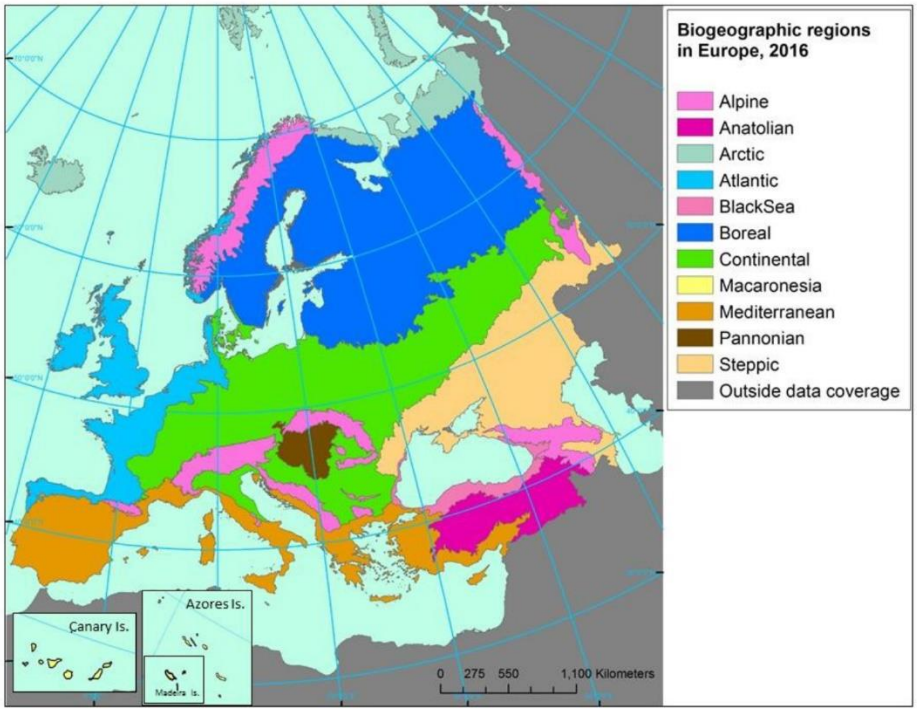

Source: This figure is adopted from a previous version of Chapter 3 of the Mapping Manual

3.3.4.2 Step 2. Obtain the O_3 concentration at the top of the canopy for the species or vegetation-specific accumulationperiod

Calculation of stomatal flux (or AOT40, see Section 3.3.7.2) is based on hourly mean O_3 concentrations in units of parts per billion (ppb volume/volume). Where O_3 concentrations require conversion from µg m^{-3} to ppb, a conversion factor appropriate for standard temperature and pressure conditions (293.15 K, 101325 Pa) of 2 µg m^{-3} per ppb can be applied. Alternatively, the equations described in detail in Gerosa et al. (2012) could be used if temperature and atmospheric pressure are available.

In this step, the O_3 concentration at the top of the leaf canopy of the vegetation of interest is determined. This is needed because surface O_3 concentrations generally increase with increasing

height above-ground. Thus, O_3 data from monitoring stations where the inlet is placed at heights of, for example, 2 – 5 m above the ground will overestimate the O_3 concentration at the canopy height of crops or low (semi-)natural vegetation such as grasslands and will underestimate the O_3 concentration at the top of the canopy of forests.

Conversion of O_3 concentrations at measurement height to canopy height can be best achieved with an appropriate deposition model (see SBD-A). However, if suitable meteorological data are unavailable, a simple tabulation of O_3 gradients can be used (Table 3.7). This table provides the average relationship between O_3 concentrations at selected heights, derived from runs of the EMEP model over May-July, selecting noon as the representative of daytime (Simpson et al., 2012). O_3 concentrations are normalised by setting the 20 m value to 1.0. For example, with 30 ppb measured at 3 m height (above ground level) in a crop field, the concentration at 1 m would be 30.0 * (0.88/0.95) = 27.8 ppb. If measured in short grasslands at 3 m height, one would obtain 30.0 * (0.74/0.96) = 23.1 ppb at a canopy height of 0.1 m and for forests one would obtain 30.0 * (1/0.96) = 31.3 ppb at a canopy height of 20 m.

Table 3.7: Representative O_3 gradients above artificial (1 m) crop, and short grasslands (0.1 m). O_3 concentrations are normalised by setting the 20 m value to 1.0. These gradients are derived from noontime factors and are intended for daytime use only.

Measurement height above theground [m]	O_3 concentration gradient	
	Crops (where z_1=1m, g_{max} = 450 mmol O_3 m^{-2} PLA s^{-1})	**Short Grasslands and Forest Trees** (where z_1=0.1m, g_{max} =270 mmol O_3 m^{-2} PLA s^{-1})
20	1.0	1.0
10	0.99	0.99
5	0.97	0.97
4	0.96	0.97
3	0.95	0.96
2	0.93	0.95
1	0.88	0.92
0.5	0.81*	0.89
0.2	-	0.83
0.1	-	0.74

* 0.5m is below the displacement height of crops, but may be used for taller grasslands, see text.

3.3.4.3 Step 3. Calculate the hourly stomatal conductance of O_3 (g_{sto})

The core of the leaf O_3 flux model is the stomatal conductance (g_{sto}) multiplicative algorithm included in the DO_3SE model and incorporated within the EMEP O_3 deposition module (Simpson et al., 2012), proposed by Jarvis (2016) and modified by Emberson et al. (2000a, b). The multiplicative algorithm has the following formulation:

(III.1)

$$g_{sto} = g_{max} * [\min(f_{phen}, f_{O3})] * f_{light} * \max\{f_{min}, (f_{temp} * f_{VPD} * f_{SW})\}$$

Where g_{sto} is the actual stomatal conductance (mmol O_3 m^{-2} PLA s^{-1}) and g_{max} is the species-specific maximum stomatal conductance (mmol O_3 m^{-2} PLA s^{-1}).

The parameters f_{phen}, f_{O3}, f_{light}, f_{temp}, f_{VPD}, f_{SW} and f_{min} are all expressed in relative terms (i.e., they take values between 0 and 1 as a proportion of g_{max}). These parameters allow for the modifying influence on stomatal conductance to be estimated for growth stage such as flowering or release of dormancy, or phenology (f_{phen}), O_3 concentration (f_{O3}, only used for crops), and four environmental variables: light (irradiance, f_{light}), temperature (f_{temp}), atmospheric water vapour pressure deficit (VPD, a measure of air humidity, f_{VPD}) and soil water (SW; soil water potential, f_{SW}, measure of soil moisture, replaced by f_{PAW} for crops where PAW is the plant available water content); f_{min} is the relative minimum stomatal conductance that occurs during daylight hours.

Each parameter modifies the maximum stomatal conductance in different ways. For example, stomatal conductance gradually increases as temperature increases reaching an optimum and then gradually declines as temperature increases beyond the optimum, whilst stomatal conductance increases rapidly as light levels increase, reaching a maximum at relatively low light levels and is maintained at that maximum as light levels increase further. Illustrations of the modifying effect of each factor on stomatal conductance are provided (Figures 3.4-9). Hourly values of all driving variables are required to calculate gsto using Equation III.1, and in step 4 (see Box 4), the stomatal O_3 flux (Fst), with hourly time resolution. In step 5, the hourly values of F_{st} are summed to obtain the total Phytotoxic O_3 Dose above a flux-threshold Y (POD_Y). Table 3.8 lists all the input variables and parameters required to calculate POD_YSPEC and POD_YIAM and the sources of this information.

Table 3.8: Parameters included in the DO_3SE model for calculating POD_YSPEC and POD_YIAM; f_{phen} and f_{SW} are not included in POD_YIAM.

Parameter	Source	POD_YSPEC	POD_YIAM
g_{max}	Parameterisation table	√	√
f_{min}	Parameterisation table	√	√
f_{phen}	Calculated using formulae and fixedparameters in table	√	
f_{light}	Calculated using formulae and fixedparameters in table	√	√
f_{temp}	Calculated using formulae and fixedparameters in table	√	√
f_{VPD}	Calculated using formulae and fixedparameters in table	√	√
f_{SW} (or f_{PAW})	Calculated using formulae and fixedparameters in table	√ f_{PAW} can be used for crops as an alternative	*

* Included in the EMEP Model as soil moisture index (Simpson et al., 2012).

3.3.4.3.1 G_{MAX} and F_{MIN}

Species- or vegetation type-specific values are provided in the relevant parameterisation tables for g_{max} and f_{min} based on analysis of published data (see SBD-A for further details); g_{max} values provided here are in mmol O_3 m^{-2} PLA s^{-1}. These have been converted from g_{max} (water vapour) using a conversion factor of 0.663 to account for the difference in the molecular diffusivity of water vapour in relation to that of O_3 (Massman,1998; Grünhage et al., 2012); f_{min} is the minimum daylight stomatal conductance expressed as a fraction of g_{max}.

3.3.4.3.2 F_{PHEN}

The phenology function is based on two approaches depending on vegetation type:

a) For forest trees and (semi-)natural vegetation, f_{phen} is calculated according to Equations III.2a, b, c when using parameterisations based on a fixed number of days (FD; Figure 3.4a).

b) For crops, f_{phen} is calculated according to Equations III.3a, b, c, using parameterisations based on effective temperature sum accumulation (ETS).

Each pair of equations gives f_{phen} in relation to the yearly accumulation period for POD_YSPEC where A_{start} and A_{end} are the start and end of the accumulation period, respectively. The subscripts FD (e.g., A_{start_FD}) and ETS (e.g., A_{start_ETS}) refer to the fixed day and effective temperature sum method, respectively.

Figure 3.4: An illustration of the formulation of f_{phen} using a) a fixed number of days, as used for forest trees and (semi-)natural vegetation (example shown here for Mediterranean trees with summer dip in f_{phen} to simulate the effect of mid-season water photo-oxidative stress on stomatal conductance, see Equation III.23), and b) effective temperature sum accumulation, as used for crops. Note: example shown here is for wheat, with effective temperature sum accumulated from day of mid-anthesis in three steps ($f_{phen\_3\_ETS}$, $f_{phen\_4\_ETS}$ and $f_{phen\_5\_ETS}$); $f_{phen\_2\_ETS}$ can replace these three steps and is usually not used for wheat, but is used for potato and tomato (hence shown in grey colour here). For potato and tomato the effective temperature sum is accumulated from day of tuber initiation and from the day of planting at the 4th true leaf stage, respectively.

a)

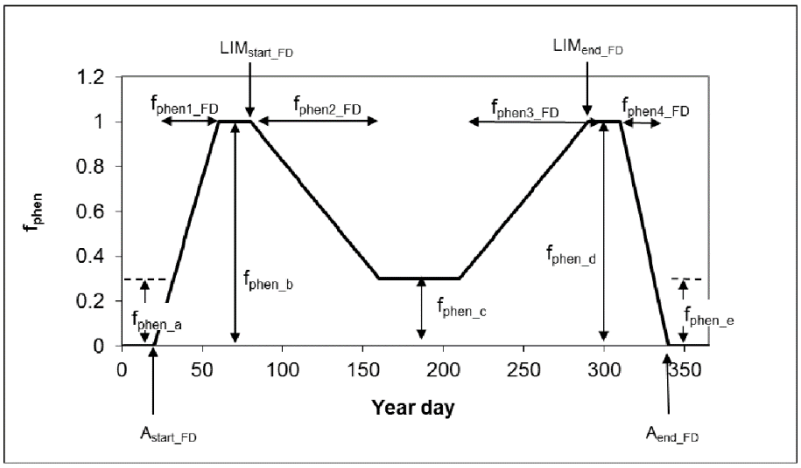

b)

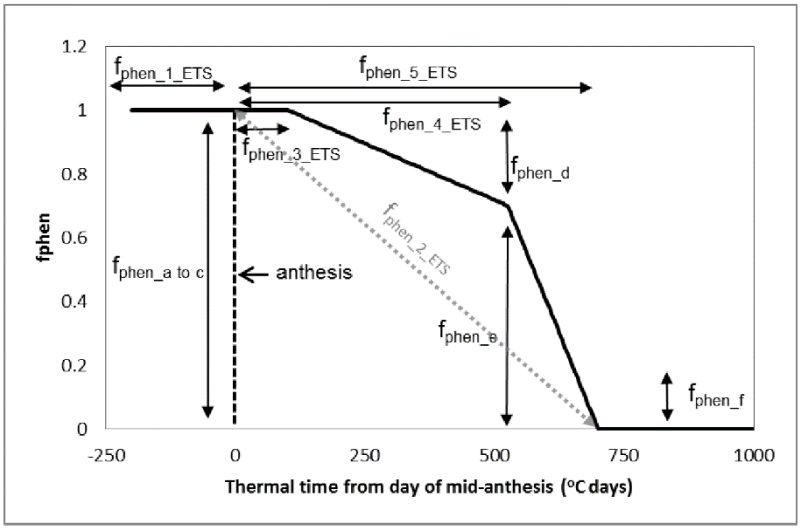

Source: This figure is adopted from a previous version of Chapter 3 of the Mapping Manual

The phenology function consists of terms describing rate changes of g_{max} ($f_{phen\_a\text{-}e}$; expressed as fractions) and time periods describing the duration from one phenology stage to another ($f_{phen\_1\text{-}5}$; expressed as days (method (a)) or growing degrees days (method (b)).

The parameters f_{phen_a} and f_{phen_e} denote the maximum fraction of g_{max} at A_{start} and A_{end}. $f_{phen\_b\text{-}d}$ and $f_{phen\_1\text{-}5}$ are species- or vegetation type-specific parameters describing the shape of the function within the accumulation period.

Method (a): based on a fixed time interval

when $A_{start\_FD} \leq yd < (A_{start\_FD} + f_{phen\_1\_FD})$

(III.2a)

$f_{phen} = (1 - f_{phen\_a}) * ((yd - A_{start\_FD})/f_{phen\_1\_FD}) + f_{phen\_a}$

when $(A_{start} + f_{phen\_1\_FD}) \leq yd \leq (A_{end} - f_{phen\_4\_FD})$

(III.2b)

$f_{phen} = 1$

when $(A_{end} - f_{phen\_4\_FD}) < yd \leq A_{end}$

(III.2c)

$f_{phen} = (1 - f_{phen\_e}) * ((A_{end} - yd)/f_{phen\_4\_FD}) + f_{phen\_e}$

where yd is the year day; A_{start} and A_{end} are the year days for the start and end of the O_3 accumulation period, respectively.

Method (b): based on temperature sum accumulation

when $A_{start\_ETS} \leq ETS < (A_{start\_ETS} + f_{phen\_1\_ETS})$

(III.3a)

$$f_{phen} = 1 - \left(\frac{1 - f_{phen\_a}}{f_{phen\_1\_ETS}}\right)\left(\left(A_{start\_ETS} + f_{phen\_1\_ETS}\right) - ETS\right)$$

when $(A_{start\_ETS} + f_{phen\_1\_ETS}) \leq ETS \leq (A_{end\_ETS} - f_{phen\_2\_ETS})$

(III.3b)

$f_{phen} = 1$

when $(A_{end\_ETS} - f_{phen\_2\_ETS}) < ETS \leq A_{end\_ETS}$

(III.3c)

$$f_{phen} = 1 - \left(\frac{1 - f_{phen\_e}}{f_{phen\_2\_ETS}}\right)\left(ETS - \left(A_{end\_ETS} - f_{phen\_2\_ETS}\right)\right)$$

where ETS is the effective temperature sum in ˚C days using a base temperature of 0 ˚C and A_{start_ETS} and A_{end_ETS} are the effective temperature sums (above a base temperature of 0 ˚C) at the start and end of the O_3 accumulation period, respectively. As such, A_{start_ETS} will be equal to 0 ˚C days. Note: A base temperature of 0 °C is currently recommended for wheat and potato.

3.3.4.3.3 F_{LIGHT}

Leaf stomata respond to light as indicated in Figure 3.5. This stomatal response is used to define f_{light} (Equation III.4). Species (for POD_YSPEC) or vegetation type specific (for POD_YIAM) values for $light_a$ are provided in the parameterisation tables.

(III.4)

$f_{light} = 1 - EXP((-light_a)*PPFD)$

where PPFD represents the photosynthetic photon flux density in units of μmol m^{-2} s^{-1}.

Figure 3.5: Illustration of the f_{light} function, using wheat as an example (Pleijel et al., 2007).

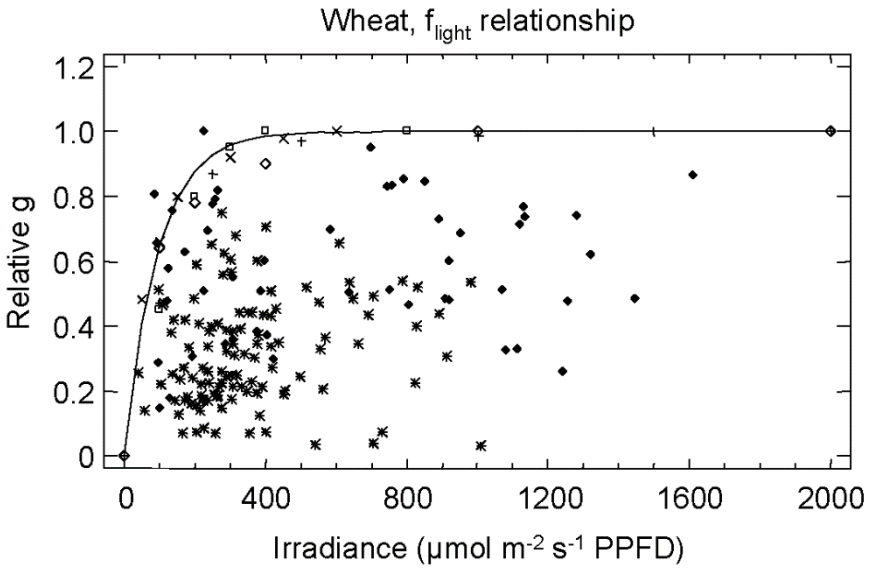

Source: This figure is adopted from a previous version of Chapter 3 of the Mapping Manual

3.3.4.3.4 F_{TEMP}

Leaf stomata respond to temperature (T, air temperature in ˚C) as indicated in Figure 3.6. This stomatal response is used to define f_{temp} (Equations III.5a,b). Species (for POD_YSPEC) or vegetation type specific (for POD_YIAM) values for T_{min} and T_{max} (the minimum and maximum temperatures at which stomatal closure occurs, respectively) and the optimum temperature (T_{opt}) are provided in the parameterisation tables.

Figure 3.6: Illustration of the f_{temp} function, using wheat as an example (Pleijel et al., 2007).

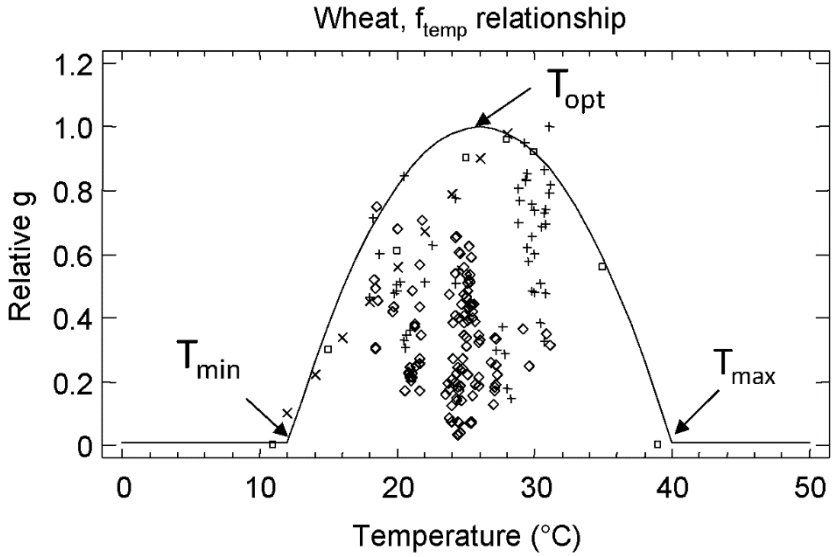

Source: This figure is adopted from a previous version of Chapter 3 of the Mapping Manual

The function used to describe f_{temp} is given in Equations III.5a,b:

when $T_{min} < T < T_{max}$

(III.5a)

$f_{temp} = \max \{f_{min}, [(T - T_{min}) / (T_{opt} - T_{min})] * [(T_{max} - T) / (T_{max} - T_{opt})]^{bt}\}$

when $T_{min} > T > T_{max}$

(III.5b)

$f_{temp} = f_{min}$

and bt is calculated as:

(III.6)

$bt = (T_{max} - T_{opt}) / (T_{opt} - T_{min})$

3.3.4.3.5 F_{VPD} and ΣVPD routine

The leaf stomatal response to air humidity is defined using vapour pressure deficit (VPD in kPa), which is the drying power of the air. VPD can be calculated from air temperature and air relative humidity. VPD (Equation III.7) is defined as the difference between the potential water vapour pressure, $e_s(T_a)$, at the prevailing air temperature T_a, and the actual water vapour pressure of the air e_a:

(III.7)

$$VPD = e_s(T_a) - e_a = e_s(T_a)(1 - h_r)$$

and can be calculated from T_a (given in °C) and relative humidity (h_r, the most often reported variable describing air humidity; Equations III8a,b)

(III.8a)

$$h_r = \frac{e_a}{e_s(T_a)}$$

once $e_s(T_a)$ has been obtained from the formula

(III.8b)

$$h_r = a\ exp\left(\frac{bT_a}{T_a + c}\right)$$

where a, b and c are empirical constants (a = 0.611 kPa, b = 17.502, c = 240.97°C). Further details can be obtained from Campbell & Norman (2000).

The response of leaf stomata to the VPD of the air surrounding the leaves is included in two ways:

c) f_{VPD}

Figure 3.7: Illustration of the f_{VPD} function, using wheat in non-Mediterranean areas as an example (Pleijel et al., 2007).

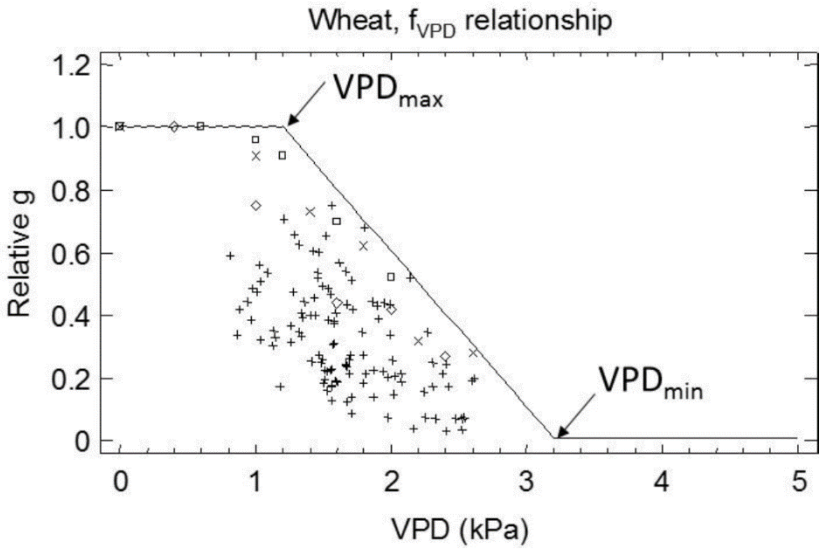

Source: This figure is adopted from a previous version of Chapter 3 of the Mapping Manual

Applicable to all species and vegetation types, this function describes the response shown in Figure 3.7. As VPD increases (i.e., the air becomes drier) above a threshold value of VPD (VPD_{max}; VPD where g_{sto} is at maximum), the stomatal pores begin to close until a maximum VPD value is reached at which the stomatal pores are fully closed (VPD_{min}) and conductance (g_{sto}) is at a minimum value. This response of the stomata to VPD is described by the f_{VPD} function (Equation III.9):

(III.9)

$$f_{VPD} = \min\{1,\max\{f_{min}, ((1-f_{min})*(VPD_{min} - VPD) / (VPD_{min} - VPD_{max})) + f_{min}\}\}$$

d) ΣVPD

For POD_YSPEC for crops, an additional effect of VPD is included. During the afternoon the temperature typically decreases, which is normally followed by a decline in VPD. The f_{VPD} function would then suggest stomatal re-opening, but this does not usually happen in crops. During the day plants lose water through transpiration faster than water is replaced by root uptake, resulting in a reduction of the plant water potential, preventing stomatal re-opening. The plant water potential recovers during the night when transpiration is low. To model this effect, the hourly VPD values during the daylight hours (when global radiation is more than 50 W m^{-2}) are summed as ΣVPD (Uddling et al., 2004). A large ΣVPD is related to large transpiration. If the ΣVPD exceeds a certain value, stomatal re-opening in the afternoon is prevented in the model:

If $\Sigma VPD \geq \Sigma VPD\_crit$, then:

$$g_{sto\_hour\_n+1} \leq g_{sto\_hour\_n}$$

where $g_{sto\_hour\_n}$ and $g_{sto\_hour\_n+1}$ are the g_{sto} values for hour n and hour n+1 respectively calculated according to Equation III.1.

ΣVPD (kPa) should be calculated for daylight hours until dawn of the next day. If ΣVPD ≥

ΣVPD_{crit} , g_{sto} calculated using Equation III.1 is valid if smaller or equal to g_{sto} of the preceding hour. If g_{sto} is larger than g_{sto} of the preceding hour, given that ΣVPD is larger than or equal to ΣVPD_{crit}, it is replaced by the g_{sto} of the preceding hour.

3.3.4.3.6 F_{SW}

For POD$_Y$IAM, f_{SW} is set to have no effect within the calculation of g_{sto}. However, the effect of soil moisture is important, and in large-scale applications surrogate indices are usually applied, such as the Soil Moisture Index in the EMEP model (Simpson et al., 2012).

For POD$_Y$SPEC, f_{SW} uses soil water potential (SWP) to determine the leaf stomatal response to soil drying. The function takes the shape indicated in Figure 3.8 and is given in Equation III.10):

(III.10)

$f_{SW} = \min\{1, \{f_{min}, ((1–f_{min})*(SWP_{min}–SWP) / (SWP_{min} – SWP_{max})) + f_{min}\}\}$

where SWP_{min} is the minimum SWP for stomatal conductance and SWP_{max} is the SWP above which conductance is maximum.

Figure 3.8: Illustration of the f_{SW} function, using soil water potential (SWP) for potato as an example.

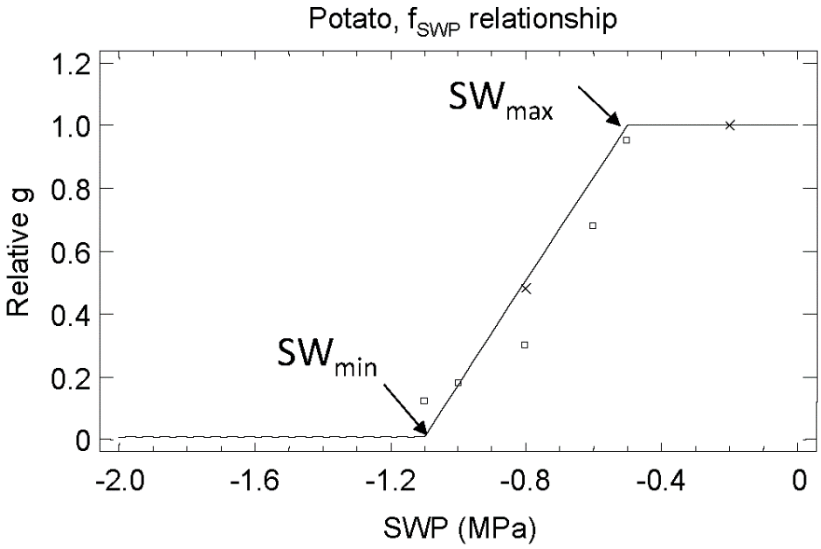

Source: This figure is adopted from a previous version of Chapter 3 of the Mapping Manual

Note: For crop species such as wheat, root zone Plant Available Water (PAW) can be used instead of SWP in f_{SW}. PAW is the amount of water in the soil (%) which is available to the plants. At PAW = 100% the soil is at field capacity, at PAW = 0% the soil is at wilting point. PAW_t is the threshold PAW, above which stomatal conductance is at a maximum, i.e., the function used to describe f_{PAW} is given in Equation III.11 and the shape of the response is indicated in Figure 3.9:

When $PAW_t \leq PAW \leq 100$ %,

$f_{PAW} = 1$

whilst, when $PAW < PAW_t$

(III.11)

$$f_{PAW} = 1 + \frac{PAW - PAW_t}{PAW_t}$$

Figure 3.9: Illustration of the f_{PAW}, using wheat as an example f_{PAW} for wheat (Grünhage et al., 2012).

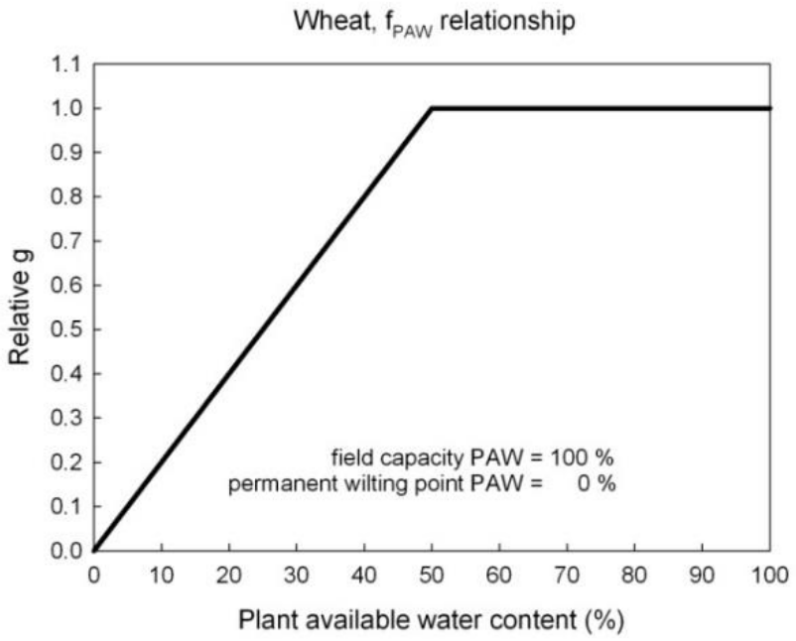

Source: This figure is adopted from a previous version of Chapter 3 of the Mapping Manual

3.3.4.3.7 F_{O3}

For wheat and potato in POD_6SPEC only, a function is included to allow for the influence of O_3 on stomatal flux by promoting premature senescence, as described for wheat by Danielsson et al. (2003) and for potato by Pleijel et al. (2002). As such, this function is used in association with the f_{phen} function to estimate g_{sto}. The f_{O3} function typically operates over a one-month period and only comes into operation if it has a stronger senescence-promoting effect in reducing stomatal conductance than normal senescence. Equations are provided for wheat and potato in Section 3.3.5.2.1.

3.3.4.4 Step 4. Modelling hourly stomatal flux of O_3 (F_{ST})

The stomatal flux of O_3 (F_{st}) is calculated based on the assumption that the concentration of O_3 at the top of the canopy represents a reasonable estimate of the concentration at the upper surface of the laminar layer for a sunlit upper canopy leaf (e.g., flag leaf for wheat). If $c(z_1)$ is the concentration of O_3 at canopy top (height z_1, unit: m), in nmol m^{-3}, then F_{st} (nmol m^{-2} PLA s^{-1}), is given by Equation 12a. Equation 15 shows how to convert the O_3 concentration from ppb to nmol m^{-3}. In order to be used correctly in Equations III.12a and III.12b, g_{sto} from equation III.1 has to be converted from units mmol m^{-2} s^{-1} to units m s^{-1}. At standard temperature (20 °C) and air pressure (1.013×10^5 Pa), the conversion is made by dividing the conductance value expressed in mmol m^{-2} s^{-1} by 41000 to give conductance in m s^{-1}.

(III.12a)

$$F_{st} = c(z_1) * \frac{1}{r_b + r_c} * \frac{g_{sto}}{g_{sto} - g_{ext}}$$

The $1/(r_b+r_c)$ term represents the deposition rate to the leaf through resistances r_b (quasi-laminar resistance) and r_c (leaf surface resistance). The fraction of this O_3 taken up by the

stomata is given by $g_{sto}/(g_{sto}+g_{ext})$, where g_{sto} is the stomatal conductance, and g_{ext} is the external leaf, or cuticular, resistance. As the leaf surface resistance, r_c, is given by $r_c = 1/(g_{sto} + g_{ext})$, we can also write Equation III.12a as:

(III.12b)

$$F_{st} = c(z_1) * g_{sto} * \frac{r_b}{r_b + r_c}$$

A value for g_{ext} has been chosen to keep consistency with the EMEP deposition modules "big-leaf" external resistance, $R_{ext} = 2500/SAI$, where SAI is the surface area index (green + senescent LAI). Assuming that SAI can be simply scaled:

(III.13)

$g_{ext} = 1/2500$ [m s^{-1}]

Consistency of the quasi-laminar boundary layer is harder to achieve, so the use of a leaf-level r_b term (McNaughton & van den Hurk, 1995) is suggested, making use of the cross-wind leaf dimension L (i.e. leaf width; unit: m) and the wind speed at height z_1, $u(z_1)$:

(III.14)

$$r_b = 1.3 * 150 * \sqrt{\frac{L}{U(Z_1)}} \; [m\, s^{-1}]$$

where the factor 1.3 accounts for the differences in diffusivity between heat and O_3.

To convert the O_3 concentration (C) at canopy height from ppb to nmol m^{-3}, the following equation should be used:

(III.15)

C [nmol m^{-3}] = C [ppb] * P/(RT)

where P is the atmospheric pressure in Pa, R is the universal gas constant of 8.31447 J mol^{-1} K^{-1} and T is the air temperature in degrees Kelvin. At standard temperature (20 °C) and air pressure (1.013×10^5 Pa), the concentration in ppb should be multiplied by 41.56 to calculate the concentration in nmol m^{-3}.

3.3.4.5 Step 5. Calculation of POD_Y (POD_YSPEC or POD_YIAM)

Hourly averaged stomatal O_3 fluxes (F_{st}) in excess of a Y threshold are accumulated over a species or vegetation-specific accumulation period using the following equation:

(III.16)

$POD_Y = \sum[(F_{st}-Y)\cdot(3600/10^6)]$ (mmol m^{-2} PLA)

The value Y (nmol m^{-2} PLA s^{-1}) is subtracted from each hourly averaged F_{st} (nmol m^{-2} PLA s^{-1}) value only when $F_{st}>Y$, during daylight hours (when global radiation is more than 50 W m^{-2}). The value is then converted to hourly fluxes by multiplying by 3600 and to mmol by dividing by 10^6 to get the stomatal O_3 flux in mmol m^{-2} PLA.

Species- or vegetation-specific flux threshold values of Y and accumulation periods are provided in the relevant sections.

3.3.4.6 Step 6. Calculation of exceedance of flux-based critical levels

If the calculated POD_Y value is larger than the flux-based critical level for O_3, then there is exceedance of the critical level ($CL_{exceedance}$). Exceedance of the critical level is calculated as follows:

(III.17)

$CL_{exceedance}$ = POD_Y – critical level

3.3.4.7 Step 7. Quantification of extent of risk and calculating percentage effect due to O_3

Quantification of the level of risk is based on the slope of flux-effect relationships, without taking the intercept of the response function into account.

For each POD_YSPEC critical level, the percentage effect is provided per mmol m^{-2} PLA, for quantifying the potential maximum magnitude of effect. Hence, the percentage effect due to O_3 impact should be calculated as follows:

(III.18a)

(POD_YSPEC – Ref10 POD_YSPEC) * % reduction per mmol m^{-2} POD_YSPEC

For POD_YIAM, the above approach can only be applied for crops, not for forest trees or (semi-) natural vegetation. Hence, the percentage effect due to O_3 impact on crop yield estimated in large-scale modelling should be calculated as follows:

(III.18b)

(POD_YIAM – Ref10 POD_YIAM) * % reduction per mmol m^{-2} POD_YIAM.

3.3.5 Species-specific flux effect relationships and critical levels for detailed assessments of risk (using POD_YSPEC)

3.3.5.1 Application

POD_YSPEC O_3 flux models have been derived for a number of crop, forest trees and (semi-) natural vegetation species using the modelling approach described in Section 3.3.4. These species-specific flux models have been used to derive flux-effect relationships and critical levels based on POD_YSPEC. Their application is described in Box 5. Additional flux models are included in SBD-A for receptors for which a robust flux model is available but a flux-effect relationship is not currently available, and are suitable for mapping risk of effects without quantification of the extent of damage.

Box 5: Applications for species-specific flux-effectrelationships and critical levels

The species-specific flux models and associated response functions and critical levels are the most biologically relevant. They can be used at any geographical scale and are particularly useful for application at the local scale to quantify the degree of risk to a specific species or a group of plant species. For several species, biogeographical region-specific flux parameterisations are included.

3.3.5.2 Crops

3.3.5.2.1 Parameterisation of the O_3 stomatal flux modelfor crops

The parameterisations recommended for use in calculating POD_6SPEC for wheat (bread wheat - *Triticum aestivum* and durum wheat - *Triticum durum;* Grünhage et al., 2012; González-Fernández et al., 2013), potato (*Solanum tuberosum*; Pleijel et al., 2007), and tomato (*Solanum*

lycopersicum; González-Fernández et al., 2014) are shown in Table 3.9. Species-specific notes to aid calculation of stomatal O_3 fluxes are found below the table.

For crops, the following additional information is required for calculating stomatal flux using the method provided in Section 3.3.4.3 and the parameterisation provided in Table 3.9:

Wheat

Timing of accumulation period

The accumulation period for wheat is 200 °C days before mid-anthesis (mid-point in flowering) to 700 °C days after mid-anthesis. The timing of mid-anthesis can be estimated using several methods, depending on application and availability of data, including:

- Observational data describing actual growth stages;
- Local agricultural statistics/information describing the timings of growth stages by region or country;
- Phenological growth models in conjunction with daily meteorological data;
- Fixed time periods (which may be moderated by climatic region or latitude) or growth stage intervals.

For European maps of risk, it is recommended that the timing of mid-anthesis is estimated by starting at the first date after the 1st of January when the temperature exceeds 0 °C, or the 1st of January if the temperature exceeds 0 °C on that date. The mean daily temperature should then be accumulated (temperature sum), and mid-anthesis is estimated to be a temperature sum of 1075 °C days, with local variation including 1256 °C days for bread wheat and 1192 °C days for durum wheat in Spain (González-Fernández et al., 2013) and 1089-1102 days for winter wheat cultivars in France (Grünhage et al., 2012). Where suitable temperature data is not available, the timing of mid-anthesis for both spring and winter wheat can be approximated as a function of latitude (degrees N) using Equation III.19:

(III.19)

Mid-anthesis = 2.57 * latitude + 40

Table 3.9: Parameterisation of the DO_3SE model for POD_6SPEC for wheat flag leaves and the upper-canopy sunlit leaves of potato and tomato.

Parameter	Units	Crop species parameterisation – POD_6SPEC				
Region (*may also be applicable in these regions*)		Atlantic, Boreal, Continental (*Pannonian, Steppic*)	Mediterranean	Mediterranean	Atlantic, Boreal, Continental (*Mediterranean, Pannonian, Steppic*)	Mediterranean
Species	Common name	**(Bread) Wheat**	**(Bread) Wheat**	**(Durum) Wheat**	**Potato**	**Tomato**
	Latin name	*Triticum aestivum*	*Triticum aestivum*	*Triticum durum*	*Solanum tuberosum*	*Solanum lycopersicum*

Parameter	Units	Crop species parameterisation – POD_6SPEC				
g_{max}	mmol O_3 m^{-2} PLA s^{-1}	500	430	410	750	330
f_{min}	fraction	0.01	0.01	0.01	0.01	0.06
light_a	-	0.0105	0.0105	0.0105	0.005	0.0125
T_{min}	°C	12	12	11	13	18
T_{opt}	°C	26	28	28	28	28
T_{max}	°C	40	39	45	39	37
VPD_{max}	kPa	1.2	3.2	3.1	2.1	1
VPD_{min}	kPa	3.2	4.6	4.9	3.5	4
ΣVPD_{crit}	kPa	8	16	16	10	-
PAW_t[i]	%	50	-	-	-	-
SWCmax[i]	% volume	-	18.6	18.0	-	-
SWCmin[i]	% volume	-	4.7	4.1	-	-
SWPmax	MPa	-	-	-	-0.5	-
SWPmin	MPa	-	-	-	-1.1	-
f_{O3}	POD_0 mmol O_3 m^{-2} PLA s^{-1} (wheat)	14	-	-	-	-
f_{O3}	AOT0, ppmh (potato)	-	-	-	40	-
f_{O3}	exponent	8	-	-	5	-
A_{start}_ETS	°C day	-	-	-	-	250[ii]
A_{end}_ETS	°C day	-	-	-	-	1500[ii]
Leaf dimension	cm	2	2	2	4	3 (leaflet width)
Canopy height	m	1	0.75	0.75	1	2
f_{phen_a}	fraction	0.3	0.0	0.0	0.4	1.0
f_{phen_b}	fraction	-	-	-	-	-
f_{phen_c}	fraction	-	-	-	-	-
f_{phen_d}	fraction	-	-	-	-	-

Parameter	Units	Crop species parameterisation – POD_6SPEC				
f_{phen_e}	fraction	0.7	0.99	0.99	0.2	0.0
$f_{phen\_1\_ETS}$	°C day	-200	-300	-300	-330	0
$f_{phen\_2\_ETS}$	°C day	0	0	0	800	2770[ii]
$f_{phen\_3\_ETS}$	°C day	100	70	100	-	-
$f_{phen\_4\_ETS}$	°C day	525	0	0	-	-
$f_{phen\_5\_ETS}$	°C day	700	550	675	-	-

The values in brackets represent "dummy" values required for DO_3SE modelling purposes. "-" = parameterisation not required for this species.

[i] Soil water content (SWC) is calculated as the soil water content available for transpiration, i.e., the actual SWC minus the SWC at the wilting point. PAWt is the threshold for plant available water (PAW), above which stomatal conductance is at a maximum.

[ii] Flux accumulation period in degree-days over a base temperature of 10 °C since the date of tomato planting in the field at the 4th true leaf stage, BBCH code of 14.

However, it should be recognised that this method is less preferable to the use of the effective temperature sum models described above since latitude is not directly related to temperature and this method will not distinguish between spring and winter wheat growth patterns.

Equation III.19 is based on data collected by the ICP Vegetation (Mills & Ball, 1998, Mills et al., 2007) from ten sites across Europe (ranging in latitude from Finland to Slovenia) describing the date of mid-anthesis of commercial winter wheat. Applying Equation III.19 across the European wheat growing region would give mid-anthesis dates ranging from the end of April to mid-August at latitudes of 35 to 65 °N, respectively. These anthesis dates fall approximately within recognised spring wheat growing seasons as described by Peterson (1965).

f_{phen}

The phenology function for wheat, based on accumulation of thermal time, should be modified as described in the equations below:

- when $(f_{phen\_2\_ETS} - f_{phen\_1\_ETS}) \leq \text{ETS} \leq (f_{phen\_2\_ETS} + f_{phen\_3\_ETS})$

  (III.20a)

  $f_{phen} = 1$

- when $(f_{phen\_2\_ETS} + f_{phen\_3\_ETS}) < \text{ETS} \leq (f_{phen\_2\_ETS} + f_{phen\_4\_ETS})$

  (III.20b)

  $$f_{phen} = 1 - \left(\frac{f_{phen\_a}}{f_{phen\_4\_ETS} - f_{phen\_3\_ETS}}\right)(ETS - f_{phen\_3\_ETS})$$

- when $(f_{phen\_2\_ETS} + f_{phen\_4\_ETS}) < \text{ETS} \leq f_{phen\_5\_ETS}$

  (III.20c)

  $$f_{phen} = f_{phen\_e} - (f_{phen\_e} / f_{phen\_5\_ETS} - f_{phen\_4\_ETS}) * (ETS - f_{phen\_4\_ETS})$$

where ETS is the effective temperature sum in ˚C days using a base temperature of 0 ˚C. As such, A_{start_ETS} (itself not defined for wheat) will be at 200 ˚C days before mid-anthesis (-200 ˚C days, as

defined by $f_{phen\_1\_ETS}$), mid-anthesis at 0 ˚C days and A_{end_ETS} (itself not defined for wheat) at 700 ˚C days after mid-anthesis (as defined by $f_{phen\_5\_ETS}$). The total temperature sum thus being 900 ˚C days.

f_{VPD}

Under Mediterranean conditions the stomata of wheat remain open under drier humidities (higher VPDs) than indicated with the parameterisations for f_{VPD} for non-Mediterannean climates (González-Fernández et al, 2013), and thus two climate region-specific f_{VPD} parameterisations are provided.

f_{PAW}

f_{PAW} is used instead of f_{SW} for wheat, see Equation III.11.

f_{O3}

The f_{O3} function typically operates over a one-month period and only comes into operation if it has a stronger senescence-promoting effect than normal senescence.

The O_3 function for spring wheat (based on Danielsson et al. (2003) but recalculated for projected leaf area - PLA) is:

(III.21)

$f_{O3} = ((1+(POD_0/14)^8)^{-1})$, where POD_0 is accumulated from A_{start}

Potato

f_{phen}

Use the thermal time equations (Equations III.3,a,b,c). Tuber initiation has the same phenology function as anthesis has for wheat (Equations III.20a,b,c). Note that A_{start_ETS} (itself not defined for potato) will be at 330 ˚C days before tuber initiation (-330 ˚C days, as defined by $f_{phen\_1\_ETS}$), tuber initiation at 0 ˚C days and A_{end_ETS} (itself not defined for potato) at 800 ˚C days after tuber initiation (as defined by $f_{phen\_2\_ETS}$). The total temperature sum thus being 1130 ˚C days.

f_{O3}

The O_3 function for potato (based on Pleijel et al., 2002) is:

(III.22)

$f_{O3} = ((1+(AOT0/40)^5)^{-1})$, where AOT0 is accumulated from A_{start}

Tomato

g_{max}

A mean value is provided in Table 3.9. Cultivar-specific values of g_{max} are provided in González-Fernández et al. (2014).

Timing of accumulation period

The accumulation period for tomato is 250 ˚C days to 1500 ˚C days after transplantation in the field over a base temperature of 10 ˚C (González-Fernández et al., 2014). The timing of transplantation into the field can vary widely depending on regions, years, cultivars and agronomic practices from March to July in the Northern Hemisphere (Battilani et al., 2012). The

tomato transplantation date can be estimated using several methods, depending on the availability of data, including:

- Observational data describing actual growth stages;
- Local agricultural statistics/information describing the timings of growth stages by region or country;
- Phenological growth models in conjunction with daily meteorological data;
- Fixed time periods (which may be moderated by climatic region or latitude) or growth stage intervals.

For European maps of risk, it is suggested that the timing of transplantation is set on a fixed date, such as the 1st of June.

3.3.5.2.2 Flux-effect relationships and critical levels for crops

Box 6: Applications for species-specific (POD_6SPEC) flux-effect relationships and critical levels for crops

The species-specific flux models and associated response functions and critical levels for ozone-sensitive crops and cultivars can be used to quantify the potential negative impacts of O_3 on the security of food supplies at the local and regional scale. They can be used to estimate yield losses, including economic losses.

The applications of the POD_YSPEC functions and critical levels for crops are described in Box 6. A flux-threshold Y of 6 (POD_6SPEC) provides the strongest flux-effect relationships for crops (Pleijel et al., 2007). O_3 effects proved to be significant at a 5% reduction of the effect parameter (Mills et al., 2011b), hence critical levels were determined for a 5% reduction of the effect based on the slope of the relationship and are summarised in Table 3.10, with further information on the sources of data provided in Annex 3, Table A2. The flux-effect relationships for wheat-yield and quality are shown in Figure 3.10, whilst those for potato yield, and tomato yield and quality are shown in Figure 3.11.

Table 3.10: POD6SPEC critical levels (CL) for crops.

Species	Effect parameter	Biogeographical region*	Potential effect at CL (% reduction)	Critical level (mmol m^{-2} PLA)**	Ref10 POD_6 (mmol m^{-2} PLA)	Potential maximum rate of reduction (%) per mmol m^{-2} PLA of POD_6SPEC***
Wheat	Grain yield	A ,B, C, M (S, P)****	5%	1.3	0.0	3.85
Wheat	1000-grain weight	A, B, C, M (S, P)****	5%	1.5	0.0	3.35
Wheat	Protein yield	A, B, C, M (S, P)****	5%	2.0	0.0	2.54

Species	Effect parameter	Biogeographical region*	Potential effect at CL (% reduction)	Critical level (mmol m^{-2} PLA)**	Ref10 POD_6 (mmol m^{-2} PLA)	Potential maximum rate of reduction (%) per mmol m^{-2} PLA of POD_6SPEC***
Potato	Tuber yield	A, B, C (M, S, P)	5%	3.8	0.0	1.34
Tomato	Fruit yield	M (A, B, C, S, P)	5%	2.0	0.0	2.53
Tomato	Fruit quality	M (A, B, C, S, P)	5%	3.8	0.0	1.30

* A = Atlantic, B = Boreal, C = Continental, M = Mediterranean, P = Pannonian, S = Steppic; Derived for regions not in brackets, but could also be applied to regions in brackets.

** Represents the (POD_6SPEC – Ref10 POD_6SPEC) required for a 5% reduction;

*** Calculate the % reduction using the following formula: (POD_6SPEC – Ref10 POD_6SPEC) * potential maximum rate of reduction;

**** Different parameterisation of DO_3SE applied for Mediterranean and non-Mediterranean regions.

Figure 3.10: **The relationship between the percentage yield of wheat and stomatal O_3 flux (POD_6SPEC) for the wheat flag leaf based on five wheat cultivars from three or four European countries (Belgium, Finland, Italy, Sweden): a) grain yield, b) 1000-grain weight, and c) protein yield. The grey area indicates the 95%-confidence interval (Grünhage et al., 2012).**

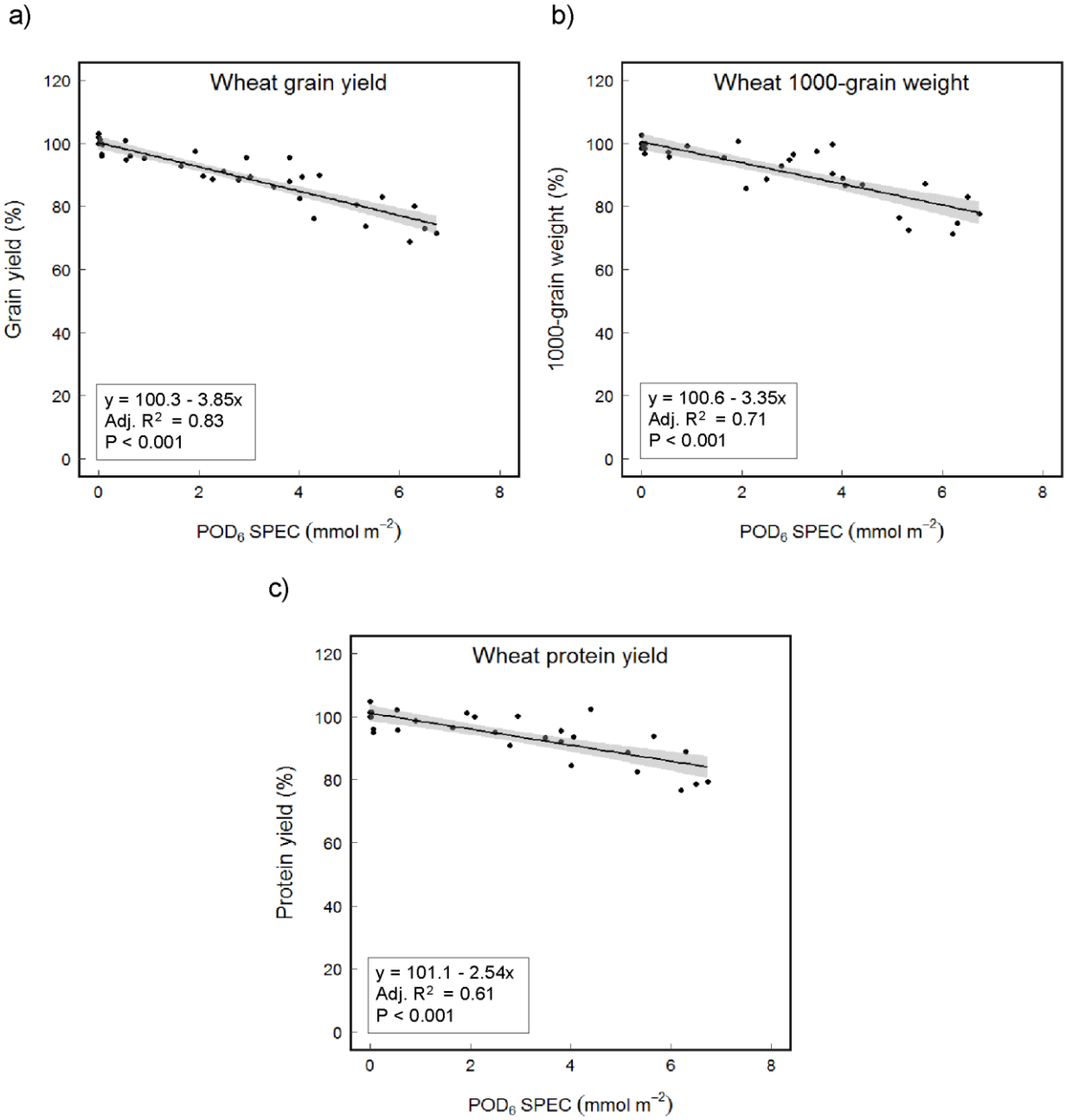

Source: This figure is adopted from a previous version of Chapter 3 of the Mapping Manual

Figure 3.11: **The relationship between the percentage a) tomato fruit yield and b) tomato fruit quality and POD_6SPEC for sunlit leaves (González-Fernández et al., 2014) based on data from Italy and Spain, and c) tuber yield of potato and POD_6SPEC for sunlit leaves (Pleijel et al., 2007) based on data from Belgium, Finland, Germany, Sweden. The grey area indicates the 95%-confidence interval.**

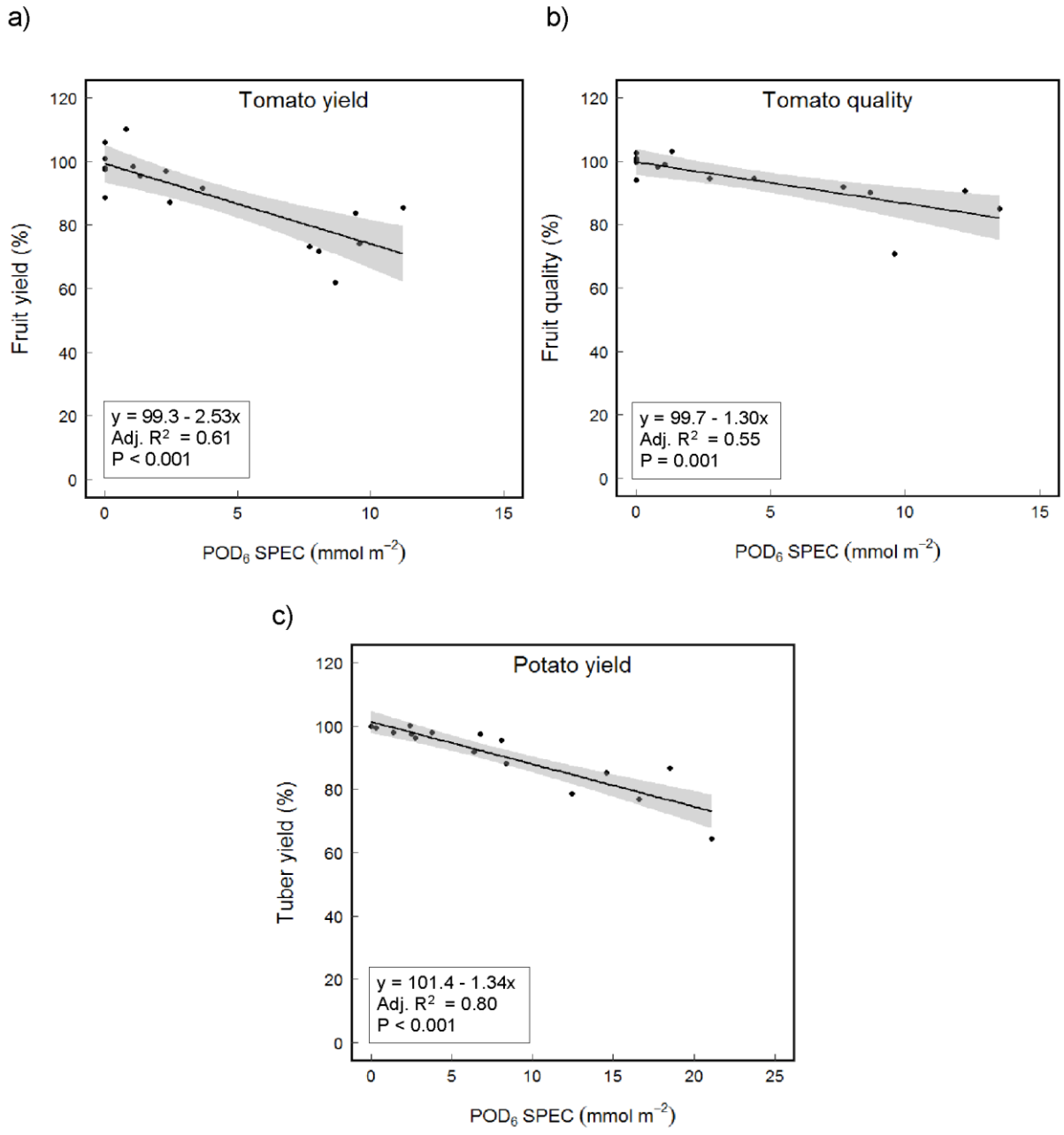

Source: This figure is adopted from a previous version of Chapter 3 of the Mapping Manual

3.3.5.3 Forest trees

3.3.5.3.1 Parameterisation of the O_3 stomatal flux model for forest trees

Species-specific stomatal flux-based critical levels are available for non-Mediterranean beech/birch (combined; *Fagus sylvatica/Betula pendula*) and Norway spruce (*Picea abies*), Mediterranean deciduous oak species (*Quercus faginea, Q. pyrenaica* and *Q. robur*) and Mediterranean evergreen species (*Pinus halepensis, Quercus ilex, Q. ballota, Ceratonia siliqua*). The parameterisation of these flux models is provided in Table 3.11 and is based on data from

mature trees species, except for Mediterranean deciduous oak species. Parameterisation of the DO_3SE model using data from young oak tree species was considered to better represent risk assessment of deciduous trees in Mediterranean areas than the previous parameterisation based on mature Mediterranean beech. Information on the sources of these parameterisations is summarised in Annex III.3 (Table A.3) and SBD-A and available in detail in Büker et al. (2015; trees in non-Mediterranean regions of Europe), Marzuoli et al. (in prep., Mediterranean broadleaf deciduous species) and Alonso et al. (in prep., Mediterranean evergreen species).

A uniform O_3 flux threshold of Y = 1 nmol m^{-2} s^{-1} PLA was adopted for use in POD_YSPEC for all tree species at the O_3 Critical Levels workshop in Madrid, November 2016, based on data and analyses as presented in Büker et al. (2015). For the majority of tree species, this threshold fulfilled the recommendations that the confidence interval of the intercept includes 100% and that the R^2 value is within 2% of the maximum R2 value (Büker et al., 2015).

For forest trees, the following additional information is required for calculating stomatal flux using the method provided in Section 3.3.4.3 and the parameterisation provided in Table 3.11.

Start (A_{start}) and end (A_{end}) of flux accumulation period

POD_1SPEC is accumulated between the start and end of the growing season. For all main receptor species, the start of the growing season is assumed to be equivalent to the start of the flux accumulation period (A_{start}) and is defined as the date of budburst/leaf emergence or the release of winter dormancy. For all main receptor species, the end of the growing season is assumed to be equivalent to the end of the flux accumulation period (A_{end}) and is defined as the onset of dormancy. For beech and birch, as well as for Norway spruce in the boreal region, A_{start} is estimated using a simple latitude model where A_{start} occurs at year day 105 at latitude 50°N, and A_{start} will alter by 1.5 days per degree latitude earlier on moving south and later on moving north. A_{end} is estimated as occurring at year day 297 at latitude 50°N, and A_{end} will alter by 2 days per degree latitude earlier on moving north and later on moving south. Leaf discolouration is assumed to occur 20 days prior to dormancy and is assumed to be the point at which f_{phen} will start to decrease from g_{max}. Between the onset of dormancy and leaf fall, g_{sto} will be assumed to be zero. The effect of altitude on phenology is incorporated by assuming a later A_{start} and earlier A_{end} by 10 days for every 1000 m a.s.l.

This latitude model agreed relatively well with ground observations from the Mediterranean (Mediavilla & Escudero, 2003; Aranda et al., 2005; Damesin & Rambal, 1995; Grassi & Magnani, 2005) and the Atlantic (Broadmeadow, pers comm.; Duchemin et al., 1999) and with remotely sensed observations for the whole of Europe (Zhang et al., 2004). The latitude model is used mainly due to its simplicity. It is understood that the modelled timing of deciduous tree budburst, at least in northern Europe, may differ from the observed timing of budburst (SBD-B, Karlsson et al., Braun et al.). Furthermore, the start of the gas exchange of coniferous tree species in northern Europe may occur at dates earlier than predicted by the latitude model (SBD-B, Karlsson et al.). The latitude model is not able to reflect changes in the climate. Hence, it is the aim that the latitude model should be replaced with a methodology that is based on meteorological parameters once a more robust model has been fully developed (SBD-B, Karlsson et al., Braun et al.).

For Norway spruce in the continental region, the growth period is determined by air temperature defined according to the f_{temp} function. The growing season is assumed to occur when air temperatures are between the T_{min} and T_{max} thresholds of the f_{temp} relationships. During such periods there is no limitation on conductance associated with leaf development stage (i.e., f_{phen} = 1).

f_{phen}

For forest trees, a modified formulation for the f_{phen} relationship as given in Equations III.2a-c is used (see below). This method allows the use of a consistent formulation irrespective of whether there is a mid-season dip in f_{phen} (to simulate the effect of mid-season photo-oxidative stress on stomatal conductance). The values in brackets for the phenology function in Table 3.11 represent "dummy" values to be used in areas where this mid-season dip does not occur:

when $yd \leq A_{start\_FD}$

(III.23a)

$f_{phen} = f_{phen\_a}$ when $A_{start\_FD} < yd \leq f_{phen1\_FD} + A_{start\_FD}$

(III.23b)

$f_{phen} = ((1-f_{phen\_a})*((yd- A_{start\_FD})/f_{phen1\_FD})+f_{phen\_a})$

when $f_{phen1\_FD} + A_{start\_FD} < yd \leq LIM_{start\_FD}$ (III.23c) $f_{phen} = f_{phen\_b}$

when $LIM_{start\_FD} < yd < LIM_{start\_FD} + f_{phen2\_FD}$

(III.23d)

$f_{phen} = (1-f_{phen\_c}) * (((f_{phen2\_FD} + LIM_{start\_FD}) - (LIM_{start\_FD} + (yd- LIM_{start\_FD}))) /f_{phen2\_FD}) + f_{phen\_c}$

when $LIM_{start\_FD} + f_{phen2\_FD} \leq yd \leq LIM_{end\_FD} - f_{phen3\_FD}$

(III.23e)

$f_{phen} = f_{phen\_c}$

when $LIM_{end\_FD} - f_{phen3\_FD} < yd < LIM_{end\_FD}$

(III.23f)

$f_{phen} = (1-f_{phen\_c}) * ((yd-(LIM_{end\_FD} - f_{phen3\_FD}))/f_{phen3\_FD}) + f_{phen\_c}$ when $LIM_{end\_FD} \leq yd \leq A_{end\_FD} - f_{phen4\_FD}$

(III.23g)

$f_{phen} = f_{phen\_d}$ when $A_{end\_FD} - f_{phen4\_FD} < yd < A_{end\_FD}$

(III.23h)

$f_{phen} = (1-f_{phen\_e}) * ((A_{end\_FD}-yd) / f_{phen4\_FD}) + f_{phen\_e}$

when $yd \geq A_{end\_FD}$

(III.23i)

$f_{phen} = f_{phen\_e}$

Table 3.11: Summary of the parameterisation of the DO_3SE model for POD_1SPEC calculations of sunlit leaves at the top of the canopy of individual tree species or groups of tree species growing in Europe. Note: Further region- and species-specific parameterisations for species can be found in SBD-A and SBD-B.

Parameter	Units	Forest tree species parameterisation - POD_1SPEC					
Region *(may also be applicable in these regions)*		Boreal		Continental (Atlantic, Steppic, Pannonian)		Mediterranean	
Forest type		Coniferous	Broadleaf deciduous	Coniferous	Broadleaf deciduous	Broadleaf deciduous	Evergreen
Tree species	Common name	**Norway spruce**	**Silver birch**	**Norway spruce**	**Beech**	**Deciduous oak species**[i, ii]	**Evergreen species**[iii]
	Latin name	*Picea abies*	*Betula pendula*	*Picea abies*	*Fagus sylvatica*		
g_{max}	mmol O_3 m^{-2} PLA s^{-1}	125	240	130	155	265	195
f_{min}	fraction	0.1	0.1	0.16	0.13	0.13	0.02
light_a	-	0.006	0.0042	0.01	0.006	0.006	0.012
T_{min}	°C	0	5	0	5	0	1
T_{opt}	°C	20	20	14	16	22	23
T_{max}	°C	200[iv]	200[iv]	35	33	35	39
VPD_{max}	kPa	0.8	0.5	0.5	1.0	1.1	2.2
VPD_{min}	kPa	2.8	2.7	3.0	3.1	3.1	4.0
ΣVPD_{crit}	kPa	-	-	-	-	-	-
PAW_t	%	-	-	-	-	-	-
SWC_{max}[v]	% volume	15	15	-	-	-	-
SWC_{min}[v]	% volume	1	1	-	-	-	-
SWP_{max}	MPa	-	-	-0.05	-0.05	-1.0	-1.0
SWP_{min}	MPa	-	-	-0.5	-1.25	-2.0	-4.5
f_{O3}	fraction	-	-	-	-	-	-
A_{start}_FD	day of year	Latitude model	Latitude model	f_{temp}[vi]	Latitude model	Latitude model	1 (Jan 1)
A_{end}_FD	day of year	Latitude model	Latitude model	f_{temp}[vi]	Latitude model	Latitude model	365 (Dec 31)
Leaf dimension	cm	0.8	5.0	0.8	7.0	4.2	3

Parameter	Units	Forest tree species parameterisation - POD_1SPEC					
Canopy height	m	20	20	20	25	20	20
f_{phen_a}	fraction	0.0	0.0	0.0	0.0	0.3	1.0
f_{phen_b}	fraction	(1.0)	(1.0)	(1.0)	(1.0)	(1.0)	(1.0)
f_{phen_c}	fraction	1.0	1.0	1.0	1.0	1.0	0.3
f_{phen_d}	fraction	(1.0)	(1.0)	(1.0)	(1.0)	(1.0)	(1.0)
f_{phen_e}	fraction	0.0	0.0	0.0	0.4	0.3	1.0
$f_{phen\_1\_FD}$	no. of days	20	20		20	15	(0)
$f_{phen\_2\_FD}$	no. of days	(200)	(200)	(200)	(200)	(200)	130
$f_{phen\_3\_FD}$	no. of days	(200)	(200)	(200)	(200)	(200)	60
$f_{phen\_4\_FD}$	no. of days	30	30	0	20	20	(0)
LIM_{start_FD}	year day	(0.0)	(0.0)	(0.0)	(0.0)	(0.0)	80 (Mar 21)
LIM_{end_FD}	year day	(0.0)	(0.0)	(0.0)	(0.0)	(0.0)	320 (Nov 16)

The values in brackets represent "dummy" values required for DO_3SE modelling purposes. "-" = parameterisation not required for this species.

[i] Mediterranean deciduous oak are represented here by Quercus robur, Q. pyrenaica and Q. faginea. Only for these tree species is the parameterisation based on young trees (Marzuoli, in prep.).

[ii] Local species-specific parameterisations can be found in scientific background document A (SBD-A).

[iii] Mediterranean evergreen species are represented here by the parameterisation for adult Quercus ilex trees.

[iv] The T_{max} value is set at 200 °C to simulate the weak response to high temperatures of Norway spruce and birch trees growing under Northern European conditions (the stomatal response is instead mediated by high VPD values). Hence, the T_{max} value should be viewed as a forcing rather than descriptive parameter.

[v] Soil water content (SWC) is calculated as the soil water content available for transpiration, i.e., the actual SWC minus the SWC at the wilting point.

[vi] For continental Norway spruce, the growing season is assumed to occur when air temperatures are between the T_{min} and T_{max} thresholds of the f_{temp} relationships. Actual data are recommended if available!

3.3.5.3.2 Flux-effect relationships and critical levels for forest trees

Box 7: Applications for species-specific (POD_1SPEC) flux-effect relationships and critical levels for forest trees

The species-group or species-specific flux models, associated response functions and critical levels for forest trees were derived from experiments with young trees and can be used to quantify the potential negative impacts of O_3 on the annual growth of the living biomass of trees at the local and regional scale. They can be used as a starting point for calculation of impacts on carbon sequestration and tree diversity.

The applications of the POD_YSPEC functions and critical levels for forest trees are described in Box 7. Methods are currently being developed for quantifying O_3 impacts on tree growth rates, such as the Net Annual Increment (NAI; SBD-B, Büker et al.). When developed, such methods should be applied to assess O_3 impacts over the entire rotation periods of trees. Flux models have been developed for the effects of O_3 on individual tree species in one year. Where effects

were reported over more than one year in experiments, the mean flux was determined by dividing the total by the number of years of O_3 exposure. Based on the exponential nature of the growth of young trees, the following procedure was applied for the correction of the biomass change in multiannual experiments:

(III.24)

$$biom_{yr} = biom^{\frac{1}{years}}$$

where $biom_{yr}$ is the corrected biomass, biom is the biomass in fractions of the control and years is the duration of the experiment in years.

The critical levels for forest trees were set to values for an acceptable biomass loss. Critical levels have been derived for either a 2% (Norway spruce) or a 4% (beech/birch, Mediterranean deciduous oaks and Mediterranean evergreen species) reduction in annual new growth (based on above ground, root, or whole tree biomass) of young trees of up to 10 years of age. For each species, data was from independent experiments conducted in two countries with three species for Mediterranean deciduous oaks; one country with four species for Mediterranean evergreen; two countries with one species for Norway spruce; and three countries with two species for beech and birch (combined in one function) (see Annex 3, Table A2). Critical levels were determined based on the slope of the flux-effect relationship and are summarised in Table 3.12.

Table 3.12: POD_1SPEC critical levels (CL) for forest tree species.

Species	Effect parameter	Biogeographical region*	Potential effect at CL (% annual reduction)	Critical level (mmol m^{-2} PLA)**	Ref10 POD_1 (mmol m^{-2} PLA)	Potential maximum rate of reduction (%) per mmol m^{-2} PLA of POD_1SPEC***
Beech and birch	Whole tree biomass	B, C (A, S, P)	4%	5.2	0.9	0.93
Norway spruce	Whole tree biomass	B, C (A, S, P)	2%	9.2	0.1	0.22
Med. deciduous oaks	Whole tree biomass	M	4%	14.0	1.4	0.32
Med. deciduous oaks	Root biomass	M	4%	10.3	1.4	0.45
Med. evergreen	Above-ground biomass	M	4%	47.3	3.5	0.09

* A: Atlantic; B: Boreal; C: Continental, S: Steppic, P: Pannonian; M: Mediterranean. Derived for regions not in brackets, but could also be applied to regions in brackets.

** Represents the (POD_1SPEC – Ref10 POD_1SPEC) required for a x% reduction

*** Calculate the % reduction using the following formula: (POD_1SPEC – Ref10 POD_1SPEC) * potential maximum rate of reduction.

The flux-effect relationships for individual tree species or groups of tree species are shown in Figure 3.12.

Figure 3.12: **The relationship between the percentage total biomass and the stomatal O_3 flux (POD_1SPEC) for sunlit leaves of a) beech (Fagus sylvatica) and silver birch (Betula pendula) based on data from Finland, Sweden and Switzerland (Büker et al., 2015), b) Norway spruce (Picea abies) based on data from France, Sweden and Switzerland (Büker et al., 2015), c) Mediterranean deciduous oak based on data from Italy and Spain (Calatayud et al., 2011; Marzuoli et al., 2016, in prep.), d) between the percentage root biomass and the stomatal O_3 flux (POD_1SPEC) for sunlit leaves of Mediterranean oak (Calatayud et al., 2011; Marzuoli et al., 2016, in prep.), and e) between the percentage of above-ground biomass and the stomatal O_3 flux (POD_1SPEC) for sunlit leaves of Mediterranean evergreen species based on data from Spain (Alonso et al., in prep). The grey area indicates the 95%-confidence interval.**

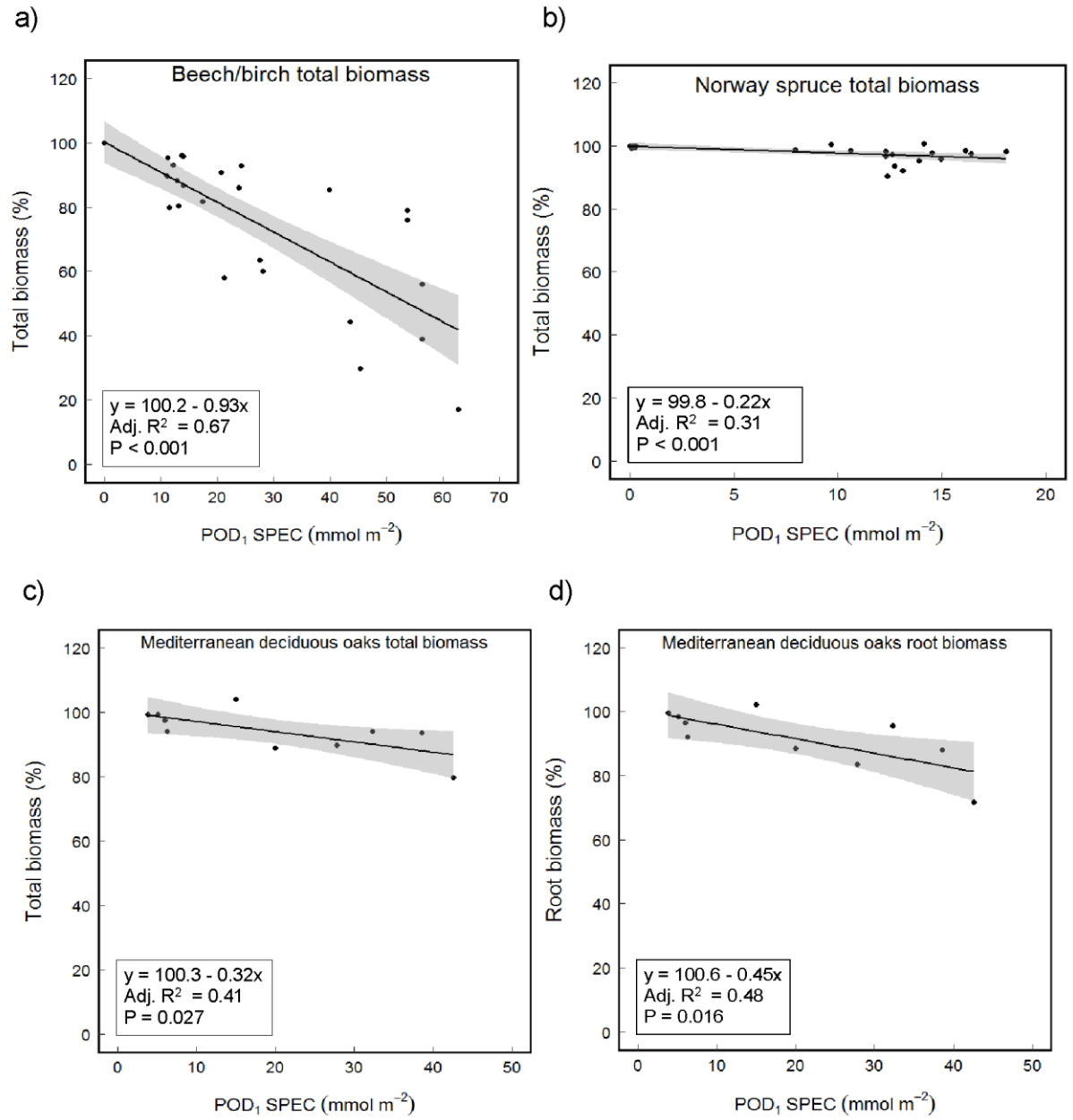

e)

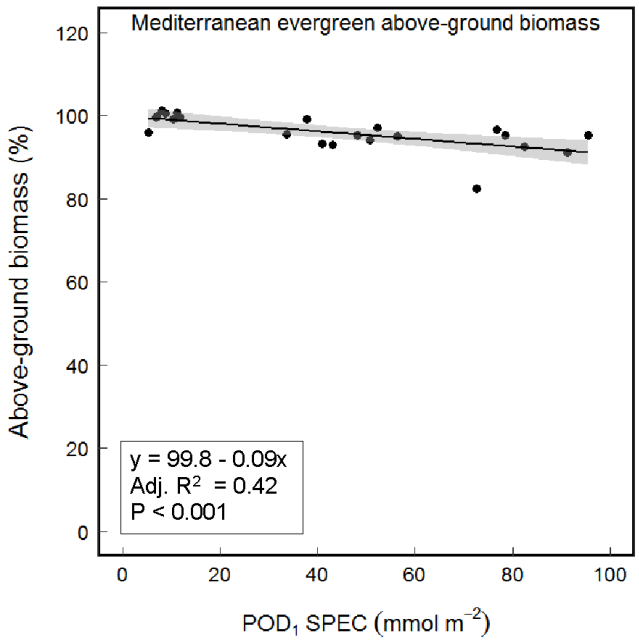

Source: This figure is adopted from a previous version of Chapter 3 of the Mapping Manual

3.3.5.4 (Semi-)natural vegetation

3.3.5.4.1 Choice of representative species and ecosystems

The (semi-)natural vegetation type includes all vegetation not planted by humans, excluding forests, but influenced deliberately or inadvertently by human actions (Di Gregorio & Jansen, 2000). This vegetation type is the most florally diverse of those considered – there are 4000+ species of (semi-)natural vegetation in Europe – making the generalisations needed for setting critical levels difficult. Although response functions and relative sensitivities have been derived for >100 species (Hayes et al., 2007; Bergmann et al., 2015), at least 98 % of (semi-)natural species remain untested.

Due to the large diversity of (semi-)natural vegetation communities across Europe in terms of ecophysiology, life form, management practices such as grazing, cutting or fertilization regime or species composition, O_3 critical levels have been established for widespread O_3 sensitive species representing broad categories of (semi-)natural vegetation plant communities. Critical levels have been established for:

- **Temperate perennial grasslands** found in Boreal, Atlantic and Continental biogeographical regions of Europe that are dominated by grasses and forbs and have little or no tree cover, and may be grazed. The majority of vegetation species are perennials, but annual species may also be present. Parameterisations and critical levels for temperate perennial grasslands may also be applicable for Pannonian and Steppic regions, but this has not been tested yet and stronger soil water limitations might be expected.
- **Mediterranean annual pastures** that are dominated by annual plants (grasses and forbs, including legumes). They include Dehesa annual pastures and other grazed annual pastures found in the Mediterranean region of Europe.

Information from field experiments to date indicates that subalpine grassland vegetation is moderately tolerant to current ambient O_3 concentrations (Bassin et al., 2013, 2015; Volk et al.,

2014). Hence, O_3 critical levels have not been established for (sub)alpine grassland communities. Currently there is insufficient data to establish a flux-based O_3 critical level for other (semi-) natural vegetation communities.

Only experiments conducted in Europe under semi-controlled conditions have been considered for critical level derivation, in which the selected species were growing in competition with other grassland species (Temperate perennial grasslands) and as single species or two-species mixtures (Mediterranean annual species) and subjected to different fertilization and cutting regimes. Several independent experiments have been included in each function.

3.3.5.4.2 Parameterisation of the O_3 stomatal flux model for (semi-)natural vegetation

Parameterisations of the DO_3SE model for representative species of (semi-)natural vegetation are shown in Table 3.13. For **temperate perennial grasslands** it is recommended to use the forbs parameterisation as an indicator of a general risk to grassland habitats. The grass parameterisation can be used to specifically assess the risk for grass species. For **Mediterranean annual pastures** it is recommended to use the legumes parameterisation as an indicator of a general risk to annual pasture habitats.

Time window

Time windows are "default" parameters that should be adjusted by the user if more appropriate local information is available. Select the accumulation period that gives the highest flux or is the most suitable season.

Canopy height

Default values are provided for general application.

EUNIS classifications

The most suitable EUNIS classes (http://eunis.eea.europa.eu/) to use are those represented by the habitats for which the critical levels have been derived.

Temperate perennial grassland:

- E2.1 Permanent mesotrophic pastures and aftermath-grazed meadows
- E2.2 Low and medium altitude hay meadows
- E2.7 Unmanaged mesic grassland
- E2.5 Meadows of the steppe zone

Mediterranean annual pasture:

- E1.3 Mediterranean xeric grassland
- E1.6 Subnitrophilous annual grassland
- E1.8 Closed Mediterranean dry acid and neutral grassland
- E7.3 Dehesa

Table 3.13: Parameterisation of the DO_3SE model for POD_1SPEC calculations for sunlit leaves at the top of the canopy for representative O_3-sensitive (semi-)natural vegetation species.

Parameter	Units	(Semi-)natural vegetation parameterisation for sunlit leaves at top of canopy - POD_1SPEC		
Region *(may also be applicable in these regions)*		Atlantic, Boreal, Continental, *(Pannonian, Steppic)*	Atlantic, Boreal, Continental, *(Pannonian, Steppic)*	Mediterranean
Land cover type		Perennial grasslands (Grass spp.)	Perennial grasslands (Forbs incl. legumes)	Annual pastures (Legume spp.)
g_{max}	mmol O_3 m^{-2} PLA s^{-1}	190	210	782
f_{min}	fraction	0.1	0.1	0.02
light_a	-	0.01	0.02	0.013
T_{min}	°C	10	10	8
T_{opt}	°C	24	22	22
T_{max}	°C	36	36	33
VPD_{max}	kPa	1.75	1.75	2.2
VPD_{min}	kPa	4.5	4.5	4.3
ΣVPD_{crit}	kPa	-	-	-
PAW_t	%	-	-	-
SWC_{max}	% volume	-	-	18.3
SWC_{min}	% volume	-	-	0.03
SWP_{max}	MPa	-0.1	-0.1	-
SWP_{min}	MPa	-1	-0.6	-
f_{O3}	fraction	-	-	-
$A_{start}\_FD^i$	day of year	91 (April 1st)	91 (April 1st)	32 (February 1st)
$A_{end}\_FD^i$	day of year	273 (September 30th)	273 (September 30th)	181 (June 30th)
Time window length	month	3	3	1.5
Leaf dimension	cm	2ii	4ii	2
Canopy height	m	0.2	0.2	0.2
f_{phen_a}	fraction	1	1	1
f_{phen_b}	fraction	1	1	1
f_{phen_c}	fraction	1	1	1

Parameter	Units	(Semi-)natural vegetation parameterisation for sunlit leaves at top of canopy - POD_1SPEC		
f_{phen_d}	fraction	1	1	1
f_{phen_e}	fraction	1	1	1
$f_{phen\_1\_FD}$	no. of days	-	-	-
$f_{phen\_2\_FD}$	no. of days	-	-	-
$f_{phen\_3\_FD}$	no. of days	-	-	-
$f_{phen\_4\_FD}$	no. of days	-	-	-
LIM_{start_FD}	year day	-	-	-
LIM_{send_FD}	year day	-	-	-

"-" = parameterisation not required for this species.

[i] Days of year given for non-leap year.

[ii] Not given, set to match wheat (grass species) and potato (forb species, including legumes).

3.3.5.4.3 Flux-effect relationships and critical levels for (semi-)natural vegetation

Box 8: Applications for species-specific (POD_1SPEC) flux-effect relationships and critical levels for (semi-)natural vegetation

The species-group specific flux models, associated response functions, and critical levels for (semi-) natural vegetation were derived from experiments with O_3-sensitive species grown in competition (temperate perennial grasslands) or as single species and two-species mixtures (Mediterranean annual pastures). Response functions and critical levels can be used to quantify the risk of potential negative O_3 impacts on biomass, and reproductive capacity. They can be used as a starting point for the calculation of impacts on carbon sequestration and plant biodiversity.

The applications of the POD_YSPEC functions and critical levels for (semi-)natural vegetation are described in Box 8. For (semi-)natural vegetation, a flux-threshold Y of 1 nmol m^{-2} s^{-1} (POD_1SPEC) was used. This threshold fulfilled the recommendations made by Büker et al. (2015), i.e., that the confidence interval of the intercept includes 100% and that the R^2 value is within 2% of the maximum R^2 value and matches the one used for forest trees.

Table 3.14: POD_1SPEC critical levels (CL) for O_3 sensitive (semi-)natural vegetation.

Species	Effect parameter	Biogeographical region*	Potential effect at CL (% reduction)	Critical level (mmol m^{-2} PLA)**	Ref10 POD_1 (mmol m^{-2} PLA)	Potential maximum rate of reduction (%) per mmol m^{-2} PLA of POD_1SPEC***
Temperate perennial grassland	Above-ground biomass	A, B, C (S, P)	10%	10.2	0.1	0.99
Temperate perennial grassland	Total biomass	A, B, C (S, P)	10%	16.2	0.1	0.62

Species	Effect parameter	Biogeographical region*	Potential effect at CL (% reduction)	Critical level (mmol m^{-2} PLA)**	Ref10 POD_1 (mmol m^{-2} PLA)	Potential maximum rate of reduction (%) per mmol m^{-2} PLA of POD_1SPEC***
Temperate perennial grassland	Flower number	A, B, C (S, P)	10%	6.6	0.1	1.54
Med. Annual pasture	Above-ground biomass	M	10%	16.9	5.2	0.85
Med. Annual pasture	Flower/ seed biomass	M	10%	10.8	4.6	1.61

* A: Atlantic; B: Boreal; C: Continental, S: Steppic, P: Pannonian; M: Mediterranean. Derived for species growing in regions not in brackets, but could also be applied to regions in brackets.

** Represents the (POD_1SPEC – Ref10 POD_1SPEC) required for a x% reduction

*** Calculate the % reduction using the following formula: (POD_1SPEC – Ref10 POD_1SPEC) * potential maximum rate of reduction.

A 10% reduction in the effects parameter was considered to be an important effect that could change ecosystem dynamics. Hence, critical levels were determined for a 10% reduction of the effect based on the slope of the relationship and are summarised in Table 3.14. The flux-effect relationships for (semi-)natural vegetation are shown in Figures 3.13 and 3.14 and further details can be found in Annex 3, Table A.4. It should be noted that the critical levels and response functions were derived from experimental data in Europe. Two sets of critical levels are provided per habitat reflecting O_3 impacts on growth or reproductive output. Users should select the most appropriate response for their requirements. POD_YSPEC-based critical levels can be used to assess the potential risk of O_3 impacts on the biomass and vitality of (semi-)natural vegetation species. These critical levels may also protect against loss of plant biodiversity, but this has not yet been confirmed.

Figure 3.13: **The relationship between the stomatal O_3 flux (POD_1SPEC) for sunlit leaves and percentage a) above-ground biomass, b) total biomass and c) flower number of temperate perennial grasslands. The grey area indicates the 95%-confidence interval. Data are from experiments conducted in the UK (Hayes et al., 2011, 2012, Hewitt et al., 2014, Wagg et al., 2012, Wyness et al., 2011) and unpublished data peer-reviewed at the Madrid Workshop, (2016).**

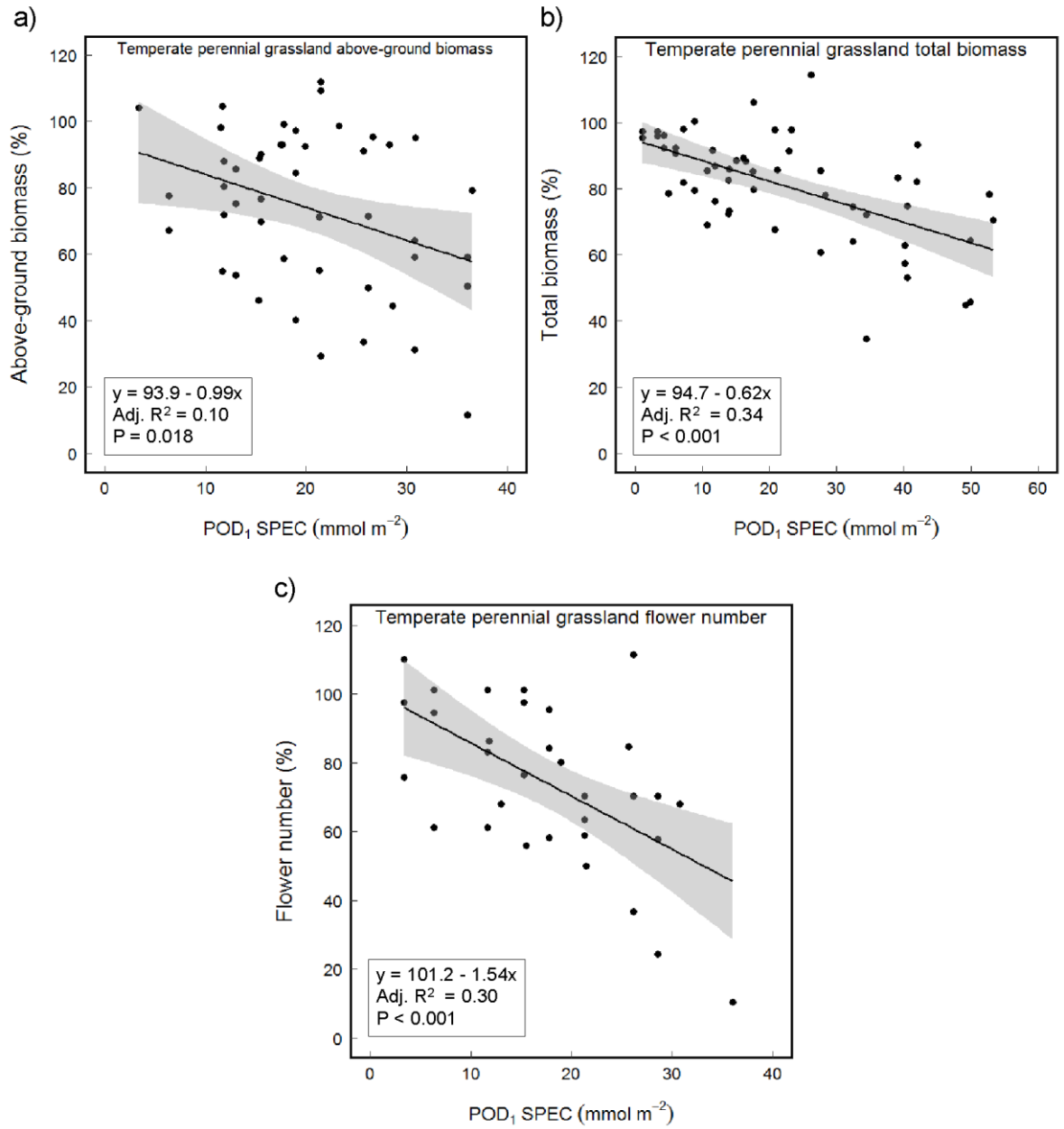

Source: This figure is adopted from a previous version of Chapter 3 of the Mapping Manual

The flux models and critical levels are the most applicable to areas where the vegetation is similar to the species/vegetation type for which a flux-based critical level has been derived (see suitable EUNIS classifications above). For other (semi-)natural vegetation communities the critical levels only provide an indication of a relative risk to these communities, except for Alpine grasslands and pastures which are rather resilient to ozone in terms of biomass growth (Volk et al., 2014).

Figure 3.14: **The relationship between the stomatal O_3 flux (POD_1SPEC) for sunlit leaves and percentage a) aboveground biomass and b) seed/flower biomass of Mediterranean annual pastures. The grey area indicates the 95%-confidence interval. Data are from experiments conducted in Spain (Gimeno et al., 2004a,b; Sanz et al., 2005, 2007, 2014, 2016).**

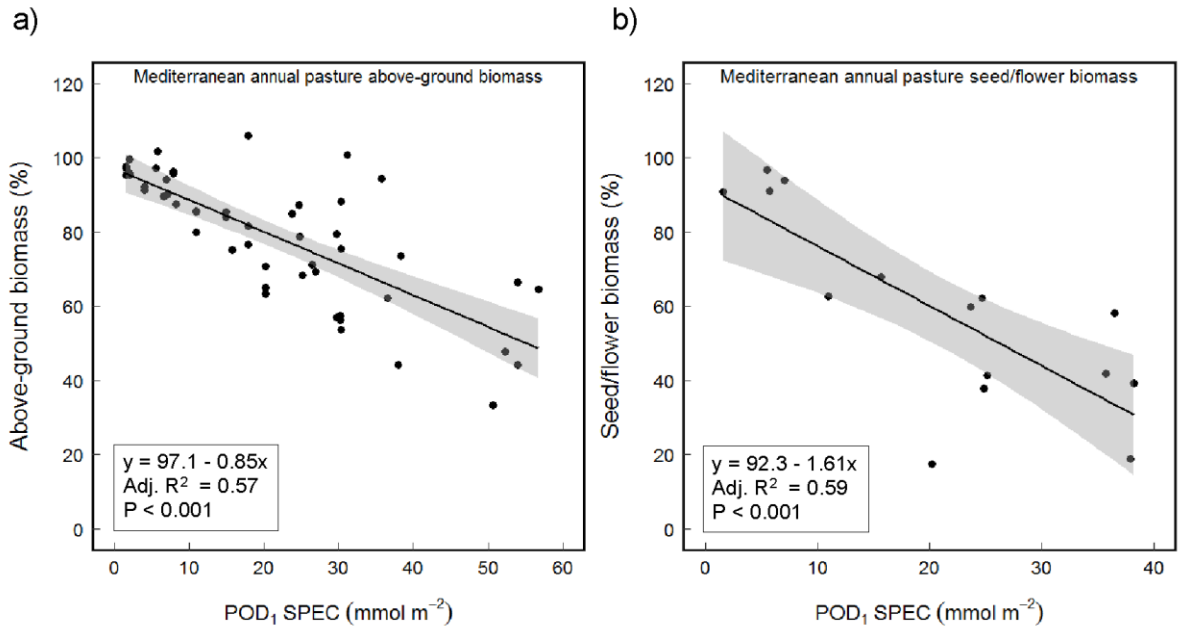

Source: This figure is adopted from a previous version of Chapter 3 of the Mapping Manual

3.3.6 Vegetation-specific flux-effect relationships and critical levels for assessing risk in large-scale integrated assessment modelling (using POD_YIAM)

3.3.6.1 Applications

The simplified flux models (POD_YIAM) and associated response functions and critical levels described in this section **are for use in integrated assessment modelling (IAM)** on a European, regional and potentially global scale for similar biogeographic regions. Using POD_YIAM, the degree of risk of damage within large scale modelling, including scenario analysis and optimisation runs within the GAINS model (**G**reenhouse Gas and **A**ir Pollution **I**nteractions and **S**ynergies) can be determined by using simplified parameterisations to represent vegetation types. POD_YIAM flux models provide an **indicative risk assessment** and are less robust than POD_YSPEC flux models. They can be applied to assess exceedance of critical levels and/or to quantify the risk of adverse O_3 impacts for the most sensitive vegetation under the worst case scenario (Box 9).

Separate simplified flux models, associated response relationships and critical levels have been defined for crops, forest trees and (semi-)natural vegetation, with parameterisations provided for Mediterranean and non-Mediterranean areas.

Text Box 9: Applications for vegetation-type flux models and critical levels, POD_YIAM

These flux models have simpler form than POD_YSPEC and have been developed specifically for use in large-scale integrated assessment modelling, including for scenario analysis and optimisation runs. Separate parametrisations are provided for Mediterranean and non-Mediterranean areas for application in risk assessments for crops, forest trees and (semi-)natural vegetation.

The flux-effect relationships can be used for:

- **Crops:** potential maximum yield loss calculation and indicative economic losses in worst case scenario.
- **Forest trees and (semi-)natural vegetation**: indicative of the potential maximum risk for estimating environmental cost, but not economic losses.

The critical levels can be used for calculating critical levels exceedances, both amount and area. For applications in a climate change context, the POD_YSPEC method is recommended as key factors, such as phenology and soil moisture, are not included in the parameterisation of POD_YIAM.

3.3.6.2 POD_YIAM-based flux-effect relationships and critical levels for crops, forest trees, and grasslands/pasture

3.3.6.2.1 Parameterisation of the O_3 stomatal flux model (POD_YIAM)

The simplified flux models suitable for IAM do not include the modifying effect of soil moisture and phenology (and O_3 in the case of crops) on the stomatal conductance, hence f_{SW} and f_{phen} (and f_{O3} for crops) are set to 1 between the start and the end of the accumulation period. Using the simplified flux models as a stand-alone application, this method would indicate the risk of O_3 damage under the worst case scenario where soil moisture is not limiting stomatal O_3 flux. However, when used within the EMEP model (Simpson et al., 2012), a simplified soil moisture index is included and further work is ongoing to optimise the applicability of the soil moisture index in soil moisture limited areas or under scenarios of climate change. The parameterisations for POD_YIAM are provided in Table 3.15.

Crops

For crops, the parameterisation for the POD_YIAM flux model is based on wheat, a sensitive crop for which abundant information exists (Table 3.15). Due to difficulties in estimating the O_3 flux using Y = 6 nmol m^{-2} s^{-1} in large scale modelling and IAM arising from the strong increase in the uncertainty in modelled POD with increasing Y, Y= 3 nmol m^{-2} s^{-1} is to be used (POD_3IAM). To accommodate the need for IAM to use a longer time period than the thermal time-based time window used for POD_6SPEC, POD_3IAM is accumulated over 90 days, centred on the timing of mid-anthesis (flowering) in wheat (see Section 3.3.5.2).

Forest trees

For forest trees, the parameterisation for the POD_1IAM flux models has been developed from the POD_1SPEC models for non-Mediterranean broadleaf deciduous species (beech - Fagus sylvatica, birch - Betula pendula, temperate oak - *Quercus petraea* and *Q. robur,* and poplar - *Populus spp.*) and Mediterranean broadleaf deciduous species (*Quercus faginea, Q. robur* and *Q. pyrenaica*). For the derivation of a flux-effect relationship, a Y value of 1 nmol m^{-2} s^{-1}.

Table 3.15: Parameterisation of the DO_3SE model for POD_YIAM calculations for the flag leaves/sunlit leaves at the top of the canopy for crops, forests, and (semi-) natural vegetation. Separate parameterisations are provided for Mediterranean and non-Mediterranean areas.

Parameter	Units	Crop parameterisation POD_3IAM		Forest trees parameterisation POD_1IAM		(Semi-)natural vegetation parameterisation POD_1IAM	
Biogeographic region		Atlantic, Boreal, Continental, Steppic, Pannonian	Mediterranean	Atlantic, Boreal, Continental, Steppic, Pannonian	Mediterranean	Atlantic, Boreal, Continental, Steppic, Pannonian	Mediterranean
Based on species		Wheat	Wheat	Beech, birch, temperate oak, poplar	Deciduous oak spp.	O_3-sensitive forbs, including legumes	O_3-sensitive legumes
g_{max}	mmol O_3 m^{-2} PLA s^{-1}	500	430	150	265	210	782
f_{min}	fraction	0.01	0.01	0.1	0.13	0.1	0.02
light_a	-	0.0105	0.0105	0.006	0.006	0.02	0.013
Tm_{in}	°C	12	13	0	0	10	8
T_{opt}	°C	26	28	21	22	22	22
T_{max}	°C	40	39	35	35	36	33
VPD_{max}	kPa	1.2	3.2	1.0	1.1	1.75	2.2
VPD_{min}	kPa	3.2	4.6	3.25	3.1	4.5	4.3
ΣVPD_{crit}	kPa	8	8	-	-	-	-
PAW_t	%	$f_{SW} = 1$	$f_{SW} = 1$	-	-	-	-
SWC_{max}	% volume	-	-	-	-	-	-
SWC_{min}	% volume	-	-	-	-	-	-
SWP_{max}	MPa	-	-	$f_{SW} = 1$	$f_{SW} = 1$	$f_{SW} = 1$	$f_{SW} = 1$
SWP_{min}	MPa	-	-	$f_{SW} = 1$	$f_{SW} = 1$	$f_{SW} = 1$	$f_{SW} = 1$
f_{O3}	fraction	1	1	-	-	-	-
A_{start}_ETS	˚C day	45 days before mid-anthesis in wheat*	45 days before mid-anthesis in wheat*	Latitude model	Latitude model	91 (April 1st)	32 (February 1st)
A_{end}_ETS	˚C day	45 days before mid-	45 days before mid-	Latitude model	Latitude model	273 (September 30th)	181 (June 30th)

Parameter	Units	Crop parameterisation POD_3IAM		Forest trees parameterisation POD_1IAM		(Semi-)natural vegetation parameterisation POD_1IAM	
		anthesis in wheat*	anthesis in wheat*				
Time window length	month	-	-	-	-	3	1.5
Leaf dimension	cm	2	2	7	4.2	4	2
Canopy height	m	1	1	20	20	0.2	0.2
f_{phen_a}	fraction	1.0	1.0	0.0	0.0	1.0	1.0
f_{phen_b}	fraction	1.0	1.0	0.0	0.0	1.0	1.0
f_{phen_c}	fraction	1.0	1.0	1.0	1.0	1.0	
f_{phen_d}	fraction	1.0	1.0	(1.0)	(1.0)	1.0	1.0
f_{phen_e}	fraction	1.0	1.0	0.0	0.0	1.0	1.0
$f_{phen\_1\_ETS}$	˚C day	-	-	-	-	-	-
$f_{phen\_2\_ETS}$	˚C day	-	-	-	-	-	-
$f_{phen\_3\_ETS}$	˚C day	-	-	-	-	-	-
$f_{phen\_4\_ETS}$	˚C day	-	-	-	-	-	-
$f_{phen\_5\_ETS}$	˚C day	-	-	-	-	-	-
$f_{phen\_1\_FD}$	no. of days	-	-	15	20	-	-
$f_{phen\_2\_FD}$	no. of days	-	-	(200)	(200)	-	-
$f_{phen\_3\_FD}$	no. of days	-	-	(200)	(200)	-	-
$f_{phen\_4\_FD}$	no. of days	-	-	20	50	-	-
LIM_{start_FD}	year day	-	-	(0.0)	(0.0)	-	-
LIM_{send_FD}	year day	-	-	(0.0)	(0.0)	-	-

The values in brackets represent "dummy" values required for DO_3SE modelling purposes. "-" = parameterisation not required for this species.

* 90d accumulation period, centred on the timing of mid-anthesis in wheat; see Section 3.3.5.2.1 for details.

(POD_1IAM) was used in agreement with POD_1SPEC (see Section 3.3.5.3). The start and the end of the accumulation period is still determined by the latitude model.

(Semi-)natural vegetation

For (semi-)natural vegetation, the parameterisation for the POD_1IAM flux models has been developed from the POD_1SPEC models for temperate perennial grasslands, using the parameterisation for forbs (including legumes) and for legumes for Mediterranean annual pasture (see Section 3.3.5.4).

3.3.6.2.2 Flux-effect relationships and critical levels for integrated assessment modelling (IAM)

The critical levels for use with POD_YIAM are shown in Table 3.16. These have been derived from response functions based on POD_3IAM for crops, and POD_1IAM for forest trees and (semi-) natural vegetation (Figure 3.15). It should be noted that for crops, the function was first derived for datasets based on 45 days (the minimum exposure period in the experiments). The values have been doubled to accommodate the longer 90-day time interval required. For crops, the effect parameter was grain yield, for forest trees it was total biomass and for (semi-)natural vegetation it was flower number (temperate perennial grasslands) or flower/seed biomass (Mediterranean annual pastures).

Table 3.16: POD_YIAM critical levels (CL) for crops, forest trees and (semi-)natural vegetation.

Vegetation type (POD_YIAM)	Effect parameter	Used to assess risk of reduction in	Biogeographical region*	Potential effect at CL (% reduction)	Critical level (mmol m^{-2} PLA)**	Ref10 PODY (mmol m^{-2} PLA)
Crops (POD_3IAM)	Grain yield	Grain yield	A, B, C, M (S, P)***	5%	7.9	0.1
Forest trees (POD_1IAM)	Total biomass	Annual growth of living biomass of trees	A, B, C (S, P)	4%	5.7	0.6
			M	4%	13.7	1.7
(Semi-) natural vegetation (POD_1IAM)						
Temperate perennial grasslands	Flower number	Vitality of species-rich grasslands	A, B, C (S, P)	10%	6.6	0.1
Med. annual pastures	Flower/ seed biomass		M	10%	10.8	4.6

A: Atlantic; B: Boreal; C: Continental, S: Steppic, P: Pannonian; M: Mediterranean. Suitable for vegetation types in regions not in brackets, but could also be applied to regions in brackets.

** Represents the (POD_YSPEC – Ref10 POD_YSPEC) required for a x% reduction

*** Separate parameterisations should be used for Mediterranean and non-Mediterranean areas.

Figure 3.15: Flux (POD_YIAM) effect relationships for application in large-scale modelling, including Integrated Assessment Modelling (IAM), a) for crops, for broadleaf deciduous trees in b) non-Mediterranean and c) Mediterranean regions, and for (semi-)natural vegetation in d) non-Mediterranean and e) Mediterranean regions.

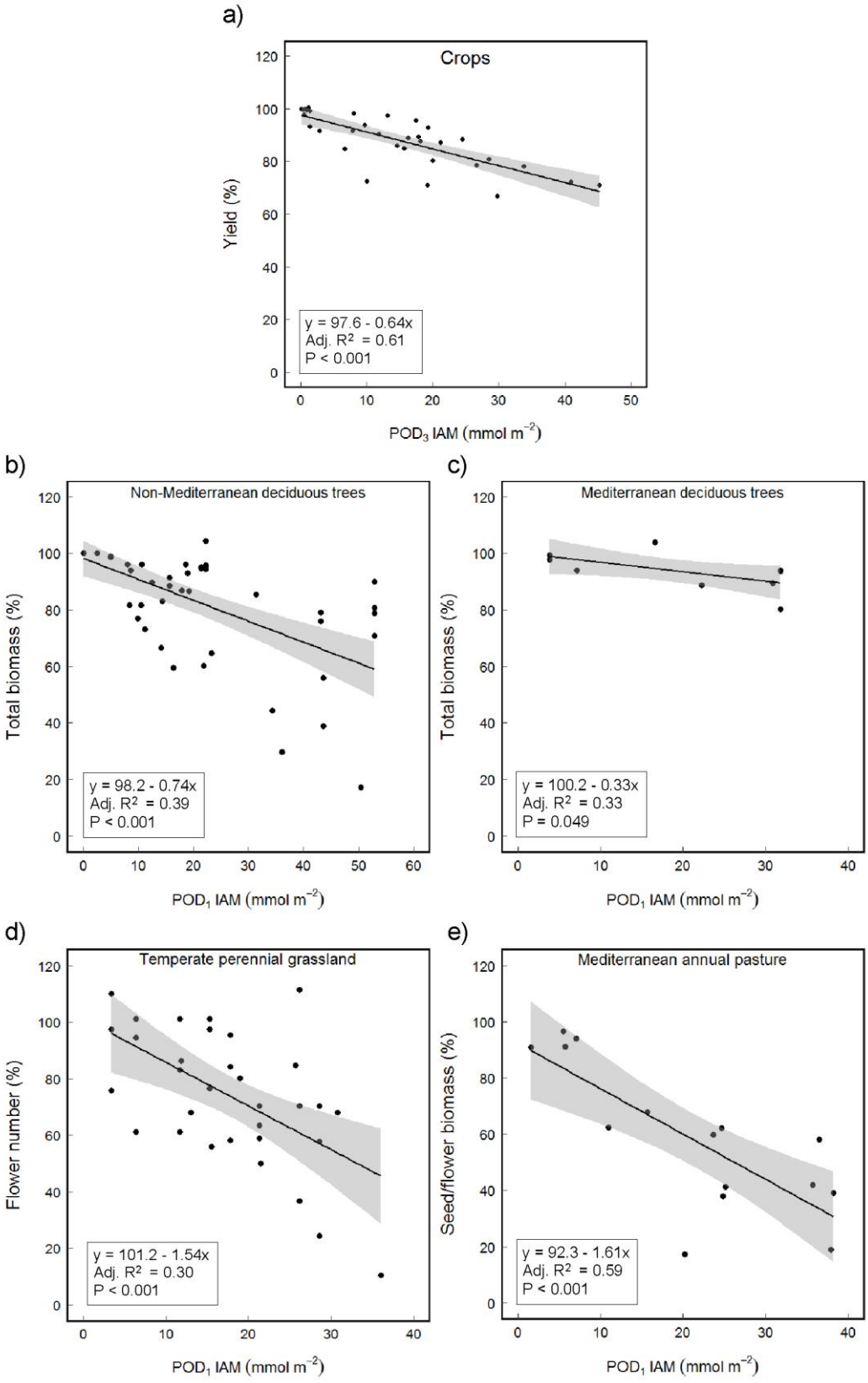

Source: This figure is adopted from a previous version of Chapter 3 of the Mapping Manual

3.3.7 Concentration-based critical levels for O_3 (AOT40)

3.3.7.1 Applications

These are based on accumulation of the hourly mean O_3 concentration at the top of the canopy over a threshold concentration of 40 ppb during daylight hours (when global radiation is more than 50 W m^{-2}) for the appropriate time-window (AOT40) and thus do not take account of the stomatal influence on the amount of O_3 entering the plant. Hence, the spatial distribution of the risk of adverse impacts on vegetation generally mimics the spatial distribution of O_3 concentration and is different from the spatial distribution of POD_Y on the pan-European scale (Mills et al., 2011a, Simpson et al., 2007). Potential applications for AOT40-based critical levels are described in box 10.

Box 10: Applications for AOT40-based critical levels

AOT40-based critical levels are suitable for estimating the risk of damage where climatic data or suitable flux models are not available and/or areas where no climatic or water restrictions to stomatal O_3 flux are expected. Critical levels are defined for agricultural and horticultural crops, forests and (semi-)natural vegetation.

3.3.7.2 AOT40 methodology for all vegetation types

It is recommended that AOT40 values for comparison with the critical levels be calculated as the mean value over the most recent five years for which appropriate quality assured data are available. For local and national risk assessment, it may also be valuable to choose the year with the highest AOT40 from amongst the five years.

In summary, the following steps are required for calculation of AOT40 and exceedance of the critical level for a given year for a specific species/vegetation type:

Step 1: The vegetation- or species-specific accumulation period is determined.

Step 2: Collate the hourly mean O_3 concentrations for the measurement height and accumulation period.

Step 3: Adjust the O_3 data from measurement height to canopy height using an appropriate model or the algorithm in this manual (see Section 3.3.4.2 and SBD-A).

Step 4: Calculate the AOT40 index by subtracting 40 from each hourly mean during daylight hours (when global radiation is more than 50 W m^{-2}) and then summing the resulting values (see example in Figure 3.16).

Figure 3.16: Calculation of O_3 accumulated over a threshold of 40 ppb (AOT40) in ppb h for Balingen (6 May, 1992). The AOT40 for this day is 383 ppb h, calculated as 17 (exceedance of 40 ppb for 11th hour) + 35 (12th hour) + 30 (13th hour) + 47 (14th hour) + 51 (15th hour) + 55 (16th hour) + 52 (17th hour) + 51 (18th hour) + 45 (19th hour). Exceedance of 40 ppb in the 20th hour is not included because it occurred after daylight (global radiation was less than 50 W m^{-2}) had ended.

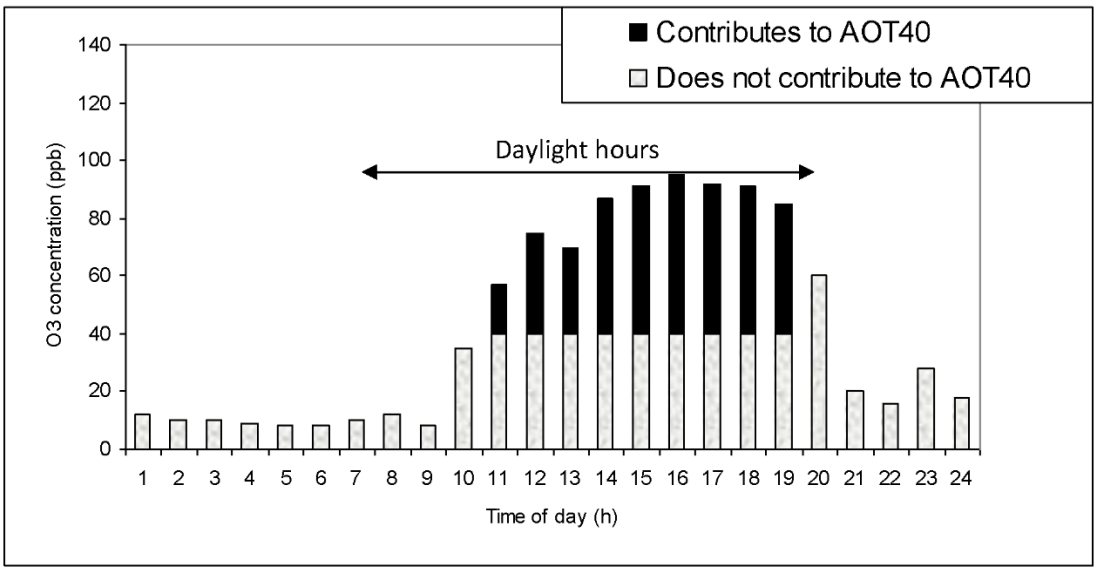

Source: This figure is adopted from a previous version of Chapter 3 of the Mapping Manual

3.3.7.3 AOT40-based critical levels for crops, forest trees, and (semi-)natural vegetation

Here we provide a summary of AOT40-based critical levels for vegetation, for further details see SBD-A.

Crops

AOT40-based critical levels have been defined for agricultural and horticultural crops, based on dose-response relationships for wheat (Mills et al., 2007) and tomato (González-Fernández et al., 2014) respectively (Table 3.17). The timing of the three-month accumulation period for agricultural crops should reflect the period of active growth of wheat and be centred on the timing of mid-anthesis (see Section 3.3.5.2.1). For horticultural crops, the timing of the start of the growing season is more difficult to define because they are repeatedly sown over several months in many regions, especially in the Mediterranean. For local application within the Mediterranean, appropriate three-month periods should be selected between March and August for eastern Mediterranean areas, and March and October for western Mediterranean areas. Since the cultivars used to derive the response function for tomato also grow in other parts of Europe, it is suggested that appropriate three-month periods are selected between the period of April to September for elsewhere in Europe.

Forest trees

AOT40-based critical levels have been defined for forest trees, based on dose-response relationships for beech and birch (Table 3.17; Karlsson et al., 2003; 2007). The default window for the accumulation of AOT40 is the 1st of April to the 30th of September for all deciduous and evergreen species in Europe. This time period does not take altitudinal variation into account and should be viewed as indicative only. The default window should only be used where local

information on the growing season is not available, with the start and end of the growing season clearly defined from measurements, the latitude model or phenological models.

(Semi-)natural vegetation

AOT40-based critical levels for (semi-)natural vegetation are applicable to all (semi-)natural vegetation. Two AOT40-based critical levels have been defined based on a limited number of sensitive species: one for communities dominated by annual, and one for communities dominated by perennial species (Table 3.17).

Table 3.17: Summary of AOT40-based critical levels for vegetation.

Vegetation type	Effect (% reduction at critical level)	Critical level (ppm h)	Accumulation period	Reference
Crops				
Agricultural	Grain yield (5%; based on wheat)	3	3 months	Mills et al, 2007
Horticultural	Fruit yield (5%; based on tomato)	8	3 months	González-Fernández et al., 2014
Trees				
	Total biomass (5%; based on beech and birch)	5	Growing season (default: 6 months)	Karlsson et al., 2003, 2007
(Semi-)natural vegetation				
Dominated by annuals	Above ground biomass (10%)	3	3 months (or growing season, if shorter)	Ashmore & Davidson, 1996; Fuhrer et al., 2003
Dominated by perennials	Effects on total above-ground or below-ground biomass and/or on the cover of individual species and/or on accelerated senescence of dominant species (10%)	5	6 months	UNECE, 2006

3.4 References

Ainsworth, E. A., 2016. Understanding and improving global crop response to ozone pollution. The Plant Journal. doi: 10.1111/tpj.13298.

Ainsworth, E.A., Yendrek, C.R., Sitch, S., Collins, W.J., Emberson, L.D., 2012. The effects of tropospheric ozone on net primary productivity and implications for climate change. Annual Review of Plant Biology 63, 637-661.

Aranda, I., Gil L., Pardos, J.A., 2005. Seasonal changes in apparent hydraulic conductance and their implications for water use of European beech (*Fagus sylvatica* L.) and sessile oak [*Quercus petraea* (Matt. Liebl)] in South Europe. Plant Ecology 179, 155-167.

Ashmore, M.R., Davison, A.W., 1996. Towards a critical level of ozone for natural vegetation. In: Kärenlampi, L. & Skärby, L., (Eds.). Critical levels for ozone in Europe: testing and finalising the concepts. UNECE Workshop Report. University of Kuopio, Department of Ecology and Environmental Science, pp. 58-71.

Ashmore, M.R., Wilson, R.B. (Eds.), 1993. Critical levels of Air Pollutants for Europe. Background Papers prepared for the ECE Workshop on critical levels, Egham, UK, 23-26 March 1992.

Bassin, S., Kach, D., Valsangiacomo, A., Mayer, J., Oberholzer, H.-R., Volk, M., Fuhrer, J., 2015. Elevated ozone and nitrogen deposition affect nitrogen pools of subalpine grassland. Environmental Pollution 201, 67-74.

Bassin, S., Volk, M., Fuhrer, J., 2007. Factors affecting the ozone sensitivity of temperate European grasslands: An overview. Environmental Pollution 146, 678-691.

Bassin, S., Volk, M., Fuhrer, J., 2013. Species composition of subalpine grassland is sensitive to nitrogen deposition, but not to ozone, after seven years of treatment. Ecosystems 16, 1105-1117.

Battilani, A., Prieto, H., Argerich, C., Campillo, C., Cantore, V., 2012. Tomato. In: Steduto, P., Hsiao, T., Fereres, E., Raes D. (Eds.) Crop yield response to water. FAO irrigation and drainage paper 66. Food and Agriculture Organization of the United Nations, Rome, pp 192-198.

Bergmann, E., Bender, J., Weigel, H.-J., 2015. Assessment of the impacts of ozone on biodiversity in terrestrial ecosystems: Literature review and analysis of methods and uncertainties in current risk assessment approaches. Part II: Literature review of the current state of knowledge on the impact of ozone on biodiversity in terrestrial ecosystems. Umwelt Bundesamt TEXTE 71/2015, Dessau-Roßlau, Germany. ISSN 1862-4804.

Braun, S., Schindler, C., Rihm, B., 2014. Growth losses in Swiss forests caused by ozone: Epidemiological data analysis of stem increment of *Fagus sylvatica* L. and *Pica abies* Karst. Environmental Pollution 192, 129-138.

Büker, P., Feng, Z., Uddling, J., Briolat, A., Alonso, R., Braun, S., Elvira, S., Gerosa, G., Karlsson, P.E., Le Thiec, D., Marzuoli, R., Mills, G., Oksanen, E., Wieser, G., Wilkinson, M., Emberson, L.D., 2015. New flux based dose–response relationships for ozone for European forest tree species. Environmental Pollution 206:163-174.

Büker, P., Morrissey, T., Briolat, A., Falk, R., Simpson, D., Tuovinen, J.-P., Alonso, R., Barth, S., Baumgarten, M., Grulke, N., Karlsson, P.E., King, J., Lagergren, F., Matyssek, R., Nunn, A., Ogaya, R., Peñuelas, J., Rhea, L., Schaub, M., Uddling, J., Werner, W., Emberson, L.D., 2012. DO3SE modelling of soil moisture to determine ozone flux to forest trees. Atmospheric Chemistry and Physics 12, 5537-5562.

Calatayud, V., Cerveró, J., Calvo, E., García-Breijo, F.J., Reig-Armiñana, J., Sanz, M.J., 2011. Responses of evergreen and deciduous Quercus species to enhanced levels. Environmental Pollution 159, 55-63.

Campbell, G.S., Norman, J.M., 2000. An introduction to environmental biosphysics (2nd edition). Springer, USA, pp. 286.

CLRTAP, 2017. Mapping critical levels for vegetation, Chapter 3 of Manual on methodologies and criteria for modelling and mapping critical loads and levels and air pollution effects, risks and trends. UNECE Convention on Long-range Transboundary Air Pollution.

Damesin, C., Rambal, S., 1995. Field study of leaf photosynthetic performance by a Mediterranean deciduous oak tree (Quercus pubescens) during a severe summer drought. New Phytologist 131, 159-167.

Danielsson, H., Pihl Karlsson, G., Karlsson, P. E., Pleijel, H., 2003. Ozone uptake modelling and flux-response relationships – assessments of ozone-induced yield loss in spring wheat. Atmospheric Environment 37, 475-485.

Di Gegorio, A., Jansen, L.J.M., 2000. Land cover classification system (LCCS): Classification concept and user manual. FAO, Rome, Italy.

Duchemin, B., Goubier, J., Courrier, G., 1999. Monitoring phenological key stages and cycle duration of temperate deciduous forest ecosystems with NOAA/AVHRR data. Remote Sensing of Environment 67, 68-82.

EEA, 2016. Biogeographical regions in Europe. http://www.eea.europa.eu/data-and-maps/data/biogeographical-regions-europe-3

Emberson, L.D., Ashmore, M.R., Cambridge, H.M., Simpson, D., Tuovinen, J.-P., 2000a. Modelling stomatal ozone flux across Europe. Environmental Pollution 109, 403-413.

Emberson, L.D., Ashmore, M.R., Simpson, D., Tuovinen, J.-P., Cambridge, H.M., 2001. Modelling and mapping ozone deposition in Europe. Water, Air and Soil Pollution 130, 577-582.

Emberson, L.D., Büker, P., Ashmore, M.R., 2007. Assessing the risk caused by ground level ozone to European forest trees: A case study in pine, beech and oak across different climate regions. Environmental Pollution 147, 454-466.

Emberson, L. D., Büker, P, Ashmore, M.R., Mills, G., Jackson, L.S., Agrawal, M., Atikuzzaman, M.D., Cinderby, S., Enghardt, M., Jamir, C., Kobayashi, K., Oanh, T.T.K., Quadir, Q.F., Wahid, A., 2009. A comparison of North American and Asian exposure–response data for ozone effects on crop yields. Atmospheric Environment 43, 1945-1953.

Emberson, L.D., Wieser, G., Ashmore, M.R., 2000b. Modelling of stomatal conductance and ozone flux of Norway spruce: comparison with field data. Environmental Pollution 109, 393-402.

Feng, Z., Hu, E., Wang, X., Jiang, L., Liu, X., 2015. Ground-level O3 pollution and its impacts on food crops in China: A review. Environmental Pollution 199, 42-48.

Franzaring, J., Kösler, J., 2023. Review of internationally proposed critical levels for ammonia - proceedings of an Expert Workshop held in Dessau and online on 28/29 March 2022. German Environment Agency. Dessau-Roßlau.

Frati L., Santoni S., Nicolardi V., Gaggi C., Brunialti G., Guttova A., Gaudino S., Pati A., Pirintsos S.A., Loppi S., 2007. Lichen biomonitoring of ammonia emission and nitrogen deposition around a pig stockfarm. Environmental Pollution 146, 311-316.

Fuhrer, J., 1994. The critical level for ozone to protect agricultural crops – An assessment of data from European open-top chamber experiments. In: Fuhrer J. & Achermann, B., (Eds). Critical Levels for Ozone. UNECE Workshop Report, Schriftenreihe der FAC Berne-Liebefeld, pp. 42-57.

Fuhrer, J., Ashmore, M.R., Mills, G., Hayes, F., Davison, A.W., 2003. Critical levels for semi-natural vegetation. In: Karlsson, P.E., Selldén, G. & Pleijel, H., (Eds). Establishing Ozone Critical Levels II. UNECE Workshop Report. IVL report B 1523. IVL Swedish Environmental Research Institute, Gothenburg, Sweden, pp. 183-198.

Fuhrer, J., Martin, M.V., Mills, G., Heald, C.L., Harmens, H., Hayes, F., Sharps, K., Bender, J., Ashmore, M.R., 2016. Current and future ozone risks to global terrestrial biodiversity and ecosystem processes. Ecology & Evolution 6, 8785-8799.

Gerosa, G., Finco, A., Marzuoli, R., Ferretti, M., Gottardini, E., 2012. Errors in ozone risk assessment using standard conditions for converting ozone concentrations obtained by passive samplers in mountain regions. Journal of Environmental Monitoring 14, 1703-1709.

Gimeno B. S., Bermejo V., Sanz J., De La Torre D., Elvira S., 2004a. Growth response to ozone of annual species from Mediterranean pastures. Environmental Pollution, 132, 297-306.

Gimeno, B.S. Bermejo, V., Sanz, J., De la Torre, D., Gil, J.M., 2004b. Assessment of the effects of ozone exposure and plant competition on the reproductive ability of three therophytic clover species from Iberian pastures. Atmospheric Environment 38, 2295-2303.

González-Fernández, I., Bermejo, V., Elvira, S., de la Torre, D., González, A., Navarrete, L., Sanz, J., Calvete, H., Garcia-Gomez, H., Lopez, A., Serra, J., Lafarga, A., Armesto, A.P., Calvo, A., Alonso, R., 2013. Modelling ozone stomatal flux of wheat under mediterranean conditions. Atmospheric Environment 67, 149-160.

González-Fernández, I., Calvo, E., Gerosa, G., Bermejo, V., Marzuoli, R., Calatayud, V., Alonso, R., 2014. Setting ozone critical levels for protecting horticultural Mediterranean crops: Case study of tomato. Environmental Pollution 185, 178-187.

Gottardini, E., Calatayud, V., Ferretti, M., Haeni, M., Schaub, M., 2016. Spatial and temporal distribution of ozone symptoms across Europe from 2002 to 2014. In: Michel, A., Seidling, W. (Eds.). Forest condition in Europe: 2016 technical report of ICP Forests. BFW-Dokumentation 23/2016. Vienna: BFW Austrian Research Centre for Forests, pp. 73-82.

Grassi, G., Magnani, F., 2005. Stomatal, mesophyll conductance and biochemical limitations to photosynthesis as affected by drought and leaf ontogeny in ash and oak trees. Plant, Cell and Environment 28, 834-849.

Grünhage, L., Pleijel, H., Mills, G., Bender, J., Danielsson, H., Lehmann, Y., Castell, J.-F., Bethenod, O., 2012. Updated stomatal flux and flux-effect models for wheat for quantifying effects of ozone on grain yield, grain mass and protein yield. Environmental Pollution 165, 147-157.

Harmens, H., G. Mills (Eds.), 2012. Ozone pollution: Impacts on carbon sequestration in Europe. Centre for Ecology & Hydrogogy, Bangor, UK. ISBN: 978-1-906698-31-7.

Hayes, F., Jones, M.L.M., Mills, G. & Ashmore, M., 2007. Meta-analysis of the relative sensitivity of semi-natural vegetation species to ozone. Environmental Pollution 146, 754-762.

Hayes, F., Mills, G., Harmens, H., Wyness, K., 2011. Within season and carry-over effects following exposure of grassland species mixtures to increasing background ozone. Environmental Pollution 159, 2420-2426.

Hayes, F., Wagg, S., Mills, G., Wilkinson, S., Davies, W., 2012. Ozone effects in a drier climate: implications for stomatal fluxes of reduced stomatal sensitivity to soil drying in a typical grassland species. Global Change Biology 18, 948-959.

Hewitt, D.K.L., Mills, G., Hayes, F., Wilkinson, S., Davies, W., 2014. Highlighting the threat from current and near-future ozone pollution to clover in pasture. Environmental Pollution 189, 111-117.

Jarvis, P.G., 1976. The interpretation of the variations in leaf water potential and stomatal conductance found in canopies in the field, Philos. Trans. R. Soc. Lond., B 273, 593-610.

Karlsson, P.E., Uddling, J., Braun, S., Broadmeadow, M., Elvira, S., Gimeno, B.S., Le Thiec, D., Oksanen, E., Vandermeiren, K., Wilkinson, M., Emberson, L., 2003. new critical levels for ozone impact on trees based on AOT40 and leaf cumulated uptake of ozone. In: Karlsson, P.E., Selldén, G., Pleijel, H., (Eds.). Establishing Ozone Critical Levels II. UNECE Workshop Report. IVL report B 1523.

Karlsson, P.E., Braun, S., Broadmeadow, M., Elvira, S., Emberson, L., Gimeno, B.S., Le Thiec, D., Novak, K., Oksanen, E., Schaub, M., Uddling, J. Wilkinson, M., 2007. Risk assessments for forest trees - the performance of the ozone flux versus the AOT concepts. Environmental Pollution 146, 608-616.

Leith I.D., van Dijk N., Pitcairn C.E.R., Wolseley P.A., Whitfield C.P., Sutton M.A., 2005. Biomonitoring methods for assessing the impacts of nitrogen pollution: refinement and testing, JNCC Report No. 386, JNCC, Peterborough, pp. 290.

Matyssek, R., Wieser, G., Calfapietra, C., De Vries, W., Dizengremel, P., Ernst, D., Jolivet, Y., Mikkelsen, T.N., Mohren, G.M.J., Le Thiec, D., Tuovinen, J.-P., Weatherall, A., Paoletti, E., 2012. Forests under climate change and air pollution: Gaps in understanding and future directions for research. Environmental Pollution, 160, 57-65.

Marzuoli, R., Monga, R., Finco, A., Gerosa, G., 2016. Biomass and physiological responses of Quercus robur (L.) young trees during 2 years of treatments with different levels of ozone and nitrogen wet deposition. Trees 30, 1995-2010.

Massman, W.J., 1998. A review of the molecular diffusivities of H_2O, CO_2, CH_4, CO, O_3, SO_2, NH_3, N_2O, NO, and NO_2 in air, O_2 and N_2 near STP. Atmospheric Environment 32, 1111-1127.

McNaughton, K.G., Van der Hurk, B.J.J.M., 1995. 'Lagrangian' revision of the resistors in the two-layer model for calculating the energy budget of a plant canopy. Boundary Layer Meteorology 74, 261-288.

Mediavilla, S., Escudero, A.E., 2003. Stomatal responses to drought at a Mediterranean site: a comparative study of co-occurring woody species differing in leaf longevity. Tree Physiology 23, 987-996.

Mills, G.E., Ball, G.R., 1998. Annual Progress Report for the ICP-Crops (September 1997-August 1998). Centre for Ecology & Hydrology, Bangor, UK.

Mills, G., Buse, A., Gimeno, B., Bemejo, V., Holland, M., Emberson, L. & Plejel, H., 2007. A synthesis of AOT40-based response functions and critical levels of ozone for agricultural and horticultural crops. Atmospheric Environment 41, 2630-2643.

Mills, G., Harmens, H. (Eds.), 2011. Ozone pollution: A hidden threat to food security. Centre for Ecology & Hydrogogy, Bangor, UK. ISBN: 978-1-906698-27-0.

Mills, G., Hayes, F., Simpson, D., Emberson, L., Norris, D., Harmens, H., Büker, P., 2011a. Evidence of widespread effects of ozone on crops and (semi-)natural vegetation in Europe (1990–2006) in relation to AOT40- and flux-based risk maps. Global Change Biology 17, 592-613.

Mills, G., Pleijel, H., Braun, S., Büker, P., Bermejo, V., Calvo, E., Danielsson, H., Emberson, L., Fernandez, I.G., Grunhage, L., Harmens, H., Hayes, F., Karlsson, P.E., Simpson, D., 2011b. New stomatal flux-based critical levels for ozone effects on vegetation. Atmospheric Environment 45, 5064-5068.

Mills, G., Wagg, S., Harmens, H. (Eds.), 2013. Ozone Pollution: Impacts on ecosystem services and biodiversity. Centre for Ecology & Hydrogogy, Bangor, UK. ISBN No. 978-1-906698-39-3.

Payne, R. J., Stevens, C. J. Dise, N.B., Gowing, D.J., Pilkington, M.G., Phoenix, G.K., Emmett, B.A., Ashmore, M.R., 2011. Impacts of atmospheric pollution on the plant communities of British acid grasslands. Environmental Pollution 159, 2602-2608.

Peterson, R.F., 1965. Wheat: Botany, cultivation, and utilization. Leonard Hill Books, London.

Pinho P., Branquinho C., Cruz C., Tang S.Y., Dias T., Rosa A.P., Máguas C., Louçãoa M.A.M., Sutton M.A., 2009. Assessment of critical levels of atmospherically ammonia for lichen diversity in cork-oak woodland, Portugal. In: Sutton M.A., Baker S., Reis S., (Eds.), Atmospheric Ammonia - Detecting emission changes and environmental impacts. Springer, Berlin, 109-119.

Pitcairn C.E.R., Leith I.D., Sheppard L.J., van Dijk N., Tang Y.S., Wolseley P.A., James P., Sutton M.A., 2004. Field intercomparison of different bio-indicator methods to assess the effects of atmospheric nitrogen deposition, in: Sutton M.A., Pitcairn C.E.R., Whitfield C.P. (Ed.), Bioindicator and biomonitoring methods for assessing the effects of atmospheric nitorgen on statutory nature conservation sites, JNCC Report 356, pp. 168-177.

Pleijel, H., 2011. Reduced ozone by air filtration consistently improved grain yield in wheat. Environmental Pollution 159, 897-902.

Pleijel, H., Danielsson, H., Emberson, L., Ashmore, M., Mills, G., 2007. Ozone risk assessment for agricultural crops in Europe: Further development of stomatal flux and flux–response relationships for European wheat and potato. Atmospheric Environment 4, 3022-3040.

Pleijel, H., Danielsson, H., Vandermeiren, K., Blum, C., Colls, J., Ojanperä, K., 2002. Stomatal conductance and ozone exposure in relation to potato tuber yield – results from the European CHIP programme. European Journal of Agronomy 17, 303-317.

Rihm B., Urech M., Peter K., 2009. Mapping ammonia emissions and concentrations for Switzerland – Effects on lichen vegetation. In: Sutton M.A., Baker S., Reis S., (Eds.), Atmospheric Ammonia - Detecting emission changes and environmental impacts. Springer, Berlin, pp. 87-92.

Sanz, J., Bermejo, V., Gimeno, B.S., Elvira, S., Alonso, R. 2007. Ozone sensitivity of the Mediterranean terophyte *Trifolium striatum* is modulated by soil nitrogen content. Atmospheric Environment 41, 8952-8962.

Sanz, J., González-Fernández, I., Calvete-Sogo, H., Lin, J.S., Alonso, R., Muntifering, R., Bermejo, V., 2014. Ozone and nitrogen effects on yield and nutritive quality of the annual legume *Trifolium cherleri*. Atmospheric Environment 94, 765-772.

Sanz, J., González-Fernández, I., Elvira, S., Muntifering, R., Alonso, R., Bermejo-Bermejo, V., 2016. Setting ozone critical levels for annual Mediterranean pasture species: Combined analysis of open-top chamber experiments. Science of the Total Environment 571, 670-679.

Sanz, J., Muntifering, R.B., Gimeno, B.S., Bermejo, V., Elvira, S., 2005. Ozone and increased nitrogen supply effects on the yield and nutritive quality of *Trifolium subterraneum*. Atmospheric Environment 39, 5899-5907.

Sheppard L.J., Leith I.D., Crossley A., van Dijk N., Fowler D., Sutton M.A., 2009. Long-term cumulative exposure exacerbates the effects of atmospheric ammonia on an ombrotrophic bog: Implications for Critical Levels. In: Sutton M.A., Baker S., Reis S., (Eds.), Atmospheric Ammonia - Detecting emission changes and environmental impacts. Springer, Berlin, 49-58.

Simpson, D., Ashmore, M.R., Emberson, L., Tuovinen, J.P., 2007. A comparison of two different approaches for mapping potential ozone damage to vegetation. A model study. Environmental Pollution 146, 715-725.

Simpson, D., Benedictow, A., Berge, H., Bergström, R., Emberson, L.D., Fagerli, H., Flechard, C.R., Hayman, G.D., Gauss, M., Jonson, J.E., Jenkin, M.E., Nýıri, A., Richter, C., Semeena, V.S., Tsyro, S., Tuovinen, J.-P., Valdebenito, Á., Wind, P., 2012. The EMEP MSC-W chemical transport model – technical description. Atmospheric Chemistry and Physics 12, 7825-7865.

Sutton M.A., Wolseley P.A., Leith I.D., van Dijk N., Tang Y.S., James P.W., Theobald M.R., Whitfield C.P., 2009. Estimation of the ammonia critical level for epiphytic lichens based on observations at farm, landscape and national scales. In: Sutton M.A., Baker S., Reis S., (Eds.), Atmospheric Ammonia - Detecting emission changes and environmental impacts. Springer, Berlin, pp. 71-86.

Temple, P.J., Bytnerowicz, A.J., Fenn, M.E., Poth, M.A., 2005. Air pollution impacts in the mixed conifer forests of Southern California. In: Kus, B.E., Beyers, J.L. (Eds.). Planning for biodiversity: Bringing research and management together. USDA Forest Service Gen. Tech. Rep. PSW-GTR-195.

Uddling, J., Pleijel, H., Karlsson, P.E., 2004. Modelling leaf diffusive conductance in juvenile silver birch, *Betula pendula*. Trees 18, 686-695.

UNECE, 2006. Report on the workshop on critical levels of ozone: further applying and developing the flux-based concept. ECE/EB.AIR/WG.1/2006/11.

UNECE, 2007. Report of workshop on atmospheric ammonia:detecting emission changes and environmental impacts. ECE/EB.AIR/WG.5/2007/3.

UNECE, 1996. Manual on methodologies and criteria for mapping critical levels/loads and geographical areas where they are exceeded. Texte 71/96, Umweltbundesamt, Berlin, Germany.

U.S. Environmental Protection Agency, 2014. Welfare risk and exposure assessment for ozone. EPA-452/R-14-005a, North Carolina, USA, pp. 7.1-7.65.

van der Eerden, L.J.M, Dueck, T.A., Posthumus, A.C., Tonneijck, A.E.G., 1994. Assessment of critical levels for air pollutant effects on vegetation: some considerations and a case study on NH3. In: Ashmore M.R., Wilson R.B.

(eds.) Critical Levels of Air Pollutants for Europe. Proceedings of the UNECE Workshop on Critical Levels, Egham, pp. 55–63.

Volk, M., Wolff, V., Bassin, S., Ammann, C., Fuhrer, J., 2014. High tolerance of subalpine grassland to long-term ozone exposure is independent of N input and climatic drivers, Environmental Pollution 189, 161-168.

Wagg, S., Mills, G., Hayes, F., Wilkinson, S., Cooper, D., Davies, W.J., 2012. Reduced soil water availability did not protect two competing grassland species from the negative effects of increasing background ozone. Environmental Pollution 165, 91-99.

WHO, 2000. Air Quality Guidelines for Europe. WHO Regional Publications, No. 91, World Health Organisation, Copenhagen. http://www.euro.who.int/en/publications

Wittig, V.E., Ainsworth, E.A., Naidu, S.L., Karnosky, D.F., Long, S.P., 2009. Quantifying the impact of current and future tropospheric ozone on tree biomass, growth, physiology and biochemistry: a quantitative meta-analysis. Global Change Biology 15, 396-424.

Wolseley P.A., James P.W., Theobald M.R., Sutton M.A., 2006. Detecting changes in epiphytic lichen communities at sites affected by atmospheric ammonia from agricultural sources. Lichenologist 38, 161-176.

Wyness, K., Mills, G., Jones, L., Barnes, J.D., Jones, D.L., 2011. Enhanced nitrogen deposition exacerbates the negative effect of increasing background ozone in *Dactylis glomerata*, but not *Ranunculus acris*. Environmental Pollution 159, 2493-2499.

Zhang, X., Friedl, M.A, Schaaf, C.B., Strahler, A.H., 2004. Climate controls on vegetation phenological patterns in northern mid- and high latitudes inferred from MODIS data. Global Change Biology 10, 1133-1145.

3.5 Annexes for chapter 3

3.5.1 Annex 1: history of the development of the included critical levels

The critical level values have been set, reviewed and revised for O_3, SO_2, NO_x and NH_3 at a series of UNECE Workshops and associated Task Force meeting of the ICP Vegetation:

- Bad Harzburg (1988; UNECE, 1988)
- Bad Harzburg (1989)
- Egham (1992; Ashmore & Wilson, 1993)
- Bern (1993; Fuhrer & Achermann, 1994)
- Kuopio (1996; Kärenlampi & Skärby, 1996)
- Gerzensee (1999; Fuhrer & Achermann, 1999)
- Gothenburg (2002; Karlsson et al., 2003)
- Obergurgl (2005; Wieser & Tausz, 2006)
- Edinburgh (2006; UNECE, 2007; Sutton et al., 2009)
- Ispra (2009)
- Tervuren (23rd ICP Vegetation Task Force Meeting, 2010, UNECE 2010; Mills et al., 2011)
- Madrid (2016); preceded by preparatory meetings in Hindås (2015) and Deganwy (2016)
- Poznan (30th ICP Vegetation Task Force Meeting, 2017; UNECE, 2017)

The earliest version of this manual (UNECE, 1996) included concentration-based critical levels that used AOTX (O_3 concentrations accumulated over a threshold of X ppb) as the O_3 parameter. However, several important limitations and uncertainties have been recognised for using AOTX. In particular, the real impacts of O_3 depend on the amount of O_3 reaching the sites of damage within the leaf, whereas AOT40-based critical levels only consider the O_3 concentration at the top of the canopy.

The Gerzensee Workshop in 1999 recognised the importance of developing an alternative approach based on the flux of O_3 from the exterior of the leaf through the stomatal pores to the sites of damage (stomatal flux or Phytotoxic Ozone Dose above a threshold flux of Y nmol m^{-2} PLA s^{-1}; POD_Y). This approach required the development of mathematical models to estimate stomatal flux, primarily from knowledge of stomatal responses to environmental factors. It was agreed at the Gothenburg Workshop in 2002 that O_3 flux-effect models were sufficiently robust for the derivation of flux-based critical levels, and such critical levels should be included in this chapter for wheat, potato, and provisionally for beech and birch combined. An additional simplified flux-based "worst-case" risk assessment method for use in large-scale and integrated assessment modelling was discussed at the Obergurgl Workshop (2005) and after further revision (approved at appropriate Task Force meetings) is included here.

At the Hindås meeting (2015), Deganwy meeting (2016), Madrid Workshop (2016), and subsequent 30th Task Force meeting of the ICP Vegetation (2017) in Poznan, the methodology, flux-effect relationships and critical levels were reviewed and revised where needed and added for new (groups of) species or vegetation types. The current version of this chapter incorporates all of these new/revised flux-based critical levels together with the updated AOT40-based critical levels (no changed made). Currently, 16 species or groups of species-specific vs (based on POD_YSPEC) and 5 vegetation type-specific critical levels (based on POD_YIAM) are included.

The critical levels and risk assessment methods for vegetation described in this chapter were prepared by leading European experts from available knowledge on impacts gaseous air pollutants on vegetation, and thus represent the current "state of knowledge".

3.5.1.1 References

Ashmore, M.R., Wilson, R.B. (Eds.), 1993. Critical levels of Air Pollutants for Europe. Background Papers prepared for the ECE Workshop on critical levels, Egham, UK, 23-26 March 1992.

Fuhrer, J., Achermann, B. (Eds,), 1994. Critical Levels for Ozone. UNECE Workshop Report, Schriftenreihe der FAC Berne-Liebefeld.

Fuhrer, J., Achermann, B. (Eds), 1999. Critical Levels for Ozone – Level II. Swiss Agency for the Environment, Forests and Landscape, Berne. Environmental Documentation No. 115.

Kärenlampi, L., Skärby, L. (Eds), (1996. Critical levels for ozone in Europe: testing and finalising the concepts. UNECE Workshop Report. University of Kuopio, Department of Ecology and Environmental Science.

Karlsson, P.E., Selldén, G., Pleijel, H. (Eds), 2003. Establishing Ozone Critical Levels II. UNECE Workshop Report. IVL report B 1523. IVL Swedish Environmental Research Institute, Gothenburg, Sweden.

Mills, G., Pleijel, H., Braun, S., Büker, P., Bermejo, V., Calvo, E., Danielsson, H., Emberson, L., Fernandez, I.G., Grunhage, L., Harmens, H., Hayes, F., Karlsson, P.E., Simpson, D., 2011. New stomatal flux-based critical levels for ozone effects on vegetation. Atmospheric Environment 45, 5064-5068.

Sutton, M.A., Reis, S., Baker, S.M.H., 2009. Atmospheric ammonia - Detecting emission changes and environmental impacts. Springer Verlag, Berlin.

UNECE, 1988. Final Draft Report of the Critical Levels Workshop, Bad Harzburg, Germany, 14-18 March 1988.

UNECE, 2007. Report of workshop on atmospheric ammonia: detecting emission changes and environmental impacts. ECE/EB.AIR/WG.5/2007/3.

UNECE, 2010. Flux-based assessment of ozone effects for air pollution policy. Technical report from the ozone workshop in Ispra, 9 – 12 November, 2009. ECE/EB.AIR/WG.1/2010/13.

UNECE, 2017. Effects of air pollution on natural vegetation and crops. Technical report from the Programme Coordinating Centre of the ICP Vegetation. ECE/EB.AIR/GE.1/2016/14 - ECE/EB.AIR/WG.1/2016/7.

Wieser, G., Tausz, M. (Eds), 2006. Proceedings of the workshop: Critical levels of ozone: further applying and developing the flux-based concept, Obergurgl, November, 2005.

3.5.2 Annex 2: terminology

Table A1: Terminology for calculating O_3 critical levels for vegetation.

Term	Abbreviation [Units]	Explanation
Terminology for flux-based critical levels		
Projected leaf area	PLA [m^2]	The projected leaf area is the total area of the sides of the leaves that are projected towards the sun. PLA is in contrast to the total leaf area, which considers both sides of the leaves. For horizontal leaves the total leaf area is simply 2*PLA.
Stomatal flux of O_3	F_{st} [nmol m^{-2} PLA s^{-1}]	Instantaneous flux of O_3 through the stomatal pores per unit projected leaf area (PLA). F_{st} can be defined for any part of the plant, or the whole leaf area of the plant, but for this manual, F_{st} refers specifically to the sunlit leaves at the top of the canopy. F_{st} is normally calculated from hourly mean values and is regarded here as the hourly mean flux of O_3 into the stomata.
Stomatal flux of O_3 above a flux threshold of Y nmol m^{-2} PLA s^{-1}	$F_{st}Y$ [nmol m^{-2} PLA s^{-1}]	Instantaneous flux of O_3 above a flux threshold of Y nmol m^{-2} PLA s^{-1}, through the stomatal pores per unit projected leaf area. $F_{st}Y$ can be defined for any part of the plant, or the whole leaf area of the plant, but for this manual $F_{st}Y$ refers specifically to the sunlit leaves at the top of the canopy. $F_{st}Y$ is normally calculated from hourly mean values and is regarded here as the hourly mean flux of O_3 through the stomata.
Phytotoxic O_3 dose above a flux threshold of Y nmol m^{-2} PLA s^{-1}	POD_Y [mmol m^{-2} PLA]	Phytotoxic O_3 dose (POD) is the accumulated flux above a flux threshold of Y nmol m^{-2} PLA s^{-1}, accumulated over a stated time period during daylight hours. Similar in mathematical concept to AOT40.
Phytotoxic O_3 dose calculated for a specific plant species or group of plant species	POD_YSPEC [mmol m^{-2} PLA]	Phytotoxic O_3 dose above a flux threshold of Y nmol m^{-2} PLA s^{-1} for a specific plant species or group of plant species (POD_YSPEC), accumulated over a stated time period during daylight hours.
Phytotoxic O_3 dose calculated for a for a vegetation type	POD_YIAM [mmol m^{-2} PLA]	Phytotoxic O_3 dose above a flux threshold of Y nmol m^{-2} PLA s^{-1} for a vegetation type for application in large-scale modelling such as integrated assessment modelling (POD_YIAM), accumulated over a stated time period during daylight hours.

Term	Abbreviation [Units]	Explanation
Reference POD_Y at constant 10 ppb O_3, representing average 'pre-industrial' O_3 concentration	Ref10 POD_Y [mmol m^{-2} PLA]	Phytotoxic O_3 dose above a flux threshold of Y nmol m^{-2} PLA s^{-1} calculated at a constant O_3 concentration of 10 ppb, accumulated over a stated time period during daylight hours.
Flux-based critical level of O_3	Flux-based CL [mmol m^{-2} PLA]	Phytotoxic O_3 dose above a flux threshold of Y nmol m^{-2} PLA s^{-1} (POD_Y), over a stated time period during daylight hours, above which direct adverse effects may occur on sensitive vegetation according to present knowledge.
Terminology for concentration-based critical levels		
Concentration accumulated over a threshold O_3 concentration of 40 ppb	AOT40 [ppm h]	The sum of the differences between the hourly mean O_3 concentration (in ppb) and 40 ppb when the concentration exceeds 40 ppb during daylight hours[1)], accumulated over a stated time period. Units of ppb and ppm are parts per billion (nmol mol^{-1}) and parts per million (µmol mol^{-1}) respectively, calculated on a volume/volume basis.
Concentration-based critical level of O_3	Concentration-based CL [ppm h]	AOT40 over a stated time period, above which direct adverse effects on sensitive vegetation may occur according to present knowledge.

3.5.3 Annex 3: Data sources and references for flux-effect relationships

3.5.3.1 Crops

Table A2 provides a summary of the data sources and O_3 flux-effect relationships for crops as described in Section 3.3.5.2.

Table A2: Date sources and response functions for agricultural crops.

Crop	Wheat	Wheat	Wheat	Potato	Tomato	Tomato
Effect parameter	Grain yield	1000 grain weight	Protein yield	Tuber yield	Fruit yield	Fruit quality
% reduction for critical level	5%	5%	5%	5%	5%	5%
Critical level (POD_6SPEC, mmol m^{-2})	1.3	1.5	2.0	3.8	2.0	3.8
Biogeographical region*	A, B, C, M (S, P)	A, B, C, M (S, P)	A, B, C, M (S, P)	A, B, C (M, S, P)	M (A, B, C, S, P)	M (A, B, C, S, P)
Countries involved in experiments	Belgium, Finland, Italy, Sweden	Belgium, Finland, Sweden	Belgium, Finland, Sweden	Belgium, Finland, Germany, Sweden	Italy, Spain	Italy, Spain

Crop	Wheat	Wheat	Wheat	Potato	Tomato	Tomato
Number of data points	36	33	33	17	17	17
Number of cultivars	5	4	4	1	5 (sensitive cultivars only)	5 (sensitive cultivars only)
Data sources	Pleijel et al., 2007	Piikki et al., 2008	Piikki et al., 2008	Pleijel et al., 2007	González-Fernández et al., 2014	González-Fernández et al., 2014
Time period	200 °C days before anthesis to 700 °C days after anthesis	200 °C days before anthesis to 700 °C days after anthesis	200 °C days before anthesis to 700 °C days after anthesis	1130 °C days starting at plant emergence	250 to 1500 °C days starting at planting in the field (at 4th true leaf stage)	250 to 1500 °C days starting at planting in the field (at 4th true leaf stage)
Response function	RY(%) = 100.3 - 3.85 x POD_6SPEC	RY(%) = 100.6 - 3.35 x POD_6SPEC	RY(%) = 101.1 - 2.54 x POD_6SPEC	RY(%) = 101.4 - 1.34 x POD_6SPEC	RY(%) = 99.3 - 2.53 x POD_6SPEC	RY(%) = 99.7 - 1.30 x POD_6SPEC
Adjusted R2	0.83	0.71	0.61	0.80	0.61	0.55
P value	<0.001	<0.001	<0.001	<0.001	<0.001	<0.001
Data curator (E-mail)	Håkan Pleijel (hakan.pleijel@bioenv.gu.se)				Ignacio González-Fernández (ignacio.gonzalez@ciemat.es)	

* A = Atlantic; B = Boreal; C, = Continental, M = Mediterranean, S = Steppic, P = Pannonian. In brackets: not derived for those regions but could be applied there too.

3.5.3.2 Forest trees

Table A3 provides a summary of the data sources and O_3 flux-effect relationships for forest trees as described in section 3.3.5.3.

Table A3: Data sources and response functions for forest trees.

Tree species	Beech and birch	Norway spruce	Deciduous oaks	Deciduous oaks	Evergreens
Effect parameter	Whole tree biomass	Whole tree biomass	Whole tree biomass	Root biomass	Above-ground biomass
% reduction for critical level	4% (annual)	2% (annual)	4% (annual)	4% (annual)	4% (annual)
Critical level (POD_1SPEC, mmol m^{-2})	5.2	9.2	14.0	10.3	47.3
Biogeographical region*	B, C (A, S, P)	B, C (A, S, P)	M	M	M

Tree species	Beech and birch	Norway spruce	Deciduous oaks	Deciduous oaks	Evergreens
Countries involved in experiments	Finland, Sweden, Switzerland	Sweden, Switzerland	Spain, Italy	Spain, Italy	Spain
Number of data points	34 (9 different experiments)	29 (8 different experiments)	10 (2 different experiments)	10 (2 different experiments)	22 (4 different experiments)
Years of experiments	1-5	1-4	2	2	1.5-3
Data sources	Braun and Flückiger, 1995; Büker et al., 2015; Karlsson et al., 2003; Oksanen, 2003; Uddling et al., 2004	Braun and Flückiger, 1995; Büker et al., 2015; Karlsson et al, 2004	Calatayud et al. 2011; Marzuoli et al. 2016 and in preparation	Calatayud et al. 2011; Marzuoli et al. 2016 and in preparation	Alonso et al., 2014 and in preparation; Barnes et al., 2000; Calatayud et al., 2011; Inclán et al., 2005; Ribas et al., 2005
Time period	Growing season	Growing season	Growing season	Growing season	Growing season
Response function	RB(%) = 100.2 – 0.93 x POD_1SPEC	RB(%) = 99.8 – 0.22 x POD_1SPEC	RB(%) = 100.3 – 0.32 x POD_1SPEC	RB(%) = 100.6 – 0.45 x POD_1SPEC	RB(%) = 99.8 – 0.09 x POD_1SPEC
Adjusted R^2	0.67	0.31	0.41	0.48	0.42
P value	<0.001	<0.001	0.027	0.016	<0.001
Data curator (e-mail)	Patrick Büker (patrick.bueker@york.ac.uk)		Riccardo Marzuoli (riccardo.marzuoli@unicatt.it)		Rocio Alonso (rocio.alonso @ciemat.es)

* A = Atlantic; B = Boreal; C, = Continental, M = Mediterranean, S = Steppic, P = Pannonian. In brackets: not derived for those regions but could be applied there too.

3.5.3.3 (Semi-)natural vegetation

Table A4 provides a summary of the data sources and O_3 flux-effect relationships for (semi-) natural vegetation as described in section 3.3.5.4.

Table A4: Data sources and response functions for (semi-)natural vegetation.

O_3-sensitive species of:	Temperate perennial grassland	Temperate perennial grassland	Temperate perennial grassland	Mediterranean annual pasture	Mediterranean annual pasture
Representative species used to derive flux-effect relationship	*Campanula rotundifolia, Trifolium pratense, Sanguisorba major, Sanguisorba*	*Campanula rotundifolia, Dactylis glomerata, Leontodon hispidus,*	*Campanula rotundifolia, Primula veris, Potentilla erecta, Scabiosa columbaria*	*Trifolium striatum, T.cherleri, T.glomeratum, T.angustifolium , T.subterraneum*	*Trifolium striatum, T. cherleri, T. subterraneu m*

O_3-sensitive species of:	**Temperate perennial grassland**	**Temperate perennial grassland**	**Temperate perennial grassland**	**Mediterranean annual pasture**	**Mediterranean annual pasture**
	officinalis, Scabiosa columbaria, Fritillaria meleagris	*Ranunculus acris*		*, Medicago minima, Biserrula pelecinus*	
Effect parameter	Above-ground biomass	Total biomass	Flower number	Above-ground biomass	Seed/flower biomass
% reduction for critical level	10%	10%	10%	10%	10%
Critical level (POD_1SPEC, mmol m^{-2})	10.2	16.2	6.6	16.9	10.8
Biogeographical regions*	A, B, C (S, P)	A, B, C (S, P)	A, B, C (S, P)	M	M
Countries involved in experiments	UK	UK	UK	Spain	Spain
Number of data points	47	53	32	51	15
Years of experiments	4	4	3	5	3
Data sources	Hayes et al., 2012; Hewitt et al., 2014; Hayes et al. unpublished	Wagg et al., 2012, Hayes et al., 2011, Wyness et al., 2011; Hayes et al., unpublished	Hayes et al., 2012; Hayes et al., 2011; Hayes et al. unpublished	Gimeno et al., 2004a; Sanz et al., 2005, 2007, 2014, 2016	Gimeno et al., 2004b; Sanz et al., 2007, 2016
Accumulation period	3 months	3 months	3 months	1.5 months	1.5 months
Time period for accumulation period	1 April to 30 Sept	1 April to 30 Sept	1 April to 30 Sept	1 February to 30 June	1 February to 30 June
Response function	RB(%) = 93.9 – 0.99 x POD_1SPEC	RB(%) = 94.7 – 0.62 x POD_1SPEC	RF(%) = 101.2 – 1.54 x POD_1SPEC	RB(%) = 97.1 – 0.85 x POD_1SPEC	RB(%) = 92.3 – 1.61 x POD_1SPEC
Adjusted R^2	0.10	0.34	0.30	0.57	0.59
P value	0.018	<0.001	<0.001	<0.001	<0.001
Data curator (e-mail)	Felicity Hayes (fhay@ceh.ac.uk)			Ignacio González-Fernández (ignacio.gonzalez@ciemat.es)	

* A = Atlantic; B = Boreal; C, = Continental, M = Mediterranean, S = Steppic, P = Pannonian. In brackets: not derived for those regions but could be applied there too.

3.5.3.4 References

Alonso, R., Elvira, S., González-Fernández, I., Calvete, H., García-Gómez, H., Bermejo, V., 2014. Drought stress does not protect *Quercus ilex* L. from ozone effects: results from a comparative study of two subspecies differing in ozone sensitivity. Plant Biology 16, 375-384.

Barnes, J.D., Gimeno, B.S., Davison, A.W., Dizengremel, P., Gerant, D., Bussotti, F., Velissariou, D., 2000. Air pollution impacts on pine forests in the Mediterranean basin. In: Ne'eman, G., Trabaud, L. (Eds.). Ecology, biogeography and management of *Pinus halepensis* and *P. Brutia* forest ecosystems in the Mediterranean basin. Leiden, The Netherlands: Backhuys Publishers, 391-404.

Braun, S., Flückiger, W., 1995. Effects of ambient ozone on seedlings of *Fagus sylvatica* L. and *Picea abies* (L.) Karst. New Phytologist 129, 33-44.

Büker, P., Feng, Z., Uddling, J., Briolat, A., Alonso, R., Braun, S., Elvira, S., Gerosa, G., Karlsson, P.E., Le Thiec, D., Marzuoli, R., Mills, G., Oksanen, E., Wieser, G., Wilkinson, M., Emberson, L.D., 2015. New flux based dose–response relationships for ozone for European forest tree species. Environmental Pollution 206, 163-174.

Calatayud, V., Cerveró, J., Calvo, E., García-Breijo, F.J., Reig-Armiñana, J., Sanz, M.J., 2011. Responses of evergreen and deciduous Quercus species to enhanced levels. Environmental Pollution 159, 55-63.

CLRTAP, 2017. Mapping critical levels for vegetation, Chapter 3 of Manual on methodologies and criteria for modelling and mapping critical loads and levels and air pollution effects, risks and trends. UNECE Convention on Long-range Transboundary Air Pollution

Gimeno B. S., Bermejo V., Sanz J., De La Torre D., Elvira S., 2004a. Growth response to ozone of annual species from Mediterranean pastures. Environmental Pollution, 132, 297-306.

Gimeno, B.S. Bermejo, V., Sanz, J., De la Torre, D., Gil, J.M., 2004b. Assessment of the effects of ozone exposure and plant competition on the reproductive ability of three therophytic clover species from Iberian pastures. Atmospheric Environment 38, 2295-2303.

González-Fernández, I., Calvo, E., Gerosa, G., Bermejo, V., Marzuoli, R., Calatayud, V., Alonso, R., 2014. Setting ozone critical levels for protecting horticultural Mediterranean crops: Case study of tomato. Environmental Pollution 185, 178-187.

Hayes, F., Mills, G., Harmens, H., Wyness, K., 2011. Within season and carry-over effects following exposure of grassland species mixtures to increasing background ozone. Environmental Pollution 159, 2420-2426.

Hayes, F., Williamson, J., Mills, G., 2012. Ozone pollution affects flower numbers and timing in a simulated BAP priority calcareous grassland community. Environmental Pollution 163, 40-47.

Hewitt, D.K.L., Mills, G., Hayes, F., Wilkinson, S., Davies, W., 2014. Highlighting the threat from current and near-future ozone pollution to clover in pasture. Environmental Pollution 189, 111-117.

Inclán, R., Gimeno, B.S., Dizengremel, P., Sánchez, M., 2005. Compensation processes of Aleppo pine (*Pinus halepensis* Mill.) to ozone exposure and drought stress. Environmental Pollution 137, 517-524.

Karlsson, P.E., Uddling, J., Braun, S., Broadmeadow, M., Elvira, S., Gimeno, B.S., Le Thiec, D., Oksanen, E., Vandermeiren, K., Wilkinson, M., Emberson, L., 2003. New Critical Levels for Ozone Impact on Trees Based on AOT40 and Leaf Cumulated Uptake of Ozone. In: Karlsson, P.E., Selldén, G., Pleijel, H., (Eds.). Establishing Ozone Critical Levels II. UNECE Workshop Report. IVL report B 1523.

Karlsson, P.E., Uddling, J., Braun, S., Broadmeadow, M., Elvira, S., Gimeno, B.S., Le Thiec, D., Oksanen, E., Vandermeiren, K., Wilkinson, M., Emberson, L., 2004. New critical levels for ozone effects on young trees based on AOT40 and simulated cumulative leaf uptake of ozone. Atmospheric Environment 38, 2283-2294.

Marzuoli, R., Monga, R., Finco, A., Gerosa, G., 2016. Biomass and physiological responses of *Quercus robur* (L.) young trees during 2 years of treatments with different levels of ozone and nitrogen wet deposition. Trees 30, 1995-2010.

Oksanen, E., 2003. Responses of selected birch (*Betula pendula* Roth) clones to ozone change over time. Plant, Cell and Environment 26, 875-886.

Piikki, K., De Temmerman, L. Ojanpera, K., Danielsson, H., Pleijel, H., 2008. The grain quality of spring wheat (*Triticum aestivum* L.) in relation to elevated ozone uptake and carbon dioxide exposure. European Journal of Agronomy 28, 245-254.

Pleijel, H., Danielsson, H., Emberson, L., Ashmore, M., Mills, G., 2007. Ozone risk assessment for agricultural crops in Europe: Further development of stomatal flux and flux–response relationships for European wheat and potato. Atmospheric Environment 4, 3022-3040.

Ribas, A., Peñuelas, J., Elvira, S., Gimeno, B.S., 2005. Ozone exposure induces the activation of leaf senescence-related processes and morphological and growth changes in seedlings of Mediterranean tree species. Environmental Pollution 134, 291-300.

Sanz, J., Bermejo, V., Gimeno, B.S., Elvira, S., Alonso, R. 2007. Ozone sensitivity of the Mediterranean terophyte *Trifolium striatum* is modulated by soil nitrogen content. Atmospheric Environment 41, 8952-8962.

Sanz, J., González-Fernández, I., Calvete-Sogo, H., Lin, J.S., Alonso, R., Muntifering, R., Bermejo, V., 2014. Ozone and nitrogen effects on yield and nutritive quality of the annual legume *Trifolium cherleri*. Atmospheric Environment 94,765-772.

Sanz, J., González-Fernández, I., Elvira, S., Muntifering, R., Alonso, R., Bermejo-Bermejo, V., 2016. Setting ozone critical levels for annual Mediterranean pasture species: Combined analysis of open-top chamber experiments. Science of the Total Environment 571, 670-679.

Sanz, J., Muntifering, R.B., Gimeno, B.S., Bermejo, V., Elvira, S., 2005. Ozone and increased nitrogen supply effects on the yield and nutritive quality of *Trifolium subterraneum*. Atmospheric Environment 39, 5899-5907.

Uddling, J., Günthardt-Goerg, M.S., Matyssek, R., Oksanen, E., Pleijel, H., Selldén, G., Karlsson, P.E., 2004. Biomass reduction of juvenile birch is more strongly related to stomatal uptake of ozone than to indices based on external exposure. Atmospheric Environment 38, 4709-4719

Wagg, S., Mills, G., Hayes, F., Wilkinson, S., Cooper, D., Davies, W.J., 2012. Reduced soil water availability did not protect two competing grassland species from the negative effects of increasing background ozone. Environmental Pollution 165, 91-99.

Wyness, K., Mills, G., Jones, L., Barnes, J.D., Jones, D.L., 2011. Enhanced nitrogen deposition exacerbates the negative effect of increasing background ozone in *Dactylis glomerata*, but not *Ranunculus acris*. Environmental Pollution 159, 2493-2499.

4 Mapping of Effects on Materials

4.1 Introduction

Please refer to this document as: CLRTAP, 2022. Mapping of effects on materials, Chapter 4 of Manual on methodologies and criteria for modelling and mapping critical loads and levels and air pollution effects, risks, and trends. UNECE Convention on Long-range Transboundary Air Pollution; accessed on [date of consultation] on Web at www.umweltbundesamt.de/en/cce-manual.

4.1.1 Aims

Atmospheric pollution is an important factor in material deterioration, including the degradation of systems used for material protection and the degradation of cultural heritage materials. Due to pollution, the lifetime of technological products is shortened. Building and other structures deteriorate more rapidly, including objects of cultural heritage that are exposed to the atmosphere. The resulting physicochemical and economic damage can be significant – not to mention the loss of unique parts of cultural heritage and the hazards that arise due to the compromised reliability of complicated technological devices. Therefore, as a result of weathering, in particular due to acidifying pollutants, a significant part of metals used in constructions and products are emitted to the biosphere with a potential hazard to the environment. Lastly, air pollution induces the soiling of glass and other materials (stone, coatings, painted surfaces etc.) that requires either a frequent potentially expensive cleaning, or maintenance operations.

This part of the manual provides methods used to assess the impact of atmospheric pollution on materials in terms of corrosion and soiling. These methods are based on studies carried out by ICP Materials since 1987. The approach initially proposed was based on results obtained after an 8-year field exposure (1987–1995, Tidblad et al., 2001). It was revised in 2005, following a multi-pollutant exposure programme (1997–2003, Kucera et al., 2007). Since then, a series of trend exposures each third year, including several materials for the evaluation of soiling effects, have been performed. These new results together with practical experiences in mapping areas of increased risk of corrosion has led to the present update, which mainly consist of new functions for soiling (4.2.3) and how they should be used for mapping (4.4) (2021).

This chapter considers the corrosive and soiling effects of gaseous SO_2, NO_x, O_3, HNO_3, particulate matter and acid rainfall in combination with climatic parameters. The chapter also aims to define procedures for mapping values of pollutants that are acceptable for buildings and materials and tolerable values for cultural and historical monuments in a way that is analogous to the methods defined elsewhere for critical levels and loads for natural ecosystems.

4.1.2 Definitions

Atmospheric deterioration of materials is a cumulative, irreversible process, which proceeds even in the absence of pollutants, which means “critical” values are not as easily defined as for some natural ecosystems. A rate of deterioration must be defined which may be considered as “acceptable” or “tolerable”, based on technical, economic, and social considerations. This approach provides the basis for mapping “acceptable areas” for corrosion and deriving areas where the acceptable pollution level/load is exceeded, in an analogous way to the maps produced for natural ecosystems. The term “acceptable” is reserved for materials used in technical constructions while “tolerable” is used in connection with degradation of cultural

heritage. Thus, in the following, “acceptable” can be replaced by “tolerable” when considering cultural heritage specifically.

Acceptable load/level. The "acceptable level or load" of pollutants for buildings and materials is the concentration or load which does not lead to an unacceptable increase in the rate of corrosion or deterioration.

Acceptable rate of corrosion or deterioration may be defined as the corrosion, which is considered "acceptable" based on technical and economic considerations and is in principle material and application dependent. The concept can, however, be simplified when developing or assessing policies within the LRTAP Convention (see 4.3.3 below).

Dose-response function. The relationship between the corrosion or deterioration rate and the levels or loads of pollutants in combination with climatic parameters.

Using the above definitions, it is possible to calculate the acceptable pollution level from the acceptable corrosion rate by using a dose-response function that relates corrosion rate to pollutant and climate exposure.

4.2 Dose-response functions

4.2.1 Introduction

Deterioration rates can be calculated using dose-response functions. The functions recommended have been derived from the field research programmes undertaken as part of the UN ECE ICP Materials Exposure Programmes and are developed primarily by considering the need of the LRTAP Convention to quantify effects of pollution. However, if other functions of the same form or of other forms are considered more suitable, then they can be used as an alternative.

This could, for example, be in particular areas where pollution is not considered the main cause of corrosion. In any case, the range of values over which the dose-response function is derived must be considered. Two sets of dose-response functions described in the following sections have been derived: functions for the SO_2 dominating situation and functions for the multi-pollutant situation. For glass soiling, only the multi-pollutant situation was considered.

4.2.2 Dose-response functions for corrosion of materials

4.2.2.1 Dose-response functions for the SO_2 dominating situation

The following equations are based on 8-year results from an exposure carried out within ICP Materials (1987–1995). They reflect the increased level of the physicochemical understanding of the corrosion mechanisms, including the synergistic effects of SO_2 and O_3 in the case of copper. The equations are valid for unsheltered exposure of materials (Tidblad et al., 2001), where r^2 denotes the explained variability and N the number of observations used in the statistical analysis.

Structural metals	r^2	N	
Weathering steel (C<0.12%, Mn 0.3-0.8%, Si 0.25-0.7%, P 0.07-0.15%, S<0.04%, Cr 0.5-1.2%, Ni 0.3-0.6%, Cu 0.3-0.55%, Al<0.01%) $ML = 34[SO_2]^{0.13} e^{\{0.020Rh + f(T)\}t^{0.33}}$ f(T) = 0.059(T-10) when T≤10°C, otherwise -0.036(T-10)	0.68	148	(4.1)
Zinc	0.84	98	(4.2)

$ML = 1.4[SO_2]^{0.22} e^{\{0.018Rh + f(T)\}t^{0.85}} + 0.029Rain[H^+]t$ f(T) = 0.062(T-10) when T≤10°C, otherwise -0.021(T-10)			
Aluminium $ML = 0.0021[SO_2]^{0.23} Rh \cdot e^{\{f(T)\}t^{1.2}} + 0.000023Rain[Cl^-]t$ f(T) = 0.031(T-10) when T≤10°C, otherwise -0.061(T-10)	0.74	106	(4.3)
Copper $ML = 0.0027\ [SO_2]^{0.32}[O_3]^{0.79} Rh \cdot e^{\{f(T)\}t^{0.78}} + 0.000023Rain[H^+]t^{0.89}$ f(T) = 0.083(T-10) when T≤10°C, otherwise -0.032(T-10)	0.73	95	(4.4)
Bronze (Cu Sn6Pb7Zn5, ISO/R 1338 (Cu 81%, Sn 5.8%, Pb 6.7%, Zn 4.5%, Ni 1.6% + trace elements) $ML = 0.026\ [SO_2]^{0.44} Rh \cdot e^{\{f(T)\}t^{0.86}} + 0.029Rain[H^+]t^{0.76} + 0.00043Rain[Cl^-]t^{0.76}$ f(T) = 0.060(T-11) when T≤11°C, otherwise -0.067(T-11)	0.81	144	(4.5)
Stone materials	**r^2**	**N**	
Limestone $R = 2.7\ [SO_2]^{0.48} e^{\{-0.18T\}t^{0.96}} + 0.019Rain[H^+]t^{0.96}$	0.88	100	(4.6)
Sandstone (White Mansfield dolomitic sandstone) $R = 2.7\ [SO_2]^{0.48} e^{\{-0.18T\}t^{0.96}} + 0.019Rain[H^+]t^{0.96}$ f(T) = 0 when T≤10°C, otherwise -0.013(T-10)	0.86	101	(4.7)
Paint coatings	**r^2**	**N**	
Coil coated galvanised steel with alkyd melamine $L = \left[\frac{5}{0.084\ [SO_2] + 0.015Rh + f(T) + 0.00082Rain}\right]^{1/0.43}$ f(T) = 0.040(T-10) when T≤10°C, otherwise -0.064(T-10)	0.73	138	(4.8)
Steel panels with alkyd $L = \left[\frac{5}{0.033\ [SO_2] + 0.013Rh + f(T) + 0.0013Rain}\right]^{1/0.41}$ f(T) = 0.015(T-11) when T≤11°C, otherwise -0.15(T-11)	0.68	139	(4.9)

where

ML = mass loss, g m^{-2}, *NOTE: see section 4.2.2.3*

R = surface recession, µm

t = exposure time, years

L = maintenance interval (lifetime), years

Rh = relative humidity, % – annual average

T = temperature, °C – annual average

$[SO_2]$ = concentration, µg m^{-3} – annual average

$[O_3]$ = concentration, µg m^{-3} – annual average

$Rain$ = amount of precipitation, mm year^{-1} – annual average

$[H^+]$ = concentration, mg l^{-1} – annual average

$[Cl^-]$ = concentration, mg l^{-1} – annual average

NOTE: the unit for $[H^+]$ is not the normal one (M) used for this denomination and the relation between pH and $[H^+]$ is therefore here $[H^+] = 1007.97 \cdot 10^{-pH} \approx 10^{3-pH}$

These equations are valid for regions without strong influence of sea salts with a total chloride content in precipitation < 5 mg l^{-1} approx., regardless of the source.

The functions for paint coatings are expressed as lifetime equations. These lifetimes can be mapped but the functions cannot at present be used for calculating acceptable levels using the concept of acceptable corrosion rates since tolerable lifetime has not yet been established for these materials.

For all these materials, and also electric contact materials and tin, data for exposure in sheltered positions are available but are of less general validity for mapping at the UNECE level since actual corrosion rates are highly dependent on the particular sheltering conditions.

4.2.2.2 Dose-response functions for the multi-pollutant situation

The following equations are based on 4-year results from the exposure within UN ECE ICP on Materials (1997–2001). These were complemented with environmental measurements of HNO_3 and particulate matter as a result from the extra effort connected to the MULTI-ASSESS project in 2002–2003. Later data of HNO_3 and particulate matter show no significant trend. They reflect the increased level of the physicochemical understanding of the corrosion mechanisms including the effect SO_2 and acid rain for all materials, the effect of nitric acid for zinc and Portland limestone, and the effect of particulate matter for carbon steel, cast bronze and Portland limestone. The functions were first derived with an inclusion of time as an independent variable (Kucera et al., 2007). However, discussions within the ICP Materials Task Force have concluded that the mapping of areas with increased risk of corrosion and calculation of acceptable levels of pollution should be based on one-year exposure. Therefore, the functions are to be only over periods of one year. Time-dependent corrosion rates are necessary for the calculation and the mapping of costs caused by atmospheric corrosion. They are described below, in the cost section.

Carbon steel

$$R = 6.5 + 0.178[SO_2]^{0.6} Rh_{60} e^{f(T)} + 0.166 Rain[H^+] + 0.076[PM_{10}] \quad (4.10)$$

f(T) = 0.15(T-10) when T<10°C, otherwise f(T) = -0.054(T-10)

Zinc

$$R = 0.49 + 0.066[SO_2]^{0.22} e^{0.018 Rh + f(T)} + 0.0057 Rain[H^+] + 0.192[HNO_3] \quad (4.11)$$

f(T) = 0.062(T-10) when T<10°C, otherwise f(T) = -0.021(T-10)

Cast Bronze

$$R = 0.15 + 0.000985[SO_2] Rh_{60} e^{f(T)} + 0.00465 Rain[H^+] + 0.00432[PM_{10}] \quad (4.12)$$

f(T) = 0.060(T-11) when T<11°C, otherwise f(T) = -0.067(T-11)

Portland limestone

$$R = 4.0 + 0.0059[SO_2] Rh_{60} + 0.054 Rain[H^+] + 0.078[HNO_3] Rh_{60} + 0.0258[PM_{10}] \quad (4.13)$$

where

Rh_{60} = Rh - 60 when Rh > 60, 0 otherwise

$[HNO_3]$ = annual average concentration, µg m^{-3}

$[PM_{10}]$ = annual average concentration, µg m^{-3}

and other symbols as in the previous section.

4.2.2.3 Units for corrosion attack of metals

Mass loss and surface recession, the two units of corrosion attack proposed, have been denoted as ML (g m^{-2}) and R (µm). It is recommended that all maps for metals are produced with the unit R (µm) with the exception of aluminium, where it is recommended to use ML (g m^{-2}). For aluminium the corrosion is localised, therefore, it would be misleading to express the results in µm since this is not reflecting the depth of local attack. For the purpose of conversion from ML to R the following densities should be used: steel (7.8 g cm^{-3}), zinc (7.14 g cm^{-3}), copper (8.93 g cm^{-3}), and bronze (8.8 g cm^{-3}).

4.2.2.4 Direct effects of ozone

The effect of ozone (O_3) on corrosion of materials is complex and there is still serious gaps of knowledge that are needed in order to characterise it. Both O_3 and NO_2 have a direct effect on the corrosion and degradation, especially on some organic materials. In recent years, the synergistic effect of SO_2 in combination with O_3 and NO_2 has been shown to lead to severely increased corrosion on several inorganic materials in laboratory exposures. In field exposures so far only the synergistic effect of SO_2 and O_3 has been shown in the UN ECE exposure programme, and only for copper, as can be inferred from the dose-response functions.

4.2.3 Dose-response functions for soiling of materials

Soiling is the visual effect that results from the darkening of exposed surfaces following the deposition and accumulation of atmospheric particles. It can be assessed by the change of optical properties of different materials, generally, as the loss of reflectance for opaque materials (such as stones, concrete, painted steel, etc.), and as the loss of transparency (i.e., transmittance, for transparent materials, such as glass). Most of the measurements were carried out on samples that were exposed in a vertical position under sheltered conditions to avoid recurring washing by rain.

For non-transparent materials, several dose-response functions were defined (Watt et al., 2008). They relate the loss of reflectance ΔR to the PM_{10} concentration ([PM_{10}] in µg m^{-3}) and time (t in days):

White painted steel

$$\Delta R = R_0\left[1 - e^{-3.96\cdot10^{-6}[PM_{10}]t}\right] \quad (4.14)$$

White plastic

$$\Delta R = R_0\left[1 - e^{-4.43\cdot10^{-6}[PM_{10}]t}\right] \quad (4.15)$$

Polycarbonate membrane

$$\Delta R = R_0\left[1 - e^{-3.47\cdot10^{-6}[PM_{10}]t}\right] \quad (4.16)$$

where

ΔR = loss of reflectance, %

R_o = reflectance from uncovered surface, %

[PM_{10}] = annual average concentration, µg m^{-3}

t = exposure time, days

There is no DRF for Portland limestone as the correlation with PM_{10} was too poor to predict a relationship with any confidence.

For transparent material, such as float glass, two kinds of dose-response functions were developed:

(1) The first one is based on multilinear regression, where haze is a temporal trend whose amplitude is controlled by $[SO_2]$, $[NO_2]$ and $[PM_{10}]$ (in µg m^{-3}) (Lombardo et al., 2010):

$$H = \frac{0.2529[SO_2]+0.1080[NO_2]+0.1473[PM_{10}]}{1+\left(\frac{382}{t}\right)^{1.86}} \quad (4.17)$$

where

H = haze, %

t = exposure time, days

and other symbols as in the previous section.

(2) The second one is based on a neural network approach (Verney-Carron et al., 2012). It corresponds to a pure statistical model that uses a non-linear parametric regression with a hyperbolic tangent function. Once set up, this function is easy to use:

$$H_{est} = 4.81H_{norm} + 5.27 \quad (4.18)$$

$$H_{norm} = 3.951 - 39.193 \tan(S_1) + 44.067 \tan(S_2) \quad (4.19)$$

$$S_1 = -1.498 - 0.145\left(\frac{t-387.18}{275.17}\right) + 0.031\left(\frac{[SO_2]-9.7}{11.82}\right) + 0.297\left(\frac{[NO_2]-33.29}{19.37}\right) + 0.28\left(\frac{[PM_{10}]-28.93}{15.68}\right) \quad (4.20)$$

$$S_2 = -1.45 - 0.073\left(\frac{t-387.18}{275.17}\right) + 0.033\left(\frac{[SO_2]-9.7}{11.82}\right) + 0.281\left(\frac{[NO_2]-33.29}{19.37}\right) + 0.261\left(\frac{[PM_{10}]-28.93}{15.68}\right) \quad (4.21)$$

where

H_{est} = estimated haze, %

H_{norm} = normalized haze, %

S_1, S_2 = 2 neurons

and other symbols as in the previous section.

The range of use of this model must be within the range of the data used to parameterize the function: a duration less than 1638 days, $[SO_2]$ less than 51.1 µg m^{-3}, $[NO_2]$ between 1.3 and 90.1 µg m^{-3}, and $[PM_{10}]$ between 5.4 and 84.3 µg m^{-3}. This model can therefore be used in rural, urban, and traffic areas.

4.3 Use of dose-response functions for mapping “acceptable corrosion rates” and “acceptable levels” for pollutants

4.3.1 Recommendations regarding the selection of functions

For the following materials, two sets of functions have been given, one for the SO_2 dominating situation and one for the multi-pollutant situation:

- Zinc
- Cast bronze

- Portland limestone

It is not possible to exactly define the SO_2 dominating situation and the multi-pollutant situation. However, it is possible to specify the recommended use of the functions:

- The multi-pollutant functions are the preferred choice. This is especially true when making maps of future scenarios and comparing the situation of today with those in the future arising from different pollution scenarios.
- The SO_2-dominating functions may be used if it can be shown that effects of other pollutants besides SO_2 and acid rain are not contributing significantly to the general appearance of maps or to conclusions. This could, for example, be the case when showing the significant improvements made in the past for Europe or when mapping areas of the world where SO_2 values are very high.

4.3.2 Recommendations regarding the use of environmental data

Any user who is considering producing maps on the pollution effects of materials based on procedures specified in this chapter should also consult the general chapters of this manual, including Chapter 1: Introduction, Outline, and General Considerations and, especially, Chapter 2: Mapping Concentration Levels and Deposition Loads. In chapter 2, the general methods of mapping, their underlying assumptions, and data requirements are given for many of the parameters needed for mapping effects on materials. Regarding the wet deposition parameters, it should be noted that the term *Rain[Cl⁻]* given in this chapter is identical to the chloride wet deposition parameter described in chapter 2. Deposition of protons (*Rain[H⁺]*) is not mentioned explicitly in chapter 2 but it should be noted that recommendation "measured solute concentrations may then be interpolated and wet deposition may be estimated from a function of the mapped solute concentration and the precipitation amount, the latter provided by the meteorological service for the country" is valid also for H^+. Annual averages of environmental parameters shall always be used in the dose-response functions but could be based either on measured or modelled values. Data valid for longer periods may also be used depending on the purpose. For example, when climatic data for a particular year is missing or when the purpose is to isolate the effect of pollutants, it is possible to use long term average data for climatic parameters (e.g., 30-year averages) as so-called "climate normals".

Values of climatic and pollution data can usually be obtained from national or international meteorological centres, international organisations (e.g., WMO), international research programmes (e.g., EMEP), or national organisations and authorities responsible for environmental protection.

4.3.2.1 Supporting function for the calculation of HNO_3

Nitric acid is a parameter that is not measured within dense monitoring networks very frequently. The availability of data is therefore limited. The following empirical function, which has been derived within the MULTI-ASSESS project (MULTI-ASSES final report), gives a good possibility of calculating the nitric acid concentrations from NO_2, O_3, relative humidity (Rh) and temperature (T).

$$HNO_3 = 516e^{\frac{-3400}{(T+273)}} \cdot ([NO_2][O_3]Rh)^{0.5} \quad (4.22)$$

4.3.3 Recommendations regarding selection of intervals for mapping corrosion attack

The acceptable rate of corrosion or deterioration (R_a), expressed in µm, or the acceptable soiling (S_a), expressed in %, was defined as being dependent on the technical and economic

considerations for the particular material and application. In reality, it is not considered practical in the context of Convention policy to do this for each individual material and for each individual application separately. Instead, it is recommended that the acceptable corrosion rate is expressed as a multiple of a constant, material dependent, "background corrosion". ICP Materials has calculated reference levels representing the background corrosion or deterioration rate (R_b) as the lower 10th percentile of observed corrosion rates in the materials exposure programme, which started in 1987 and ended in 1995. Acceptable corrosion rates can then be expressed as a multiple (n) of the background corrosion or rate:

$$R_a = n \cdot R_b \tag{4.23}$$

An appropriate n value still has to be selected based on technical/economic consideration but will then be independent of material.

Acceptable rate of corrosion can be used to produce maps. They will show where corrosion exceeds the acceptable deterioration rate (R_a) for simple samples of material. Thus, no correction is implemented for the form in which the material is used (e.g., the type of component). Practical n values 1.5, 2.0, and 2.5 are recommended following discussion at the 24th meeting of the Task Force (2008), and corresponding R_a values are given in table 4.1. Targets for protecting materials of infrastructure and cultural heritage monuments for 2050 and 2020 have been given in "Indicators and targets for air pollution effects" (ECE/EB.AIR/WG.1/2009/16) corresponding to n=2.5 (2020) and n=2.0 (2050).

Table 4.1. Recommended class boundaries to be used for mapping corresponding to *n* values of 1.0 (background corrosion rate), 1.5, 2.0 and 2.5.

Material	*n* = 1.0	*n* = 1.5	*n* = 2.0	*n* = 2.5	
Limestone	3.2	5.0	6.4	8	µm, first year exposure
Sandstone	2.8	4.0	5.5	7	µm, first year exposure
Copper	0.32	0.5	0.64	0.8	µm, first year exposure
Bronze	0.25	0.4	0.5	0.6	µm, first year exposure
Zinc	0.45	0.7	0.9	1.1	µm, first year exposure
Carbon steel and weathering steel	8.5	12	16	20	µm, first year exposure
Aluminium*	0.09	0.14	0.18	0.22	g m^{-2}, first year exposure

*Aluminium undergoes localised corrosion, but the corrosion rates were calculated as uniform corrosion. Maximum pit depth is a better indication of potential damage, but this characteristic cannot be evaluated after the first year of exposure.

Today, most European sites have corrosion values in the range corresponding to those given in Table 4.1. However, intervals for higher corrosion attack also need to be specified in order to map corrosion in areas with high levels of pollution whether in or outside Europe, or to map situations observed in the past. The ISO standard 9223 specifies intervals of corrosion values for the following metallic materials: carbon steel, zinc, copper, and aluminium; see Table 4.2. Although these intervals correspond to different n values, the variation is not so large and the corresponding approximate n values are 5.0, 10, and 20. Therefore, it is recommended that these n values be used for mapping high corrosion values for materials other than carbon steel, zinc, copper, and aluminium. For carbon steel, zinc, copper, and aluminium, the C classes given in Table 4.2 are recommended when mapping areas with high corrosion rates.

Table 4.2 ISO 9223 corrosivity categories.

Material	C1	C2	C3	C4	C5	CX	
Carbon steel	<1,3	1,3–25	25–50	50–80	80–200	200–700	µm, first year exposure
Zinc	<0,1	0,1–0,7	0,7–2,1	2,1–4,2	4,2–8,4	8,4–25	µm, first year exposure
Copper	<0,1	0,1–0,6	0,6–1,3	1,3–2,8	2,8–5,6	5,6–10	µm, first year exposure
Aluminium[#]		<0,6	0,6-2	2–5	5–10	>10	g m^{-2}, first year exposure

[#]Aluminium undergoes localised corrosion, but the corrosion rates were calculated as uniform corrosion. Maximum pit depth is a better indication of potential damage, but this characteristic cannot be evaluated after the first year of exposure due to passivation effects and decreasing corrosion rates.

4.3.4 Recommendations regarding grid size

It is recommended that countries make use of best available data and generate information at appropriate national scales. It is advisable to produce maps with high resolution (small grid size), preferably 1 km^2 or smaller, especially for mapping of effects in urban areas. Such resolution enables the consideration of differences between urban and rural conditions in levels of pollution, in relevant climatic characteristics (such as temperature and relative humidity) and may include both long-range transported pollutants and local emissions.

However, for regional European assessments, pollutant effects on materials may be mapped using EMEP grid areas (0.1° x 0.1° Lat-Long currently). It is thus advisable to use a grid network that coincides with the EMEP network or, preferably, a smaller network that is a fraction of the EMEP size.

4.3.5 Recommended maps

Several maps may be used to illustrate the effects of air pollution on materials:

- Maps showing the geographical distribution of some of the most important environmental parameters and their combinations used in the dose-response functions: [SO_2], [O_3], T, Rh, Rain, pH, Cl^-, Rain[H^+].
- Maps showing combinations of important parameters illustrating important effects related to materials damage that are not possible to express in terms of a specific material. This could, for example, be time of wetness (TOW), calculated as a combination of temperature and relative humidity parameters (Tidblad et al., 2000) or other “heritage climatology” parameters, such as the number of freeze-thaw cycles (Brimblecombe, 2010).
- Material damage maps for selected materials should preferably be produced using the recommendations in 4.3.3. These maps will enable the identification of areas exceeding acceptable/tolerable corrosion rates.
- Maps can also be made showing the contribution of wet deposition to the total corrosion effect or ratio between corrosion effect of wet and dry deposition.

Maps showing acceptable/tolerable pollution levels/loads of individual pollutants (SO_2, O_3, HNO_3, PM_{10}, H^+) can be made but levels of other pollutants need to be specified. A common approach is to assume that these are unchanged.

Another possibility is to use target values. These give information on the pollutant deposition that would lead to a given (chosen) acceptable level of corrosion or soiling for a given year (the target). For example, if we assume that PM_{10} levels are below 20 µg m^{-3} annual mean (as recommended by WHO Air quality guidelines, global update 2005), and that pH levels are equal to those in 2000, it is possible to calculate acceptable SO_2 levels for carbon steel using equation 4.11 for 2020 (R=20 µm) and 2050 (R=16 µm). Assisting maps of temperature, relative humidity and precipitation (long-term averages) and pH (for the year 2000) would be needed.

4.4 Use of dose-response functions for mapping "acceptable soiling rates"

For the mapping of soiling rates and costs, a background rate and suggested tolerable and acceptable rates (thresholds) in the years 2020 and 2050 can be used.

For non-transparent materials (white painted steel and plastic), and polycarbonate membrane (Equations 4.14 to 4.16) the lifetimes are calculated until 30% loss of reflection, for a selected PM10 background scenario. It is suggested to use threshold cleaning intervals of 10 years (in year 2020) and 15 years (in 2050). The cleaning interval in the background is expected to typically be between 30 and 40 years. A tolerable soiling threshold of 30% loss of reflection is suggested based on the research of Brimblecombe and Grossi (2005), and on the following considerations:

- The threshold is chosen to protect buildings sensitive to soiling of light colour.
- The threshold represents a perceived reflectance where about 30% of respondents find the surface dirty.
- The unprompted dirtiness response is expected to be considerably lower than 30% of the respondents.

For glass soiling, both functions can be used provided that the concentration ranges are respected for the neural network DRF.

For the soiling of modern glass, it is recommended to use a lifetime between cleaning in the background of 1500 days (~ 4 years), and a threshold lifetime for 2050 calculated from a haze value of 1% for cultural heritage (and in sensitive situations), and from a haze value of 3% for technical constructions and the general stock of buildings. In instances when a haze value of 3% is never reached by Equations (4.14, 4.15 or 4.16), or only reached at cleaning intervals longer than 1500 days, the cleaning interval is set to 1500 days and the rate and cost over background is set equal to zero (Grøntoft et al., 2019). Depending on the pollution, 1% haze would, typically, be reached in some months up to a year, whereas 3% haze was found to be reached in one year for the average of the ICP stations between 2002 and 2014.

4.5 Use of dose response functions for calculation and mapping of costs resulting from corrosion

One additional important goal of the mapping activities in the field of materials is the calculation of cost of damage caused by air pollutants to materials. While it is not recommended to assess the absolute cost, it is possible to estimate the difference in cost between two alternative scenarios using the following equation:

$$\Delta C = C \cdot S \cdot (L_{S1}^{-1} - L_{S2}^{-1}) \quad (4.25)$$

where AC is the cost difference, C is the cost per surface area of material for maintenance/replacement/cleaning, S is the surface area of material, Ls1 is the maintenance

interval (lifetime) for scenario 1 and Ls2 is the maintenance interval for scenario 2. If Equation 4.16 is to be used for estimating the cost of corrosion or soiling due to pollutants in the present situation, the present pollution situation (scenario 1) should be used to calculate Ls1 and the background corrosion (scenario 2) to calculate Ls2. When calculating the lifetime from the background scenario, it is recommended one use the time dependence from the dry deposition term given in Equations 4.1–4.7, which means t0.85 for zinc and t0.86 for bronze in the multi-pollutant situation. For carbon steel, a time dependence of t0.54 is recommended. It is not recommended to use Equations 4.8–4.9 for cost calculations when it comes to the paint coatings, since the evaluations are based on damage from an intentionally made scratch, which may be regarded as a form of accelerated testing. At present, the practical functions described in Kucera et al. 1993 are the only ones available for use, but these have not been verified by ICP Materials. A UN/ECE Workshop on economic evaluation of air pollution abatement and damage to buildings (including cultural heritage) took place in Stockholm on 23–25 January 1996 (Proc. UNECE Economic Workshop, 2007). The proceedings of the workshop summarised the state of the art and is given in the reference list together with a selection of other important publications: Kucera et al, 1993, Ecotec, 1986, Tolstoy et al., 1989 and Cowell and ApSimon, 1996. In the ECOTEC study of 1986, building identikits for Birmingham (UK), Dortmund (Germany), and Cologne (Germany) were compiled. For Stockholm (Sweden), Sarpsborg (Norway), and Prague (Czech Republic), statistically based inventories of outdoor material surfaces were compiled by Kucera et al., 1993. These studies include percentage values of the most common construction materials and their distribution, which in absence of stock at risk data may provisionally be used as default values. Later, Tidblad et al., 2010 made an updated review on the economic assessment of corrosion and soiling of materials (including cultural heritage) that included references to several national studies and also several EU projects, such as REACH, ExternE and ExternE Transport, and CULT-STRAT. The CULT-STRAT project resulted in a book titled The Effects of Air Pollution on Cultural Heritage with a chapter on economic evaluation (Watt et al., 2009a).

Mapping of damage costs will be similar to mapping of acceptable levels/loads but will include data on the stock of material in each mapping unit and the economic costs associated with the deterioration of these materials (e.g., replacement or repair costs). The change in the rate of deterioration can be used to estimate the cost associated with the deterioration and, furthermore, to undertake a cost benefit analysis of pollutant emission reduction scenarios in the mapping area.

4.5.1 Assessment of stock of materials at risk

So far, materials have not been included in integrated assessment modelling and are not included in the multi-pollutant protocol. Part of the explanation for this may be the lack of stock at risk data. Several stock at risk studies have, however, been performed during the years, the most intensive period being from 1990 to 1996 with several important studies in individual countries that, in the end, enabled the estimate of Cowell and ApSimon (1996) on the cost of damage to buildings by atmospheric pollution in Europe. These studies, many others, and an overview of methodologies for assessing stock at risk were recently presented in the ICP Materials report 61 “Assessment of stock of materials at risk including cultural heritage” by Tidblad et al. in 2010. Furthermore, the CULT-STRAT book mentioned above also included a chapter on stock at risk (Watt et al., 2009b).

4.5.2 Sources of uncertainty

The main sources of uncertainty for estimation of corrosion costs will result from

- assessment of the stock of materials at risk;
- translation of dose-response functions obtained by exposure of test specimens to damage functions that consider the exposure situation on a construction and rational maintenance practice;
- characterisation of reduced service lifetime and quantification of costs associated with reduced service lifetime;
- assessment of environmental data and their extrapolation to each mapping square that consider the importance of the difference in local environment in populated and rural areas; and
- use of yearly mean values of pollution parameters which do not consider the effect of fluctuations of pollutant levels.

4.6 Concluding remarks

Mapping atmospheric corrosivity was first done in the past to identify effect of emission on metals in the vicinity of industrial emission sources. These maps could be done by simply plotting SO_2 isolines, which would be almost identical to corrosion isolines. With more knowledge and changing pollution situation more parameters have successively been added to dose-response functions, including the effect of climate (time of wetness, temperature, relative humidity), precipitation (acid rain), other gaseous pollutants (O_3, HNO_3), and particulate pollution.

Corrosivity maps are useful for material selection and for appropriate selection of protection methods in industrial applications for bare as well as coated metals. Furthermore, the use of indicator materials can show potential effects on cultural heritage, as is illustrated in the "Guidance document on health and environmental improvements using new knowledge, methods and data" (ECE/EB.AIR/2013/8) which gives materials corrosion and soiling risks for individual countries in the ECE region.

It is our hope that this document will stimulate further mapping of corrosion by using a standardised methodology within and also outside of Europe in order to facilitate comparison of maps produced at different geographical resolutions, geographical scales, and time scales.

4.7 References

Brimblecombe P. and Grossi C. M., 2005. Aesthetic thresholds and blackening of stone buildings, Science of the total environment 349, 175–189.

Brimblecombe P., 2010: "Heritage Climatology", in Climate change and cultural heritage, Proc. Ravello Int. Workshop, ISBN 978-88-7228-601-2, Edipuglia, Italy.

CLRTAP, 2022. Mapping of effects on materials, Chapter 4 of Manual on methodologies and criteria for modelling and mapping critical loads and levels and air pollution effects, risks and trends. UNECE Convention on Long-range Transboundary Air Pollution.

Cowell and Apsimon H., 1996: "Estimating the cost of damage to buildings by acidifying atmospheric pollution in Europe", Atmos. Env., Vol. 30, pp. 2959–2968.

Ecotec (1986) Identification and Assessment of Materials Damage to Buildings and Historic Monuments by Air Pollution. Report to the UK Department of the Environment. Ecotec Consulting Ltd., Birmingham.

Grøntoft T., Verney-Carron A., and Tidblad J. (2019) Cleaning Costs for European Sheltered White Painted Steel and Modern Glass Surfaces due to Air Pollution since the Year 2000. Atmosphere 10, 167, 31 pp.

Kucera V., Henriksen J., Knotkova D., and Sjöström C., 1993: "Model for Calculations of Corrosion Costs Caused by Air Pollution and its Applications in three Cities", Proc. 10th European Corros. Congr., Barcelona.

Kucera V., J. Tidblad, K. Kreislova, D. Knotkova, M. Faller, D. Reiss, R. Snethlage, T. Yates, J. Henriksen, M. Schreiner, M. Melcher, M. Ferm, R.-A. Lefèvre and J. Kobus, "UN/ECE ICP materials dose-response functions for the multi-pollutant situation," Water, Air, & Soil Pollution: Focus, vol. 7, 2007, pp. 249–258.

Lombardo T., Ionescu A., Chabas A., Lefèvre R.-A., Ausset P. and Candau Y., 2010. Dose-response function for the soiling of silica-soda-lime glass due to dry deposition, Science of the total environment 408, 976–984.

MULTI-ASSESS final report, http://www.corr-institute.se/MULTI-ASSESS/

Tolstoy N., Andersson G., Sjöström C and Kucera V. 1989: "External building materials – quantities and degradation." Statens institut för byggnadsforskning, Gävle. ISBN 91-540-9315-5.

Tidblad, J., Mikhailov, A.A. and Kucera, V., 2000. Model for the prediction of the time of wetness from average annual data on relative air humidity and air temperature. Protection of Metals (Russia), 36(6), 533–540.

Tidblad, J., Kucera, V., Mikhailov, A. A., Henriksen, J., Kreislova, K., Yates, T., Stöckle, B. and Schreiner, M., 2001. UN ECE ICP Materials. Dose-response functions on dry and wet acid deposition effects after 8 years of exposure. Water, air and soil pollution, 130(1-4 III), 1457–1462.

Tidblad J., T. Yates, S. Doytchinov, M. Faller, and K. Kreislova, UNECE International co-operative programme on effects on materials, including historic and cultural monuments. Report No 61 Assessment of stock of materials at risk including cultural heritage., Swerea KIMAB AB, Stockholm, Sweden., 2010.

Tidblad J., Faller M., Grøntoft T., Kreislova K., Varotsos C., De la Fuente D., Lombardo T., Doytchinov S., Brüggerhoff S. and Yates T., 2010: UNECE International co-operative programme on effects on materials, including historic and cultural monuments. Report No 65 Economic assessment of corrosion and soiling of materials including cultural heritage, Swerea KIMAB AB, Stockholm, Sweden.

UN/ECE Economic Workshop, 1997: "Economic Evaluation of Air Pollution Damage to Materials." Proceedings of the UN ECE Workshop on Economic Evaluation of Air Pollution Abatement and Damage to Buildings including Cultural Heritage, Eds V. Kucera, D. Pearce and Y.-W. Brodin, Report 4761, Swedish Environmental Protection Agency, Stockholm, Sweden, 1997.

Verney-Carron A., Dutot A.L., Lombardo T., Chabas A., 2012. Predicting changes of glass optical properties in polluted atmospheric environment by a neural network model, Atmospheric Environment 54, 141–148.

Watt J., Jarrett D. and Hamilton R., 2008. Dose-response functions for the soiling of heritage materials due to air pollution exposure, Science of the total environment 400, 415–424.

Watt J., Navrud S., Slizkova Z. and Yates T., 2009a: "Economic Evaluation", in The effects of air pollution on cultural heritage. Springer (book chapter), pp. 189–214.

Watt J., Doytchinov S., Lefevre R.-A., Ionescu A., Dela Fuente D., Kreislova K and Screpanti A., 2009b: "Stock at risk", in The effects of air pollution on cultural heritage. Springer (book chapter), pp. 147–188.

5 Mapping critical loads for ecosystems

Last update by the CCE in 2024.

Please refer to this document as: CLRTAP, 2024. Mapping critical loads for ecosystems, Chapter 5 of Manual on methodologies and criteria for modelling and mapping critical loads and levels and air pollution effects, risks, and trends. UNECE Convention on Long-range Transboundary Air Pollution; accessed [date of consultation] at www.umweltbundesamt.de/en/cce-manual.

5.1 Introduction

Critical loads are related to indirect, soil-mediated effects of elevated deposition and are defined as **"a quantitative estimate of an exposure to one or more pollutants below which significant harmful effects on specified sensitive elements of the environment do not occur according to present knowledge" (Nilsson and Grennfelt 1988).**

The use of critical loads to provide intelligence on the impacts of air pollution for the support of abatement strategies and policies is termed "the critical load approach" (de Vries et al., 2015a).

The basic idea of the critical load approach is to balance the depositions which an ecosystem is exposed to with the capacity of this ecosystem to buffer the input (e.g., the acidity input buffered by the weathering rate), or to remove it from the system (e.g., nitrogen by harvest) without harmful effects within or outside the system.

The general definition of a critical load applies to different receptors (e.g., terrestrial ecosystems, groundwater, aquatic ecosystems, and/or human health). 'Sensitive elements' can be part of or the whole of an ecosystem or of ecosystem development processes, such as their structure and function. Critical loads have been defined for several pollutants and effects resulting from their deposition. In this chapter, the focus is on critical loads of acidity, nutrient nitrogen, and heavy metals.

Critical loads can be derived from:

- Field experiments with an aim to establish dose response relationships between the input (deposition) of a pollutant and ecosystem impacts. These so-called "empirical critical loads" are described in sections 5.2.1 and 5.2.2 with respect to eutrophication and acidification, respectively. Empirical critical loads for heavy metals have not been considered.
- Steady-state mass balance models in which critical loads are derived on the basis of a given chemical criterion in the soil solid phase, soil solution and/or surface water.

Critical load modelling in terrestrial and aquatic ecosystems is described in sections 5.3 and 5.4 respectively, addressing both acidification and eutrophication. In the following two subchapters, the modelling of critical loads of heavy metals (section 5.5) and for biodiversity (section 5.6) are considered. Both sulphur and nitrogen compounds contribute to the total deposition of acidity. The acidity input has to be considered in this balance regardless of whether it is due to sulphur or nitrogen depositions. Thus, the ratio between sulphur and nitrogen may vary without change in the acidity load.

In the context of a multi-pollutant multi-effects approach it is desirable to consider all effects simultaneously as far as possible. For eutrophication and acidification, this has been done using so-called critical load functions. These are described in detail in section 5.3.

An overview of critical load methods, data, and applications can be found in De Vries et al. (2015a; 2015b). This book focuses on the science behind critical loads and methods to understand *future consequences* of atmospheric depositions that exceed these thresholds.

The assessment of "future consequences", (i.e., whether "significant harmful effects on specified sensitive elements of the environment" occurs), depends on the time duration and magnitude of atmospheric depositions that exceed critical loads. Inversely, when exceedance does not occur, recovery of a sensitive (element of) environment may occur if the critical load was exceeded in the past. This assessment of future consequences requires the use of so-called dynamic models. In fact, a future state of the environment can serve as a basis for dynamic models to "back-calculate" a critical load. This can be regarded as a third method to obtain critical loads in addition to the aforementioned empirical and modelled critical loads. However, since critical loads are steady-state quantities, the use of dynamic models for the sole purpose of deriving critical loads may be inadequate. On the other hand, if dynamic models are used to simulate the transition to a steady state for the comparison with critical loads, care has to be taken that the steady-state version of the dynamic model is compatible with the critical load model. This third method is not described in this chapter. Dynamic modelling in general is addressed in chapter 6.

This chapter compiles descriptions of the methods to assess empirical and steady-state critical loads for eutrophication and acidification. It also describes how to calculate critical loads for heavy metals.

5.2 Databases

5.2.1 The European background database

With the aim of providing European maps and databases to the relevant bodies under the LRTAP Convention, the CCE collects and collates national data on critical loads for eutrophication and acidification for European terrestrial ecosystems. For meaningful applications, a complete European coverage with critical load is required. If a country does not provide national data, the CCE fills the gaps with critical load from a so-called European background database (EU-DB) of critical load. The EU-DB was developed by the CCE in collaboration with Wageningen University & Research and is regularly updated based on the latest scientific findings. Over the years, the CCE has maintained and updated the EU-DB with information provided by parties, especially following calls for data. The last major update of the EU-DB was completed in 2021. Detailed information can be found in Reinds et al. (2021), which is available online (https://www.umweltbundesamt.de/sites/default/files/medien/5750/publikationen/2021-07-12_doku_03-2021-critical_load.pdf).

In 2013, the WGE "requested that the European Background Database would be used by the CCE for effect-based assessments, after CCE have checked with National Focal Centres (NFCs) that national data are not available, unless countries request the CCE not to carry out calculations for a given parameter on their national territory" (ECE/EB.AIR/WG.1/2013/2).

The EU-DB contains data on ecosystem characteristics for the calculation of SMB critical loads, applying the equations given in chapter 5.4, and for running simple dynamic models. The parameters included in the EU-DB describe geographic and climatic variables, base cation deposition and weathering rates, nutrient uptake, nitrogen transformations, and cation exchange. Critical load computations are restricted to (semi-)natural habitats, i.e. forests, mires, bogs and fens, natural grasslands and heathland, scrub and tundra. In a first step, the geographic variables (1) land cover (see section 5.2.2), (2) soil, (3) forest growth region, (4) distance to coast, and (5) Natura 2000 delineation are gridded in an ArcMap Pro procedure in Python to

rasters with a resolution of 0.01° × 0.01° for each country separately. In a second step, the meteorological data is processed using the statistic software R. Critical loads are computed from South to North through Europe preparing meteorological data, computing hydrology and critical load for all receptors between -12 and 42 degrees longitude. For further details regarding data and methods see Reinds et al. (2021).

5.2.2 The harmonised land cover map

The land cover map is a major input data for the calculation of critical loads for eutrophication and acidification of terrestrial ecosystems. The spatial extent of the map covers all countries in Europe, the Caucasus and Central Asia. The harmonised land cover map depicts the **E**uropean **N**ature **I**nformation **S**ystem (EUNIS) classes.

In total, this harmonised land cover map represents 218 EUNIS classes, from which 204 classes represent EUNIS level 3. The classification of EUNIS level 1 and 2 classes is based on CORINE Land Cover 2018 and Ecosystem Type Map v3.1 for European countries covered by CORINE Land Cover Maps. The Copernicus Global Land Cover Map is applied for European countries not-covered by CORINE Land Cover Maps. The Global Potential Natural Vegetation (GPNV) maps and the Harmonized World Soil Database (HWSD) are applied to further disaggregate Level 2 classes towards Level 3. More than 700,000 points from the European Vegetation Archive (EVA) classified at EUNIS Level 3 were provided by the expert system for automatic classification of European vegetation plots to EUNIS habitats. The map is compatible with the EMEP grid. A detailed description about the map is available in the report from Gebhardt (2023). The report and the map are available from the CCE. For the report, please visit the CCE website (https://www.umweltbundesamt.de/en/publikationen/creation-of-a-harmonized-land-cover-map-as-an) and for the map contact the CCE@uba.de.

Figure 5: Updated European EUNIS Level 2 habitat map (Gebhardt, 2023)

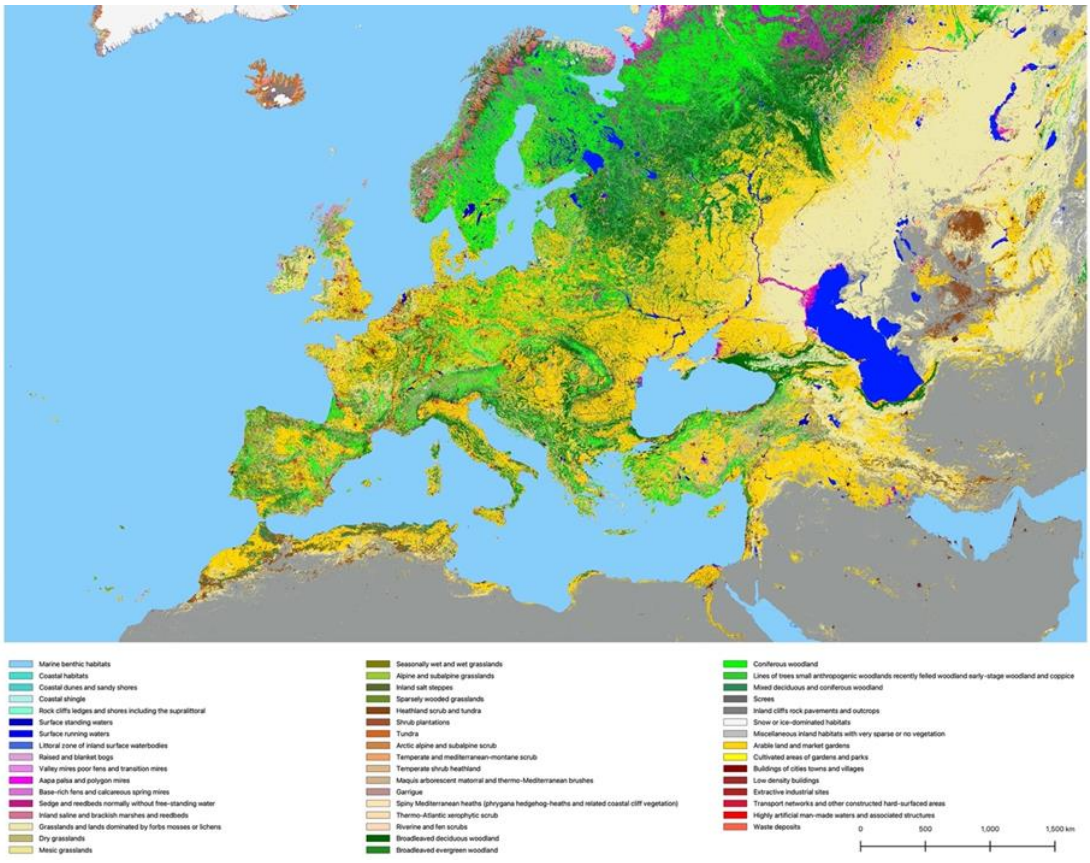

5.3 Empirical critical loads

Empirical critical loads are based on field observations and experiments (i.e., empirical evidence) with the aim to establish dose response relationships between the input (deposition) of a pollutant and ecosystem impacts (see also Bobbink et al., 2015; Hettelingh et al., 2015a). These observations may be carried out on experimental sites with addition or reduction of pollutants. An alternative is to establish dose-response relationships from gradient studies, (i.e., by using a wide range of actual depositions for sites for which information on impacts is available). Gradient studies can include data from a range of clean areas to polluted ones, or sites that are studied over a long period of time during which deposition levels are known to have increased or decreased. Empirical critical loads have mainly been developed for eutrophication of terrestrial ecosystems (section 5.2.1). Some are proposed for acidification (section 5.2.2), but the approach has not been applied to heavy metals.

The text in this section is from the 2004 Mapping Manual (CLRTAP, 2004), updated using sections and data from Bobbink et al. (2022).

5.3.1 Empirical critical loads for nutrient nitrogen

5.3.1.1 Short- and long-term impacts of nitrogen on ecosystems

Depositions of ammonia (NHx) and nitrogen oxides (NOy) have strongly increased in Europe in the second half of the 20th century. This is related to increasing emissions over time of reduced ammonia, especially in agriculture, and to nitrogen oxide emissions from various industrial processes (energy, transport, etc.).

The availability of nutrients is one of the most important abiotic factors, which determine the plant species composition in ecosystems. Nitrogen is the limiting nutrient for plant growth in many natural and semi-natural ecosystems, especially in oligotrophic and mesotrophic habitats. Most of the plant species living under such conditions are adapted to nutrient-poor conditions and can only survive or compete successfully on soils with low nitrogen availability (Bobbink et al., 2022). In addition, the nitrogen cycle in ecosystems and between the different compartments in the environment is complex, as is illustrated by the “nitrogen cascade” (Figure 5.2, Galloway et al., 2003; Sutton et al., 2011). This cycle is strongly regulated by physical, chemical, biological, and microbiological processes. As a result of increased air-borne nitrogen pollutants, many changes may therefore occur in soil-based processes, plant growth, and in inter-species relationships in each ecosystem.

Figure 5.2: Simplified view of the nitrogen cascade, highlighting the transfer of nitrogen species between the different compartments of the environment and their environmental impacts (blue boxes). Arrows in blue represent intended anthropogenic flows of reactive nitrogen (N_r), all other arrows represent unintended flows (adapted from Sutton et al., 2011).

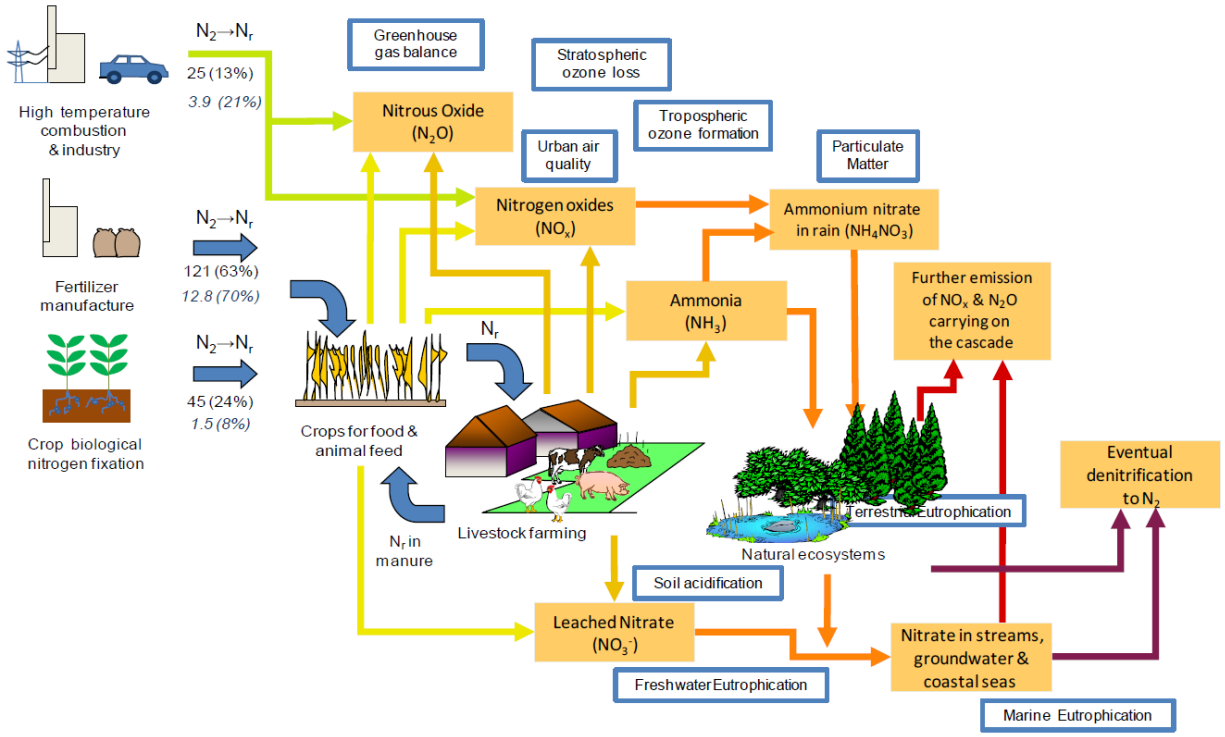

Source: This figure is adopted from a previous version of Chapter 5 of the Mapping Manual

The series of events which occur when nitrogen inputs increase in an area with originally low background deposition rates is highly complex. Many ecological processes interact and operate at different temporal and spatial scales. As a consequence, high variations in sensitivity to atmospheric nitrogen deposition have been observed among different natural or semi-natural ecosystems. The following main effect "categories" can be distinguished:

- Direct toxicity of nitrogen gases and aerosols to individual species (see nitrogen critical levels).
- Accumulation of nitrogen compounds, resulting in increased nitrogen availability and changes of species composition or relative abundance.
- Long-term negative effect of ammonium and ammonia.
- Soil-mediated effects of acidification.
- Increased susceptibility to secondary stress and disturbance factors such as drought, frost, pathogens, or herbivores.

5.3.1.2 Updating and reviewing procedures for empirical critical loads

5.3.1.2.1 Organisation

Under the Convention on Long-range Transboundary Air Pollution (LRTAP), empirical critical loads of nitrogen for natural and semi-natural terrestrial ecosystems and wetland ecosystems

were first presented in a background document for the 1992 workshop on critical loads held under the UNECE LRTAP Convention at Lökeberg (Sweden) (Bobbink et al. 1992). After detailed discussions before and during the meeting, the proposed values were set at that meeting (Grennfelt and Thörnelöf 1992). Additional information from the period 1992–1995 was evaluated and summarised in an updated background paper (Bobbink et al. 1996) and published as Annex III in a previous version of the Mapping Manual (UBA 1996). The updated nitrogen critical loads were discussed and accepted at an expert meeting held in December 1995 in Geneva (Switzerland). They were also used in the Air Quality Guidelines for Europe (2nd edition) of the World Health Organisation (WHO 2000).

New insights into, and data on, the impacts of nitrogen deposition on natural and semi-natural ecosystems are made available by continuing research. Therefore, relevant information gathered over the years has been discussed, evaluated, and approved by consensus in 2002, at an expert meeting held under the LRTAP Convention in Berne (Switzerland, Achermann and Bobbink 2003), in 2007 at a LRTAP Convention workshop on critical loads of nitrogen in low-deposition areas (Stockholm, Sweden), in 2010 at an expert meeting held under the LRTAP Convention in Noordwijkerhout (The Netherlands), and in 2021 at an LRTAP Convention workshop on the review and revision of empirical critical loads for Europe in Berne (Bobbink et al., 2022). All expert propositions for critical loads and levels were adopted by ICP M&M and WGE.

5.3.1.2.2 Procedure followed to define empirical critical loads and levels

The procedure followed to update empirical critical loads and levels is an iterative process, as presented in Figure 5.3. Initially, in both 1992 and 1996, empirical nitrogen critical loads were evaluated for specific receptor groups of natural and semi-natural ecosystems based on observed changes in the structure and function of ecosystems, as has been reported in a range of publications. For each updating procedure, in 2002, 2007, 2011 and 2022, the most recent European publications on the effects of nitrogen in natural and semi-natural ecosystems were reviewed. Peer-reviewed publications, book chapters, nationally published papers, and “grey” reports of institutes or organisations, if available by request, were incorporated. Results from field addition experiments and mesocosm studies, from correlative or retrospective field studies, and, in few cases, dynamic ecosystem modelling were relevant in this respect. Draft documents were written by a small team of authors for each relevant ecosystem (identified since 2007 as a EUNIS class, cf. following section) and included a table presenting critical loads and levels. Finally, these draft documents were the basis for expert meetings. There, the participants discussed, commented, and added information and data to both documents and tables. These were finally approved by the ICP M&M and the WGE at their following annual meeting. All proceedings and details can be found in Bobbink et al., 2022 and references therein.

Figure 5.3: Schematic representation of the critical loads and levels up-dating procedure (adapted from Bobbink et al., 2022).

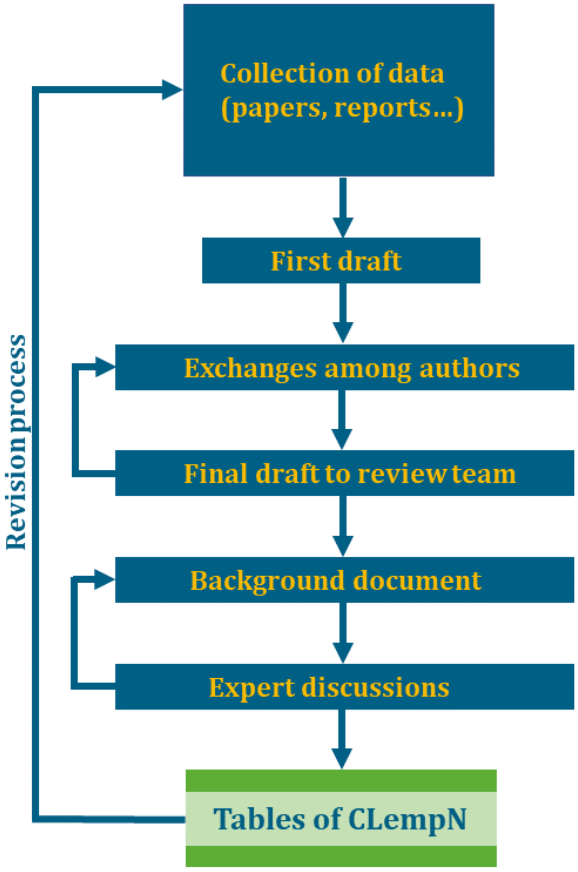

Source: Bobbink et al., 2022

5.3.1.2.3 Ecosystem classification

To harmonise the mapping procedure between countries and ecosystems, the receptor groups of natural and semi-natural ecosystems were classified and ordered according to the EUNIS habitat classification for Europe (Chytrý et al., 2020). For an introduction to the use of the EUNIS classification see Moss, 2008 and the supporting website (http://eunis.eea.europa.eu/). An illustration of the use of the EUNIS classification with respect to empirical nitrogen critical loads can be found in Hall et al. (2003).

In general, the ecosystems used in the 2022 updating procedure were classified mostly down to level 3 or 4 of the EUNIS hierarchy. The EUNIS codes have been included in the critical loads and levels tables. Also, Natura 2000 habitat types were related to EUNIS classification (see Appendix 1 in Bobbink et al., 2022) for correspondences between the EUNIS and the Natura 2000 classifications).

Finally, empirical critical loads were compiled (see Table 5.1) by Bobbink et al. (2022) for the following seven EUNIS habitat classes (EUNIS level 1 code between brackets):

- Marine habitats **(MA)**
- Coastal habitats **(N)**

- Inland surface water habitats **(C)**
- Mire, bog, and fen habitats **(Q)**
- Grassland and tall forb habitats **(R)**
- Heathland, scrub, and tundra habitats **(S)**
- Woodland and forests habitats **(T)**

The other habitats (unvegetated or sparsely vegetated habitats, including caves, agricultural and urban zones) have little relevance in the context of long-range atmospheric pollution for setting critical loads and levels for nitrogen.

5.3.1.3 Procedure to follow to assess and attribute critical loads on a territory

It is recommended that the empirical nitrogen critical loads updated in 2022 (Table 5.1) are used to update (national) databases of empirical critical loads.

5.3.1.3.1 Required data

High-resolution maps of sensitive ecosystems of high conservation value[13], and/or or ecosystems whose functions are to be protected, are needed per country to map nitrogen critical loads for these systems.

Countries are advised to identify those receptor ecosystems of high sensitivity within the mentioned EUNIS classification relating to their individual interest. Effort should be directed to producing high-resolution maps of sensitive ecosystems.

5.3.1.3.2 The empirical critical load values

Table 5.1. provides recommendations for empirical critical load ranges that apply to ecosystems following their EUNIS classification. In this table, each critical load is associated with effects that may occur when the critical load (range) is exceeded. This may be useful for assessing expected impacts of nitrogen deposition with respect to empirical critical load and for comparing results to field observations.

Table 5.1: Overview of empirical N critical loads (kg N ha^{-1} yr^{-1}) to natural and (semi-)natural ecosystems (column 1), classified according to EUNIS (column 2), as established in 2011 (column 3), and as revised in 2022 (column 4). The reliability is indicated by ## reliable; # quite reliable and (#) expert judgement (column 5). Column 6 provides a selection of effects that may occur when critical loads are exceeded. Finally, changes with respect to 2011 are indicated as values in bold.

Ecosystem type	EUNIS code	2011 kg N ha^{-1} yr^{-1}	2022 kg N ha^{-1} yr^{-1}	2022 reliability	Indication of exceedance
Marine habitats (MA)					
Atlantic upper-mid salt marshes	MA223	20-30	10-20	(#)	Increase in dominance of graminoids; decline positive indicator species

[13] Such as, but not exclusively, Special Areas of Conservation in Natura 2000 network, as defined in the EU, or areas of Special Conservation Interest as defined under the Berne Convention.

Ecosystem type	EUNIS code	2011 kg N ha^{-1} yr^{-1}	2022 kg N ha^{-1} yr^{-1}	2022 reliability	Indication of exceedance
Atlantic mid-low salt marshes	MA224	20-30	10-20	(#)	Increase in late successional species; decline positive indicator species
Atlantic pioneer salt marshes	MA225	20-30	20-30	(#)	Increase in late successional species; increase in productivity species
Coastal habitat (N)					
Shifting coastal dunes	N13, N14	10-20	10-20	#	Biomass increase; increased N leaching; reduced root biomass
Coastal dune grasslands (grey dunes)	N15	8-15	5-15	##	Increased biomass and cover of graminoids and mesophilic forbs; decrease in oligotrophic species including lichens; increased tissue N; increased N leaching; soil acidification
Coastal dune heaths	N18, N19	10-20	10-15	#	Increased plant production; increased N leaching; accelerated succession; typical lichen C:N decrease; increased yearly increment *Calluna*
Moist and wet dune slacks	N1H	10-20	5-15	#	Increased cover of graminoids and mesophilic forbs; decrease in oligotrophic species; increased Ellenberg N
Dune-slack pools (freshwater aquatic communities of permanent Atlantic and Baltic or Mediterranean and Black Sea dune-slack water bodies)	N1H1, N1J1	10-20	10-20	(#)	Increased biomass and rate of succession
Inland surface water habitats (C) [a]					
Permanent oligotrophic lakes, ponds, and pools (including soft-water lakes)	C1.1	3-10	2-10 [b]	##	Increased algal productivity and a shift in nutrient limitation of phytoplankton from N to P; shifts in macrophyte community

Ecosystem type	EUNIS code	2011 kg N ha^{-1} yr^{-1}	2022 kg N ha^{-1} yr^{-1}	2022 reliability	Indication of exceedance
Alpine and sub-Arctic clear water lakes	C1.1		2-4	##	Increased algal productivity and a shift in nutrient limitation of phytoplankton from N to P
Boreal clear water lakes	C1.1		3-6	##	Increased algal productivity and a shift in nutrient limitation of phytoplankton from N to P
Atlantic soft water bodies	C1.1, elements C1.2	3-10	5-10	##	Change in species composition of macrophyte communities
Permanent dystrophic lakes, ponds, and pools	C1.4	3-10	5-10 [c]	(#)	Increased algal productivity and a shift in nutrient limitation of phytoplankton from N to P
Mire, bog and fen habitats (Q)					
Raised and blanket bogs	Q1	5-10	5-10	##	Increase in vascular plants; decrease in bryophytes; altered growth and species composition of bryophytes; increased N in peat and peat water
Valley mires, poor fens, and transition mires	Q2	10-15	5-15	##	Increase in sedges and vascular plants; negative effects on bryophytes
Palsa and polygon mires	Q3		3-10	(#)	Increase in graminoids, tissue N concentrations and decomposition rate
Rich fens	Q41-Q44	15-30	15-25	#	Increase in tall vascular plants (especially graminoids); decrease in bryophytes
Arctic-alpine rich fens	Q45	15-25	15-25	(#)	Increase in vascular plants; decrease in bryophytes
Grasslands and tall forb habitats (R)					
Semi-dry Perennial calcareous grassland (basic meadow steppe)	R1A	15-25	10-20	##	Increase in tall grasses; decline in diversity; change in species composition; increased mineralisation; N leaching; surface acidification
Mediterranean closely grazed dry grasslands, or	R1D or R1E or	15-25	5-15	(#)	Increased production; dominance by graminoids; changes to soil crusts; changes to soil nutrient cycling

Ecosystem type	EUNIS code	2011 kg N ha^{-1} yr^{-1}	2022 kg N ha^{-1} yr^{-1}	2022 reliability	Indication of exceedance
Mediterranean tall perennial dry grassland or Mediterranean annual-rich dry grassland	R1F				
Lowland to montane, dry to mesic grassland usually dominated by *Nardus stricta*	R1M	10-15	6-10	##	Increase in graminoids; decline of typical species; decrease in total species richness
Oceanic to subcontinental inland sand grassland on dry acid and neutral soils or Inland sanddrift and dune with siliceous grassland	R1P or R1Q	8-15	5-15	(#)	Decrease in lichens; increase in biomass
Low and medium altitude hay meadows	R22	20-30	10-20	(#)	Increase in tall grasses; decrease in diversity; decline of typical species
Mountain hay meadows	R23	10-20	10-15	#	Increase in nitrophilous graminoids; changes in diversity; decline of typical species
Moist or wet mesotrophic to eutrophic hay meadow	R35	15-25	15-25	(#)	Increase in tall graminoids; decreased diversity; decrease in bryophytes
Temperate and boreal moist and wet oligotrophic grasslands	R37	10-20	10-20	#	Increase in tall graminoids; decreased diversity; decrease in bryophytes
Moss and lichen dominated mountain summits	(Earlier E4.2)	5-10	5-10	#	Change in species composition; effects on bryophytes or lichens
Temperate acidophilous alpine grasslands	R43	5-10	5-10	#	Changes in species composition; increase in plant production
Arctic-alpine calcareous grassland	R44	5-10	5-10	#	Changes in species composition; increase in plant production

Ecosystem type	EUNIS code	2011 kg N ha^{-1} yr^{-1}	2022 kg N ha^{-1} yr^{-1}	2022 reliability	Indication of exceedance
Heathland, scrub, and tundra habitats (S)					
Tundra	S1	3-5	3-5 [d]	#	Changes in biomass; physiological effects; changes in bryophyte species composition; decrease in lichen species richness
Arctic, alpine, and subalpine scrub habitats	S2	5-15	5-10 [d]	#	Decline in lichens; bryophytes and evergreen shrubs
Lowland to montane temperate and submediterranean *Juniperus* scrub	S31		5-15	(#)	Shift in vegetation community composition; reduced seed viability
Northern wet heath	S411				
'U' *Calluna*-dominated wet heath (upland)	S411	10-20	5–15[e]	##	Decreased heather dominance; decline in lichens and mosses; increased N leaching
'L' *Erica tetralix*-dominated wet heath (lowland)	S411	10-20	5-15 [e]	##	Transition from heather to grass dominance; decrease in heather cover; shift in vegetation community composition
Dry heaths	S42	10-20	5-15 [e]	##	Transition from heather to grass dominance; decline in lichens; changes in plant biochemistry; increased sensitivity to abiotic stress
Maquis, arborescent matorral and thermo-Mediterranean scrub	S5	20-30	5-15	(#)	Change in plant species richness and community composition; nitrate leaching; acidification of soil
Garrigue	S6		5-15	#	Changes in species composition; decline in shrub cover; increased invasion of annual herbs
Forest habitats (T)					

Ecosystem type	EUNIS code	2011 kg N ha^{-1} yr^{-1}	2022 kg N ha^{-1} yr^{-1}	2022 reliability	Indication of exceedance
Broadleaved deciduous forest	T1	10-20	10-15	##	Changes in soil processes; nutrient imbalance; altered composition mycorrhiza and ground vegetation
Fagus forest on non-acid and acid soils	T17, T18	10-20	10-15	(#)	Changes in ground vegetation and mycorrhiza; nutrient imbalance; changes in soil fauna
Mediterranean *Fagus* forest on acid soils	T18		10-15	(#)	Annual height and volume tree growth; analogy to temperate *Fagus* forest
Acidophilous *Quercus* forest	T1B	10-15	10-15	(#)	Decrease in mycorrhiza; loss of epiphytic lichens and bryophytes; changes in ground vegetation
Carpinus and *Quercus* mesic deciduous forest	T1E	15-20	15-20	(#)	Changes in ground vegetation
Mediterranean evergreen *Quercus* forest	T21	10-20	10-15	(#)	NO_3 in soil water and streams
Coniferous forests	T3	5-15	3-15	##	Changes in soil processes; nutrient imbalance; altered composition mycorrhiza and ground vegetation; increase in mortality with drought
Temperate mountain *Picea* forest; Temperate mountain *Abies* forest	T31, T32	10-15	10-15	(#)	Decreased biomass of fine roots; nutrient imbalance; decrease in mycorrhiza; changed soil fauna
Mediterranean mountain *Abies* forest	T33		10-15	(#)	Tree foliar stoichiometry; tree physiology; soil N losses
Temperate continental *Pinus sylvestris* forest	T35	5-15	5-15	#	Changes in ground vegetation and mycorrhiza; nutrient imbalances; increased N_2O and NO emissions
Mediterranean montane *Pinus sylvestris-Pinus nigra* forest	T37		5-17	(#)	Lichen chemistry and community changes in Mediterranean mixed-conifer forests in USA
Mediterranean lowland to submontane *Pinus* forest	T3A	3-15	5-10	(#)	Reduction in fine-root biomass; shift in lichen community

Ecosystem type	EUNIS code	2011 kg N ha^{-1} yr^{-1}	2022 kg N ha^{-1} yr^{-1}	2022 reliability	Indication of exceedance
Dark taiga	T3F	5-10	3-5 [f]	##	Changes in epiphytic lichen and ground-layer bryophyte communities; increase in free-living algae; decline in N-fixation
Pinus sylvestris light taiga	T3G	5-10	2-5 [f]	#	Changes in epiphytic lichen and ground-layer bryophyte communities; increase in free-living algae; decline in N-fixation

a) The lower part of the $CL_{emp}N$ range should be applied for lakes in small catchments (with high lake to catchment ratios), because these are most exposed to atmospheric deposition, given that a relatively high fraction of their N inputs is deposited directly on the lakes and is not retained in the catchments. Similarly, the lower part of the range should be applied for lakes in catchments with thin soils, sparse vegetation, and/or with a high proportion of bare rock.

b) This $CL_{emp}N$ should only be applied to oligotrophic waters with low alkalinity and with no significant agricultural or other human inputs. Apply the lower end of the range to clear-water sub-Arctic and alpine lakes, the middle range to boreal lakes, and the higher end of the range to Atlantic soft waters.

c) This $CL_{emp}N$ should only be applied to waters with low alkalinity and with no significant agricultural or other direct human inputs. Apply the lower end of the range to boreal dystrophic lakes.

d) Use towards high end of range if phosphorus limited, and towards lower end if phosphorus is not limiting.

e) Use towards high end of range with high intensity management and use towards lower end of range with low intensity management.

f) Mainly based on N deposition impacts on lichens and bryophytes.

5.3.1.3.3 Ranges and reliability

The empirical nitrogen critical loads are expressed as a range for each ecosystem class, because of:

- The variability of thresholds (critical loads) between measurement sites above which impacts have been established or below which impacts have not been established;
- The differences between treatment concentrations compared to the levels at which effects occurred during addition experiments;
- Site-specific uncertainties in total atmospheric deposition values.

The reliability of the presented nitrogen critical load figures is associated to each critical load, as before (Achermann and Bobbink, 2003, Bobbink et al. 1996, Bobbink and Hettelingh 2011), as indicated by the symbols:

- ##: reliable: when a number of published papers of various studies show comparable results;
- #: quite reliable: when the results of some studies are comparable;
- (#): expert judgement: when no (robust or reliable) empirical data are available for this type of ecosystem. The nitrogen critical load is then based upon expert judgement and knowledge of ecosystems, which are likely to be more or less comparable with this ecosystem.

Additional qualitative information, in comparison to recommendations provided in Achermann and Bobbink (2003), on how to interpret the agreed ranges of critical loads in specific situations for an ecosystem was assigned to a number of modifying factors. However, short of agreement on how to quantify modifying factors for assessments on broad regional scales, consensus was reached to use the minimum value of the ranges of empirical critical loads in every EUNIS class to enable the comparison of their exceedances between different air pollution abatement scenarios. This approach is an implementation of the precautionary principle. The details of the methodology used to derive values for empirical critical load ranges are given in Bobbink et al., 2022 and in the references therein.

5.3.1.4 Summary of empirical critical loads for eutrophication

This section is adapted from Bobbink et al., 2022.

- Empirical critical loads described in this section have been revised at a workshop on the review and revision of empirical critical loads and dose-response relationships that was held under the LRTAP Convention, in Berne, from the 26th to the 28th of October 2021. The workshop was hosted by the Swiss Federal Office for the Environment (BAFU) (see Bobbinket al., 2022).
- The workshop had the objective to review and revise the empirical critical loads of nitrogen for natural and semi-natural ecosystems, which were set at the previous expert workshop held in Noordwijkerhout from the 23rd to the 25th of June 2010 (see Bobbink and Hettelingh, 2011), based on additional scientific information available for the period from 2010 to 2021, as presented in a new and updated background document (Bobbink et al., 2022).
- The following classes according to the EUropean Nature Information System (EUNIS) were addressed: marine habitats (EUNIS class MA), coastal habitats (EUNIS class N), inland surface waters (EUNIS class C), mires, bogs, and fens (EUNIS class Q), grasslands and lands dominated by forbs, mosses or lichens (EUNIS class R), heathland, scrubland, and tundra (EUNIS class S), woodland, forest, and other wooded land (EUNIS class T).
- Statistically and biologically significant outcomes of field addition experiments and mesocosm studies were the basis for the assessment of empirical N critical loads. Only studies which have independent N treatments and realistic N loads and durations (below 100 kg N ha^{-1} yr^{-1}; more than 2 years) were used for the updating and refinement of critical load values.
- Studies with higher nitrogen additions or shorter experimental periods were only interpreted with respect to the understanding of effects mechanisms, possible nitrogen limitation or sensitivity of the system. The methods used in these studies were carefully scrutinised to identify factors related to the experimental design or data analysis, which may constrain their use in assessing critical loads. This includes evaluation of the precision of the estimated values of background deposition at the experimental site.

- Empirical critical loads for levels 2 and 3 of the EUNIS classification were agreed on for a range of deposition values for all EUNIS classes, including forest and woodland habitats (EUNIS class T). The reliability of empirical critical loads was qualitatively established, distinguishing between 'reliable', 'quite reliable', and 'expert judgement', symbolised by ##, #, and (#), respectively.

5.3.1.5 Recommendations about empirical critical loads for eutrophication from the Berne workshop

- More research and data are required to establish a $CL_{emp}N$ for the following ecosystems: several grasslands and steppe meadows; all Mediterranean vegetation types; wet (swamp) forests; many mires and fens and several coastal habitats; in addition, more research is needed for all distinguished EUNIS habitat types that have an 'expert' judgement rating.
- Impacts of N enrichment in (sensitive) freshwater and shallow marine ecosystems (including coastal waters) need further research.
- More well-designed gradient studies with both (very) low and high N loads are needed, especially in EUNIS habitat types that are hardly investigated. Furthermore, combining the results of both experimental and gradients studies increases the reliability of the $CL_{emp}N$.
- More research is needed on the differential effects of the deposited N forms (NO_x or NH_y) to be able to determine the critical loads for oxidised and reduced nitrogen separately in the future.
- To refine the current $CL_{emp}N$, long-term experiments (10-20 years) with a high N addition frequency of between 5 and 50 kg N ha^{-1} yr^{-1} in regions with low background, deposition is crucial. This would increase the reliability of the derived $CL_{emp}N$ if the lowest treatment level does not exceed the current critical load.
- Climate change and nitrogen deposition are likely to have strong interactive effects on ecosystem functioning, with climate change altering ecosystem responses to nitrogen deposition and vice versa. More experimental studies are needed to investigate these interactions, as well as more gradient studies that explicitly examine the impacts of nitrogen deposition in combination with climatic gradients.

Overall, it remains crucial to understand the long-term effects of increased nitrogen deposition on ecosystem processes in a representative range of ecosystems. It is thus very important to quantify the effects of nitrogen loads by manipulation of nitrogen inputs in long-term ecosystem studies in unaffected and affected areas. These data are essential to validate the set of empirical critical loads, but also to develop existing and new robust dynamic ecosystem models and/or multiple correlative species models, which are reliable enough to assess nitrogen impacts on (semi-)natural ecosystems and to predict (natural) recovery rates for nitrogen-affected systems.

5.3.2 Empirical critical loads for acidity

Empirical approaches assign an acidity critical load to soils on the basis of soil mineralogy and/or chemistry. For example, at the Critical Loads Workshop at Skokloster (Nilsson and Grennfelt 1988), soil forming materials were divided into five classes on the basis of the dominant weatherable minerals. A critical load range, rather than a single value, was assigned to each of these classes according to the amount of acidity that could be neutralised by the base cations produced by mineral weathering (Table 5.2).

Table 5.2: Mineralogical classification of soil materials and soil critical loads.

Minerals controlling weathering	Critical load range
Quartz, K-feldspar	<200
Muscovite, Plagioclase, Biotite (<5%)	200–500
Biotite, Amphibole (<5%)	500–1000
Pyroxene, Epidote, Olivine (<5%)	1000–2000
Carbonates	>2000

The classification of soil materials developed at Skokloster (Table 5.2) used a relatively small range of primary silicate minerals and carbonates. A larger range of minerals has been classified by Sverdrup and Warfvinge (1988a) and Sverdrup et al. (1990). The following mineral classes have been identified:

- Very fast weathering minerals include carbonate minerals that have the potential to dissolve very rapidly, in a geological perspective. The group includes calcite, dolomite, magnesite, and brucite.
- Fast weathering minerals include the silicate minerals with the fastest weathering rate. The group comprises minerals such as anorthite and nepheline, olivine, garnet, jadeite, and diopside. A soil with a major content of these minerals would be resistant to soil acidification. Intermediate weathering minerals include enstatite, hypersthene, augite, hornblende, glaucophane, chlorite, biotite, epidote, and zoisite.
- Slow weathering minerals include albite, oligoclase, labradorite, and illite. Soils with a majority of such minerals will be sensitive to soil acidification.
- Very slow weathering minerals include K-feldspar, muscovite, mica, montmorillonite, and vermiculite. Soils with a majority of these minerals will be sensitive to soil acidification.
- Inert minerals are those that dissolve so slowly or provide so little neutralising substance that they may be considered as inert regarding soil acidification. This includes minerals such as quartz, rutile, anatase, kaolinite, and gibbsite.

For each of the above mineral classes, weathering rates for soils with different mineral contents have been proposed (Table 5.3, Sverdrup et al. 1990).

Table 5.3: Weathering rates (in eq/(ha·m)/yr) for four selected mineral classes of soil material based on a soil depth of one meter – to convert to critical load values multiply by soil thickness in meters.

Mineral class	Average soil mineral class content			
	100%	30%	3%	0.3%
Very fast weathering	25000	15000	10000	3000
Fast weathering	15000	10000	3000	300
Intermediate weathering	10000	3000	300	30
Slow weathering	600	200	20	-

Mineral class	Average soil mineral class content			
	100%	30%	3%	0.3%
Very slow weathering	300	100	10	-
Inert	100	100	-	-

In addition, a number of modifying factors (such as precipitation, vegetation, soil drainage) were identified that would enable the critical load value to be adjusted within the ranges (Table 5.4, after Nilsson and Grennfelt, 1988). For example, some factors could make the soil more sensitive to acidification, requiring that the critical load be set to the lower end of the range, while other factors could make the soil less sensitive, setting the critical load at the upper end of the range.

Table 5.4: Modifying factors causing an increase or decrease in critical loads.

Modifying factor	Effect on critical load	
	Decrease	*Increase*
Precipitation	High	Low
Vegetation	Coniferous forest	Deciduous forest
Elevation, slope	High	Low
Soil texture	Coarse-sandy	Fine
Soil drainage	Free	Impeded
Soil sulphate adsorption capacity	Low	High
Base cation deposition	Low	High

The information shown in Table 5.2 toTable 5.4 provide the basis on which empirical acidity critical loads can be assigned to soils. If mineralogical data are available for the units of a soil map, critical loads can be assigned to each unit and a critical loads map produced.

An example of the development of a critical load map at the national scale using empirical approaches is given by Hornung et al. (1995). In the UK, this approach has been used to define acidity critical loads for non-forest ecosystems by setting a critical load that will protect the soil upon which the habitat depends (Hall et al. 1998, 2003). The critical load is effectively the base cation weathering rate, with the leaching of acid neutralising capacity (ANC) set to zero and can be used in the calculations of the maximum critical loads of sulphur and nitrogen (see section 5.3.2).

Other methods of estimating base cation weathering are discussed in section 5.3.2.

5.4 Modelling critical loads for terrestrial ecosystems

The purpose of a model-based approach to calculating critical loads is to link, via mathematical equations, a chemical criterion (critical limit) with the maximum deposition(s) 'below which significant harmful effects on specified sensitive elements of the environment do not occur', (i.e., for which the criterion is not violated). In most cases, the 'sensitive element of the environment' will be of a biological nature (e.g., the vitality of a tree; the species composition of a heather ecosystem) and thus the criterion should be a biological one. However, there is a dearth of simple yet reliable models that adequately describe the whole chain from deposition to

biological impact. Therefore, chemical criteria are used instead, and simple chemical models are used to derive critical loads. This simplifies the modelling process, but shifts the burden to find, or derive, appropriate (soil) chemical criteria (and critical limits) with proven (empirical) relationships to biological effects. The choice of the critical limit is an important step in deriving a critical load, and much of the uncertainty in critical load calculations stems from the uncertainty in the link between soil chemistry and biological impact.

In the following we consider only steady-state models and concentrate on the so-called Simple Mass Balance (SMB) model (Posch et al. 2015) as the standard model for calculating critical loads for terrestrial ecosystems under the LRTAP Convention (Sverdrup et al. 1990, Sverdrup and De Vries 1994). The SMB model is a single-layer model, in other words, the soil is treated as a single homogeneous compartment. Furthermore, it is assumed that the soil depth is at least the depth of the rooting zone, which allows us to neglect the nutrient cycle and to deal with net growth uptake only. Additional simplifying assumptions include:

- all evapotranspiration occurs on the top of the soil profile;
- percolation is constant through the soil profile and occurs only vertically;
- physico-chemical constants are assumed uniform throughout the whole soil profile;
- internal fluxes, such as weathering rates, nitrogen immobilisation etc.;
- are independent of soil chemical conditions (such as pH).

Since the SMB model describes steady-state conditions, it requires long-term averages for input fluxes. Short-term variations (e.g., episodic, seasonal, inter-annual, due to harvest and as a result of short-term natural perturbations) are not considered but are assumed to be included in the calculation of the long-term mean. In this context, 'long-term' is defined as about 100 years, (i.e., at least one rotation period for forests). Ecosystem interactions and processes like competition, pests, herbivore influences etc. are not considered in the SMB model. Although the SMB model is formulated for undisturbed (semi-)natural ecosystems, the effects of extensive management, such as grazing and the burning of moor, could be included.

Besides the single-layer SMB model, there exist multi-layer steady-state models for calculating critical loads. Examples are the MACAL model (De Vries 1988) and the PROFILE model (Warfvinge and Sverdrup 1992b), which has, at its core, a model for calculating weathering rates from total mineral analyses. These models will not be discussed here, and the interested reader is referred to the literature.

In the following sections we will derive the SMB model for critical loads of nutrient nitrogen (eutrophication) and critical loads of acidifying sulphur and nitrogen.

5.4.1 Critical loads of nutrient nitrogen (eutrophication)

5.4.1.1 Model derivation

The starting point for calculating critical loads of nutrient N with the SMB model is the mass balance of total nitrogen (N) for the soil compartment under consideration (inputs = sinks + outputs):

(V.1)

$$N_{dep} + N_{fix} = N_{ad} + N_i + N_u + N_{de} + N_{eros} + N_{fire} + N_{vol} + N_{le}$$

where:

N_{dep} = total N deposition

N_{fix} = N 'input' by biological fixation

N_{ad} = N adsorption

N_i = long-term net immobilisation of N in soil organic matter

N_u = net removal of N in harvested vegetation and animals

N_{de} = flux of N to the atmosphere due to denitrification

N_{eros} = N losses through erosion

N_{fire} = N losses in smoke due to fires, whether wild or controlled

N_{vol} = N losses to the atmosphere via NH3 volatilisation

N_{le} = leaching of N below the root zone

The units used are eq/ha/yr (or $mol_c ha^{-1} a^{-1}$ in proper SI nomenclature).

The following assumptions lead to a simplification of eq. V.1:

- Nitrogen adsorption (e.g., the adsorption of NH_4 by clay minerals) can temporarily lead to an accumulation of N in the soil, however it is stored/released only when the deposition *changes* and can thus be neglected in steady state considerations.
- Nitrogen fixation is negligible in most forest ecosystems, except for N-fixing species.
- The loss of N due to fire, erosion and volatilisation is small for most ecosystems in Europe, and therefore neglected in the following discussion. Alternatively, one could replace N_i by $N_i + N_{eros} + N_{fire} + N_{vol} - N_{fix}$ in the subsequent equations.
- The leaching of ammonium (NH_4) can be neglected in all forest ecosystems due to preferential uptake and complete nitrification within the root zone (i.e., $NH_{4,le}$=0, N_{le}=$NO_{3,le}$).

Under these simplifying assumptions eq. V.1 becomes:

(V.2)

$$N_{dep} = N_i + N_u + N_{de} + N_{le}$$

From this equation, a critical load is obtained by defining an acceptable limit to the leaching of N, $N_{le(acc)}$, the choice of this limit depends on the 'sensitive element of the environment' that is to be protected. If an acceptable leaching is inserted into eq. V.2, the deposition of N becomes the critical load of nutrient nitrogen, $CL_{nut}(N)$:

(V.3)

$$CL_{nut}(N) = N_i + N_u + N_{de} + N_{le(acc)}$$

When deriving the critical load of nutrient N as eq. V.3 it is assumed that the sources and sinks do not depend on the deposition of N. This is unlikely to be the case and thus all quantities should be taken 'at critical load'. However, to compute 'denitrification at critical load' one needs to know the critical load, the very quantity one wants to compute. The only clean way to avoid this circular reasoning is to establish a functional relationship between deposition and the sink of N, insert this function into eq. V.2, and solve for the deposition in order to obtain the critical load. This has been done for denitrification; in the simplest case denitrification is linearly related to the net input of N (De Vries et al. 1993, 1994):

(V.4)

$$N_{de} = \begin{cases} f_{de} \cdot (N_{dep} - N_i - N_u), & if\ N_{dep} > N_i + N_u \\ 0, & else \end{cases}$$

where f_{de} ($0 \leq f_{de} < 1$) is the so-called denitrification fraction, a site-specific quantity. This formulation implicitly assumes that immobilisation and uptake are faster processes than denitrification. Inserting this expression for N_{de} into eq. V.2 and solving for the deposition leads to the following expression for the critical load of nutrient N:

(V.5)

$$CL_{nut}(N) = N_i + N_u + \frac{N_{le(acc)}}{1 - f_{de}}$$

An alternative, non-linear, equation for the deposition-dependence of denitrification has been proposed by Sverdrup and Ineson (1993) based on the Michaelis-Menten reaction mechanism and includes a dependence on soil moisture, pH, and temperature. Also, in this case $CL_{nut}(N)$ can be calculated explicitly. For further details the reader is referred to Posch et al. (1993).

More generally, it would be desirable to have deposition-dependent equations (models) for all N fluxes in the critical load equation. However, these either do not exist or are so involved that no simple explicit expression for $CL_{nut}(N)$ can be found. Although this does not matter in principle, it would reduce the appeal and widespread use of the critical load concept. Therefore, when calculating critical loads from eq. V.3 or eq. V.5, the N fluxes should be estimated as long-term averages derived from conditions not influenced by elevated anthropogenic N inputs.

5.4.1.2 The acceptable leaching of inorganic nitrogen

The value set for the acceptable leaching of inorganic N depends on the 'harmful effects' that should be avoided. These include eutrophication, vegetation changes, nutrient imbalances, and plant sensitivity to frost and diseases. There are two approaches to estimate the acceptable N leaching. Option (a) is based on acceptable N concentrations in soil solution combined with runoff amounts and option (b) sets absolute values for acceptable annual N-leaching amounts. Option (b) can be chosen if option (a) is not meaningful, (e.g., due to high precipitation amounts) or in polar/sub polar regions.

(a) The acceptable N leaching (in eq/ha/yr) can be calculated based on an acceptable N concentration and the precipitation surplus percolating from the root zone:

(V.6)

$$N_{le(acc)} = Q \cdot [N]_{acc}$$

where $[N]_{acc}$ is the acceptable N concentration (eq/m^3) and Q is the precipitation surplus (in m^3/ha/yr). Values for acceptable N concentrations derived from combined modelling and observation approaches are given in Table 5.5 (adapted from De Vries et al. 2007). To convert the values in Table 5.5 to eq/m^3 divide them by 14.

The use of the N concentrations in Table 5.5 in high precipitation areas can lead to very high nitrate leaching amounts accompanied by substantial losses of base cations. This nutrient loss can lead to a gradual decrease of the base saturation with the risk to induce nutrient imbalances in the vegetation. Using the values in Table 5.5 in high precipitation areas may finally also lead to critical loads of nutrient nitrogen being much higher than the empirical critical loads of nitrogen set for specific ecosystems (see Section 5.2, Table 5.1). (b) The acceptable inorganic N leaching flux can be estimated based on long-term observations in catchment and plot studies and has to be formulated as total annual output and expressed as a long-term average. In the case of forest

ecosystems, this would be at least over a rotation period. The values should reflect the conditions in mostly undisturbed and undamaged natural ecosystems in order to meet the underlying concepts for setting critical loads formulated at the UNECE workshops held in Lökeberg (Grennfelt and Thörnelöf 1992) and in Grange-over Sands (Hornung et al. 1994) which include the avoidance of nitrogen saturation in the long-term and thus the prevention of concomitant effects like nutrient imbalances, biodiversity changes, and increase of overall ecosystem instability. Enhanced N leaching is considered as an indication of N saturation (Aber et al. 1989, Grennfelt and Thörnelöf 1992).

Much of the data available on the total annual leaching of nitrogen from European catchment and plot studies has been brought together by Hornung et al. (1990), Dise, and Wright (1995). The following ranges of values are largely based on these reviews and also include information from North America. They are recommended in the absence of relevant national datasets as already agreed upon in the 1996 version of the Mapping Manual.

- Boreal and temperate heaths and bogs: 0-0.5 kg N ha^{-1} yr^{-1} (inorganic N); losses of organic N can be larger, but few data are currently available (there is an urgent need for more data on organic N outputs from a range of ecosystems).
- Managed coniferous forest: 0.5-1.0 kg N ha^{-1} yr^{-1}.
- Intensive coniferous plantations: 1-3 kg N ha^{-1} yr^{-1}. (Can be significantly larger if open drains are dug prior to planting).
- Temperate deciduous forests: 2-4 kg N ha^{-1} yr^{-1}.
- Temperate grasslands: 1-3 kg N ha^{-1} yr^{-1}.
- Mediterranean forests: 1-2 kg N ha^{-1} yr^{-1}.

To convert the values to eq multiply them by 71.428.

Table 5.5: Critical (acceptable) nitrogen concentrations in soil solution for calculating CLnut(N).

Impact	$[N]_{acc}$ (mgN/L)
Vegetation changes in forested ecosystems (data established in Sweden):1	
Lichens to cranberry (lingonberries)	0.2–0.4[1]
Cranberry to blueberry	0.4–0.6[1]
Blueberry to grass	1–2[1]
Grass to herbs	3–5[1]
Vegetation changes (data established in The Netherlands):2	
Ground vegetation in coniferous forest	2.5–4[2]
Ground vegetation in deciduous forest	3.5–6.5[2]
Grass lands	3[2]
Heath lands	3–6[2]
Other impacts on forests:	

Impact	$[N]_{acc}$ (mgN/L)
Nutrient imbalances	0.2–0.4[3]
Elevated nitrogen leaching/N saturation	1[4]
Fine root biomass/root length	1–3[5]
Sensitivity to frost and fungal diseases	3–5[6]

[1] In the 2004 version of the Mapping Manual, the use of critical N concentrations was not limited to Northern Europe. This study, however, shows that its derivation is limited to forests in Scandinavia based on an inverse use of the SMB model, using empirically derived critical N loads and backcalculating the concentrations (see Annex 9 of de Vries et al. 2007).

[2] This refers to the range in median values derived with SMART-NTM using a dynamic and a steady state approach. The actual range is much larger and varies often as much as the median value (variation coefficient of 100%). For grassland, the value only refers to the study using a dynamic modelling approach (see text for reasons). The results officially apply only to the Netherlands.

[3] Actually, the range of 0.2-0.4 $mg.l^{-1}$ is given for deciduous trees, whereas the value of 0.2 is given for conifers. It is, however, likely that this range also applies for conifers and therefore, both forest types are lumped in this table.

[4] Based on a differentiation between undisturbed and "leaky" forest sites by Stoddard (1994).

[5] Based on a relationship between root biomass and dissolved N concentration in Matzner and Murrach (1995).

[6] Based on a relationship between dissolved N concentration and a critical N concentration in the needles of 18 $g.kg^{-1}$, above which the sensitivity to frost and fungal diseases increases.

The advice of national experts should be sought when deciding on the most appropriate value. Clear fellings, fire, and large-scale disturbances can lead to short-term high nitrogen leakage, however, they do not necessarily change the critical load. In any case, it is recommended that critical loads of nitrogen resulting from the use of acceptable N leaching values according to the approaches (a) or (b) should be compared with the ecosystem-specific empirical critical loads for nitrogen given in Chapter 5.3 in order to check the plausibility of the results from the mass balance approach. In view of the precautionary principle, it is recommended to use the lowest of the obtained critical load values.

5.4.1.3 Sources and derivation of input data

The obvious sources of input data for calculating critical loads are measurements at the site under consideration. However, in many cases these will not be available. A discussion on N sources and sinks can be found in Hornung et al. (1995) and UNECE (1995). Some data sources and default values and procedures to derive them are summarised below.

5.4.1.3.1 Nitrogen immobilisation

Ni refers to the long-term net immobilisation (accumulation) of N in the root zone, i.e., the continuous build-up of stable C-N compounds in (forest) soils. In other words, this immobilisation of N should not lead to significant changes in the prevailing C/N ratio. This has to be distinguished from the high amounts of N accumulated in the soils over many years (decades) due to the increased deposition of N, leading to a decrease in the C/N ratio in the topsoil. Using data from Swedish forest soil plots, Rosén et al. (1992) estimated the annual N immobilisation since the last glaciation at 0.2–0.5 kg N/ha/yr (14.286–35.714 eq/ha/yr). Similar rates of 0.2 – 0.8 kg N/ha/yr (14.286–57.142 eq/ha/yr) have also been calculated by Höhle et al. (2017) based on German, French and Swiss soil data.

For estimating site specific long-term net N immobilisation, measured N stocks in soil, for example from the ICP Forests network, may be used. The average rate of N immobilisation calculated as the ratio of the N stock divided by soil age may be regarded as the maximal acceptable value for a sustainable long-term net N immobilisation. Nevertheless, N

immobilisation is not a linear process. Most net N immobilisation occurs in an early state of soil development (Egli et al. 2012, Olsen 1958, Jenny 1965, Lichter 1998) which is already completed in many soils in Europe. For soils in a dynamic equilibrium state (e.g., soils with A-B-C horizons) in undisturbed environments, a net N immobilisation close to zero can be assumed. It should be pointed out, however, that higher values (closer to present-day immobilisation rates) have been used in critical load calculations. Nevertheless, there is no consensus yet on long-term sustainable immobilisation rates.

5.4.1.3.2 Nitrogen uptake

The uptake flux N_u equals the long-term average removal of N from the ecosystem. For unmanaged ecosystems (e.g., national parks) the long-term (steady-state) net uptake is basically zero, whereas for managed forests it is the long-term net growth uptake. The harvesting practice is of crucial importance, whether stems only, stems plus (parts of) branches, or stems plus branches plus leaves/needles (whole-tree harvesting) are removed. The uptake of N is then calculated as:

(V.7)

$$N_u = \frac{N\ removedin\ harvestedbiomass\ (eq/ha)}{intervalbetween\ harvests(rotationperiod)(yr)}$$

The amount of N in the harvested biomass (stems and branches) can be calculated as following:
ρp

(V.8)

$$N_u = k_{gr} \cdot \rho_{st} \cdot (ctN_{st} + fbr,st \cdot ctN_{br})$$

where k_{gr} is the average annual growth rate (m³/ha/yr), ρ_{st} is the density of stem wood (kg/m³), ctN is the N content in stems (subscript st) and branches (subscript *br*) (eq/kg), and $f_{br,st}$ is the branch-to-stem ratio (kg/kg). The contribution of branches should be neglected in case of stem removal.

Values for the density of stem wood of most trees are in the range of 400–500 kg/m³ for conifers and 550–700 kg/m³ for deciduous trees. The branch-to-stem ratio is about 0.15 kg/kg for conifers and 0.20 kg/kg for deciduous trees (Kimmins et al. 1985, De Vries et al. 1990). According to Swedish data (Rosén 1990; see also Reinds et al. 2001) the contents of N in stems are 1 g/kg for conifers and 1.5 g/kg in deciduous trees, whereas in branches of all tree species the N content is 4 g/kg in the south and 2 g/kg in the north. In a recent report Jacobsen et al. (2002) have summarised the results of a large number of studies on that subject, and Table 5.6 shows the average element contents in 4 major tree species, both for stems and branches. For N, the values have to be multiplied by 1/14=0.07143 to obtain the N contents in eq/kg.

Table 5.6: Mean (and standard deviation) of the element contents in stems and branches (both incl. bark) of four tree species (Jacobsen et al. 2002); the number of data points ranges from 6 to 32.

Tree species	Contents (g/kg) in stems (incl. bark)				Contents (g/kg) in branches (incl. bark)			
	N	Ca[a)]	Mg	K	N	Ca	Mg	K
Oak	2.10	2.47	0.18	1.05	6.19	4.41	0.44	2.00
quercus spp	(0.46)	(1.42)	(0.07)	(0.51)	(1.02)	(0.65)	(0.14)	(0.47)
Beech	1.54	1.80	0.26	1.04	4.27	4.02	0.36	1.50

Tree species	Contents (g/kg) in stems (incl. bark)				Contents (g/kg) in branches (incl. bark)			
	N	Ca[a)]	Mg	K	N	Ca	Mg	K
fagus sylv.	(0.25)	(1.12)	(0.09)	(0.13)	(1.36)	(1.91)	(0.13)	(0.44)
Spruce	1.22	1.41	0.18	0.77	5.24	3.33	0.53	2.39
picea abies	(0.49)	(0.40)	(0.06)	(0.43)	(1.66)	(1.06)	(0.27)	(1.35)
Pine	1.09	1.08	0.24	0.65	3.61	2.07	0.43	1.67
pinus sylv.	(0.30)	(0.30)	(0.09)	(0.28)	(1.28)	(0.65)	(0.11)	(0.68)

[a)] Note that for Ca data points from calcareous sites are included in the statistics.

Growth rates used should be long-term average values that are typical for the site. It must be noted that recent growth rates are higher due to increased N input. Therefore, it is recommended to use older investigations (yield tables), preferably from before 1960–70. An example of how to use national inventory information to compute forest growth (and critical loads) in Germany can be found in Nagel and Gregor (1999).

Net uptake of N in non-forest natural and (semi-)natural ecosystems is insignificant unless they are used for extensive grazing. For example, in the United Kingdom net removal of N in sheep (mutton/wool) due to extensive grazing is between 0.5 and 2.0 kgN/ha/yr, depending on site fertility and grazing density.

5.4.1.3.3 Denitrification

Dutch and Ineson (1990) reviewed data on rates of denitrification. Typical values of N_{de} for boreal and temperate ecosystems are in the range of 0.1–3.0 kgN/ha/yr (=7.14–214.3 eq/ha/yr), where the higher values apply to wet(ter) soils; rates for well drained soils are generally below 0.5 kgN/ha/yr.

With respect to deposition-dependent denitrification, values for the denitrification fraction f_{de} have been given by De Vries et al. (1993) based on data from Breeuwsma et al. (1991) and Steenvorden (1984): f_{de}=0.8 for peat soils, 0.7 for clay soils, 0.5 for sandy soils with gleyic features and f_{de}=0–0.1 for sandy soils without gleyic features. Reinds et al. (2001) related the denitrification fraction to the drainage status of the soil according to Table 5.7:

Table 5.7: Denitrification fraction f_{de} as a function of the soil drainage (Reinds et al. 2001).

Drainage status	Excessive	Good	Moderate	Imperfect	Poor	Very poor
f_{de}	0	0.1	0.2	0.4	0.7	0.8

5.4.1.3.4 Precipitation surplus

The precipitation surplus Q is the amount of water percolating from the root zone. It is conveniently calculated as the difference between precipitation and actual evapotranspiration, and it should be the long-term climatic mean annual value. In many cases evapotranspiration will have to be calculated by a model using basic meteorological input data (precipitation, temperature, radiation etc.). For the basics of modelling evapotranspiration see Monteith and Unsworth (1990) and for an extensive collection of models see Burman and Pochop (1994). Historical time series of meteorological data can be found on the website of the Climate Change Research Unit of the University of East Anglia (www.cru.uea.ac.uk/data).

5.4.2 Critical loads of acidity

5.4.2.1 Model derivation: the simple mass balance (smb) model

The starting point for deriving critical loads of acidifying S and N for soils is the charge balance of the ions in the soil leaching flux (De Vries 1991, Posch et al. 2015):

(V.9)

$$H_{le} + Al_{le} + BC_{le} + NH_{4,le} = SO_{4,le} + NO_{3,le} + Cl_{le} + HCO_{3,le} + RCOO_{le}$$

where the subscript le stands for leaching, *Al* stands for the sum of all positively charged aluminium species, *BC* is the sum of base cations (*BC=Ca+Mg+K+Na*) and *RCOO* is the sum of organic anions. A leaching term is given by $X_{le}=Q\cdot[X]$, where [*X*] is the soil solution concentration of ion X and Q is the precipitation surplus. All fluxes are expressed in equivalents (moles of charge) per unit area and time (eq/ha/yr). The concentrations of OH and CO_3 are assumed zero, which is a reasonable assumption even for calcareous soils. The leaching of Acid Neutralising Capacity (ANC) is defined as:

(V.10)

$$ANC_{le} = HCO_{3,le} + RCOO_{le} - H_{le} - Al_{le}$$

Combination with eq. V.9 yields:

(V.11)

$$BC_{le} + NH_{4,le} - SO_{4,le} - NO_{3,le} - Cl_{le} = ANC_{le}$$

This shows the alternative definition of ANC as "sum of (base) cations minus strong acid anions". For more detailed discussions on the processes and concepts of (soil) chemistry encountered in the context of acidification see the books by Reuss and Johnson (1986) or Ulrich and Sumner (1991).

Chloride is assumed to be a tracer. In other words, there are no sources or sinks of Cl within the soil compartment, and chloride leaching is therefore equal to the Cl deposition (subscript dep):

(V.12)

$$Cl_{le} = Cl_{dep}$$

In a steady-state situation the leaching of base cations has to be balanced by the net input of base cations. Consequently, the following equation holds:

(V.13)

$$BC_{le} = BC_{dep} + BC_w + Bc_u$$

where the subscripts *w* and *u* stand for weathering and net growth uptake (i.e., the net uptake by vegetation that is needed for long-term average growth); *Bc=Ca+Mg+K*, reflecting the fact that Na is not taken up by vegetation. Base cation input by litterfall and Bc removal by maintenance uptake (needed to re-supply base cations in leaves) is not considered here, assuming that both fluxes are equal (in a steady-state situation). Also, the finite pool of base cations at the exchange sites (cation exchange capacity, CEC) is not considered. Although cation exchange might buffer incoming acidity for decades, its influence is only a temporary phenomenon, which cannot be accounted for when considering long-term steady-state conditions.

The leaching of sulphate and nitrate can be linked to the deposition of these compounds by means of mass balances for S and N. For S this reads (De Vries 1991):

(V.14)

$S_{le} = S_{dep} - S_{ad} - S_i - S_u - S_{re} - S_{pr}$

where the subscripts *ad, i, re* and *pr* refer to adsorption, immobilisation, reduction, and precipitation, respectively. An overview of sulphur cycling in forests by Johnson (1984) suggests that uptake, immobilisation, and reduction of S is generally insignificant. Adsorption (and in some cases precipitation with Al complexes) can temporarily lead to a strong accumulation of sulphate (Johnson et al. 1979, 1982). However, sulphate is only stored or released at the adsorption complex when the input (deposition) *changes*, since the adsorbed S is assumed in equilibrium with the soil solution S. Only dynamic models can describe the time pattern of ad- and desorption of sulphate, but under steady-state conditions, S ad- and desorption and precipitation/mobilisation are not considered. Since sulphur is completely oxidised in the soil profile, $SO_{4,le}$ equals S_{le}, and consequently:

(V.15)

$SO_{4,le} = S_{dep}$

For nitrogen, the mass balance in soil is (see Sec. 5.3.1):

(V.16)

$N_{le} = N_{dep} + N_{fix} - N_{ad} - N_i - N_u - N_{de} - N_{eros} - N_{fire} - N_{vol}$

where the subscripts *fix* refers to fixation of N, *de* to denitrification, and *eros*, *fire* and *vol* to the loss of N due to erosion, forest fires and volatilisation, respectively. N_i is the long-term immobilisation of N in the root zone, and N_u the net growth uptake (see above). Furthermore, the leaching of NH_4 can be neglected in almost all forest ecosystems due to (preferential) uptake and complete nitrification within the root zone (i.e., $NH_{4,le}$=0). Under these various assumptions eq. V.16 simplifies to:

(V.17)

$N_{le} = NO_{3,le} = N_{dep} - N_i - N_u - N_{de}$

Inserting eqs. 5.12, 5.13, 5.15, and 5.17 into eq. V.11 leads to the following simplified charge balance for the soil compartment:

(V.18)

$S_{dep} + N_{dep} = BC_{dep} - Cl_{dep} + BC_w - Bc_u + N_i + N_u + N_{de} - ANC_{le}$

Strictly speaking, we should replace $NO_{3,le}$ in the charge balance not by the right-hand side of eq. V.17, but by $\max\{N_{dep}-N_i-N_u-N_{de},0\}$, since leaching cannot become negative; the same holds true for base cations. Nevertheless, this would lead to unwieldy critical load expressions. Therefore, one should proceed with eq. V.18 keeping this constraint in mind.

Since the aim of the LRTAP Convention is to reduce *anthropogenic* emissions of S and N, sea-salt derived sulphate should not be considered in the balance. To retain charge balance, this is achieved by applying a sea-salt correction to sulphate, chloride, and base cations, using either Cl or Na as a tracer, whichever can be (safely) assumed to originate from sea-salts only. Denoting sea-salt corrected depositions with an asterisk, one has either Cl^*_{dep}=0 or Na^*_{dep}=0, respectively. For procedures to compute sea-salt corrected depositions, see 5.9.4 (Annex 4).

For given values for the sources and sinks of S, N and Bc, eq. V.18 allows the calculation of the leaching of ANC, and thus assessment of the acidification status of the soil. Conversely, critical loads of S, $CL(S)$, and N, $CL(N)$, can be computed by defining a critical ANC leaching, $ANC_{le,crit}$:

(V.19)

$$CL\ (S) + CL\ (N) = BC^*_{dep} - Cl^*_{dep} + BC_w - Bc_u + N_i + N_u + N_{de} - ANC_{le,crit}$$

A so-called critical load of potential acidity has earlier been defined (see Sverdrup et al. 1990) as:

(V.20)

$$C_L(Ac_{pot}) = BC_W - Bc_u + N_i + N_u + N_{de} - ANC_{le,crit}$$

with $Ac_{pot} = S_{dep}+N_{dep}-BC^*_{dep} + Cl^*_{dep}$.

The term 'potential' is used since NH3 is treated as a potential acid due to the assumed complete nitrification. $CL(Ac_{pot})$ has been defined to have no deposition terms in its definition, since Bc and Cl deposition are not really an ecosystem property and can (and often do) change over time. However, since these depositions are partly of non-anthropogenic origin (e.g., Saharan dust) and since they are not subject to emission reduction negotiations, they are kept in the critical load definition for convenience.

A further distinction has been made earlier (see, e.g., Sverdrup and De Vries 1994) between 'land use acidity' $Bc_u-N_i-N_u-N_{de}$ and 'soil acidity' which is used to define a so-called critical load of actual acidity as:

(V.21)

$$CL(A) = BC_W - ANC_{le,crit}$$

The reason for making this distinction was to exclude all variables that may change in the long term, such as uptake of Bc and N, which are influenced by forest management, and N immobilisation and denitrification, which may change due to changes in the hydrological regime. There are two problems with this reasoning: (a) the remaining terms in eq. V.21 are also liable to change (e.g., ANC leaching depends on precipitation surplus, see below), and (b) uptake and other N processes are a defining part of the ecosystem (vegetation) itself. In other words, $CL(A)$ may be a critical load of *soil* acidity, but it is rarely the soil that is the 'sensitive element' that needs to be protected. The sensitive element is usually the vegetation growing on that soil. Nevertheless, quantities such as $CL(A)$ are computed and reported, and they can have a role as useful short-hand notation for the variables involved.

Note that eq. V.19 does not give a unique critical load for S or N. However, nitrogen sinks cannot compensate incoming sulphur acidity, and therefore the maximum critical load for sulphur is given by:

(V.22)

$$CL_{max}(S) = BC^*_{dep} - Cl^*_{dep} + BC_W - Bc_u - ANC_{le,crit} = BC^*_{dep} - Cl^*_{dep} - Bc_u + CL(A)$$

as long as N deposition is lower than all the N sinks, termed the minimum critical load of N. In other words, as long as:

(V.23)

$$N_{dep} \leq CL_{mn}\ (N) = N_i + N_u + N_{de}$$

Finally, the maximum critical load of nitrogen (in the case of zero S deposition) is given by:
(V.24)

$$CL_{max}\ (N) = CL_{min}\ (N) + CL_{max}\ (S)$$

The three quantities $CL_{max}\ (S)$, $CL_{min}\ (N)$, and $CL_{max}(N)$ define the *critical load function* (CLF; depicted in Figure 5.4(a)). Every deposition pair (N_{dep}, S_{dep}) lying on the CLF are critical loads of acidifying S and N.

Figure 5.4: Critical load function (CLF) of sulphur and acidifying nitrogen, defined by the three quantities $CL_{max}(S)$, $CL_{min}(N)$, and $CL_{max}(N)$. (a) with constant denitrification N_{de}, and thus a 45° slope of the CLF; (b) with deposition-dependent denitrification, resulting in a smaller $CL_{min}(N)$ and a flatter slope, depending on f_{de}. The grey area below the CLF denotes deposition pairs resulting in an ANC leaching greater than ANC_{ecrit} (non-exceedance of critical loads; see Chapter 7).

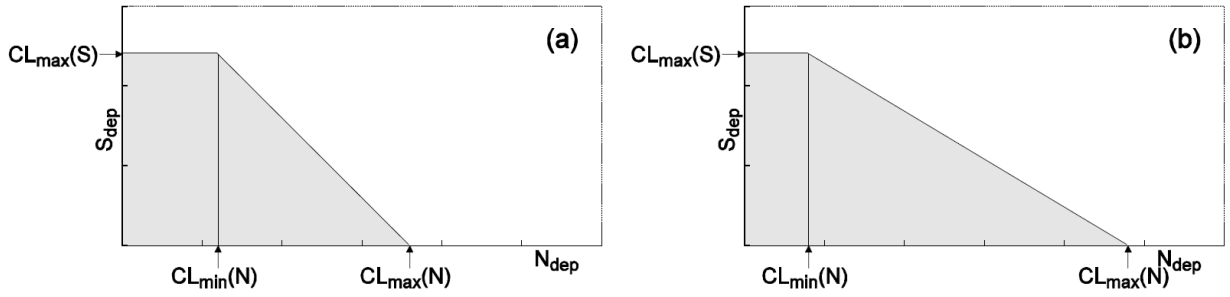

Source: This figure is adopted from Chapter 5 of a previous version of the Mapping Manual

Deriving critical loads as shown above assumes that the sources and sinks of N do not depend on the N deposition, though this is unlikely to be true. As in section 5.3.1, we also consider the case of denitrification being linearly related to the net input of N. Substituting eq. V.4 for N_{de} into the equations above results in the following expressions for CL_{mn} (N) and $CL_{max}(N)$:

(V.25)

$$CL_{min}\,(N) = N_i + N_u$$

and

(V.26)

$$CL_{max}(N) = CL_{min}(N) + \frac{CL_{max}(S)}{1 - f_{de}}$$

where f_{de} $(0 \leq f_{de} < 1)$ is the denitrification fraction; CL_{max} (S) remains the same (eq. V.22). An example of a critical load function with $f_{de} > 0$ is shown in Figure 5.4(b).

5.4.2.2 Chemical criteria and the critical leaching of acid neutralising capacity

The leaching of Acid Neutralising Capacity (ANC) is defined in eq. V.10. In the simplest case bicarbonate (HCO_3) and organic anions (RCOO) are neglected since in general they do not contribute significantly at low pH values (but see section 5.3.2.4). In this case the ANC leaching is given by:

(V.27)

$$ANC_{le} = -H_{le} - A_{le} = -Q \cdot ([H]+[Al])$$

where Q is the precipitation surplus in m^3/ha/yr (see section 5.3.1.3 for data).

It is within the calculation of ANC_{le} that the critical chemical criterion for effects on the receptor is set. Selecting the most appropriate method of calculating ANC_{le} is important, since the different methods may result in very different critical loads. If, for the same ecosystem, critical loads are calculated using different criteria, the final critical load is the minimum of all those calculated. The main decision in setting the criterion will depend on whether the receptor considered is more sensitive to unfavourable pH conditions or to the toxic effects of aluminium. ANC_{le} can then be calculated by either setting a hydrogen ion criterion (i.e., a critical soil solution pH) and calculating the critical aluminium concentration, or vice versa.

The relationship between $[H]$ and $[Al]$ is described by an (apparent) gibbsite equilibrium:

(V.28)

$$[Al] = K_{gibb} \cdot [H]^3$$

or

$$[H] = ([Al]/K_{gibb})^{cl/3}$$

where K_{gibb} is the gibbsite equilibrium constant (see below). Eq. V.28 is used to calculate the (critical) Al concentration from a given proton concentration, or vice versa. Different critical chemical criteria are listed below together with the equations for calculating $ANC_{le,crit}$. In this context the reader could also consult the minutes of an Expert Workshop on 'Chemical Criteria and Critical Limits' (UNECE 2001, Hall et al. 2001).

5.4.2.2.1 Aluminium criteria

Aluminium criteria are generally considered most appropriate for mineral soils with a low organic matter content. The three commonly used criteria are a) critical aluminium concentration, b) critical base cation to aluminium ratio and c) aluminium mobilisation rate.

a) Critical aluminium concentration:

Critical limits for Al have been suggested for forest soils (e.g., $[Al]_{crit}$=0.2 eq/m^3). These are:

b) Critical base cation to aluminium ratio:

Most widely used for soils is the connection between soil chemical status and plant response (damage to fine root) via a critical molar ratio of the concentrations of base cations (Bc=Ca+Mg+K) and Al in soil solution, denoted as $(Bc/Al)_{crit}$. Values for a large variety of plant species (trees, shrubs, flowering plants, grasses, crop plants) can be found in Sverdrup and Warfvinge (1993a). They are based either on observations made in laboratory experiments and/or in field studies addressing effects on growth parameters (root growth, stem growth, biomass growth) as endpoints. An exemplary dose-response curve for biomass growth of Norway spruce is shown in Figure 5.5. The response functions generally show that the more the *Bc/Al* ratio in the soil solution is below a plant-specific limit, the more pronounced the reduction in growth. Setting a critical *Bc/Al ratio* depends on the accepted growth reduction and varies between plant species. *Bc/Al* ratios for especially useful for drinking water (ground water) protection, (e.g., the EC drinking water standard for $[Al]$ of maximally 0.2 mg/L, or about 0.02 eq/m^3). $ANC_{le,crit}$ can then be calculated as:

(V.29)

$$ANC_{le,crit} = -Q \cdot (([Al]_{crit}/K_{gibb})^{1/3} + [Al]_{crit})$$

examples of European trees and herbs selected from Sverdrup and Warfvinge (1993a) in relation to different growth reduction are given in Table 5.8. The values show that the accepted growth reduction at $(Bc/Al)_{crit}$=1, which has commonly been used previously[14], can be relatively large.

[14] Based on experimental data of Norway spruce showing 20% growth reduction at $(Bc/Al)_{crit}$=1.2 under laboratory conditions, see Figure 5.5 (Sverdrup and Warfvinge, 1993)

Figure 5.5: Dose-response curve for the relationship between Bc/Al ratio and biomass growth derived from experimental studies with Norway spruce (Sverdrup and Warfvinge, 1993).

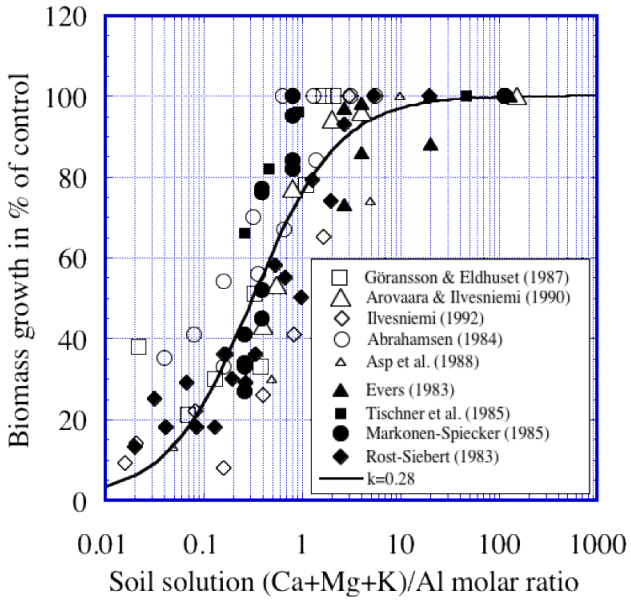

Source: This figure is adopted from a previous version of Chapter 5 of the Mapping Manual

Table 5.8: BC/Al values in relation to different growth reductions for examples of European trees and herbs (from Sverdrup and Warfvinge, 1993).

Latin name	Trivial name	$(BC/Al)_{Crit}$: % growth impact			
		20%	**10%**	**5%**	**2%**
Coniferous trees					
Picea abies	Norway spruce	1.2	2.7	5.7	15
Pinus sylvestris	Scots pine	1.2	1.8	3	5
Deciduous trees					
Fagus sylvatica	European beech	0.6	0.8	1.2	2.5
Quercus robur	Oak				
Betula pendula	Silver birch				
Ground vegetation					
Deschampsia flexuosa	Wavy hairgrass	0.5	1.2	2.5	6.4
Calluna vulgaris	Common heather	0.8	1.8	3.8	10

Furthermore, the ratio $(Bc/Al)_{crit}$=1 may allow acidification to such an extent that the risk for growth reductions is no longer negligible and leads to an unacceptable decrease of the soil base saturation. Arp and Ouimet (2001) examined the observed and calculated relationships between base saturation, pH values, and Bc/Al ratios in organic and mineral soils of forests in Eastern Canada and concluded that, at a $(Bc/Al)_{crit}$ value of 1, the base saturation can be nearly zero. Consequently the Canadian experts used a $(Bc/Al)_{crit}$=10 for the calculation of the critical loads of acidity for forests (Ouimet et al. 2006). Very low base saturation at Bc/Al ratios below 10 have

also been observed in Swiss Forests monitoring sites (Graf et al. 2004, Braun 2013). As an example, according to the observed relationships, a Bc/Al ratio of 4 corresponds approximately to a base saturation of 5%.

Thus, it is recommended to carefully evaluate the relationship between Bc/Al ratios and base saturation when setting critical limit values. It might also be justified to set first of all a critical limit value for base saturation before addressing the Bc/Al ratio, since different tree species have different requirements in terms of base saturation (Puhe and Ulrich 2001). Harmful effects in forest ecosystems, such as decreased rooting depths and increased uprooting during storms, are documented when base saturation is below certain limit values (Braun et al. 2003, Braun et al. 2005). For effects-based relationships regarding the base saturation see Chapter 5.3.2.2.3.

The critical Al leaching is calculated from the leaching of Bc (compare eq. V.13):

(V.30)

$$AL_{le,crit} = 1.5 \cdot \frac{Bc_{le}}{(Bc/Al)_{crit}} = 1.5 \cdot \frac{Bc_{dep} + Bc_w - Bc_u}{(Bc/Al)_{crit}}$$

The factor 1.5 arises from the conversion of mols to equivalents when one assumes that K is divalent. Using eqs.V.27 and V.28, this yields for the critical ANC leaching:

(V.31)

$$ANC_{le,crit} = Q^{2/3} \cdot \left(1.5 \cdot \frac{Bc_{dep} + Bc_w - Bc_u}{K_{gibb} \cdot (Bc/Al)_{crit}}\right)^{1/3} - 1.5 \cdot \frac{Bc_{dep} + Bc_w - Bc_u}{(Bc/Al)_{crit}}$$

Note that the expression $Bc_{le}=Bc_{dep}+Bc_w-BC_u$ has to be non-negative. It has been suggested that it should be above a minimum leaching or, more precisely, there is a minimum concentration of base cations in the leacheate, below which they cannot be taken up by vegetation. In other words, Bc_{le} is set equal to max($Bc_{dep}+Bc_w- BC_u$, $Q\cdot[Bc]_{min}$), with $[Bc]_{min}$ in the order of 0.01eq/m³.

Alternatively, if considered more appropriate, a critical molar ratio of calcium to aluminium in soil solution can be used, by replacing all the *Bc*-terms in eq. V.31 with *Ca*-terms.

c) Critical aluminium mobilisation rate:

Critical ANC leaching can also be calculated using a criterion to prevent the depletion of secondary Al phases and complexes which may cause structural changes in soils and a further pH decline. Aluminium depletion occurs when the acid deposition leads to an Al leaching in excess of the Al produced by the weathering of primary minerals. Thus, the critical leaching of Al is given by:

(V.32)

$$Al_{le,crit} = Al_w$$

where Al_w is the weathering of Al from primary minerals (eq/ha/yr). The weathering of Al can be related to the Bc weathering via:

(V.33)

$$Al_w = p \cdot BC_W$$

where p is the stoichiometric ratio of Al to BC weathering in primary minerals (eq/eq), with a default value of p=2 for typical mineralogy of Northern European soils (range: 1.5-3.0). The critical leaching of ANC becomes then:

(V.34)

$$ANC_{le,crit} = Q^{2/3} \cdot \left(\frac{p \cdot Bc_w}{K_{gibb}}\right)^{1/3} - p \cdot Bc_w$$

5.4.2.2.2 Hydrogen ion criteria

A proton criterion is generally recommended for soils with a high organic matter content. Two such criteria are listed below.

a) Critical pH:

A critical pH limit is set at a pH below which the receptor is adversely affected. For example, in some soils, a pH limit of $pH(H_2O)_{crit} = 4.2$ (corresponding to $[H]_{crit} \approx 0.0631$ eq/m^3) avoids considerable increase of Al concentration in soil solution (Lindsay 1979, Ulrich 1981). Critical pH values can be found for different plant species (Sverdrup and Warfvinge 1993a). For aluminium effects see chapter 5.3.2.2.1 on aluminium criteria. $ANC_{le,crit}$ can then be calculated as:

(V.35)

$$ANC_{le,crit} = -Q \cdot ([H]_{crit} + K_{gibb} \cdot [H]^3_{crit})$$

b) Critical base cation to proton ratio:

For organic soils which do not contain Al-(hydr)oxides, such as peat lands, it is suggested to use a critical molar base cation to proton ratio $(Bc/H)_{crit}$. The critical ANC leaching is then given by (no Al leaching):

(V.36)

$$ANC_{le,crit} = -0.5 \cdot \frac{Bc_{dep} + Bc_w - Bc_u}{(Bc/H)_{crit}}$$

where the factor 0.5 comes from converting mols to equivalents. For organic soils the weathering in eq. V.36 will probably be negligible (Bc_w=0). Values suggested for $(Bc/H)_{crit}$ are expressed as multiples of $(Bc/Al)_{crit}$, these multiples range from 0.3 for deciduous trees and ground vegetation, to 1 for spruce and pine (Sverdrup and Warfvinge, 1993).

5.4.2.2.3 Critical base saturation

Base saturation, or the fraction of base cations at the cation exchange complex, is an indicator of the acidity status of a soil, and one may want to keep the base saturation above a certain level to avoid nutrient deficiencies. The UNECE workshop held at York (UK) in 2001 recommended to include base saturation as a potential criterion in the Mapping Manual (see Hall et al. 2001, UNECE 2001). Based on field observations in Swiss forest ecosystems, effects-based base saturation values were found between 20% and 40% below which harmful effects in forest ecosystems, such as decreased rooting depths and increased uprooting during storms in Switzerland were documented (Braun et al. 2003, Braun et al. 2005). More frequent forest storm damages on acidic soils were also found by Mayer et al. (2005) on sites in France, southern Germany, and Switzerland, with comparable explanatory power of pH and base saturation.

To relate base saturation to ANC requires the description of the exchange of cations between the exchange complex and the soil solution. Two descriptions are the most commonly used in dynamic soil models: the Gapon and the Gaines-Thomas exchange model. For a comparison between different exchange models and the implications for the relationship between base saturation and soil solution concentrations see Reuss (1983).

As an example, we consider the description of the exchange between H, Al and Bc=Ca+Mg+K as implemented in the Very Simple Dynamic (VSD) and the SAFE model (see Posch et al. 2003a and Chapter 6). For both models the critical concentration $[H]_{crit}$ can be found as a solution of an equation of the type:

(V.37)

$$A \cdot [H]^{p}_{crit} + B \cdot [H]_{crit} = 1 - E_{Bc,crit}$$

where the coefficients A, B and the exponent p are given in Table 5.8.

In general, eq. V.37 is non-linear and will have to be solved numerically. Only for the Gapon model and the gibbsite equilibrium (a=3, $K_{Alox} = K_{gibb}$) it becomes a linear equation with the solution:

(V.38)

$$[H]_{crit} = K_{Gap} \cdot \sqrt{[Bc]} \cdot \left(\frac{1}{E_{Bc,crit}} - 1 \right)$$

with

$$K_{Gap} = \frac{1}{k_{HBc} + k_{AlBc} \cdot K_{gibb}^{1/3}}$$

where k_{HBc} and k_{AlBc} are the two (site-specific) selectivity coefficients describing cation exchange, and $[Bc]=Bc_{le}/Q$ as above. $[Al]_{crit}$ is then computed from the gibbsite equilibrium (eq. V.28) and from that the critical ANC leaching can be obtained via eq. V.29. Values of selectivity coefficients for a range of Dutch soil types and combinations of exchangeable ions are given by De Vries and Posch (2003).

In Figure 5.6, the critical ANC leaching is shown for a range of constants K_{Gap}. This range encompasses a wide range of values for the exchange constants. The figure shows that ANC leaching is very sensitive to low values of the critical base saturation.

Base saturation is also used as criterion in the New England Governors/Eastern Canadian Premiers 'Acid Rain Action Plan' for calculating sustainable S and N depositions to upland forests with the SMB model (NEG/ECP 2001).

Table 5.8: Coefficients in eq. V.37 for the Gapon and Gaines-Thomas exchange model.

Exchange model	A	p	B
Gapon	$K_{Alox}^{1/3} \cdot k_{AlBc} \cdot E_{Bc,crit}/\sqrt{[Bc]}$	a/3	$k_{HBc} \cdot E_{Bc,crit}/\sqrt{[Bc]}$
Gaines-Thomas	$K_{Alox} \cdot \sqrt{K_{AlBc} \cdot \left(E_{Bc,crit}/\sqrt{[Bc]}\right)^3}$	a	$\sqrt{K_{HBc} \cdot E_{Bc,crit}/[Bc]}$

Note: The generalised relationship $[Al]=K_{Aiox}[H]^a$ has been used (see below).

Figure 5.6: Critical ANC leaching (as defined by eq. V.27, for Q=1 m/yr) as a function of the critical base saturation, E_{Bccrit}, for [Bc]=0.02eq/m^3, $K_{gbb}=10^8$ (mol/L)$^{-2}$ (=300 (eq/m^3)$^{-2}$) and K_{Gap}=0.005 (leftmost curve), 0.01, 0.03 and 0.05 (eq/m^3)^{12} (rightmost curve).(To obtain ANC_{ecrit} for arbitrary Q, multiply the values on the vertical axis by Q in m/yr; see also Figure 5.7 below).

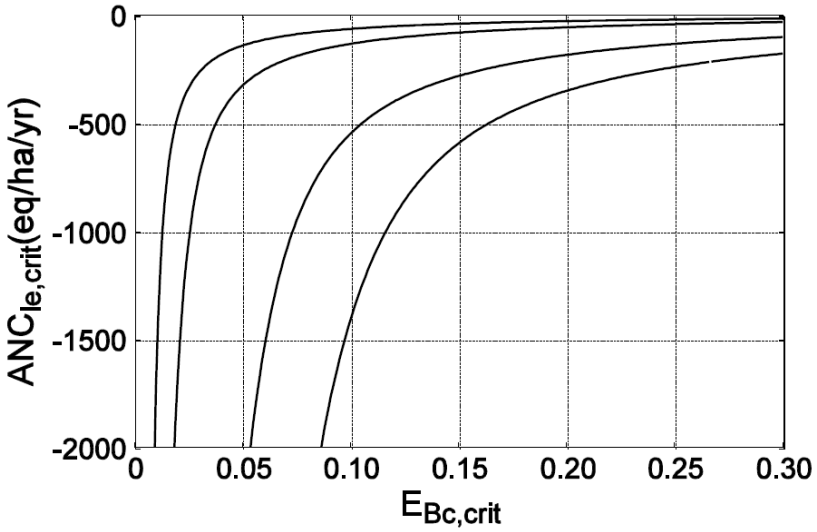

Source: This figure is adopted from a previous version of Chapter 5 of the Mapping Manual

5.4.2.3 Sources and derivation of input data

The obvious sources of input data for calculating critical loads of acidity are measurements at the site under consideration. However, in many cases these will not be available. For data on the different N quantities see section 5.3.1. Some data sources and default values for the other variables, and procedures to derive them, are summarised below.

5.4.2.3.1 Gibbsite equilibrium constant (K_{gibb})

The equilibrium constant relating the Al concentration to pH (eq. V.28) depends on the soil. Table 5.9 presents ranges of K_{gibb} (and pK_{gibb}=–log$_{10}$(K_{gibb} in (mol/L)$^{-2}$) as a function of the soil organic matter content. A widely used default value is $K_{gibb}=10^8$(mol/L)$^{-2}$=300 m^6/eq^2.

Table 5.9: Ranges for K_{gibb} as a function of soil organic matter content.

Soil type; layer	Organic matter (%)	K_{gibb} (m^6/eq^2)	$-pK_{gibb}$
Mineral soils; C-layer	<5	950–9500	8.5–9.5
Soils with low organic matter; B/C layers	5–15	300–3000	8–9
Soils with some organic material; A/E layers	15–30	100	7.6
Peaty and organic soils; organic layers	>70	9.5	6.5

If sufficient empirical data are available to derive the relationship between [H] and [Al], these should be used in preference to the gibbsite equilibrium (see Sec. 5.3.2.4).

5.4.2.3.2 Base cation and chloride deposition

The base cation and chloride depositions entering the critical load calculations should be the deposition after all feasible abatement measures have been taken (ideally the non-anthropogenic deposition), and they should be sea-salt corrected. Observations on a European scale are available from the EMEP Chemical Coordinating Centre (www.emep.int) or from national sources. See Chapter II for more details.

5.4.2.3.3 Base cation weathering

5.4.2.3.3.1 Introduction

Weathering here refers to the release of base cations from minerals in the soil matrix due to chemical dissolution (Ca, Mg, K, Na), and the neutralisation of acidity and production of alkalinity connected to this process. This has to be distinguished from the denudation of base cations from ion exchange complexes (cation exchange) and the degradation of soil organic matter. It is also distinguished from the mechanical weathering, where solid particles are broken up from large to smaller particles, and when solid particles are removed from a soil. Many methods for determining weathering rates have been suggested, and here we list those with the highest potential for regional applications in order of decreasing complexity. There are several levels of weathering rate mapping. The following list is in order of complications for soils:

- Use an integrated model, based on these mechanisms and processes
  - for soils profiles (terrestrial ecosystems), exemplified by models like the Swedish PROFILE.
  - for catchments, exemplified by:
    - the ForSAFE or the PROFILE models modified for catchments and based on geochemical kinetics and watershed hydrology;
    - the use of MAGIC on streams and lakes to find a weathering rate for the catchment as a part of the calibration procedure. Note that this is a catchment rate and not necessarily a soil profile rate.
- Use a model and data supported look-up table based on mineralogy, using a number of site adaption factors for soil wetness, texture, and temperature, such as Table 5.10 for soils.
- Use a simple empirical model based on total analysis, with optional adaptation for soil wetness, texture, and temperature (Equations V.42a-e):
  - for soils;
  - when using a catchment modification routine for recalculating soil weathering rates to catchment weathering rates.
- Using the very simple Skokloster table (Table 5.17) with optional adaptation for soil wetness, texture, and temperature.
- Using a simple empirical correlation based on soil type and texture (Equation V.39).
- Make an estimate with some other method described in the literature, provided the data is available for it (section 5.3.2.3.3.4.)

Weathering of minerals is the result of chemical reactions at the mineral surfaces exposed to liquid. Normally the rate equation takes the shape of an area multiplied with an expression for

the chemical reactions rate. Base cations, aluminium, and silica are released in the reaction, reactants like H^+, water, carbon dioxide, organic acids, and OH^- ions are consumed in the process.

The dynamic model ForSAFE contains PROFILE on the inside (Sverdrup et al. 2007, Belyazid et al. 2011d, Phelan et al. 2014) and may be used for estimating weathering rates as a function of time. The French WITCH model has a simplified PROFILE model inside. These are dynamic models, and the reader will find more on them in the section about dynamic models. They are different in the respect that they give a weathering rate that varies with time instead of a constant value.

Further information on the different approaches described in this section may be found in Annex 1.

5.4.2.3.3.2 The calculation of weathering rates with the PROFILE model

5.3.2.3.3.2.1 Soil profiles and very small catchments

Figure 5.7: The weathering rate increases up to a depth of about 0.5-0.6 meters. The diagram to the left shows the weathering rate distributed among minerals, the diagram to the right shows the total rate as a function of depth down a soil profile. One can see how it reaches a maximum at about a 0.5-0.6 m depth and then decreases. The example shows the weathering rate at catchment F1 at the Gårdsjön Research site, Sweden (Sverdrup et al., 1996).

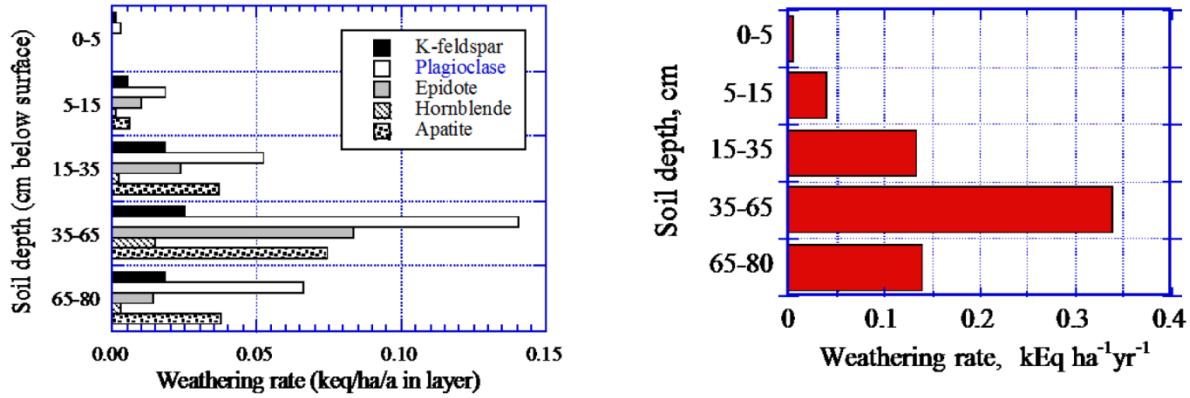

Source: This figure is adopted from a previous version of Chapter 5 of the Mapping Manual

Weathering rates can be computed with the multi-layer steady-state model PROFILE (Sverdrup and Warfvinge 1993b, Warfvinge and Sverdrup 1992b, 1995) and may be used for estimating weathering rates as a function of time. The model is based on geochemical mechanisms and the resulting kinetic equations, using geological properties like mineralogy, exposed surfaces, etc. Basic input data are the mineralogy of the site or a total element analysis, from which the mineralogy is derived by a normative procedure (Uppsala-model) or the A2M code (Posch and Kurz 2007). Generic weathering rates of each mineral are modified inside the model by the concentration of protons, base cations, aluminium, and organic anions as well as the partial pressure of CO_2 and temperature. The total weathering rate is proportional to soil depth and the wetted surface area of all minerals present. For the theoretical foundations of the weathering rate model see Sverdrup (1990).

5.3.2.3.3.2.2 Watersheds and lakes

The MAGIC model is used for lakes, which implicitely takes the watershed into account. The MAGIC model does not include a weathering rate model inside. But the MAGIC model may, be used as an automated budget study, when it is assumed that all else is correctly estimated, estimating a residual term that may be interpreted as being made up of the weathering rate in the catchment.

Since there is no weathering rate model inside, the weathering estimate obtained from MAGIC is a fixed number.

5.3.2.3.3.3 Simplified approaches to weathering rate estimations

5.3.2.3.3.3.1 The mineralogy correlations

This method is based on the fact that the weathering rate in a soil depends on several factors:

- The content of weatherable minerals in the soil (expressed as % dry weight content). Table 5.10 lists the most weatherable mineral groups in a normal soil. Note that quartz has the weathering rate 0.
- The surface area of these minerals exposed to soil solution, which is related to the soil texture. The wetter the climate is, the higher this is, the drier it is, the slower the weathering rate. We suggest three soil moisture classes (C_{sw}):
  - Dry (C_{sw} = 0.7)
  - Normal (C_{sw} = 1.0)
  - Wet (C_{sw} = 1.3)
- The amount of soil material per unit land, depending on the average soil density, related to how packed the soil is and how much organic material there is in it.
- The temperature at the site. The colder the temperature, the slower the weathering goes, and the opposite when it gets warmer Equation (V.42).

Table 5.10 shows a look-up table for a soil with an average soil texture (TX) of 1.1 million m^2 per m^3 soil and a soil depth of 0.5 meter (a default thickness of the forest root zone, comparable to the Gårdsjön F1 site, Sweden), based on mineral dry weight content in the soil. The weathering rate is obtained by summing up the contributions from each mineral. Weathering rate is expressed in eq/ha/yr in the given expressions. The construction of the table was assisted by estimations using PROFILE at about 100 sites in Northern Europe and 72 sites in Maryland, United States. The texture (TX) of a soil may be calculated with a simple formula (in million m^2 per m^3 soil):

(V.39)

$$TX = 0.3 * X_{sand} + 2.2 * X_{silt} + 8*X_{clay}$$

The classification into sand, silt, and clay is often used and available in many. The Nordic Forest soil field texture class is the test where a soil sample is placed in the palm of the hand. Therefore, a small amount of water is added to the soil and a sausage shape is created by rolling the water and soil as thin as possible in the palm of ones hand. For this the texture class is judged. The method was calibrated at Lund University in 1992 against measured samples. For further information, see Sverdrup and Warfvinge (1993b) and Warfvinge and Sverdrup (1993). The weathering rate ($W_{BC,Soil}$) will be the sum of the weathering rates from Table 5.10, with terms for adjusting for soil wetness, soil texture, large passive stones, soil density, and temperature when it is different from an annual average of 8°C (Sverdrup et al. 1990, Sverdrup 1990 and Sverdrup and Warfvinge 1996):

(V. 40)

$$W_{BC,Soil} = C_{sw} * (1 - S) * \frac{TX}{1.2} * \frac{\rho_{Soil}}{1200} * \frac{z}{0.5} \left(\sum_{i=1}^{n=minerals\ in\ the\ soil} W_{Minarals,i} \right) * 10 \left(\frac{A}{281} - \frac{A}{273 - T} \right)$$

where C_{sw} is the soil moisture class correction factor, S is the value of the pebble and stone weight fraction, and z is the soil depth (in m) for which weathering is considered (the factor adjusts for soil depth different than the 0.5 m the Table 5. 10). The factor A depends on the mineral and the reaction, but a generic value of A=3600 will work fine for most soils (Sverdrup and Warfvinge 1996). This adjustment is valid in the range 0.2–0.8 m. Stones larger than 2 mm do not participate significantly in the weathering and thus are eliminated from the calculation.

Table 5.10: Look-up table for a soil with an average soil texture of 1.1 million m^2 per m^3 soil and a depth of 0.5 m, based on mineral dry weight content in the soil, at an annual average temperature of 8°C. Weathering rates are in eq/ha/yr. The table assumes soil moisture to be the same as at Gårdsjön (Class = normal above). The table was updated by Sverdrup in 2016.

Mineral	$W_{Minerals}$, units are eq/ha/yr The weathering rate at this % weight content of the listed mineral			
	100	10	5	1
Calcite	82000	8200	4100	820
Apatite	17000	1700	850	170
Epidote	8800	880	440	88
Hornblende	2630	263	132	26
Pyroxene	2060	206	103	21
Albite	1680	168	84	17
Plagioclase	1340	134	67	13
Oligoclase	1240	124	62	12
Garnet	1160	116	58	11
Chlorite	1050	105	53	11
Biotite	930	93	47	9
Vermiculite	560	56	28	6
K-Feldspar	480	48	24	5
Muscovite	300	30	15	3
Illite	300	30	15	3

Table 5.11: Soil texture based on the formula in V.39 and data from the Swedish critical loads database (Warfvinge and Sverdrup 1993, updated by Sverdrup 2016).

Dutch texture class	Standard forest soil texture class	Name	%			TX Calculated approximate surface area, million m^2 m^{-3}
			Sand	Silt	Clay	
1	1	Coarse moraine	80	20	0	0.68
1	2	Forest moraine	70	28	2	0.97
1	3–4	Silty soil	60	35	5	1.35
1	4–6	Fine silty soil	40	50	10	2.02
2	7	Coarse clay soil	30	50	20	2.79
3	8	Clayey soil	10	50	40	4.33
4	9	Clay soil	5	35	60	5.59
5	10	Fine clay soil	1	24	75	6.53

Table 5.12: Default values for soil specific densities for entry into Equations V.40 and V.43.

Soil layer description		Classification of soil and their density, kg m^{-3}		
Name	z, meter	High organic content soil	Podzolic type of soil	Heavy soils compact clay soils
Organic layer	0-0.15	300	300	300
Leached layer	0.15-0.35	600	700	900
B-layer	0.35-0.65	900	1100	1200
C-layer	0.65-0.80	1000	1200	1300
Mineral soil	0.80-1.50	1000	1350	1400
Mineral soil	1.50-2.00	1000	1350	1400
Mineral soil	2.00-2.50	1000	1350	1400

Table 5.13: Guideline for selecting rooting depth in the weathering estimation. For catchment weathering, the weathering rate available to the stream or lake considered is relevant. See also Sverdrup and Warfvinge (1995), Sverdrup et al. (2007) and Belyazid et al. (2011a) for lists with rooting depth (updated by Sverdrup 2016).

Classification	Surficially rooted plants	Shallowly rooted plants	Intermediate rooted plants	Deeply rooted plants
Rooting depth	0–0.20 m	0.25–0.35 m	0.45–0.55 m	0.55–0.80 m
Typical plants	Tree seedlings, Norway spruce on acid soils, ground plant seedlings	Norway spruce, Silver fir, Red Spruce, Red Cedar	Birch, Scots pine, Beech, Aspen, Popular	Oaks, ash singular pine and spruce trees, trees in arid areas

Classification	Surficially rooted plants	Shallowly rooted plants	Intermediate rooted plants	Deeply rooted plants
Typical ground vegetation	Lichens, moss	Heather and ling, many grasses and herbs	Dry area grasses and plants	Grain, drought-resistant grasses

5.3.2.3.3.3.2 Mineralogy estimation, valid for larger catchments and groundwater.

One empirical model is outlined here. Figure GG shows how the weathering rate (at catchment F1 at Gårdsjön, Sweden) increases towards a 0.5–0.6 meter depth. Further down in the soil, the weathering rate declines because of retarding effects from base cation, aluminium, and silica concentrations in the weathering kinetics. This implies that the soil weathering rates cannot readily be scaled to watersheds and catchments in a linear way. At a 2-3 meter soil depth, in coarse soils and moraines, the weathering rate will have declined to quite low levels. The catchment weathering rate ($W_{Catchment}$) in eq/ha/yr is:

(V. 41)

$$W_{Catchment} = \sum_{\substack{i=top\\layer}}^{\substack{n=Bottom\\layer}} \left(W_{Soil\ profile,i} * X_{Soil,i}\right)$$

where $X_{soil,i}$ is the fraction of the total catchment area covered by soil layer i. The different soil layer weathering rates $W_{soil,I}$ may be calculated using, for instance, the PROFILE model. The weathering products entering the stream necessitates data on how the weight of the soil layers are distributed across the catchment with respect to soil depth. Then, the soil layer coverage in the catchment must be derived, either from field data, or, for regional assessments, from known generic distributions.

5.3.2.3.3.3.3 The total base cation content correlation

The total base cation content correlation uses relationships between estimates, weathering rates of base cations, and the total content of the respective element in the soil, with an additional correction for temperature. For Ca, Mg, Na, and K the equations are (Sverdrup et al. 1990, Sverdrup and Warfvinge 1996) in eq/ha/yr:

(V.42a)

$W_{ca} = z\ (0.1\ \%CaO \cdot (768+104 \cdot T) - 0.08)$

(V.42b)

$W_{Mg} = Z \cdot (0.212 \cdot \%MgO \cdot (768+104 \cdot T) - 0.09)$

(V.42c)

$W_{Na} = z\ 0.037 \cdot \%Na_2O \cdot (768+104 \cdot T)$

(V.42d)

$W_K = z \cdot 0.021 \cdot \%K_2O \cdot (768+104 \cdot T)$

where z is the soil thickness (in m), %CaO, %MgO, $\%Na_2O$, and $\%K_2O$ are the base cation soil content expressed as % dry weight of the soil and T is the annual average temperature in °C. For critical loads for plants, z is the rooting depth (examples in Table 5.13).

Adding together equations V.42a-d) the weathering rate of base cations is given by equation V.42e.

Another empirical expression available for the total weathering rate based on correlating total analysis to observed weathering rates is provided by equation V.42f (Sverdrup et al., 1990; Sverdrup et al 1990, 1995).

Note the following:

- Plants take up Mg, Ca, and K but not Na, thus the weathering of Na does not contribute to uptake.
- All the weathering (Na, K, Mg, Ca) contribute to neutralization of acidity.

These equations were empirically derived for Nordic soils which were tested at Gardsjon, Sweden, but derived from about 100 soils from Northern Europe, Central Europe, and Northern America, (Sverdrup et al 1996), and seem to work reasonably well in most glaciated areas where they have been tested. To select relevant soil depth, check with Table 5.13. For critical loads for plants, only the weathering available to the root zone is of interest. Additional corrections can be made for soil wetness, soil texture, and amount of large stones and pebbles that do not contribute to weathering in the soil. These correction factors may be significant in all coarser soils. They lead to equation V.43.

(V.42e)

$$W_{BC} = z * (0.1 * (768 + 104 * T) * (\%\ CaO + 2.12 * \%\ MgO + 0.37 * \%\ Na_2O + 0.21 * \%\ K_2O) - 0.17)$$

(V.42f)

$$W_{BC} = z * (0.1 * (768 + 104 * T) * (\%\ CaO + \%\ MgO + \%\ Na_2O + \%\ K_2O) - 0.37)$$

(V.43)

$$W_{BC,Soil} = C_{sw} * (1 - S) * \frac{TX}{1.2} * \frac{\rho_{Soil}}{1200} * \left(W_{Ca} + W_{Mg} + W_K + W_{Na}\right)$$

where C_{SW} is the soil wetness class, ρ_{Soil} is the bulk density of the soil in kg m^{-3}, TX is the texture expressed in million m^2 mineral surface per m^3, W_{Ca}, …, W_{NA} are to be taken from eqs.V.42a-d.

If the soil wetness class cannot be set, take the value C_{SW} = 1. If the bulk density is not known and cannot be easily estimated, it is set to ρ_{Soil} = 1200. If the texture value is not known or cannot be estimated, it is set to TX = 1.1.[15]

5.3.2.3.3.3.4 The soil type – texture approximation

Since mineralogy controls weathering rates, weathering rate classes were assigned to European (forest) soils by Sverdrup et al., (1990) using the PROFILE model and later again by de Vries et al. (1993), based on texture class and parent material class. Note that some countries have their own local texture class classification and that it can be different than the ones presented here. Texture classes are defined as a function of their clay and sand content. From texture and parent material class (Table 5.14 and Table 5.15), the weathering rate class is obtained from Table 5.16 (modified from de Vries et al. 1993). The approximate weathering rate (in eq/ha/yr) for a non-calcareous soil of depth z (in meters) is then computed as:

(V.44)

[15] Earlier, the manual contained an equation developed by Olsson et al (1993). The equations were developed without considering soil depth, a parameter used in the critical load calculation. It is thus not applicable to critical load calculations.

$$W_{BC} = z * 500(W_{Class} - 0.5) * 10\left(\frac{A}{281} - \frac{A}{273 - T}\right)$$

where W_{class} is the weathering rate class, T (°C) is the average annual (soil) temperature and A=3600 K (Sverdrup 1990). Note that in this equation, the temperature correction is given as a power to 10 whereas it was an exponential in equation V.39 of the 2004 Mapping Manual**.**

For calcareous soil, for which critical loads for acidity are not really of interest, one could set, for example, W_{class}=20 in eq. V.44, or read it out of Table 5.10 or Table 5.17. Using the FAO soil classification (FAO 1981), the parent material class has been defined for each soil type in Table 5.15 (updated from de Vries et al. 1993).

The above procedure provides weathering rates for BC=Ca+Mg+K+Na which is equal to the neutralization power of the soil. However, for computing the critical ANC leaching according to eq. V.31 based on what is active in protecting plants in the BC/Al ratio, the weathering rate for Bc=Ca+Mg+K is needed. W_{Bc} can be approximated by multiplying W_{Bc} with a factor between 0.70 for poor sandy soils and 0.85 for rich sandy soils with 0.75 on the average. Van der Salm et al. (1998) (for texture classes 2-5, see Table 5.12) and de Vries (1994) (for texture class 1) provide regression equations for weathering rates of Ca, Mg, K, and Na as a function of the sand (and silt) content of the soil, which can be used to split W_{Bc} into individual weathering rates.

The correlation of these approximate values to observed weathering rates is not strong across Europe, but the use of these values is useful if they are applied in cumulative distributions of weathering rates for critical loads. They will give the approximate right pattern on a large-scale but are difficult to validate in single points. This is because the mistakes made are symmetrically distributed around the median and thus cancel out in cumulative distributions to a significant degree.

Table 5.14: Soil texture classes as a function of their clay and sand content (Eurosoil 1999). This is primarily designed for agricultural soils and soils with high clay content, which are suitable to the plains of coastal and central Europe. It is less suitable for hilly terrain, mountains, and the coarser soils of northern glaciated areas in general. The texture class is defined also in Table 5.11 and used in Table 5.16.

Texture class	Name	Definition
1	Coarse	clay < 18 % and sand ≥ 65 %
2	Medium	clay < 35% and sand > 15 %, but clay ≥ 18 % if sand ≥ 65 %
3	medium fine	clay < 35% and sand < 15 %
4	Fine	35 % ≤ clay < 60 %
5	very fine	clay ≥ 60 %

Table 5.15: Parent material classes for common FAO soil types (Posch et al. 2003b).

Parent material	FAO soil type
Acidic: sand, gravel, granite, quartzite, gneiss (schist, shale, greywacke, coarse glacial till), silicious sandstones.	Ah, Ao, Ap, B, Ba, Bd, Be, Bf, Bh, Bm, Bx, D, Dd, De, Dg, Gx, I, Id, Ie, Jd, P, Pf, Pg, Ph, Pl, Po, Pp, Q, Qa, Qc, Qh, Ql, Rd, Rx, U, Ud, Wd

Parent material	FAO soil type
Intermediate: Granodiorite, granitic with some dark minerals, loess, fluvial and marine sediments (schist, shale, greywacke, fine glacial till)	A, Af, Ag, Bv, C, Cg, Ch, Cl, G, Gd, Ge, Gf, Gh, Gi, Gl, Gm, Gs, Gt, H, Hg, Hh, Hl, J, Je, Jm, Jt, L, La, Ld, Lf, Lg, Lh, Lo, Lp, Mo, R, Re, V, Vg, Vp, W, We
Basic: Mafic minerals, gabbro, basalt, dolomite, limestone, volcanic deposits, carbonaceous sandstones	F, T, Th, Tm, To, Tv
Organic soils, peats	O, Od, Oe, Ox

Table 5.16: Weathering rate classes (WClass) as a function of texture and parent material classes (Posch et al. 2003b).

Parent material	Texture class Table 5.11 or Table 5.14				
	1	2	3	4	5
Acidic	1	3	3	6	6
Intermediate	2	4	4	6	6
Basic	2	5	5	6	6
Organic	Class 6 for Oe and class 1 for other organic soils				

5.3.2.3.3.3.5 The Skokloster assignment

The Skokloster assignment is a method devised at the Critical Loads Workshop at Skokloster (Sweden, Table 1, p. 40 in Nilsson and Grennfelt 1988). Some details can be found in the section on empirical acidity critical loads (section 5.2.2). However, this method can be used to make rough estimates of the weathering rate of a soil and used as input data for the SMB method or to constrain models that do not have their own weathering rates such as MAGIC or VSD. Large-scale patterns are usually displayed correctly, but small-scales tend to be inaccurate. It is not very accurate on a site-by-site basis.

Table 5.17: An updated version of the Skokloster table from 1988 (Sverdrup and Warfvinge (1988b), Grennfelt and Nilsson (1988), updated by Sverdrup 2016).

Mineral class	Type of soils	Weathering, 10^3 eq/ha/yr. % content of minerals			
		100%	30%	3%	0.3%
Very fast weathering	Calcareous soils, fine-grained dark mineral dominated soils, basic basaltic, and mafic minerals	25	15	10	3
Fast weathering	Dark mineral dominated soils, basic basaltic, mafic minerals, and traces of carbonate minerals from deeper layers	15	10	3	0.3
Intermediate	Fine-grained normal soils, brown soils, rich soils for agriculture, very fine-grained granitic soils	5	2	0.2	0.05
Slow weathering	Granitic and gneissic materials, most coarse soils, and old weathered soils	2	0.6	0.2	0.02

Mineral class	Type of soils	Weathering, 10_3 eq/ha/yr.			
		% content of minerals			
		100%	30%	3%	0.3%
Near inert	Tropical weathered soils, quartzitic soils, high content of quartz, and slow weathering minerals	0.3	0.2	0.05	0.01

5.3.2.3.3.4 Other methods

When specialised data is available there are a number of ways the weathering can be estimated. None of the methods are particularly well suitable for large-scale weathering rate mapping. The methods are:

- Historic weathering rate
  - The ZrO_2 or TiO_2 depletion method, assuming zircon or rutile to be inert to determine lost mass and divide by soil age. In Scandinavia, this varies from 14,000 years in the south to 8,000 years in the north.
  - The mineralogy depletion method, using either quartz or the soil profile bottom composition as standard (Sverdrup and Warfvinge 1988a, 1988c, 1995, Sverdrup et al., 1995, Sverdrup 1990).
  - The profile depletion method, using bedrock composition as standard based on quantitative mineralogy or total analysis of the underlying bedrock, assuming this to be the origin of the soil minerals.
- Present weathering rate
  - The Sr-isotope method (Calcium weathering only), where Sr is used as a tracer in a budget study.
  - Budget studies.
    - Weathering rates can also be estimated from budget studies of small catchments (see, e.g., Paces 1983) where the fluxes have been measured. Be aware that budget studies can easily overestimate weathering rates where there is significant cation release due to weathering of the bedrock. Other confounding factors are net release of base cations from decomposition of organic matter because of climate change and leaching from ion exchange complex because of acid soil water (lack of steady state with respect to acid rain).
    - Calibration of a model biogeochemical model, fitting the weathering rate. This is in essence a budget study. MAGIC is an example of such a model.
- Base mineral index, a crude estimate based on the content of dark and heavy minerals (Sverdrup et al., 1990).

Other methods are listed and described in Sverdrup et al. (1990), Warfvinge and Sverdrup (1993) and Sverdrup and Warfvinge (1996) and Sverdrup et al., (1995).

5.3.2.3.3.5 Normative reconstruction of mineralogy from total analysis.

The mineralogy can be backcalculated from the total analysis made on a soil. The UPPSALA model was developed for this purpose in Sweden. It has since been used for many sites in central

and northern Europe and in North America. Despite its large simplifications, it seems to perform quite well when it is tested (Warfvinge and Sverdrup 1992, 1993, Sverdrup and Warfvinge 1992, 1993, Sverdrup et al., 1990). For converting total analysis databases to mineralogy, it was quite useful. The UPPSALA model is a normative backcalculation model for reconstructing the mineralogy from the total analysis. The model assumes prior knowledge of the stoichiometric composition of the minerals. The mineral names are groupings of soil minerals.

The following data are needed: Total analysis (full digestion without residual) expressed as weight % of CaO, MgO, N_2O, K_2O, AL_2O_3, P_2O5, SiO_2. If Fe_2O_3 is available, it may be useful for further distinction. If some determination exists of which minerals are present or absent, then that may be of assistance for estimating minerals like hornblende, biotite, pyroxenes or olivines. The mineral groups are as follows:

- K-feldspar is assumed to have a 10% albite feldspar component. The K-feldspars are sanidine, orthoclase, and microcline.
- The plagioclase group has been assumed to be oligoclase with 15% anorthite component.
- All phosphorus has been attributed to the apatite group.
- The hornblende group includes all amphiboles.
- The muscovite group comprise muscovite and di-octahedral secondary or altered minerals like sericite and lightly weathered illites.
- The chlorite group comprise trioctahedral clay minerals, biotite, and glauconite. If Fe_2O_3 is available, that may be used to differentiate between biotite (with iron) and chlorite (without iron).
- The epidote group comprises all epidotes, zoisites, garnets, olivines and pyroxenes.
- The vermiculite group comprise vermiculite, montmorillonite, and weathered illites.
- The quartz group is just quartz, all the silica that cannot be accounted for in other minerals.
- The model is executed as an ordered sequence in 11 steps in a spreadsheet as shown in Table 5.18, giving 9 different minerals.

Potassium is put into the K-Feldspar group and the muscovite group and a little in plagioclase (1, 2, 5). Magnesium is put into chlorite group, and hornblende (4, 5, 6). Sodium is put into the plagioclase, apatite, epidote, and hornblende groups. From residual aluminium (9) we make the vermiculite group (10, 11). All SO_2 bound into the created minerals is subtracted from the SO_2 in the total analysis, and what is left is assigned to quarts (8). The calculation is checked by calculating the amount of quartz (8), and only such sites which lie within the range 95–105% are accepted. It is advisable to keep track of how much of the oxides that are used up in each step on a parallel sheet. When no more adequate ions are available for the formation of a mineral, then the content of that mineral is set to zero. If more sophisticated estimates are required, the A2M procedure could be used (Posch and Kurz 2007).

Table 5.18: The 11 steps of the UPPSALA model.

1	K-Feldspar	=	Max(0,5.88*K_2O – 0.588*Na_2O)
2	Plagioclase	=	Max(0,11.1*Na_2O – 0.22*K – Feldspar)
3	Apatite	=	2.24*P_2O_5

1	K-Feldspar	=	Max(0,5.88*K_2O – 0.588*Na_2O)
4	Hornblende	=	Max(0,6.67*CaO – 3.67*Apatite – 0.2*Plagioclase)
5	Muscovite	=	Max(0,2.08*K_2O – 0.208*Na_2O)
6	Chlorite	=	Max(0,3.85*MgO – 0.39*Hornblende – 0.39*Muscovite)
7	Epidote	=	Max(0,0.1*Hornblende + 0.03*Plagioclase – 0.3)
8	Quartz	=	SiO_2 – 0.63*Plagioclase – 0.68*K – Feldspar – 0.38*Muscovite – 0.33*Chlorite – 0.45*Hornblende – 0.42*Epidote
9	Al-residual	=	Al_2O_3 – 0.1*Plagioclase – 0.1*K – Feldspar-0.26*Muscovite – 0.09*Chlorite – 0.01*Hornblende – 0.025*Epidote
10	Delta	=	Quartz+Plagioclase + K-Feldspar + Muscovite + Chlorite + Hornblende + Epidote +Apatite
11	Vermiculite	=	Min(Al-residual, Max(0,(100%-Delta)))]

5.4.2.3.4 Base cation uptake

The uptake flux of base cations, Bc_u, entering the critical load calculations is the long-term average removal of base cations from the ecosystem. The [2]uptake fluxes should be calculated for the individual base cations (Ca, Mg and K) separately. The considerations and calculations are exactly the same as for the uptake of N (see Section 5.3.1). Average contents of Ca, Mg, and K in stems and branches can be found in Table 5.8 (see also Jacobsen et al. 2002). Values have to be multiplied by 2/40.08, 2/24.31, and 1/39.10 for Ca, Mg and K, respectively, to obtain contents in eq/kg.

The (long-term) net uptake of base cations is limited by their availability through deposition and weathering (neglecting the depletion of exchangeable base cations). Furthermore, base cations will not be taken up below a certain concentration in soil solution, nor due to other limiting factors, such a temperature. Thus, the values entering critical load calculations should be constrained by:

$$Y_u \leq Y_{dep}, + Y_w - Q \cdot [Y]_{min}$$

(V.45) for

$$Y = Ca, Mg, K$$

This is preferable to constraining the sum $Bc_u = Ca_u + Mg_u + K_u$ (see eq. V.31). Suggested values are 5 meq/m³ for $[Ca]_{min}$ and $[Mg]_{min}$, and zero for $[K]_{min}$ (Warfvinge and Sverdrup 1992). It should also be considered that vegetation takes up nutrients in fairly constant (vegetation-specific) ratios. Thus, when adjusting the uptake value for one element, the values for the other elements (including N) should be adjusted proportionally.

5.4.2.4 Possible extensions to the SMB model

In the following section, three suggestions are made for generalising the SMB model, with the idea of improving the critical load calculations but also with the aim to enhance the compatibility with dynamic models. All three suggestions are 'backwards compatible', (i.e., by setting key parameters to zero the original SMB model is obtained). For an earlier discussion of these extensions see also Posch (2000).

a) Generalisation of the Al-H relationship

In the SMB model the relationship between Al concentration and pH is described as gibbsite equilibrium (see eq. V.21). However, Al concentrations, especially in the topsoil, can be influenced by the complexation of Al with organic matter (Cronan et al. 1986, Mulder and Stein 1994). Therefore, the gibbsite equilibrium in the SMB model could be generalised by:

(V.46)

$$[Al] = K_{Alox} \cdot [H]^a$$

with equilibrium constant K_{Alox} and exponent a. Obviously, the gibbsite equilibrium is a special case of eq. V.46 (setting a=3 and K_{Alox}=K_{gibb}). The exponent a and K_{Alox} depend on the soil type and especially on the soil horizon. As an example, in Table 5.19 values for K_{Alox} and a are presented for different soil groups and soil depths derived from several hundred Dutch forest soil solution samples (see Van der Salm and De Vries 2001).

Table 5.19: Estimated values of K_{Alox} and the exponent a based on regression between pAl and pH in the soil solution of Dutch forests (N = number of samples).

Soil type	Depth (cm)	$\log_{10} K_{Alox}$ [a)]	*a*	*N*
All	humus layer	-1.03	1.17	275
Sandy soils	0–10	3.54	2.26	274
	10–30	5.59	2.68	377
	30-100	7.88	3.13	271
Loess	0-10	-0.38	1.04	45
soils	10-30	3.14	1.83	46
	30-100	4.97	2.21	40
Clay	all depths	4.68	2.15	152
Peat	all depths	1.41	1.85	163

a) Values for K_{Alox} are derived from [*Al*] and [*H*] in mol/L; the unit of K_{Alox} depends on a and is $(mol/L)^{1-a}$.

The data in Table 5.19 show that a standard gibbsite equilibrium constant and a=3 is reasonable for (Dutch) sandy soils. Very different values, however, are obtained for peat soils and, to a lesser extent, also for loess and clay soils, especially for shallow parts of the soil, where the organic matter content is highest. Data from intensive forest monitoring plots show that there is a strong correlation between a and $\log_{10}K_{Alox}$ (De Vries et al. 2003, p. 118), which emphasises that these two parameters cannot be chosen independently.

Figure 5.8 shows the relationship between [H] and [Al] as well as its logarithmic form for different values of K_{Alox} and a. Defining pX=$-\log_{10}[X]$, with [*X*] given in mol/L, one has pH=$3-\log_{10}([H])$, if [*H*] is expressed in eq/m³; and for [*Al*] in eq/m³ the relationship is pAl=$3-\log_{10}([Al]/3)$.

Figure 5.8: Relationships between H and Al concentration in eq/m³ (left) and in their logarithmic forms (right) for K_{Alox}= 10^1, a=2 and K_{Alox}=$10^{4.5}$, a=1.3 (solid lines) as well as three gibbsite equilibria (a=3) with K_{gibb}=10^7, 10^8 and 10^9 (dashed lines). Note: [H]=0.1 eq/m³ corresponds to pH=4.

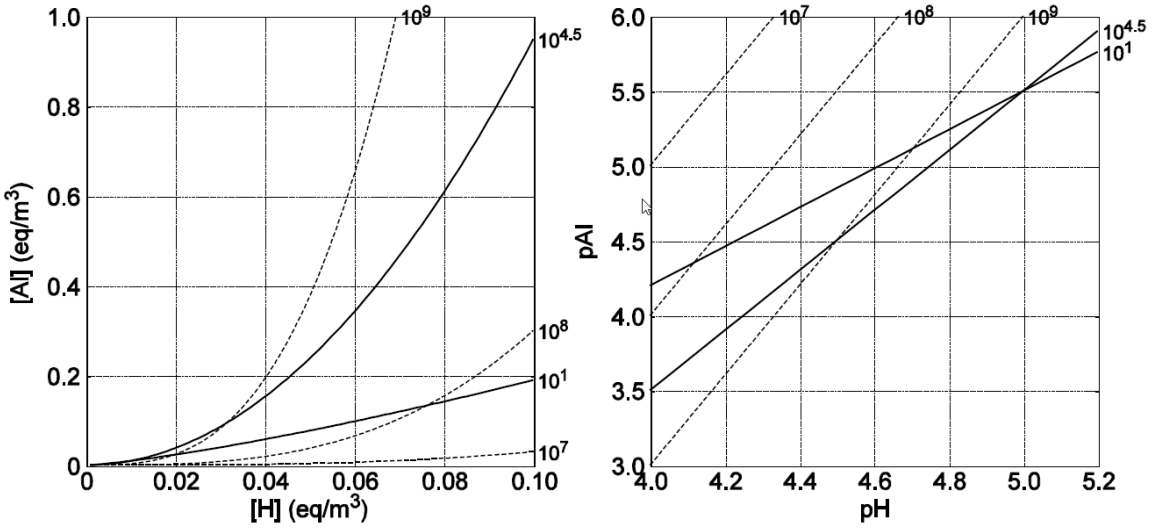

Source: This figure is adopted from a previous version of Chapter 5 of the Mapping Manual

Note that, when using eq. V.46 instead of eq. V.28, the formulae for $ANC_{le,crit}$ have to be adapted as well (mostly replacing the exponent 3 by a and 1/3 by $1/a$).

b) Including bicarbonate leaching

The charge balance (eq. V.9) and the definition of ANC leaching in eq. V.10 also includes the leaching of bicarbonate anions ($HCO_{3,le}$=Q·[HCO_3]). The concentration of bicarbonates is a function of the pH:

(V.47)

$$[HCO_3] = \frac{K_1 \cdot K_H \cdot p_{CO2}}{[H]}$$

where K_1 is the first dissociation constant, K_H is Henry's constant and p_{CO2} is the partial pressure of CO_2 in the soil solution (in atm). The two constants are weakly temperature-dependent, and the value for their product at 8°C is $K_1 \cdot K_h$ =$10^{-1.7}$=0.02 eq²/m⁶/atm. For systems open to the atmosphere, p_{CO2} is about 370 ppm or 3.7·10^{-4} atm (in the year 2000). However, in soils p_{CO2} is generally higher (ranging from 10^{-2} to 10^{-1} atm, Bolt and Bruggenwert 1976), due to respiration and oxidation of below-ground organic matter. Respiratory production of CO_2 is highly temperature dependant (e.g., Witkamp 1966); based on soil temperature and mean growing season soil p_{CO2}, Gunn and Trudgill (1982) derived the following relationship:

(V.48)

$$\mathrm{Log}_{10} p_{CO2} = -2.38 + 0.031 \cdot T$$

where T is the (soil) temperature (°C). Brook et al. (1983) present a similar regression equation based on data for 19 regions of the world. In the absence of data or such relationships, the following default ranges have been suggested (Bouten et al., 1987): 5–10 times atmospheric pressure in the organic layer, 5–15 times atmospheric pressure in the E-layer, 15–20 times atmospheric pressure in the B-layer and 15-30 times atmospheric pressure in the upper C-layer.

For p_{CO2}=0.0055 atm (about 15 times the partial CO_2 pressure in air) and Q=0.3 m/yr, eq. V.47 yields a bicarbonate leaching of almost 100 eq/ha/yr at pH=5.5, not always a negligible quantity. Therefore, it would make sense to include the bicarbonate leaching into the SMB model. Not only would this make critical loads more compatible with steady-state solutions of dynamic models, but it is also the only way to allow the ANC leaching to obtain positive values. Eq. V.27 would than read:

(V.49)

$$ANC_{le} = -H_{le} - Al_{le} + HCO_{3,le} = Q \cdot ([HCO_3] - [H] - [Al])$$

All chemical criteria could be used since bicarbonate leaching could always be calculated from H_{le} via eq. V.47. We illustrate the influence of bicarbonates on the ANC leaching by re-drawing Figure 5.6, but now using eq. V.49 to calculate the ANC leaching. Comparing Figure 5.9 with Figure 5.6 illustrates that, depending on the parameters of the site, bicarbonate leaching can make a significant contribution to the overall ANC leaching.

Figure 5.9: Critical ANC leaching (for Q=1 m/yr) including bicarbonate leaching as a function of the critical base saturation, $E_{Bc,crit}$, using the same parameters as in Figure 5.5.

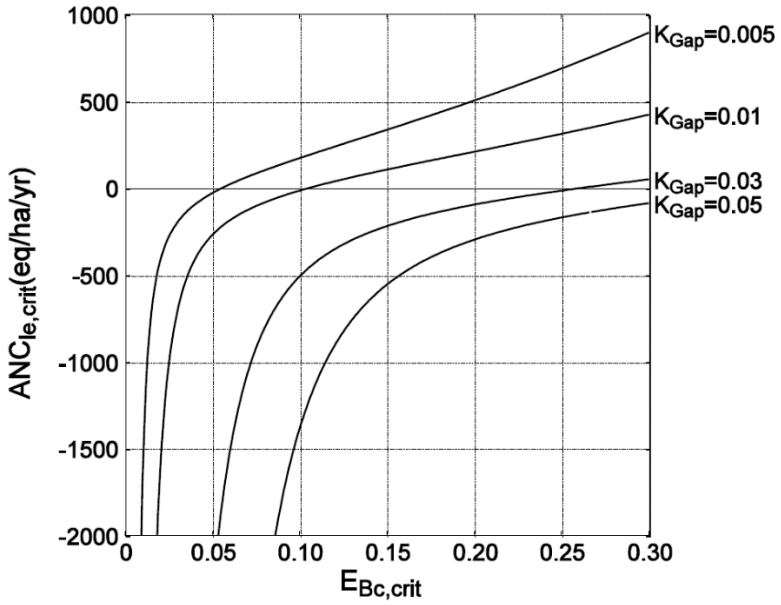

Source: This figure is adopted from a previous version of Chapter 5 of the Mapping Manual

c) Including the dissociation of organic acids

The charge balance (eq. V.9) and the definition of ANC leaching in eq. V.10 also include the leaching of organic anions ($RCOO_{le}$). This has been neglected in the SMB model for (at least) two reasons: (i) to keep the SMB model simple, and/or (ii) due to the assumption that the negatively charged organic anion concentration balances the positively charged organic Al-complexes. However, this does not hold for a wide range of pH values, and at sites with high concentrations of organic matter the contribution of organic anions to ANC leaching can be considerable.

Since it is difficult to characterise (let alone model) the heterogeneous mixture of naturally occurring organic solutes, so-called 'analogue models' are used. The simplest assumes that only monovalent organic anions are produced by the dissociation of dissolved organic carbon:

(V.50)

$$[RCOO^-] = \frac{m \cdot DOC \cdot K_1}{K_1 + [H]}$$

where *DOC* is the concentration of dissolved organic carbon (in molC/m³), *m* is the concentration of functional groups (the 'charge density', in mol/molC) and K_1 the dissociation constant. Both *DOC* and *m* are site-specific quantities. While *DOC* estimates are often available, data for *m* are less easy to obtain. For example, Santore et al. (1995) report values of *m* between 0.014 for topsoil samples and 0.044 mol/molC for a B-horizon in the Hubbard Brook experimental forest in New Hampshire.

Since a single value of K_1 does not always model the dissociation of organic acids satisfactorily, Oliver et al. (1983) have derived an empirical relationship between K_1 and pH:

(V.51)

with a=0.96, b=0.90 and c =0.039 (and m=0.120 mol/molC). Note that eq. V.51 gives K_i in mol/L. In Figure 5.10, the fraction of *m-DOC* dissociated as a function of *pH* is shown for the Oliver model and a monoprotic acid with a 'widely-used' value of pK_i=4.5.

$pK_1 = -\log_{10} K_1 = a + b \cdot pH - c \cdot (pH)^2$

Figure 5.10: Fraction of organic acids (m-DOC) dissociated as a function of pH for the Oliver model (solid line) and the mono-protic model (eq.5.46) with pK_1=4.5 (dashed line).

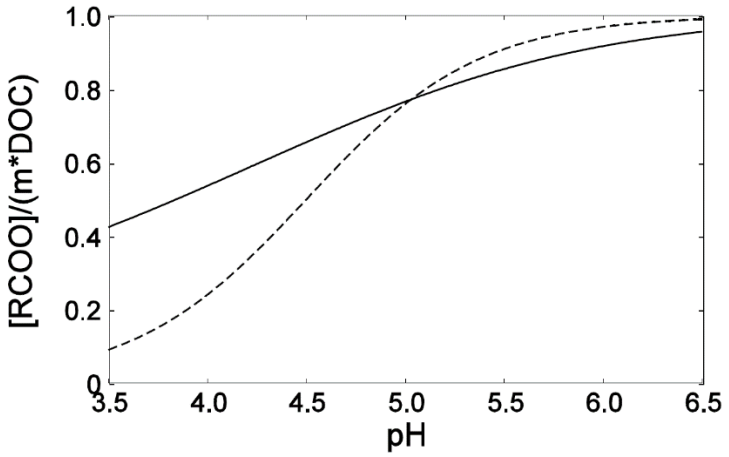

Source: This figure is adopted from a previous version of Chapter 5 of the Mapping Manual

Figure 5.9 shows that, depending on the amount of DOC, the contribution of organic anions to the ANC leaching, even at fairly low pH, can be considerable.

Other models for the dissociation of organic acids have been suggested and are utilised in dynamic models, such as di- and tri-protic analogue models (see, e.g., Driscoll et al. 1994), or more detailed models of the speciation of humic substances, such as the WHAM model (Tipping 1994). Any model could be used for the calculation of critical loads as long as the dissociation depends only on $[H]$, so that a critical leaching of organic anions can be derived from $[H]_{crit}$ (or $[Al]_{crit}$).

5.5 Critical loads for aquatic ecosystems

The purpose of critical loads for aquatic ecosystems (Posch et al. 2015; Curtis et al. 2015) is to estimate the maximum deposition(s) below which 'significant harmful effects' on biological species do not occur. Similar to terrestrial ecosystems, the links between water chemistry and

biological impacts cannot be modelled adequately at present (see also Wright and Lie 2002). As such, water quality criteria are generally used to derive critical loads for aquatic ecosystems.

In this section we deal only with the modelling of critical loads of acidity for aquatic ecosystems. The models are restricted to freshwater systems since models for marine ecosystems do not seem to exist. Empirical critical loads of nitrogen for eutrophication for fresh waters, as well as coastal and marine habitats, can be found in section 5.2.

The following description is largely based on the review by Henriksen and Posch (2001) but amended with new or additional information where available. Three models for calculating critical loads of acidifying N and S deposition are described. Models of critical loads for surface waters also include their terrestrial catchments to a greater or lesser extent. Therefore, it is advised to consult section 5.3 for some of the terminology and variables used in the context of critical loads for soils.

5.5.1 The steady-state water chemistry (SSWC) model

5.5.1.1 Model derivation

The critical load of a lake or stream can be derived from present day water chemistry using the SSWC model, if weighted annual mean values, or estimates thereof, are available. It assumes that all sulphate (SO_4^{2-}) in runoff originates from sea salt spray and anthropogenic deposition (no adsorption or retention). The model uses Acid Neutralising Capacity (ANC) as the variable linking water chemistry to sensitive indicator organisms in freshwaters.

In the SSWC model (Sverdrup et al. 1990, Henriksen et al. 1992, Henriksen and Posch 2001; Curtis et al. 2015) a critical load of acidity, $CL(A)$, is calculated from the principle that the acid load should not exceed the non-marine, non-anthropogenic base cation input and sources and sinks in the catchment minus a buffer to protect selected biota from being damaged, in other words:

(V.52)

$$CL(A) = BC^*_{dep} + BC_w - Bc_u - ANC_{limit}$$

where BC^*_{dep} (BC=Ca+Mg+K+Na) is the sea-salt corrected (with Cl as a tracer; see Chapter 2) non-anthropogenic deposition of base cations, Bc_w is the average weathering flux, Bc_u (Bc=Ca+Mg+K) is the net long-term average uptake of base cations in the biomass (i.e., the annual average removal of base cations due to harvesting), and ANC_{limit} the lowest ANC-flux that does not damage the selected biota. Since the average flux of base cations weathered in a catchment and reaching the lake is difficult to measure or to compute from available information, a critical load equation that uses water quality data alone has been derived.

In pre-acidification times the non-marine flux of base cations from the lake, BC^*_0, is given by (all parameters are expressed as annual fluxes, e.g., in eq/m²/yr):

(V.53)

$$BC^*_0 = BC^*_{dep} + BC_w - Bc_u$$

Thus, we have for the critical load from eq. V.52:

(V.54)

$$CL(A) = BC^*_0 - ANC_{limit} = Q \cdot ([BC^*]0 - [ANC]_{limit})ds$$

where the second identity expresses the critical load in terms of the catchment runoff Q (in m/yr) and concentrations ($[X]= X/Q$). To estimate the pre-acidification flux of base cations we start with the present flux of base cations, BC^*_t, given by:

(V.55)

$$BC^*_t = BC^*_{dep} + BC_w - Bc_u + BC_{exc}$$

where BC_{exc} is the release of base cations due to ion-exchange processes. Assuming that deposition, weathering rate, and net uptake have not changed over time, we obtain BC_{exc} by subtracting eq. V.49 from eq. V.55:

(V.56)

$$BC_{exc} = BC^*_t - BC^*_0$$

This present-day excess production of base cations in the catchment is related to the long-term *changes* in inputs of non-marine acid anions by the so-called F-factor (see below):

(V.57)

$$BC_{exc} = F \cdot (\Delta SO^*_4 + \Delta NO_3)$$

For the pre-acidification base cation flux we thus get from eq. V.56 ($\Delta X = X_t - X_0$):

(V.58)

$$BC^*_0 = BC^*_t - F \cdot (SO^*_{4,t} - SO^*_{4,0} + NO_{3,t} - NO_{3,0})$$

The pre-acidification nitrate concentration, $NO_{3,0}$, is generally assumed zero.

5.5.1.2 The F-factor

According to eqs.V.56 and V.57, and using concentrations instead of fluxes, the F-factor is defined as the ratio of change in non-marine base cation concentrations due to changes in strong acid anion concentrations (Henriksen 1984, Brakke et al. 1990):

(V. 59)

$$F = ([BC^*]_t - [BC^*]_0)/([SO^*_4]_t - [SO^*_4]_0 + [NO_3]_t - [NO_3]_0)$$

where the subscripts t and 0 refer to present and pre-acidification concentrations, respectively. If F=1, all incoming protons are neutralised in the catchment (only soil acidification), at F=0 none of the incoming protons are neutralised in the catchment (only water acidification). The F-factor was estimated empirically to be in the range 0.2–0.4, based on the analysis of historical data from Norway, Sweden, USA, and Canada (Henriksen 1984). Brakke et al. (1990) later suggested that the F-factor should be a function of the base cation concentration:

(V.60)

$$F = \sin\left(\frac{\pi}{2}[BC^*]_t/[S]\right)$$

where $[S]$ is the base cation concentration at which F=1; and for $[BC^*]_t > [S]$ F is set to 1. For Norway $[S]$ has been set to 400 meq/m^3 (ca. 8 mgCa/L) (Brakke et al. 1990).

In eq. V. 60 the present base cation concentration is used for practical reasons. To render the F-factor independent from the present base cation concentration (and to simplify the functional form), Posch et al. (1993) suggested the following relationship between F and the pre-acidification base cation concentration $[BC^*]_0$:

(V.61)

$F = 1 - \exp(-[BC^*]_0/[B])$

where $[B]$ is a scaling concentration estimated to be 131 meq/m³ from paleolimnological data from Finland (Posch et al. 1993). Inserting this expression into eq. V.55 gives a non-linear equation for $[BC^*]_0$ which has to be solved by an iterative procedure. The two expressions for the F-factor give similar results when used to calculate critical loads for surface waters in Norway (see Henriksen and Posch 2001).

The use of the F-factor, defined as a function of the base cation concentration (Henriksen 1984), was originally derived from Norwegian lake data. In Norway the range of runoff is wide (0.3–5 m/yr), with an average of about 1 m/yr. In other Nordic countries, such as Sweden and Finland, runoff is low compared to most of Norway. The weathering rate of a catchment is largely dependent on the bedrock and overburden. Thus, catchments with similar bedrock and overburden characteristics should have similar weathering rates. If one catchment has a high runoff (e.g., 2 m/yr), and another one has a low runoff (e.g., 0.3 m/yr), their base cation fluxes will be similar, but their concentrations will differ considerably. Thus, in the F-factor (eq. V.60) the BC-flux should be used instead of the concentration (Henriksen and Posch 2001):

(V.62)

$$F = \sin\left(\frac{\pi}{2} Q \cdot [BC^*]_t / S\right)$$

where S is the base cation flux at which F=1. For Norway, S has been estimated at 400 meq/m²/yr. Again, if $Q \cdot [BC^*]_t > S$, F is set to 1. Similarly, fluxes could be introduced for the formulation in eq. V.61.

5.5.1.3 The non-anthropogenic sulphate concentration

The pre-acidification sulphate concentration in lakes, $[SO^*_4]_0$, is assumed to consist of a constant atmospheric contribution and a geologic contribution proportional to the concentration of base cations (Brakke et al. 1989):

(V.63)

$[SO^*_4]_0 = a + b \cdot [BC^*]_t$

The coefficients in this equation, estimated for different areas and by different authors, are summarised in Table 5.20.

Table 5.20: Constants to estimate the non-anthropogenic sulphate concentration with eq. V.63, derived from empirical data (N is the number of samples and r is the correlation coefficient).

a (meq/m³)	*b*	*N*	*r*	Reference
15	0.16	143	0.38	Lakes, Norway (Brakke et al 1989)
8	0.17	289	0.78	Lakes, Norway (Henriksen and Posch 2001)
5	0.05	n.g.	n.g.	Groundwater, Sweden (Wilander 1994)
14	0.10	61	0.29	Lakes, Finland (Posch et al. 1993)
19	0.08	251	0.66	Lakes, N. Norway+Finland+Sweden (Posch et al. 1997)
9.5	0.08	60	0.66	Lakes, Ireland (Aherne et al. 2002)

Details on the procedures and data sources for estimating these coefficients can be found in the references given. In Henriksen and Posch (2001) it is shown that the exceeded area for Norwegian lakes (in 1994) is influenced very little by the choice of coefficients for calculating non-anthropogenic sulphate. Similar results have been reported for Irish lakes (Aherne and Curtis 2003).

Larssen and Høgåsen (2003) suggested that the atmospheric contribution in eq. V.63 be derived from background S deposition, as estimated by atmospheric transport models:

(V.64)

$$[SO^*_4]_0 = S_{dep,0}/\ Q + b \cdot [BC^*]_t$$

For southern Norway, $S_{dep,0}$ is about 50 mgS/m²/yr from the EMEP long-range transport model, (i.e., about 3 meq/m²/yr). With Q varying between 0.5 and 1 m/yr, this results in an atmospheric contribution to $[SO^*_4]_0$ of about 3–6 meq/m³.

The SSWC model has been developed for and is particularly applicable to dilute oligotrophic waters located on granitic and gneissic bedrock with thin overburden, such as large parts of Fennoscandia, Scotland, Canada, and Ireland. In such areas, surface waters are generally more sensitive to acid inputs than soils. The model assumes that all sulphate in runoff originates from deposition alone, except for a small geologic contribution. In areas where the geological conditions lead to more alkaline waters, the SSWC model has to be modified, since significant amounts of sulphate from geological sources can be present in the runoff water. A modification for this kind of conditions has been developed for Slovakia (Závodský et al. 1995).

5.5.1.4 The ANC-limit

Lien et al. (1996) analysed the status of fish and invertebrate populations in the context of surface water acidification and loss of ANC in Norwegian lakes and streams. The data for fish came from populations in 1,095 lakes, mostly from the regional lake survey carried out in 1986 (Henriksen et al. 1988, 1989). The critical level of ANC varied among fish species, with Atlantic salmon being the most sensitive, followed by brown trout. They concluded that Atlantic salmon appeared to be a good indicator for acidification of rivers, and trout seemed to be a useful indicator for acidification of lakes. Based on an evaluation of fish and invertebrate populations, a critical lower limit of $[ANC]$=20 meq/m³ was suggested as the tolerance level for Norwegian surface waters (Lien et al. 1996; see Figure 5.11). This limit has been widely used (Kola, northern Russia: Moiseenko 1994; southern central Alps: Boggero et al. 1998; China: Duan et al. 2000); however, it has been set to zero in the United Kingdom (CLAG 1995) and to 40 meq/m³ in south-central Ontario, Canada (Henriksen et al. 2002).

Figure 5.11: Relationship between the ANC concentration in lake water and the probability for damage and extinction of fish (brown trout) populations in lakes, derived from Norwegian data (after Lien et al. 1996).

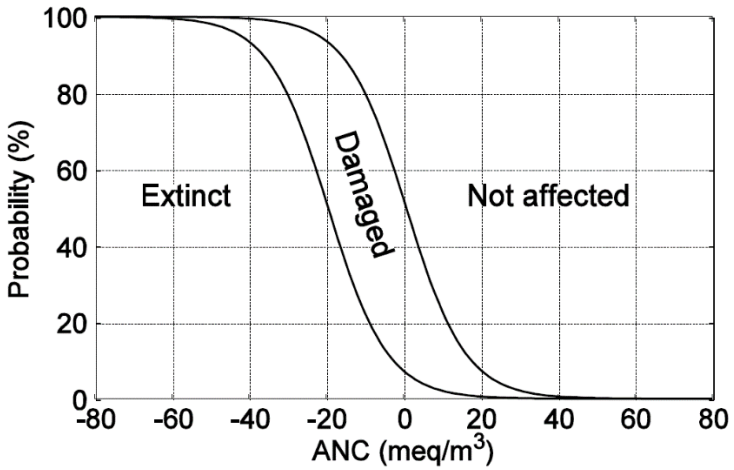

Source: This figure is adopted from a previous version of Chapter 5 of the Mapping Manual

Lydersen et al. (2004) argued that the ANC-limit should be corrected with the amount of organic acids present in the lake. They also showed that the fit between observed fish status and ANC can be (slightly) improved, if an 'organic acid adjusted' ANC, $[ANC]_{oaa}$, is used. Using critical limits for $[ANC]_{oaa}$, the critical ANC-limit is obtained as:

(V.65)

$$[ANC]_{limit} = [ANC]_{oaa,limit} + \frac{1}{3} \cdot m \cdot TOC$$

where $m \cdot TOC$ is the total organic carbon expressed in meq/m³ (m being the charge density). Values for $[ANC]_{oaa,limit}$ for different fish species can be found in Lydersen et al. (2004).

Figure 5.10 indicates that in the ANC range 0–50 meq/m³ there is a decreasing probability from about 50% to 0% of damage to fish populations. The lakes studied receive very low to very high (for Norway) levels of deposition, thus including a wide range of affected lakes. This implies that for a given ANC-value lakes of varying sensitivity exist, receiving varying amounts of deposition. This could reflect that fish have responded to the same ANC differently in different lakes, indicating that a catchment-dependent ANC-limit would be more appropriate than a fixed value for all lakes. In other words, every lake has its own characteristic ANC-limit (in the range shown in Figure 5.11). Less sensitive lakes (i.e., lakes with higher critical loads) should have a higher ANC-limit, since less sensitive ecosystems will have a higher biological variety/diversity and thus require a higher ANC-limit to keep that diversity intact. The simplest functional relationship with this feature is a linear relationship between $[ANC]_{limit}$ and the critical load CL:

(V.66)

$$[ANC]_{limit} = k \cdot CL$$

This gives the following implicit equation for the critical load (see eq. V.54):

(V.67)

$$CL = Q \cdot ([BC^*]_0 - k \cdot CL)$$

which yields after re-arranging for CL:

(V.68)

$CL = Q \cdot [BC^*]_0/(1 + k \cdot Q)$

and thus from eq. V.66:

(V.69)

$[ANC]_{limit} = k \cdot Q \cdot [BC^*]_0/(1 + k \cdot Q)$

This is a special case of a more general expression derived earlier using somewhat different arguments (Henriksen et al. 1995). They derived a k-value by assuming that for a critical load of 200 meq/m²/yr the ANC-limit should not exceed 50 meq/m³, resulting in k = 50/200 = 0.25 yr/m (see eq. V.66). In addition, 50 meq/m³ was set as upper boundary for $[ANC]_{limit}$. The value of k was derived from experience in the Nordic countries and, as such, reflects the geology, deposition history, and biological diversity (fish species) of that region. For different regions other k-values may be more appropriate.

The lake-dependent ANC-limit has also been derived for the organic acid adjusted ANC-limit, resulting in the expression (Hindar and Larssen 2005):

(V.70)

$$[ANC]_{oaa,limit} = k \cdot Q \cdot \left([BC^*]_0 - \frac{1}{3} \cdot m \cdot TOC\right)/(1 + k \cdot Q)$$

Inserting this expression into eq. V.65 gives the ANC-limit for the CL calculation. Also, the k-value has been adjusted to k = 0.2, and the upper boundary to 40 meq/m³ (Hindar and Larssen 2005).

5.5.2 The empirical diatom model

The empirical diatom model is an alternative approach to the SSWC model and is developed from paleolimnological data (Battarbee et al. 1995). Diatom assemblages in cores from acidified lakes usually show that prior to acidification the diatom flora, and therefore water chemistry, changed little over time. The point of acidification is indicated by a shift towards a more acidophilous diatom flora. Diatoms are amongst the most sensitive indicators of acidification in freshwater ecosystems; hence it can be argued that the point of change in the diatom record indicates the time at which the critical load for the site was exceeded.

The acidification status (as defined by diatom analyses) of 41 sites in the United Kingdom (UK) was compared to site sensitivity (defined by lake-water calcium concentrations) and current deposition loading. The optimal separation of acidified and non-acidified sites is given by a $[Ca]$: S_{dep} ratio of 94:1 (Battarbee et al. 1995), acidified sites having a ratio less than 94:1. This critical ratio, determined by logistic regression, can be used to define critical sulphur loads for any site, including streams. Critical load values are calculated from preacidification calcium concentrations using the F-factor (Brakke et al. 1990). For example, the critical sulphur load for a lake with a $[Ca]_0$-value of 40 meq/m³ is approximately 0.43 keq/ha/yr.

The diatom model has been adapted to provide critical loads, and critical load exceedances, for total acidity (sulphur and nitrogen). Exceedance values for total acidity require a measure of the fraction of deposited nitrogen leached to the surface waters. This is calculated from the differences between the ratios of sulphate/nitrate in the water and in the deposition at the site. In this way the fraction of the nitrogen deposition contributing to acidification, a_w, is added to the value of sulphur deposition to provide a total 'effective' acid deposition:

(V 71)

$$a_N = \frac{S^*_{dep}}{N_{dep}} \Big/ \frac{[SO_4^*]}{[NO_3]}$$

This model assumes equilibrium between sulphur deposition and sulphate in water, and only applies to sites with no additional catchment nitrogen inputs. The diatom model has been re-calibrated for total acidity loads by substituting total effective acid deposition for sulphur deposition. The resulting critical ratio is 89:1, slightly lower than when considering sulphur alone. The basic equation for the critical load of total acidity in the empirical diatom model is therefore as follows:

(V.72)

$$CL(A) = \frac{[Ca^*]_0}{89}$$

where $CL(A)$ is in keq/ha/yr and $[Ca^*]_0$ in meq/m³. The pre-acidification Ca-concentration is calculated as:

(V.73)

$$[Ca^*]_0 = [Ca^*]_t - F \cdot ([SO^*_4]_t - [SO^*]_0 + [NO_3]_t - [NO_3]_0)$$

with

(V.74)

$$F_{Ca} = \sin\left(\frac{\pi}{2}[Ca^*]_t / [S_{Ca}]\right)$$

and $[S_{Ca}]$ is the Ca-concentration at which F_{Ca}=1. It can vary between 200 and 400 meq/m³, depending on location. In the UK, critical loads mapping exercise a value of $[S_{Ca}]$=40 meq/m³ has been used, and in waters with $[Ca^*]_t > [S_{Ca}]$, F_{Ca} was set to 1. The pre-acidification nitrate concentration, $[NO_3]_0$, is assumed zero. The pre-acidification sea-salt corrected sulphate concentration, $[SO_4^*]_0$, is estimated according to eq. V.63 (Brakke et al.1989).

The diatom model has been calibrated using sites and data from the UK. However, a major advantage of the approach is that predictions for any lake can be validated by analysing diatoms in a sediment core. In this way the applicability of the model to sites outside the UK can be tested.

5.5.3 The first-order acidity balance (FAB) model

The First-order Acidity Balance (FAB) model for calculating critical loads of sulphur (S) and nitrogen (N) for a lake considers sources and sinks within the lake and its terrestrial catchment. The original version of the FAB model has been developed and applied to Finland, Norway, and Sweden in Henriksen et al. (1993) and further described in Posch et al. (1997). A modified version was first reported in Hindar et al. (2000) and is described in Henriksen and Posch (2001). A comprehensive summary can also be found in Posch et al. (2012b). The FAB model is designed to be equivalent to the Simple Mass Balance model for a catchment, and it largely follows its derivation (see section 5.4), the main difference being that the leaching of ANC is modelled according to the SSWC model (see section 5.5.1).

5.5.3.1 Model derivation

The lake and its catchment are assumed small enough to be properly characterised by average soil and lake water properties. With A we denote the total catchment area (lake + terrestrial catchment), A_l is the lake area, A_f the forested area and A_g the area covered with grass/heath land. We have $A_l + A_f + A_g \leq A$, and a non-zero difference represents a land area on which no transformations of the deposited ions take place ('bare rock').

The starting point for the derivation of the FAB model is the charge balance ('acidity balance') in the lake water running off the catchment:

(V.75)

$$S_{runoff} + N_{runoff} = BC^*_{runoff} - ANC_{runoff}$$

where BC^* stands for the sum of (non-marine) base cations and ANC is the acid neutralising capacity. In the above equation we assume that the quantities are total amounts per time (e.g., eq/yr). In order to derive critical loads, we have to link the ions in the lake water to their depositions, taking into account their sources and sinks in the terrestrial catchment and in the lake.

For X = S, N and BC the mass balance in the lake is given by:

(V.76)

$$X_{runoff} = X_{in} - X_{ret}, \quad X = S, N, BC$$

where X_{in} is the total amount of ion X entering the lake and X_{ret} the amount of X retained in the lake. The in-lake retention of S and N is assumed to be proportional to the input of the respective ion into the lake:

(V.77)

$$X_{ret} = \rho_X \cdot X_{in}, \quad X = S, N$$

where $0 \le p_x \le 1$ is a dimensionless retention factor. Thus, the mass balances for the lake become:

(V.78)

$$X_{runoff} = (1 - \rho_X) \cdot X_{in}, \quad X = S, N$$

The total amount of sulphur entering the lake is given by:

(V.79)

$$S_{in} = A \cdot S_{dep}$$

where S_{dep} is the total deposition of S per unit area. Immobilisation, reduction, and uptake of sulphate in the terrestrial catchment are assumed negligible. Sulphate ad/desorption is not considered since we model steady-state processes only. Eq. V.79 states that all sulphur deposited onto the catchment enters the lake, and no sources or sinks are considered in the terrestrial catchment.

In the case of nitrogen, we assume that immobilisation and denitrification occur both in forest and grass/heath land soils, whereas net uptake occurs in forests only (equalling the annual average amount of N removed by harvesting); the deposition onto the remaining area (lake + 'bare rocks') enters the lake unchanged. Thus, the amount of N entering the lake is:

(V.80)

$$N_{in} = (A - A_f - A_g) \cdot N_{dep} + A_f \cdot (N_{dep} - N_i - N_u - N_{de})_+ + A_g \cdot (N_{dep} - N_i - N_{de})_+$$

where N_{dep} is the total N deposition, N_i is the long-term net immobilisation of N (which may include other long-term steady-state sources and sinks; see Chapter 5.3), N_{de} is N lost by denitrification, and N_u the net growth uptake of N, all per unit area. The symbol $(x)_+$ or x_+ is a short-hand notation for max(x, 0), i.e., $x_+ = x$ for $x > 0$ and $x_+ = 0$ for $x \le 0$. The effects of nutrient cycling are ignored, and the leaching of ammonium is considered negligible, implying its complete uptake and/or nitrification in the terrestrial catchment.

While immobilisation and net growth uptake are assumed independent of the N deposition, denitrification is modelled as a fraction of the available N:

(V.81)

$$N_{de} = \begin{cases} f_{de} \cdot (N_{dep} - N_i - N_u)_+, & on\ A_f \\ f_{de} \cdot (N_{dep} - N_i)_+, & on\ A_g \end{cases}$$

where $0 \le f_{de} < 1$ is the (soil-dependent) denitrification fraction. The above equation assumes that denitrification is a slower process than immobilisation and growth uptake. Inserting eq. V.81 into eq. V.80 one obtains:

(V.82)

$$N_{in} = (A - A_f - A_g) \cdot N_{dep} + A_f \cdot (1 - f_{de}) \cdot (N_{dep} - N_i - N_u)_+ + A_g \cdot (1 - f_{de}) \cdot (N_{dep} - N_i)_+$$

If sufficient data for quantifying the sources and sinks of base cations in the catchment, such as deposition, weathering, and uptake, are available, the runoff of base cations (BC^*_{runoff}) could be described in the same way as S and N. This would be in analogy to the derivation of the SMB model for (forest) soils. Alternatively, water quality data can be used to quantify the runoff of base cations and ANC, as is done in the SSWC model (see section 5.5.1).

To arrive at an equation for critical loads, a link has to be established between a chemical variable and effects on aquatic biota. The most commonly used criterion is the so-called ANC-limit (see above), (i.e., a minimum concentration of ANC derived to avoid 'harmful effects' on fish):

$$ANC_{runoff,crit} = A \cdot Q \cdot [ANC]_{limit}.$$

Defining $L_{crit} = (BC^*_{runoff} - ANC_{runoff,crit})/A$, inserting eq. V.79 and V.82 into eq. V.78 and eq. V.75 and dividing by A yields the following equation to be fulfilled by critical depositions (loads) of S and N:

(V.83)

$$(1 - \rho_S) - S_{dep} + (1 - \rho_N) \cdot \{(1 - f - g) \cdot N_{dep} + f \cdot (1 - f_{de}) \cdot (N_{dep} - N_i - N_u)_+ + g \cdot (1 - f_{de}) \cdot (N_{dep} - N_i)_+\} = L_{crit}$$

where we have defined:

(V.84)

$$f = A_f/A, \quad g = A_g/A$$

$$\Rightarrow \quad 1 - f - g \ge r \quad \text{with } r = A_l/A$$

Eq. V.83 defines a function in the (N_{dep}, S_{dep})-plane, the so-called critical load function, and in the following we will look at this function in more detail. The general form of the critical load function is:

(V.85)

$$a_S \cdot S_{dep} + a_N \cdot N_{dep} = L_N + L_{crit}$$

with

(V.86)

$$a_S = 1 - \rho_S,\ a_N = (1 - \rho_N) \cdot b_N,\ L_N = (1 - \rho_N) \cdot M_N$$

The quantity M_N and the dimensionless coefficient b_N depend on N_{dep}:

(a) $N_{dep} \leq N_i$: In this case $(N_{dep}-N_i)_+ = 0$ and $(N_{dep}-N_i-N_u)_+ = 0$, which means that all N falling onto forests and grassland is immobilised and only the N deposition falling directly onto the lake and 'bare rocks' contributes to the leaching of N:

(V.87)

$b_N = b_1 = 1 - f - g$, $M_N = M_1 = 0$

(b) $N_i < N_{dep} \leq N_i + N_u$: In this case $(N_{dep}-N_i)_+ = N_{dep}-N_i$, but $(N_{dep}-N_i-N_u)_+ = 0$, meaning that all N deposition falling onto forests is immobilised or taken up, but N falling onto the other areas is (partially) leached:

(V88)

$b_N = b_2 = 1 - f - g \cdot f_{de}$,

$M_N = M_2 = (1 - f_{de}) \cdot g \cdot N_i$

(c) $N_{dep} > N_i + N_u$: Some N deposition is leached from all areas:

(V.89)

$b_N = b_3 = 1 - (f + g) \cdot f_{de}$,

$M_N = M_3 = (1 - f_{de}) \cdot [(f + g) \cdot N_i + f \cdot N_u]$

The maximum critical load of sulphur is obtained by setting $N_{dep} = 0$ in eq .V.83:

(V.90)

$CL_{max}(S) = L_{crit}/a_S$

Setting $S_{dep} = 0$ and considering the three different cases for N_{dep}, gives the following expression for the maximum critical load for nitrogen:

(V.91)

$CL_{max}(N) = \min\{(L_{crit}/1 - \rho_N) + M_i)/\ b_i, \text{ i} = 1,2,3\}$

Figure 5.12: Piece-wise linear critical load function of S and acidifying N for a lake as defined by catchment properties. Note the difference with the critical load function for soils (see Figure 5.4). The grey area below the CL function denotes deposition pairs resulting in an ANC leaching greater than $Q \cdot [ANC]_{limit}$ (non-exceedance of critical loads; see Chapter 7).

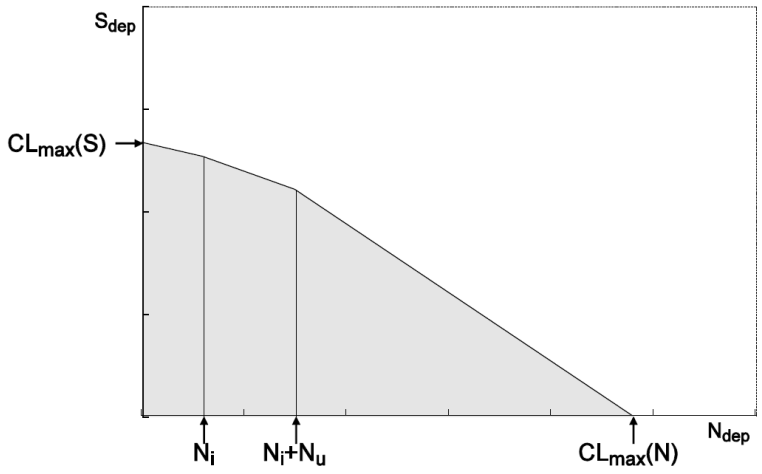

Source: This figure is adopted from a previous version of Chapter 5 of the Mapping Manual

5.5.3.2 Systems of lakes

The above derivation of the FAB model is for small headwater lakes only. Critical loads are generally calculated for such lakes, since lakes with many upstream lakes tend to have larger catchments, and several (implicit) assumptions of the FAB model (e.g., uniform depositions) will be violated. Nevertheless, in some areas systems of lakes can be found on a small scale, and therefore a model for such systems is desirable.

When computing the critical load of acidity with the SSWC model (which uses annual average lake water chemistry) for a lake receiving runoff from upstream lakes, one implicitly computes *the critical load for that lake including all its upstream lakes*, since water samples taken from (the outlet of) the lowest lake is a mixture of the water of that lake and all its upstream lakes. Consequently, when applying the FAB model to such a lake, one has to be aware that one also computes the critical load for the whole system of lakes and thus must consider the catchment and lake characteristics of all lakes in the system. To do this in a more explicit way, two methods for computing the critical load of a system of lakes have been developed (Hindar et al. 2000). Both require the same input data, but they differ in the complexity of the calculations involved. The formulae will not be derived here, and the interested reader is referred to the literature (see also Hindar et al. 2001), where also the differences between the methods are demonstrated using data from lake systems in the Killarney Provincial Park in Ontario, Canada. An application to lakes in the Muskoka River catchment (which are also located in Ontario, Canada) can be found in Aherne et al. (2003).

5.5.4 Input data

In addition to the data required for the SSWC and diatom model (runoff and concentrations of major ions in the lake runoff water), the FAB model also needs information on (a) the area of lake, catchment and different land cover classes, (b) terrestrial nitrogen sinks, and (c) parameters for in-lake retention of N and S.

5.5.4.1 Runoff

The runoff Q is the amount of water leaving the catchment at the lake outlet, expressed in m/yr. It is derived from measurements or can be calculated as the difference between precipitation and actual evapotranspiration, averaged over the catchment area. A longterm climatic mean annual value should be taken. Sources for data and models for evapotranspiration can be found in section 5.5.

5.5.4.2 Ion concentrations

In addition to runoff, the concentrations of major ions in the runoff water, (i.e., sulphate, nitrate, and base cations), are needed to calculate SSWC critical loads, and these come from the analysis of representative water samples.

The critical load for a site should be calculated with yearly flow-weighted average chemistry and yearly average runoff. Since such values are not available for a large number of lakes, critical loads are mostly calculated on the basis of a single sample considered representative of yearly flow-weighted averages. A sample collected shortly after the fall circulation of a lake is generally assumed to fulfil this purpose. To check this claim, Henriksen and Posch (2001) compared critical load values calculated from yearly flow-weighted average concentrations with critical loads calculated from a single fall value for sites for which long-term data series are available. Results for seven Norwegian catchments show that the single fall value is fairly representative for the annual average chemistry. Similarly, results from eight Canadian catchments show that a

single spring sample is fairly representative of the annual average chemistry (Henriksen and Dillon 2001).

5.5.4.3 Lake and catchment characteristics

The area parameters A, A_i, A_f and A_g, which are needed in the FAB model, can generally be derived from both digital and paper maps.

5.5.4.4 Terrestrial nitrogen sinks

The uptake of N can be computed from the annual average amount of N in the harvested biomass if there is no removal of trees from the catchment, N_u=0.

N_i is the long-term annual immobilisation (accumulation) rate of N in the catchment soil. Note that at present immobilisation may be substantially higher due to elevated N deposition.

The denitrification fraction f_{de} depends on the soil type and its moisture status. In earlier FAB applications it has been estimated from the fraction of peat-lands, f_{peat}, in the catchment by f_{de}=0.1+0.7·f_{peat} (Posch et al. 1997).

For more details on these parameters see section 5.4.

5.5.4.5 In-lake retention of N and S

Concerning in-lake processes, the retention factor for nitrogen ρ_N (see eq. V.77) is modelled by a kinetic equation (Kelly et al. 1987):

(V.92)

$$\rho_N = \frac{s_N}{s_N + z/\tau} = \frac{s_N}{s_N + Q/r}$$

where z is the mean lake depth, τ is the lake's residence time, r is the lake: catchment ratio (=A_l/A) and S_N is the net mass transfer coefficient. There is a lack of observational data for the mass transfer coefficients, especially from European catchments, but Dillon and Molot (1990) give a range of 2–8 m/yr for S_N. Values for Canadian and Norwegian catchments are given in Kaste and Dillon (2003).

An equation analogous eq. V.92 for ρ_S with a mass transfer coefficient s_S is used to model the in-lake retention of sulphur. Baker and Brezonik (1988) give a range of 0.2–0.8 m/yr for s_s.

5.6 Critical loads of cadmium, lead and mercury

5.6.1 General methodological aspects of mapping critical loads of heavy metals

5.6.1.1 Calculation of different types of critical loads

The method to calculate critical loads of heavy metals is based on the balance of all relevant metal fluxes in and out of a considered ecosystem in a steady state situation (De Vries et al. 2015c; Hettelingh et al., 2015c) In order to keep the approach compatible with the simple mass balance approach used for nitrogen and acidity, the internal metal cycling within an ecosystem is ignored, such that calculations can be kept as simple as possible. As a consequence, the critical load of a metal can be calculated from the sum of tolerable outputs from the considered system in terms of net metal uptake and metal leaching.

The assumption of a steady-state signifies that the concentration in the system does not change in time because the amount of heavy metal entering the system is equal to the amount that leaves the system. The validity of this assumption depends on the magnitude of the time scales

of the various input and output processes. If, for example, a metal sorbs very strongly to the soil, it may take a long time (up to hundreds of years), before a steady-state is reached. This has to be kept in mind when comparing a present load with the critical load (De Vries and Bakker 1998). Critical loads of cadmium (Cd), lead (Pb) and mercury (Hg) can be calculated in dependence on the receptors and the metal of concern. Critical limits of these heavy metals addressing either ecotoxicological ecosystem effects or human health effects are derived with specific approaches. Critical loads on the basis of such limits should be calculated separately for aquatic and terrestrial ecosystems. Consequently, four types of critical loads can be derived for each metal. An overview is provided in Table 5.21, though it is not a complete review of possible effects of these metals. Indicators of effects on ecosystems listed in Table 5.21 are mainly ecotoxicological effects. Secondary poisoning through the food chain has also been studied (De Vries et al. 2003). These effects give partly more stringent critical limits; however, their modelling includes more uncertainties and is therefore not considered in this manual.

Critical loads for terrestrial ecosystems addressing human health effects can be calculated, either in view of not violating food quality criteria in crops or in view of ground water protection (keeping quality criteria for drinking water of WHO 2004). An appropriate indicator for critical load calculations addressing human health effects via food intake is the Cd content in wheat. Keeping a conservative food quality criterion for wheat, as described in section 5.5.2.2.1, simultaneously protects against effects on human health via other food and fodder crops (including also the quality of animal products, since the pathway of Cd to wheat leads to the lowest critical Cd content in soils according to De Vries et al. (2003)). Such critical load calculations are, in principle, also possible for lead, and for other food and fodder crops, if the soil-plant transfer can be described with sufficient accuracy and can be done in addition on a voluntary basis.

Among terrestrial ecosystems, critical loads of Cd and Pb are to be calculated from the viewpoint of ecotoxicology for areas covered by non-agricultural land (forests, semi-natural vegetation) or agricultural land (arable land and grassland). Organic forest (top)soils are considered as the only critical receptor with respect to atmospheric Hg pollution, based on knowledge on effects on microbial processes and invertebrates (Meili et al. 2003a). The critical exposure of terrestrial ecosystems to atmospheric Hg pollution can be calculated in much the same way as for Pb and Cd by a simple mass balance, as discussed in section 5.5.2.1. For aquatic ecosystems the critical limits of Pb and Cd are related to ecotoxicological effects, while human health effects by this pathway are less relevant and therefore not considered here. Critical limits of Hg refer to both human health effects (Hg concentration in fish and other animals that serve as a food source to humans) and ecotoxicological effects, since microbiota and higher wildlife itself may also be affected.

Although it might be useful to calculate and map each of the different types of critical loads and the critical *Hg* level in precipitation separately for comparison purposes, the aim is ultimately to provide maps for at most four critical loads per metal (or *Hg* level, respectively) related to:

- Ecotoxicological effects for all terrestrial ecosystems.
- Human health effects for all terrestrial ecosystems.
- Ecotoxicological effects for all aquatic ecosystems.
- Human health effects for all aquatic ecosystems.

If different indicators within each category (map) have been considered (e.g., *Cd* in wheat and *Cd* in soil drainage water in view of ground water protection for human health), the final map

should indicate the minimum critical *Cd* load for both effects to human health. The reason for providing different critical loads for different types of ecosystems is because the critical load for terrestrial ecosystems does not automatically protect aquatic ecosystems, which recieve much or most of their metal load by drainage from the surrounding soils, and vice versa.

A critical load indicates only the sensitivity of an ecosystem against the anthropogenic input of the metal of interest. It implies a potential risk at sites where the critical load is exceeded. In agricultural ecosystems, the exceedance of critical loads of heavy metals is not only determined by atmospheric inputs (being generally the only source in non-agricultural ecosystems), but by total inputs, including fertilizer and animal manure inputs.

Table 5.21: Four types of critical loads of Pb, Cd, Hg, related receptors and indicators.

Receptor ecosystem	Critical loads related to	Metals of concern	Land cover types to be considered	Indicator addressed by the critical limit
1) Terrestrial[*)]	a) Human health effects	Cd, Pb, Hg	Arable land	Metal content in food/fodder crops
		Cd, Pb, Hg	Grassland	Metal content in grass, animal products (cow, sheep)
		Cd, Pb, Hg	Arable land, grassland, non-agricultural land	Total metal concentration in soil water below the rooting zone (aiming at ground water protection)
	b) Ecosystem functioning	Pb, Cd	Non-agricultural land, arable land, grassland,	Free metal ion concentration in soil solution in view of effects on soil microorganisms, plants and invertebrates
		Hg	Forests only	Total metal concentration in humus layer in view of effects on soil micro-organisms and invertebrates
2) Aquatic	a) Human health effects	Hg	Freshwaters	Metal concentration in fish
	b) Ecosystem functioning	Pb, Cd, Hg	Freshwaters	Total metal concentration in freshwaters in view of effects on algae, crustacea, worms, fish, top predators

[*)] In italics: these calculations can be done in addition on a voluntary basis. To perform such calculations, more information on the derivation of critical limits based on critical metal contents in food/fodder crops and in animal products is given in Annex 2 and 3, respectively, of the background document (De Vries et al. 2005).

5.6.1.2 Limitations in sites that allow critical load calculations

Critical load calculations can not be carried out for sites with:

- negative water balances – since there is no leaching but a seepage influx of water, leading to accumulation of salts and very high *pH* (however, such regions do hardly occur in Europe);
- and soils with reducing conditions (e.g., wetlands), because the transfer functions do not apply for such soils. In the topsoil to which the critical load calculations apply, such situations do, however, hardly occur apart from waterlogged soils where the simplified critical load calculation can not be applied anyhow because of a deviating hydrology.

Weathering inputs of metals are neglected due to i) low relevance of such inputs and ii) high uncertainties of respective calculation methods. It is, however, recommended to use estimates of weathering rate to identify sites with a high geogenic metal input, where natural weathering may already exceed the critical load. This should be considered when critical limits and loads exceedances are to be interpreted. For methods to calculate weathering rates, see De Vries and Bakker (1998) and Hettelingh et al. (2002). More information on how sites with high geogenic contents of metals can be identified are described in Farret et al. (2003). The most important information is summarised in Annex 6 of the background document (De Vries et al. 2004b).

5.6.1.3 Definitions and symbols / abbreviations used in critical load calculations

General definitions of critical loads, critical levels and exceedances, and others can be found in the related chapters of the Modelling and Mapping Manual. The following definitions refer specifically to the application in the context of critical loads of heavy metals.

5.6.1.3.1 Definitions

The receptor is a living element of the environment that is subject to an adverse effect. It can be a species of interest, including human beings, or several species considered representative of a larger group (e.g., plants, soil invertebrates, fish, algae, etc.), or the whole ecosystem (typically the subject of interest in the critical load approach).

The critical limit is a concentration threshold within the ecosystem, based on adverse effects, (i.e., it is a short expression of "effect-based critical limit"). Below this critical limit significant harmful effects on human health or specified sensitive elements of the environment do not occur, according to present knowledge. To avoid confusion, limits that are not based on effects should not be called "critical limits".

The critical load is the highest total metal input rate (deposition, fertilisers, other anthropogenic sources) below which harmful effects on human health as well as on ecosystem structure and function will not occur at the site of interest in a long-term perspective, according to present knowledge. The critical load is derived from the critical limit through a biogeochemical flux model, assuming steady-state for the fluxes as well as chemical equilibrium (which is a theoretical situation in an undetermined future, consistent with concepts of sustainability). For this purpose, the critical limit has to be transformed to a critical total concentration of the metal in the output fluxes by water (leaching from the soil or outflow from an aquatic ecosystem).

5.6.1.3.2 Some general symbols and abbreviations

M = a flux of a metal M

[M] = a content (in soil, plants, other biota) or a concentration (in a liquid) of a metal M

$[M]_{(crit)}$ = a critical content (in soil, plants, other biota) or a critical concentration (in a liquid) of a metal M, not explicitly explained in Table 5.18 for all the individual contents or concentrations

f = a fraction

c = a factor for conversion of units, not explained in the table

$_{sdw}$ = in soil drainage water

$_{sw}$ = in surface water

Table 5.22: Symbols and abbreviations used in the calculation of critical loads of heavy metals.

$[M]_{SPM,sdw}$ or $[M]_{SPM,sw}$	Concentration of metal bound to suspended particulate matter in soil drainage water, or in surface water, respectively	[mg kg^{-1}]
$[Hg]_{OM}$	Concentration of Hg, normalised for $[OM]_s$	[mg (kg OM)$^{-1}$]
$[Hg]_{Pike}$	Hg concentration in the flesh of 1 -kg pike	[mg kg^{-1} fw]
$[Hg]_{Bio}$	Hg concentration in biota, e.g., fish flesh	[mg kg^{-1} fw]
$[Hg]_{Prec}$	Hg concentration in precipitation	[ng l-1]
[clay]	Clay content of the soil	[(kg clay) kg^{-1}] or [%]
$[OM]_s$	Organic matter content of the soil	[(kg OM) kg^{-1}] or [%]
$[DOM]_{sdw}$ or $[DOC]_{sdw}$	Concentration of dissolved organic matter or dissolved organic carbon, respectively, in soil drainage water	[g m^{-3}] or [mg l^{-1}]
$[TOC]_{sw}$	Concentration of total organic carbon in surface water	[g m^{-3}] or [mg l^{-1}]
$[TP]_{sw}$	Concentration of total phosphorus in surface water	[µg l^{-1}] or [mg l^{-1}]
$[SPM]_{sdw}$ or $[SPM]_{sw}$	Concentration of suspended particulate matter in soil drainage water or in surface water, respectively	(kg m^{-3})
pH_{sdw} or pH_{sw}	pH value in soil drainage water or in surface water	[-]

5.6.1.4 Stand-still approach versus calculation of critical limit exceedance

The harmonised methodological basis for a first preliminary calculation and mapping of critical loads of Cd and *Pb* related to ecotoxicological effects (Hettelingh et al. 2002), was based on a guidance document (De Vries et al. 2002). In this document, a standstill approach was also included as an alternative to the effect-based approach, which aims at avoiding any (further) accumulation of heavy metals in the soil. This method is, however, not included in this manual since it implies the continued addition of metals on historically polluted soils with high leaching rates. The current leaching may then already imply significant effects, both on terrestrial as well as aquatic ecosystems receiving the drainage water from the surrounding soils, and is thus not per se acceptable in the long term. Furthermore, it leads to critical load exceedance at soils which strongly adsorb heavy metals, whereas the effect occurs through the soil solution.

Instead, it is suggested to calculate critical concentrations of metals in the soil, the soil drainage water or the surface water based on the critical limits and compare these to the present soil or water metal concentrations to assess the critical limit exceedance in the present situation. This implies that one has to map the present metal concentrations in the country (expressed as total or reactive soil contents, total dissolved concentrations, or even free ion concentrations). Such a comparison can be seen as an intermediate step for dynamic models for heavy metals (Groeneberg et al., 2015; De Vries et al., 2015c). If the present soil metal content exceeds the critical concentration (limit), the metal input has to be less than the critical load to reach the critical concentration at a defined time penod. In the reverse case, the metal input can be larger than the critical load for a defined time period not exceeding during that period the critical concentration. However, only keeping the critical load will not lead to exceedance of the critical

limit in the long run. More information on how to calculate the critical concentration is given in the background document (De Vries et al, 2005).

5.6.2 Terrestrial ecosystems

5.6.2.1 Simple steady-state mass balance model and related input data

5.6.2.1.1 Steady-state mass balance model

The method to calculate critical loads of heavy metals for terrestrial ecosystems is focusing, in particular, on the upper soil layer. The critical load of a metal can be calculated as the sum of tolerable outputs from this considered soil layer by harvest and leaching minus the natural inputs by weathering release (De Vries and Bakker, 1998). Because weathering causes only a minor flux of metals in topsoils, while uncertainties of such calculations are very high, the model was further simplified by assuming that weathering is negligible within the topsoil outside ore-rich areas. As mentioned in the introduction of this chapter, the calculation of weathering rates is recommended to identify areas, where the natural input exceeds tolerable outputs. Such sites can be excluded from the database, subject to decision by the National Focal Centres.

The described approach implies that the critical load equals the net uptake by forest growth or agricultural products plus an acceptable metal leaching rate:

(V.93)

$CL(M) = M_u + M_{le(crit)}$

where:

$CL(M)$ = critical load of a heavy metal M (g ha^{-1} a^{-1})

M_u = metal net uptake in harvestable parts of plants under critical load conditions (g ha^{-1} a^{-1})

$M_{le(crit)}$ = critical leaching flux of heavy metal M from the considered soil layer (g ha^{-1} a^{-1}), whereby only the vertical drainage flux is considered

The notation has been related to the critical load equations for acidity and nutrient nitrogen: *M* stands for flux of a heavy metal and can be substituted by the chemical symbol of the individual metal *(Cd, Pb, Hg)* under consideration. The critical metal leaching $M_{le(crit)}$ refers to the total vertical leaching rate, including dissolved, colloidal, and particulate (metal) species in the drainage water. For a critical load, the critical metal leaching is based on a critical (toxic) metal concentration in soil or the (free ion or total) metal concentration in soil water.

In mass balance models for *Hg*, re-emission (volatilization) of deposited *Hg* occurs as an additional flux. This flux can, however, be ignored when calculating critical loads of *Hg*, because this re-emission is treated as part of the atmospheric net deposition in the modelling by EMEP MSC-E (Ryaboshapko et al. 1999, Ilyin et al. 2001). Therefore, in order to avoid double consideration in the calculation of critical load exceedances, it should be excluded from the critical loads model.

Appropriate and consistent calculation of critical loads for terrestrial ecosystems requires a consistent definition of the topsoil compartment and its boundaries. The depth can be a variable. Relevant boundaries have been derived by considering, on the one hand, the expected probability of adverse impacts on the main target groups of organisms (plants, soil invertebrates, soil microbiota), or ground water quality and, on the other hand, the occurrence and location of relevant metal fluxes within the soil profile:

- For *Pb* and *Cd* it is assumed that ecotoxicological effects as well as the main proportion of uptake by plants occur in (from) the organic layer (O horizon) and the humus rich (top)soil horizons (A_h, A_p). Therefore, the depth of the biological active topsoil (z_b) should be considered for arable lands, grasslands, and forests as far as the critical load calculations are addressing ecotoxicological effects or the protection of food/fodder quality, respectively. For forest soils covered by an organic layer, the critical loads for both the organic layer and the upper mineral horizon should be calculated separately. In these cases, the most sensitive of both layers should be presented in the critical loads map. For all terrestrial ecosystems the maximum depth of the topsoil (z_b) to be considered is the lower boundary of the uppermost mineral horizon (in most soil classification systems called the A-horizon).

Default values of z_b are:

for forests: 0.1 m (O and/or A_h horizon)

for grassland: 0.1 m (A_h horizon)

for arable: 0.3 m (A_p horizon, plough layer).

- Regarding *Hg*, the critical receptor in terrestrial ecosystems is the organic topsoil (mor or humus layer) of forest soils (O-horizon excluding litter, which is sometimes divided into L, F, and H horizons), where microbial processes are suspected to be affected. For calculating the critical load of *Hg* in forests, the topsoil is therefore defined as the humus layer, excluding underlying mineral soil layers.

Note that for calculations of critical loads with respect to protection of groundwater quality, the entire soil column has to be included. However, it is preliminarily not planned within the critical loads work to model the whole pathway of the metal flux with drainage water, considering the binding capacity of layers between rooting zone and upper groundwater. Therefore, for simplification, the critical leaching of metals from the viewpoint of ground water protection is calculated by multiplying the drainage water flux below the rooting zone (soil depth = z) with the critical limit for drinking water (see 5.5.2.2.2).

5.6.2.1.2 Heavy metal removal from the topsoil by net growth and harvest of plants

For critical load calculations, the removal of heavy metals refers to a future steady-state level where critical limits in the ecosystem compartments are just reached (critical loads conditions). The calculation of a critical removal of metals on the basis of a critical concentration for soil solution is hardly practical, since for many metals there are no clear relationships between concentrations in soil solution (or even free metal ions) and the content of the metals in harvestable part of the plants. One of several reasons is the plant specific exclusion of metals from root uptake or accumulation in specific tissues (detoxification). An exception is the transfer of *Cd* from soil to wheat grains, used to calculate critical loads related to food quality criteria (see V.5.2.2.1). Therefore, a simplified approach is proposed to describe the tolerable removal of heavy metals by biomass net uptake. The average yield (or growth increment) of harvestable biomass is multiplied with the heavy metal content in harvestable plant parts and with a factor to account for the fraction of metal uptake from the relevant soil layer relative to the uptake from the total rooting zone:

(V.94)

$$M_u = f_{Mu} \cdot Y_{ha} \cdot [M]_{ha}$$

where:

M_u = metal net uptake in harvestable parts of plants under critical load conditions (g ha^{-1} a^{-1}) (see Eq. V.93).

f_{Mu} = fraction of metal net uptake within the considered soil depth (z_b or z), accounting also for metal uptake due to deposition on vegetation surfaces (–); in calculations of critical loads to protect ground water, f_{Mu} = 1, otherwise f_{Mu} is a value between 0 and 1.

Y_{ha} = yield of harvestable biomass (dry weight) (kg ha^{-1} a^{-1}).

$[M]_{ha}$ = metal content of the harvestable parts of the plants (g kg^{-1} dw), including also metals deposited on vegetation surfaces (when the metal content is given in mg kg^{-1} dw, the value has to be divided by 1000).

As a default approximation, a root uptake factor ($f_{Mu,zb}$) of 1 can be used for all ecosystem types, assuming that most uptake of nutrients and pollutants occurs in the top soil. In forests values around 80 % have been reported for uptake from the humus layer alone (based on lead isotopes in Scots pine, Bindler et al. 2003). Thus, for calculations referring to the humus layer, $f_{Mu,zb}$ may be 0.8, but, if the top of the underlying mineral soil is included in the calculations, $f_{Mu,zb}$ is likely to approach 1, also in forests. If $_{Mu,zb}$ is 1, the uptake from the upper horizon is equal to that of the entire rooting depth (assumed to be limited to the depth where 90 % of the root biomass is distributed). This implies that there is no difference in the uptake calculation of critical loads related to ecotoxicological effects and in view of ground water protection. More detailed values of $f_{Mu,zb}$ may be used, if information is available.

Data on yields for forests can, in principle, be obtained from the database of critical loads of acidity and nutrient nitrogen. Data on yields in agro-ecosystems are available from related statistics of the countries. The spatial pattern can be derived using information on land use as well as on soil quality and climate.

To get data on metal contents in harvestable biomass, studies from relatively unpolluted areas should be used. Median values (or averages) of metals contents in plants from such databases do in general not exceed quality criteria for food and fodder crops or phyto-toxic contents, respectively. Related fluxes can therefore be considered as tolerable. When appropriate national data are not available, the default values or ranges in Table 5.23 can be used for orientation, (e.g., the average of a range).

If critical loads related to quality criteria of food or fodder are to be calculated, the critical concentrations in the harvestable plant parts should be multiplied with the yields (net crop removal), with consideration for arable land the coverage by the crops of interest, in order to calculate the tolerable output of metals by biomass harvest.

If contents are available for different harvested parts of the plants (e.g., stem and bark), a mass weighted mean should be used. Beware that only the net uptake is calculated. For instance, for agricultural land, the amount of metals in stalks or the leaves of beets remaining on the field should not be considered. The removal of heavy metals in this case is the product of the yield of grains/beets and the mean contents in these parts of the plants. For forest ecosystems, only the net increment should be considered, but not the uptake into needles, leaves, etc., which also remain in the system.

Table 5.23: Ranges of mean values (averages, medians) of contents of Pb, Cd, and Hg in biomass for various species (harvestable parts).

Land use	Species	Metal content in harvestable plant parts, [M]ha [mg kg-1 dw]		
		Pb	Cd	Hg
Grassland	mixed grassland species	1.0–3.0	0.05–0.25	0.01–0.1
Arable land	wheat (grains) other cereals (grains) potato sugar beet maize	0.1 0.1–0.3 0.73 1.0 3.8	0.08 0.02–0.06 0.23 0.25 0.2	0.01 0.01 0.02 0.02 0.04
Coniferous forest	spruce, pine, fir, douglas, Central Europe Northern Europe	0.5–10 0.1/0.2**	0.1–0.5 0.02/0.04**	0.01–0.05* 0.004/0.008**
Deciduous forest	oak, beech, birch, poplar	0.5–10	0.05–0.5	

*) *Hg* in spruce stems ≈ 10-20% of needle content (Schütze and Nagel 1998)

**) Northern Sweden (Alriksson et al. 2002 and unpublished), for spruce stems without/with bark. Other data sources: De Vries and Bakker (1998), Nagel et al. (2000), Jacobsen et al. (2002)

In ecosystems with appreciable precipitation surplus or with a very limited growth, the removal of metals by harvest may often be very low compared to metal losses by leaching at critical load. In these cases, the uptake calculation does not deserve high efforts. Instead, it is better to concentrate on sophisticated calculations for the critical leaching rate.

5.6.2.1.3 Critical leaching of heavy metals from the soil

The critical leaching flux of a heavy metal from the regarded soil layer can be calculated according to the equation:

(V.95)

$$M_{le(crit)} = c_{le} \cdot Q_{le} \cdot [M]_{tot,sdw(crit)}$$

where:

$M_{le(crit)}$ = critical leaching flux of heavy metal from the topsoil *(g ha^{-1} a^{-1})* (see eq. V.93)

Q_{le} = flux of drainage water leaching from the regarded soil layer defined as above *(m a^{-1})*.
$[M]_{tot.sdw(crit)}$ = critical total concentration of heavy metal in the soil drainage water *(mg m^{-3})* (derived from critical limits, see 5.5.2.2).

c_{le} = *10 g mg^{1} m^{2} ha.*, factor for appropriate conversion of flux units.

5.6.2.1.3.1 Flux of drainage water

In order to calculate critical loads in view of groundwater protection the data on precipitation surplus from the database on critical loads of acidity and nutrient nitrogen can be used. Deviating from this, the proportion of transpiration removing water from the upper horizons *(O, and /or A_h, A_p)* has to be accounted for by using a scaling (root uptake) factor when critical loads with respect to ecotoxicological effects or to food/fodder quality are addressed.

The drainage water flux leaching from the topsoil at the bottom of the topsoil *(Q_{ezb})* at steady state can be calculated according to:

(V.96a)

$$Q_{le,zb} = P - E_i - E_s - f_{Et,zb} \cdot E_t$$

where:

P = precipitation *(m a^{-1})*

E_i = interception evaporation *(m a^{-1})*

E_s = actual soil evaporation within the topsoil defined as above *(m a^{-1})*

E_t = actual plant transpiration *(m a^{-1})*

$f_{Et,zb}$ = scaling or root uptake factor, fraction of water uptake within the topsoil (–)

This approach assumes that soil evaporation *(E_s)* only takes place down to the depth Z_b. Interception evaporation can be calculated as a function of the precipitation (De Vries et al. 1991). For sites without detailed water balance data, the annual mean water percolation Q_{le} can also be determined by the long-term mean annual temperature (mainly determining the potential evapotranspiration, E_{pot}*)* and precipitation (mainly influencing the actual evapotranspiration, E_{act}) according to:

(V.96b)

$$Q_{le,zb} = P_m - f_{E,zb} \cdot (P_m^{-2} + (e^{(0.063 \cdot T_m)} \cdot E_{m,pot})^{-2})^{-1/2}$$

where:

P_m = annual mean precipitation (*m a^{-1}*, data adjusted for common measurement bias)

T_m = annual mean air temperature *(°C)*

$E_{m,pot}$ = annual mean potential

Evapotranspiration in humid areas at T_m = *0°C;* $E_{m,pot} \approx$ *0.35 m a^{-1}* in forests, possibly less in other terrestrial ecosystems.

$f_{E,zb}$ = fraction of total annual mean evapotranspiration above zb (–); $f_{E,zb} \approx 0.8$ for the organic top soil layer of forests.

For forested areas, this relationship is supported by data not only on river runoff but also on soil percolation (e.g., based on Michalzik et al. 2001), which together suggest that about 80% or more of the total evapotranspiration takes place above or within the organic topsoil layer. Thus, the mean water flux from the organic top layer.

(Q) can easily be estimated from annual means of precipitation *(P)* and air temperature *(T)*, which are two traditional climate normals available in traditional climate maps (see background document, De Vries et al, 2005):

In European forest regions, $Q_{le,zb}$ is typically *0.–0.6 m a^{-1}*, but may reach >*2 m a^{-1}* in coastal mountain regions. The standard parameter uncertainty is on the order of *±0.1 m a* (i.e., about ±30%) at the landscape scale. Depending on climate, Q_{le} can account for 10 to 90% of P in temperate-boreal forests but is usually close to half. In very dry regions the percentage of Q_{ie} relative to P can become very low. With eq. V.96b, Q_{le} almost never drops below 0.1 m^{-1} in Europe (considering EMEP-50 km grid square means). For eq. V.96a, a suggested minimum value is 5 % of the precipitation. This seems a reasonable lower value since there are always periods during the year with downward percolation and a situation of no leaching hardly (or

never) occurs on a yearly basis. The use of monthly water balances is not advised as the effect of all seasonal variations is not included in the critical limits, since these represent annual or long-term means, in line with the critical load approach for acidity.

5.6.2.1.3.2 Critical total dissolved or total concentrations of heavy metals in soil drainage water

Information on the derivation of critical total dissolved concentrations of heavy metals in soil drainage water, $[M]_{dis,sdw(crit)}$, either directly, through transfer functions (plant soil solution) or through $[M]_{tree,sdw(crit)}$ is given in the next section (5.5.2.2), with background information on used approaches in the Annexes 2 and 3. The critical total dissolved metal concentrations related to ecotoxicological effects in soils require some specific considerations. These critical total metal concentrations in soil solution are determined as the sum of the critical concentration of the free metal ion M^{2+}, $[M]_{free,sdw(crit)}$, and the metals bound to dissolved inorganic complexes $[M]_{DIC,sdw}$ such as MOH^{*}, HCO_3, MCl^{+}, and to dissolved organic matter, $[M]_{DOM,sdw}$, according to:

(V.97)

$$[M]_{dis,sdw(crit)} = [M]_{free,sdw(crit)} + [M]_{DIC,sdw} + [M]_{DOM,sdw} + [DOM]_{sdw}$$

where:

$[M]_{dis,sdw(crit)}$ = critical total dissolved metal concentration in soil drainage water *(mg m^{-3})*

$[M]_{free,sdw(crit)}$ = critical free metal ion concentration in soil drainage water *(mg m^{-3})*

$[M]_{DIC,sdw}$ = concentration of metal bound to dissolved inorganic complexes in soil drainage water *(mg m^{-3})*

$[M]_{DOM,sdw}$ = concentration of metal bound to dissolved organic matter in soil drainage water *(mg.kg^{-1})*

$[DOM]_{sdw}$ = concentration of dissolved organic matter in soil drainage water *(kg m^{-3})*

Geochemical equilibrium partitioning of the heavy metal between the different fractions is assumed. Furthermore, the water draining from the soil also contains metals bound to suspended particulate matter, $[M]_{SPM,sdw}$, according to:

(V.98)

$$[M]_{tot,sdw(crit)} = [M]_{dis,ss(crit)} + [M]_{SPM,sdw} \cdot [SPM]_{sdw}$$

where:

$[M]_{tot,sdw(crit)}$ = critical total metal concentration in soil drainage water *(mg m^{-3})*

$[SPM]_{sdw}$ = concentration of suspended particulate matter in soil drainagewater *(kg m^{-3})*

In the calculations, we suggest the particulate fraction be neglected to get comparable values of critical concentrations for the different effects pathways (see section 5.5.2.2.3). In this manual, the description of methods is adapted to the use of the critical total dissolved metal concentrations, $[M]_{dis,sdw(crit)}$, beeing equal to total metal concentrations in soil solution, implicitly assuming that the concentration of metals bound to suspended particulate matter is negligible *($[SPM]_{sdw} = 0$)*, (i.e., $[M]_{dis,sdw(crit)}$ equals $[M]_{tot,sdw(crit)}$).

5.6.2.2 Critical dissolved metal concentrations derived from critical limits in terrestrial ecosystems

Critical total concentrations of the heavy metals *Cd*, *Pb,* and *Hg* in the soil solution, $[M]_{dis,sdw(crit)}$, depend on the target to be protected. These values have to be derived from critical limits (see Table 5.15):

- Critical metal contents in plants *(Cd, Pb, Hg)* in view of human health or animal health effects through intake of plant products.
- Critical metal concentrations in ground water *(Cd, Pb, Hg)* in view of human health effects through intake of drinking water.
- Critical concentrations of free metal ions in soil solution *(Cd, Pb)* in view of ecotoxicological effects on soil microorganisms, plants, and invertebrates.
- Critical metal contents in the soil *(Hg)* in view of ecotoxicological effects on soil micro-organisms and invertebrates in the forest humus layer.

The critical total dissolved concentration of a heavy metal in the soil drainage water *($[M]_{dis,sdw(crit)}$)* includes both the free metal ions and the metals bound to dissolved inorganic and organic complexes (eq. V.97).

The derivation of the critical total dissolved concentrations to be applied in eq. V.95 is explained below.

5.6.2.2.1 Critical dissolved concentrations of Cd, Pb, and Hg in view of critical plant metal contents

Starting from the idea to derive critical total *Cd, Pb,* and *Hg* concentrations in soil solution related to human health effects on the basis of critical limits for plant metal contents (food quality criteria) for food crops on arable land De Vries et al. (2003) provided an overview on selected soil-plant relationships of *Cd, Pb,* and *Hg*. It shows that only for *Cd* significant relationships *($R^2$of^3 0.5)* are available.

5.6.2.2.1.1 Cadmium

Starting with a critical *Cd* content in plant one may derive a critical dissolved metal concentration by a plant – soil solution relationship. Such a relationship was derived in the Netherlands by applying a regression of *Cd* contents in wheat to calculated soil solution concentrations that were derived by using measured total soil contents and soil properties and application of a transfer function, relating total concentrations in solution to the soil metal content (Romkens et al. 2004). By applying such a function, regression relationships were derived for *Cd* in plant (wheat grains) as a function of *Cd* in soil solution and vice versa as described in Table 5.24. The best estimate of a critical *Cd* concentration might be the mean of both estimates.

The EU regulation (EG) No.466/2001 uses a limit for *Cd* of *0.2 mg kg^{-1}* fresh weight in wheat grains. This limit was derived with the principle "**A**s **L**ow **A**s **R**easonably **A**chievable" (ALARA) and is therefore not based on effects. However, there are many indications that the critical limit of *0.1 mg kg^{-1}* fresh weight, which was used in the EU before 2001, is more appropriate for the protection of the human health (for these arguments see De Vries et al. 2003, 2005, 2007a).

Table 5.24 provides the parameters for the transfer functions as well as results based on the critical limit of *0.1 mg kg^{-1}* fresh weight (results for the EU limit of *0.2 mg kg^{-1}* fresh weight is given in brackets). If the mean of both results of transfer function application is used, the resulting critical total concentration is approximately *0.8 mg m^{-3}* (or *4 mg m^{-3}*). The most conservative estimate equals approximately *0.6 mg m^{-3}* (or *1.75 mg m^{-3}*).

A more sophisticated and consistent way would be to:

- first derive a critical "pseudo" total soil metal content, by applying soil – plant relationships in the inverse way (derive a critical total soil content from a critical plant content);

- then apply a transfer function relating "pseudo" total metal contents to reactive metal contents (Annex 2, eq. A2.3);
- followed by a transfer function relating the free ion metal activity in solution to the reactive metal content (Annex 2, eq. A2.4 or eq. A2.5);
- followed by a calculation of total concentrations from free metal ion activities with a chemical speciation model (i.e., the W6S-MTC2 model, section 5.5.2.2.3).

Please note that the current version of W6S-MTC2 is designed to calculate $M_{(sdw)crit}$ based only on the critical limits relating to ecotoxicological effects and not to food quality.

Table 5.24: Values for the intercept (int) and the parameter a in the regression relationships relating Cd in plant (wheat grains) as a function of Cd in soil solution and vice versa. The table also gives the percentage variation explained (R^2), the standard error of the result (se) and the resulting critical total dissolved Cd concentration when applying a critical Cd content in wheat of 0.1 mg kg^{-1} fresh weight (0.12 mg kg^{-1} dry weight) and in brackets the value when applying the limit of 0.2 mg kg^{-1}fresh weight (EG No 466/2001).

Relationship	Intercept	a	R^2	Se	$log[Cd]_{dis,sdw(crit)}$ [$mmol.l^{-1}$]	$[Cd]_{dis,sdw(crit)}$ [$mg.m^{-3}$]
Cd_{plant} – $Cd_{solution}$[1]	1.05	0.39	0.62	0.25	-5.03 (-4.26)	1.05 (6.16)
$Cd_{solution}$ – Cd_{plant}[2]	-3.82	1.57	0.62	0.50	-5.28 (-4.81)	0.59 (1.75)

[1] log(Cd plant) = Int + a*log(Cd soil solution)

[2] log(Cd soil solution) = Int + a*log(Cd plant)

5.6.2.2.1.2 Lead and mercury

For *Pb* and *Hg* in food crops, backcalculation to soil content is not possible, because there are no relationships between content of soil and contents in plants for those metals. For *Pb* and *Hg*, direct uptake from the atmosphere by plants has to be considered. Methods for such calculations, based on data from De Temmerman and de Witte (2003a,b) are provided in Annex 5 of the background document (De Vries et al. 2005).

Critical concentrations given here are those in use in 2004. Since then, the EU regulation No 466/2001 has been updated by the EU regulation No. 1881/2006. The relevance of using the new regulatory values is to be assessed within the WGE prior to a potential update of the values recommended here.

5.6.2.2.2 Critical dissolved concentrations of Cd, Pb and Hg aiming at ground water protection

The critical total *Cd*, *Pb,* and *Hg* concentration in soil solution related to human health effects can also be based on quality criteria (critical limits) for drinking water (WHO 2004) for all terrestrial ecosystems (see Table 5.21). In line with the decisions of the Expert Meeting on Critical Limits that was held in 2002 in Berlin, the protection of ground water for potential use as drinking water resource should also be addressed in critical load calculations. The Technical Guidance Document for Risk Assessment (http://ecb.jrc.it) suggests in chapter 3.1.3 that in the first instance the concentration in soil pore water can be used as an estimate of the concentration in ground water. The WHO guideline includes the following quality criteria for *Cd*, *Pb,* and *Hg* in view of drinking water quality:

Pb: 10 mg m^{-3}

Cd: 3 mg m^{-3}

Hg: 1 mg m^{-3} (for total mercury)

These values can directly be included as $[M]_{dis,sdw(crit)}$ in the critical load calculation.

2011 WHO recommendations for drinking waters are 6 mg m-3 for inorganic mercury (WHO 2011). As for updated EU regulations, these values may be included in the CLd methodology once discussed within the ICP M&M.

5.6.2.2.3 Critical dissolved concentrations of Cd and Pb related to ecotoxicological effects

Critical limits related to the ecotoxicological effects of *Cd* and *Pb* are related to impacts on soil micro-organisms, plants, and invertebrates for both agricultural land (arable land, grassland) and non-agricultural land (forests, natural non-forested ecosystems; see Table 5.21. The critical concentrations used in this manual are based on the following approach:

- use of ecotoxicological data (NOEC and LOEC data) for the soil metal content using experiments with information on soil properties (clay and organic matter content and soil *pH*) as well;
- calculation of critical free metal ion concentrations (critical limits) in soil solution on the basis of the ecotoxicological soil data (NOECs and LOECs) and soil properties, using transfer functions relating the reactive soil metal content to the free metal ion concentration;
- calculation of the critical total dissolved metal concentrations $[M]_{dis,sdw(crit)}$ from critical limits for free metal ion concentrations using a chemical speciation model.

5.6.2.2.3.1 Calculation of critical free metal ion concentrations from critical soil reactive metal contents

Soil toxicity data collated and accepted under the terms of current EU Risk Assessment procedures were used (Draft Risk Assessment Report *Cd* (July 2003) see http://ecb.jrc.it, Voluntary Risk Assessment for *Pb*),. The data covered chronic population-level effects on soil plants, soil-dwelling invertebrates, and microbial processes. The toxicity endpoints were quoted mainly in terms of an added metal dose. In using added doses, the assumption is made that the added metal is entirely in reactive forms over the course of the toxicity experiment.

The transfer functions for the calculation of free metal ion concentration from reactive soil metal content, used in the derivation of free ion critical limit functions, are given in Annex 2. Soil properties needed in this function are organic matter and soil solution *pH*. In the derivation, soil *pH* values measured by chemical extraction (by H_2O, KCl, or $CaCl_2$) were used to estimate soil solution *pH* by application of regressions given in Annex 10 of the background document (De Vries et al. 2005), assuming that the *pH* in soil solution equals pH_{sdw}. EU Risk Assessment procedures do not require the organic matter content of the soil to be specified for data to be accepted. However, such data were not usable for the calculation of critical free metal ion concentrations from critical soil metal contents since the transfer functions utilised require these data (see Annex 2) and were thus removed from the databases.

The bioavailability of metals does not only depend on the free metal ion concentration but also on the concentration of other cations, particularly H^+. This was considered when deriving critical limits as a function of the *pH* in soil drainage water (pH_{sdw}). The derived critical limit functions were:

(V.99)

$$\log[Cd]_{free,sdw(crit)} = -0.32 \cdot pH_{sdw} - 6.34$$

(V.100)

$$\log[Pb]_{free,sdw(crit)} = -0.91 \cdot pH_{sdw} - 3.80$$

More information on the approach and the toxicity data is given in Lofts et al. (2004) and in De Vries et al. (2004). A summary can be found in the background document (De Vries et al. 2005).

5.6.2.2.3.2 Calculation of total dissolved metal concentrations from free metal ion concentrations

To calculate critical loads for soils from the critical limit functions, it is necessary to know the total concentration of metal in soil drainage water that corresponds to the free ion critical limit. In Annex 3, an overview is given of the calculation procedure using the WHAM model. Results thus obtained with this model for an assumed standard CO_2 pressure of 15 times the atmospheric pressure of 0.3 mbar (4.5 mbar) are given in Tables 5.19 and 5.20. WHAM also includes the fraction of suspended particulate matter, which strictly is not part of the soil solution. The total concentration is therefore related to soil drainage water. When $[SPM]_{sdw} = 0$, the value of $[M]_{tot,sdw(crit)}$ equals that of $[M]_{dis,sdw(crit)}$ (see eq. V.98). For reasons of consistency with the other approaches (see eq V.97), in which the critical value refers to $M]_{dis,sdw(crit)}$, it is advised to apply the results with $[SPM]_{sdw} = 0$. Furthermore, there are high uncertainties in the data on *SPM* in soil solution. Table 5.25 shows that, in most cases, the impact of suspended particulate matter on the total *Cd* concentration in soil drainage water (even at a concentration of $50\ mg\ l^{-1}$) is small, but for *Pb* it can be large (cf. Table 5.26).

5.6.2.2.3.3 Use of pH and DOC values to be considered in the calculation of critical metal concentrations

Some parameters in the critical load calculation depend on the status of the soil, in particular the acidification status *(pH)* and the concentration of *DOC* (see also the tables 5.19 and 5.20). In the following subsections, recommendations are provided, which status of soil conditions should be considered, when $M_{dis,sdw(crit)}$ is derived from critical limits for free metal ion concentrations, as presented in the tables 5.25 and 5.26.

Table 5.25: Look-up table to derive values of the total critical Cd concentrations in soil drainage water $[Cd]_{tot,sdw(crit)}$ at a CO_2 pressure that equals 15 times the CO_2 pressure of the air.

			$[Cd]_{tot,sdw(crit)}$ ($mg.m^{-3}$), being $[Cd]_{dis,sdw(crit)}$ ($mg.m^{-3}$) at SPM=0									
OM	SPM	DOC	pH	pH	pH	pH	pH	pH	pH	pH	pH	pH
%dw	$mg.l^{-1}$	$mg.l^{-1}$	3.5	4.0	4.5	5.0	5.5	6.0	6.5	7.0	7.5	8.0
10	0	0	4.04	2.79	1.92	1.34	0.94	0.68	0.51	0.43	0.47	0.75
10	0	5	4.04	2.80	1.93	1.38	1.04	1.08	0.91	0.66	0.61	0.80
10	0	15	4.04	2.81	1.97	1.47	1.23	1.83	1.68	1.13	0.88	0.91
10	0	50	4.05	2.86	2.12	1.80	1.89	4.08	4.03	2.74	1.85	1.30
10	0	100	4.07	2.94	2.36	2.29	2.80	6.76	6.86	4.94	3.22	1.85
10	50	0	4.06	2.82	1.95	1.38	1.00	0.76	0.61	0.57	0.67	1.02

			$[Cd]_{tot,sdw(crit)}$ ($mg.m^{-3}$), being $[Cd]_{dis,sdw(crit)}$ ($mg.m^{-3}$) at SPM=0									
10	50	5	4.06	2.82	1.96	1.42	1.10	1.16	1.02	0.81	0.80	1.07
10	50	15	4.06	2.84	2.00	1.51	1.29	1.91	1.79	1.28	1.08	1.18
10	50	50	4.07	2.89	2.15	1.85	1.94	4.15	4.14	2.88	2.05	1.57
10	50	100	4.08	2.96	2.39	2.33	2.85	6.84	6.97	5.08	3.42	2.12
50	0	0	3.98	2.74	1.91	1.34	0.94	0.68	0.51	0.43	0.47	0.75
50	0	5	4.02	2.81	2.02	1.52	1.26	1.09	0.91	0.66	0.61	0.80
50	0	15	4.11	2.94	2.24	1.89	1.85	1.86	1.68	1.13	0.88	0.91
50	0	50	4.45	3.48	3.01	3.06	3.69	4.16	4.03	2.74	1.85	1.30
50	0	100	5.06	4.29	4.07	4.59	5.96	6.89	6.86	4.94	3.22	1.85
50	50	0	4.03	2.81	2.00	1.45	1.11	0.90	0.81	0.84	1.03	1.51
50	50	5	4.07	2.87	2.10	1.64	1.42	1.31	1.21	1.08	1.17	1.57
50	50	15	4.16	3.00	2.32	2.01	2.01	2.08	1.98	1.54	1.44	1.68
50	50	50	4.50	3.54	3.09	3.18	3.85	4.38	4.33	3.15	2.41	2.06
50	50	100	5.11	4.35	4.16	4.71	6.12	7.11	7.16	5.35	3.78	2.61

Table 5.26: Look-up table to derive values of the total critical Pb concentrations in soil drainage water $[Pb]_{tot,sdw(crit)}$ at a CO_2pressure that equals 15 times the CO_2pressure of the air.

			$[Pb]_{tot,sdw(crit)}$ ($mg.m^{-3}$), being $[Pb]_{dis,sdw(crit)}$ ($mg.m^{-3}$) at SPM=0									
OM	SPM	DOC	pH	pH	pH	pH	pH	pH	pH	pH	pH	pH
%dw	$mg.l^{-1}$	$mg.l^{-1}$	3.5	4.0	4.5	5.0	5.5	6.0	6.5	7.0	7.5	8.0
10	0	0	34.72	11.41	3.83	1.32	0.46	0.17	0.08	0.09	0.23	0.72
10	0	5	34.80	11.55	4.02	1.57	0.77	0.86	1.12	1.29	1.36	1.64
10	0	15	34.96	11.83	4.42	2.09	1.38	2.18	3.16	3.67	3.61	3.47
10	0	50	35.52	12.82	5.83	3.92	3.42	6.25	10.04	11.87	11.47	9.89
10	0	100	36.33	14.25	7.92	6.51	6.21	11.39	19.36	23.30	22.68	19.07
10	50	0	37.33	14.50	7.43	5.53	5.41	5.98	6.88	8.08	9.60	11.71
10	50	5	37.41	14.64	7.62	5.79	5.72	6.66	7.92	9.27	10.73	12.63
10	50	15	37.57	14.92	8.02	6.31	6.33	7.98	9.97	11.66	12.98	14.46
10	50	50	38.13	15.91	9.43	8.14	8.37	12.05	16.84	19.86	20.84	20.89

			$[Pb]_{tot,sdw(crit)}$ ($mg.m^{-3}$), being $[Pb]_{dis,sdw(crit)}$ ($mg.m^{-3}$) at SPM=0									
10	50	100	38.94	17.34	11.52	10.74	11.16	17.19	26.17	31.29	32.05	30.06
50	0	0	32.85	11.08	3.80	1.31	0.46	0.17	0.08	0.09	0.23	0.72
50	0	5	34.36	12.59	5.32	2.74	1.63	0.89	1.12	1.29	1.36	1.64
50	0	15	37.41	15.65	8.37	5.51	3.80	2.25	3.16	3.67	3.61	3.47
50	0	50	48.44	26.65	18.69	14.44	10.52	6.45	10.04	11.87	11.47	9.89
50	0	100	65.13	42.22	32.86	26.13	18.94	11.76	19.36	23.30	22.68	19.07
50	50	0	39.22	18.51	12.51	11.53	12.45	14.27	16.57	19.45	22.94	27.36
50	50	5	40.73	20.03	14.03	12.96	13.63	14.95	17.61	20.64	24.06	28.27
50	50	15	43.78	23.08	17.07	15.74	15.78	16.30	19.66	23.03	26.31	30.11
50	50	50	54.80	34.07	27.42	24.65	22.51	20.51	26.54	31.24	34.18	36.53
50	50	100	71.49	49.66	41.61	36.34	30.92	25.82	35.86	42.66	45.38	45.70

5.5.2.2.3.3.1 pH values

If possible, it is recommended to use the pH at steady-state, assuming the implementation of the most recent regulations (such as the revised Gothenburg protocol). It may be necessary to run dynamic models to obtain this steady-state pH value.

Alternatively, and pragmatically, the present soil solution pH may be used. It is then assumed that present pH is (almost) equal to future pH under most recent regulations. If the present pH in soil solution is not available, soil solution pH may be derived from pH in water or pH in salt extracts through regression functions. Linear relation coefficients are given in Table 5.20 assuming no effect of soil type on the relationship. These relations can be used to calculate the soil solution pH which is needed in the critical load calculations and also in the transfer functions relating reactive metal contents to free metal ion concentrations.

A last approach is to use the pH at the critical acid load, however, it is not recommended. This pH is easier to calculate but may strongly deviate from pH at steady-state. Furthermore, the calculation of the critical load pH is rather uncertain as it depends on arbitrary choices. These relations can be used to calculate the soil solution pH which is needed in the critical load calculations and also in the transfer functions relating reactive metal contents to free metal ion concentrations.

More detailed information is given in Annex 10 in the background document (De Vries et al. 2005). This includes relationships as a function of soil type. Ranges in the present and steady-state critical soil pH for various combinations of land use, soil type and soil depth are also provided there.

Table 5.27: Results of linear regression analyses of the pH in soil solution against pH-H_2O, pH-$CaCl_2$ and pH-KCl. (pHsoil solution = α pH-X + β, with X = H2O, CaCl2 or KCl).

Explaining variable	N[1)]	Slope (α)[2)]	Intercept (β)[2)]	se $_{Yest}$[3)]	R^2adj[4)]
pH-H_20	1145	1.0462	-0.2847	0.453	0.84
pH-KCl	905	0.9692	0.6233	0.491	0.80
pH-$CaCl_2$	413	0.8834	1.317	0.741	0.49

1) Number of samples

2) All coefficients are significant at p > 0,999

3) se $_{Yest}$: Standard error of estimated Y

4) R^2adj: Adjusted R^2

5.5.2.2.3.3.2 DOC concentrations

The concentration of dissolved organic matter *(DOM)* in soils is nowadays frequently determined in climaterelated studies. Concentrations of *DOM* are usually determined by analysis of carbon *(DOC)* which accounts for half of the weight of soil organic matter *(DOM = 2 x DOC)*. However, long-term data on soil solutions are rarely available at sufficient density for mapping region-specific means and variability's; they may need to be estimated from studies elsewhere. Ranges in *DOC* values for major forest types and soil layers, by means of the 5-, 50-and 95 percentiles, are presented in Annex 11 of the background document (De Vries et al. 2005) on the basis of *DOC* values from approximately 120 Intensive Monitoring plots in Europe. In general, the results show a clear decrease in *DOC* concentrations going from the humus layer (median value of 40 *mg* l^{-1}) into the mineral subsoil. Furthermore, the values are slightly higher in coniferous forests compared to deciduous forests.

Relationships of *DOC* concentrations with vegetation type, hydrology, growth conditions, or soil properties may be expected, which would be useful to improve estimates for different sites and regions. The data for the mineral soil (De Vries et al. 2005) were thus used to derive relationships with available site characteristics and soil data that may affect the *DOC* concentrations, including the type of forest, (coniferous or deciduous forests), texture class (indication for soil type), temperature, *pH* and the contents of *C* and *N*, including the *C/N* ratio. Results thus obtained are given in the background document (De Vries et al, 2005). The results show a good relationship with the site and soil characteristics in the subsoil (below 30cm) but the relationships were much worse in the topsoil (above 30cm). In the topsoil there was a clear positive relationship with *C/N* ratio and temperature, while the correlated values of the individual *C* and *N* concentrations were negatively and positively related to *DOC*, respectively. The relationships are, however, too weak to be very useful. This is in line with the limited number of studies in the literature, from which no significant relationship could be discerned (Michalzik et al. 2001).

Based on the available data the following default values for calculating critical loads of *Pb* and *Cd*, or critical levels of atmospheric *Hg* pollution, respectively, are suggested (see background document, Annex 11):

Forest organic layer (O horizon):

$[DOC]_{sdw}$ = 35 mg l^{-1} ($[DOM]_{sdw}$ = 70 mg l^{-1}).

Forest mineral topsoil (0-10 cm):

$[DOC]_{sdw}$ = 20 mg l^{-1} ($[DOM]_{sdw}$ = 40 mg l^{-1}).

Grass land (0-10 cm):

$[DOC]_{sdw}$ = 15 mg l^{-1} ($[DOM]_{sdw}$ = 30 mg l^{-1}).

Arable land (0-30 cm):

$[DOC]_{sdw}$ = 10 mg l^{-1} ($[DOM]_{sdw}$ = 20 mg l^{-1})

5.6.2.2.4 Critical dissolved concentrations of hg related to ecotoxicological effects in soils

5.6.2.2.4.1 Critical limit for the soil

With respect to *Hg*, critical limits refer only to effects on soil micro-organisms and invertebrates in the humus layer of forests. The suggested critical limit for *Hg* is that the concentration in the humus layer (O-horizon) of forest soils after normalization with respect to the organic matter content should not exceed *0.5 mg kg (org)*$^{-1}$ (Meili et al. 2003a). Because of the strong association of *Hg* with organic matter leaving virtually no free ions, the exposure of biota to *Hg* is controlled by the competition between biotic and other organic ligands, and the contamination of all types of organic matter is determined by the supply of organic matter relative to the supply of *Hg* at a given site (Meili 1991a, 1997, cf. biodilution). Therefore, the critical limit for *Hg* in soils is set for the organically bound *Hg* rather than for the free ion concentration, also in solution.

Critical total mercury concentrations in soil solution can be calculated by using a transfer function for *Hg* from soil-to-soil solution, while assuming a similar critical *Hg/org* ratio in the solid phase and in the liquid phase, at least in oxic environments where binding to sulphides is negligible. Various reasons supporting this are given in Meili (1991a, 1997, 2003b), De Vries et al. (2003), and Åkerblom et al. (2004).

5.6.2.2.4.2 Transfer function for mercury

The critical leaching of *Hg* from the humus layer ($M_{le(crit)}$ in eq. V.93) is related to the mobility and *Hg* content of dissolved organic matter because of the strong affinity of *Hg* for living and dead organic matter and the resulting lack of competition by inorganic ligands in this layer (e.g., Meili 1991, 1997). Because of the strong association of *Hg* with organic matter leaving virtually no free ions (apparently far less than one per km^2 of topsoil, based on Skyllberg et al. 2003), the biogeochemical turnover of *Hg* is controlled by the competition between biotic and other organic ligands. Therefore, *Hg/OM* ratios are a useful tool for calculating critical limits, loads, and associated transfer functions (Meili et al. 2003a). This is the basis of the transfer function to derive total *Hg* concentrations in percolating (top)soil water ($[M]_{dis,sdw(crit)}$ in eq. V.95, *mg m*$^{-3}$) as follows:

(V.101)

$$[Hg]_{dis,sdw(crit)} [Hg]_{OM(crit)} \cdot f_f \cdot [DOM]_{sdw} \cdot c_{sdw}$$

where:

$[Hg]_{dis,sdw(crit)}$ = critical total *Hg* concentration in soil drainage water *(mg m*$^{-3}$*)*

$[Hg]_{OM(crit)}$ = critical limit for *Hg* concentration in solid organic matter *(OM)*, or the *Hg/OM* ratio in organic *(top)soils ($[Hg]_{OM(crit)}$=0.5 mg (kg OM)*$^{-1}$*)*

f_f = fractionation ratio, describing the *Hg* contamination of organic matter in solution *(DOM)* relative to that in solids *(OM) (–)*,

$[DOM]_{sdw}$ = concentration of dissolved organic matter in soil drainage water *(g m*$^{-3}$*)*

C_{sdw} = *10*$^{-3}$ *kg g*$^{-1}$, factor for appropriate conversion of mass units

The scale-invariant fractionation or transfer factor f_f describes the *Hg* partitioning between organic matter in solids and organic matter in solution and is defined as the ratio between the *Hg* content of *DOM* and that of *OM* (Meili et al. 2003a, Meili et al. 2003b). Preliminary studies in Sweden suggest that the *Hg* concentration in *DOM* is of similar magnitude as that in *OM*, and that 1 may be used as a default value for f_f until deviations from unity prove to be significant (Åkerblom et al. 2004).

5.6.2.2.4.3 Critical concentration for the soil drainage water:

Based on the *Hg* limit of *0.5 mg kg*$^{-1}$ *OM* and a *DOM* concentration of *70 mg l*$^{-1}$ *(DOC = 35 mg l*$^{-1}$*)*, the critical steady state concentration of total *Hg* in soil drainage water is *35 ng l*$^{-1}$ or *0.035 ug l*$^{-1}$ (see eq. V.101). This concentration is consistent with that derived by a different approach at the watershed scale (Meili et al. 2003a) and is similar to high-end values presently observed in soil solutions and surface freshwaters (Meili, 1997; Meili et al. 2003b; Åkerblom et al. 2004). Note that this ecosystem limit for soil water is much lower than the drinking water limit above, but still higher than that for surface freshwaters where *Hg* limits for fish consumption usually are exceeded at surface water concentrations of *1-5 ng l*$^{-1}$.

5.6.3 Aquatic ecosystems

5.6.3.1 Critical loads of cadmium and lead

5.6.3.1.1 Simple steady-state mass balance model and related input data

In principle, the simple steady-state mass balance approach can be used for *Cd*, *Pb* and *Hg* but it has been decided to restrict the approach in first instance to *Cd* and *Pb* and use a different, precipitation-based approach for *Hg*, as described in section 5.5.3.2.

5.6.3.1.1.1 Steady-state mass balance model in stream waters

As with terrestrial ecosystems, the critical load of *Cd* and *Pb* for freshwaters is the acceptable total load of anthropogenic heavy metal inputs corresponding to the sum of tolerable outputs from the catchment by harvest and outflow, minus the natural inputs by weathering release in the catchment but adding the retention in the surface water (De Vries et al. 1998). There is no need to consider net release in catchment soils if the net weathering (weathering minus occlusion) is negligible. Since the estimation of net release in soils includes high uncertainties, it is preliminarily assumed to be negligible.

In the initial manual on the calculation of critical loads of heavy metals for aquatic ecosystems (De Vries et al. 1998), the default method presented to calculate critical loads of heavy metals for soils included in-lake metal retention, including all relevant metal fluxes, namely sedimentation, resuspension, and exchange processes in the lake (infiltration, diffusion and bioirrigation), while assuming a steady state situation (DeVries et al. 1998). To keep the approach as simple as possible, and also to stay as close as possible to the simple mass balance approach for nitrogen and acidity, this model can be simplified by neglecting weathering in the catchment and lumping transient exchange processes at the sediment-water interface and the net effect of sedimentation and resuspension in one retention term according to De Vries et al. (1998):

(V.102)

$$CL(M) = M_u + M_{ret(crit)} \cdot A_l / A_c + M_{lo(crit)}$$

where:

M_u = removal of heavy metal by biomass harvesting or net uptake in the catchment (g ha^{-1}a^{-1})

$M_{ret(crit)}$ = net retention of heavy metal in the lake at critical load (g ha^{-1}a^{-1})

$M_{lo(crit)}$ = critical lateral outflow of heavy metal from the whole catchment (g $ha^{-1}a^{-1}$)

A_l = lake area (ha)

A_c = catchment area (ha)

When critical loads of *Cd* and *Pb* for stream waters are calculated, there is no need to consider net retention, leading to the following critical load calculation:

(V.103)

$$CL(M) = M_u + M_{lo(crit)}$$

Because the estimation of net retention for lakes includes high uncertainties, it is recommended one calculate preliminarily aquatic critical loads for stream waters only, for which the retention in surface water is negligible. It furthermore leads to the lowest critical loads and thus implies the protection of lakes as well. Finally, when calculating critical loads for lakes, one may also assume that net retention of metals in lakes is negligible, implying the assumption that the overall release or retention of metals in a catchment, including the lake sediment, is negligible.

5.6.3.1.1.2 Heavy metal removal by net uptake

The assessment of these data is comparable for those in terrestrial ecosystems (see eq. V.94), but now the uptake or release refers to the complete catchment. This implies that no further reduction factors need to be applied to relate the uptake in the root zone/catchment to the mineral topsoil. The equation for net uptake is thus equal to eq. V.94 with f_{Mu} being equal to 1.

5.6.3.1.1.3 Critical output of heavy metals from the aquatic system

The critical lateral outflow can be described as the product of the lateral outflow flux of water and the critical limit for the total concentration of the heavy metal in the surface water according to:

(V.104)

$$M_{lo(crit)} = 10 \cdot Q_{lo} \cdot [M]_{tot,sw(crit)}$$

where:

Q_{lo} = lateral outflow flux of water from the whole catchment area *(m a^{-1})*

$[M]_{tot,sw(crit)}$ = critical limit for the total concentration (dissolved and in suspended particles) of heavy metal in surface water *(mg m^{-3})*

Q_{lo}, which sometimes is denoted as the hydraulic load in the literature can be derived for a lake on the basis of the flow from the aquatic system, *Q ($m^{-3}a^{-1}$)* divided by the catchment area *(m^2)*. The total concentration of metals can be calculated as:

(V.105)

$$[M]_{totsw(crit)} = [M]_{dis,sw(crit)} + [M]_{SPM,sw(crit)} \cdot [SPM]_{sw}$$

where:

$[M]_{dis,sw(crit)}$ = critical dissolved concentration of a heavy metal in surface water *(mg m^{-3})*

$[M]_{SPM,sw(crit)}$ = critical total content of a heavy metal in suspended particles *(mg kg^{-1})*

$[SPM]_{sw}$ = concentration of suspended particulate matter in surface water *(kg m^{-3})*

Data on the lateral outflow of lakes can be derived from the *S&N* critical loads database. The critical load depends on the critical limit used. In the initial manual for aquatic ecosystems (De Vries et al. 1998), it was argued that critical limits referring to the free metal ion activity in

surface water are most appropriate. This idea has been further developed by Lofts et al. (unpublished data), but has not been adopted here, for reasons which will be given in 5.5.3.1.2. Instead, critical limits referring to total dissolved metal concentrations have been adopted. It is necessary to include a solid-solution transfer function (see Annex 2) to calculate the critical metal concentration in suspended particles and hence the critical total aqueous metal concentration.

Information on how to estimate the critical net in-lake retention when calculating critical metal loads for lakes is given in the background document to this manual (De Vries et al. 2005). Like for terrestrial ecosystems, it is recommendable to calculate weathering rates (here at least for a depth of 1 m) to account for the influence of natural processes in comparison to atmospheric deposition in order to evaluate critical loads and critical limits exceedances. Information on how to calculate weathering within the catchment is given in Annex 6 of the background document (De Vries et al. 2005).

5.6.3.1.2 Critical total dissolved cadmium and lead concentrations in aquatic ecosystems

5.6.3.1.2.1 Critical limits for total dissolved concentrations

Analysis of aquatic ecotoxicological data by Lofts et al. (unpublished) suggested overlap between aquatic and terrestrial toxic endpoint concentrations at a given *pH*. Hence it was suggested that common critical limits be applied for both soils and freshwaters, by using the critical limit functions derived in 5.5.2.2 for toxic effects on the soil ecosystem. However, although there is no theoretical reason why the sensitivities of soil and water organisms to metals should not be similar (assuming that uptake of the free ion from the aqueous phase is the significant mechanism leading to toxicity) this approach has not been adopted for the following reasons:

- The aquatic toxicity data for *Cd* covered a more restricted *pH* range than for the terrestrial toxicity data (*pH* 6.9 to 8.7 compared to *pH* 3.2 to 7.9). Therefore, although overlap of points was seen within the *pH* range covered by the aquatic toxicity data, no data were available to validate the theory of overlap below *pH* 6.9.
- Observed overlapping of points for *Pb* was less than for any of the metals studied (*Cu* and *Zn* in addition to *Cd* and *Pb*). Most of the aquatic toxicity data gave free *Pb* endpoints higher than those observed for soils.

For these reasons, it was decided not to use the free ion approach for aquatic critical limits and instead to express the critical limits as the total dissolved metal *(mg m^{-3})*.

A summary of preliminary effect-based critical limits is given in Table 5.24. The values for *Cd* are based on the EU Risk Assessment Report for *Cd* (Risk assessment Cadmium metal CAS-No. 7440-43-9). The values for *Pb* are based on Crommentuijn et al. (1997) for the value suggested for use in the 2004 call for data, and on a substance data sheet on *Pb* and its compounds (2003) for the value to be used with the 2005 update of Annex 3. There are also critical limits related to secondary poisoning, but these values are not yet recommended for use because they require further substantiation and discussion.

The value of *0.38 mg m^{-3}*, taken from EU Risk Assessment Report for *Cd*, is based on the 5-percentile cut-off value of chronic toxicity data from 168 reliable tests on single species and 9 multi-species studies. An assessment factor of 2 is further introduced in the report, leading to a critical limit of *0.19 mg m^{-3}*, but this approach was not accepted in this manual. For *Cd*, a relationship with water hardness has also been found in the EU Risk Assessment Report. Since 2004, it has been also accepted to take the influence of hardness on the toxicity of cadmium into account, using 3 hardness classes (with hardness *H* in *mg $CaCO_3$ l^{-1}*) according to *0.16 mg m^{-3}* if *H*

<100, 0.30 mg m^{-3} if *100<H <200* and *0.50 mg m^{-3}* if *H >200*, using no assessment factor (see also the background document to the manual, De Vries et al, 2005).

For *Pb*, the critical limit of *11 mg m^{-3}* is based on Crommentuijn et al. (1997), whereas the value of *5 mg m^{-3}* (range of *2.1–9.3 mg m^{-3})* is based on the 5-percentile cut-off value of chronic toxicity data, calculated with the method of Aldenberg & Jaworska, using 3 data sets of selected (i) freshwater and saltwater NOECs/EC10s (30 values). (ii) freshwater NOECs/EC10s (19 values) and (iii) saltwater NOECs/EC10s (11 values). In the substance data sheet on *Pb*, an assessment factor of 3 is further introduced, but this approach was not accepted in this manual. At a workshop of ICP Waters on heavy metals, 2002, in Lillehammer (Skjelkvale and Ulstein, 2002) a range of *1–11 mg m^{-3} was* suggested in dependence on water chemistry, with low values referring to clear softwaters.

Table 5.28: Recommended critical limits for dissolved Cd and Pb concentrations surface waters.

Metal	Critical dissolved concentration (mg m^{-3})	
	Value used before 2005	Value used since the 2005 update of Annex 3
Cd	0.38 [1]	0.16 if H < 100 [2] 0.30 if 100 < H < 200 and 0.50 if H > 200
Pb	11	5

[1] A comparable critical limit is suggested in the RAR on Cd for the protection of top predators, namely 0.26 mg m-3. This value is based on a critical limit for the intake of Cd of 160 µg Cd /kg food (wet weight) of the predator, being the quality standard for biota tissue with respect to secondary poisoning. However, this value is yet considered too uncertain to be used in the critical load calculations.

[2] H = hardness in mg $CaCO_3$ l^{-1}

Regulation update:

The recommended values for use in this manual are the ones that were agreed upon when the 2004 version of the manual was prepared. Since then, new EU legislations (Directive 2013/39/UE) have been published. They are mentioned here for information. The values in the table below are not compatible with data used in the Annex 3 of this section.

Metal	Critical dissolved concentration (mg m^{-3})	
	mg.m^{-3}	Water hardness
Cd	≤0.08 0.08 0.09 0.15 0.25	[$CaCO_3$] < 40 mg/l 40 < [$CaCO_3$] < 50 mg/l 50 < [$CaCO_3$] < 100 mg/l 100 < [$CaCO_3$] <200 mg/l 200 mg/l < [$CaCO_3$]
Pb	1.3[2]	5
Hg	0.07[3]	

[1] Annual Averages of Environmental Quality Standards for inland surface waters as in Directive 2013/39/EU 2013.

[2] This Environmental Quality Standard applies to lead bioavailable fraction.

[3] Maximum allowable concentrations for inland waters.

The critical limit of *5 mg* m^{-3} is in the middle of this range and thus consistent. A much lower critical limit is suggested in substance data sheet on *Pb* for the protection of human health using a critical limit of *200 µg Pb* kg^{-1} muscle meat of fish (food standard set by Commission Regulation (EC) No. 466/2001) and the protection of predators in freshwater and saltwater environments from secondary poisoning (near *0.4 µg Pb* l^{-1}). However, this value is considered too uncertain to be used in the critical load calculations.

Although not presently used, a preliminary critical limit for *Hg* can be found in the substance data sheet on *Hg* and its compounds (2003). As with *Pb*, this value is based on the 5-percentile cut-off value of chronic toxicity data, using 3 data sets of selected (i) freshwater and saltwater, (ii) freshwater and (iii) saltwater, leading to a value of *0.142 mg* m^{-3} (90 percentile range of *0.056–0.281 mg* m^{-3}). In the substance data sheet on *Hg*, an assessment factor of 4 is further introduced, but this approach was not accepted in this manual. A reliable quality standard to protect top predators from secondary poisoning can not be given, but the value is much lower than those for ecotoxicological effects. The value of *0.035 mg* m^{-3} presented earlier for soils is likely to be an upper limit for secondary poisoning.

5.6.3.1.2.2 Calculation of critical limits for total aqueous concentrations

In order to calculate critical loads of metals for freshwater ecosystems it is necessary to know the total aqueous concentration at the critical limit, (i.e. the concentration of dissolved metal and of metal bound to suspended particulate matter *(SPM)*). There are various possible approaches to derive adsorbed metal contents on suspended particles *($[M]_{SPMsw}$)* from total dissolved metal concentrations in surface water *($[M]_{tot,sw}$)*. The simplest approach is an empirical linear approach (K_d-value) relating both contents and concentrations, while accounting for the impact of major properties of the suspended particles influencing the sorption relationship. However, K_d values for a given metal may vary substantially from place to place and so the K_d approach is not appropriate when calculating metal contents on suspended particles from a large number of different locations.

An alternative approach, which uses as far as possible data and models used elsewhere in this manual, is to take a two-stage approach:

- Calculate the critical free ion concentration from the critical dissolved metal concentration.
- Calculate the critical particle-bound metal from the critical free ion.
- Sum the critical particle-bound and dissolved metal to obtain the critical total metal.

Step 1 uses a complexation model (e.g., WHAM) to calculate the critical free ion concentration from the critical dissolved metal concentration. Step 2 uses a transfer function to calculate the particle-bound metal from the free ion. This transfer function is given in Annex 2. The calculation of the critical total aqueous concentration is presented in Annex 3.

In Annex 3, the procedure given applies to the values given in Table 5.22 (considering water hardness for *Cd* and *5 mg* m^{-3} for *Pb*). Use of different values implies a rerun of the WHAM model.

5.6.3.1.2.3 Surface water chemistry data

Data needed to calculate the total dissolved metal concentration are the concentration of suspended particles in the water compartment, *$[SPM]_{sw}$*, the *pH* and *DOC* concentrations of surface water. The concentration of *SPM* in the surface water (*kg* m^{-3} or *g* l^{-1}) depends on the turbulence of the water, which in turn depends on the geological setting (incl. land use) and water flow velocity (i.e., wind speed for lakes). The concentration of suspended particles may thus vary considerably and generally ranges from 1 to 100 *g* m^{-3}. The average concentration for

Dutch surface waters, for example, is 30 *g* m^{-3}, and for a dataset of lowland UK rivers (*n* = 2490) it is 30.6 *g* m^{-3} with a range of <0.1 to 890 *g* m^{-3}, while Scandianavian waters typically show much lower values.

pH and *DOC* values for lakes largely depend on the landscape surrounding the lakes including the parent material (its sensitivity to acid inputs). Typical *DOC* values for clear water lakes are below 5 *mg* l^{-1}, whereas for humic lakes, values can be higher than 50 *mg* l^{-1}. Values for the *pH* generally vary between 5 and 7. Both *pH* and *DOC* are standard measurements in lake surveys and a wealth of data can be derived from those surveys.

When calculating in-lake retention in deriving critical loads for lakes, data on characteristics such as the lake, catchment area, and the net retention rate are needed. For more information we refer to the background document (De Vries et al. 2005) and an earlier manual (De Vries et al. 1998).

5.6.3.2 Critical levels of mercury in precipitation

Critical loads of atmospheric pollution for aquatic ecosystems (lakes and rivers) may be approached by a mass balance approach involving a wide variety of processes both within the water column and in the surrounding watershed. Alternatively, the steady state partitioning of pollutants in a constant environment can be formulated without any need for mass balance considerations or detailed understanding of ecosystem processes. This can be achieved by linking critical receptors, such as fish, directly to the main immissions through transfer functions (TF) describing the relationship of their *Hg* concentrations at steady state, as described below.

5.6.3.2.1 Derivation of critical levels of mercury in precipitation referring to a standard fish

5.6.3.2.1.1 Basic concept

Hg concentrations in fish show a wide variation, about 30-fold both within and among sites (Meili 1997). A standardized value for a given site (lake or river) can be obtained by referring to a commonly caught piscivorous fish with a total body weight of 1 kg, in particular pike (*Esox lucius*). Using a 1-kg pike as a standard receptor, the mean *Hg* concentration in fish flesh can be related to the mean *Hg* concentration in precipitation at a given site as follows:

(V.106)

$$[Hg]_{Pike} = C_{bp} \cdot [Hg]_{Prec} \cdot TF_{HgSite}$$

where:

$[Hg]_{Pike}$ = *Hg* concentration in the flesh of 1-kg pike *(mg* kg^{-1} *fw)*

$[Hg]_{Prec}$ = *Hg* concentration in precipitation *(ng* l^{-1}*)*

TF_{HgSite} = site-specific transfer function *(l* kg^{-1} *fw)* referring to the transfer of atmospheric *Hg* to fish flesh in a watershed at steady state

C_{bp} = 10^{-6} *mg* ng^{-1}, factor for appropriate conversion of units.

The critical level of atmospheric pollution $([Hg]_{Prec(crit)})$ can thus be calculated as follows:

(V.107)

$$[Hg]_{Prec(crit)} = [Hg]_{Pike(crit)} / (TF_{HgSite} \cdot C_{bp})$$

where:

$[Hg]_{Pike(crit)}$ = critical *Hg* concentration in the flesh of 1-kg pike (0.3 *mg* kg^{-1} *fw*)

$[Hg]_{Prec(crit)}$ = critical *Hg* concentration in precipitation *(ng* l^{-1}*)*

C_{bp} =10^{-6} *mg ng*$^{-}$, factor for appropriate conversion of flux units

Regarding the critical limit for mercury in pike of 0.3 *mg kg*$^{-1}$ *fw*, we refer to the background document of the manual (De Vries et al. 2005).

5.6.3.2.1.2 The transfer function TF_{HgSite}

TF_{HgSite} addresses the wide variation of *Hg* concentrations among ecosystems in response to a given atmospheric *Hg* input at steady state. It accounts for a variety of complex processes including both terrestrial and aquatic aspects related to the biogeochemistry of *Hg* in lakes and rivers (Meili et al. 2003a), thus accounting for both fluxes and transformations of *Hg* (e.g., sorption, volatilization, net methylation, bioavailability, biodilution, biomagnification). For mapping of watershed sensitivity, TF_{HgSite} is preferably expressed as a function of basic physical chemical parameters. *Hg* concentrations in fish are generally highest in nutrient-poor softwaters in acidic watersheds rich in wetlands (e.g., Verta et al. 1986, Hakanson et al. 1988, Meili 1991a, 1994, 1996a, 1997). Such differences can be described by empirical relationships to address regional and local differences in watershed biogeochemistry, based on variables for which data are commonly available (e.g., from other studies under the LRTAP Convention), such as surface water *pH* or concentrations of organic carbon or nutrients (the latter being of particular relevance for mercury). Two alternative formulations capturing part of the large variation in TF_{HgSite} are:

(V.108a)

$$TF_{HgSite} \approx TF_{HgRun} \cdot ([TOC]_{sw}^{+1}) / (400[TP]_{sw}^{+6})$$

(V.108b)

$$TF_{HgSite} \approx TF_{HgRun} \cdot e^{-(pHsw-6)/2}$$

where:

$[TOC]_{sw}$ = concentration of total organic carbon in surface water *(mg l*$^{-1}$*)*

$[TP]_{sw}$ = concentration of total phosphorus in surface water *(mg l*$^{-1}$*)*

pH_{sw} = *pH* in surface water

TF_{HgRun} = transfer function *(l kg*$^{-1}$ *fw)* referring to the transfer of atmospheric *Hg* to fish flesh via runoff in a reference watershed at steady state.

The first formulation (V.108a) is most appropriate and should be used when concentrations of total organic carbon and total phosphorus in surface water are available, which is often the case from routine monitoring of surface waters. The alternative formulation based on *pH* alone (V.108b) is less adequate but can be used if data access is limited.

TF_{HgRun} can be quantified from adequate data sets in various ways (see Annex 13 of the background document, De Vries et al. 2005). If such data are not available, a value of 250 000 *l kg*$^{-1}$ *fw* can be used for TF_{HgRun} referring to the standard fish (1 kg, in particular pike, *Esox lucius*) at steady state (Meili et al. 2003a, cf. Verta et al. 1986, Meili 1991a). An important aspect to consider when quantifying TF_{HgRun} (or other steady state parameters) from field data is that present environmental *Hg* concentrations are not in steady state with the present level of atmospheric pollution.

5.6.3.2.2 Derivation of critical levels of mercury in precipitation referring to other organisms

5.6.3.2.2.1 Basic concept

The *Hg* concentration in any fish or other organism, serving as food for humans and fish-based wildlife such as birds and mammals, can be related to the *Hg* concentration in 1-kg pike according to:

(V.109)

$$[Hg]_{Bio} = [Hg]_{Pike} \cdot TF_{HgBio}$$

where:

$[Hg]_{Bio}$ = *Hg* concentration in any biota, (e.g., fish flesh) *(mg kg^{-1} fw)*

TF_{HgBio} = organism-specific transfer function addressing the typical *Hg* partitioning within food webs (–)

The critical level of atmospheric pollution $([Hg]_{Prec(crit)})$ can thus be calculated from a combination of eq. V.107 and eq. V.109 as follows:

(V.110)

$$[Hg]_{Prec(crit)} = [Hg]_{Bio(crit)} / (TF_{HgBio} \cdot TF_{HgSite} \cdot C_{bp})$$

where:

$[Hg]_{Bio(crit)}$ = critical *Hg* concentration in any biota, (e.g., fish flesh) *(mg kg^{-1} fw)*

C_{bp} = see above

TF_{HgBio} is useful for two purposes:

(1) to estimate values for 1-kg pike for sites/regions in which only mercury concentrations in other organisms are available,

(2) to convert critical load maps referring to 1-kg pike into maps for other target organisms of local/regional interest.

5.6.3.2.2.2 The transfer function TF_{HgBIO}

TF_{HgBio} addresses the wide variation of *Hg* concentrations among organisms within food webs, by describing the typical deviation from the standard fish. Among commonly available variables, body weight is the most powerful single predictor of fish *Hg* levels, also across species. The variation in TF_{HgBio} can be described as follows:

(V.110)

$$TF_{HgBio} \approx f_{HgY} + f_{HgW} W^{2/3}$$

where:

f_{HgY} = value for very young fish and other small animals (–); $f_{HgY} \approx 0.13$

f_{HgW} = species-specific slope coefficient (–)

$f_{Hgw} \approx 0.2...2$ (Table 5.29)

W = total body fresh weight *(kg fw)*

For many freshwater fish used for human consumption, this will generate estimates of mean *Hg* concentrations at a given fish size that differ less than 2-fold from observed means. Species-specific slope coefficients (f_{Hgw}) for some common freshwater fish are given in Table 5.29 for the

typical case that the value for very young fish and other small animals (f_{HgY}) can be maintained at 0.13. For any fish species (e.g. for unexplored sites or for unknown future fish populations), a first approximation differing less than 3-fold from observed size-class means can be made based on body weight alone, using the parameter for the standard fish, pike (f_{Hgw} = *0.87*, Table 5.29). If fish weight data are not available, total body weight (*W* in kg) can be estimated from total body length by applying a species-specific shape factor (f_{LW}, Table 5.29) according to:

(V.112)

$$W \approx f_{LW} \cdot L^{3.1}$$

Where *L* = length of the fish (cm).

Table 5.29: Coefficients for size conversion (f_{LW}) and normalization of Hg concentrations (f_{Hgw}) in freshwater fish, some standard fish weights (W) for consumption, and the related value for TF_{HgBio}.

Fish taxa			f_{LW}	f_{HgW}	W	TF_{HgBio}
pike	*Esox lucius*	Esocidae	$3.8\ 10^{-6}$	0.87	1.0	1
pike-perch, zander	*Stizostedion lucioperca*	Percidae	$6.4\ 10^{-6}$	1.2	1.0	1.3
perch	*Perca fluviatilis*	Percidae	$7.9\ 10^{-6}$	1.9	0.3	1.0
trout	*Salmo trutta*	Salmonidae	$7.2\ 10^{-6}$	0.4	0.3	0.3
Arctic char	*Salvelinus alpinus*	Salmonidae	$6.8\ 10^{-6}$	0.7	0.3	0.4
whitefish	*Coregonus spp.*	Coregonidae	$6\ 10^{-6}$	<0.4...>2		
burbot	*Lota lota*	Lotidae	$5\ 10^{-6}$	0.9	0.3	0.5
bream	*Abramis brama*	Cyprinidae	$8\ 10^{-6}$	0.25	0.3	0.2
roach	*Rutilus rutilus*	Cyprinidae	$6.8\ 10^{-6}$	0.6...1.2		

Table 5.29 is meant as a reference that can be expanded and adapted for local use, based on additional field data from systems where several coexisting species have been analyzed. Note that for compatibility of transfer functions and for inter-regional comparisons, the value of TF_{HgBio} refers to a 1-kg pike, which should be maintained as a reference receptor with a value of ${}^{TF}HgBio^{=1}$.

5.6.4 Limitations in the present approach and possible future refinements

In general, the uncertainties in measurement as well as in modelling are higher with respect to trace elements than for main nutrient elements. In particular the following uncertainties of the models should be mentioned:

- The steady-state of metal inputs and outputs on the level of the critical limit is a theoretical situation. In dependence of the actual status of a site (or area) it may take years to centuries (e.g., for calcareous soils) to reach this steady-state. This should be considered when critical loads and their exceedances are to be interpreted. To consider the processes of metal accumulation or loss from soils over time, dynamic approaches would be needed (see for an overview Bonten et al., 2015). Although such models are already suggested, they are not yet considered here, because they still need further sophistication. There is some inconsistency between the calculation of the critical leaching and the tolerable removal of the metals with biomass because types of critical limits and their mode of use are different for both fluxes.

- The uptake of heavy metals by plants is not constant over time but varies strongly with changes in pollution and is at present likely lower than indicated above at steady state at the level of critical concentrations.
- Possible effects of thinning of the metal concentration due to high mass fluxes of biomass harvest (high yields) are not considered due to missing knowledge.
- The delivery of heavy metals to the available pools of soils and surface waters is excluded from the mass balance equation due to high uncertainties of the available calculation approach. However, since the same approach is used to identify sites with high natural inputs it may happen that one site is excluded, while another site with an insignificant lower weathering rate will stay in the database.
- The approaches taken to calculate critical limits for ecotoxicological effects are different for terrestrial and aquatic ecosystems. Given the likelihood that terrestrial and freshwater organisms (with the exception of surface-dwelling soil invertebrates such as snails) are exposed to metal in a similar manner (i.e., via the solution phase), a common approach to deriving critical limits, if not common values or functions for the limits, is scientifically desirable.
- The critical limit derivation includes several uncertainties, as e.g. differences between results from laboratory or field, which are (deviating e.g. from OECD methodologies) not taken into account by the use of "uncertain factors".
- Organisms can be affected by different pathways, which could only partly considered here.
- The vertical flux of metals bound to particulate matter suspended in the drainage water, may be remarkable in certain soils, this holds in particular for *Pb*. It was, however, not recommended to consider this, in order to be consistent with other parts of the manual.
- The seasonal variation of soil parameters such as *pH*, *DOC* cannot be accounted for in the models.

5.7 Modelling critical loads for biodiversity

5.7.1 Introduction

The critical load concept has been developed as a measure of the good ecological state of an ecosystem in the long-term in relation to air pollutants. Initially this indicator has been based on chemical characteristics of soils. On the other hand, empirical critical loads considered the effects of atmospheric pollution on specific functions of an ecosystem or its overall good condition.

At its 25th session in 2007, the Executive Body encouraged the Working Group on Effects "... to increase its work on quantifying effects indicators, in particular for biodiversity. These should also be linked to the integrated assessment modelling activities" (ECE/EB.AIR/91, para. 31). This has been confirmed in the Long-term Strategy of the Convention till 2020 which "set a vision for the next 10 years and beyond to address the remaining issues from existing activities and to meet emerging challenges with the aim of delivering a sustainable optimal long-term balance between the effects of air pollution, climate change and biodiversity" (ECE/EB.AIR/2010/4, para 6a). This has been thus explained in the 2012-2014 call for data issued by the CCE (CCE 2012).

Responding to this request from the EB in 2007, the ICP M&M embarked on developing methods and data for biodiversity indicators that can be used for policy support through integrated assessment modelling. Preliminary results were reported in the CCE status reports as soon as 2008 (Hettelingh et al. 2008). Following this, ICP M&M, the CCE and M&M NFCs have continued their activity on biodiversity indicators as reported every year in CCE status reports (Hettelingh et al. 2009; Posch et al. 2011, 2012a; Slootweg et al. 2010). This was a logical methodological evolution that aimed at linking critical loads to biodiversity. These new developments, based on recent scientific findings, are described in this section. Under the WGE, different ICPs have also undertaken to develop indicators linking atmospheric pollution to biodiversity changes, as shown in Harmens et al. (2013).

The work undertaken under ICP M&M, and more widely by the WGE, meet general preoccupations about the observed loss of biodiversity at the world scale (cf. http://www2.epa.gov/nutrientpollution, http://www.initrogen.org, Sutton et al. 2011). Also, pollution deposition, in particular nitrogen, is included in the threats to biodiversity listed by the Convention on Biological Diversity (CBD, decisions VII/30 in 2004 and VIII/15 in 2006). Nitrogen deposition has been shown to be above critical loads for a significant number of protected areas across the world, indicating that nitrogen deposition is a one of the drivers of biodiversity loss (Bleeker et al., 2011). Assessments for the revision of the Gothenburg protocol evaluated that, in 2005, over 57 % of the EMEP area the critical loads for eutrophication were exceeded (WGE 2013).

Published in 2010, the CBD "strategic plan for biodiversity 2011-2020" translated its decisions into the Aichi Targets (in particular "Target 8: By 2020, pollution, including from excess nutrients, has been brought to levels that are not detrimental to ecosystem function and biodiversity"). In 2011, its Subsidiary Body on Scientific, Technical and Technological Advice recommended that this target was supported by indicators expressing the trends in pressures from pollution such as "trends in water quality in aquatic ecosystems"; "trends in pollution deposition rate"; "trends in emission to the environment of pollutants relevant for biodiversity"; and "trends in ozone levels in natural ecosystems" (Target 8, recommendation XV/1, CBD 2011).

At the European level, the pan-European initiative, launched in January 2005, developed a set of indicators to assess progress towards CBD 2010 biodiversity target in Europe, the Streamlining European 2010 Biodiversity Indicators (SEBI 2010, http://biodiversity.europa.eu/topics/sebi-indicators). One of these indicators, in line with the Aichi target 8, is the critical load exceedance for nitrogen (SEBI 09).

The EU Biodiversity Strategy for 2020 (EC, 2011), adopted through a European Parliament resolution in 2012, emphasizes the importance of the SEBI indicators for implementing and assessing policy efficiency. Its target 2, action 7, encourages member states to "Ensure no net loss of biodiversity and ecosystem services".

For Europe, the EU specified six 2020-biodiversity targets. In particular for EU Member States, results of this work could contribute and support the EU 2020 headline target "halting the loss of biodiversity and the degradation of ecosystem services in the EU by 2010, and restoring them in so far as feasible, while stepping up the EU contribution to averting global biodiversity loss". This objective has been abbreviated in the EU to "no net loss of biodiversity and ecosystem services" (EU 2011, p.12, Target 2, Action 7) which was simplified to "no net loss of biodiversity" for the purpose of this call. For more detailed background information, NFCs may wish to consult the documents listed in the CCE Call for Contributions of 2011-2012 (to be found at: http://wge-cce.org/Activities/Call_for_Data).

5.7.2 Objectives

In this context, ICP M&M and CCE have promoted the development of modelling tools based on biodiversity metrics (instead of a physico-chemical indicator) and integrating the effects of climate change. These tools may calculate nitrogen critical loads in relation to an acceptable change in plant species diversity or predict change in vegetation under different scenarios. Available approaches, used by ICP M&M NFCs, are briefly described below.

At the ICP M&M meeting and CCE workshop in 2012 in Warsaw (Poland), NFCs have furthermore been encouraged to choose indicators that may provide a measure of "no net loss of biodiversity" for sensitive plant species or ecosystems that are of relevance for individual countries. In this context an approach is adopted that is similar to previous calls for ICP M&M relative to critical loads data. The reason is that in their response to calls for critical loads data, countries are free to decide on the sensitive ecosystems for which they wish to include critical loads in the European critical load database. This way of harmonisation of information on impacts provides a level playing field for the comparison, by policy analysts, of impacts generated from emission reduction scenarios that are simulated in integrated assessment.

In this way, the use of future "no net loss of biodiversity" indicators in integrated assessment models becomes similar to the manner in which the Europen critical loads database is implemented and used in effect-based scenario analyses.

Following the 2012-2014 call for data (Slootweg et al. 2014), the ICP M&M discussions concluded that a common indicator, preliminarily named "habitat suitability indicator", should be used by all NFCs, in addition to indicators that meet specific national requirements. This indicator should be calculated using lists of species characteristic of EUNIS habitats.

The most recent information on the development of "no net loss of biodiversity indicators" and "habitat suitability indicators" can be found on the ICP M&M and CCE websites (http://icpmapping.org/ and http://wge-cce.org/) and described in the CCE Status Report 2014 (Slootweg et al. 2014).

These indicators are to be calculated from a number of tools and models that are made available through the CCE for NFCs to carry out their calculations. NFCs are encouraged to make use of them especially when they do not have at their disposal more accurate or detailed national tools equivalent to the ones listed here. These tools and models are briefly described in the following sections. Further information is to be found in the CCE Status Reports, in particular the 2009 and 2014 reports.

5.7.3 Vegetation models to predict biodiversity changes

Vegetation models simulate vegetation developments or changes in relation to abiotic conditions (nutrients, basic cations, light or water availability, soil acidity, temperature, etc.). These conditions are provided by models such as VSD+ (see chapter 6.3).

Vegetation models have been developed and tested under ICP M&M for several years (see, for instance, De Vries et al. 2010 for a comparison of 4 of them; Bonten et al. 2015). In the following sections, some of these approaches are presented. Models are sorted in alphabetical order. Further details on the models are to be found in the bibliographic references and in particular in De Vries et al. (2015a).

5.7.3.1 BERN

The BERN model (Schlutow et al. 2015) simulates the potential plant community composition depending on the geo-chemical soil's characteristics and climatic conditions. It uses fuzzy

functions for 7 different factors (soil water content, base saturation or pH, C:N ratio, climatic water balance, vegetation period, solar radiation, and temperature). These functions represent the ecological niche under pristine or semi-natural conditions (Schlutow and Huebener 2003, Nagel et al. 2012).

5.7.3.2 MOVE

The MOVE model assesses changes in plant species occurrence due to changes in abiotic site conditions. This statistical model is based on response curves that define the probability of occurrence of plant species along environmental gradients (De Vries et al. 2007; Latour and Reiling 1993; Latour et al. 1994; Van Dobben et al. 2010, Van Dobben et al. 2015).

GBMOVE is an application to the UK to this model. This simulates the interactions between 1,130 UK plant species through a set of multiple logistic regression niche models. This is an empirical model based on extensive survey dataset (Rowe et al. 2009; Smart et al. 2010).

5.7.3.3 PROPS

The PROPS model estimates the probability of plant species occurrence as a function of environmental factors. It is associated to a database including over 40,000 vegetation relevés. At some of the sites, soil parameters such as pH and C/N ratio have been measured as well. The PROPS model has been coupled to the biogeochemical model VSD+ (Reinds et al. 2012; Bonten et al. 2015).

5.7.3.4 Sumo

In SUMO, the biomass development of five functional plant types is simulated as a function of nitrogen availability, light interception, and management. This process-based model simulates the change in biomass distribution over functional types during the succession from almost bare soil via grassland or heathland to various forest types (Wamelink et al., 2009).

The SUMO model has been coupled with the biogeochemical model SMART2 (Wamelink et al. 2009).

5.7.3.5 Veg

The Veg model (Belyazid et al., 2015) estimates the composition of the ground vegetation community using abiotic conditions at a particular site (Reinds et al. 2013). The composition of the ground vegetation community is simulated in the Veg module by distributing the available ground area (a representative 1 m^2) over the plant species that would be able to establish at the site, given its abiotic conditions. For each species a 'niche window' is estimated by the model. This niche window is the combined limits of N and Bc concentrations in the soil solution, soil solution pH, soil moisture, air temperature, and light intensity reaching the ground vegetation (light below tree canopy in case trees are present), within which a species could become established at a certain site. Usually, site conditions are favourable enough for several species to be present simultaneously. The model then calculates the relative ground area occupied by each species, depending on their vigour in response to site conditions and their respective competitiveness. The plant species compete by growing roots to different soil depths and by shading other plants above ground. The root depth and shading are given as inputs for each indicator plant species (Belyazid et al. 2009; Belyazid et al. 2011b; Belyazid et al. 2011c; Sverdrup et al. 2007).

The model requires a list of indicator plant species, which is typically based on input from biologists and ecologists familiar with the ecosystem to be modelled, which can be found on the "Veg Table". It contains information on plant species present in the different EUNIS classes.

Initially compiled on the basis of Northern Europe plant relevés (Sverdrup et al., 2007), this table has been enriched or adapted by different countries. It thus progressively adapts to different European eco-regions (e.g., Braun et al. 2012; Nagel et al. 2012; Probst et al., 2012; Probst et al., 2014; Probst et al. 2015).

The Veg model has been coupled with the biogeochemical ForSafe (Belyazid et al. 2015) and VSD+ (Bonten et al. 2015) models.

5.8 References

Achermann B, Bobbink R (eds) (2003) Empirical critical loads for nitrogen, expert workshop, Berne, 11–13 November 2002., Swiss Agency for the Environment, Forests and Landscape (SAEFL), Berne, Switzerland, 1–327 pp.

Aherne J, Kelly-Quinn M, Farrell EP (2002) A survey of lakes in the Republic of Ireland: Hydrochemical characteristics and acid sensitivity. Ambio 31: 452–459.

Aherne J, Curtis CJ (2003) Critical loads of acidity for Irish lakes. Aquatic Sciences. 65: 21–35.

Aherne J, Posch M, Dillon PJ, Henriksen A (2004) Critical loads of acidity for surface waters in south-central Ontario, Canada: Regional application of the First-order Acidity Balance (FAB) model. Water, Air and Soil Pollution: Focus 4: 25–36.

Åkerblom S, Meili M, Bringmark L, Johansson K (2004) Determination of the fractionation factor (ff) in forest soil describing the Hg content of organic matter in solution relative to that in solids based on field data from Sweden. Background Document on Critical Loads of Heavy Metals, UN/ECE-CLRTAP-ICP Modelling and Mapping, 6 pp.

Akselsson, C., Holmquist, J., Alveteg, M., Kurz, D., Sverdrup, H. (2004). Scaling and mapping regional calculations of soil chemical weathering. Water, Air and Soil Pollution Focus 4:671–681.

Akselsson, C., Sverdrup, H., Holmqvist, J. (2005). Estimating weathering rates of Swedish forest soils in different scales, using the PROFILE model. Journal of Sustainable Forestry. 21:119–131.

Akselsson, C., Holmqvist, J., Kurz, D., Sverdrup, H., (2006). Relations between elemental content in till, mineralogy of till and bedrock mineralogy in the province of Småland, Southern Sweden. Geoderma 136:643–659.

Alriksson A, Eriksson H, Karltun E, Lind T, Olsson M (2002) Carbon pools and sequestration in soil and trees in Sweden, based on data from national soil and forest inventories. In: M Olsson (ed): Land Use Strategies for Reducing Net Greenhouse Gas Emissions (LUSTRA), Progress Report 1999–2002, pp. 30–36. Swedish University of Agricultural Sciences, Uppsala, Sweden.

Arp PA, Ouimet R (2001) Sustaining the soil base saturation. Appendix 2 in: Protocol for assessment and mapping of forest sensitivity to S and N deposition, p. 29–41. New England Governors/Eastern Canadian Premiers. Acid Rain Action Plan 2001. Action Item 4: Forest Mapping Research Project.

Baker LA, Brezonik PL (1988) Dynamic model of in-lake alkalinity generation. Water Resources Research 24: 65–74.

Batterbee RW, Allot TEH, Juggins S, Kreiser AM (1995) Estimating the base critical load: The diatom model. In: CLAG (1995) op. cit., pp.3–6.

Belyazid S, Kurz D, Sverdrup H, Braun S, Rhim B (2009) Developing a method for estimating critical loads of nitrogen deposition under a changing climate, based on biological indicators. In Hettelingh J-P, Posch M, Slootweg J (eds): Progress in the modelling of critical thresholds, impacts to plant species diversity and

ecosystem services in Europe. CCE Status Report 2009, Coordination Centre for Effects (CCE) Bitlhoven, The Netherlands, pp. 57–67.

Belyazid, S., Kurz, D., Braun, S., Sverdrup, H., Rihm, B., Hettelingh, J.P. (2011a) A dynamic modelling approach for estimating critical loads of nitrogen based on plant community changes under a changing climate. Environmental Pollution 159:789–801.

Belyazid S, Posch M, Kurz D (2011b) Appendix B: Manual for setting flora parameters for the Veg model. In Posch M, Slootweg J, Hettelingh J-P (eds): Modelling critical thresholds and temporal changes of geochemistry and vegetation diversity, CCE Status Report 2011, Bilthoven, The Netherlands. pp. 181–184.

Belyazid S, Posch M, Kurz D (2011c) Progress in vegetation and soil chemistry modelling. In Posch M, Slootweg J, Hettelingh J-P (eds) Modelling critical thresholds and temporal changes of geochemistry and vegetation diversity, CCE Status Report 2011, Bilthoven, The Netherlands. pp. 53–58.

Belyazid, S., Sverdrup, H., Kurz, D., Braun, S. (2011d) Exploring ground vegetation change for different scenarios and methods for estimating critical loads for biodiversity using the ForSAFE-VEG model in Switzerland and Sweden. Water, Air and Soil Pollution, 216:289–317

Belyazid S, Sverdrup HU, Kurz D, Braun S (2015) Use of an integrathed soilvegetation model to assess impacts of atmospheric deposition and climate change on plant species diversity. Chapter 12 in: De Vries W, Hettelingh J-P, Posch M (eds) Critical Loads and Dynamic Risk Assessments of Nitrogen, Acidity and Metals for Terrestrial and Aquatic Ecosystems. Springer, pp. 327–358.

Berendse F, Beltman B, Bobbink R, Kwant M, Schmitz MB (1987) Primary production and nutrient availability in wet heathland ecosystems. Acta Oec./Oecol. Plant. 8: 265–276.

Bindler R, Renberg I, Klaminder J, Emteryd O (2004) Tree rings as Pb pollution archives? A comparison of 206Pb / 207Pb isotope ratios in pine and other environmental media. Sci. Total Environ. 319: 173–183.

Bleeker A, Hicks WK, Dentener E, Galloway J, Erisman JW (2011) N deposition as a threat to the World's protected areas under the Convention on Biological Diversity. Environmental Pollution 159(10): 2280–2288.

Bobbink R, Boxman D, Fremstad E, Heil G, Houdijk A, Roelofs J (1992) Critical loads for nitrogen eutrophication of terrestrial and wetland ecosystems based upon changes in vegetation and fauna. In: Grennfelt and Thörnelöf (1992), op. cit., pp. 111–159.

Bobbink R, Hornung M, Roelofs JGM (1996) Empirical nitrogen critical loads for natural and semi-natural ecosystems. In: UBA (1996) op. cit., Annex III (54 pp).

Bobbink R, Hornung M, Roelofs JGM (1998) The effects of air-borne pollutants on species diversity in natural and seminatural European vegetation. Journal of Ecology 86: 717–738.

Bobbink R, Ashmore M, Braun S, Flückiger W, Van den Wyngaert IJJ (2003) Empirical nitrogen critical loads for natural and semi-natural ecosystems: 2002 update. In: Achermann and Bobbink (2003), op. cit., pp 43–170.

Bobbink R, and Hettelingh, J. P., eds. (2011) Review and revision of empirical critical loads and dose response relationships. Bobbink, R., and Hettelingh, J. P., Coordination Center for Effects (CCE); National institute for public health and the environment (RIVM), Bilthoven, The Netherlands. pp. 1–243.

Bobbink R, Tomassen H, Weijters M, Van den Berg L, Strengbom J, Braun S, Nordin A, Schütz K, Hettelingh J.-P (2015). Effects and empirical critical loads of nitrogen for Europe. Chapter 4 in: De Vries W, Hettelingh J-P, Posch M (eds) Critical Loads and Dynamic Risk Assessments of Nitrogen, Acidity and Metals for Terrestrial and Aquatic Ecosystems. Springer, pp. 85–127.

Bobbink R, Loran C, Tomassen H, eds. (2022) Review and revision of empirical critical loads of nitrogen for Europe. German Environment Agency, Dessau-Roßlau.

Boggero A, Barbieri A, De Jong J, Marchetto A, Mosello R (1998) Chemistry and critical loads of Alpine lakes in Canton Ticino (southern central Alps) Aquatic Science 60: 300–315.

Bolt GH, Bruggenwert MGM (eds) (1976) Soil Chemistry. Part A. Basic Elements. Elsevier, Amsterdam, The Netherlands, 281 pp.

Bonten L, Mol-Dijkstra JP, Wiegger R, Reinds GJ (2012) GrowUp: A tool for computing forest Growth, nutrient Uptake and litterfall. In: Posch M, Slootweg J, Hettelingh J-P (eds): Modelling and mapping of atmospherically-induced ecosystem impacts in Europe. CCE Status Report 2012, Bilthoven, The Netherlands. pp. 43–48.

Bonten LTC, Reinds GJ, Groenenberg JE, De Vries W, Posch M, Evans CD, Belyazid S, Braun S, Moldan F, Sverdrup HU, Kurz D, (2015) Dynamic geochemical models to assess deposition impacts and target loads of acidity for soils and surface waters. Chapter 8 in: De Vries W, Hettelingh J-P, Posch M (eds) Critical Loads and Dynamic Risk Assessments of Nitrogen, Acidity and Metals for Terrestrial and Aquatic Ecosystems. Springer, pp. 225–251.

Bouten W, De Vre FM, Verstraten JM, Duysings JJHM (1984) Carbon dioxide in the soil atmosphere: simulation model parameter estimation from field measurements. In: E Eriksson (ed): Hydrochemical Balances of Freshwater Systems. IAHS-AISH 150, Uppsala, Sweden, pp. 23–30.

Brakke DF, Henriksen A, Norton SA (1989) Estimated background concentrations of sulfate in dilute lakes. Water Resources Bulletin 25(2): 247253.

Brakke DF, Henriksen A, Norton SA (1990) A variable F-factor to explain changes in base cation concentrations as a function of strong acid deposition. Verh. Internat. Verein. Limnol. 24: 146–149.

Braun S, Schindler C, Volz R, Flückiger W (2003) Forest damages by the storm 'Lothar' in permanent observation plots in Switzerland: the significance of soil acidification and nitrogen deposition. Water, Air and Soil Pollution 142: 327–340.

Braun S, Cantaluppi L, Flückiger W (2005) Fine roots in stands of Fagus sylvatica and Pices abies along a gradient of soil acidification. Environmental Pollution 137: 574–579.

Braun S, Kurz D, Kohli L, Roth T, Rihm B (2012) National report: Switzerland. In: Posch M, Slootweg J, Hettelingh J-P (eds): Modelling and mapping of atmospherically-induced ecosystem impacts in Europe. CCE Status Report 2012, Bilthoven, The Netherlands. pp. 125–138.

Braun S (2013) Untersuchungen über die Zusammensetzung der Bodenlösung, Bericht 2012, http://www.iap.ch/publikationen/untersuchungen_zusammensetzung_bodenloesung_iap_bericht_2012.pdf

Breeuwsma A, Chardon JP, Kragt JF, De Vries W (1991) Pedotransfer functions for denitrification. Final Report of the project 'Nitrate in Soils', DG XII, European Community, Brussels, pp. 207–215.

Brook GA, Folkoff ME, Box EO (1983) A world model of carbon dioxide. Earth Surface Processes and Landforms 8: 79–88.

Burman R, Pochop LO (1994) Evaporation, Evapotranspiration and Climatic Data. Developments in Atmospheric Science 22, Elsevier, Amsterdam, 278 pp.

CBD (2011) Recommendation XV/1. Indicator framework for the Strategic Plan for Biodiversity 2011-2020 and the Aichi Biodiversity Targets. Convention on biological diversity, Subsidiary body on scientific, technical and technological advice XV/1, 11 p.

CCE (2012) Modelling and Mapping regional "no net loss of biodiversity". CCE Call for Data 2012-2014. Coordination Center for Effects, National Institute of Public Health and Environmental Protection (RIVM), 7 pp.

Cinderby S, Emberson L, Owen A, Ashmore M (2007) LRTAP land cover map of Europe. In: Slootweg J, Posch M, Hettelingh J-P (eds) cCe Progress Report 2007, Bilthoven, The Netherlands, pp. 59–70.

Chytrý M et al. (2020) EUNIS Habitat Classification: Expert system, characteristic species combinations and distribution maps of European habitats. Appl. Veg. Sci.: 23: 648-675.

CLAG (Critical Loads Advisory Group) (1995) Critical loads of acid deposition for United Kingdom freshwaters. ITE Edinburgh/Department of the Environment, London, United Kingdom, 80 pp.

CLRTAP (2004) Manual on methodologies and criteria for modelling and mapping critical loads and levels and air pollution effects, risks and trends. UNECE Convention on Long-range Transboundary Air Pollution; accessed at www.umweltbundesamt.de/en/cce-manual.

CLRTAP (2017) Mapping critical loads for ecosystems, Chapter 5 of Manual on methodologies and criteria for modelling and mapping critical loads and levels and air pollution effects, risks and trends. UNECE Convention on Long-range Transboundary Air Pollution.

Crommentuijn T, Polder MD, Van de Plassche EJ (1997) Maximum permissible concentrations and negligible concentrations for metals, taking background concentrations into account. Report 601501 001, National Institute for Public Health and the Environment, Bilthoven, The Netherlands, 157 pp.

Cronan CS, Walker WJ, Bloom PR (1986) Predicting aqueous aluminium concentrations in natural waters. Nature 324: 140–143.

Curtis CJ, Posch M, Aherne J, Folster J, Forsius M, Larssen T, Moldan F (2015) Assessment of critical loads of acidity and their exceedances for European lakes. Chapter 17 in: De Vries W, Hettelingh J-P, Posch M (eds) Critical Loads and Dynamic Risk Assessments of Nitrogen, Acidity and Metals for Terrestrial and Aquatic Ecosystems. Springe, p439–462.

Davies CE, Moss D (2002) EUNIS habitat classification, Final Report. CEH Monks Wood, United Kingdom.

Davies CE, Moss D, Hill MO (2004) EUNIS habitat classification revised 2004. European Environment Agency, European topic centre on nature protection and biodiversity.

De Temmerman L, de Witte T (2003a) Biologisch onderzoek van de verontreiniging van het milieu door zware metalen te Hoboken groeiseizoen 2001. Internal report Centrum voor onderzoek in diergeneeskunde en agrochemie C.O.D.A, Tervuren.

De Temmerman L, De Witte T (2003b) Biologisch onderzoek van de verontreiniging van het milieu door kwik en chloriden te Tessenderlo en van kwik te Berendrecht. Internal report Centrum voor onderzoek in diergeneeskunde en agrochemie C.O.D.A, Tervuren. EG No. 466/2001: COMMISSION REGULATION (EC) No 466/2001 of 8 March 2001 setting maximum levels for certain contaminants in foodstuffs, Official Journal of the European Commission No. L 77.

De Vries W (1988) Critical deposition levels for nitrogen and sulphur on Dutch forest ecosystems. Water, Air and Soil Pollution 42: 221–239.

De Vries W (1991) Methodologies for the assessment and mapping of critical loads and of the impact of abatement strategies on forest soils. Report 46, DLO Winand Staring Centre, Wageningen, The Netherlands, 109 pp.

De Vries W (1994) Soil response to acid deposition at different regional scales. PhD thesis, Agricultural University Wageningen, Wageningen, The Netherlands, 487 pp.

De Vries W, Bakker DJ (1998) Manual for calculating critical loads of heavy metals for terrestrial ecosystems. Guidelines for critical limits, calculation methods and input data. DLO Winand Staring Centre, Report 166, Wageningen, The Netherlands, 144 pp.

De Vries W, Posch M, Reinds GJ, Kämäri J (1993) Critical loads and their exceedance on forest soils in Europe. Report 58 (revised version), DLO Winand Staring Centre, Wageningen, The Netherlands, 116 pp.

De Vries W, Reinds GJ, Posch M (1994) Assessment of critical loads and their exceedances on European forests using a one-layer steady-state model. Water, Air and Soil Pollution 72: 357–394.

De Vries W, Bakker DJ, Sverdrup HU (1998) Manual for calculating critical loads of heavy metals for aquatic ecosystems. Guidelines for critical limits, calculation methods and input data. DLO Winand Staring Centre, Report 165, Wageningen, The Netherlands, 91 pp.

De Vries W, Hol A, Tjalma S, Voogd JC (1990) Literature study on the amounts and residence times of elements in forest ecosystems (in Dutch) Rapport 94, DLO Winand Staring Centre, Wageningen, The Netherlands, 205 pp.

De Vries W, Posch M (2003) Derivation of cation exchange constants for sand loess, clay and peat soils on the basis of field measurements in the Netherlands. Alterra-Rapport 701, Alterra Green World Research, Wageningen, The Netherlands, 50 pp.

De Vries W, Reinds GJ, Posch M, Sanz MJ, Krause GhM, Calatayud V, Renaud JP, Dupouey JL, Sterba H, Vel EM, Dobbertin M, Gundersen P, Voogd JCH (2003) Intensive Monitoring of Forest Ecosystems in Europe. Technical Report 2003, EC-UNECE, Brussels and Geneva, 161 pp.

De Vries W, Schütze G, Lofts S, Meili M, Römkens PFAM, Farret R, De Temmerman L, Jakubowski M (2003) Critical limits for cadmium, lead and mercury related to ecotoxicological effects on soil organisms, aquatic organisms, plants, animals and humans. In: Schütze et al. (2003) op. cit., pp. 29–78.

De Vries W, Lofts S, Tipping E., Meili M., Groenenberg JE, Schütze G (2004) Impact of Soil Properties on Critical Concentrations of Cadmium, Lead, Copper, Zinc, and Mercury in Soil and Soil Solution in View of Ecotoxicological Effects. Reviews of Environmental Contamination and Toxicology 191: 47–89.

De Vries W, Schütze G, Lofts S, Tipping E, Meili M, Groenenberg JE, Römkens PFAM (2005) Calculation of critical loads for cadmium, lead and mercury. Background document to Mapping Manual Chapter 5.5, 143 pp.

De Vries W, Kros H, Reinds GJ, Wamelink W, Van Dobben H, Bobbink R, Smart S, Evans CD, Schlutow A, Kraft P, Belyazid S, Sverdrup H, Van Hinsberg A, Posch M, Hettelingh J-P (2007) Developments in deriving critical limits and modelling critical loads of nitrogen for terrestrial ecosystems in Europe. Alterra-Report 1382, Alterra, Wageningen, The Netherlands, 206 pp.

De Vries W, Wamelink GWW, Van Dobben H, Kros J, Reinds GJ, Mol-Dijkstra JP, Smart SM, Evans CD, Rowe EC, Belyazid S, Sverdrup HU, Van Hinsberg A, Posch M, Hettelingh J-P, Spranger T, Bobbink R (2010) Use of dynamic soil-vegetation models to assess impacts of nitrogen deposition on plant species composition: an overview. Ecological Applications 20(1): 60–79.

De Vries W, Hettelingh J-P, Posch M (eds) (2015a) Critical Loads and Dynamic Risk Assessments of Nitrogen, Acidity and Metals for Terrestrial and Aquatic Ecosystems. Springer, 662p.

De Vries W, Hettelingh J.-P., Posch M (2015b) The history and current state of critical loads and dynamic modelling assessments. Chapter 1 in: De Vries W, Hettelingh J-P, Posch M (eds) Critical Loads and Dynamic Risk Assessments of Nitrogen, Acidity and Metals for Terrestrial and Aquatic Ecosystems. Springer, pp. 1–11.

Vries W, Groenenberg JE, Posch M (2015c) Mass balance approaches to assess critical loads and target loads of metals for terrestrial and aquatic ecosystems. Chapter 7 in: De Vries W, Hettelingh J-P, Posch M (eds) Critical Loads and Dynamic Risk Assessments of Nitrogen, Acidity and Metals for Terrestrial and Aquatic Ecosystems. Springer, pp. 207–222.

De Wit, H. A., and Lindholm, M. (2010) Nutrient enrichment effects of atmospheric N deposition on biology in oligotrophic surface waters – a review. NIVA, Norwegian institute for Water Research, Oslo, Norway. Rep. No. 6007 – 2010 ICP Waters report 101/2010, 39 p.

Dillon PJ, Molot LA (1990) The role of ammonium and nitrate retention in the acidification of lakes and forested catchments. Biogeochemistry 11: 23–43.

Directive 2013/39/EU (2013) Directive 2013/39/EU of the European Parliament and of the Council of 12 August 2013 amending Directives 2000/60/EC and 2008/105/EC as regards priority substances in the field of water policy. European Parliament.

Dise NB, Wright RF (1995) Nitrogen leaching from European forests in relation to nitrogen deposition. Forest Ecology and Management 71: 153–161.

Dittmar, W. (1884). Report on research into the composition of ocean water, collected by H.M.S. Challenger, during the years 1873–1876. Physics and Chemistry 1: 1-251.

Driscoll CT, Lehtinen MD, Sullivan TJ (1994) Modeling the acid-base chemistry of organic solutes in Adirondack, New York, lakes. Water Resources Research 30: 297–306.

Duan L, Hao J, Xie S, Du K (2000) Critical loads of acidity for surface waters in China. Science of the Total Environment 246: 1–10.

Dutch J, Ineson P (1990) Denitrification of an upland forest site. Forestry 63: 363–377.

EC (2011) Our life insurance, our natural capital: an EU biodiversity strategy to 2020. Communication from the commission to the European Parliament, the Council, the Economic and Social Committee and the Committee of the Regions, European Commission, Brussels, Belgium. COM(2011) 244 final, 17 p.

Egli, M., Favilli, F., Krebs, R., Pichler, B., Dahms, D. (2012): Soil organic carbon and nitrogen accumulation rates in cold and alpine environments over 1Ma. Geoderma 183: 109–123.

Eurosoil (1999) Metadata: Soil Geographical Data Base of Europe v.3.2.8.0. Joint Research Centre, Ispra, Italy.

FAO (1981) FAO-Unesco Soil Map of the World, 1:5.000.000; Volume V Europe, Unesco-Paris, 199 pp.

Farret R (2003) General Methodology. In: Schütze et al. (2003) “Expert meeting on critical limits for heavy metals and methods for their application”, pp. 103–107.

Galloway JN, Aber JD, Erisman JW, Seitzinger SP, Howarth RW, Cowling EB, Cosby BJ (2003) The nitrogen cascade. BioScience, 53: 4, 341.

Gebhardt S (2023) Creation of a harmonized land cover map as an example for the entire region of the Geneva Air Pollution Convention. Final report. CCE, UBA, Dessau-Roßlau, Germany.

Graf Pannatier E, Walthert L, Blaser P (2004) Solution chemistry in acid forest soils: Are the BC:Al ratios as critical as expected in Switzerland? J. Plant Nutr. Soil Sci. 167: 160–168.

Grennfelt P, Thörnelöf E (eds), (1992), Critical Loads for Nitrogen – a workshop report, Workshop held under the LRTAP Convention (UNECE) in Lökeberg, Sweden 1992, Nordic Council of Ministers, Copenhagen, Nord 1992:41. 428 pp.

Groenenberg JE, Romkens P, Comans RNJ, Luster J, Pampura T, Shotbolt L, Tipping E, De Vries W (2010) Transfer functions for solid-solution partitioning of cadmium, copper, nickel, lead and zinc in soils: derivation of relationships for free metal ion activities and validation with independent data. European Journal of Soil Science 61: 58–73.

Groenenberg JE, Tipping E, Bonten LTC, De Vries W (2015) Dynamic geochemical models to assess deposition impacts of metals for soils and surface waters Chapter 9 in: De Vries W, Hettelingh J-P, Posch M (eds) Critical Loads and Dynamic Risk Assessments of Nitrogen, Acidity and Metals for Terrestrial and Aquatic Ecosystems. Springer, pp. 253–268.

Gunn J, Trudgill ST (1982) Carbon dioxide production and concentrations in the soil atmosphere: a case study from New Zealand volcanic ash soils. Catena 9: 81–94.

Häkanson L, Nilsson A, Andersson T (1988) Mercury in fish in Swedish lakes. Environmental Pollution 49: 145–162.

Hall J, Ashmore M, Curtis C, Doherty C, Langan S, Skeffington R (2001) UN/ECE expert workshop: Chemical criteria and critical limits. In: Posch et al. (2001) op. cit., pp. 67–71.

Hall J, Bull K, Bradley I, Curtis C, Freer-Smith P, Hornung M, Howard D, Langan S, Loveland P, Reynolds B, Ullyett J, Warr T (1998) Status of UK critical loads and exceedances. Part 1: Critical loads and critical load maps. Report prepared under DETR/NERC Contract EPG1/3/116. http://critloads.ceh.ac.uk

Hall J, Ullyett J, Heywood E, Broughton R, Fawehinmi J & UK experts (2003) Status of UK critical loads: critical loads methods, data and maps. Report prepared under Defra/NERC contract EpG 1/3/185. http://critloads.ceh.ac.uk

Hall J, Davies C, Moss D (2003) Harmonisation of ecosystem definitions using the EUNIS habitat classification. In Achermann B, Bobbink R (eds) Empirical critical loads for nitrogen. Expert workshop, Berne, 11-13 November 2002, Swiss Agency for the Environment, Forests and Landscape (SAEFL), Bern, Switzerland. pp. 171–195.

Harmens H, Fischer R, Forsius M, Hettelingh J-P., Holen S, Le Gall A C, Lorenz M, Lundin L, Mills G, Moldan F, Posch M, Seifert I, Skjelkvåle BL, Slootweg J, Wright RF (2013) Benefits of air pollution control for biodiversity and ecosystem services. Report by the Working Group on Effects. Working Group on Effects, Convention on Long-range Transboundary Air Pollution, 48 pp.

Henriksen A (1984) Changes in base cation concentrations due to freshwater acidification. Verh. Internat. Verein. Limnol. 22: 692–698.

Henriksen A, Dillon PJ (2001) Critical load of acidity in south-central Ontario, Canada: I. Application of the Steady-State Water Chemistry (SSWC) model. Acid Rain Research Report 52/01, Norwegian Institute for Water Research, Oslo, Norway, 31 pp.

Henriksen A, Posch M (2001) Steady-state models for calculating critical loads of acidity for surface waters. Water, Air and Soil Pollution: Focus 1: 375–398.

Henriksen A, Dillon PJ, Aherne J (2002) Critical loads of acidity for surface waters in south-central Ontario, Canada: Regional applications of the Steady-State Water Chemistry (SSWC) model. Canadian Journal of Fisheries and Aquatic Sciences 59: 1287–1295.

Henriksen A, Lien L, Traaen TS, Sevaldrud IS, Brakke DF (1988) Lake acidification in Norway – Present and predicted chemical status. Ambio 17: 259–266.

Henriksen A, Lien L, Rosseland BO, Traaen TS, Sevaldrud IS (1989) Lake acidification in Norway – Present and predicted fish status. Ambio 18: 314–321.

Henriksen A, Kämäri J, Posch M, Wilander A (1992) Critical loads of acidity: Nordic surface waters. Ambio 21: 356–363.

Henriksen A, Forsius M, Kämäri J, Posch M, Wilander A (1993) Exceedance of critical loads for lakes in Finland, Norway and Sweden: Reduction requirements for nitrogen and sulfur deposition. Acid Rain Research Report 32/1993, Norwegian Institute for Water Research, Oslo, Norway, 46 pp.

Henriksen A, Posch M, Hultberg H, Lien L (1995) Critical loads of acidity for surface waters – Can the ANClimit be considered variable? Water, Air and Soil Pollution 85: 2419–2424.

Hettelingh J-P, Slootweg J, Posch M, Dutchak S, Ilyin I (2002) Preliminary modelling and mapping of critical loads of cadmium and lead in Europe. Report 259101011, CCE & EMEP MSC-East, RIVM, Bilthoven, The Netherlands, 127 pp.

Hettelingh J-P, Posch M, Slootweg J (2007) Tentatively exploring the likelihood of exceedances: Ensemble assessment of Impacts (EAI) In: Slootweg J, Posch M, Hettelingh J-P (eds): Critical loads of nitrogen and dynamic modelling., Coordination Centre for Effects (CCE), Bilthoven, The Netherlands. pp. 53–58.

Hettelingh J-P, Posch M, Slootweg J (2008) Critical load, dynamic modelling and impact assessment in Europe. CCE Status Report. Coordination Centre for Effects, Netherlands Environmental Assessment Agency, Bilthoven, The Netherlands. Rep. No. ISBN 978-90-6960-211-0, 231 pp.

Hettelingh J-P., Posch M, Slootweg J (eds) (2009) Progress in the modelling of critical thresholds, impacts to plant species diversity and ecosystem services in Europe: CCE Status Report 2009, Coordination Center for Effects (CCE) Bitlhoven, The Netherlands. 130 pp.

Hettelingh J-P, Stevens CJ, Posch M, Bobbink R, De Vries W, (2015a). Assessing the impacts of nitrogen deposition on indicator values of plant species in Europe. Chapter 23 in: De Vries W, Hettelingh J-P, Posch M (eds) Critical Loads and Dynamic Risk Assessments of Nitrogen, Acidity and Metals for Terrestrial and Aquatic Ecosystems. Springer, pp. 573–586.

Hettelingh J-P, Posch M, Slootweg J, Reinds GJ, De Vries W, Le Gall A-C, Maas R (2015b) Effects-based integrated assessment modelling for the support of European air pollution abatement policies. Chapter 25 in: De Vries W, Hettelingh J-P, Posch M (eds) Critical Loads and Dynamic Risk Assessments of Nitrogen, Acidity and Metals for Terrestrial and Aquatic Ecosystems. Springer, pp. 613–635.

Hettelingh J-P, Schütze G, De Vries W, Denier van der Gon H, Ilyin I, Reinds GJ, Slootweg J, Travnikov O (2015c) Critical loads of cadmium, lead and mercury and their exceedances in Europe, Chapter 21 in: De Vries W, Hettelingh J-P, Posch M (eds) Critical Loads and Dynamic Risk Assessments of Nitrogen, Acidity and Metals for Terrestrial and Aquatic Ecosystems. Springer, pp. 523–546.

Hindar A, Larssen T (2005) Modification of ANC and critical load computations taking into account strong organic acids. NIVA-Report 5030-2005, Norwegian Institute for Water Research, Oslo, 38 pp. (in Norwegian).

Hindar A, Posch M, Henriksen A (2001) Effects of in-lake retention of nitrogen on critical load calculations. Water, Air and Soil Pollution 130: 1403–1408.

Hindar A, Posch M, Henriksen A, Gunn J, Snucins E (2000) Development and application of the FAB model to calculate critical loads of S and N for lakes in the Killarney Provincial Park (Ontario, Canada) Report SNO 4202–2000, Norwegian Institute for Water Research, Oslo, Norway, 40 pp.

Höhle, J., Wellbrock N. (2017) Background paper – Immobilisation of nitrogen: Literature review and analysis of German, French and Swiss soil data, Report from the Thünen Institute of Forest Ecosystems, Germany. 20 pp.

Hornung M, Roda F, Langan SJ (eds) (1990) A review of small catchment studies in Western Europe producing hydrochemical budgets. Air Pollution Research Report 28. Commission of the European Communities. Brussels. ISBN 2-87263-040-6.

Hornung M, Bull KR, Cresser M, Hall J, Langan SJ, Loveland P, Smith C (1995) An empirical map of critical loads of acidity for soils in Great Britain. Environmental Pollution 90: 301–310.

Hornung M, Sutton MA, Wilson RB (eds) (1995) Mapping and Modelling of Critical Loads for Nitrogen: A Workshop Report. Proceedings of the Grange-over-Sands Workshop 24–26 October 1994. Institute for Terrestrial Ecology, United Kingdom, 207 pp.

Ilyin I, Ryaboshapko A, Afinogenova O, Berg T, Hjellbrekke AG (2001) Evaluation of transboundary transport of heavy metals in1999. Trend analysis. EMEP Report 3/2001, EMEP Meteorological Synthesizing Centre – East, Moscow.

Jacobsen C, Rademacher P, Meesenburg H, Meiwes KJ (2002) Gehalte chemischer Elemente in Baumkompartimenten, Niedersächsische Forstliche

Versuchsanstalt Göttingen, im Auftrag des Bundesministeriums für Verbraucherschutz, Ernährung und Landwirtschaft (BMVEL), Bonn, 80 pp.

Jenny, H. (1965): Bodenstickstoff und seine Abhängigkeit von Zustandsfaktoren. Zeitschrift für Pflanzenernährung, Düngung, Bodenkunde Band 109, Heft 2: 97–112.

Johansson M, Tarvainen T (1997) Estimation of weathering rates for critical load calculations in Finland. Environmental Geology 29(3/4): 158–164.

Johnson DW (1984) Sulfur cycling in forests. Biogeochemistry 1: 29–43.

Johnson DW, Cole DW, Gessel SP (1979) Acid precipitation and soil sulfate adsorption properties in a tropical and in a temperate forest soil. Biotropica 11: 38–42.

Johnson DW, Henderson GS, Huff DD, Lindberg SE, Richter DD, Shriner DS, Todd DE, Turner J (1982) Cycling of organic and inorganic sulphur in a chestnut oak forest. Oecologia 54: 141–148.

Joki-Heiskala P, Johansson M, Holmberg M, Mattson T, Forsius M, Kortelainen P, Hallin L (2003) Long-term base cation balances of forest mineral soils in Finland. Water, Air and Soil Pollution 150: 255–273.

Kaste Ø, Dillon PJ (2003) Inorganic nitrogen retention in acid-sensitive lakes in southern Norway and southern Ontario, Canada – a comparison of mass balance data with and empirical N retention model. Hydrological Processes 17: 2393–2407.

Kelly CA, Rudd JWM, Hesslein RH, Schindler DW, Dillon PJ, Driscoll CT, Gherini SA, Hecky RE (1987) Prediction of biological acid neutralization in acid-sensitive lakes. Biogeochemistry 3: 129–140.

Kimmins JP, Binkley D, Chatarpaul L, De Catanzaro J (1985) Biogeochemistry of temperate forest ecosystems: Literature on inventories and dynamics of biomass and nutrients. Information Report PI-X47E/F, Petawawa National Forestry Institute, Canada, 227 pp.

Larssen T, Høgåsen T (2003) Critical loads and critical load exceedances in Norway (in Norwegian with English Appendix) NIVA Report 4722-2003, Norwegian Institute for Water Research, Oslo, Norway, 23 pp.

Latour JB, Reiling R (1993) A multiple stress model for vegetation ("MOVE"): a tool for scenario studies and standard-setting. Science of The Total Environment, 134, Supplement, 1513–1526.

Latour JB, Reiling R, Slooff W (1994) Ecological Standards for Eutrophication and Desiccation – Perspectives for a Risk Assessment. Water Air and Soil Pollution, 78(3-4): 265–277.

Lichter, J. (1998) Rates of weathering and chemical depletion in soils across a chronosequence of Lake Michigan sand dunes. Geoderma 85: 255–282.

Lien L, Raddum GG, Fjellheim A, Henriksen A (1996) A critical limit for acid neutralizing capacity in Norwegian surface waters, based on new analyses of fish and invertebrate responses. The Science of the Total Environment 177: 173–193.

Lindsay WL (1979) Chemical Equilibria in Soils. Wiley, Chichester, New York.

Lofts S, Spurgeon DJ, Svendsen C, Tipping E (2003) Deriving soil critical limits for Cu, Zn, Cd and Pb: a method based on free ion concentration, Environmental Science and Technology, 38, 3623–3631.

Lydersen E, Larssen T, Fjeld E (2004) The influence of total organic carbon (TOC) on the relationship between acid neutralizing capacity (ANC) and fish status in Norwegian lakes. The Science of the Total Environment 326: 63–6.

Lyman, J. & Fleming, R.H. (1940). Composition of sea water. Journal of Marine Research 3: 134-146.

Mayer P, Brang P, Dobbertin M, Hallenbarter D, Renaud J-P, Walthert L, Zimmermann S (2005) Forest storm damage is more frequent on acidic soils. Ann. For. Sci. 62: 303–311.

Meili M (1991a) The coupling of mercury and organic matter in the biogeochemical cycle – towards a mechanistic model for the boreal forest zone. Water, Air and Soil Pollution 56: 333–347.

Meili M (1991b) Mercury in boreal forest lake ecosystems. Acta Universitatis Upsaliensis 336, Chapter 8.

Meili M (1994) Aqueous and biotic mercury concentrations in boreal lakes: model predictions and observations. In: CJ Watras and JW Huckabee (eds) Mercury Pollution: Integration and Synthesis. CRC Press, Lewis Publishers Inc., Boca Raton FL, Chapter I.8, pp. 99–106.

Meili M (1997) Mercury in lakes and rivers. Metal Ions in Biological Systems 34: 21–51.

Meili M, Malm O, Guimarães JRD, Forsberg BR, Padovani CR (1996a) Mercury concentrations in tropical (Amazon) and boreal freshwater fish: natural spatial variability and pollution effects. 4th International Conference on Mercury as a Global Pollutant, Hamburg, Germany, 4–8 Aug. 1996. Book of Abstracts, GkSs, p. 403.

Meili M, Bishop K, Bringmark L, Johansson K, Munthe J, Sverdrup H, De Vries W (2003a) Critical levels of atmospheric pollution: criteria and concepts for operational modelling of mercury in forest and lake ecosystems. The Science of the Total Environment 304: 83–106.

Meili M, Åkerblom S, Bringmark L, Johansson K, Munthe J (2003b) Critical loads and limits of heavy metals in ecosystems: Some Swedish contributions to European modelling efforts, Background document presented at the Editorial Meeting of the Expert Panel on Critical Loads of Heavy Metals under UNECE-CLRTAP-ICP Modelling and Mapping, Paris, 9–10 April 2003, 22 pp.

Michalzik B, Kalbitz K, Park JH, Solinger S, Matzner E (2001) Fluxes and concentrations of dissolved organic carbon and nitrogen – a synthesis for temperate forests. Biogeochemistry 52: 173–205.

Moiseenko T (1994) Acidification and critical load in surface waters: Kola, Northern Russia. Ambio 23: 418–424.

Monteith JL, Unsworth M (1990) Principles of Environmental Physics (2nd edition) Arnold, London, 291 pp.

Moss D (2008) EUNIS habitat classification – a guide for users. European Environment Agency, European topic centre for biological diversity 27 pp.

Mulder J, Stein A (1994) The solubility of aluminum in acidic forest soils: long-term changes due to acid deposition. Geochimica et Cosmochimica Acta 58: 85–94.

Nagel H-D, Gregor H-D (eds) (1999) Ökologische Belastungsgrenzen – Critical Loads & Levels (in German) Springer, Berlin, 259 pp.

Nagel H-D, Becker R, Eitner H, Kunze F, Schlutow A, Schütze G (2000) Kartierung von Critical Loads für den Eintrag von Säure und eutrophierenden Stickstoff in Waldökosysteme und naturnahe waldfreie Ökosysteme zur Unterstützung von UNECE-Protokollen, Abschlussbericht zum Forschungsprojekt 297 73 011 im Auftrag des Umweltbundesamtes Berlin.

Nagel H-D, Schlutow A, Scheuschner T (2012) National report: Germany. In: Posch M, Slootweg J, Hettelingh J-P (eds): Modelling and mapping of atmospherically-induced ecosystem impacts in Europe. CCE Status Reports, cCe, Bilthoven, The Netherlands. pp. 81–88.

NEG/ECP (2001) Protocol for Assessment and Mapping of Forest Sensitivity to Atmospheric S and N Deposition, prepared by the NEG/ECP Forest Mapping Group, New England Governors/Eastern Canadian Premiers, 'Acid Rain Action Plan 2001, Action Item 4: Forest Mapping Research Project', 79 pp.

Nilsson J, Grennfelt P (1988) Critical loads for sulphur and nitrogen. Nordic council of Ministers, Report from a workshop held at Skokloster, Sweden, 19–24 March 1988. Miljorapport 15. 418 pp.

Oliver BG, Thurman EM, Malcolm RL (1983) The contribution of humic substances to the acidity of colored natural waters. Geochimica et Cosmochimica Acta 47: 2031–2035.

Olson, J. (1958). Rates of Succession and Soil Changes on Southern Lake Michigan Sand Dunes. Botanical Gazette, 119(3): 125–170. Retrieved from http://www.jstor.org/stable/2473440

Olsson M, Rosén K, Melekrud P-A (1993) Regional modelling of base cation losses from Swedish forest soils due to whole-tree harvesting. Applied Geochemistry, Suppl. Issue No.2, pp. 189–194.

Ouimet R, Arp PA, Watmough SA, Aherne J, Demerchant I (2006) Determination and mapping critical loads of acidity and exceedances for upland forest soils in Eastern Canada. Water, Air, and Soil Pollution 172: 57–66.

Paces T (1983) Rate constants of dissolution derived from the measurements of mass balance in hydrological catchments. Geochimica et Cosmochimica Acta 47: 1855–1863.

Phelan, J., Belyazid, S., Kurz, D., Guthrie, S., Cajka, J., Sverdrup, H., Waite, R., (2014). Estimation of soil base cation weathering rates with the PROFILE model to determine critical loads of acidity for forested ecosystems in Pennsylvania, USA; Pilot application of a potential National methodology. Water, Air and Soil Pollution, 225: 2109–2128. DOI 10.1007/s11270-014-2109-4.

Posch M (2000) Critical loads of acidity: Possible modifications. In: M Holmberg (ed) Critical Loads Calculations: Developments and Tentative Applications. TemaNord 2000:566, Nordic Council of Ministers, Copenhagen, pp.8–19.

Posch M, Reinds GJ (2005) The European Background database. In Posch M, Slootweg J, Hettelingh J-P (eds): European Critical loads and Dynamic Modelling: CCE status report 2005, Coordination Centre for Effects (CCE) Bitlhoven, The Netherlands. pp. 63–70.

Posch M, Kurz D (2007). A2M – A program to compute all possible mineral modes from geochemical analyses. Computers & Geosciences 33: 563–572; DOI: 10.1016/j.cageo.2006.08.007

Posch M, Forsius M, Kämäri J (1993) Critical loads of sulfur and nitrogen for lakes I: Model description and estimation of uncertainty. Water, Air and Soil Pollution 66: 173–192.

Posch M, Hettelingh J-P, Sverdrup HU, Bull K, De Vries W (1993) Guidelines for the computation and mapping of critical loads and exceedances of sulphur and nitrogen in Europe. In: RJ Downing, J-P Hettelingh, PAM de Smet (eds) Calculation and Mapping of Critical Loads in Europe. CCE Status Report 1993, RIVM Report 259101003, Bilthoven, The Netherlands, pp. 25–38.

Posch M, Kämäri J, Forsius M, Henriksen A, Wilander A (1997) Exceedance of critical loads for lakes in Finland, Norway and Sweden: Reduction requirements for acidifying nitrogen and sulfur deposition. Environmental Management 21(2): 291–304.

Posch M, De Smet PAM, Hettelingh J-P, Downing RJ (eds) (2001) Modelling and Mapping of Critical Thresholds in Europe. CCE Status Report 2001, RIVM Report 259101010, Bilthoven, Netherlands, iv+188 pp. See also http://wge-cce.org/

Posch M, Hettelingh J-P, Slootweg J (eds) (2003a) Manual for dynamic modelling of soil response to atmospheric deposition. RIVM Report 259101012, Bilthoven, The Netherlands, 69 pp. See also http://wge-cce.org/

Posch M, Reinds GJ, Slootweg J (2003b) The European background database. In: M Posch, J-P Hettelingh, J Slootweg, RJ Downing (eds) Modelling and Mapping of Critical Thresholds in Europe. CCE Status Report 2003, RIVM Report 259101013, Bilthoven, The Netherlands, pp. 37–44. See also http://wge-cce.org/

Posch M, Slootweg J, Hettelingh J-P (eds) (2011) Modelling critical thresholds and temporal changes of geochemistry and vegetation diversity. CCE Status Report 2011, Bilthoven, The Netherlands. 186 pp.

Posch M, Slootweg J, Hettelingh J-P (eds) (2012a) Modelling and mapping of atmospherically-induced ecosystem impacts in Europe. CCE Status Report 2012, Bilthoven, The Netherlands, 144 pp.

Posch M, Aherne J, Forsius M, Rask M (2012b). Past, present, and future exceedance of critical loads of acidity for surface waters in Finland. Environmental Science & Technology 46: 4507–4514.

Posch M, De Vries W, Sverdrup HU (2015) Mass balance models to derive critical loads of nitrogen and acidity for terrestrial and aquatic ecosystems. Chapter 6 in: De Vries W, Hettelingh J-P, Posch M (eds) *Critical Loads and Dynamic Risk Assessments of Nitrogen, Acidity and Metals for Terrestrial and Aquatic Ecosystems*. Springer, pp. 171–205.

Probst A, Mansat A, Gaudio N (2012) National report: France. In: Posch M, Slootweg J, Hettelingh J-P (eds): Modelling and mapping of atmospherically-induced ecosystem impacts in Europe. CCE Status Reports 2012, Bilthoven, The Netherlands. pp. 73–80.

Probst A, Rizzetto S, Gaudio N, Mansat A (2014) French National Focal Centre report. In: Slootweg J, Posch M, Hettelingh J-P, Mathijssen L (eds) Modelling and Mapping the impacts of atmospheric deposition on plant species diversity in Europe, CCE Status Report 2014, Bilthoven, The Netherlands, pp 73–86.

Probst A, Obeidy C, Gaudio N, Belyazid S, Gégout J-C, Alard D, Corket E, Party J-P, Gauquelin T, Mansat A, Nihlgård B, Leguédois S, Sverdrup H (2015) Evaluation of plant-responses to atmospheric nitrogen deposition in France using integrated soil-vegetation models. Chapter 12 in: De Vries W, Hettelingh J-P, Posch M (eds) *Critical Loads and Dynamic Risk Assessments of Nitrogen, Acidity and Metals for Terrestrial and Aquatic Ecosystems*. Springer, pp. 327–358.

Puhe J and Ulrich B (2001) Global Climate Change and Human Impacts on Forest Ecosystems. Ecological Studies 143, Berlin, Heidelberg, Springer. 592 pp.

Reinds GJ, Posch M, De Vries W (2001) A semi-empirical dynamic soil acidification model for use in spatially explicit integrated assessment models for Europe. Alterra Report 084, Alterra Green World Research, Wageningen, The Netherlands, 55 pp.

Reinds GJ (2007) Background database for computing critical loads for the EECCA countries, Turkey and Cyprus. In: Slootweg J, Posch M, Hettelingh J-P (eds) Critical loads of nitrogen and dynamic modelling. CCE Progress Report 2007 CCE, Bilthoven, The Netherlands, pp. 89–102.

Reinds GJ, Bonten L, Mol-Dijkstra JP, Wamelink GWW, Goedhart P (2012) Combined effects of air pollution and climate change on species diversity in Europe: First assessments with VSD+ linked to vegetation models. In: Posch M, Slootweg J, Hettelingh J-P (eds): Modelling and mapping of atmospherically-induced ecosystem impacts in Europe. CCE Status Report 2012, Bilthoven, The Netherlands, pp. 49–62.

Reinds GJ, Thomas D, Posch M, Slootweg J (2021) Critical loads for eutrophication and acidification for European terrestrial ecosystems. Final report. CCE, UBA, Dessau-Roßlau, Germany.

Resolution of 20 April 2012 (2012) Our life insurance, our natural capital: an EU biodiversity strategy to 2020. European Parliament, 2011/2307(INI).

Reuss JO (1983) Implications of the calcium-aluminum exchange system for the effect of acid precipitation on soils. Journal of Environmental Quality 12(4): 591–595.

Reuss JO, Johnson DW (1986) Acid Deposition and the Acidification of Soils and Waters. Ecological Studies 59, Springer, New York, 119 pp.

Römkens PFAM, Groenenberg JE, Bril J, De Vries W (2001) Derivation of partition relationships to calculate Cd, Cu, Pb, Ni and Zn solubility and activity in soil solutions: an overview of experimental results. Summary of an Alterra Report.

Rosén K (1990) The critical load of nitrogen to Swedish forest ecosystems. Department of Forest Soils, Swedish University of Agricultural Sciences, Uppsala, Sweden, 15 pp.

Rosén K, Gundersen P, Tegnhammar L, Johansson M, Frogner T (1992) Nitrogen enrichment in Nordic forest ecosystems – The concept of critical loads. Ambio 21: 364–368.

Rowe E, Emmett BA, Smart SM (2009) A single metric for defining biodiversity damage using Habitat Directive criteria. In: Hettelingh J-P, Posch M, Slootweg J (eds) Progress in the modelling of critical thresholds, impacts to plant species diversity and ecosystem services in Europe. CCE Status Report 2009 CCE, Bitlhoven, The Netherlands. pp. 101–107.

Ryaboshapko A, Ilyin I, Gusev A, Afinogenova O, Berg T, Hjellbrekke AG 1999: Monitoring and modelling of lead, cadmium and mercury transboundary transport in the atmosphere of Europe. EMEP Report 3/99, Meteorological Synthesizing Centre – East, Moscow.

Santore RC, Driscoll CT, Aloi M (1995) A model of soil organic matter and its function in temperate forest soil development. In: WW McFee, JM Kelly (eds) Carbon Forms and Functions in Forest Soils. Soil Science Society of America, Madison, Wisconsin, pp. 275–298.

Sauvé S, McBride M, Hendershot W et al. (1998) Soil solution speciation of lead(II): effects of organic matter and pH Soil Sci. Soc. Am. J., 62, 618–621.

Sauvé S, Norvell W, McBride, Hendershop W (2000) Speciation and complexation of cadmium in extracted soil solutions Environ. Sci. Technol., 34, 291–296.

Schlutow A, Huebener P (2003) The BERN model: Bioindicator for ecosystem regeneration within natural conditions. In: Achermann B, Bobbink R (eds) Empirical critical loads for nitrogen, expert workshop, Berne, 11–13 November 2002, Swiss Agency for the Environment, Forests and Landscape (SAEFL), Berne, Switzerland, pp 305–314.

Schlutow A, Dirnböck T, Pecka T, Scheuschner T (2015) Use of an empirical model approach for modelling trends of ecological sustainability. Chapter 14 in: De Vries W, Hettelingh J-P, Posch M (eds) *Critical Loads and Dynamic Risk Assessments of Nitrogen, Acidity and Metals for Terrestrial and Aquatic Ecosystems*. Springer, pp. 381–400.

Schütze G, Nagel H-D (1998) Kriterien für die Erarbeitung von Immissionsminderungszielen zum Schutz der Böden und Abschätzung der langfristigen räumlichen Auswirkungen anthropogener Stoffeinträge auf die Bodenfunktionen, Abschlußbericht UBA-FKZ 104 02 825, in UBA-Texte 19/98, Umweltbundesamt, Berlin.

Schütze G, Lorenz U, Spranger T (2003) Expert meeting on critical limits for heavy metals and methods for their application, 2–4 December 2002 in Berlin, Proceedings, UBA Texte 47/2003, Umweltbundesamt, Berlin.

SEPA (2000) Environmental quality criteria: lakes and running waters. Swedish Environmental Protection Agency, Report 5050, 102 pp.

Skjelkvåle BL, Ulstein M (2002) Proceedings from the workshop on heavy metals (Pb, Cd, Hg) in surface waters: Monitoring and biological impact. 18–20 March 2002, Lillehammer, Norway, ICP Waters Report 67/2002, Norwegian Institute for Water Research, NIVA, Oslo.

Skyllberg U, Qian J, Frech W, Xia K, Bleam WF, (2003) Distribution of mercury, methyl mercury and organic sulphur species in soil, soil solution and stream of a boreal forest catchment. Biogeochemistry 64: 53–76.

Slootweg J, Posch M, Hettelingh J-P (2008) Summary of national data. In: Hettelingh J-P, Posch M, Slootweg J (eds) Critical load, dynamic modelling and impact assessment in Europe. CCE Status Report 2008, PBL Netherlands Environmental Assessment Agency, Bilthoven, The Netherlands, pp. 29–50.

Slootweg J, Posch M, Warrink A (2009) Status of the harmonised European land cover map. In: J-P Hettelingh, Posch M, Slootweg J (eds) Progress in the modelling of critical thresholds, impacts to plant species diversity and ecosystem services in Europe. CCE Status Report 2009CCE. Bitlhoven, The Netherlands. pp. 31–34.

Slootweg J, Posch M, Hettelingh J-P (eds) (2010) Progress in the modelling of critical thresholds and dynamic modelling, including impacts on vegetation in Europe. CCE Status Report 2010, Bilthoven, The Netherlands, 182 pp.

Slootweg J, Posch M, Hettelingh J-P (2011) Summary of national data. In: Posch M, Slootweg J, Hettelingh J-P (eds) Modelling critical thresholds and temporal changes of geochemistry and vegetation diversity. CCE Status Report 2011, Bilthoven, Netherlands, pp. 29–42.

Slootweg J, Posch M, Hettelingh J-P, Mathijssen L (eds) (2014) Modelling and Mapping the impacts of atmospheric deposition on plant species diversity in Europe, CCE Status Report 2014. RIVM Report 2014-0075, ISBN 978-90-6960-276-9, https://www.umweltbundesamt.de/en/cce-status-reports?parent=68093.

Smart SM, Scott WA, Whitaker J, Hill MO, Roy DB, Critchley CN, Marini L, Evans C, Emmett BA, Rowe EC, Crowe A, Le Duc M, Marrs RH (2010) Empirical realised niche models for British higher and lower plants – development and preliminary testing. Journal of Vegetation Science 21(4): 643–656.

Steenvorden J (1984) Influence of changes in water management on water quality (in Dutch) Report 1554, Institute for Land and Water Management, Wageningen, The Netherlands.

Sutton MA, Howard CM, Erisman JW, Billen G, Bleeker A, Grennfelt P, Van Grinsven HJM, Grizzetti B, (eds) (2011) The European Nitrogen Assessment: Sources, Effects and Policy Perspectives. Cambridge University Press, Cambridge, UK, 612 pp.

Sverdrup H (1990) The Kinetics of Base Cation Release due to Chemical Weathering. Lund University Press, Lund, Sweden, 246 pp.

Sverdrup H, Warfvinge P (1988a) Weathering of primary silicate minerals in the natural soil environment in relation to a chemical weathering model. Water, Air and Soil Pollution 38: 387–408.

Sverdrup, H., Warfvinge, P. (1988b) Assesment of critical loads of acid deposition on forest soils, In: Critical loads for sulphur and nitrogen, Nilsson, J. and Grennfelt, P. (Eds) Nordic Council of Ministers and The United Nations Economic Commission for Europe (ECE), Stockholm Nordic Council of Ministers Miljorapport 1988:15:81–130.

Sverdrup, H., Warfvinge, P. (1988c). Chemical weathering of minerals in the Gårdsjon catchment in relation to a model based on laboratory rate coefficients. In: Critical loads for sulphur and nitrogen, Nilsson, J. and Grennfelt, P. (Eds) Nordic Council of Ministers and The United Nations Economic Commission for Europe (UN/ECE). Stockholm, Nordic Council of Ministers Miljörapport 1988:15:131–150.

Sverdrup, H. and Warfvinge, P. (1992). PROFILE-A mechanistic geochemical model for calculation of field weathering rates. In: Kharka, Y. and Maest, A. (Eds.), Proceedings of the 7th International Symposium on water-rock interaction, Utah, 13–19 July 1992, 44–48. Balkemaa Publishers.

Sverdrup H, Ineson P (1993) Kinetics of denitrification in forest soils. Compuscript, 18 pp.

Sverdrup H, Warfvinge P (1993a) The effect of soil acidification on the growth of trees, grass and herbs as expressed by the (Ca+Mg+K)/Al ratio. Reports in Ecology and Environmental Engineering 2, Lund University, Lund, Sweden, 177 pp.

Sverdrup, H., Warfvinge, P. (1993b). Calculating field weathering rates using a mechanistic geochemical model-PROFILE. Journal of Applied Geochemistry, 8:273–283.

Sverdrup H, De Vries W (1994) Calculating critical loads for acidity with the simple mass balance method. Water, Air and Soil Pollution 72: 143–162.

Sverdrup, H. and Warfvinge, P., (1995). Estimating field weathering rates using laboratory kinetics. In: White, A.F., Brantley, S.L., (Eds.), Chemical weathering rates of silicate minerals. Mineralogical Society of America, Washington DC. *Reviews in Mineralogy*, 31:485–541.

Sverdrup H, De Vries W, Henriksen A (1990) Mapping Critical Loads. Environmental Report 1990:14 (NORD 1990:98), Nordic Council of Ministers, Copenhagen, 124 pp.

Sverdrup, H.U., Johnson, M.W. & Fleming, R.H. (1946). The Oceans – Their Physics, Chemistry and General Biology. New York: Prentice-Hall, 1087 pp.

Sverdrup H, Belyazid S, Nihlgard B, Ericson L (2007) Modelling change in ground vegetation response to acid and nitrogen pollution, climate change and forest management in Sweden 1500-2100 A.D. Water Air & Soil Pollution: Focus 7(1-3): 163–179.

Technical Guidance Document on Risk Assessment in support of Commission Regulation (EC) No 1488/94 on Risk Assessment for existing substances, TGD European Chemicals Bureau, Institute for Health and Consumer Protection, European Commission Joint Research Centre.

Tipping E (1994) WHAM – A chemical equilibrium model and computer code for waters, sediments, and soils incorporating a discrete site/electrostatic model of ion-binding by humic substances. Computers & Geosciences 20(6): 973–1023.

Tipping E (1998) Humic ion-binding Model IV: an improved description of the interactions of protons and metal ions with humic substances. Aquatic Geochemistry 4: 3–48.

Tipping E, Lofts S, Smith EJ, Shotbolt L, Ashmore MR, Spurgeon D, Svendsen C (2003a) Information and proposed methodology for determining critical loads of cadmium and lead; a UK contribution. Backround document presented at the Editorial Meeting of the Expert Panel on Critical Loads of Heavy Metals under ICP Modelling and Mapping, Paris, 9–10 April 2003.

Tipping E, Rieuwerts J, Pan G, Ashmore MR, Lofts S, Hill MTR, Farrago ME, Thornton I (2003b) The solid-solution partitioning of heavy metals (Cu, Zn, Cd, Pb) in upland soils of England and Wales. Environmental Pollution 125: 213–225.

UBA (1996) Manual on Methodologies and Criteria for Mapping Critical Levels/Loads and Geographical Areas where they are exceeded. UNECE Convention on Long-range Transboundary Air Pollution, Federal Environmental Agency, Berlin.

Ulrich B (1981) Ökologische Gruppierung von Böden nach ihrem chemischen Bodenzustand. *Zeitschrift für Pflanzenernährung und Bodenkunde* 144: 289–305.

Ulrich B, Sumner ME (eds) (1991) Soil Acidity. Springer, Berlin, 224 pp.

UNECE (1995) Calculation of critical loads of nitrogen as a nutrient. Summary report on the development of a library of default values. Document EB.AIR/WG.1/R.108, United Nations Economic Commission for Europe, Geneva, 7 pp.

UNECE (2001) Workshop on chemical criteria and critical limits. Document EB.AIR/WG.1/2001/13, United Nations Economic Commission for Europe, Geneva, 8 pp.

Utermann J, Duewel O, Gaebler H-E, Hindel R (2000) Beziehung zwischen Totalgehalten und königswasser-extrahierbaren Gehalten von Schwermetallen in Böden. In: Rosenkranz D, Einsele G, Bachmann G, Harreß M (Eds): Handbuch Bodenschutz, Loseblattsammlung, Erich Schmidt-Verlag, Berlin, Kennzahl 1600.

Van Dam D (1990) Atmospheric deposition and nutrient cycling in chalk grassland. PhD Thesis, University of Utrecht, Utrecht, The Netherlands, 119 pp.

Van Dobben H, Posch M, Wamelink GWW, Hettelingh J-P, De Vries W (2015) Plant species diversity indicators for use in the computation of critical loads and dynamic risk assessments. Chapter 3 in: De Vries W, Hettelingh J-P, Posch M (eds) *Critical Loads and Dynamic Risk Assessments of Nitrogen, Acidity and Metals for Terrestrial and Aquatic Ecosystems*. Springer, pp. 59–81.

Van der Salm C, De Vries W (2001) A review of the calculation procedure for critical acid loads for terrestrial ecosystems. The Science of the Total Environment 271: 11–25.

Van der Salm C, Köhlenberg L, De Vries W (1998) Assessment of weathering rates in Dutch loess and river-clay soils at pH 3.5, using laboratory experiments. Geoderma. 85: 41–62.

Van Dobben H, Hettelingh J-P, Wamelink GWW, De Vries W, Slootweg J, Reinds GJ (2010) Plant species diversity indicators for impacts of nitrogen and acidity and methods for their simulation: an oververview. In: Slootweg J, Posch M, Hettelingh J-P (eds): Progress in modelling of critical thresholds and dynamic modelling, including impacts on vegetation in Europe. CCE Status Report 2010, RIVM, Bilthoven, Netherlands, pp. 55–63.

Verta M, Rekolainen S, Mannio J, Surma-Aho K (1986) The origin and level of mercury in Finnish forest lakes. Finnish National Board of Waters, Helsinki, Publications of the Water Research Institute 65: 21–31.

Walther B (1998) Development of a process-based model to derive methane emissions from natural wetlands for climate studies. Dissertation im Fachbereich Geowissenschaften der Universität Hamburg, Examensarbeit Nr. 60, Max-Planck-Institut für Meteorologie, Hamburg.

Wamelink GWW, Van Dobben HF, Berendse F (2009) Vegetation succession as affected by decreasing nitrogen deposition, soil characteristics and site management: A modelling approach. Forest Ecology and Management 258(8): 1762–1773.

Warfvinge P, Sverdrup H (1992a) Calculating critical loads of acid deposition with PROFILE – A steady-state soil chemistry model. Water, Air and Soil Pollution 63: 119–143.

Warfvinge, P., Sverdrup, H. (1992b) Modelling regional mineralogy and weathering rates. In: Y. Kharka and A. Maest (Eds.), *Proceedings of the 7th International Symposium on water-rock interaction*, held in Utah, 13–19 July, 1992, 49–53.

Warfvinge P, Sverdrup H (1995) Critical loads of acidity to Swedish forest soils. Reports in Ecology and Environmental Engineering 5, Lund University, Lund, Sweden, 104 pp.

Weast, R.C., Lide, D.R., Astle, M.J. & Beyer, W.H. (Eds.) (1989). CRC Handbook of Chemistry and Physics (70th edition). Boca Raton, FL, USA: CRC.

Weng LP, Temminghoff EJM, Lofts S, Tipping E, Van Riemsdijk WH (2002) Complexation with dissolved organic matter and solubility control of metals in a sandy soil. Environ. Sci. Technol. 36, 4804–4810

WGE (2013) Guidance document on health and environmental improvements using new knowledge, methods and data. Report to the 32nd Executive Body meeting UN-ECE Convention on Long range Transboundary Air Pollution, Working Group on Effects, Geneva, Switzerland. ECE/EB.AIR/2013/8, 14 p.

WHO (2000) Air Quality Guidelines for Europe, Second Edition. WHO Regional Publications, European Series, No. 91. World Health Organisation, Regional Office for Europe, Copenhagen, 273 pp.

WHO (2004) Guidelines for Drinking Water Quality – Third Edition, Vol. 1 – Recommendations, World Health Organisation, Geneva.

Wilander A (1994) Estimation of background sulphate concentrations in natural surface waters in Sweden. Water Air and Soil Pollution 75: 371–387.

Witkamp M (1966) Decomposition of leaf litter in relation to environment, microflora, and microbial respiration. Ecology 47(2): 194–201.

Wright RF, Lie MC (eds) (2002) Workshop on models for biological recovery from acidification in a changing climate, 9–11 September 2002 in Grimstad, Norway. Acid Rain Research Report 55/02, Norwegian Institute for Water Research (NIVA), Oslo, Norway, 42 pp.

Závodský D, Babiaková G, Mitosinková M, Pukanèiková K, Roneák P, Bodis D, Rapant S, Mindás J, Skvarenina J, Cambel B, Rehák S, Wathne BM, Henriksen A, Sverdrup H, Tørseth K, Semb A, Aamlid D (1995) Mapping critical level/loads for the Slovak Republic. Acid Rain Research Report 37/1995. Norwegian Institute for Water Research (NIVA), Oslo, Norway, 74 pp.

5.9 Annexes

5.9.1 Annex 1: Complementary information on available models

5.9.1.1 Steady state modeling of weathering rates

1988-1995; Warfvinge P. and Sverdrup, H.; The single site version of **PROFILE** model for calculation and mapping of critical loads and rates of field chemical weathering. It is the world's most used soil model, it has been validated and is used operationally in more than 50 countries worldwide. It uses laboratory kinetics and kinetic coefficients to predict field weathering rates. PROFILE remains in operation from its launch 25 years ago and is still the only existing field verified model for chemical weathering of soil minerals under field conditions that demonstrably works and yields verifiable results. Archived. Fortran 77 older source code version available upon request for PC and Apple from Harald Sverdrup (hus@hi.is). Hypercard version no longer operable.

1992-present; Sverdrup, H., Warfvinge, P., Alveteg, M., Walse, C., Kurz, P., Posch, M., Belyazid, S.; **RegionalPROFILE**. A regionalized version of the PROFILE model, used for creating weathering rate maps for soils and catchments across regions and countries, as well as a key tool for critical loads for forest soils. Updated versions available upon request from Salim Belyazid (salim.belyazid@natgeo.su.se) or Dani Kurz (geo-science@bluewin.ch).

2000; Sverdrup, H. and Alveteg, M., **CLAY-PROFILE.** Specialized for volcanic soils and clayey agricultural soils. No longer operable. Archived. Fortran 77 source code available upon request from Harald Sverdrup (hus@hi.is) or Salim Belyazid (salim.belyazid@natgeo.su.se).

5.9.1.2 Dynamic modeling of weathering

1987-2008; Warfvinge P., Sverdrup, H., Alveteg, M., Walse, C., Martinsson, L.: The **SAFE** model and its helper routine **MakeDep**, a generally applicable dynamic soil chemistry and acidification model. Used worldwide for acidification research and critical loads. FORTRAN code. Retired model, replaced by the **ForSAFE** model system. Archived. No longer maintained.

1995-1996; Rietz, F., Sverdrup, H., Warfvinge, P.; **SkogsSAFE**; A long term model for simulating soil genesis and mineralogy dynamics in soils since glaciation (14,000 years ago to the present). FORTRAN code. Source code available upon request from Harald Sverdrup (hus@hi.is) or Salim Belyazid (salim.belyazid@natgeo.su.se).

1996-2004; Sverdrup, H., Wallman P., Belyazid, S., Alveteg, M., Walse, C., Martinsson, L.: Directed the development of **ForSAFE** and **ForSAFE-VEG**, an integrated biogechemical forest ecosystem model for growth, nitrogen, and carbon cycling. FORTRAN code. Published and available from Salim Belyazid (salim.belyazid@natgeo.su.se) or Dani Kurz (geo-science@bluewin.ch)

5.9.1.3 Mineralogy estimation

1990; Sverdrup, H., Melkerud, P. A., Kurz, D.: The **UPPSALA** model for reconstruction of soil mineralogy from soil total analysis data. Very simple model, spreadsheet based. Available upon request from Harald Sverdrup (hus@hi.is).

1998; Sverdrup, H. and Erdogan, B. **Turkey** mineral depletion model (TMD), a simple model for estimating the soil mineralogy from bedrock geology and estimates of soil age. Can be used when the soil was created in-situ over very long time. Not applicable in glaciated areas. Written in STELLA®. Archived, available upon request from Harald Sverdrup (hus@hi.is).

2005-2010; Kurz, D. and Posch, M.; **A2M** ("Analysis to Mineralogy"), A mathematical procedure (not a model!) to derive all possible mineralogies from a total chemical analysis for any pre-

defined set of (potential) minerals. Available upon request from Max Posch (max.posch@rivm.nl) or Dani Kurz (geo-science@bluewin.ch).

5.9.2 Annex 2: Transfer functions for lead and cadmium for the conversion of metal concentrations in different soil phases

Need of transfer functions in deriving critical dissolved metal concentrations

In principle, transfer functions are not needed when performing a critical load calculation. Transfer functions have been used to derive critical limits for free metal ion concentrations from NOEC data, referring to reactive soil metal contents. When applying critical limits for free metal ion concentrations, related to ecotoxicological effects, no transfer function is needed any more, since $[M]_{(sdw)crit}$ can be obtained directly, either by reference to the look up tables or by use of the W6S-MTC2 program (see section 5.5.2.2.3). In case of ground water protection, total dissolved critical concentrations can be used directly (see section 5.5.2.2.2). In the case of using critical limits, referring to the metal content in plants, an empirical relationship can be used to derive the total dissolved critical concentrations in soil solution, at least for *Cd* (See Table 6).

Using the more sophisticated and consistent way to derive soil solution concentrations from critical plant contents does, however, require transfer functions according to the following:

- First derive a critical "pseudo" total soil metal content, by applying soil-plant relationships in the inverse way (derive a critical total soil content from a critical plant content);
- then apply a transfer function relating pseudo-total metal contents to reactive metal contents (Annex 2, eq. A2.3);
- followed by a transfer function relating the free ion metal activity in solution to the reactive metal content (Annex 2, eq. A2.4 or eq. A2.5).

Furthermore, all the transfer functions listed below are needed for the calculation of a critical soil limit (from a given critical limit function for the soil solution) and are also used to compare this to the present soil metal content to assess the critical limit exceedance in the present situation. This requires a map of the present soil metal content in the country. Inversely, one may calculate the present dissolved metal concentration from the present soil metal content, using the transfer functions described below and compare this to the critical limit function for the soil solution (see section 5.5.1.4).

Transfer functions to calculate pseudo-total from total contents of Cd and Pb

In some countries, true total metal concentrations are measured, whereas most or nearly all countries use "pseudo-total" concentrations. Utermann et al. (2000) provided transfer functions to calculate *pseudo-total* contents of heavy metals (here aqua regia extract $[M]_{AR}$) from total contents (here $[M]_{HF}$), according to:

(A2.1)

$$\log_{10}[M]_{AR} = a_0 + a_1 \cdot \log_{10}[M]_{HF}$$

where:

$[M]_{AR}$ = *pseudo-total* content of heavy metal *M* in soil provided as Aqua Regia extraction *(mg kg-1)*

$[M]_{HF}$ = total content of heavy metal *M* in soil, provided as *HF*-extraction *(mg kg-1)*

Values for a_0 and a_i are given in Tables A2.1 and A2.2. The correlations are depending on metal and substrate. In general, total, and *pseudo-total* contents are very similar. For backcalculations

of total contents from *pseudo-total* contents, different functions are to be used (see background document, De Vries et al 2005, Annex 7). These functions are not provided here since those calculations are not needed in the present calculation of critical loads.

Table A2.1: Relationship between cadmium (Cd) content in soils extractable by aqua regia (AR) and total contents in dependence on the parent material.

Parent material	a_0	a_1	n	R^2	range of validity	
					Cd (HF)	(mg kg^{-1})
basic and intermediate igneous rock	0.13	1.41	25	0,94	0,25	1,12
boulder clay	0.09	1.38	26	0.91	0.07	0.39
limestone	-0.15	1.24	25	0.91	0.26	1.86
loess or loessic loam	-0.15	1.26	25	0.91	0.07	0.88
marl stone	-0.05	1.24	25	0.93	0.10	0.98
sand	-0.02	1.26	37	0.89	0.04	0.65
sandy loess	0.29	1.78	36	0.82	0.06	0.29
acid igneous and metamorphic rock	-0.09	1.08	25	0.80	0.09	0.63
quartzitic sand stones and conglomerates	-0.11	1.23	25	0.81	0.07	0.60
clay stone, hard argillaceous and silty slates	-0.05	1.33	25	0.96	0.14	1.88
all parent materials	-0.12	1.19	274	0.91	0.04	1.88

Table A2.2: Relationship between lead (Pb) content in soils extractable by aqua regia (AR) and total contents extractable by HF in dependence on the parent material.

Parent material	a_0	a_1	n	R^2	range of validity	
					Pb (HF)	(mg kg^{-1})
basic and intermediate igneous rock	-0.20	1.11	25	0.97	5.6	113.6
boulder clay	-0.54	1.32	26	0.95	8.3	49.5
limestone	-0.02	0.99	22	0.88	24.8	132.7
loess or loessic loam	-0.42	1.22	24	0.91	15.1	91.8
marl stone	-0.03	0.95	25	0.94	5.5	124.0
sand	-0.54	1.31	49	0.91	2.7	76.7
sandy loess	-0.72	1.46	43	0.97	6.0	75.9
acid igneous and metamorphic rock	-0.84	1.44	25	0.84	14.6	106.1

Parent material	a_0	a_1	n	R^2	range of validity	
					Pb (HF)	(mg kg^{-1})
quartzitic sand stones and conglomerates	-0.55	1.28	25	0.88	12.6	109.2
clay stone, hard argillaceous and silty slates	-0.11	1.05	25	0.98	13.9	270.3
all parent materials	-0.45	1.24	289	0.95	2.7	270.3

Transfer functions to calculate reactive contents from pseudo-total contents of Cd and Pb.

The reactive metal concentration *$[M]_{re}$ (mol kg^{-1})* can be related to the *pseudo-total* concentration extracted with Aqua Regia *$[M]_{AR}$ (mol kg^{-1})* according to:

(A2.3)

$$\log[M]_{re} = ß_0 + ß_1 \cdot \log[M]_{AR} + ß_2 \cdot \log(\%[OM]_s) + ß_3 \cdot \log(\%[clay])$$

Regression relations were derived from a Dutch dataset containing 630 soil samples which were both extracted with *0.43 Mol l^{-1} HNO_3* and Aqua Regia. The dataset consists of a large variety of soil types with a wide variety in soil properties, such as the organic matter and clay content. The dataset comprises both polluted and unpolluted soils. Results are shown in Table A2.3 and suggest that reactive contents typically are more than half of *pseudo-total* contents.

Table A2.3: Relationship between lead (Pb) content in soils extractable by aqua regia (AR) and total contents extractable by HF in dependence on the parent material.

Metal	ß0	ß1	ß2	ß3	R^2	se-yest[1)]
Cd	0.225	1.075	0.006	-0.020	0.82	0.26
Pb	0.063	1.042	0.024	-0.122	0.88	0.17

1) The standard error of the y-estimate on a logarithmic basis

Transfer functions to calculate free Cd and Pb ion concentrations from reactive Cd and Pb contents used in the derivation of critical limits for free Cd and Pb ion concentrations

Critical concentrations of soil metal are frequently higher than ambient soil concentrations. Therefore, a transfer function should, if possible, be calibrated over a range of soil metal concentrations which is the whole range of critical receptor concentrations observed. This is relevant, since the derived critical limit functions are dependent upon the transfer functions.

For calibration of direct transfer functions for *Cd* and *Pb*, data were drawn from four sources:

- Sauvé et al. (1998). Soil metal and labile *Pb* in *Pb*-contaminated soils of various origins. Free *Pb* concentrations were estimated by measurement of labile *Pb* using differential pulse anodic stripping voltammetry (DPASV) and speciation calculations.
- Sauvé et al. (2000). Soil metal and labile *Cd* in *Cd*-contaminated soils of various origins. Free *Cd* concentrations were estimated by measurement of labile *Cd* using differential pulse anodic stripping voltammetry (DPASV) and speciation calculations.
- Weng et al. (2002). Soil metal and free ion concentrations in sandy Dutch soils. Free *Cd* and *Pb* concentrations were estimated by the Donnan membrane technique.

- Tipping et al. (2003a). Soil metal and free ion concentrations in UK upland soils. Free Cd and Pb were estimated by using the WHAM6 speciation model (Tipping, 1998) to speciate the soil solution.

The data were fitted to the following transfer function (termed as c-Q relationship):

(A2.4)

$\log[M]_{free,sdw} = a + b \cdot \log[OM]_s + c \cdot pH_{sdw} + m \cdot \log[M]_{re}$

where:

$[M]_{free,sdw}$ = the free metal ion concentration *(mol l^{-1})*

$[M]_{re}$ = the reactive metal content in the solid phase *(mol l^{-1})*

$[OM]_s$ = organic matter (%)

pH_{sdw} = soil drainage water *pH*

Calculated values of the parameters are given in Table A21.4.

Table A2.4: Values for the regression coefficients for the free ion concentration – reactive metal content relationship (eq. A2.4) and statistical measures R^2 and se(Y) based on results of studies carried out in Canada, the Netherlands, and the UK. Values in brackets are the standard errors for the coefficients.

Metal	a	b $([OM])_s$	c (pH_{sdw})	m $(lOg[M]_{re})$	R^2	se(Y)
Cd	-0.08 (0.65)	-0.60 (0.08)	-0.53 (0.03)	0.60 (0.06)	0.624	0.53
Pb	4.32 (0.49)	-0.69 (0.07)	-1.02 (0.03)	1.05 (0.06)	0.854	0.60

Transfer functions to calculate reactive Cd and Pb contents from free Cd and Pb ion concentrations used in the derivation of critical Cd and Pb contents on suspended particles in aquatic ecosystems

This transfer function (termed as Q-c relationship) has been derived using the same soil data set used to calculate the transfer function relating the free ion to the soil reactive metal (see Table A2.4). The expression for the Q-c relation is:

(A2.5)

$\log[M]_{re} = a + b \cdot \log[OM]_s + c \cdot pH_{sw} + m \cdot \log[M]_{free,sw}$ (A2.5)

where

$[M]_{free,sw}$= the free metal ion concentration in surface water (mol l^{-1})

$[M]_{re}$ = the reactive metal content in the solid phase (mol g^{-1})

$[OM]_s$= organic matter (%), here the organic matter content of the suspended particles

pH_{sw}= the pH of the surface water Calculated values of the parameters are given in Table A2.5.

Use of transfer functions in the manual

The direct transfer function for the calculation of the free ion concentration from the soil reactive metal content (the c-Q relation) is used for the calculation of the *pH*-dependent critical limit functions (see section 5.5.2.2.3), in order to express the endpoint metal dose in toxicity

experiments as the free ion concentration. The transfer function for the calculation of the soil reactive metal content from the free metal ion concentration (the Q-c relation) is used to calculate the critical *SPM*-bound metal ($[M]_{SPM}$ *(crit)*) in surface waters (see section 5.5.2.2.3 and Annex 3).

Table A2.5: Values for the regression coefficients for the reactive metal content – free ion concentration relationship (eq. 8) and statistical measures R^2 and se(Y) based on results of studies carried out in Canada, the Netherlands, and the UK. Values in brackets are the standard errors for the coefficients.

Metal	a	b $([OM])_s$	c (pH_{sdw})	m $(lOg[M]_{free,sw})$	R^2	se(Y)
Cd	-6.42 (0.41)	0.64 (0.07)	0.45 (0.04)	0.58 (0.06)	0.507	0.52
Pb	-5.42 (0.21)	0.55 (0.06)	0.70 (0.03)	0.61 (0.03)	0.698	0.45

5.9.3 Annex 3: Calculation of total metal concentration from free metal ion concentrations using the wham model

The metal in soil drainage water comprises the following metal species:

Metal species	Symbol
Metal free ion M^{2+}	$[M]_{free,sdw}$
Inorganic complexes MOH^+, $MHCO_3$, MCl^+ etc	$[M]_{DIC,sdw}$
Metal bound to *DOM*	$[M]_{DOM,sdw}$
Metal bound to *SPM*	$[M]_{SPM,sdw}$

Here, *DOM* is dissolved organic matter, and *SPM* is suspended particulate matter. The total concentration of metal in soil drainage water does not refer simply to dissolved components ($[M]_{free,sdw}$, $[M]_{DIC,sdw}$, and $[M]_{DOM,sdw}$), but also includes $[M]_{SPM,sdw}$. Data on *SPM* concentration in soil drainage waters may be scarce, and in many cases the contribution of *SPM* to the metal leaching is only small. Thus, this flux can be neglected preliminarily. The calculation model includes, however, the possibility of metal being leached from the soil in association with particulates.

Given the activity or concentration of M^{2+}, the concentrations of the other metal species can be estimated by applying an equilibrium speciation model. The calculation has to consider the dependence of the metal speciation on *pH* and competitive effects due to major cationic species of *Mg*, *Al*, *Ca,* and *Fe*. For this purpose, a custom version of the Windermere Humic Aqueous Model version 6 (WHAM6; Tipping 1998) speciation model, termed W6S MTC2, has been produced. A more detailed description of the model calculation steps is given in the background document (De Vries et al. 2005). NFCs may calculate critical dissolved metal concentrations from the free ion concentration by one of three methods:

8. Linear interpolation in the look-up tables (chapter 5.5.2.2.3). The look-up tables list critical dissolved metal concentrations (calculated using W6S-MTC2) for various combinations of *pH*, concentrations of soil organic matter, dissolved organic carbon $([DOC]_{sdw})$ and suspended particulate matter *(SPM)* and partial CO_2 pressure (pCO_2).

9. Sending suitably formatted files to the Centre for Ecology & Hydrology (CEH), Lancaster, Ed Tipping (ET@CEH.AC.UK), who will perform the computations with W6S-MTC2. Instructions for preparing suitably formatted files for this purpose are given below.
10. Using the W6S-MTC2 program themselves. Instructions for use are given with the program, which can be obtained by contacting Ed Tipping (see above).

NFCs that wish values of $M_{tot,sdw(crit)}$ to be calculated by should submit files to the CEH Lancaster, Ed Tipping (ET@CEH.AC.UK). The data should simply be entered into an Excel workbook, under the following headings.

code	pH	% OM	PCO_2	DOC	SPM

code the user's identifier of the site

pH soil solution pH

% OM the soil organic matter content

pCO_2 the soil pCO_2 expressed as a multiple of the atmospheric value

DOC concentration of dissolved organic carbon in mg l^{-1}

SPM concentration of suspended particulate matter in mg l^{-1}

- Please see the background document (Annex 8 and 9) regarding the selection of *pH* and pCO_2 values. If data on *DOC* concentration are not available, a standard value of 20 *mg* l^{-1} will be assumed.
- If data on pCO_2 are not available, a value of 15 x atmospheric will be assumed.
- If data on *SPM* are not available, a value of zero will be assumed.

Please note that it is necessary to recalculate values of soil *pH* (measured in *KCl*, $CaCl_2$, H_2O) to soil solution *pH*, as mentioned in the main text, before applying the look-up tables or creating input files for W6S-MTC2. Annex 3: Calculation of critical total Cd and Pb concentrations in surface water related to ecotoxicological effects.

This Annex was first published as Appendix 12 of the background document (De Vries et al. 2005) and became part of the manual by decision of the 22th Task Force on ICP Modelling and Mapping (April 2006, in Bled, Slovenia). It replaces the original version of Annex 3 (October 2004).

The calculation of the critical total aqueous concentration comprises the following steps:

11. Estimate the critical free metal ion concentration from the critical dissolved concentration (critical limit).
12. Calculate the metal bound per unit mass of suspended particulate matter *(SPM)*.
13. Calculate the water hardness.
14. Sum the total dissolved and particulate concentrations.

The critical free metal ion concentrations *([M]free, crit) (mol* l^{-1}*)* are calculated using WHAM6, for waters of different *pH*, *DOC,* and pCO_2, making the same assumptions as are used for calculating total metal from free-ion critical limits (for the look-up tables, see 5.5.2.2.3). These assumptions also lead to hardness values (*H* = hardness in *mg CaCO3* l^{-1}). In the calculations the critical dissolved concentrations used depend on the water hardness in case of *Cd* (*0.16 mg* m^{-3} if $H < 100$, *0.30 mg* m^{-3} if $100 < H < 200$ and *0.50 mg* m^{-3} if $H > 200$), whereas a value of *5 mg* m^{-3} was used for *Pb*. Note that, here, all waters are assumed to be "normal" with respect to dissolved *Al* (i.e., acid bog-waters are not included).

Free ion activities corresponding to these limits (taking into account the variation in the *Cd* critical limit with water hardness) were calculated with WHAM6 for a range of solution conditions covering most natural freshwaters. They can be expressed in terms of multiple regression equations at different *pH* values, according to:

$$\log [M]_{free,crit} = A \cdot [DOC] + B \cdot pCO2 + C \quad (A3.1)$$

where *[DOC]* is in *mg* l^{-1} and pCO_2 is a multiple of the atmospheric pCO_2. Root mean square errors in *log [M]free,crit* between the WHAM6 values and the regression values are *< 0.12* for *Cd* and *< 0.18* for *Pb*. The regression coefficients are given in Tables A3.1 and A3.2. Linear interpolation can be performed to obtain coefficients for intermediate *pH* values.

Step 1

Table A3.1 Regression coefficients for estimating critical free Cd^{2+} concentrations.

pH	A	B	C
4	-0.0004	0.0000	-8.87
5	-0.0053	-0.0001	-8.87
6	-0.0258	0.0040	-8.93
7	-0.0344	0.0189	-9.05
8	-0.0196	0.0466	-9.18
9	-0.0010	-0.0742	-9.44

Table A3.2 Regression coefficients for estimating critical free Pb^{2+} concentrations.

pH	A	B	C
4	-0.0020	0.0000	-7.66
5	-0.0231	0.0000	-7.70
6	-0.0546	0.0062	-8.19
7	-0.0681	0.0261	-9.33
8	-0.0641	0.0349	-10.33
9	-0.0160	-0.1303	-11.41

Step 2

The critical *SPM*-bound metal (*[M]SPM (crit), mol.*g^{-1}) is calculated using the Q-c relations derived in Annex 2, eq. A2.4 (Table A2.4). In this way, we do calculate the critical reactive metal content on the suspended particles. This is considered appropriate by limiting the critical load approach to processes and fluxes of geochemically reactive metals. This implies that actual loads should also be related to the reactive fraction of the total input. Deposition measurements practices aim at extraction of reactive species (not total metal). Therefore, we assume that, since EMEP models are calibrated to measurements, the currently mapped concentration/ deposition data (called "total") can be regarded as geochemically reactive metals.

Before proceeding to Step 3 *[M]SPM (crit)* must be converted to units of *mg* kg^{-1} by multiplying with the molar weight and a factor 10_6 to transfer from *g* g^{-1} to *mg* kg^{-1}

[Cd]SPM(crit) (mg kg^{-1}) = [Cd]SPM(crit) (mol g^{-1}) · ($112 \cdot 10^6$) (A3.2a)

[Pb]SPM(crit) (mg kg^{-1}) = [Pb]SPM(crit) (mol g^{-1}) · ($207 \cdot 10^6$) (A3.2b)

Step 3

Using the assumptions about water composition (see Step 1), water hardness (*mg CaCO3* l^{-1}) is given by regression equations in the following form:

hardness = A · [DOC] + B · pCO2 + C (A 3.3)

where *[DOC]* is in *mg* l^{-1} and *pCO2* is a multiple of the atmospheric *pCO2*. The regression coefficients are given in Table A3.3. Linear interpolation can be performed to obtain coefficients for intermediate *pH* values.

Table A3.3 Regression coefficients for estimating water hardness.

pH	A	B	C
4	0.00	0.00	0.00
5	0.11	0.02	-0.37
6	0.23	0.34	-0.14
7	0.31	3.4	-0.12
8	0.36	38.2	-6.84
9	0.43	1020	-966

Step 4

The total metal concentration in surface water at the critical limit is given by: [M]tot, sw(crit) = [M]dis,sw(crit) + [M]SPM (crit) · [SPM]sw (A3.4) where *[M]dis, sw(crit)* is the critical dissolved concentration (*mg* m^{-3} or *µg* l^{-1}) (see Table 5.24 in the main text), *[M]SPM(crit)* is the critical concentration bound to *SPM* calculated in Step 2 (*mg.kg*$^{-1}$), and *[SPM]sw* is the *SPM* concentration in surface water (*kg* m^{-3}).

FULL CALCULATION EXAMPLE #1

pH = 6

DOC = 8 mg l^{-1}

pCO2 = 4 times atmospheric

SPM = 50 mg l^{-1}

% OM = 20

Step 1

Log [Cd]free(crit) = (-0.0258 · 8) + (0.0040 · 4) + (-8.93)
= -0.206 + 0.016 – 8.93
= <u>-9.12</u>

log [Pb] free(crit) = (-0.0546 · 8) + (0.0062 · 4) + (-8.19)
= -0.437 + 0.025 – 8.19
= <u>-8.60</u>

Step 2

log [Cd]SPM (crit) = -6.42 + (0.45 · 6) + (0.64 · 1.30) + (0.58 · -9.12)
= -6.42 + 2.70 + 0.832 – 5.29
= -8.178 [Cd]SPM (crit)
= $6.64 \cdot 10^{-9}$ (mol g^{-1}) · 112 · 10^{6}
= 7.43 mg kg^{-1}

log [Pb]SPM (crit) = -5.42 + (0.70 · 6) + (0.55 · 1.30) + (0.61 · -8.60)
= -5.42 + 4.20 + 0.715 – 5.25
= -5.755

[Pb]SPM (crit) = $1.76 \cdot 10^{-6}$ (mol g^{-1}) · 207 · 10^{6}
= 364 mg kg^{-1}

Step 3

HARDNESS = (0.23 · 8) + (0.34 · 4) + (-0.14)
= 1.84 + 1.36 – 0.14 = 3.1

Therefore

[Cd]sw(crit) = 0.16 µg l^{-1}

[Pb]sw(crit) = 5 µg l^{-1}

Step 4

[Cd]tot, sw(crit) = 0.16 + [(50 / 1000) · 7.43)] µg l^{-1}
= 0.53 µg l^{-1}

[Pb]tot, sw(crit) = 5 + [(50 / 1000) · 364)] µg l^{-1}
= 23 µg l^{-1}

FULL CALCULATION EXAMPLE #2

pH = 8

DOC = 1 mg l^{-1}

pCO2 = 10 times atmospheric

SPM = 10 mg l^{-1}

% OM = 20

Step 1

Log [Cd]free(crit) = (-0.0196 · 1) + (0.0466 · 10) + (-9.18)
= -0.020 + 0.466 – 9.18
= <u>-8.73</u>

log [Pb] free(crit) = (-0.0641 · 1) + (0.0349 · 10) + (-10.33) .
= -0.064 + 0.349 – 10.33
= <u>-10.05</u>

Step 2

log [Cd]SPM (crit) = -6.42 + (0.45 · 8) + (0.64 · 1.30) + (0.58 · -8.73)
= -6.42 + 3.60 + 0.832 – 5.06
= -7.048

[Cd]SPM (crit) = $8.95 \cdot 10^{-8}$ mol g^{-1} · 112 · 10^{6}
= 10.0 mg kg^{-1}

log [Pb]SPM (crit) = -5.42 + (0.70 · 8) + (0.55 · 1.30) + (0.61 · -10.05)
= -5.42 + 5.60 + 0.715 – 6.13
= -5.235

[Pb]SPM (crit) = $5.82 \cdot 10^{-6}$ mol $g^{-1} \cdot 207 \cdot 10^{6}$
= 1205 mg kg^{-1}

Step 3

HARDNESS = (0.36 · 1) + (38.2 · 10) + (-6.84)
= 0.36 + 382 – 6.84
= 376

Therefore,

[Cd]sw(crit) = 0.50 µg l^{-1}

[Pb]sw(crit) = 5 µg l^{-1}

Step 4

[Cd]tot, sw(crit) = 0.50 + [(10/1000) · 10)] µg l^{-1}
= 0.60 µg l^{-1}

[Pb]tot, sw(crit) = 5 + [(10 / 1000) · 1205)] µg l^{-1}
= 17 µg l^{-1}

5.9.4 Annex 4: Correcting depositions for sea salts

Acidity critical loads are often compared with *anthropogenic* S deposition, (i.e., the contribution due to sea spray is not included). If this is the case, the critical load of S has to be reduced by the S deposition originating from sea salts, in other words:

$CL_{max}(S^*) = CL_{max}(S) - SO4_{, dep, ss}$

where the asterisk indicates a sea salt corrected quantity and the subscript 'ss' stand for sea salt derived. Ignoring ions such as Br, F, Sr, boric acid, and bicarbonate, which occur only in traces in seawater (and which we thus ignore), the charge balance of sea salt derived deposition reads:

$SO_{4, dep, ss} = BC_{dep, ss} - Cl_{dep, ss}$

Subtracting this from the critical load equation ($CL_{max}S = BC_{dep} - Cl_{dep} + BC_w - Bc_u - ANC_{le,crit}$) yields for the sea salt corrected critical load:

$CL_{max}(S^*) = BC^*_{dep} - Cl^*_{dep} + BC_w - Bc_u - ANC_{le,crit}$

How are those sea salt derived depositions obtained for a given location? First, the amounts of those ions in ocean water (unaffected by land drainage) are remarkably constant. This has been established by Dittmar (1884); and Dittmar's results were so consistent that later investigations introduced only minor changes, mostly with respect to more accurate atomic weights. Here we report the values given in Sverdrup et al. (1946), which are in turn based on data by Lyman & Fleming (1940). Table A4.1 lists the amounts of the six major ions in seawater, their atomic weights, and the calculated equivalents.

Table A4.1 Major ions in seawater and their abundance.

Ion	Amount in seawater[a] (g/kg)	Molecular weight of ion[b] (mol/g)	Equivalents in seawater (eq/kg)
Ca^{2+}	0.4001	40.078	0.01997

Ion	Amount in seawater[a] (g/kg)	Molecular weight of ion[b] (mol/g)	Equivalents in seawater (eq/kg)
Mg^{2+}	1.2720	24.305	0.10467
K^{+}	0.3800	39.098	0.00972
Na^{+}	10.5561	22.990	0.45916
Cl^{-}	18.9799	35.453	0.53545
SO_4^{2-}	2.6486	96.064	0.05514

[a]Sverdrup et al. (1946; p. 173); [b]Weast et al. (1989)

Secondly, it is assumed that either the sodium or the chloride deposition at a given location derives only from sea salts. Using their globally constant ratio in sea water, the depositions of base cations, sulphur, and chloride (given in equivalents) are corrected according to:

$$X^*_{dep} = X_{dep} - r_{XY}\, Y_{dep}$$

where $X = Ca, Mg, K, Na, Cl$ or SO_4, $Y = Na$ or Cl and r_{XY} is the ratio of ions X to Y in seawater. Ratios r_{XY} can by computed from the last column of Table A4.1 and are shown in Table A4.2 with 3-decimal accuracy. Note that if Na (Cl) is chosen to correct for sea salts, $Na^*_{dep}=0$ ($Cl^*_{dep}=0$).

Table A4.2 Ion ratios r_{XY} = [X]/[Y] (in eq/eq) in seawater (computed from Table A4.1).

	X					
Y	Ca	Mg	K	Na	Cl	SO_4
Na	0.043	0.228	0.021	1	1.166	0.120
Cl	0.037	0.195	0.018	0.858	1	0.103

It should be noted that the above procedure assumes that all quantities involved disperse in the atmosphere in the same way, which is not entirely true, especially for chloride. Nevertheless, given the dearth of dispersion modelling results for sea salts, the above procedure is widely used for locations not too far from the sea.

6 Dynamic modelling

Last updated in 2015 with inputs from Richard Wright, Luc Bonten, Max Posch and Anne Christine Le Gall, from initial text by M. Posch and J. Aherne, Mapping Manual 2004.

Please refer to this document as: CLRTAP, 2015. Dynamic modelling, Chapter 6 of Manual on methodologies and criteria for modelling and mapping critical loads and levels and air pollution effects, risks and trends. UNECE Convention on Long-range Transboundary Air Pollution; accessed on [date of consultation] on Web at www.umweltbundesamt.de/en/cce-manual.

6.1 Introduction

Target load is the logical extension of critical load. Critical loads are based on a steady-state concept, they are the constant depositions an ecosystem can tolerate in the long run, (i.e., after it has equilibrated with these depositions). However, many ecosystems are not in equilibrium with present or projected depositions, since there are processes ('buffer mechanisms') at work, which delay the reaching of an equilibrium (modelled as steady-state) for years, decades or even centuries. By definition, critical loads do not provide any information on these time scales. Target loads take these time delays into account. Dynamic models are needed to assess time delays of damage in regions where critical loads continue to be exceeded and time delays of recovery in regions where critical loads cease being exceeded. The purpose of this Chapter is to explain the use (and constraints) of dynamic modelling in support of the effects-oriented work under the LRTAP Convention. This chapter is a shortened and updated version of the 'Dynamic Modelling Manual' published earlier by the CCE (Posch et al. 2003). It has been further updated in 2015 to take into account new methodologies and model developments and improvements.

For the sake of simplicity and in order to avoid the somewhat vague term 'ecosystem', we refer in this sequel to non- calcareous (forest) soils. However, most of the considerations hold for surface water systems as well, since their water quality is strongly influenced by properties of, and processes in, catchment soils. A report dealing specifically with the dynamic modelling of surface waters on a regional scale has been prepared under the auspices of the ICP Waters (Jenkins et al. 2002).

6.1.1 Why dynamic modelling?

In the causal chain from deposition of strong acids to damage to key indicator organisms there are two major links that can give rise to delays. Biogeochemical processes can delay the chemical response in soil, and biological processes can further delay the response of indicator organisms, such as damage to trees in forest ecosystems. The static models to determine critical loads consider only the steady-state condition, in which the chemical and biological response to a (new) (constant) deposition is complete. Dynamic models, on the other hand, attempt to estimate the time required for a new (steady) state to be achieved.

In the steady-state situation, only two cases can be distinguished when comparing deposition to critical load: (1) the deposition is below critical load(s) (i.e., does not exceed critical load) and (2) the deposition is greater than critical load(s) (i.e., there is critical load exceedance). In the first case there is no (apparent) problem (i.e., no reduction in deposition is deemed necessary). In the second case there is, by definition, an increased risk of damage to the ecosystem. Thus, a critical load serves as a warning as long as there is exceedance, since it states that deposition should be reduced. However, it is often assumed that reducing deposition to (or below) critical loads immediately removes the risk of 'harmful effects' or, in other words the chemical criterion

(e.g., the Al/Bc-ratio[16][17]) that links the critical load to the (biological) effect(s), immediately attains a non-critical (safe) value, and that there is immediate biological recovery as well. But the reaction of soils, especially their solid phase, to changes in deposition is delayed by (finite) buffers, the most important being the base cation pool of the soil cation exchange complex. These buffer mechanisms can delay the attainment of a critical chemical parameter, and it might take decades or even centuries, before an equilibrium (steady-state) is reached. These finite buffers are not included in the critical load formulation, since they do not influence the steady-state, but only the time to reach it. Therefore, dynamic models are needed to estimate the times involved in attaining a certain chemical state in response to deposition scenarios (e.g. the consequences of 'gap closures' in emission reduction negotiations). In addition to the delay in chemical recovery, there is likely to be a further delay before the 'original' biological state is reached even if the chemical criterion is met (e.g., Al/Bc<1), it will take time before biological recovery is achieved.

Figure 6.1 summarises the possible development of a (soil) chemical and biological variable in response to a 'typical' temporal deposition pattern. Five stages can be distinguished:

Stage 1: Deposition was and is below the critical load (CL) and the chemical and biological variables do not violate their respective criteria. As long as deposition stays below the CL, this is the 'ideal' situation.

Stage 2: Deposition is above the CL, but (chemical and) biological criteria are not violated because there is a time delay before this happens. No damage has yet occurred despite exceedance of the CL. The time between the first exceedance of the CL and the first violation of the biological criterion (the first occurrence of actual damage) is termed the Damage Delay Time ($DDT=t_3-t_1$).

Stage 3: The deposition is above the CL and both the chemical and biological criteria are violated. Measures (emission reductions) have to be taken to avoid a (further) deterioration of the ecosystem status.

Stage 4: Deposition is below the CL, but the (chemical and) biological criteria are still violated and thus recovery has not yet occurred. The time between the first non- exceedance of the CL and the subsequent non-violation of both criteria is termed the Recovery Delay Time ($RDT=t_6-t_4$).

Stage 5: Deposition is below the CL and both criteria are no longer violated. This stage is similar to Stage 1 and only at this stage can the ecosystem be considered to have recovered.

Stages 2 and 4 can be subdivided into two sub-stages each: Chemical delay times ($DDT_c=t_2-t_1$ and $RDT_c=t_5-t_4$; dark grey in Figure 6.1) and (additional) biological delay times ($DDT_b=t_3-t_2$ and $RDT_b=t_6-t_5$; light grey). Very often, due to the lack of operational biological response models, damage and recovery delay times mostly refer to chemical recovery alone and this is used as a surrogate for overall recovery. It is also important to note that recovery does not follow the same, (inverse) path of damage, since there is a so-called hysteresis in these natural systems (see, e.g., Warfvinge et al. 1992).

[16] Bc = Ca + Mg + K

[17] In Chapter 5 (and elsewhere) the Bc/Al-ratio is used. However, this ratio becomes infinite when the Al concentration approaches zero. To avoid this inconvenience, its inverse, the Al/Bc-ratio, is used here.

Figure 6.1: **Typical past and future development of the acid deposition effects on a soil chemical variable (Al/Bc-ratio) and the corresponding biological response in comparison to the critical values of those variables and the critical load derived from them. The delay between the (non)exceedance of the critical load, the (non)violation of the critical chemical criterion and the crossing of the critical biological response is indicated in grey shades, highlighting the Damage Delay Time (DDT) and the Recovery Delay Time (RDT) of the system.**

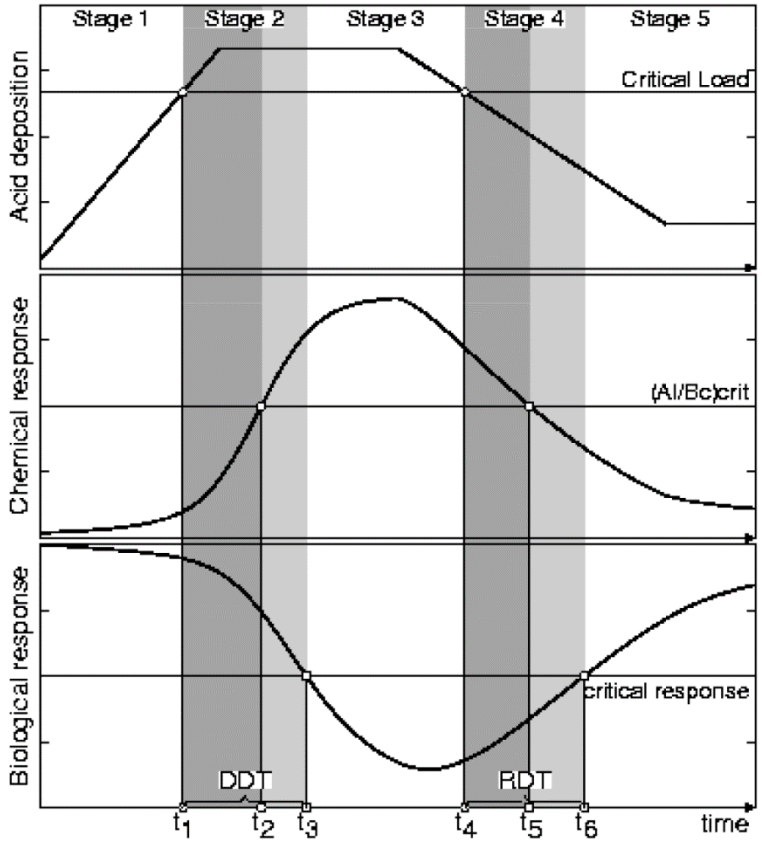

Source: This figure is adopted from a previous version of Chapter 6 of the Mapping Manual

6.1.2 Constraints for dynamic modelling under the LRTAP Convention

Steady-state models (critical loads) have been used to negotiate emission reductions in Europe. In this context, an emission reduction is judged successful if deposition no longer exceeds the critical load. To gain insight into the time delay between the attainment of non-exceedance and actual chemical (and biological) recovery, dynamic models are needed. Thus, if dynamic models are to be used to assess recovery with respect to negotiated targets under the LRTAP Convention or other national or international regulations, they should be compatible with the steady-state models used for calculating critical loads. In other words, when critical loads are used as input to the dynamic model, the (chemical) parameter chosen as the criterion in the critical load calculation has to attain the critical value after the dynamic simulation has reached steady-state. But this also means that concepts and equations used in the dynamic model should be an extension of the concepts and equations employed in deriving the steady- state model. For example, if critical loads are calculated with the Simple Mass Balance (SMB) model (see Chapter 5), this model should be the steady-state version of the dynamic model used (e.g., the VSD model, see below).

Due to a lack of (additional) data, it may be impossible to run dynamic models on all sites in a country for which critical loads have been calculated. The selection of the subset of sites, at which dynamic models are applied, should be sufficiently representative to allow comparison with results obtained with critical loads.

6.2 Basic concepts and equations

Dynamic models of acidification are based on the same principles as steady-state models: the charge balance of the ions in the soil solution, mass balances of the various ions, and equilibrium equations. However, whereas in steady-state models only infinite sources and sinks are considered (such as base cation weathering), the inclusion of the finite sources and sinks of major ions into dynamic models is crucial, since they determine the long-term (slow) changes in soil (solution) chemistry. The three most important processes involving finite buffers and time-dependent sources/sinks are cation exchange, nitrogen retention and sulphate adsorption.

A short description of the models mentioned in this section can be found in section 6.3.

6.2.1 Charge and mass balances

As mentioned above, we consider non-calcareous forest soils as ecosystem, although most of the considerations hold also for non-calcareous soils covered by (semi-)natural vegetation subjected to acidification. Since we are interested in applications on a large regional scale (for which data are scarce) and long-time horizons (decades to centuries with a time step of one year), we make the same simplifying assumption as for the SMB model (see Chapter 5). We assume that the soil is a single homogeneous compartment and its depth is equal to the root zone. This implies that internal soil processes (such as weathering and uptake) are evenly distributed over the soil profile, and all physico-chemical constants are assumed uniform in the whole profile. Furthermore, we assume the simplest possible hydrology: The water leaving the root zone is equal to precipitation minus evapotranspiration; more precisely, percolation is constant through the soil profile and occurs only vertically.

As for the SMB model, the starting point is the charge balance of the major ions in the soil water, leaching from the root zone (cf. eq.V.9):

(VI.1)

$$SO_{4,le} + NO_{3,le} - NH_{4,le} - BC_{le} + Cl_{le} = H_{le} + Al_{le} - HCO_{3,le} - RCOO_{le} = -ANC_{le}$$

where BC=Ca+Mg+K+Na and RCOO stands for the sum of organic anions. Eq.VI.1 also defines the acid neutralising capacity, ANC. The leaching term is given by $X_{le}=Q\cdot[X]$ where $[X]$ is the soil solution concentration (eq/m³) of ion X and Q (m/yr) is the water leaving the root zone.

The concentrations $[X]$ of an ion in the soil compartment, and thus its leaching X_{le}, are either obtained from equilibrium equations with $[H]$, such as $[Al]$, $[HCO_3]$, and $[RCOO]$ (see eqs. V.42, V.43 and V.45), or from mass balance equations. The latter describe the change over time of the total amount of ion X per unit area in the soil matrix/soil solution, X_{tot} (eq/m²):

(VI.2)

$$\frac{d}{dt}X_{tot} = X_{in} - X_{le}$$

where X_{in} (eq/m²/yr) is the net input of ion X (sources minus sinks, except leaching).

With the simplifying assumptions used in the derivation of the SMB model, the net input of sulphate and chloride is given by their respective deposition:

(VI.3)

$SO_{4,in} = S_{dep}$ and $Cl_{in} = Cl_{dep}$

For base cations the net input is given by (Bc=Ca+Mg+K):

(VI.4)

$BC_{in} = BC_{dep} + BC_w - Bc_u$

where the subscripts dep, w, and u stand for deposition, weathering and net uptake, respectively. Note, that S adsorption and cation exchange reactions are not included here, they are included in X_{tot} and described by equilibrium equations (see below). For nitrate and ammonium, the net input is given by:

(VI.5)

$NO_{3,in} = NO_{x,dep} + NH_{4,ni} - NO_{3,i} - NO_{3,u} - NO_{3,de}$

(VI.6)

$NH_{4,in} = NH_{3,dep} - NH_{4,ni} - NH_{4,i} - NH_{4,u}$

where the subscripts *ni, i,* and de stand for nitrification, net immobilisation and denitrification, respectively. In the case of complete nitrification one has $NH_{4,in}=0$ and the net input of nitrogen is given by:

(VI.7)

$NO_{3,in} = N_{in} = N_{dep} - N_i - N_u - N_{de}$

6.2.2 From steady state (critical loads) to dynamic models

Steady-state means there is no change over time in the total amounts of ions involved (i.e., see eq.VI.2):

(VI.8)

$$\frac{d}{dt} X_{tot} = 0 \Rightarrow X_{le} = X_{in}$$

From eq.VI.7 the critical load of nutrient nitrogen, $CL_{nut}(N)$, is obtained by specifying an acceptable N-leaching, $N_{le,acc}$. By specifying a critical leaching of ANC, $ANC_{le,crit}$, and inserting eqs. VI.3, VI.4 and VI.7 into the charge balance (eq. VI.1), one obtains the equation describing the critical load function of S and N acidity, from which the three quantities $CL_{max}(S)$, $CL_{min}(N)$ and $CL_{max}(N)$ can be derived (see Chapter 5).

To obtain time-dependent solutions of the mass balance equations, the term X_{tot} in eq. VI.2 the total amount (per unit area) of ion X in the soil matrix/soil solution system has to be specified. For ions, which do not interact with the soil matrix, X_{tot} is given by the amount of ion X in solution alone:

(VI.9)

$X_{tot} = \Theta \cdot z \cdot [X]$

where z (m) is the soil depth under consideration (root zone) and Θ (m^3/m^3) is the (annual average) volumetric water content of the soil compartment. The above equation holds for chloride. For every base cation Y participating in cation exchange, Y_{tot} is given by:

(VI.10)

$$Y_{tot} = \Theta \cdot z \cdot [Y] + \rho \cdot z \cdot CEC \cdot E_Y$$

where ρ is the soil bulk density (g/cm^3), CEC the cation exchange capacity (meq/kg) and E_Y is the exchangeable fraction of ion Y.

The (long-term) changes of the soil N pool are mostly caused by net immobilisation, and N_{tot} is given by:

(VI.11)

$$N_{tot} = \Theta \cdot z \cdot [N] + \rho \cdot z \cdot N_{pool}$$

If there is no ad/desorption of sulphate, $SO_{4,tot}$ is given by eq. VI.9. If sulphate adsorption cannot be neglected, it is given by:

(VI.12)

$$SO_{4,tot} = \Theta \cdot z \cdot [SO_4] + \rho \cdot z \cdot SO_{4,ad}$$

When the rate of Al leaching is greater than the rate of Al mobilisation by weathering of primary minerals, the remaining part of Al has to be supplied from readily available Al pools, such as Al hydroxides. This causes depletion of these minerals, which might induce an increase in Fe buffering which in turn leads to a decrease in the availability of phosphate (De Vries 1994). Furthermore, the decrease of those pools in podzolic sandy soils may cause a loss in the structure of those soils. The amount of aluminium is in most models assumed to be infinite and thus no mass balance for Al is considered.

Inserting these expressions into eq. VI.2 and observing that $X_{le}=Q\cdot[X]$, one obtains differential equations for the temporal development of the concentration of the different ions. Only in the simplest cases can these equations be solved analytically. In general, the mass balance equations are discretised and solved numerically, with the solution algorithm depending on the model builders' preferences.

6.2.3 Finite buffers

Finite buffers of elements in the soil are not included in the derivation of critical loads, since they do not influence the steady state. However, when investigating the state of soils over time as a function of changing deposition patterns, these finite buffers govern the long-term (slow) changes in soil (solution) chemistry. In the following we describe the most important ones in turn.

6.2.3.1 Cation exchange

Generally, the solid phase particles of a soil carry an excess of cations at their surface layer. Since electro-neutrality has to be maintained, these cations cannot be removed from the soil, but they can be exchanged against other cations (e.g., those in the soil solution). This process is known as cation exchange and every soil (layer) is characterised by the total amount of exchangeable cations per unit mass (weight), the "cation exchange capacity" (CEC, measured in meq/kg). If X and Y are two cations with charges m and n, then the general form of the equations used to describe the exchange between the liquid- phase concentrations (or activities) [X] and [Y] and the equivalent fractions E_X and E_Y at the exchange complex is:

(VI.14)

$$\frac{E_X^i}{E_Y^j} = K_{XY} \cdot \frac{[X^{m+}]^n}{[Y^{n+}]^m}$$

where K_{XY} is the exchange (or selectivity) constant, a soil-dependent quantity. Depending on the powers i and j different models of cation exchange can be distinguished: For *i=n* and *j=m* one obtains the Gaines-Thomas exchange equations, whereas for *i=j=mn*, after taking the *mn*-th root, the Gapon exchange equations are obtained.

The number of exchangeable cations considered depends on the purpose and complexity of the model. For example, Reuss (1983) considered only the exchange between Al and Ca (or divalent base cations). In general, if the exchange between *N* ions is considered, *N*–1, exchange equations (and constants) are required, all the other (*N*–1)(*N*–2)/2 relationships and constants can be easily derived from them. In the VSD/VSD+ and SAFE models, the exchange between aluminium, divalent base cations and protons is considered. The exchange of protons is important, if the cation exchange capacity (CEC) is measured at high pH- values (pH=6.5). In the case of the Bc-Al-H system, the Gaines-Thomas equations read:

(VI.15)

$$\frac{E_{Al}^2}{E_{Bc}^3} = K_{AlBc} \cdot \frac{[Al^{3+}]^2}{[Bc^{2+}]^3} \quad \text{and} \quad \frac{E_H^2}{E_{Bc}} = K_{HBc} \cdot \frac{[H^+]^2}{[Bc^{2+}]}$$

where Bc=Ca+Mg+K, with K treated as divalent. The equation for the exchange of protons against Al can be obtained from eqs.VI.15 by division:

(VI. 16)

$$\frac{E_H^2}{E_{Al}} = K_{HAl} \cdot \frac{[H^+]^2}{[Al^{3+}]^3} \quad \text{and} \quad K_{HAl} = \sqrt{K_{HBc}^3 / K_{AlBc}}$$

The corresponding Gapon exchange equations read:

(VI.17)

$$\frac{E_{Al}}{E_{Bc}} = k_{AlBc} \cdot \frac{[Al^{3+}]^{1/3}}{[Bc^{2+}]^{1/2}} \quad \text{and} \quad \frac{E_H}{E_{Bc}} = k_{HBc} \cdot \frac{[H^+]}{[Bc^{2+}]^{1/2}}$$

Again, the H-Al exchange can be obtained by division (with kHAl=kHBc/kAlBc). Charge balance requires that the exchangeable fractions add up to one:

(VI.18)

$$E_{Bc} + E_{Al} + E_H = 1$$

The sum of the fractions of exchangeable base cations (here E_{Bc}) is called the base saturation of the soil. It is the time development of the base saturation, which is of interest in dynamic modelling. In the above formulations the exchange of Na, NH_4 (which can be important in high NH_4 deposition areas) and heavy metals is neglected (or subsumed in the proton fraction).

Care has to be exercised when comparing models, since different sets of exchange equations are used in different models. Whereas eqs. VI.15 are used in the VSD and VSD+ model, the SAFE model employs the Gapon exchange equations (eqs. VI.17), however with exchange constants $k'_{X/Y}=1/k_{XY}$. In the MAGIC model the exchange of Al with all four base cations is modelled separately with Gaines- Thomas equations, without explicitly considering H-exchange. This is because the equation for dissolution of the solid phase Al-hydroxide is identical to that of Al- H+ exchange. Including both in MAGIC would be redundant.

6.2.3.2 Nitrogen immobilisation

In the calculation of critical loads, the (acceptable, sustainable) long-term net immobilisation (i.e., the difference between immobilisation and mineralisation) is assumed to be constant.

However, it is well known, that the amount of N immobilised is (at present) in many cases larger than this long-term value. Thus, a sub-model describing the nitrogen dynamics in the soil is part of most dynamic models. For example, the MAKEDEP model, which is part of the SAFE model system (but can also be used as a stand-alone routine) describes the N-dynamics in the soil as a function of forest growth and deposition.

According to Dise et al. (1998) and Gundersen et al. (1998) the forest floor C/N-ratios may be used to assess risk for nitrate leaching. Gundersen et al. (1998) suggested threshold values of >30, 25 to 30, and <25 to separate low, moderate, and high nitrate leaching risk, respectively. This information has been used in several models, such as VSD and MAGIC (version 7) to calculate nitrogen immobilisation as a fraction of the net N input, linearly depending on the C/N-ratio in the mineral topsoil.

In addition to the long-term constant net immobilisation, $N_{i,acc}$, the net amount of N immobilised is a linear function of the actual C/N-ratio, CN_t, between a prescribed maximum, CN_{max}, and a minimum C/N-ratio, CN_{min},:

(VI.19)

$$N_{i,t} = \begin{cases} N_{in,t}, & CN_t \geq CN_{max} \\ \dfrac{CN_t - CN_{min}}{CN_{max} - CN_{min}} \cdot N_{in,t}, & CN_{min} < CN_t < CN_{max} \\ 0, & CN_t \leq CN_{min} \end{cases}$$

where $N_{in,t}$ is the available N (e.g., $N_{in,t}=N_{dep,t}- -N_{u,t}-N_{i,acc}$). At every time step the amount of immobilised N is added to the amount of N in the top soil, which in turn is used to update the C/N-ratio. The total amount immobilised at every time step is then $N_i=N_{i,acc}+N_{i,t}$. The above equation states that when the C/N- ratio reaches the minimum value, the annual amount of N immobilised equals the acceptable value $N_{i,acc}$ (see Figure 6.2). This formulation is compatible with the critical load formulation for $t \rightarrow \infty$.

Figure 6.2: Amount of N immobilised (left) and resulting C/N-ratio in the topsoil (right) for a constant net input of N of 1 eq/m²/yr (initial C_{pool} = 4000 gC/m²), $N_{i,acc}$ = 1 kg/ha/yr).

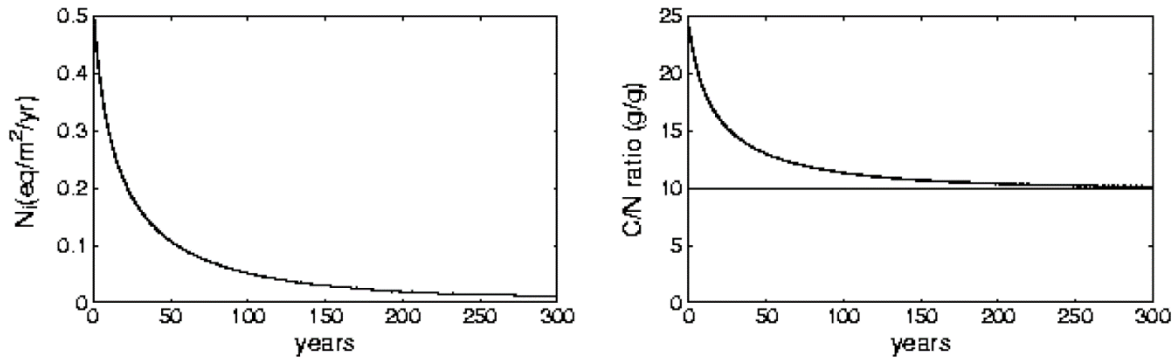

Source: This figure is adopted from a previous version of Chapter 6 of the Mapping Manual

6.2.3.3 Sulphate adsorption

The amount of sulphate adsorbed, $SO_{4,ad}$ (meq/kg), is often assumed to be in equilibrium with the solution concentration and is typically described by a Langmuir isotherm (e.g., Cosby et al. 1986):

(VI.20)

$$SO_{4,ad} = \frac{[SO_4]}{S_{1/2} + [SO_4]} \cdot S_{max}$$

where S_{max} is the maximum adsorption capacity of sulphur in the soil (meq/kg) and $S_{1/2}$ is the half-saturation concentration (eq/m³).

6.2.4 From soils to surface waters

The processes discussed so far are assumed to occur in the soil solution while it is in contact with the soil matrix. To calculate surface water concentrations, it is assumed that the water leaves the soil matrix and is exposed to the atmosphere (Cosby et al. 1985, Reuss and Johnson 1986). When this occurs, excess CO_2 in the water degasses. This shifts the carbonate-bicarbonate equilibria and changes the pH (see eq. V.43). Surface water concentrations are thus calculated by resolving the system of equations presented above at a lower partial pressure of CO_2 (e.g., mean p_{CO2} of $8 \cdot 10^{-4}$ atm for 37 lakes, Cole et al. 1994) while ignoring exchange reactions, nitrogen immobilisation and sulphate adsorption.

Since exchanges with the soil matrix are precluded, the concentration of the base cations and the strong acid anions (SO_4, NO_3 and Cl) will not change as the soil water becomes surface water. As such, ANC is conservative (see eq. VI.1).

In lakes additional processes occur, and several of these are included in dynamic models such as MAGIC. In-lake, retention of NO_3 and SO_4 by denitrification and sulphate reduction, respectively, at the sediment water interface and retention in sediment or loss as gaseous phase to the atmosphere are the most important of these processes (Dillon and Molot 1990, Kaste and Dillon 2003).

6.2.5 Biological response models

Just as there are delays between changes in acid deposition and changes in surface (or soil) water chemistry, there are delays between changes in chemistry and the biological response. Because the goal in recovery is to restore good or healthy populations of key indicator organisms, the time lag in response is the sum of the delays in chemical and biological response (see Figure 6.1). Thus, dynamic models for biological response are needed. In the following a summary is provided of existing models and ideas.

6.2.5.1 Terrestrial ecosystems

A major drawback of most dynamic soil acidification models is the neglect of biotic interactions. For example, vegetation changes are mainly triggered by a change in N cycling (N mineralisation; Berendse et al. 1987). Furthermore, the enhancement of diseases by elevated N inputs, such as heather beetle outbreaks, may stimulate vegetation changes. Consequently, dynamic soil-vegetation models, which include such processes, have a better scientific basis for the assessment of critical and target N loads. Such an approach has been developed to model eutrophication (see section 5.3). Amongst older models, are CALLUNA (Heil and Bobbink 1993) and ERICA (Berendse 1988). The model CALLUNA integrates N processes by atmospheric deposition, accumulation and sod removal, with heather beetle outbreaks and competition

between species, to establish the critical N load in lowland dry-heathlands (Heil and Bobbink 1993). The wet-heathland model ERICA incorporates the competitive relationships between the species *Erica* and *Molinia*, the litter production from both species, and nitrogen fluxes by accumulation, mineralisation, leaching, atmospheric deposition and sheep grazing. At present, there are also several forest-soil models that calculate forest growth impacts in response to atmospheric deposition and other environmental aspects, such as meteorological changes (precipitation, temperature) and changes in CO_2 concentration. Examples are the models NAP (Van Oene 1992), ForSVA (Oja et al. 1995), and Hybrid (Friend et al. 1997).

Statistical models have been developed to assess the relationship between the species diversity of the ecosystem and abiotic aspects related to acidification and eutrophication. An example is the vegetation model MOVE (Latour and Reiling 1993), that predicts the occurrence probability of plant species in response to scenarios for acidification, eutrophication, and desiccation. Input to the model comes from the output of the soil model SMART2 (Kros et al. 1995), being an extension of the SMART model (De Vries et al. 1989). The SMART2 model predicts changes in abiotic soil factors indicating acidification (pH), eutrophication (N availability), and desiccation (moisture content) in response to scenarios for acid deposition and groundwater abstraction, including the impact of nutrient cycling (litterfall, mineralisation and uptake). MOVE predicts the occurrence probability of around 700 species as a function of three abiotic soil factors, including nitrogen availability, using regression relationships. Since combined samples of vegetation and environmental variables are rare, the indication values of plant species by Ellenberg (1985) are used to assess the abiotic soil conditions. Deduction of values for the abiotic soil factors from the vegetation guarantees ecological relevance. Combined samples of vegetation with environmental variables are used exclusively to calibrate Ellenberg indication values with quantitative values of the abiotic soil factors. A calibration of these indication values to quantitative values of the abiotic soil factors is necessary to link the soil module to the vegetation module.

A comparable statistical model is the NTM model (Wamelink et al. 2003, Schouwenberg et al. 2000), that was developed to predict the potential conservation value of natural areas. Normally conservation values are calculated on the basis of plant species or vegetation types. As with MOVE, NTM has the possibility to link the vegetation and the site conditions by using plant ecological indicator values. NTM uses a matrix of the habitats of plant species defined on the basis of moisture, acidity and nutrient availability. The model was calibrated using a set of 160,252 vegetation relevées. A value index per plant species was defined on the basis of rarity, decline, and international importance. This index was used to determine a conservation value for each relevée. The value per relevée was then assigned to each species in the relevée and regressed on the Ellenberg indicator values for moisture, acidity and nutrient availability (Ellenberg 1985) using a statistical method (P-splines). The model has these three Ellenberg indication values as input for the prediction of the potential conservation value. A potential conservation value is calculated for a combination of the abiotic conditions and vegetation structure (ecotope). Therefore, four vegetation types are accounted for, each represented by a sub-model of NTM: heathland, grassland, deciduous forest, and pine-forest. Use of those models in dynamic modelling assessments is valuable to gain more insight in the effect of deposition scenarios on terrestrial ecosystems.

6.2.5.2 Aquatic ecosystems

As with terrestrial ecosystems, biological dose/response models for surface waters have not generally focused on the time- dynamic aspects. For example, the relationship between lake ANC and brown trout population status in Norwegian lakes used to derive the critical limit for surface waters is based on synoptic (once in time) surveys of ANC and fish status in a large number of

lakes. Similarly, the invertebrate indices (Raddum 1999) and diatom response models (Battarbee et al. 1996) do not incorporate dynamic aspects. Additional information on dose/response comes from traditional laboratory studies of toxicity (chronic and acute) and reproductive success.

Information on response times for various organisms comes from studies of recovery following episodes of pollution, for example, salmon population following a chemical spill in a river. For salmon, full recovery of the population apparently requires about 10 years after the water chemistry has been restored.

There is currently no available time-dynamic process-oriented biological response models for effects of acidification on aquatic and terrestrial organisms, communities or ecosystems. Such models are necessary for a full assessment of the length of time required for recovery of damage from acidification.

There are several types of evidence that can be used to empirically estimate the time delays in biological recovery. The whole-lake acidification and recovery experiments conducted at the Experimental Lakes Area (ELA) in north-western Ontario, Canada, provide such information at realistic spatial and temporal scales. These experiments demonstrate considerable lag times between the achievement of acceptable water quality following a decrease in acid inputs, and achievement of acceptable biological status. The delay times for various organisms are at least several years. In the case of several fish species, irreversible changes may have occurred (Hann and Turner 2000, Mills et al. 2000).

A second source of information on biological recovery comes from liming studies. Over the years such studies have produced extensive empirical evidence on rate of response of individual species as well as communities following liming. There has been little focus, however, on the processes involved.

Finally, there is recent documentation of recovery in several regions at which acid deposition has decreased since the 1980s and 1990s. Lakes close to the large point- source of sulphur emissions at Sudbury, Ontario, Canada, show clear signs of chemical and biological recovery in response to substantial decreases in emissions beginning in the late 1970s (Keller and Gunn 1995). Lakes in the nearby Killarney Provincial Park (Ontario, Canada) also show clear signs of biological recovery during the past 20 years (Snucins et al. 2001). Also, recent results compiled by ICP Waters have shown recovery processes (Garmo et al., 2014; Skjelkvåle, 2008). Here there are several biological factors that influence the rate of biological recovery such as:

1. fish species composition and density;
2. dispersal factors such as distance to intact population and ability to disperse;
3. existence of resting eggs (for such organisms such as zooplankton);
4. existence of precluding species – (i.e., the niche is filled).

Knowledge on models for biological recovery in surface waters has been reviewed in a workshop in 2002 (Wright and Lie 2002) and is commonly discussed at ICP Waters meetings.

Development of biological response models must also consider the frequency and severity of harmful episodes, such as pH shocks during spring snowmelt, or acidity and aluminium pulses due to storms with high seasalt inputs. These links between episodic water chemistry and biological response at all levels (organisms, community, and ecosystem) are poorly quantified and thus not yet ready to be incorporated into process-oriented models.

6.3 Available dynamic models

In the previous sections the basic processes involved in soil acidification have been summarised and expressed in mathematical form, with emphasis on slow (long-term) processes. Over the past 25 years, the resulting equations, or generalisations and variants thereof, together with appropriate solution algorithms and input-output routines have been packaged into soil acidification models, mostly known by their (more or less formal) acronyms.

There is no shortage of soil (acidification) models, but most of them are not designed for regional applications. A comparison of 16 models can be found in a special issue of the journal 'Ecological Modelling' (Tiktak and Van Grinsven, 1995). These models emphasise either soil chemistry (such as SMART, SAFE, and MAGIC) or the interaction with the forest (growth). There are very few truly integrated forest-soil models. An example is the forest model series ForM-S (Oja et al. 1995), which is implemented not in a 'conventional' Fortran code, but is realised in the high-level modelling software STELLA. A more recent comparison of the models VSD, SAFE and MAGIC (and PnET- BGC) can be found in Tominaga et al. (2010).

The following selection is biased towards models which have been widely used and which are simple enough to be applied on a (large) regional scale. Only a short description of the models is given as details can be found in the references cited. It should be emphasised that the term 'model' used here refers, in general, to a model system (i.e., a set of (linked) software and databases) which consists of pre-processors for input data (preparation) and calibration, post-processors for the model output, and – in general the smallest part – the actual model itself.

An overview of the various models is given in Table 6.1 and a short description below. The first three models are soil models of increasing complexity, whereas the MAGIC model is generally applied at the catchment level. Application at the catchment level, instead of on a single (forest) plot, has implications for the derivation of input data. For example, weathering rates have to represent the average weathering of the whole catchment, data that is difficult to obtain from soil parameters. Thus, in MAGIC catchment, weathering is calibrated from water quality data.

Table 6.1: Overview of dynamic models that have been (widely) applied on a regional scale.

Model	Essential process descriptions	Layers	Essential model inputs
VSD	ANC charge balance Mass balances for BC and N (complete nitrification assumed)	One	CL input data + CEC, base saturation C/N-ratio
VSD+	VSD model + Separate mass balances for NH_4 and NO_3, nitrification; N fixation Explicit organic C and N dynamics Ca and Mg carbonate equilibrium	One	VSD model + organic C and N inputs (litterfall, root turnover, harvest residues)
SAFE	VSD model + Separate weathering calculation Element cycling by litterfall Root decay Mineralisation and root uptake	Several	VSD model + Input data for PROFILE litterfall rate parameters describing mineralisation and root uptake
MAGIC	VSD model + SO_4 sorption Al speciation/complexation Aquatic chemistry	Several (mostly one used)	VSD model + S_{max} and $S_{1/2}$ pK values for several Al reactions parameters for aquatic chemistry

6.3.1 The VSD model

The basic equations presented in section 6.2 have been used to construct a **V**ery **S**imple **D**ynamic (VSD) soil acidification model. The VSD model is designed as the simplest extension of the SMB model for critical loads. In addition to the equations included in the SMB model, it includes cation exchange and N immobilisation as well as a mass balance for cations and nitrogen as described above. However, it resembles the model presented by Reuss (1980) which does not consider nitrogen processes. The model is described in Posch and Reinds (2009) and a single-site version is available from the CCE website (www.wge-cce.org).

The VSD model consists of a set of mass balance equations, describing the soil input- output relationships, and a set of equations describing the rate-limited and equilibrium soil processes, as described in section 6.2. The soil solution chemistry in VSD depends solely on the net element input from the atmosphere (deposition minus net uptake minus net immobilisation) and the geochemical interaction in the soil (CO_2 equilibria, weathering of carbonates and silicates, and cation exchange). Soil interactions are described by simple rate- limited (zero-order) reactions (e.g., uptake and silicate weathering) or by equilibrium reactions (e.g. cation exchange). It models the exchange of Al, H and Ca+Mg+K with Gaines-Thomas or Gapon equations. Solute transport is described by assuming complete mixing of the element input within one homogeneous soil compartment with a constant density and a fixed depth. Since VSD is a single layer soil model neglecting vertical heterogeneity, it predicts the concentration of the soil water leaving this layer (the rootzone). The annual water flux percolating from this layer is taken equal to the annual precipitation excess. The time step of the model is one year, i.e. seasonal variations are not considered.

6.3.2 The VSD+ model

The VSD+ model (Bonten et al. 2015) is an extension of the VSD model. An explicit description of organic C and N turnover has been included to better predict N eutrophication and C sequestration and be able to link the model to vegetation biodiversity models. For C sequestration, VSD+ uses the equations of the RothC-26.3 model (Coleman and Jenkinson 2005). This model consists of five soil C pools. Two pools contain fresh organic input from litterfall, root turnover, and harvest residues, whereby one of these pools assembles easily decomposable plant material and the other pool stands for recalcitrant material. For the three other pools, one resembles soil microbial C, one is humified material and the last one is inert organic material. Mineralisation and transfer of C to a next pool is described by single order differential equations, with a fixed reference rate constant for each pool that is adjusted for temperature and soil moisture. Nitrogen mineralization and immobilization follows the turnover of the C pools, depending on the C:N ratios of the five organic matter compartments. The C:N ratio of the pool with easily decomposable plant material depends on the C:N ratio of the total organic C input. The C:N ratio of the humified pool is adjusted depending on N deposition, N uptake, and transfer of N from other pools. The C:N ratios for the three other pools are fixed. Input for this explicit C and N model are the total organic C and N inputs.

Also different from the VSD model, the VSD+ model no longer assumes full nitrification, but includes a first order differential equation for nitrification. Also, denitrification is modelled with a first order equation. Nitrification and denitrification rates are calculated from reference rate constants that are modified for temperature, soil moisture, and soil pH.

The final difference with VSD is that VSD+ includes equations for Ca and/or Mg carbonates equilibrium, which allows VSD+ to be easier used for calcareous soils, especially for N eutrophication effects (acidification does not play a big role for these soils).

6.3.3 The SAFE model

The SAFE (**S**oil **A**cidification in **F**orest **E**cosystems) model has been developed at the University of Lund (Warfvinge et al. 1993) and a recent description of the model can be found in Alveteg (1998) and Alveteg and Sverdrup (2002). The main differences to the VSD/VSD+ and MAGIC models are: (a) weathering of base cations is not a model input, but it is modelled with the PROFILE (sub-)model, using soil mineralogy as input (Warfvinge and Sverdrup 1992); (b) SAFE is oriented to soil profiles in which water is assumed to move vertically through several soil layers (usually 4), (c) Cation exchange between Al, H, and (divalent) base cations is modelled with Gapon exchange reactions, and the exchange between soil matrix and the soil solution is diffusion limited. The standard version of SAFE does not include sulphate adsorption although a version in which sulphate adsorption is dependent on sulphate concentration and pH has been developed (Martinson et al. 2003).

The SAFE model has been applied to many sites and more recently also regional applications have been carried out for Sweden (Alveteg and Sverdrup 2002) and Switzerland (SAEFL 1998, Kurz et al. 1998, Alveteg et al. 1998).

6.3.4 The MAGIC model

MAGIC (**M**odel of **A**cidification of **G**roundwater **I**n **C**atchments) is a lumped- parameter model of intermediate complexity, developed to predict the long- term effects of acidic deposition on soils and surface water chemistry (Cosby et al. 1985a, b, c, 1986). The model simulates soil solution chemistry and surface water chemistry to predict the monthly and annual average concentrations of the major ions in lakes and streams. MAGIC represents the catchment with aggregated, uniform soil compartments (one or two) and a surface water compartment that can be either a lake or a stream. MAGIC consists of (1) a section in which the concentrations of major ions are assumed to be governed by simultaneous reactions involving sulphate adsorption, cation exchange, dissolution-precipitation-speciation of aluminium, and dissolution-speciation of inorganic and organic carbon, and (2) a mass balance section in which the flux of major ions to and from the soil is assumed to be controlled by atmospheric inputs, chemical weathering inputs, net uptake in biomass and losses to runoff. At the heart of MAGIC is the size of the pool of exchangeable base cations in the soil. As the fluxes to and from this pool change over time owing to changes in atmospheric deposition, the chemical equilibria between soil and soil solution shift to give changes in surface water chemistry. The degree and rate of change in surface water acidity thus depend both on flux factors and the inherent characteristics of the affected soils.

The soil layers can be arranged vertically or horizontally to represent important vertical or horizontal flow paths through the soils. If a lake is simulated, seasonal stratification of the lake can be implemented. Time steps are monthly or yearly. Time series inputs to the model include annual or monthly estimates of: (1) deposition (wet plus dry) of ions from the atmosphere; (2) discharge volumes and flow routing within the catchment; (3) biological production, removal and transformation of ions; (4) internal sources and sinks of ions from weathering or precipitation reactions; and (5) climate data. Constant parameters in the model include physical and chemical characteristics of the soils and surface waters, and thermodynamic constants. The model is calibrated using observed values of surface water and soil chemistry for a specified period.

MAGIC has been modified and extended several times from the original version from 1984. In particular, organic acids have been added to the model (version 5; Cosby et al. 1995a), nitrogen processes have been added based on the C/N ratio of soil (version 7; Cosby et al. 2001) and most

recently, N retention in soil is described as a microbial-driven process (i.e., the C/N ratio of the soil no longer governs the N immobilisation) (Oulehle et al., 2012).

The MAGIC model has been extensively applied and tested over the past 30 years at many sites and in many regions around the world. Overall, the model has proven to be robust, reliable and useful in a variety of scientific and managerial activities.

6.4 Input data and model calibration

Running a dynamic model is usually the least time- or resource-consuming step in an assessment. It takes time to interpret model output, but most time-consuming is the acquisition and preparation of input data. Rarely can field, laboratory, or literature data be directly used as model inputs. They have to be pre-processed and interpreted, often with the help of other models. Especially for regional applications, not all model inputs are available (or directly usable) from measurements at sites, and interpolations and transfer functions have to be derived and used to obtain the necessary input data. When acquiring data from different sources of information, it is important to keep a record of the 'pedigree' (i.e., the entire chain of information, assumptions and (mental) models used to produce a certain number). Also, the uncertainty of the data should be assessed, recorded and communicated.

As with critical loads, for the policy support of the effects-oriented work under the LRTAP Convention, output of dynamic models will most usefully represent not a particular site, but a larger area, such as a forest instead of a single tree stand. Therefore, certain variables should be 'smoothed' to represent that larger area. For example, (projected) growth uptake of nutrients (nitrogen and base cations) should reflect the (projected) average uptake of the forest over that area, and not the succession of harvest and re- growth at a particular spot.

6.4.1 Input data

The input data required to run dynamic models depend on the model, but essentially all of them need the following (minimum) data, which can be roughly grouped into in- and output fluxes, and soil properties. Note that this grouping of the input data depends on the model considered. For example, weathering has to be specified as a (constant) input flux in the VSD/VSD+ models, whereas in the SAFE model it is internally computed from soil properties and depends on the state of the soil (e.g., the pH). Some of the input data are also needed in the SMB model to calculate critical loads, and are described in Chapter 5. This chapter thus focuses on additional data and parameters needed to run dynamic models. The most important soil parameters are the cation exchange capacity (CEC), the base saturation, and the exchange (or selectivity) constants describing cation exchange, as well as parameters describing nitrogen retention and sulphate ad/desorption, since these parameters determine the long-term behaviour (recovery) of soils.

Ideally, all input data are directly derived from measurements. This is usually not feasible for regional applications, in which case input data have to be derived from relationships (transfer functions) with basic (map) information. In this chapter, we provide information on the input data needed for running the VSD model and thus, by extension, also other models. Descriptions and technical details of the input data for those models can be found in Posch and Reinds (2009) for the VSD model, in Bonten et al (2015) for the VSD+ model, in Cosby et al. (1985a, 2001) for the MAGIC model and in Alveteg and Sverdrup (2002) for the SAFE model.

In most of the (pedo-)transfer functions presented here, soils – or rather soil groups – are characterised by a few properties, mostly organic carbon and clay content of the mineral soil (see also Figure 6.3). The organic carbon content, C_{org}, can be estimated as 0.5 or 0.4 times the

organic matter content in the humus or mineral soil layer, resp. If C_{org}>15%, a soil is considered a peat soil. Mineral soils are called sand (or sandy soil) here, if the clay content is below 18% (coarse textured soils; see also Table 6.6), otherwise it is called a clay (or clayey/loamy soil). Loess soils are soils with more than 50% *silt*, i.e. *clay*+*sand*<50% (since *clay*+*silt*+*sand*=100%).

Figure 6.3: Illustration of the basic composition of a soil profile: soil water, organic matter (organic carbon) and the mineral soil, characterised by its clay, silt, and sand fraction (clay+silt+sand=100%).

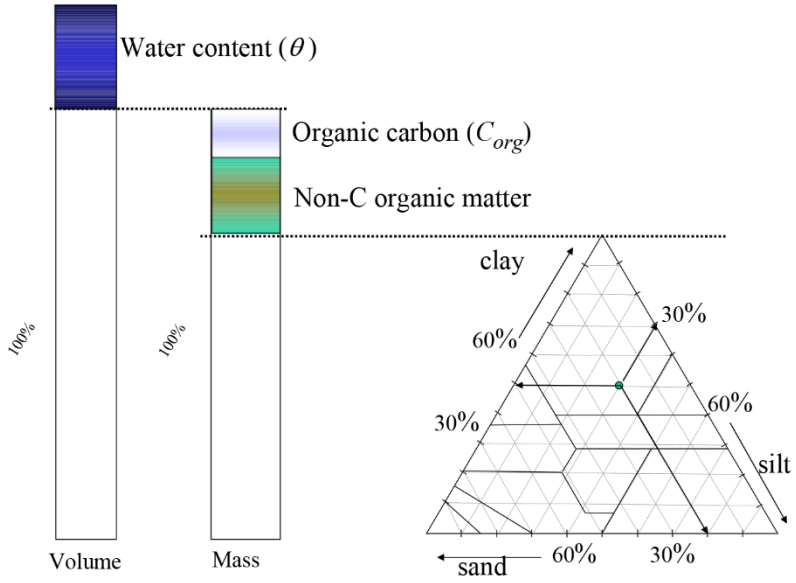

Source: This figure is adopted from a previous version of Chapter 6 of the Mapping Manual

6.4.1.1 Averaging soil properties

For single layer soil models, such as VSD, VSD+, or MAGIC, the profile averages of certain soil parameters are required, and in the sequel formulae for the average bulk density, cation exchange capacity, and base saturation are derived.

For a given soil profile it is assumed that there are measurements of bulk density ρ_l (g/cm³), cation exchange capacity CEC_l (meq/kg), and base saturation $E_{BC,l}$ for n (homogeneous) soil horizons with thickness z_l (l=1,..., n). Obviously, the total thickness (soil depth) z is given by:

(VI.21)

$$z = \sum_{l=1}^{n} z_l$$

The mean bulk density ρ of the profile is derived from mass conservation (per unit area):

(VI.22)

$$\rho = \frac{1}{z} \sum_{l=1}^{n} z_l \cdot \rho_l$$

The average cation exchange capacity *CEC* has to be calculated in such a way that the total number of exchange sites (per unit area) is given by $z \cdot \rho \cdot CEC$. This implies the following formula for the profile average cation exchange capacity:

(VI.23)

$$CEC = \frac{1}{z \cdot \rho} \sum_{l=1}^{n} z_l \cdot \rho_l \cdot CEC_l$$

And for the profile average base saturation E_{BC} one then gets:

(VI.24)

$$CEC = \frac{1}{z \cdot \rho \cdot CEC} \sum_{l=1}^{n} z_l \cdot \rho_l \cdot CEC_l \cdot E_{BC,l}$$

Note that for aquatic ecosystems, these parameters have to be averaged over the terrestrial catchment area as well.

6.4.1.2 Data also used for critical load calculations

In this section we describe those input data which are also used in critical load calculations (see chapter 5) For further details the reader is referred to that chapter, especially sections 5.3.1.3 and 5.3.2.3.

Whereas for critical loads and exceedance calculations, data are needed at a specific point in time (or at steady-state), their past and future temporal development is needed for dynamic modelling.

6.4.1.2.1 Deposition

Non-anthropogenic (steady-state) base cation and chloride deposition are incorporated into the definition of the critical load of acidity. For dynamic model times, a series of past and future depositions are needed. However, at present there are no projections available for these elements on a European scale. Thus, in most model applications (average) present base cation and chloride depositions are assumed to hold also in the future (and past).

Sulphur and nitrogen depositions enter only the exceedance calculations of critical loads. In contrast, their temporal development is the driving force of every dynamic model. Time series for the period 1880–1990 of S and N deposition on the EMEP-150 grid have been computed using published estimates of historical emissions (Schöpp et al. 2003) and 12-year average transfer matrices derived from the EMEP/MSC-W lagrangian atmospheric transport model. Equivalent datasets have been prepared for the EMEP 50x50 km^2 as well as the latest 10x10 km^2 grids.

Scenarios for future sulphur and nitrogen deposition are provided by integrated assessment modellers, based on atmospheric transport modelling by EMEP.

In case the deposition model provides only grid average values, a local deposition (adjustment) model could compute the local deposition from the grid average values, especially for forest soils, where the actual (larger) deposition depends on the type and age of trees (via the 'filtering' of deposition by the canopy). An example of such a model is the MAKEDEP model, which is also part of the SAFE model system (Alveteg and Sverdrup 2002).

6.4.1.2.2 Uptake

Long-term average values of the net growth- uptake of nitrogen and base cations by forests are also needed to calculate critical loads. Data sources and calculation procedures are given in Chapter 5. In simple dynamic models these processes are described as a function of actual and projected forest growth. To this end, additional information on forest age and growth rates is needed, and the amount of data needed depends largely on whether the full nutrient cycle is modelled or whether only net sources and sinks are considered.

When considering net removal by forest growth, as in the VSD and MAGIC models, the yield (forest growth) at a certain age can be derived from yield tables for the considered tree species. The element contents in stems (and possibly branches) should be the same as used in the critical load calculations (see, e.g., Table 5.2). If the nutrient cycle is modelled, as in the SAFE model, data are needed on litterfall rates, root turnover rates, including the nutrient contents in litter (leaves/needles falling from the tree), and fine roots. Such data are highly dependent on tree species and site conditions. Compilations of such data can be found in De Vries et al. (1990) and Jacobsen et al. (2002).

6.4.1.2.3 Water flux and soil moisture

Water flux data that are needed in one- layer models are limited to the precipitation surplus leaving the root zone (see Chapter 5), whereas multi- layer models require water fluxes for each soil layer down to the bottom of the root zone. For simple dynamic models, water fluxes could be calculated by a separate hydrological model, running on a daily or monthly time step with aggregation to annual values afterwards. An example of such a model is WATBAL (Starr 1999), which is a capacity-type water balance model for forested stands/plots running on a monthly time step and based on the following water balance equation:

(VI.25)

$$Q = P - ET \pm \Delta SM$$

where Q = precipitation surplus, P = precipitation, ET = evapotranspiration, and $\pm\Delta SM$ = changes in soil moisture content. WATBAL uses relatively simple input data, which is either directly available (e.g., monthly precipitation and air temperature) or which can be derived from other data using transfer functions (e.g., soil available water capacity).

In any dynamic model, that includes a mass balance for elements, information on the soil moisture content is also needed. This is also output from a hydrological model (see SM in eq.6.25) or has to be estimated from other site properties. An approximate annual average soil moisture content θ (m^3/m^3) can be obtained as a function of the clay content (see Brady 1974):

(VI.26)

$$\theta = \min\{0.04 + 0.0077 \cdot \ clay, 0.27\}$$

Namely, for clay contents above 30% a constant value of 0.27 is assumed. It should be noted that most models are quite insensitive to the value of θ.

6.4.1.2.4 Base cation weathering

The various possibilities to assess weathering rates of base cations, which are a key input also to critical load calculations, are discussed and cited in Chapter 5.

6.4.1.2.5 Mineralisation and (de-)nitrification

Rate constants (and possibly additional parameters) for mineralisation, nitrification, and denitrification are needed in detailed models, but simple models mostly use factors between

zero and one, which compute nitrification and denitrification as fraction of the (net) input of nitrogen.

As with the calculation of critical loads (SMB model), in the VSD model complete nitrification is assumed (nitrification fraction equals 1.0), and denitrification fractions can be found in Table 5.3. Mineralisation is not considered explicitly, but included in the net immobilisation calculations.

For the complete soil profile, the nitrification fraction in forest soils varies mostly between 0.75 and 1.0. This is based on measurements of NH_4/NO_3 ratios below the root-zone of highly acidic Dutch forests with very high NH_4 inputs in the early nineties, which were nearly always less than 0.25 (De Vries et al. 1995). Generally, 50% of the NH_4 input is nitrified above the mineral soil in the humus layer (Tietema et al. 1990). Actually, the nitrification fraction includes the effect of both nitrification and preferential ammonium uptake.

6.4.1.2.6 AL-H equilibrium

The constants needed to quantify the equilibrium between [Al] and [H] in the soil solution are discussed and presented in Chapter 5 (Table 5.9), since they are also needed for critical load calculations. For models including the complexation of Al with organic anions, such as MAGIC, relevant parameters can be found (e.g., in Driscoll et al. (1994)).

6.4.1.3 Data needed to simulate cation exchange

In all dynamic soil models, cation exchange is a crucial process (see section 6.2.3.1). Data needed to allow exchange calculations are:

- The pool of exchangeable cations, being the product of layer thickness, bulk density, cation exchange capacity (CEC) and exchangeable cation fractions;
- Cation exchange constants (selectivity coefficients).

These data are preferably taken from measurements. Such measurements are generally made for several soil horizons. For single-layer models, such as VSD, these data have to be properly averaged over the entire soil depth (rooting zone; see eqs. VI.21 – VI.24).

In the absence of measurements, the various data needed to derive the pool of exchangeable cations for major forest soil types can be derived by extrapolation of point data, using transfer functions between bulk density, CEC and base saturation and basic land and soil characteristics, such as soil type, soil horizon, organic matter content, soil texture, etc.

6.4.1.3.1 Soil bulk density

If no measurements are available, the soil bulk density ρ (g cm^{-3}) can be estimated from the following transfer function:

(VI.27)

$$\rho = \begin{cases} 1/\left(0.625 + 0.05 \cdot C_{org}\right), & C_{org} \leq 5\% \\ 1.55 - 0.0814 \cdot C_{org}, & 5\% < C_{org} < 15\% \\ 0.725 - 0.337 \cdot \log_{10} C_{org}, & C_{org} \geq 15\% \end{cases}$$

where C_{org} is the organic carbon content and *clay* the clay content (both in %). The top equation for mineral soils is based on data by Hoekstra and Poelman (1982), the bottom equation for peat(y) soils is derived from Van Wallenburg (1988) and the central equation is a linear interpolation (for *clay*=0) between the two.

6.4.1.3.2 Cation exchange capacity (CEC)

The value of the CEC depends on the soil pH at which the measurements are made. Consequently, there is a difference between unbuffered CEC values measured at the actual soil pH and buffered values measured at a standard pH, such as 6.5 or 8.2. In the VSD (and many other) models the exchange constants are related to a CEC that is measured in a buffered solution in order to standardise to a single pH value (e.g., pH=6.5, as upper limit of non-calcareous soils). The actual CEC can be calculated from pH, clay and organic carbon content according to (after Helling et al. 1964):

(VI.28)

$$CEC(pH) = (0.44 \cdot\ pH + 3.0) \cdot clay + (5.1 \cdot\ pH - 5.9) \cdot C_{org}$$

where CEC is the cation exchange capacity (meq/kg), clay is the clay content (%) and C_{org} the organic carbon content (%). The pH in this equation should be as close as possible to the measured soil solution pH. For sandy soils the clay content can be set to zero in eq. VI.28. Typical average clay contents as a function of the texture class, presented on the FAO soil classification (FAO 1981), are given in Table 6.2. Values for C_{org} range from 0.1% for arenosols (Qc) to 50% for peat soils (Od).

Table 6.2: Average clay contents and typical base saturation as a function of soil texture classes (see Table 6.6).

Texture class	Name	Definition	Average clay content (%)	Typical base saturation (%)
1	coarse	clay < 18% and sand ≥ 65%	6	5
2	medium	clay < 35% and sand ≥ 15%; but clay ≥ 18% if sand ≥ 65%	20	15
3	medium fine	clay < 35% and sand < 15%	20	20
4	fine	35% ≤ clay < 60%	45	50
5	very fine	clay ≥ 60%	75	50
9	organic soils	Soil types O	5	10-70

Computing CEC ($pH_{measured}$) (i.e., the CEC from eq. VI.28) using measured (site- specific) C_{org}, $clay$ and pH does not always match the measured CEC, $CEC_{measured}$, and thus computing CEC at pH=6.5, CEC (6.5), would not be consistent with it. Nevertheless, eq. VI.28 can be used to *scale* the measured CEC to a value at pH=6.5 (i.e. the value needed for modelling), in the following manner:

(VI.29)

$$CEC_{pH=6.5} = CEC_{measured} \cdot \frac{CEC(6.5)}{CEC(pH_{measured})}$$

This method of scaling measured data with the ratio (or difference) of model output is widely used in global change work to obtain, for example, climate-changed (meteorological) data consistent with observations.

6.4.1.3.3 Exchangeable base cation fraction (base saturation)

In most models, a lumped expression is used for the exchange of cations, distinguishing only between H, Al and base cations (VSD, VSD+, and SAFE). As with the clay content, data for the

exchangeable cation fractions, or in some cases only the base saturation, can be based on information on national soil information systems, or in absence of these, on the FAO soil map of Europe (FAO 1981). Base saturation data vary from 5-25% in relatively acid forest soils to more than 50% in well buffered soils. A very crude indication of the base saturation as a function of the texture class of soils is given in the last column of Table 6.2. This relationship is based on data from forest soils given in FAO (1981) and in Gardiner (1987). A higher texture class reflects a higher clay content implying an increase in weathering rate, which implies a higher base saturation. For organic soils, the base saturation is put equal to 70% for eutric histosols (Oe) and 10% for dystric histosols (Od).

Ideally, only measured CEC and exchangeable cation data are used. However, when data on the initial base saturation of soils are not available for regional (national) model applications, one may derive them from a relationship with environmental factors. Such an exercise was carried out using a European database with approximately 5,300 soil chemistry data for the organic layer and the forest topsoil (0-20 cm) collected on a systematic 16×16 km^2 grid (ICP Forest level-I grid; Vanmechelen et al. 1997). The regression relationship for the estimated base saturation EBC (expressed as a fraction with values between 0 and 1) is:

(VI.30a)

$$E_{BC} = \frac{1}{1 + e^{-B}}$$

(VI.30b)

$$B = a_0 + a_1(soilgroup) + a_2(treespecies) + a_3 \cdot altitude + a_4 \cdot \ln(age) + a_5 \cdot temperature + a_6(temperature)^2 + a_7 \cdot \ln(precipitation) + \sum_{k=8}^{k=11} a_k \cdot \ln(deposition_k) + \sum_{k=12}^{k=15} a_k \cdot \mathrm{lt}(depositionfraction_k)$$

where 'ln' is the natural logarithm, lt(x)=ln(x/(1–x)), and the a_k's are the regression coefficients. The regression analysis was carried out using a so-called select-procedure. This procedure combines qualitative predictor variables, such as tree species and/or soil type, with quantitative variables and combines forward selection, starting with a model including one predictor variable, and backward elimination, starting with a model including all predictor variables. The 'best' model was based on a combination of the percentage of explained variance (which should be high) and the number of predictor variables (which should be low). More information on the procedure is given in Klap et al. (2004). Results of the analyses are given in Table 6.3. The explained variance for base saturation was approximately 45%.

Note: When data are not available, one may also calculate base saturation as the maximum of (i) a relation with environmental factors as given above and (ii) an equilibrium with present deposition levels of SO_4, NO_3, NH_4, and BC. Especially in southern Europe, where acid deposition is relatively low and base cation input is high, the base saturation in equilibrium with the present load can be higher than the value computed according to eq. VI.30.

Table 6.3: Coefficients for estimating base saturation and the C/N-ratio in the mineral topsoil (0- 20cm) and the organic layer (after Klap et al. 2004; Note: (a) the star denotes sea-salt corrected depositions, (b) depositions<0.1 should be set to 0.1 to avoid underflow in the equations).

Predictor variable	Base saturation (mineral topsoil)	C/N-ratio (organic layer)	C/N-ratio (mineral topsoil)	Coefficients in eqs.6.30 and 6.31
Constant	3.198	3.115	1.310	a_0
Soil group:				
sandy soils	0	0	0	a_1
loamy/clayey soils	0.297	-0.807	-0.279	a_1
peat soils	0.534	-0.025	-0.312	a_1
Tree species:				
pine	0	0	0	a_2
spruce	-0.113	-0.158	-0.093	a_2
oak	0.856	-0.265	-0.218	a_2
beech	0.591	-0.301	-0.218	a_2
Site conditions:				
Altitude [m]	-0.00014	-0.00008	-0.000136	a_3
Age [yr]	0	0.025	0.096	a_4
Meteorology:				
Temperature [°C]	0	-0.0078	-0.041	a_5
Temperature^2 [°C^2]	0	0.00095	0.0014	a_6
Precipitation [mm/yr]	0	0.178	0.194	a_7
Deposition:				
Na [eq/ha/yr]	-0.223	0	0.080	a_8
N-tot (=NO_y+NH_z) [eq/ha/yr]:				
sandy soils	0	-0.150	-0.019	a_9
loamy/clayey soils	0	-0.032	0	a_9
peat soils	0	-0.136	0	a_9
Acid (=So_x^* +N-tot) [eq/ha/yr]	-1.025	0	0	a_{10}
Bc* (=Ca^*+Mg^*+K^*) [eq/ha/yr]	0.676	0	0	a_{11}
Deposition fractions:				
NH_z/*Acid* [-]:				
sandy soils	0	0	0	a_{12}

Predictor variable	Base saturation (mineral topsoil)	C/N-ratio (organic layer)	C/N-ratio (mineral topsoil)	Coefficients in eqs.6.30 and 6.31
loamy/clayey soils	-0.494	0	0	α_{12}
peat soils	-0.896	0	0	α_{12}
NH_z/N-tot [-]	0	0.102	0.120	α_{13}
Ca^*/Bc^* [-]	1.211	0	0	α_{14}
Mg^*/Bc^* [-]	0.567	0	0	α_{15}

6.4.1.3.4 Exchange constants (selectivity coefficients)

In many exchange models the cations are lumped to H, Al, and base cations (as in VSD, VSD+, and SAFE), but in MAGIC every base cation (Ca, Mg, K, Na) is modelled separately. Furthermore, cation exchange in VSD, VSD+, and MAGIC is based upon Gaines-Thomas equations; in SAFE it is described by Gapon exchange reactions, whereas in the VSD and VSD+ models the user can choose between the two. Exchange constants can be derived from the simultaneous measurement of the major cations (H, Al, Ca, Mg, K, and Na) at the adsorption complex and in the soil solution.

In contrast to the other dynamic soil models, MAGIC takes a different approach to estimating both weathering rates and selectivity coefficients for base cations. MAGIC assumes that at some time in the past (i.e., year 1850), the ecosystem was at steady-state with the output flux of each base cation in runoff (soil leachate) equal to weathering plus deposition. The user thus chooses an initial set of values for weathering and % base cation saturation, runs the model forward in time to the present driven by an historical sequence of deposition and compares the simulated values for % base cation saturation and concentration of base cation in runoff with those measured for the present-day reference year. If these do not agree, then the user goes back and, by trial-and-error, changes the initial values such that the simulated agree with the observed for each of the four base cations in the reference year. This trial-and-error procedure has been automated for MAGIC with a program named “MAGICOPT”.

Using more than 800 such measurements from Dutch soils, extensive tables of exchange constants have been derived for sand, loess, clay, and peat soils, together with their standard deviations and correlations for all combinations of H, Al, and base cations (De Vries and Posch 2003). The data show the high affinity of the complex for protons compared to all other monovalent cations, and that the relative contributions of K, Na, and NH4 on the adsorption complex are very low. Results for the logarithms ($\log_{10}$) of the exchange constants used in the VSD model, both for the ‘Gaines-Thomas mode’ and the ‘Gapon mode’, together with their standard deviation (‘stddev’) are given in Tables 6.4 to 6.7. For a conversion to other units see Annex III.

It should be noted that exchange constants vary widely and are unknown for most sites. Therefore, in most models (SAFE, MAGIC, but also VSD) they are calibrated against measurements of base saturation (and soil solution concentrations).

Table 6.4: Mean and standard deviation of logarithmic *Gaines-Thomas* exchange constants of *H* against *Ca+Mg+K* as a function of soil depth for sand, loess, clay, and peat soils $(mol/l)^{-1}$.

Layer	Sand		Loess		Clay		Peat	
(cm)	Mean	stddev	Mean	Stddev	Mean	stddev	Mean	stddev
0-10	5.338	0.759	5.322	0.692	6.740	1.464	4.754	0.502
10-30	6.060	0.729	5.434	0.620	6.007	0.740	4.685	0.573
30-60	6.297	0.656	-	-	6.754	0.344	5.307	1.051
60-100	6.204	0.242	5.541	0.579	7.185	-	5.386	1.636
0-30	5.236	0.614	5.386	0.606	6.728	1.373	4.615	0.439
0-60	5.863	0.495	-	-	6.887	1.423	4.651	0.562

Table 6.5: Mean and standard deviation of logarithmic *Gaines-Thomas* exchange constants of *Al* against *Ca+Mg+K* as a function of soil depth for sand, loess, clay, and peat soils (mol/l).

Layer	Sand		Loess		Clay		Peat	
(cm)	Mean	stddev	Mean	Stddev	Mean	stddev	Mean	stddev
0-10	2.269	1.493	1.021	1.147	1.280	1.845	0.835	1.204
10-30	3.914	1.607	1.257	0.939	-0.680	1.152	0.703	0.968
30-60	4.175	1.969	-	-	-3.070	0.298	0.567	1.474
60-100	2.988	0.763	1.652	1.082	-2.860	-	0.969	1.777
0-30	2.306	1.082	0.878	1.079	0.391	1.555	0.978	0.805
0-60	2.858	1.121	-	-	-0.973	1.230	0.666	0.846

Table 6.6 : Mean and standard deviation of logarithmic *Gapon* exchange constants of *H* against *Ca+Mg+K* as a function of soil depth for sand, loess, clay, and peat soils $(mol/l)^{-1/2.}$

Layer	Sand		Loess		Clay		Peat	
(cm)	Mean	stddev	Mean	Stddev	Mean	stddev	Mean	stddev
0-10	3.178	0.309	3.138	0.268	3.684	0.568	2.818	0.199
10-30	3.527	0.271	3.240	0.221	3.287	0.282	2.739	0.175
30-60	3.662	0.334	-	-	3.521	0.212	2.944	0.382
60-100	3.866	0.125	3.232	0.251	3.676	-	3.027	0.672
0-30	3.253	0.311	3.170	0.206	3.620	0.530	2.773	0.190
0-60	3.289	0.340	-	-	3.604	0.654	2.694	0.170

Table 6.7: Mean and standard deviation of logarithmic *Gapon* exchange constants of *Al* against *Ca+Mg+K* as a function of soil depth for sand, loess, clay, and peat soils (mol/l)$^{1/6}$.

Layer	Sand		Loess		Clay		Peat	
(cm)	Mean	stddev	Mean	Stddev	Mean	stddev	Mean	stddev
0-10	0.306	0.440	0.190	0.546	-0.312	0.738	-0.373	0.350
10-30	0.693	0.517	0.382	0.663	-0.463	0.431	-0.444	0.255
30-60	0.819	0.527	-	-	-1.476	0.093	-0.740	0.336
60-100	1.114	0.121	0.390	0.591	-1.795	-	-0.867	0.401
0-30	0.607	0.472	0.221	0.647	-0.609	0.731	-0.247	0.404
0-60	0.199	0.633	-	-	-1.054	0.362	-0.551	0.210

6.4.1.4 Data needed for balances of nitrogen, sulphate, and aluminium

6.4.1.4.1 C/N-ratio

Data for the C/N-ratio generally vary between 15 in rich soils where humification has been high to 40 in soils with low N inputs and less humification. Values can also be obtained from results of a regression analysis similar to that of the base saturation according to:

(VI.31)

$$\ln(C/N-ratio) = a_0 + a_1(soilgroup) + a_2(treespecies) + a_3 \cdot altitude + a_4 \cdot \ln(age) + a_5 \cdot temperature + a_6(temperature)^2 + a_7 \cdot \ln(precipitation) + \sum_{k=8}^{k=11} a_k \cdot \ln(deposition_k) + \sum_{k=12}^{k=15} a_k \cdot \mathrm{lt}(depositionfraction_k)$$

where 'ln' is the natural logarithm and lt(x) = ln(x/(1–x)). Results of the analysis, which was performed with the same data sets as described in the section on base saturation, are given in Table 6.3; and more information on the procedure is given in Klap et al. (2004).

6.4.1.4.2 Sulphate sorption capacity and half- saturation constant

Values for the maximum sorption capacity for sulphate, S_{max}, can be related to the content of oxalate extractable Al (meq kg^{-1}) according to (Johnson and Todd 1983):

(VI.32)

$$S_{max} = 0.02 \cdot Al_{ox}$$

Estimates for the oxalate extractable Al content are given below. Adsorption or half- saturation constants for sulphate, $S_{1/2}$, can be derived from literature information (e.g., Singh and Johnson 1986, Foster et al. 1986). A reasonable average value is 1.0 eq/m^3.

6.4.1.4.3 AL-hydroxide content

Data for the oxalate extractable Al content (the content of readily available Al- hydroxide) are often available in national soil information systems, such as the soil information system of the Netherlands. In sandy soils the Al-hydroxide content (in meq/kg) mostly varies between 100-

200 for A-horizons, between 200-350 for B- horizons, and between 50-150 for C- horizons (parent material, De Vries 1991).

6.4.1.5 Model calibration

If all input parameters, initial conditions, and driving forces were known, the chosen model would describe the future development of the soil chemical status for any given deposition scenario. However, in most cases several of the parameters are poorly known, and thus many models (i.e. the badly known parameters in the model) have to be 'calibrated'. The method of calibration varies with the model and/or the application.

In standard applications of both the MAGIC and SAFE model it is assumed that in pre-acidification times (say 1850) the input of ions is in equilibrium (steady-state) with the soil (solution) chemistry. Furthermore, it is assumed that the deposition history of all (eight) ions is known (properly reconstructed).

In SAFE, weathering rates and uptake/net removal of N and base cations are computed within the model (see above). Only simulated (present) base saturation is matched with observations (in every soil layer) by adjusting the cation exchange selectivity coefficient(s). Matching simulated and observed soil solution concentrations is not part of the standard calibration procedure.

The calibration of MAGIC is a sequential process whereby firstly the input and output of those ions assumed to act conservatively in the catchment are balanced (usually only Cl). Next, the anion concentrations in surface waters are matched by adjusting catchment net retention (of N) and soil adsorption (of S) if appropriate. Thirdly, the four individual major base cation concentrations in the stream and on the soil solid phase (expressed as a percentage of cation exchange capacity) are matched by adjusting the cation exchange selectivity coefficients and the base cation weathering rates. Finally, surface water pH, Al, and organic anion concentrations are matched by adjusting the aluminium solubility coefficient and total organic acid concentration in surface water.

Both in MAGIC and SAFE automatic calibration routines are an important part of the overall model system. For the VSD and VSD+ model, a Bayesian calibration routine has been implemented, the details of which can be found in Reinds et al. (2008) and Posch and Reinds (2009) and in the help-file of the 'VSD/VSD+-Studio' software (available at www.wge-cce.org).

6.5 Model calculations and presentation of model results

As stated above, the most demanding part is not the actual running of a model, but the derivation and preparation of input data (files) and the model initialisation/calibration. However, especially for regional applications (i.e. runs for many sites), additional work is required to embed the model – often designed for single site applications – into a suitable (data base) framework which allows the efficient handling of model inputs and outputs.

6.5.1 Use of dynamic models in integrated assessment

Most usefully for the review of the Gothenburg Protocol, a link should be established between the dynamic models and integrated assessment (models). In the following several modes of interaction with integrated assessment (IA) models are identified.

6.5.1.1 Scenario analyses

Deposition scenario output from IA models are used by the 'effects community' (ICPs) as input to dynamic models to analyse their impact on (European) soils and surface waters, and the results (recovery times etc.) are reported back.

Presently available dynamic models are well suited for this task. The question is how to summarise the resulting information on a European scale. Also, the 'turn-around time' of such an analysis (i.e. the time between obtaining deposition scenarios and reporting back dynamic model results) may be long as it could involve the work of several subsidiary bodies under the LRTAP Convention.

6.5.1.2 Response functions

Response functions are pre-processed dynamic model runs for a large number of plausible future deposition patterns from which the results for every (reasonable) deposition scenario can be obtained by interpolation. Such response functions encapsulate a site's temporal behaviour to reach a certain (chemical) state and linking them to IA models allows to evaluate the site's response to a broad range of deposition patterns.

An example is shown in Figure 6.4: It shows the isolines of years ('recovery isochrones') in which Al/Bc=1 is attained for the first time for a given combination of percent deposition reduction (vertical axis) and implementation year (horizontal axis). The reductions are expressed as percentage of the deposition in 2010 after implementation of the Gothenburg Protocol and the implementation year refers to the full implementation of that additional reduction. For example, a 44% reduction of the 2010 deposition that is fully implemented by the year 2020 will result in a (chemical) recovery by the year 2040 (dashed line in Figure 6.4). Note that for this example site no recovery is possible, unless deposition is reduced more than 18% of the 2010 level.

Figure 6.4: Example of 'recovery isochrones' for a single site. The vertical axis gives the additional reduction in acidifying deposition after the implementation of the Gothenburg Protocol in 2010 (expressed as percentage of the 2010 level) and the horizontal axis the year at which these additional reductions are fully implemented. The isolines are labelled with the first year at which Al/Bc=1 is attained for a given combination of percent reduction and implementation year.

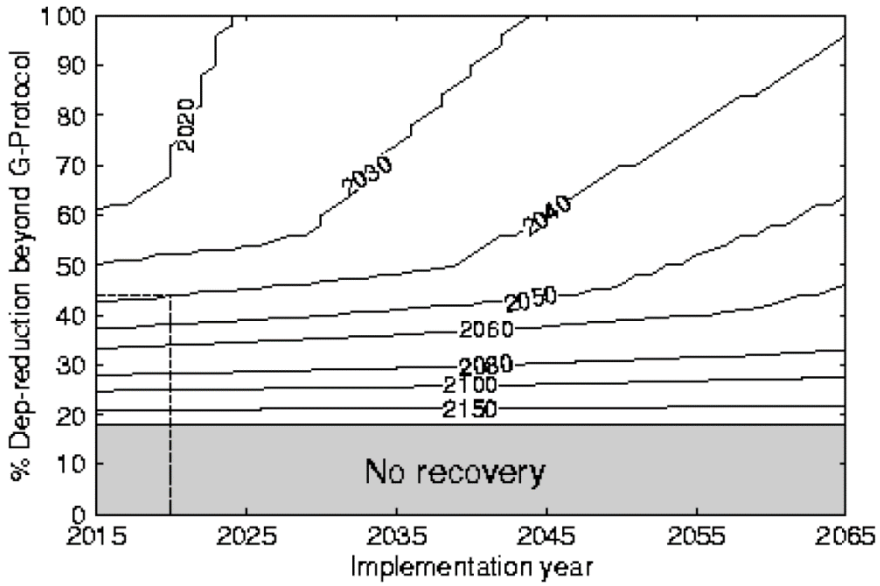

Source: This figure is adopted from a previous version of Chapter 6 of the Mapping Manual

Figure 6.5: Required deposition reductions (target loads) for a site as a function of the target year, i.e., the year in which recovery is achieved (see also Figure 6.4). The implementation year of the reductions is 2020. Note that for reductions above 74% the recovery happens already before the implementation year.

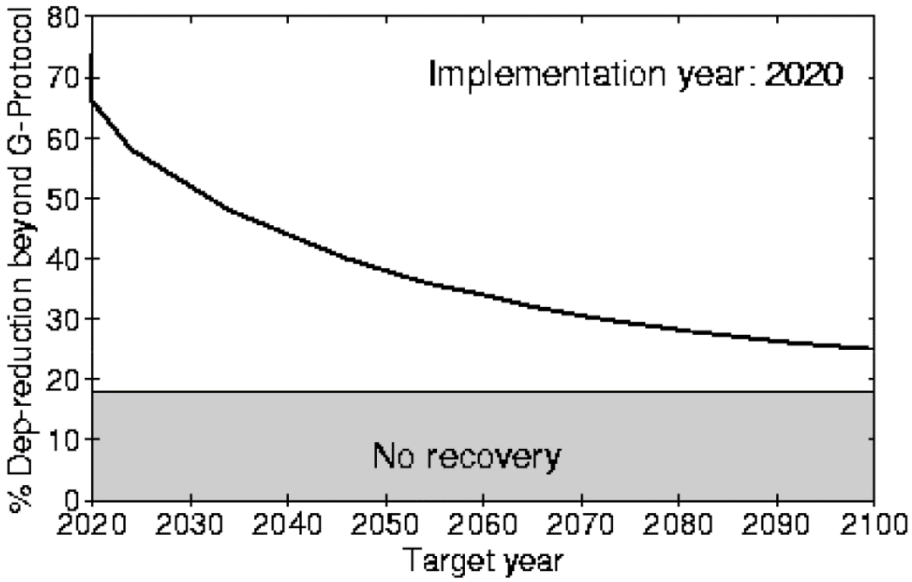

Source: This figure is adopted from a previous version of Chapter 6 of the Mapping Manual

During the negotiations of protocols or of their review, a recurrent question to integrated assessment modellers is: What is the maximum deposition allowed to achieve recovery (i.e., reach and sustain) a desired chemical state (e.g., Al/Bc=1) in a prescribed year? Such a deposition is called a **target load** and, in the case of a single pollutant, target loads can, in principle, be read from information as presented in Figure 6.4. In Figure 6.5, target loads (expressed as percent deposition reductions from the 2010 level) are shown explicitly as function of the target year for the (fixed) implementation year 2020. In the case of a single pollutant, this is the type of information to be linked to integrated assessment models.

However, in the case of acidity, both N and S deposition determine the soil chemical state and it will not be possible to obtain unique pairs of N and S deposition to reach a prescribed target (similar to critical load functions for acidity). Thus, **target loads** functions have to be derived with dynamic models for a series of target years and agreed upon implementation years. These target load functions, or suitable statistics derived from them, are passed on to the integrated assessment modellers who evaluate their feasibility of achievement (in terms of costs and technological abatement options available).

The determination of response functions, such a target loads, requires no changes to existing models *per se*, but rather additional work, since dynamic soil model have to run many times and/or 'backwards' (i.e. in an iterative mode). A further discussion of the problems and possible pitfalls in the computation of target loads is provided in the next section (see also Jenkins et al. 2003).

6.5.1.3 Integrated dynamic model

The 'most intimate' link would be the integration of a dynamic model into an integrated assessment model (e.g., GAINS). In this way it could be an integral part of all scenario analyses and optimisation runs. Widely used models, such as MAGIC or SAFE, are not easily incorporated into integrated assessment models, and they might be still too complex to be used in

optimisation runs. Alternatively, a very simple dynamic model could be incorporated into an integrated assessment model, capturing the essential, long-term features of dynamic soil models. This would be comparable to the process that led to the simple ozone model included in GAINS, which was derived from the complex photo- oxidant model of EMEP. However, even this would require a major effort, not the least of which is the creation of a European database to run the model.

6.5.2 Target load calculations

As outlined above, target loads, or target load functions in the case of acidification, are a way to link dynamic models with integrated assessment models, not least due to their similarity with critical load functions (see chapter 5). If a target load exists, there exists also an infinite variety of deposition paths to reach that target load. To bring order into this multitude and to make results comparable, we define a target load as a deposition path characterised by three numbers (years): (i) the protocol year, (ii) the implementation year, and (iii) the target year (see Figure 6.6). If needed, these terms are proceeded by the term 'dynamic modelling' ('DM') to distinguish them from similar terms used in integrated assessment circles.

In contrast to scenario analyses, the computation of target loads is not straightforward. After specifying the target year and the year of implementation of the (yet unknown) target load, the dynamic model has to be run iteratively until the deposition (= target load) is found which is required to reach the desired chemical status in the specified target year. The following examples demonstrate the different cases that can arise when calculating target loads and what can happen when doing such calculations 'blindly'. For the sake of simplicity, we use a single pollutant (deposition), but the conclusions hold for target load functions as well.

As an example, Figure 6.7 shows the deposition history (left) and the resulting molar Al/Bc-ratio (right) as simulated (by the VSD model) for three different soils, solely distinguished by their CEC (40, 60 and 80 meq/kg). In two cases the Al/Bc- ratio in the year 2010 is above the critical value (=1), while for CEC=80 it stayed below it during the past. To investigate the future behaviour of the soils, we let the deposition drop to the critical load (which is independent of the CEC) during the 'implementation period' (marked by two vertical lines in Figure 6.7). Obviously, for CEC=80, the Al/Bc-ratio stays below one, whereas for CEC=60 it drops below one within the first decade and then slowly rises again towards the critical value. For CEC=40, the Al/Bc-ratio stays well above the critical value, approaching it asymptotically over time. In all three cases the approach to the critical value is very slow.

Figure 6.6: **Deposition paths for calculating target loads by dynamic models (DM) are characterised by three key years. (i) The year up to which the (historic) deposition is fixed (*protocol year*); (ii) the year in which the emission reductions leading to a target load are fully implemented (*DM implementation year*); and (iii) the years in which the chemical criterion is to be achieved.**

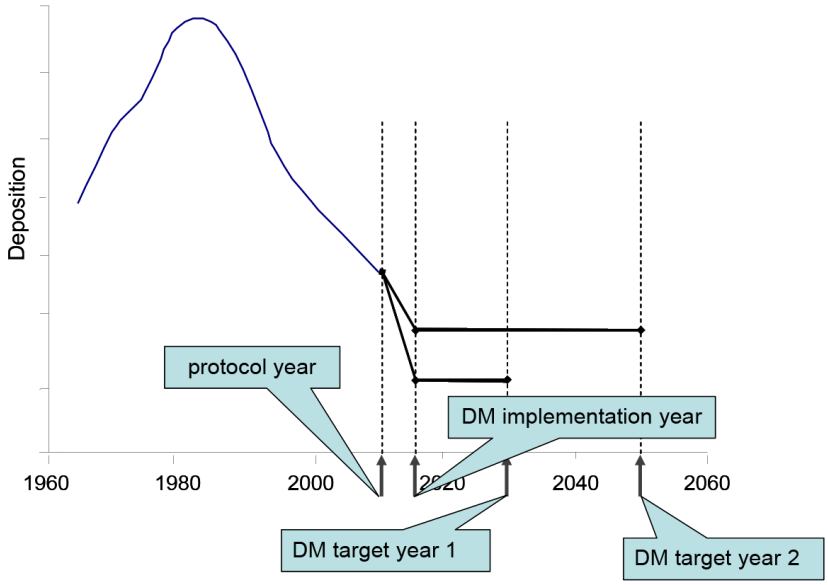

Source: This figure is adopted from a previous version of Chapter 6 of the Mapping Manual

Figure 6.7: **Temporal development of acidifying deposition (left) and corresponding molar Al/Bc- ratio (right) for 3 soils varying in CEC. The two vertical lines separate 50 years of 'history', 10 years (2010-2020) of implementation, and the future. Also shown are the critical load and the critical value $(Al/Bc)_{crit}$=1 as thin horizontal lines. The deposition drops to the critical load within the implementation period and the Al/Bc-ratios (slowly) approach the critical value.**

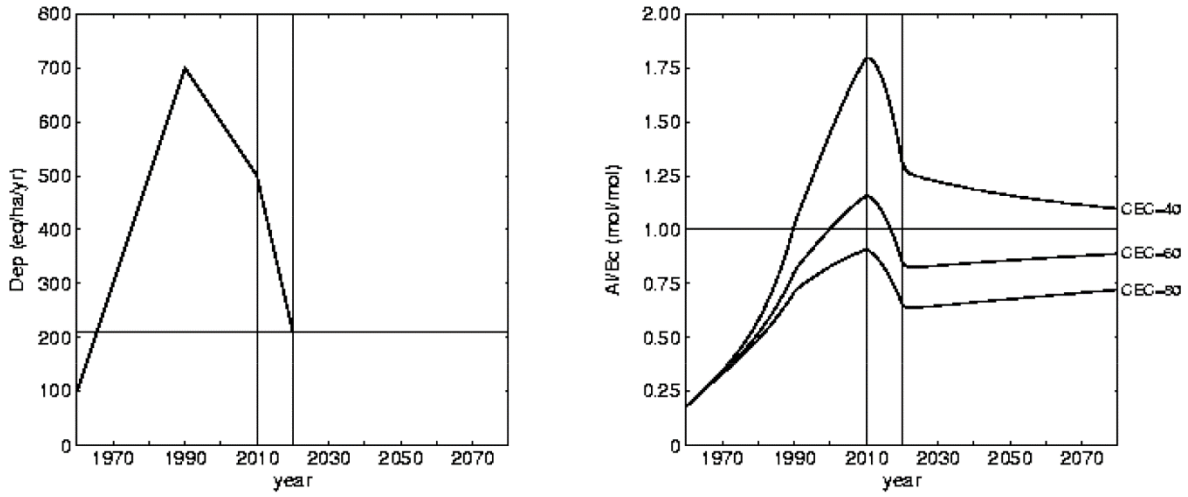

Source: This figure is adopted from a previous version of Chapter 6 of the Mapping Manual

Next, we look at target load calculations for these three soils. Figure 6.8 shows the results of target load calculations for 40 years, in other words, achieving $(Al/Bc)_{crit}$=1 in the year 2050. For CEC=40 meq/kg the target load is smaller than the critical load, as one would expect. For CEC=60 and 80, however, the computed target loads are higher than the critical load. As

Figure 6.8 illustrates, this does not make sense: After reaching the critical limit, these two soils deteriorate and the Al/Bc-ratio gets larger and larger. Since target loads are supposed to protect also *after* the target year, we stipulate that *whenever a calculated target load is higher than the critical load it has to be set equal to the critical load*.

In the light of the above considerations we define that ***a target load is the deposition for which a pre-defined chemical or biological status is reached in the target year and maintained (or improved) thereafter.***

Figure 6.8: Target loads (with 2050 as target year) for three soils and the resulting Al/Bc-ratio (left). Note that for CEC=60 and 80 the target load is higher than the critical load, even when $(Al/Bc)_{crit}<1$ at present (for CEC=80). Clearly, in such cases target load calculations don't make sense.

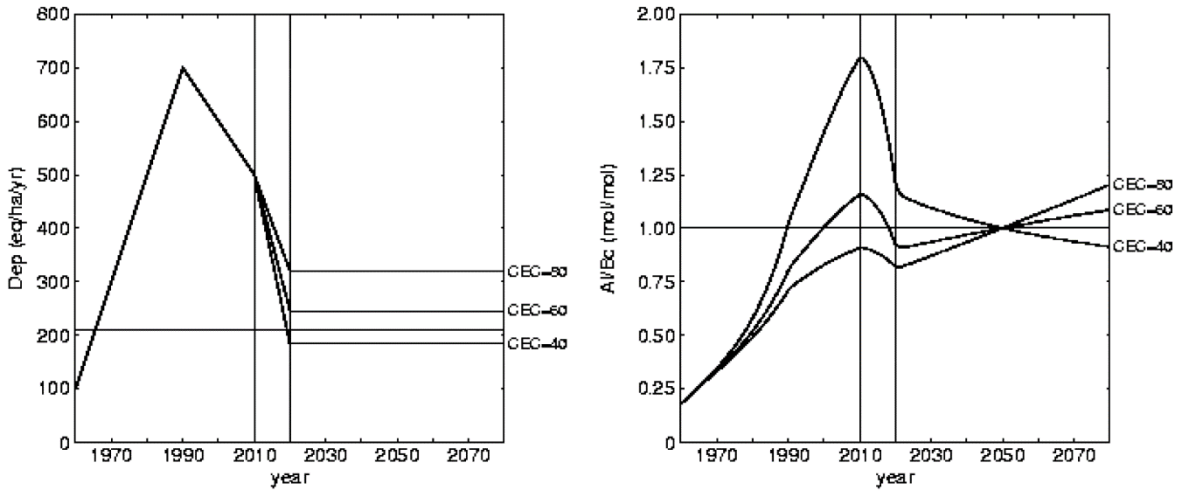

Source: This figure is adopted from a previous version of Chapter 6 of the Mapping Manual

Figure 6.9: Flow chart of the procedure to calculate a target load, avoiding the pitfalls mentioned in the text (e.g., computing a target load that allows violation of the criterion after the target year).

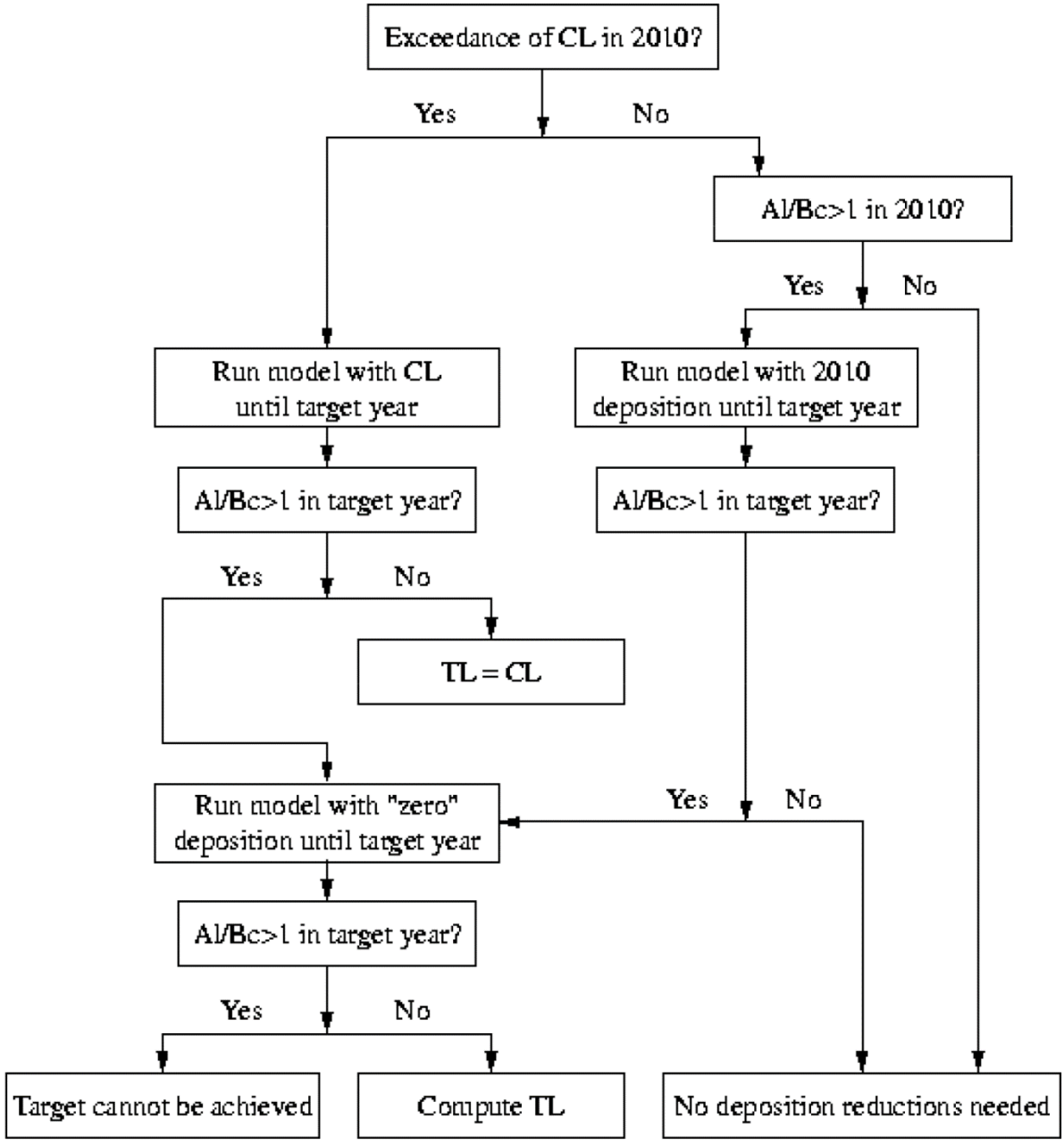

Source: This figure is adopted from a previous version of Chapter 6 of the Mapping Manual

In view of this, the steps to be considered for calculating a target load are shown in the flow chart in Figure 6.9. The first check at every site is whether the critical load (CL) is exceeded in the reference year (2010 in this case). If the answer is 'yes' (as for the soils with CEC=40 and 60 in Figure 6.7), the next step is to run the dynamic model with the deposition equal to the critical load. If in the target year the chemical criterion is no longer violated (e.g., Al/Bc≤1), the target load equals the critical load (TL=CL).

If, after running the model with the critical load as deposition, the criterion is still violated in the target year, the model has to be run with "zero" deposition until the specified target year. "Zero" deposition means a deposition small enough as not to contribute to acidification (or

eutrophication). In the case of nitrogen, this would mean that N_{dep} is set equal to $CL_{min}(N)$, thus avoiding problems, such as, for example, negatively influencing forest growth in case of zero N deposition.

If, after running the model with "zero" deposition, the criterion is still violated in the target year, then the target cannot be met in that year. In such a case recovery can only be achieved in a later year. Otherwise, a target load exists and has to be calculated; its value lies somewhere between zero and the critical load.

If the critical load is not (or no longer) exceeded in the implementation year (here 2010, as for the soil with CEC=80 in Figure 6.7), this does *not* mean that the risk of damage to the ecosystem is already averted – it only means that *eventually*, maybe after a very long time, the chemical criterion is no longer violated. Only if, in addition, the chemical criterion is not violated in 2010, no further emission reductions are required for that ecosystem. Also, if the model is run with the 2010 deposition until the target year and the criterion is no longer violated in that year, no further emission reductions are required.

In the implementation of the above procedure, one could skip the step in which the model is run with the critical load as deposition (in case of exceedance in 2010) and immediately start with target load calculations (if a target load exists). It is only afterwards that it is checked if this target load is greater than the CL (and set it equal to the CL) (see the soil with CEC=60 in Figure 6.8). However, in view of the fact that TL calculations require iterative model runs, and also to avoid surprises due to round-off errors, it makes good sense to include that intermediate step.

An issue requiring attention in all target load calculations is the assumptions about finite nitrogen buffers. If it is, for example, assumed that a soil can immobilise N for, say, the next 50 years more than assumed in the critical load calculations, then target loads can be higher than the critical load. This might cause confusion and demands careful explanations.

The above considerations hold also in the case of two pollutants, such as S and N in the case of acidification. The result is then not a single value for a target load, but a so- called **target load function** consisting of all pairs of deposition (N_{dep}, S_{dep}) for which the target is achieved in the selected year. This concept is very similar to the critical load function (see Chapter 5). In Figure 6.10, examples of target load functions are shown for a set of target years.

When summarising target load calculations for ecosystems in a grid square (or region), it is important not only to report sites for which target load (functions) could been derived, but all cases (and their areas). In other words, the sites for which (i) no further deposition reductions are necessary, (ii) a target load has been calculated, and (iii) no target load exists (for the given target year). Note that in case (i), the deposition at the time of the implementation year (2010 in the example here) needs to be below (or equal to) the critical load.

Figure 6.10: Example of target load functions for a site for five different target years. Also shown is the critical load function of the site (dashed line). Note that any meaningful target load function has to lie below the critical load function, i.e., require stricter deposition reductions than achieving critical loads.

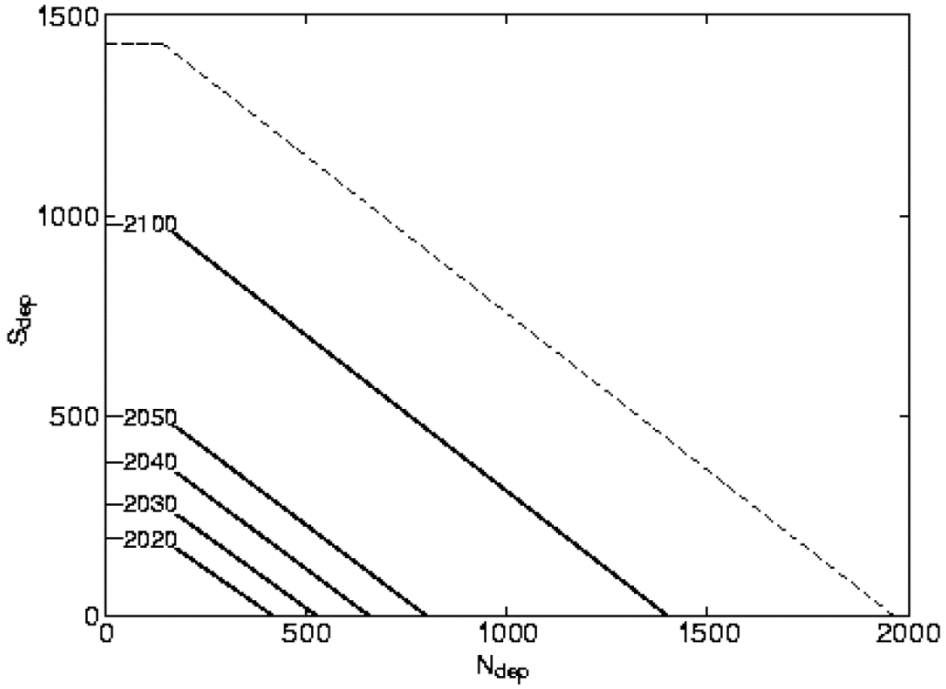

Source: This figure is adopted from a previous version of Chapter 6 of the Mapping Manual

6.5.2.1 Presentation of model results

Figure 6.11: Example of percentile traces of a regional dynamic model output. From it, seven percentiles (5, 10, 25, 50, 75, 90, and 95%) can be read for every time step.

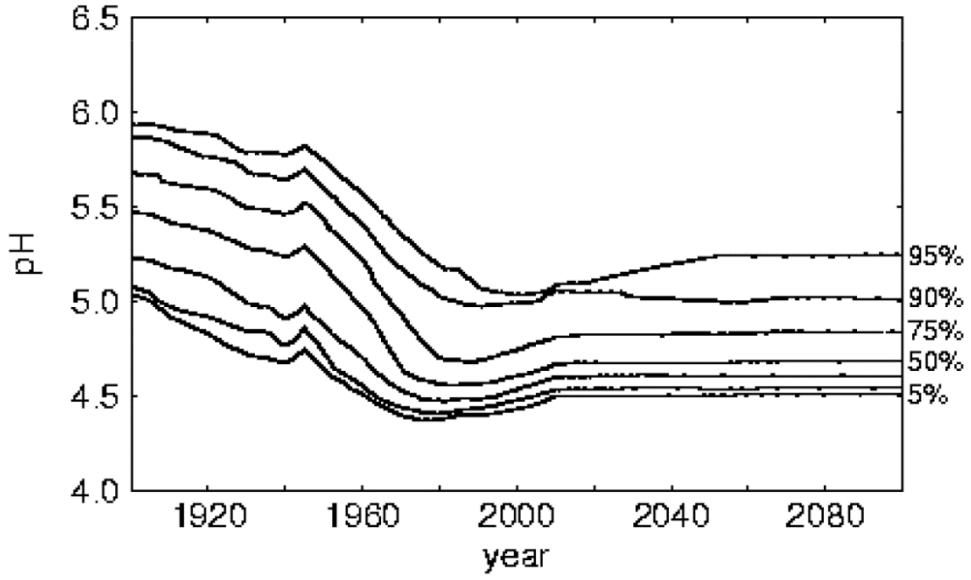

Source: This figure is adopted from a previous version of Chapter 6 of the Mapping Manual

For single site applications of dynamic models, the obvious way to present model output are graphs of the *temporal development of* the most relevant soil *chemical variables*, such as base saturation or the concentrations of ions in the soil solution (e.g., Al/Bc-ratio), in response to given deposition scenarios. In regional (European) applications, however, this kind of information has to be summarised. This can be done in several ways, for example, by displaying the temporal development of selected percentiles of the distribution of the variable(s) of interest (see Figure 6.11). Another way is to show a sequence of maps displaying the variable of interest in, say five-year intervals ('map movies'). These and other options are discussed and illustrated in Evans et al. (2001), Jenkins et al. (2002), and Moldan et al. (2003).

Maps can represent single sites only if their number does not become too large. If the number of sites reaches the thousands, statistical descriptors (means, percentiles) have to be used to represent the model output. For example, for a given target year the percentage of ecosystems in a grid square for which the target is achieved under a given deposition scenario can be displayed in a map format, very much in the same way as protection percentages (derived from protection isolines) have been displayed for critical load exceedances. Procedures for calculating percentiles and 'target load' isolines can be found in Chapter 8.

6.6 References

Alveteg M (1998) Dynamics of forest soil chemistry. PhD thesis, Reports in Ecology and Environmental Engineering 3:1998, Department of Chemical Engineering II, Lund University, Lund, Sweden, 81 pp.+appendices

Alveteg M, Sverdrup H, Kurz D (1998) Integrated assessment of soil chemical status. 1. Integration of existing models and derivation of a regional database for Switzerland. *Water, Air and Soil Pollution* 105: 1-9

Alveteg M, Sverdrup H (2002) Manual for regional assessments using the SAFE model (draft version 8 April 2002). Department of Chemical Engineering II, Lund University, Lund, Sweden; see also www2.chemeng.lth.se

Battarbee RW, Allott TEH, Juggins S, Kreiser AM, Curtis C, Harriman R (1996) Critical loads of acidity to surface waters – an empirical diatom-based palaeolimnological model. *Ambio* 25: 366-369

Berendse F, Beltman B, Bobbink R, Kwant M, Schmitz MB (1987) Primary production and nutrient availability in wet heathland ecosystems. *Acta Oec./Oecol. Plant.* 8: 265-276

Berendse F (1988) The nutrient balance of vegetation on dry sandy soils in the context of eutrophication via the air. Part 1: A simulation model as an aid for the management of wet heathlands (in Dutch). Centre for Agrobiological Research, Wageningen, The Netherlands, 51 pp

Bonten LTC, Reinds GJ, Posch M, (2015) A simple model to calculate effects of atmospheric deposition on soil acidification, eutrophication and C- sequestration. *Environmental Modelling & Software* (submitted)

Brady NC (1974) *The Nature and Properties of Soils* (8th edition). MacMillan, New York, 693 pp

CLRTAP, 2015. Dynamic modelling, Chapter 6 of Manual on methodologies and criteria for modelling and mapping critical loads and levels and air pollution effects, risks and trends. UNECE Convention on Long-range Transboundary Air Pollution.

Cole JJ, Caraco NF, Kling GW, Kratz TK (1994) Carbon dioxide supersaturation in the surface waters of lakes. *Science* 265: 1568-1570

Coleman K, Jenkinson DS (2005) RothC - A model for the turnover of carbon in soil. Model description and users guide. Rothamsted Research: Harpenden, UK;
http://rothamsted.ac.uk/sites/default/files/users/kcoleman/RothC_guide_DOS.pdf

Cosby BJ, Hornberger GM, Galloway JN, Wright RF (1985a) Modeling the effects of acid deposition: Assessment of a lumped parameter model of soil water and streamwater chemistry. *Water Resources Research* 21(1): 51-63

Cosby BJ, Wright RF, Hornberger GM, Galloway JN (1985b) Modeling the effects of acid deposition: Estimation of long-term water quality responses in a small forested catchment. *Water Resources Research* 21(11): 1591-1601

Cosby BJ, Hornberger GM, Galloway JN, Wright RF (1985c) Time scales of catchment acidification: A quantitative model for estimating freshwater acidification. *Environmental Science & Technology* 19:1144-1149

Cosby BJ, Hornberger GM, Wright RF, Galloway JN (1986) Modeling the effects of acid deposition: Control of long-term sulfate dynamics by soil sulfate adsorption. *Water Resources Research* 22(8): 1283-1291

Cosby BJ, Ferrier RC, Jenkins A, Wright RF (2001) Modelling the effects of acid deposition: refinements, adjustments and inclusion of nitrogen dynamics in the MAGIC model. *Hydrology and Earth System Sciences* 5(3): 499-517

De Vries W, Posch M, Kämäri J (1989) Simulation of the long-term soil response to acid deposition in various buffer ranges. *Water, Air and Soil Pollution* 48: 349-390

De Vries W, Hol A, Tjalma S, Voogd JC (1990) Stores and residence times of elements in a forest ecosystem: a literature study (in Dutch). DLO-Staring Centrum, Rapport 94, Wageningen, The Netherlands, 205 pp

De Vries W (1991) Methodologies for the assessment and mapping of critical loads and the impact of abatement strategies on forest soils. DLO Winand Staring Centre for Integrated Land, Soil and Water Research, Report 46, Wageningen, The Netherlands, 109 pp

De Vries W, Reinds GJ, Posch M, Kämäri J (1994) Simulation of soil response to acidic deposition scenarios in Europe. *Water, Air and Soil Pollution* 78: 215-246

De Vries W (1994) Soil response to acid deposition at different regional scales. Field and laboratory data, critical loads and model predictions. PhD Thesis, Agricultural University, Wageningen, The Netherlands, 487 pp

De Vries W, Van Grinsven JJM, Van Breemen N, Leeters EEJM, Jansen PC (1995) Impacts of acid atmospheric deposition on concentrations and fluxes of solutes in Dutch forest soils. *Geoderma* 67: 17-43

De Vries W, Posch M (2003) Derivation of cation exchange constants for sand loess, clay and peat soils on the basis of field measurements in the Netherlands. Alterra-rapport 701, Alterra Green World Research, Wageningen, The Netherlands, 50 pp

Dillon PJ, Molot LA (1990) The role of ammonium and nitrate retention in the acidification of lakes and forested catchments. *Biogeochemistry* 11: 23-43

Dise NB, Matzner E, Gundersen P (1998) Synthesis of nitrogen pools and fluxes from European forest ecosystems. *Water, Air and Soil Pollution* 105: 143-154

Driscoll CT, Lehtinen MD, Sullivan TJ (1994) Modeling the acid-base chemistry of organic solutes in Adirondack, New York, lakes. *Water Resources Research* 30: 297-306

Ellenberg H (1985) Veränderungen der Flora Mitteleuropas unter dem Einfluss von Düngung und Immissionen. *Schweizerische Zeitschift für das Forstwesen* 136: 19-39

Evans C, Jenkins A, Helliwell R, Ferrier R, Collins R (2001) Freshwater Acidification and Recovery in the United Kingdom. Centre for Ecology and Hydrology, Wallingford, United Kingdom, 80 pp

FAO (1981) FAO-Unesco Soil Map of the World, 1:5,000,000. Volume V Europe. Unesco, Paris 1981, 199 pp

Friend AD, Stevens AK, Knox RG, Channel MGR (1997) A process-based terrestrial biosphere model of ecosystem dynamics (Hybrid v3.0). *Ecological Modelling* 95: 249-287

Foster NW, Morrison IK, Nicolson JA (1986) Acid deposition and ion leaching from a podzolic soil under hardwood forest. *Water, Air and Soil Pollution* 31: 879-889

Gardiner MJ (1987) Representative data for major soil units in the EEC soil map. An Foras Taluntais, Ireland. Internal Report, 486 pp

Garmo, Ã. y., Skjelkvåle, B. L., Wit, H., Colombo, L., Curtis, C., Fölster, J., Hoffmann, A., Hruska, J., Hogåsen, T., Jeffries, D., Keller, W. B., Kram, P., Majer, V., Monteith, D. T., Paterson, A. M., Rogora, M., Rzychon, D., Steingruber, S., Stoddard, J., Vuorenmaa, J., and Worsztynowicz, A. (2014). Trends in Surface Water Chemistry in Acidified Areas in Europe and North America from 1990 to 2008. *Water, Air, & Soil Pollution C7 - 1880*, 225, 3, 1-14.

Gundersen P, Callesen I, De Vries W (1998) Nitrate leaching in forest ecosystems is controlled by forest floor C/N ratio. *Environmental Pollution* 102: 403-407

Hann BJ, Turner MA (2000) Littoral microcrustacea in Lake 302S in the Experimental Lakes Area of Canada: acidification and recovery. *Freshwater Biology* 43: 133-146

Heil GW, Bobbink R (1993) 'CALLUNA' a simulation model for evaluation of impacts of atmospheric nitrogen deposition on dry heathlands. *Ecological Modelling* 68: 161-182

Helling CS, Chesters G, Corey RB (1964) Contribution of organic matter and clay to soil cation exchange capacity as affected by the pH of the saturating solution. *Soil Sci. Soc. Am. J.* 28: 517-520

Hoekstra C, Poelman JNB (1982) Density of soils measured at the most common soil types in the Netherlands (in Dutch). Report 1582, Soil Survey Institute, Wageningen, The Netherlands, 47 pp

Jacobsen C, Rademacher P, Meesenburg H, Meiwes KJ (2002) Element contents in tree compartments – Literature study and data collection (in German). Report, Niedersächsische Forstliche Versuchsanstalt, Göttingen, Germany, 80 pp

Jenkins A, Larssen T, Moldan F, Posch M, Wright RF (2002) Dynamic modelling of surface waters: Impact of emission reduction – possibilities and limitations. ICP-Waters Report 70/2002, Norwegian Institute for Water Research (NIVA), Oslo, Norway, 42 pp

Jenkins A, Cosby BJ, Ferrier RC, Larssen T, Posch M (2003) Assessing emission reduction targets with dynamic models: deriving target load functions for use in integrated assessment. *Hydrology and Earth System Sciences* 7(4): 609-617

Johnson DW, Todd DE (1983) Relationships among iron, aluminium, carbon, and sulfate in a variety of forest soils. *Soil Sci. Soc. Am. J.* 47: 792-800

Kaste Ø, Dillon PJ (2003) Inorganic nitrogen retention in acid-sensitive lakes in southern Norway and southern Ontario, Canada: a comparison of mass balance data with an empirical N retention model. *Hydrological Processes* 17: 2393-2407

Keller W, Gunn JM (1995) Lake water quality improvements and recovering aquatic communities. In: Gunn JM (ed), *Restoration and Recovery of an Industrial Region*, Springer Verlag, New York, pp.67-80

Klap JM, Brus DJ, De Vries W, Reinds GJ (2004) Assessment of site-specific estimates of critical deposition levels for nitrogen and acidity in European forest ecosystems using measured and interpolated soil chemistry. (in prep)

Kros J, Reinds GJ, De Vries W, Latour JB, Bollen M (1995) Modelling of soil acidity and nitrogen availability in natural ecosystems in response to changes in acid deposition and hydrology. Report 95, DLO Winand Staring Centre, Wageningen, The Netherlands, 90 pp

Kurz D, Alveteg M, Sverdrup H (1998) Integrated assessment of soil chemical status. 2. Application of a regionalized model to 622 forested sites in Switzerland. *Water, Air and Soil Pollution* 105: 11-20

Latour JB, Reiling R (1993) A multiple stress model for vegetation (MOVE): a tool for scenario studies and standard setting. *Science of the Total Environment* Supplement 93: 1513-1526

Martinson L, Alveteg M, Warfvinge P (2003) Parameterization and evaluation of sulfate adsorption in a dynamic soil chemistry model. *Environmental Pollution* 124(1): 119-125

Mills KH, Chalanchuk SM, Allan DJ (2000) Recovery of fish populations in Lake 223 from experimentalacidification. *Can. J. Fish. Aquat. Sci.* 57: 192-204

Moldan F, Beier C, Holmberg M, Kronnäs V, Larssen T, Wright RF (2003) Dynamic modelling of soil and water acidification: Display and presentation of results for policy purposes. Acid Rain Research Report 56/03, Norwegian Institute for Water Research (NIVA), Oslo, Norway, 62 pp

Oja T, Yin X, Arp PA (1995) The forest modelling series ForM-S: applications to the Solling spruce site. *Ecological Modelling* 83: 207-217

Oulehle F, Cosby BJ, Wright RF, Hruška J, Kopácek J, Krám P, Evans CD, Moldan F (2012) Modelling soil nitrogen: The MAGIC model with nitrogen retention linked to carbon turnover using decomposer dynamics. *Environmental Pollution* 165: 158-166

Posch M, Hettelingh J-P, Slootweg J (eds) (2003) Manual for dynamic modelling of soil response to atmospheric deposition. RIVM Report 259101012, Bilthoven, The Netherlands, 69 pp; see also www.wge-cce.org

Posch M, Reinds GJ (2009) A very simple dynamic soil acidification model for scenario analyses and target load calculations. *Environmental Modelling & Software* 24: 329-340

Raddum GG (1999) Large scale monitoring of invertebrates: Aims, possibilities and acidification indexes. In: GG Raddum, BO Rosseland, J Bowman (eds) Workshop on Biological Assessment and Monitoring; Evaluation and Models. ICP-Waters Report 50/99, Norwegian Institute for Water Research, Oslo, Norway, pp.7-16

Reinds GJ, Van Oijen M, Heuvelink GBM, Kros H (2008) Bayesian calibration of the VSD soil acidification model using European forest monitoring data. *Geoderma* 146: 475-488

Reuss JO (1980) Simulation of soil nutrient losses due to rainfall acidity. *Ecological Modelling* 11: 15-38.

Reuss JO (1983) Implications of the calcium-aluminium exchange system for the effect of acid precipitation on soils. *Journal of Environmental Quality* 12(4): 591-595

Reuss JO, Johnson DW (1986) *Acid Deposition and the Acidification of Soils and Waters.* Ecological Studies 59, Springer, New York, 119 pp

SAEFL (1998) Acidification of Swiss forest soils - Development of a regional dynamic assessment. Environmental Documentation No.89, Swiss Agency for the Environment Forest and Landscape (SAEFL), Berne, Switzerland, 115 pp

Schöpp W, Posch M, Mylona S, Johansson M (2003) Long-term development of acid deposition (1880-2030) in sensitive freshwater regions in Europe. *Hydrology and Earth System Sciences* 7(4): 436-446

Schouwenberg EPAG, Houweling H, Jansen MJW, Kros J, Mol-Dijkstra JP (2000) Uncertainty propagation in model chains: a case study in nature conservancy. Alterra Report 001, Alterra Green World Research, Wageningen, The Netherlands, 90 pp

Singh BR, Johnson DW (1986) Sulfate content and adsorption in soils of two forested watersheds in southern Norway. *Water, Air and Soil Pollution* 31: 847-856

Skjelkvåle, B. L. (2008). ICP Waters: Monitoring effects of long-range transboundary air pollution on surface waters in Europe and North-America since 1985. Version for comments, Norwegian Institute for Water Research, NIVA, Oslo, Norway. p.

Snucins S, Gunn JM, Keller W, Dixit S, Hindar A, Henriksen A (2001) Effects of regional reductions in sulphur deposition on the chemical and biological recovery of lakes within Killarney Park, Ontario, Canada. *Journal of Environmental Monitoring and Assessment* 67: 179-194

Starr M (1999) WATBAL: A model for estimating monthly water balance components, including soil water fluxes. In: S Kleemola, M Forsius (eds) 8th Annual Report, UNECE ICP Integrated Monitoring, Finnish Environment Institute, Helsinki, Finland. *The Finnish Environment* 325: 31-35

Tietema A, Duysings JJHM, Verstraten JM, Westerveld JW (1990) Estimation of actual nitrification rates in an acid forest soil. In: AF Harrison, P Ineson, OW Heal (eds) *Nutrient cycling in terrestrial ecosystems; Field methods, application and interpretation.* Elsevier Applied Science, London and New York, pp.190-197

Tiktak A, Van Grinsven JJM (1995) Review of sixteen forest-soil-atmosphere models. *Ecological Modelling* 83: 35-53

Tominaga K, Aherne J, Watmough SA, Alveteg M, Cosby BJ, Driscoll CT, Posch M, Pourmokhtarian A, (2010) Predicting acidification recovery at the Hubbard Brook Experimental Forest, New Hampshire: Evaluation of four models. *Environmental Science & Technology* 44(23): 9003-9009

Ulrich B (1981) Ökologische Gruppierung von Böden nach ihrem chemischen Bodenzustand. *Z. Pflanzenernähr. Bodenk.* 144: 289-305

Vanmechelen L, Groenemans R, Van Ranst E (1997) Forest soil condition in Europe. Results of a large-scale soil survey. EC-UN/ECE, Brussels, Geneva, 261 pp

Van Oene H (1992) Acid deposition and forest nutrient imbalances: a modelling approach. *Water, Air and Soil Pollution* 63: 33-50

Van Wallenburg C (1988) The density of peaty soils (in Dutch). Internal Report, Soil Survey Institute, Wageningen, The Netherlands, 5 pp

Wamelink GWW, Ter Braak CJF, Van Dobben HF (2003) Changes in large- scale patterns of plant biodiversity predicted from environmental economic scenarios. *Landscape Ecology* 18: 513-527

Warfvinge P, Sverdrup H (1992) Calculating critical loads of acid deposition with PROFILE - A steady-state soil chemistry model. Water, Air and Soil Pollution 63: 119-143

Warfvinge P, Holmberg M, Posch M, Wright RF (1992) The use of dynamic models to set target loads. *Ambio* 21: 369-376

Warfvinge P, Falkengren-Grerup U, Sverdrup H, Andersen B (1993) Modelling long-term cation supply in acidified forest stands. *Environmental Pollution* 80: 209-221

Wright RF, Lie MC (eds) (2002) Workshop on models for biological recovery from acidification in a changing climate, 9-11 September 2002 in Grimstad, Norway. Acid Rain Research Report 55/02, Norwegian Institute for Water Research (NIVA), Oslo, Norway, 42 pp

7 Exceedance calculations

Last updated in 2015 by Max Posch, CCE, from the initial text of the Mapping Manual 2004.

Please refer to this document as: CLRTAP, 2015. Exceedance calculations, chapter 7 of Manual on methodologies and criteria for modelling and mapping critical loads and levels and air pollution effects, risks, and trends. UNECE Convention on Long-range Transboundary Air Pollution; accessed on [date of consultation] on Web at www.umweltbundesamt.de/en/cce-manual.

7.1 Introduction

In this chapter the calculation of exceedances (i.e. the comparison of critical loads/levels with depositions/ concentrations, is described). In section 7.2, the basic definition of an exceedance is given, including some historical remarks on the origin and use of the word 'exceedance'. In Section 7.3, the concept of a conditional critical load of S and N is introduced, which allows treating these two acidifying pollutants separately, and thus also makes exceedance calculations straightforward.

In Section 7.4 the exceedance of critical loads is defined that involves two pollutants simultaneously; in Section 7.5 exceedances are regionalised by defining the Average Accumulated Exceedance (AAE). Finally, in Section 7.6, the exceedances of surface water critical loads are considered. Most of the material presented here is based on Posch et al. (1997, 1999, 2001).

7.2 Basic definitions

The word 'exceedance' is defined as "the amount by which something, especially a pollutant, exceeds a standard or permissible measurement" (The American Heritage Dictionary of the English Language, Fourth Edition 2000) and is a generally accepted term within the air pollution discipline. Interestingly, the Oxford English Dictionary (OED) database has an example of 'exceedance' from 1836 (Quinion 2004) – 36 years before Robert Angus Smith was credited with coining the term 'acid rain' (Smith 1872). However, the term 'acid rain' (in French) had already been used in 1845 by Ducros in a scientific journal article (Ducros 1845).

Critical loads and levels are derived to characterise the vulnerability of ecosystem (parts, components) in terms of a deposition or concentration. If the critical load of pollutant X at a given location is smaller than the deposition of X at that location, the critical load is said to be exceeded, and the difference is called *exceedance*[18]. In mathematical terms, the exceedance *Ex* of the critical load $CL(X)$ is given as:

(VII.1)

$$Ex(X_{dep}) = X_{dep} - CL(X)$$

where X_{dep} is the deposition of pollutant X. In the case of the critical level, the comparison is with the respective concentration quantity. If the critical load is greater than or equal to the deposition, one says that it is not exceeded or there is non- exceedance of the critical load.

An exceedance defined by eq. VII.1 can obtain positive, negative or zero value. Since it is in most cases sufficient to know that there is non-exceedance, without being interested in the magnitude of non- exceedance, the exceedance can be also defined as:

[18] When comparing deposition(s) to target load (functions), one does not talk about the exceedance, but the 'non-achievement' of a target load.

(VII.2)

$$Ex(X_{dep}) = max\{0, X_{dep} - CL(X)\}$$
$$= \begin{cases} X_{dep} - CL(X), & X_{dep} > CL(X) \\ 0, & X_{dep} \leq CL(X) \end{cases}$$

An example of the application of this basic equation is the exceedance of the critical load of nutrient N (see Chapter 5), which is given by:

(VII.3)

$$Ex_{nut}\,(N_{dep}) = N_{dep} - CL_{nut}(N)$$

It should be noted that exceedances differ fundamentally from critical loads, as exceedances are time dependent. One can speak of *the* critical load of X for an ecosystem, but not of *the* exceedance of it. For exceedances the time (or the deposition) for which they have been calculated has to be reported, since – especially in integrated assessment – it is exceedances due to (past or future) *anthropogenic* depositions that are of interest.

Of course, the time-invariance of critical loads and levels has its limitations, certainly when considering a geological time frame. Even during shorter time periods, such as decades or centuries, one can anticipate changes in the magnitude of critical loads due to global (climate) change, which influences the processes from which critical loads are derived. An early example of a study of the (first-order) influence of temperature and precipitation changes on critical loads of acidity and nutrient N in Europe can be found in Posch (2002).

The exceedance of a critical load is often misinterpreted as the amount of excess leaching, that is the amount leached above the critical/acceptable leaching. This is generally *not* the case as exemplified by the exceedance of the critical load of nutrient N. The excess leaching due to the deposition N_{dep}, Ex_{le}, is given as:

(VII.4)

$$Ex_{le}(N_{dep}) = N_{le} - N_{le,acc}$$

Inserting the mass balance of N and the deposition-dependent denitrification one obtains for the excess leaching (eqs.V.2– V.5):

(VII.5)

$$Ex_{le}(N_{dep}) = (1 - f_{de}) \cdot (N_{dep} - CL_{nut}(N)) = (1 - f_{de}) \cdot Ex_{nut}(N_{dep})$$

which shows that a deposition reduction of 1 eq/ha/yr reduces the leaching of N by only $1–f_{de}$ eq/ha/yr. Only in the simplest case, in which all terms of the mass balances are independent of depositions, does the change in leaching equal the change in deposition.

7.3 Conditional critical loads of N and S

The non-uniqueness of the critical loads of S and N acidity makes both their implementation into integrated assessment models and their communication to decision makers more difficult. However, if one is interested in reductions of only one of the two pollutants, a unique critical load can be derived, and thus also a unique exceedance according to eq. VII.1 can be calculated.

If emission reductions deal with nitrogen only, a unique critical load of N for a *fixed* sulphur deposition S_{dep} can be derived from the critical load function. This is the so-called **conditional critical load of nitrogen**, CL($N|S_{dep}$), and it is computed as:

(VII.6)

$$L\left(N|S_{dep}\right) = \begin{cases} CL_{min}(N), & S_{dep} \geq CL_{max}(S) \\ CL_{max}(N) - \alpha \cdot S_{dep}, & S_{dep} < CL_{max}(S) \end{cases}$$

with

(VII.7)

$$\alpha = \frac{CL_{max}(N) - CL_{min}(N)}{CL_{max}(s)}$$

In Figure 7.1a, the procedure for calculating $CL(N|S_{dep})$ is depicted graphically.

Figure 7.1: Examples of computing (a) conditional critical loads of N for different S deposition values S1 and S2, and (b) conditional critical loads of S for different N deposition values N1 and N2.

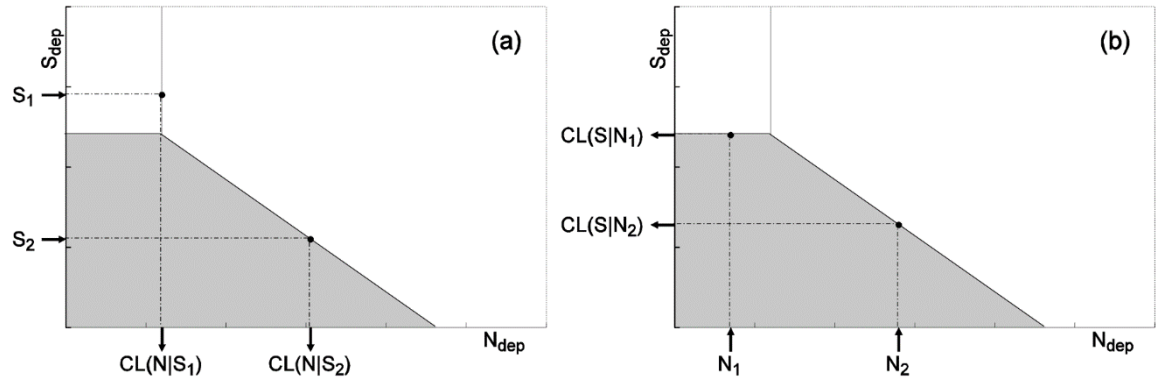

Source: This figure is adopted from Chapter 7 of the previous version of the Mapping Manual

In an analogous manner **a conditional critical load of sulphur**, $CL(S|N_{dep})$, for a fixed nitrogen deposition N_{dep} can be computed as:

(VII.8)

$$CL\left(S|N_{dep}\right) = \begin{cases} 0, & N_{dep} \geq CL_{max}(N) \\ \dfrac{CL_{max}(N) - N_{dep}}{\alpha}, & CL_{min}(N) < N_{dep} < CL_{max}(N) \\ CL_{max}(S), & N_{dep} \leq CL_{min}(N) \end{cases}$$

where α is given by eq. VII.7. The procedure for calculating $CL(S|N_{dep})$ is depicted graphically in Figure 7.1b. Setting $N_{dep} = CL_{nut}(N)$, the resulting conditional critical load has been termed minimum **critical load of sulphur**: $CL_{min}(S) = CL(S|CL_{nut}(N))$.

When using conditional critical loads, the following caveats should be kept in mind:

a) A conditional critical load can be considered a true critical load only when the chosen deposition of the other pollutant is kept constant.

If the conditional critical loads of both pollutants are considered simultaneously, care has to be exercised. It is *not* necessary to reduce the exceedances of both, but only one of them to reach non-exceedance for both pollutants. Recalculating the conditional critical load of the other pollutant generally results in non-exceedance. However, if $S_{dep} > CL_{max}(S)$ or $N_{dep} >$

$CL_{max}(N)$, depositions have to be reduced at least to their respective maximum critical load values, irrespective of the conditional critical loads.

7.4 Two pollutants

As shown in Chapter 5, there is no unique critical load of N and S in the case of acidity or in the case of a critical load function derived from multiple criteria related to N and S. Consequently, there is no unique exceedance, although non- exceedance is easily defined (as long as its amount is not important). This is illustrated in Figure 7.2: Let the point E denote the (current) deposition of N and S. By reducing N_{dep} substantially, one reaches the point Z_1 and thus non-exceedance without reducing S_{dep}. On the other hand one can reach non-exceedance by only reducing S_{dep} (by a smaller amount) until reaching Z_3; finally, with a reduction of both N_{dep} and S_{dep}, one can reach non-exceedance as well (e.g., point Z_2).

Figure 7.2: The N-S critical load function defined by two points (four values): (CLN_{min}, CLS_{max}) and (CLN_{max}, CLS_{min}) (thick line). The grey-shaded area below the critical load function defines deposition pairs (N_{dep}, S_{dep}) for which there is non-exceedance. The points E and Z1-Z3 demonstrate that non-exceedance can be attained in different ways, i.e., there is no unique exceedance.

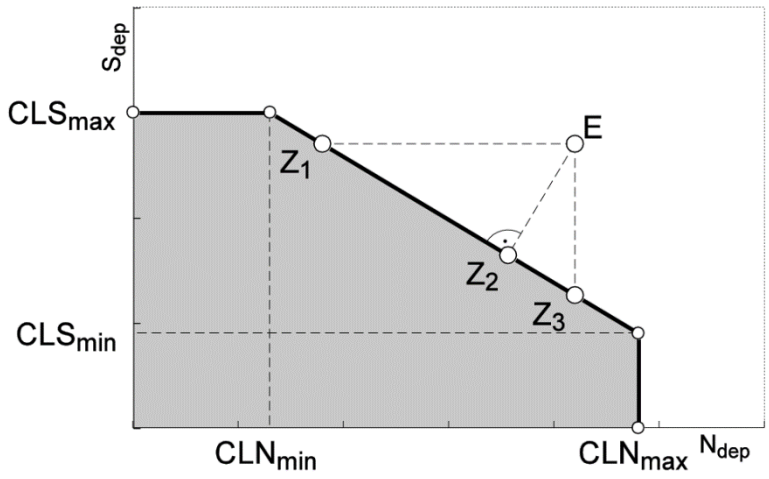

Source: This figure is adopted from a previous version of Chapter 7 of the Mapping Manual

Intuitively, the reduction required in N and S deposition to reach point Z_2 (see Figure 7.2) (i.e., the shortest distance to the critical load function, seems a good measure for exceedance). Thus, we *define* the exceedance for a given pair of depositions (N_{dep}, S_{dep}) as the sum of the N and S deposition reductions required to reach the critical load function by the 'shortest' path.
Figure 7.3 depicts the cases that can arise, if the deposition falls …

a) … on or below the critical load function (Region 0). In this case the exceedance is defined as zero (non- exceedance);

… Region 1 (e.g., point E_1): An S deposition reduction does not help; an N deposition reduction is needed: the exceedance is defined as $N_{dep}–CL_{max}N$;

… Region 2 (e.g., point E_2): the exceedance in this region is defined as the sum of N and S deposition reduction needed to reach the corner-point point Z_2;

… Region 3 (e.g., point E_3): the exceedance is given by the sum of N and S deposition reduction, *ExN+ExS*, required to reach the point Z_3, with the line $E_3–Z_3$ perpendicular to the CLF;

... Region 4 (e.g., point E_4): the exceedance is defined as the sum of N and S deposition reduction needed to reach the corner-point Z_4;

... Region 5 (e.g., point E_5): an N deposition reduction does not help; an S deposition reduction is needed: the exceedance is defined as $S_{dep} - CL_{max}S$.

Figure 7.3: Illustration of the different cases for calculating the exceedance for a given critical load function.

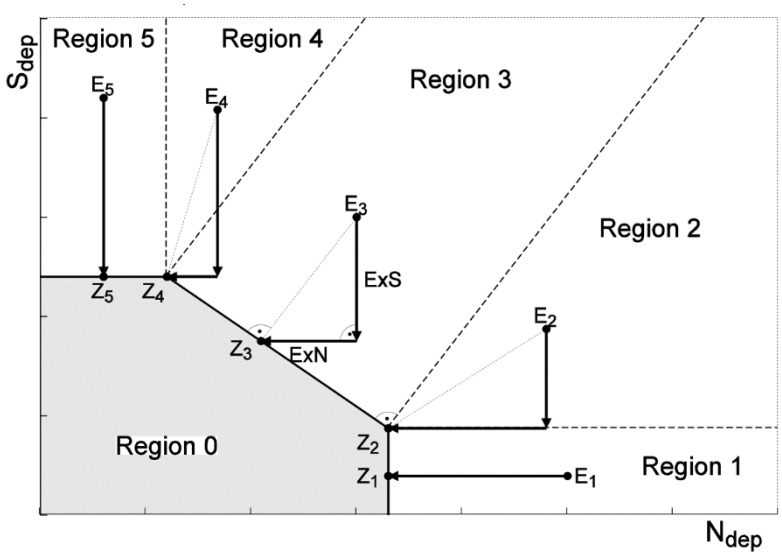

Source: This figure is adopted from a previous version of Chapter 7 of the Mapping Manual

The exceedance function can be described by the following equation (the coordinates of the point Z_3 are denoted by (N_0, S_0); see also Figure 7.2):

(VII.9)

$$(N_{dep}, S_{dep}) = \begin{cases} 0, & (N_{dep}, S_{dep}) \in Region\ 0 \\ N_{dep} - CLN_{max}, & (N_{dep}, S_{dep}) \in Region\ 1 \\ N_{dep} - CLN_{max} + S_{dep} - CLS_{min}, & (N_{dep}, S_{dep}) \in Region\ 2 \\ N_{dep} - N_0 + S_{dep} - S_0, & (N_{dep}, S_{dep}) \in Region\ 3 \\ N_{dep} - CLN_{min} + S_{dep} - CLS_{max}, & (N_{dep}, S_{dep}) \in Region\ 4 \\ S_{dep} - CLS_{max}, & (N_{dep}, S_{dep}) \in Region\ 5 \end{cases}$$

The function thus defined fulfils the criteria of a meaningful exceedance function: it is zero, if there is non-exceedance, positive when there is exceedance, and increases in value when the point (N_{dep}, S_{dep}) moves away from the critical load function.

The computation of the exceedance function requires the estimation of the coordinates of the point (N_0, S_0) on the critical load function. If (x_1, y_1) and (x_2, y_2) are two arbitrary points of a straight line g and (x_e, y_e) another point (not on that line), then the coordinates $(x_0, y_0) = (N_0, S_0)$ of the point obtained by intersecting the line passing through (x_e, y_e) and perpendicular to g (called the 'foot' or 'foot of the perpendicular') are given by:

(VII.10a)

$x_0 = (d_1 s + d_2 v)/d^2$ and $y_0 = (d_2 s - d_1 v)/d^2$

with

(VII.10b)

$d_1 = x_2 - x_1$, $d_2 = y_2 - y_1$, $d^2 = d_1^2 + d_2^2$

(VII.10c)

$$\begin{cases} s = x_e d_1 + y_e d_2 \\ v = x_1 d_2 - y_1 d_1 = x_1 y_2 - y_1 x_2 \end{cases}$$

The final difficulty in computing the $Ex(N_{dep}, S_{dep})$ is to determine into which of the regions (Region 0 through Region 5 in Figure 7.3) a given pair of deposition (N_{dep}, S_{dep}) falls. Without going into the details of the geometrical considerations, a FORTRAN subroutine is listed below, which returns the number of the region as well as *ExN* and *ExS*. The correspondences of the 4 quantities – CLN_{min}, CLS_{max}, CLN_{max}, and CLS_{min} – with the classical critical load function for acidity, defined by $CL_{max}S$, $CL_{min}N$ and $CL_{max}N$, intersected with the nutrient N critical load $CL_{nut}N$ (or $CL_{emp}N$) are:

$CLN_{min} = CL_{min}N$

$CLN_{max} = CL_{max}S$

and, if $CL_{nut}N < CL_{max}N$:

$$\begin{cases} CLN_{max} = CL_{nut}N \\ CLS_{min} = CL_{max}S \times \dfrac{CL_{max}N - CL_{nut}N}{CL_{max}N - CL_{min}N} \end{cases}$$

otherwise

$$\begin{cases} CLN_{max} = CL_{nut}N \\ CLS_{min} = 0 \end{cases}$$

(see also Posch et al. 2014).

```
subroutine exceedNS (CLNmin,CLSmax,CLNmax,CLSmin,depN,depS,ExN,ExS,ireg)
!
! Returns the exceedances ExN and ExS (Ex=ExN+ExS) for N and S depositions
! depN and depS and the CLF defined by (CLNmin,CLSmax) and (CLNmax,CLSmin).
! The "region" in which (depN,depS) lies, is returned in ireg.
!
implicit none
!
real, intent(in) : : CLNmin, CLSmax, CLNmax, CLSmin, depN, depS
real, intent(out) : : ExN, ExS
integer, intent(out) : : ireg
!
```

```
real : : dN, dS, dd, s, v, xf, yf
!
ExN = -1; ExS = -1; ireg = -1
if (CLNmin < 0 .or. CLSmax < 0 .or. CLNmax < 0 .or. CLSmin < 0) return
ExN = depN; ExS = depS; ireg = 9
! CLN = CLNmax
if (CLSmax == 0 .and. CLNmax == 0) return
! CLS = CLSmin
dN = CLNmin-CLNmax dS = CLSmax-CLSmin
if (depS <= CLSmax .and. depN <= CLNmax .and. &
& (depN-CLNmax)*dS <= (depS-CLSmin)*dN) then ! non-exceedance:
ireg = 0
ExN = 0; ExS = 0
else if (depS <= CLSmin) then
ireg = 1
ExN = depN-CLNmax; ExS = 0
else if (depN <= CLNmin) then
ireg = 5
ExN = 0; ExS = depS-CLSmax
else if (-(depN-CLNmax)*dN >=(depS-CLSmin)*dS) then
ireg = 2
ExN = depN-CLNmax; ExS = depS-CLSmin
else if (-(depN-CLNmin)*dN <= (depS-CLSmax)*dS) then
ireg = 4
ExN = depN-CLNmin; ExS = depS-CLSmax
else
ireg = 3
dd = dN*dN+dS*dS
s = depN*dN+depS*dS
```

```
v = CLNmax*dS-CLSmin*dN xf = (dN*s+dS*v)/dd

yf = (dS*s-dN*v)/dd

ExN = depN-xf; ExS = depS-yf

end if

return

end subroutine exceedNS
```

7.5 The average accumulated exceedance (AAE)

To summarise exceedances in a grid cell (e.g., for mapping) or country/region (for tabulation) one could resort to standard statistical quantities, such as mean, or any percentile of the distribution of individual exceedance values (see Chapter 8). Alternatively, the so-called Average Accumulated Exceedance (Posch et al. 2001) has been used, especially in integrated assessment, which is defined as follows.

Let Ex_i be the exceedance for ecosystem i with area A_i, then we define the accumulated exceedance (AE) of n ecosystems on a region (grid cell) as:

(VII.11)

$$AE = \sum_{i=1}^{n} A_i E_i$$

For a given deposition, AE is total amount (in eq/yr) deposited in excess over the critical loads in the region in a given year. This function is thus strongly determined by the total ecosystem area in a grid cell. In order to minimise this dependence and to obtain a quantity which is directly comparable to depositions (in eq/ha/yr), we define the *average accumulated exceedance* (AAE) by dividing the AE function by the total ecosystem area:

(VII.12)

$$AEE = AE \Big/ \sum_{i=1}^{n} A_i$$

Instead of the total ecosystem area, one could also think of dividing by another area (e.g. the area exceeded for a given (fixed) deposition scenario). However, recalculating the AAE with new areas when depositions change can lead to inconsistencies: the new AAE could be larger, despite declining deposition – as can be shown with simple examples.

7.6 Surface waters

Since exceedance calculations for the critical loads for surface waters require special considerations due to the peculiarities of (some of) the models, they are treated here separately. The three critical load models mentioned are described in chapter 5.

7.6.1 The SSWC model

In the SSWC model, sulphate is assumed to be a mobile anion (i.e., leaching equals deposition), whereas N is assumed to a large extent to be retained in the catchment by various processes.

Therefore, only the so-called present-day exceedance can be calculated from the leaching of N, N_{le}, which is determined from the sum of the measured concentrations of nitrate and ammonia in the runoff. This present exceedance of the critical load of acidity is defined as (Henriksen and Posch 2001):

(VII.13)

$$Ex(A) = S_{dep} + N_{le} - CL(A)$$

where $CL(A)$ is the critical load of acidity as computed with eq.V.50. No N deposition data are required for this exceedance calculation. However, $Ex(A)$ quantifies only the exceedance at present rates of retention of N in the catchment. Nitrogen processes are modelled explicitly in the FAB model (see below), and thus it is the only surface water model that can be used for comparing the effects of different N deposition scenarios. In the above derivation we assumed that base cation deposition and net uptake did not change over time.

If there is increased base cation deposition due to human activities or a change in the net uptake due to changes in management practices, this has to be taken into account in the exceedance calculations by subtracting that anthropogenic $BC^*_{dep} - Bc_u$ from $S_{dep} + N_{le}$.

7.6.2 The empirical diatom model

For the diatom model the exceedance of the critical load of acidity is given by:

(VII.14)

$$Ex(A) = S_{dep} + f_N \cdot N_{dep} - CL(A)$$

where f_N is the fraction of the N deposition contributing to acidification (see eq.V.66).

7.6.3 The FAB model

In the FAB model, a critical load function for surface waters is derived in the same way as in the SMB model for soils, and the same considerations hold as given in Section 7.4.

Again, there is no unique exceedance for a given pair of depositions (N_{dep}, S_{dep}), but an exceedance can be *defined* in an analogous manner as above (see also Henriksen and Posch 2001).

7.7 References

CLRTAP, 2015. Exceedance calculations, Chapter 7 of Manual on methodologies and criteria for modelling and mapping critical loads and levels and air pollution effects, risks and trends. UNECE Convention on Long-range Transboundary Air Pollution.

Ducros M (1845) Observation d'une pluie acide. *Journal de Pharmacie et de Chimie* 3(7): 273-277

Henriksen A, Posch M (2001) Steady- state models for calculating critical loads of acidity for surface waters. *Water, Air and Soil Pollution: Focus* 1: 375-398

Posch M, Hettelingh J-P, De Smet PAM, Downing RJ (eds) (1997) Calculation and mapping of critical thresholds in Europe. Status Report 1997, Coordination Centre for Effects, RIVM Report 259101007, Bilthoven, Netherlands, iv+163 pp. www.wge-cce.org

Posch M, De Smet PAM, Hettelingh J-P, Downing RJ (eds) (1999) Calculation and mapping of critical thresholds in Europe. Status Report 1999, Coordination Centre for Effects, RIVM Report 259101009, Bilthoven, Netherlands, iv+165 pp. www.wge-cce.org

Posch M, Hettelingh J-P, De Smet PAM (2001) Characterization of critical load exceedances in Europe. *Water, Air and Soil Pollution* 130: 1139-1144

Posch M (2002) Impacts of climate change on critical loads and their exceedances in Europe. *Environmental Science and Policy* 5(4): 307-317

Posch M, Hettelingh J-P, Slootweg J, Reinds GJ (2014) Deriving critical loads based on plant diversity targets. Chapter 3 in: Slootweg J, Posch M, Hettelingh J-P, Mathijssen L (eds), Modelling and mapping the impacts of atmospheric deposition on plant species diversity in Europe: CCE Status Report 2014. RIVM Report 2014-0075, Coordination Centre for Effects, Bilthoven, Netherlands, pp. 41-46; www.wge-cce.org

Quinion M (2004) "The example I quoted [on www.worldwidewords.org] is known to the compilers of the OED (who will be writing an entry for 'exceedance' at some point) from their in-house database of unpublished citations. They didn't provide me with a full citation, only with the date" (personal communication to Julian Aherne in July 2004). – As of January 2014, no entry for 'exceedance' had yet been prepared for the OED (email by David Simpson from 25 Jan 2014).

Smith RA (1872) *Air and Rain: The Beginnings of a Chemical Climatology*. Longmans, Green & Co., London, 600 pp.

8 General mapping issues

Last updated in 2015 by Max Posch and Anne Christine Le Gall, Chairwoman of the Task Force on Modelling and Mapping from initial text by M. Posch and J. Aherne (Mapping Manual 2004 and various CCE reports) and from documentation on EMEP.

Please refer to this document as: CLRTAP, 2015. General mapping issues, Chapter VIII of Manual on methodologies and criteria for modelling and mapping critical loads and levels and air pollution effects, risks and trends. UNECE Convention on Long-range Transboundary Air Pollution; accessed on [date of consultation] on Web at www.umweltbundesamt.de/en/cce-manual.

In this chapter procedures are described for summarising results of critical load and exceedance calculations and presenting them on a regional scale. The objective of the text below is to show the (mathematical and methodological) links between the calculation of critical loads and integrated assessment modelling.

The material presented here is a summary of the material from CCE Status Reports (see Posch et al. 1995, 1997, 1999). It is complemented by recent EMEP documentation (EMEP 2013; Simpson et al. 2012). Page VIII - 5

In Section 8.1, the grid systems used by EMEP are defined; in Section 8.2 methods for the calculation of percentiles (in one and two dimensions) are presented. In Section 8.3 the uses of critical loads in integrated assessment is discussed, including different gap closure methods used to evaluate the differences between a reference scenario (such as past or present situation) and scenarios proposed for future policies.

8.1 Geographic grid systems

To make critical loads usable and useful for the work under the LRTAP Convention, one has to be able to compare them to deposition estimates. Deposition of sulphur and nitrogen compounds have earlier been reported by EMEP on a 150 × 150 km² grid covering (most of) Europe, then depositions have become available on a 50 × 50 km² grid. Both are special cases of the so-called polar stereographic projection, which is described in the following. The latest grid used by EMEP has geographical coordinates ("latitude- longitude grid", cf. section 8.1.2).

8.1.1 The polar stereographic projection

In the polar stereographic projection each point on the Earth's sphere is projected from the South Pole onto a plane perpendicular to the Earth's axis and intersecting the Earth at a fixed latitude ϕ_0 (see Figure A-1 in the CCE Status Report 2001, p. 182.). Consequently, the coordinates x and y are obtained from the geographical longitude λ and latitude ϕ (in radians) by the following equations:

(VIII.1)

$$x = x_p + M \cdot \tan\left(\frac{\pi}{4} - \frac{\phi}{2}\right) \cdot \sin(\lambda - \lambda_0)$$

And

(VIII.2)

$$y = y_p - M \cdot \tan\left(\frac{\pi}{4} - \frac{\phi}{2}\right) \cdot \cos(\lambda - \lambda_0)$$

where (x_p, y_p) are the coordinates of the North Pole; λ_0 is a rotation angle (i.e., the longitude parallel to the *y*-axis); and M is the scaling of the *x*-*y* coordinates. In the above definition, the x-values increase and the *y*- values decrease when moving towards the equator. For a given unit length (grid size) d in the *x*-*y* plane the scaling factor *M* is given by:

(VIII.3)

$$M = \frac{R}{d} \cdot (1 + \sin \phi_0)$$

where *R* (= 6370 km) is the radius of the Earth. The inverse transformation (i.e., longitude and latitude as function of *x* and *y)* is given by:

(VIII.4)

$$\lambda = \lambda_0 + \arctan\left(\frac{x - x_p}{y_p - y}\right)$$

and

(VIII.5)

$$\phi = \frac{\pi}{2} + \arctan(r/M)$$

with

$$r = \sqrt{(x - x_p)^2 + (y - y_p)^2}$$

The *arctan* in eq. VIII.5 gives the correct longitude for quadrant 4 ($x>x_p$ and $y<y_p$) and quadrant 3 ($x<xp$ and $y<y_p$); π (=180°) has to be added for quadrant 1 ($x>x_p$ and $y>y_p$) and subtracted for quadrant 2 ($x<x_p$ and $y>y_p$). Note that quadrant 4 is the one covering (most of) Europe.

Every stereographic projection is a so- called conformal projection, as such, an angle on the sphere remains the same in the projection plane, and vice versa. However, the stereographic projection distorts areas (even locally), in other words, it is not an equal-area projection (see below).

We define a **grid cell** (*i,j*) as a square in the *x*-*y* plane with side length *d* (see eq. 8.3) and centre point as an integral part of *x* and *y*, therefore:

(VIII.6)

$i = \text{nint}(x)$ and $j = \text{nint}(y)$

where 'nint' is the nearest integer (rounding function). Consequently, the four corners of the grid cell have coordinates (*i*±½, *j*±½*).*

8.1.2 Grids used for critical loads mapping under lrtap convention

8.1.2.1 The latitude-longitude grid

The latitude-longitude grid is a plane projection of the EMEP domain based on the World Geodesic System (WGS84, revised in 2004). This grid system is widely used for GPS. This gridding combines information on the shape of the earth, the (nominal) sea level and altitude. In principle, the origin of this gridding system is the mass centre of the earth. However, the two dimension grid used for mapping critical loads at regional scale is done on a two dimensional grid, the origin of the grid is the intersect between the Greenwich meridian and the equator.

In 2012, at the 36th session of the EMEP Steering Body, the EMEP centres suggested to increase spatial resolution of reported emissions. This new grid is defined in a geographic coordinate system (WGS84) with grid cells at about 28 km x 28 km. The new domain covers the geographic area between 30°N-82°N latitude and 30°W-90°E longitude (Figure 8.1, Dore and Vidič, 2012).

This evolution represents a balance between political needs (requests for detailed information at country level), scientific needs (links with biodiversity and climate changes), and technical feasibility (availability of meteorological and emission data at finer scale, computation time) as of 2014 and for the following years.

Figure 8.1: The EMEP domain over Europe. "Current": Polar-stereographic domain (used since 2008). "New": Latitude-longitude domain (proposed in 2012 (Dore and Vidič, 2012) leading to EB decision 2012/13).

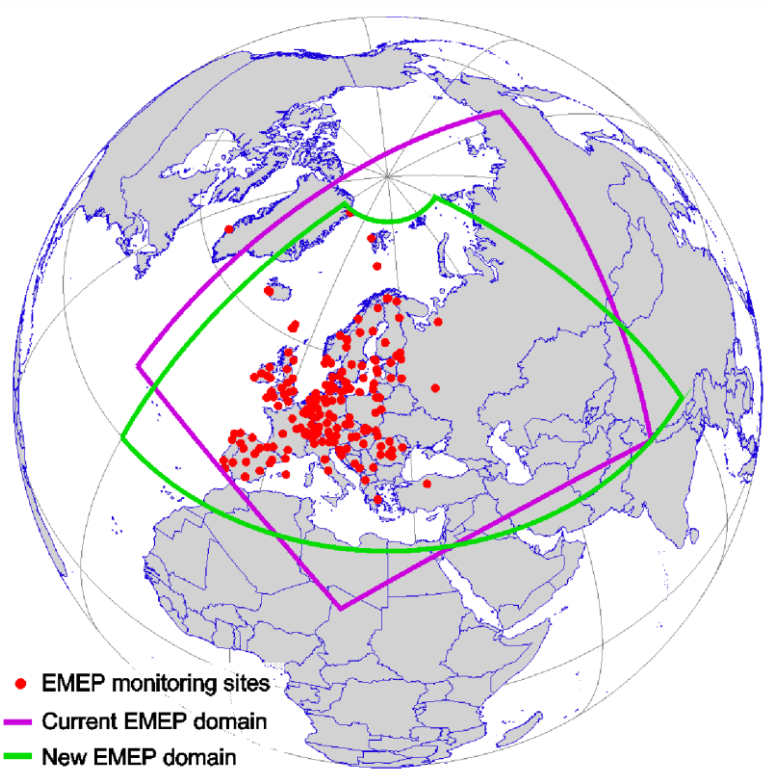

Source: This figure is adopted from a previous version of Chapter 8 of the Mapping Manual

8.1.2.2 The 50×50 km² grid (EMEP50 grid)

The eulerian dispersion model of EMEP/MSC-W produces concentration and deposition fields on a 50 × 50 km² grid with the parameters (see also www.emep.int):

(VIII.7)

$d = 50$ km, $(x_p, y_p) = (8,110)$,

$\phi_0 = \pi/3 = 60°$ N, $\lambda_0 = -32°$ (i.e. 32° W)

yielding M=237.7314...

This 50 x 50 km² gridding of the EMEP area has been used from 1999 to the beginning of 2013. The domain has been extended from the area covered by the initial 150 x 150 km² grid to that presented in *Figure 8.2* in 2008.

Figure 8.2: The EMEP150 grid (solid lines) and EMEP50 grid (dashed lines). The numbers at the bottom and to the right are EMEP150 grid indices; those at the top and to the left are EMEP50 grid indices (every third).

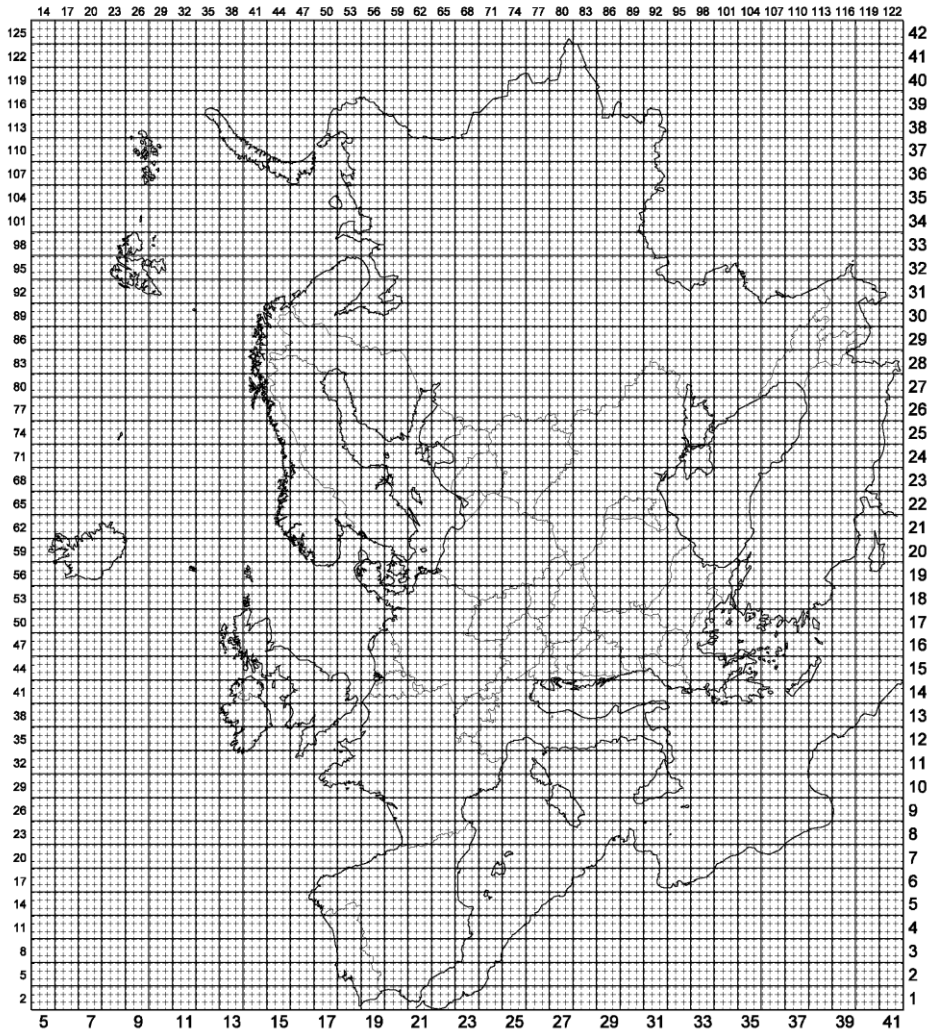

Source: This figure is adopted from a previous version of Chapter 8 of the Mapping Manual

8.1.2.3 The 150×150 km² grid (EMEP150 grid)

The coordinate system used by EMEP/MSC-W for the (old) lagrangian long-range transport model was defined by the following parameters (Saltbones and Dovland 1986):

(VIII.8)

$d = 150$ km, $(x_p, y_p) = (3,37)$,

$\phi_0 = \pi/3 = 60°\text{N}$, $\lambda_0 = -32°$ (i.e. 32° W)

which yields M=79.2438... .

An EMEP150 grid cell (i, j) contains 3×3=9 EMEP50 grid cells (m,n) with all combinations of the indices m=3i–2, 3i–1, 3i and n=3j–2, 3j–1, 3j. The part of the two EMEP grid systems covering Europe is also shown in Figure 8.2.

This gridding of the EMEP area had been used until 1997.

To convert a point (*xlon*, *ylat*), given in degrees of longitude and latitude, into EMEP coordinates (*emepi*, *emepj*), the following FORTRAN subroutine can be used:

```
subroutine llemep (xlon,ylat,par,emepi,emepj)
!
! This subroutine computes for a point (xlon,ylat), where xlon is the
! longitude (<0 west of Greenwich) and ylat is the latitude in degrees,
! its EMEP coordinates (emepi,emepj) with parameters given in par().
!
! par(1) ... size of grid cell (km)
! (par(2),par(3)) = (xp,yp) ... EMEP coordinates of the North Pole
!
real(4) xlon, ylat, par(*), emepi, emepj
!
data Rearth /6370./ ! radius of spherical Earth (km)
data xlon0 /-32./ ! = lambda_0
data drm /1.8660254/ ! = 1+sin(pi/3) = 1+sqrt(3)/2
data pi180 /0.017453293/ ! = pi/180
data pi360 /0.008726646/ ! = pi/360
!
em = (Rearth/par(1))*drm
tp = tan((90.-ylat)*pi360)
rlamp = (xlon-xlon0)*pi180
emepi = par(2)+em*tp*sin(rlamp)
emepj = par(3)-em*tp*cos(rlamp)
                                                                    return
end subroutine llemep
```

EMEP50 coordinates are obtained by calling the above subroutine with *par*(1)=50, *par*(2)=8 and *par*(3)=110; and EMEP150 coordinates are obtained with *par*(1)=150, *par*(2)=3 and *par*(3)=37. Conversely, the EMEP coordinates of a point can be converted into its longitude and latitude with the following subroutine:

```
subroutine emepll (emepi,emepj,par,xlon,ylat)
```

```
!
! This subroutine computes for a point (emepi,emepj) in the EMEP
! coordinate system, defined by the parameters in par(), its
! longitude xlon and latitude ylat in degrees.
!
! par(1) ... size of grid cell (km)
! (par(2),par(3)) = (xp,yp) ... EMEP coordinates of the North Pole
!
real(4) emepi, emepj, par(*), xlon, ylat
!
data Rearth /6370./ ! radius of spherical Earth (km)
data xlon0 /-32./ ! = lambda_0
data drm /1.8660254/ ! = 1+sin(pi/3) = 1+sqrt(3)/2
data pi180 /57.2957795/ ! = 180/pi
data pi360 /114.591559/ ! = 360/pi
!
emi = par(1)/(Rearth*drm) ! = 1/M
ex = emepi-par(2)
ey = par(3)-emepj
if (ex == 0. .and. ey == 0.) then ! North Pole
xlon = xlon0 ! or whatever
else
xlon = xlon0+pi180*atan2(ex,ey)
endif
r = sqrt(ex*ex+ey*ey)
ylat = 90.-pi360*atan(r*emi)
                                                                    return
end subroutine emepll
```

8.1.3 The area of an EMEP grid cell

As mentioned above, the stereographic projection does not preserve areas. For example, a 50 × 50 km² EMEP grid cell is 2,500 km² only in the projection plane, but never on the globe. The area A of an EMEP grid cell with lower-left corner (x_1, y_1) and upper- right corner (x_2, y_2) is given by:

(VIII.9)

$$A(x_1, y_1, x_2, y_2) = 2R^2 \cdot \begin{Bmatrix} I(u_2, v_2) - I(u_1, v_2) \\ -I(u_2, v_1) + I(u_1, v_1) \end{Bmatrix}$$

where $u_1 = (x_1 - x_p)/M$, etc.; and $I(u, v)$ is the double integral (see Posch et al. 1997 for details):

(VIII.10)

$$I(u,v) = \iint \frac{2dudv}{(1+u^2+v^2)^2}$$
$$= \frac{v}{\sqrt{1+v^2}} \cdot \arctan\frac{u}{\sqrt{1+v^2}}$$
$$+ \frac{u}{\sqrt{1+u^2}} \cdot \arctan\frac{v}{\sqrt{1+u^2}}$$

These two equations allow the calculation of the area of the EMEP grid cell (i, j) by setting (x_1, y_1) = $(i–½, j–½)$ and (x_2, y_2) = $(i+½, j+½)$.

The following FORTRAN functions compute the area of an EMEP grid cell for arbitrary grid indices (i, j), for the EMEP50 or the EMEP150 grid, depending on the parameters in *par*() (see above):

```
real function aremep (par,i,j)
!
! Returns the area (in km2) of an ax-parallel cell with
! centerpoint (i,j) in the EMEP grid defined by par().
!
! par(1) ... size of grid cell (km)
! (par(2),par(3)) = (xp,yp) ... EMEP coordinates of the North Pole
!
integer(4) i, j
real(4) par(*)
!
external femep
!
data Rearth /6370./ ! radius of spherical Earth (km)
data drm /1.8660254/ ! = 1+sin(pi/3) = 1+sqrt(3)/2
```

```
!
x1 = real(i)-0.5
y1 = real(j)-0.5
emi = par(1)/(Rearth*drm) ! = 1/M
u1 = (x1-par(2))*emi
v1 = (y1-par(3))*emi
u2 = u1+emi
v2 = v1+emi
ar0 = 2.*Rearth*Rearth
aremep = ar0*(femep(u2,v2)-femep(u1,v2)-femep(u2,v1)+femep(u1,v1))
                                                                    return
end function aremep
!
real function femep (u,v)
!
! Function used in computing the area of an EMEP grid cell.
!
real(4) u, v
!
ui = 1./sqrt(1.+u*u)
vi = 1./sqrt(1.+v*v)
femep = v*vi*atan(u*vi)+u*ui*atan(v*ui)
                                                                    return
end function femep
```

The area distortion ratio α, i.e. the ratio between the area of a small rectangle in the EMEP grid and its corresponding area on the globe is obtained as (Posch et al. 1999):

(VIII.11)

$$\alpha = \left(\frac{1+\sin\phi}{1+\sin\phi_0}\right)^2$$

which shows that the distortion ratio depends on the latitude ϕ only, and (small) areas are undistorted (i.e., α =1, only at ϕ=ϕ_0=60°).

8.2 Comparing critical loads: cumulative distribution functions, percentiles, and protection isolines

Cumulative distribution functions and percentiles allow a statistical description of critical loads and other parameters used by countries.

Cumulative distribution functions are useful to assess and compare the range of critical loads values and of other parameters. Percentiles allow excluding extreme values and thus increase the robustness of the assessments. In this section, we first define and investigate different methods for calculating percentiles of a cumulative distribution function (cdf) given by a finite number of values. Then we generalise the concept of a percentile to the case in which the cdf is defined by a set of *functions* (critical load functions), resulting in the so-called percentile function (protection isoline).

8.2.1 Cumulative distribution function

Assume we have critical load values, x_i, for n ecosystems. We sort these values in ascending order, resulting in a sequence $x_1 \le x_2 \le \ldots \le x_n$. Each value is accompanied by a weight (area) A_i (i=1,...,n), characterizing the size (importance) of the respective ecosystem. From these we compute normalized weights w_i according to:

(VIII.12)

$$w_i = A_i \Big/ \sum_{j=1}^{n} A_j , \qquad i = 1, \ldots, n$$

resulting in:

(VIII.13)

$$\sum_{i=1}^{n} w_i = 1$$

The cumulative distribution function (cdf) of these n critical load values is then defined by:

(VIII.14)

$$F(x) = \begin{cases} 0, & x < x_1 \\ W_k, & x_k \le x < x_{k+1} \\ 1, & x \ge x_n \end{cases}$$

with

(VIII.15)

$$W_k = \sum_{j=1}^{n} w_i , \qquad i = 1, \ldots, n$$

$F(x)$ is the probability of a critical load being smaller than (or equal to) x (i.e., 1–$F(x)$ is the fraction of ecosystems protected). With this definition $F(x)$ has the mathematical properties of a cdf: F is a monotonously increasing right-continuous function with $F(-\infty)$=0 and $F(\infty)$=1. In

Figure 8.3, an example of a cdf is shown. Note that the function assumes only a finite number of values.

Figure 8.3: (a) Example of a cumulative distribution function for n=5 data points ($x_1<x_2<x_3<x_4<x_5$, with weights $w_1=2/15$, $w_2=4/15$, $w_3=5/15$, $w_4=1/15$, $w_5=3/15$). The filled (empty) circles indicate whether a point is part (not part) of the function. (b) The same cdf is drawn by connecting all points, the way a cdf is usually displayed.

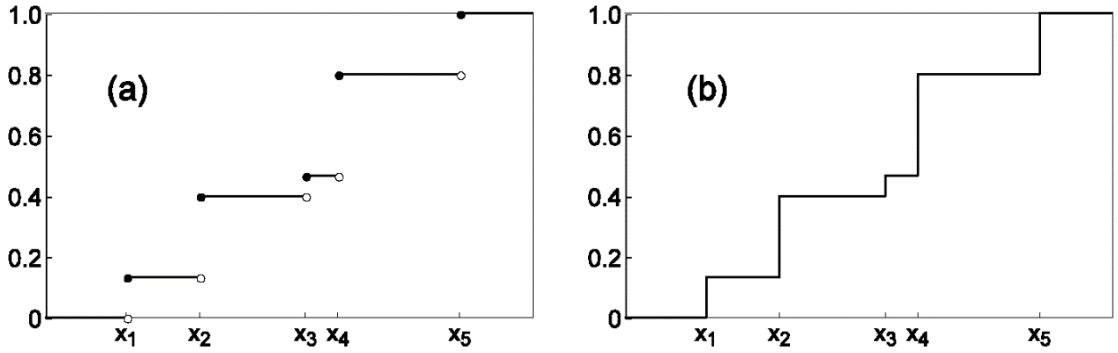

Source: This figure is adopted from a previous version of Chapter 8 of the Mapping Manual

8.2.2 Quantiles and percentiles

All ecosystems in a region (grid cell) are protected, if deposition stays below the smallest critical load values. However, to discard outliers and to account for uncertainties in the critical load calculations, but also to ensure that a sufficient percentage of ecosystems are protected, (low) percentiles of the cdf are compared to the deposition.

The q-th ***quantile*** ($0 \le q \le 1$) of a cdf F, denoted by x_q, is the value satisfying:

(VIII.16)

$$F(x_q) = q$$

which means that x_q, viewed as a function of q, is the inverse of the cdf (i.e. $x_q=F^{-1}(q)$).

Percentiles are obtained by scaling quantiles to 100, therefore the p-th percentile is the $(p/100)$-th quantile. Other terms used are *median* for the 50-th percentile, lower, and upper *quartile* for the 25-th and 75-th percentile, respectively. Note that the p-th percentile critical load protects $100–p$ percent of the ecosystems.

Computing quantiles (i.e. the inverse of a cdf given by a finite number of points) poses a problem: due to the discrete nature of the cdf, a unique inverse simply does not exist.

For many values of q no value x_q exists at all so that eq. VIII.16 holds; and for the n values x_i such a value exists (i.e., $q=F(x_i)$), but the resulting quantile is not unique – every value between x_i and x_{i+1} could be taken (see Figure 8.2). Therefore, the cdf is approximated (interpolated) by a function which allows solving eq. VIII.16 for every q. There is neither a unique approximation, nor is there a single accepted way for calculating percentiles: Posch et al. (1993) discuss six methods for calculating percentiles. Note that commonly definitions are given for data with identical weights (i.e. $w_i=1/n$), but the generalization to arbitrary weights is mostly straightforward. It should be also noted that the differences between different approximation methods vanish when the number of points becomes very large (and all weights small).

In the following we have a closer look at two types of quantile functions: (a) those derived from linearly interpolating the cdf, and (b) those using the empirical cdf. After defining their equations for arbitrary weights we discuss their advantages and disadvantages.

8.2.2.1 Linear interpolation of the cdf

In this case, the quantile function is the inverse of the linearly interpolated cdf given by:

(VIII.17)

$$x_q = \begin{cases} x_1, & q \le w_1 = W_1 \\ x_k + (x_{k+1} - x_k) \cdot \dfrac{q - W_k}{w_{k+1}}, & x_k \le x < x_{k+1} \\ & k = 1, \dots, n \end{cases}$$

where the W_k are defined in eq. VIII.15. An example is shown in Figure 8.4a.

Figure 8.4: Examples of the two quantile functions discussed in the text. Values and weights are the same as in Figure 8.4. The filled (empty) circles indicate whether a point is part (not part) of the function. The thin horizontal lines indicate the cumulative distribution function. Note that for almost all values of q (e.g., q=0.35) the resulting quantile is smaller in (a) than in (b).

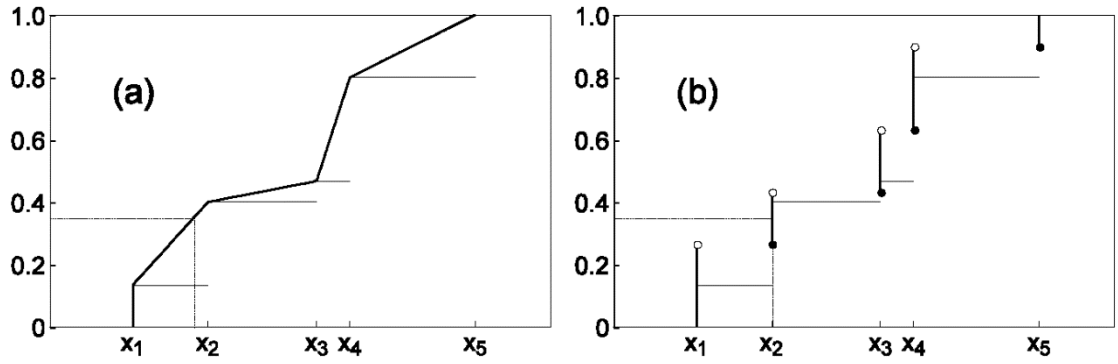

Source: This figure is adopted from a previous version of Chapter 8 of the Mapping Manual

The advantage of this quantile function is that it is continuous, that is to say, a small change in q leads to only a small change in the resulting quantile x_q. However, it has the following three disadvantages:

a) In case of two (or more) identical data points, the definition of the quantile function is not unique: for identical critical load values the shape of the interpolation function depends on the order of the weights (see Figures 8.5 a,a'). This could be resolved by sorting the weights of identical data points according to size (smallest first, as in Figures 8.5a.b). This minimizes the difference to the empirical distribution function (see below) but requires fairly complicated (and time- consuming) routines for the actual computations.

Figure 8.5: **Examples of the two quantile functions discussed in the text. Values and weights are the same as in Figure 8.2, except that $x_3=x_4$ (compare Figure 8.5). Note, that for the linearly interpolated quantile function (a,a') its shape depends on the order of the weights for the identical values.**

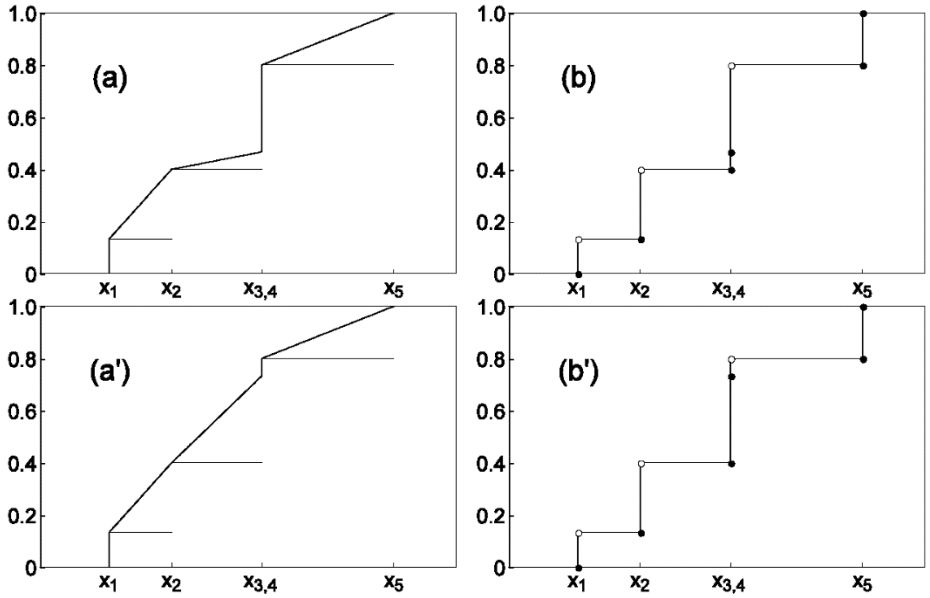

Source: This figure is adopted from a previous version of Chapter 8 of the Mapping Manual

b) As mentioned above, a critical load xq is selected to protect the (1–q)-th fraction of the ecosystems within a given region (grid cell). However, for the linear interpolated quantile function certain choices of q result in xq -values which are below the actual value needed to protect a fraction 1–q of the ecosystems (see example in Figure 8.4). This is protective for the ecosystems but may lead to higher costs for abatement.

c) The computation of quantiles is not order-preserving when using linear interpolation. We say the order is preserved by a quantile function, if the following holds for two cdfs:

(VIII.18)

$F1(x) \leq F2(x)$ for all $x \Rightarrow xq(1) \leq xq(2)$ for all q

In other words, the smaller cdf leads to smaller quantiles. In Figure 8.5a, an example is shown with two data sets for the same n ecosystems, x1,...,xn and y1,...,yn with common weights w1,...,wn and the property xi < yi for i=1,...,n (e.g., CLmin's and CLmax's). But for certain values of q it turns out that xq > yq when computed by linear interpolation (Fig. 8.6a).

Figure 8.6: Example of two quantile functions for 3 values each (x_1, x_2, x_3 and y_1, y_2, y_3) and common weights w_1, w_2, w_3 and the property $x_i<y_i$ for i=1,2,3. However, in case (a) the median $x_{0.5}$ is greater than the median $y_{0.5}$.

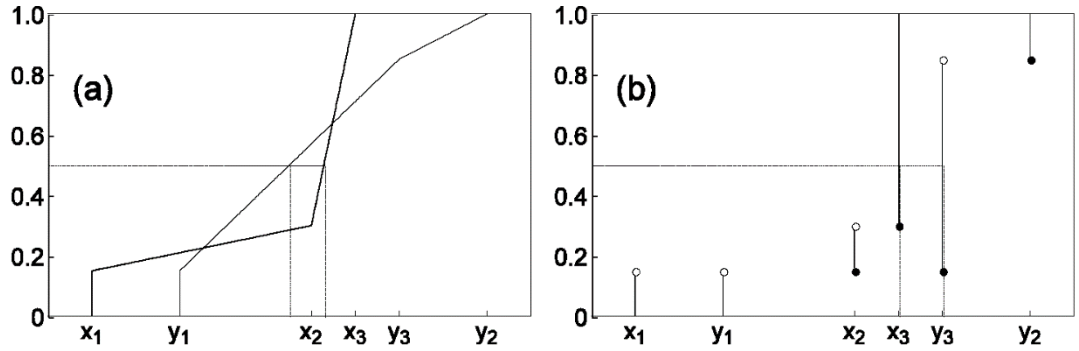

Source: This figure is adopted from a previous version of Chapter 8 of the Mapping Manual

8.2.2.2 Empirical distribution function

In this case the quantile function assumes only values defining the cdf:

(VIII.19)

$$x_q = \begin{cases} x_1, & q \le w_1 = W_1 \\ x_k, & W_{k-1} \le q < W_k, k = 2, \dots, n-1 \\ x_n, & q \ge W_{n-1} \end{cases}$$

An example of this quantile function is shown in Figure 8.5b. The disadvantage of this quantile function is that it is not continuous. A very small change in q may lead to a significant change in the quantile x_q (jump from x_i to $x_{i''1}$).

However, none of the disadvantages of the linear interpolation holds for this function, but:

a) identical values do not lead to ambiguities (see Figures 8.5b, b');

b) the quantile x_q protects (at least) a fraction q of the ecosystems (see Figure 8.4b); and

c) the computation of quantiles is order- preserving (see eq. VIII.18 and Figure 8.6b).

It is especially property (c) which makes the empirical distribution function the only viable choice for computing percentiles. The following FORTRAN subroutine computes the q-quantile of a given vector of data with a corresponding vector of weights. The data have to be sorted in ascending order, but the weights do not have to be normalised to one.

```
subroutine qantilcw (q,num,vec,wei,xq)

!

! This subroutine computes the q-quantile xq of the num values in vec()

! - sorted in ascending order - with corresponding weights wei()

! from the empirical distribution function.

!

integer(4) num
```

```
real(4) q, vec(*), wei(*), xq
!
if (num == 0) stop 'Quantile of nothing?!'
if (q < 0. .or. q > 1.) stop 'q outside [0,1]!'
!
wsum = wei(1)
do k = 2,num
wsum = wsum+wei(k)
if (vec(k) < vec(k-1)) stop 'Data not sorted!'
end do
!
qw = q*wsum
sum = 0.
do k = 1,num
sum = sum+wei(k)
if (qw < sum) then
xq = vec(k)
                                                                    return
end if
end do
xq = vec(num) ! if q=1
                                                                    return
end subroutine qantilcw
```

8.2.3 Percentile functions and protection isolines

In this section, we generalize of the concept of cumulative distribution function (cdf) and quantile (percentile) to the case when the data (e.g., critical loads) are given as a function (rather than as single values), which is the case when considering two pollutants (e.g., sulphur and nitrogen in the case of acidification), leading to the so- called percentile function or (ecosystem) protection isoline.

In the following we assume that a (critical load) function is defined by a set of pairs of values (nodes) (x_j,y_j), $(j=1,...,m)$, and the function is given by connecting (x_1,y_1) with (x_2,y_2) etc., in this way generating a polygon in the x-y plane. We denote this polygon by:

(VIII.21)

$\boldsymbol{f} = [(x_1,y_1),...,(x_m, y_m)]$

For the values x and y we assume that:

(VIII.22)

$0 = x_1 \le x_2 \le ... \le x_m$ and $y_1 \ge y_2 \ge ... \ge y_m = 0$

The nodes on the polygon are numbered from left to right, starting on the y-axis and ending on the x-axis. Eq. VIII.22 also ensures that the polygon is monotonically decreasing, when considered as a function of x or y[19]. With the notation $(x,y)<\boldsymbol{f}$ we mean that the point (x,y) lies below the polygon (i.e., critical loads are not exceeded).

Considering the critical load for S and N acidity the critical load function for an ecosystem is defined by 3 values, namely $CL_{min}(N)$, $CL_{max}(N)$, and $CL_{max}(S)$, and as a polygon with m=3 nodes it is written according to eq. VIII.21 as:

(VIII.23)

$\boldsymbol{CLF} = [(0, CL_{max}(S)),(CL_{min}(N), CL_{max}(S)),(CL_{max}(S),0)]$

where we assumed that the N-deposition is plotted along the x-axis and the S- deposition along the y-axis.

Now we assume that we have n critical load functions $\boldsymbol{f}_1,...,\boldsymbol{f}_n$ with respective weights $w_1,...,w_n$ (Σw_i=1). In general, it will not be possible to sort these critical load functions. In other words, it is not possible to say that $\boldsymbol{f}_i$ is larger or smaller than $\boldsymbol{f}_j$, because $CL_{max}(S)$ for $\boldsymbol{f}_i$ could be larger and $CL_{max}(N)$ smaller than the corresponding values for $\boldsymbol{f}_j$ (see Figure 8.7 for examples). Nevertheless, we can define a cumulative distribution function F in the following way:

(VIII.24)

$$F(x,y) = \sum_{(x,y)<f_i} w_i$$

meaning that for a given point (x,y) we sum all weights w_i for which $(x,y)<\boldsymbol{f}_i$, (i.e., for which there is no exceedance). Obviously $0 \le F(x,y) \le 1$, and F has also otherwise all properties of a (two-dimensional) cdf. A percentile p is now easily defined as the intersection of such a function with a horizontal plane at height $q=p/100$. The result (projected onto the x-y plane) is a curve, more precisely a polygon which has the property defined in eq. VIII.22. Let $\boldsymbol{f}_q$ be the quantile (percentile) function for a given q, then every point (x,y) (i.e., every pair of N and S deposition), with $(x,y)<\boldsymbol{f}_q$ protects (at least) a fraction of $1-q$ of the ecosystems; and $\boldsymbol{f}_q$ is also called a (*ecosystem*) *protection isoline*. Note that protection isolines for the same set of polygons (critical load functions) do not intersect (although they might partly coincide), and for $r<s$ $\boldsymbol{f}_r$ lies below $\boldsymbol{f}_s$.

Since an exact computation of a percentile function is hardly feasible (especially in case of a large number of critical load functions), we have to use an approximate method (see Figure 8.7): we draw rays through the origin of the x-y plane (i.e., lines with a constant S:N deposition ratio) and compute the intersections of these rays with all critical load functions (small circles in Figure 8.7a). For each ray the intersection points are sorted according to their distance from the origin and the chosen quantiles of these distances are calculated according to eq. VIII.19. Finally, the resulting quantile values are connected to obtain the percentile functions (protection

[19] Alternatively, the numbering could start on the x-axis, etc.

isolines). Obviously, the more rays are used in this procedure the more accurate are the protection isolines. As Figure VIII.8b shows, a protection isoline need not be convex.

Figure 8.7: Computation of protection isolines: (a) set of critical load functions and intersection of these CL-functions with rays from the origin (small circles); (b) computing the percentiles (*q*=0.25, 0.50 and 0.75 in this case) along each ray (small diamonds) and connecting them to obtain the protection isolines (thick [red] lines).

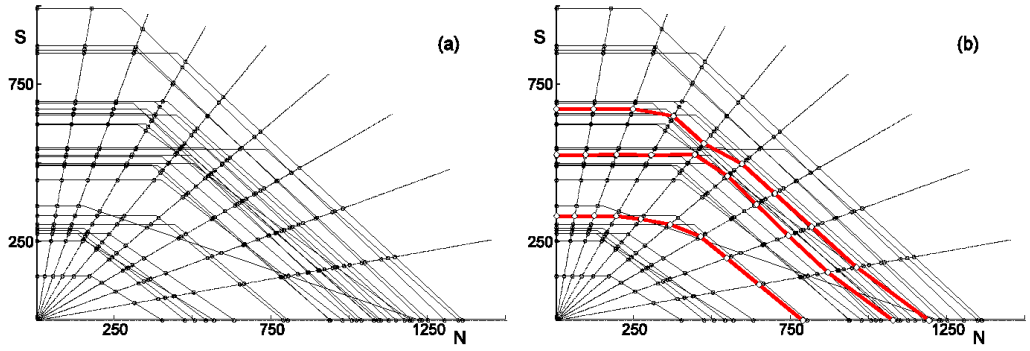

Source: This figure is adopted from a previous version of Chapter 8 of the Mapping Manual

8.3 Critical load exceedances used in integrated assessment modelling

8.3.1 Gap closure methods

Except for the earliest protocols, integrated assessment modellers have used uniform *percentage* reductions of the excess deposition (so-called *gap closures*) to define emission reduction scenarios. In the following we summarize the different gap closure methods used and illustrate them for the case of a single pollutant. This section follows largely Posch et al. (2001).

In the 1994 Sulphur Protocol, only sulphur was considered an acidifying pollutant (N deposition was fixed; it determined, together with N uptake and immobilization, the sulphur fraction). Furthermore, considering the uncertainties in the CL calculations, it was decided to use the 5-th percentile of the critical load cdf in a grid cell as the only value representing the ecosystem sensitivity of that cell. The exceedance was simply the difference between the (current) S deposition and that 5-th percentile critical load. This is illustrated in Figure 8.8a): Critical loads and deposition are plotted along the horizontal axis and the (relative) ecosystem area along the vertical axis. The thick solid and the thick broken lines are two examples of critical load cdfs (which have the same 5-th percentile critical load, indicated by 'CL'). 'D0' indicates the (present) deposition, which is higher than the CLs for 85% of the ecosystem area. The difference between 'D0' and 'CL' is the exceedance in that grid cell. It was decided to reduce the exceedance everywhere by a fixed percentage (i.e., to 'close the gap' between (present) deposition and (5-th percentile) critical load). In Figure 8.8a, a *deposition gap closure* of 60% is shown as an example. As can be seen, a fixed deposition gap closure can result in very different improvements in ecosystem protection percentages (55% vs. 22%), depending on the shape of the critical load cdf.

Figure 8.8: **Cumulative distribution function (thick solid line) of critical loads and different methods of gap closure: (a) deposition gap closure, (b) ecosystem gap closure, and (c) accumulated exceedance (AE) gap closure. The thick dashed line in (a) and (b) depict another cdf, illustrating how different ecosystem protection follows from the same deposition gap closure (a), or how different deposition reductions are required to achieve the same protection level (b).**

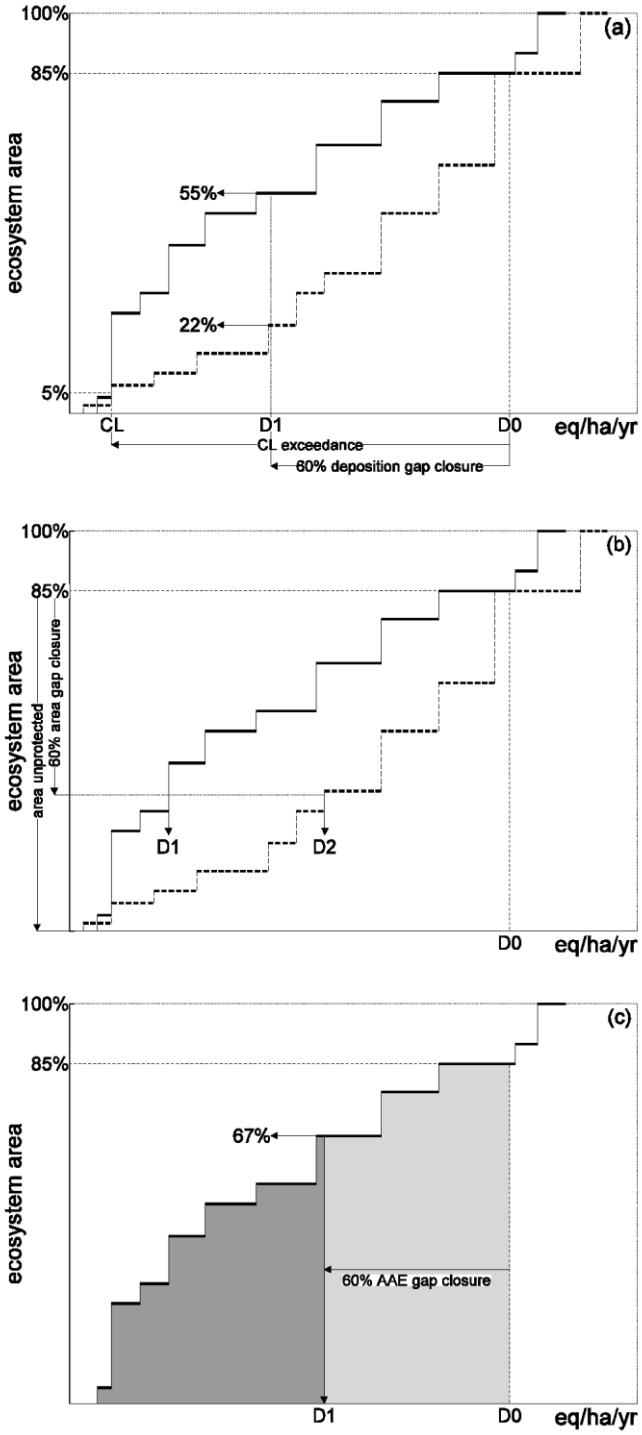

Source: This figure is adopted from a previous version of Chapter 8 of the Mapping Manual

When considering all critical loads within a grid cell (and not only the 5-th percentile), it was suggested to use an *ecosystem area gap* closure instead of the deposition gap closure. This is illustrated in Figure 8.8b: for a given deposition 'D0' the ecosystem area unprotected, as such, with deposition exceeding the critical loads can be read from the vertical axis. After agreeing to a certain (percent) reduction of the unprotected area (i.e., 60%), it is easy to compute for a given cdf the required deposition reduction ('D1' and 'D2' in Figure 8.8b). Another important reason to use the ecosystem area gap closure is that it can be easily generalized to two (or more) pollutants, which is not the case for a deposition-based exceedance. This generalization became necessary for the negotiations of the 1999 Gothenburg Protocol, as both N and S contribute to acidification. Critical load values have been replaced by critical load functions and percentiles replaced by ecosystem protection isolines (see above). However, the use of the area gap closure becomes problematic if only a few critical load values or functions are given for a grid cell. In such a case the cdf becomes highly discontinuous, and small changes in deposition may result in either no increase in the protected area at all or large jumps in the area protected.

To remedy the problem with the area gap closure caused by discontinuous cdfs, the accumulated exceedance (AE) concept has been introduced (see above). In the case of one pollutant, the AE is given as the area under the cdf of the critical loads (the entire grey-shaded area in Figure 8.8c). Deposition reductions are now negotiated in terms of an AE (or AAE) *gap closure*, also illustrated in Figure 8.8c: a 60% AE gap closure is achieved by a deposition 'D1' which reduces the total grey area by 60%, resulting in the dark grey area; also the corresponding protection percentage (67%) can be easily derived. The greatest advantage of the AE and AAE is that it varies smoothly as deposition is varied, even for highly discontinuous cdfs, thus facilitating optimization calculations in integrated assessment. The advantages and disadvantages of the three gap closure methods described above are summarized in the following table.

Table 8.1: Advantages and disadvantages of the different gap closure methods used to define emission scenarios for policies in 1994, 1997 and 1999.

	Advantages	Disadvantages
Deposition gap closure (used for the 1994 Sulphur Protocol)	• Easy to use even for discontinuous cdfs (e.g. grid cells with only one CL).	• Takes only one CL value (e.g. 5th percentile) into account. • May result in no increase in protected area. • Difficult to define for two pollutants.
Ecosystem area gap closure (used for the EU 1997 Acidification Strategy)	• In line with the goals of CL use (maximum ecosystem protection). • Easy to apply to any number of pollutants.	• Difficult (or even impossible) to define a gap closure for discontinuous cdfs (e.g. grid cells with only one CL).
Accumulated Exceedance (AE) gap closure (used for the 1999 Gothenburg Protocol)	• AE (and AAE) is a smooth and convex function of deposition even for discontinuous cdfs.	• AE stretches the limits of the critical load definition. * • Exceedance definition not unique for two or more pollutants.

* It assumes a linear damage function. However, this feature could also be an advantage.

8.3.2 Linear emission-exceedance relationships

The change to higher resolutions of the EMEP grid and the introduction of new pollutants (in particular PM) has led to a significant increase of required calculations for optimization exercises of scenarios. In order to keep computing times at a workable level, the methodology to calculate critical loads exceedances has been simplified. The new approach has been inspired by the Life Cycle Impact Analysis (LCIA) community which uses the simplest approach possible, as such, a linear relationship between emission (changes) and impact (changes) on ecosystems. Models and factors are described and defined in Posch et al. (2005).

In practice, linear relationships are defined between the emission and the average accumulated exceedances for each country. This linearization requires deposition fields computed exactly with a full atmospheric transport model for the reference scenario (for instance "current legislation" scenario). The coefficients of the linear relationship are "impact" or "damage" factors. They are site or country dependent. The impact factors are computed by changing the emission of one pollutant at the time in a given source region, compared to the reference scenario, leaving the emissions of the other pollutants and all other source regions unchanged (further details in Posch et al. 2005).

The approach makes it feasible to assess several policy scenarios. Errors on the results remain small if the assessed scenario remains close to the reference scenario: tests have shown that when the emissions are reduced by up to 20%, the linear model produces good approximations. Besides, approximations become poor when exceedances become close to 0.

8.4 References

CLRTAP, 2015. General mapping issues, Chapter VIII of Manual on methodologies and criteria for modelling and mapping critical loads and levels and air pollution effects, risks and trends. UNECE Convention on Long-range Transboundary Air Pollution.

Dore CJ, Vidič S (2012) Considerations of changing the EMEP Grid. Document prepared by the EMEP Centres MSC-W, MSC-E, CEIP and CIAM, EMEP, Geneva, Switzerland. 9 pp.

EMEP (2013) Transboundary Acidification, Eutrophication and Ground Level Ozone in Europe in 2011. Norwegian Meteorological Institute, Oslo, Norway, 205 pp.

Posch M, Kämäri J, Johansson M, Forsius M (1993) Displaying inter- and intra- regional variability of large-scale survey results. *Environmetrics* 4: 341-352

Posch M, De Smet PAM, Hettelingh J-P, Downing RJ (eds) (1995) Calculation and mapping of critical thresholds in Europe. Status Report 1995, Coordination Centre for Effects, RIVM Report 259101004, Bilthoven, Netherlands, iv+198 pp.

Posch M, Hettelingh J-P, De Smet PAM, Downing RJ (eds) (1997) Calculation and mapping of critical thresholds in Europe. Status Report 1997, Coordination Centre for Effects, RIVM Report 259101007, Bilthoven, Netherlands, iv+163 pp.

Posch M, De Smet PAM, Hettelingh J-P, Downing RJ (eds) (1999) Calculation and mapping of critical thresholds in Europe. Status Report 1999, Coordination Centre for Effects, RIVM Report 259101009, Bilthoven, Netherlands, iv+165 pp. www.wge-cce.org

Posch M, Hettelingh J-P, De Smet PAM (2001) Characterization of critical load exceedances in Europe. *Water, Air and Soil Pollution* 130: 1139-1144

Posch M, Hettelingh J-P, Heyes C (2005) Use of critical loads in integrated assessment modelling. In: M Posch, J Slootweg, J-P Hettelingh (eds), European Critical loads and dynamic modelling: CCE Status Report 2005. RIVM Report259101016, Coordination Centre for Effects, Bitlhoven, The Netherlands, pp. 71-76

Saltbones J, Dovland H (1986) Emissions of sulphur dioxide in Europe in 1980 and 1983. EMEP/CCC Report 1/86, Norwegian Institute for Air Research, Lillestrøm (now in Kjeller), Norway

Simpson D, Benedictow A, Berge H, Bergström R, Emberson LD, Fagerli H, Flechard CR, Hayman GD, Gauss M, Jonson JE, Jenkin ME, Nyiri A, Richter C, Semeena VS, Tsyro S, Tuovinen JP, Valdebenito A, Wind P (2012) The EMEP MSC-W chemical transport model - technical description. *Atmospheric Chemistry and Physics* 12(16): 7825-7865.